HERBAL MEDICINES IN THE TREATMENT OF LIVER DISEASES - EFFICACY, ACTION MECHANISMS AND CLINICAL APPLICATION

EDITED BY: Yanling Zhao, Ping Liu and Yibin Feng

frontiers Research Topics

About Frontiers

Frontiers is more than just an open-access publisher of scholarly articles: it is a pioneering approach to the world of academia, radically improving the way scholarly research is managed. The grand vision of Frontiers is a world where all people have an equal opportunity to seek, share and generate knowledge. Frontiers provides immediate and permanent online open access to all its publications, but this alone is not enough to realize our grand goals.

Frontiers Journal Series

The Frontiers Journal Series is a multi-tier and interdisciplinary set of open-access, online journals, promising a paradigm shift from the current review, selection and dissemination processes in academic publishing. All Frontiers journals are driven by researchers for researchers; therefore, they constitute a service to the scholarly community. At the same time, the Frontiers Journal Series operates on a revolutionary invention, the tiered publishing system, initially addressing specific communities of scholars, and gradually climbing up to broader public understanding, thus serving the interests of the lay society, too.

Dedication to Quality

Each Frontiers article is a landmark of the highest quality, thanks to genuinely collaborative interactions between authors and review editors, who include some of the world's best academicians. Research must be certified by peers before entering a stream of knowledge that may eventually reach the public - and shape society; therefore, Frontiers only applies the most rigorous and unbiased reviews.
Frontiers revolutionizes research publishing by freely delivering the most outstanding research, evaluated with no bias from both the academic and social point of view. By applying the most advanced information technologies, Frontiers is catapulting scholarly publishing into a new generation.

What are Frontiers Research Topics?

Frontiers Research Topics are very popular trademarks of the Frontiers Journals Series: they are collections of at least ten articles, all centered on a particular subject. With their unique mix of varied contributions from Original Research to Review Articles, Frontiers Research Topics unify the most influential researchers, the latest key findings and historical advances in a hot research area! Find out more on how to host your own Frontiers Research Topic or contribute to one as an author by contacting the Frontiers Editorial Office: frontiersin.org/about/contact

HERBAL MEDICINES IN THE TREATMENT OF LIVER DISEASES - EFFICACY, ACTION MECHANISMS AND CLINICAL APPLICATION

Topic Editors:
Yanling Zhao, Fifth Medical Center of the PLA General Hospital, China
Ping Liu, Shanghai University of Traditional Chinese Medicine, China
Yibin Feng, The University of Hong Kong, SAR China

Table of Contents

Check for updates

Calculus Bovis Sativus Improves Bile Acid Homeostasis via Farnesoid X Receptor-Mediated Signaling in Rats With Estrogen-Induced Cholestasis

Dong Xiang, Jinyu Yang, Yanan Liu, Wenxi He, Si Zhang, Xiping Li, Chenliang Zhang* and Dong Liu*

Department of Pharmacy, Tongji Hospital Affiliated, Tongji Medical College, Huazhong University of Science and Technology, Wuhan, China

Cholestatic diseases are characterized by toxic bile acid (BA) accumulation, and abnormal BA composition, which subsequently lead to liver injury. Biochemical synthetic *Calculus Bovis Sativus* (CBS) is derived from natural *Calculus Bovis*, a traditional Chinese medicine, which has been used to treat hepatic diseases for thousands of years. Although it has been shown that CBS administration to 17α-ethinylestradiol (EE)-induced cholestatic rats improves bile flow and liver injury, the involved underlying mechanism is largely unknown. In this study, we showed that CBS administration to EE-induced cholestatic rats significantly decreased serum and hepatic BA levels and reversed hepatic BA composition. DNA microarray analysis suggested that the critical pathways enriched by CBS treatment were bile secretion and primary BA synthesis. These findings led us to focus on the effects of CBS on regulating BA homeostasis, including BA transport, synthesis and metabolism. CBS enhanced hepatic BA secretion by inducing efflux transporter expression and inhibiting uptake transporter expression. Moreover, CBS reduced BA synthesis by repressing the expression of BA synthetic enzymes, CYP7A1 and CYP8B1, and increased BA metabolism by inducing the expression of metabolic enzymes, CYP3A2, CYP2B10, and SULT2A1. Mechanistic studies indicated that CBS increased protein expression and nuclear translocation of hepatic and intestinal farnesoid X receptor (FXR) to regulate the expression of these transporters and enzymes. We further demonstrated that beneficial effects of CBS administration on EE-induced cholestatic rats were significantly blocked by guggulsterone, a FXR antagonist. Therefore, CBS improved BA homeostasis through FXR-mediated signaling in estrogen-induced cholestatic rats. Together, these findings suggested that CBS might be a novel and potentially effective drug for the treatment of cholestasis.

Keywords: *Calculus Bovis Sativus*, cholestasis, FXR, 17α-ethinylestradiol, bile acid

INTRODUCTION

Cholestatic liver diseases, including estrogen-induced cholestasis, primary biliary cholangitis (PBC), and primary sclerosing cholangitis (PSC), result from intrahepatic accumulation of toxic bile acids (BAs) that cause liver injury and ultimately lead to fibrosis and cirrhosis (Trauner et al., 2017). When treatment is delayed, many patients would require a liver transplantation at the end-stage of cholestatic diseases (Wang et al., 2017). Estrogens and their metabolites are known to cause intrahepatic cholestasis in susceptible women during pregnancy as well as administration of oral contraceptives and postmenopausal hormone replacement therapy (Li et al., 2017). Currently, only few therapies to effectively treat cholestatic diseases are available, and the curative effect is limited (Jansen et al., 2017). Thus, developing novel therapeutic strategies for treating and managing cholestatic liver diseases is of utmost importance.

Considering clinical implications, experimental cholestasis induced by 17α-ethynylestradiol (EE) administration in rodents has been widely used to investigate the underlying molecular/cellular mechanisms involved in estrogen-induced cholestasis (Zhang et al., 2018). In experimental animals, treatment with EE decreased bile flow and BA synthesis, thereby leading to accumulation of high levels of BAs and an abnormal BA composition in the liver (Fischer et al., 1996). BA homeostasis is tightly controlled by hepatic nuclear receptors, including the farnesoid X receptor (FXR, NR1H4), pregnane X receptor (PXR, NR1I2), vitamin D receptor (VDR, NR1I1), constitutive androstane receptor (CAR, NR1I3), liver X receptor (LXR, NR1H3), and the peroxisome proliferator-activated receptor α (PPARα, PPARA) (Zollner and Trauner, 2009). Importantly, FXR is one of the main mediators in the liver and intestine and regulates BA transporters and enzymes to maintain BA homeostasis Li and Chiang, 2013. Ligand-activated FXR promoted BA secretion through inducing the expression of efflux transporters, including bile salt export pump (BSEP, ABCB11) and multidrug resistance-associated protein 2 (MRP2, ABCC2), and reduced BA reabsorption via decreasing the expression of uptake transporters, such as Na$^+$-dependent taurocholate cotransport peptide (NTCP), and sodium-independent organic anion transporters (OATPs) (Halilbasic et al., 2013). In addition, FXR inhibited cholesterol 7α-hydroxylase (CYP7A1) and microsomal sterol 12α-hydroxylase (CYP8B1) to reduce BA synthesis and induce CYP3A2 (a homolog of human CYP3A4) and sulfotransferase family 1E member 1 (SULT1E1) to promote BA detoxification (Chiang, 2013). In previous studies, it has been demonstrated that targeting FXR is promising for treating cholestatic liver diseases (Beuers et al., 2015).

Calculus Bovis is a traditional Chinese medicine, which has been widely used in Oriental and Southeast Asian countries, especially China, to relieve fever, alleviate inflammation, maintain sedation, and recover gallbladder function (Chen, 1987). Due to the extremely scarce resources (gallstones of *Bos Taurus domesticus Gmelin*), and high prices, countless studies have strived to substitute natural *Calculus Bovis*. According to the formation principle of gallstones *in vivo* and the methods of biochemical synthesis, *Calculus Bovis Sativus* (CBS) is cultivated from bovine bile *in vitro* by modern bioengineering techniques. CBS is an ideal substitute, which is identical in terms of properties and components and has been included in the Pharmacopoeia of the People's Republic of China since 2005 Edition (Feng et al., 2015). According to pharmacopeia, CBS has a definite chemical profile, containing cholic acid, deoxycholic acid, and bilirubin as its principal bioactive components. As reported, CBS has been successfully used to treat many severe liver diseases, such as hepatic cancer, hepatitis B, and non-alcoholic fatty liver disease in both humans and experimental animals (Liu et al., 2010; Bai and Zhao, 2011; Cheng et al., 2014). In our previous study, we showed that CBS exerted beneficial effects on EE-induced cholestatic rats, at least in part by improving functions of MRP2, breast cancer resistance protein (BCRP), and P-glycoprotein (P-gp) (Liu et al., 2014).

In the present study, we aimed to fully understand the hepatoprotective effects of CBS on EE-induced cholestasis and investigated the underlying mechanisms involved. We utilized DNA microarray to screen the critical pathways involved in CBS treatment and studied the effects of CBS on hepatic BA composition as well as regulatory functions on BA synthesis, metabolism, and transport. The findings of our study suggested that FXR-mediated signaling plays a critical role in the beneficial effects of CBS on EE-induced cholestasis.

MATERIALS AND METHODS

Chemicals and Reagents

Calculus Bovis Sativus was provided by Wuhan Jianmin Dapeng Pharmaceutical Co., Ltd. (Lot: 2016-05-16, Wuhan, China), and the same preparation and lot number was used in our previous study (He et al., 2017). We also successfully established a liquid chromatography-tandem mass spectrometry (LC-MS/MS) approach to determine the main components in CBS, and subsequently established a quality control method to ensure the stability, uniformity, and quality of CBS (Feng et al., 2015; He et al., 2017). EE was purchased from Sigma-Aldrich (St. Louis, MO, United States, purity ≥98%). Guggulsterones (GS) was purchased from Dibo biochemical Co., Ltd. (Shanghai, China). Standards for BAs for cholic acid (CA), deoxycholic acid (DCA), chenodeoxycholic acid (CDCA), β-muricholic acid (β-MCA), taurocholic acid (TCA), taurodeoxycholic acid (TDCA), β-tauromuricholic acid (Tβ-MCA), and tauroursodeoxycholic acid (TUDCA) were obtained from Steraloids (Newport, RI, United States). The internal standard (IS) was from Isoreag (Shanghai, China). Antibodies directed against NTCP, FXR, CYP7A1, LXR, VDR, CAR, PXR, PPARα, CK19, Lamin B, and β-actin were purchased from Absin Biochemical Company (Shanghai, China). An antibody directed against BSEP was obtained from Santa Cruz Biotechnology (Santa Cruz, CA, United States) and an antibody directed against MRP2 was obtained from Abcam (Cambridge, United Kingdom). All other chemical agents used were from analytical grade or HPLC grade.

Animals and Treatments

The present study was conducted in strict accordance with the National Institutes of Health guide for the care and use of laboratory animals (Muhler et al., 2011). The animal protocol was approved by the Ethical Committee on Animal Experimentation of the Tongji hospital (Tongji, Wuhan, China). Male Sprague-Dawley rats, 8 weeks of age and weighing 220 ± 20 g were obtained from the Center of Experimental Animal of Hubei Province (Wuhan, China). All animals were housed under standard laboratory conditions at a temperature of 25 ± 2°C and a 12-h light/dark cycle. To induce cholestatic rats, EE (5 mg/kg) was subcutaneously injected for five consecutive days. Non-cholestatic control rats received the EE vehicle (propylene glycol). CBS (150 mg/kg) or vehicle (0.5% sodium carboxymethyl cellulose) was administered to rats by oral gavage once per day for five consecutive days with co-administration of EE or EE vehicle. GS, an FXR antagonist, was dissolved as previous described (Meng et al., 2015), and rats were injected intraperitoneally with 10 mg/kg of GS 4 h prior to CBS or vehicle treatment. Body weight was recorded daily. Animals were fasted overnight and sacrificed randomly between 8:00 and 11:00 am. Blood, bile, liver, and ileum samples were collected for further analyses.

Serum Biochemistry Assay and Histology

Serum levels of alanine aminotransferase (ALT), aspartate aminotransferase (AST), alkaline phosphatase (ALP) as well as serum and hepatic levels of total bile acid (TBA) were determined using commercial kits (JianCheng, Nanjing, China) according to the manufacturer's instructions. After rats were sacrificed, livers were collected, fixed in 4% formaldehyde, embedded in paraffin, sectioned at 5 μm, and stained with hematoxylin and eosin (H&E). Images were taken by EVOS FL Auto microscope (Life Technologies, Carlsbad, CA, United States) and Olympus microscope (Olympus, Tokyo, Japan).

DNA Microarray Analysis

Total RNA of three randomly chosen livers from non-cholestatic, EE, and EE+CBS rats was isolated by a Takara RNAiso Plus kit and purified using an RNeasy Mini Kit (Qiagen, GmBH, Darmstadt, Germany) following the manufacturer's instructions. Total RNA was amplified and labeled by an Agilent Quick Amp Labeling Kit. Each slide was hybridized with Agilent Whole Rat Genome Oligo Microarray (4 × 44K). Data were collected by Agilent Feature Extraction software 10.7 (Agilent Technologies, Santa Clara, CA, United States) and then filtered for significant detection (Student's t-test, $p < 0.05$, and fold change >1.2 or <0.8). Technical support was provided by Biotechnology Corporation (Shanghai, China) for determining the whole gene expression profile. Gene ontology (GO) and Kyoto encyclopedia of genes and genomes (KEGG) analyses of differentially expressed genes were performed by using the common public online database DAVID Bioinformatics Resources 6.8 Tools[1].

---

[1]https://david.ncifcrf.gov

Analysis of Bile Acids in the Liver by Liquid Chromatography-Tandem Mass Spectrometry

In brief, approximately 100 mg of liver tissue was homogenized in 4 volumes of methanol-water (50:50 v/v). A total of 150 μL of liver homogenate was added to 20 μL IS (5 μmol/L d4-GCDCA) and 1 mL of ice-cold alkaline acetonitrile (containing 5% $NH_3 \cdot H_2O$ v/v), then samples were vortexed and shaken for 60 min, and centrifuged at 12,000 × g for 10 min at 4°C. Subsequently, supernatants were evaporated and reconstituted in 100 μL methanol. A high-performance liquid chromatography (HPLC; LC-20AD, Shimadzu, Japan) system coupled to an Applied Biosystems 4000 Q trap (AB Sciex, CA, United States) mass spectrometer with electrospray ionization source (ESI) was used. Chromatographic separation of BAs was performed using a C18 column (3.5 μm, 2.1 mm × 150 mm, Symmetry®Waters, MA, United States). The mobile phase consisted of A (water with 10 mM ammonium acetate and 0.1% formic acid) and B (methanol with 10 mM ammonium acetate and 0.1% formic acid). A gradient elution was used, starting with 60% B for the first 2 min, then linearly increased to 90% B in 38 min, and kept constant for 5 min. All BAs were detected in the negative ionization mode with the following mass spectrometer source settings: ion spray voltage = −4500 V; ionsource heater = 300°C; source gas 1 = 40 psi; source gas 2 = 40 psi, and curtain gas = 20 psi. Data were collected and analyzed using Analyst 1.6.1 software (AB Sciex, CA, United States).

Quantitative Real-Time PCR Assay

Total RNA from liver and intestine was extracted using TRIzol Reagent (Invitrogen, CA, United States) according to the manufacturer's instructions. Total RNA was reverse transcribed into cDNA using PrimeScript™ RT Master Mix (Takara, Dalian, China), and then obtained cDNA was used as a template for real-time PCR amplification, performed by using SYBR Green (Takara, Dalian, China) and forward/reverse primer pairs for the tested genes. Independent reactions were performed in triplicate using an ABI StepOne Plus system (Applied Biosystems, CA, United States). Threshold cycle values were normalized to β-actin. Both forward and reverse primers used are presented in **Supplementary Table 1**.

Western Blot Analysis

Western blot analysis of membrane and total protein samples was performed as described in our previous study (Liu et al., 2014). In brief, nuclear protein samples from hepatic and intestinal tissues were extracted following standard protocols (Beyotime Institute of Biotechnology, Shanghai, China). Proteins were subjected to SDS–PAGE, then transferred to PVDF membranes. After blocking for 1 h with 5% non-fat milk in TBST, membranes were incubated overnight at 4°C with primary antibodies directed against MRP2, BSEP, NTCP, CYP7A1, FXR, LXR, VDR, CAR, PXR, PPARα, Lamin B, and β-actin. Next, membranes were incubated with horseradish peroxidase (HRP)-conjugated antibodies
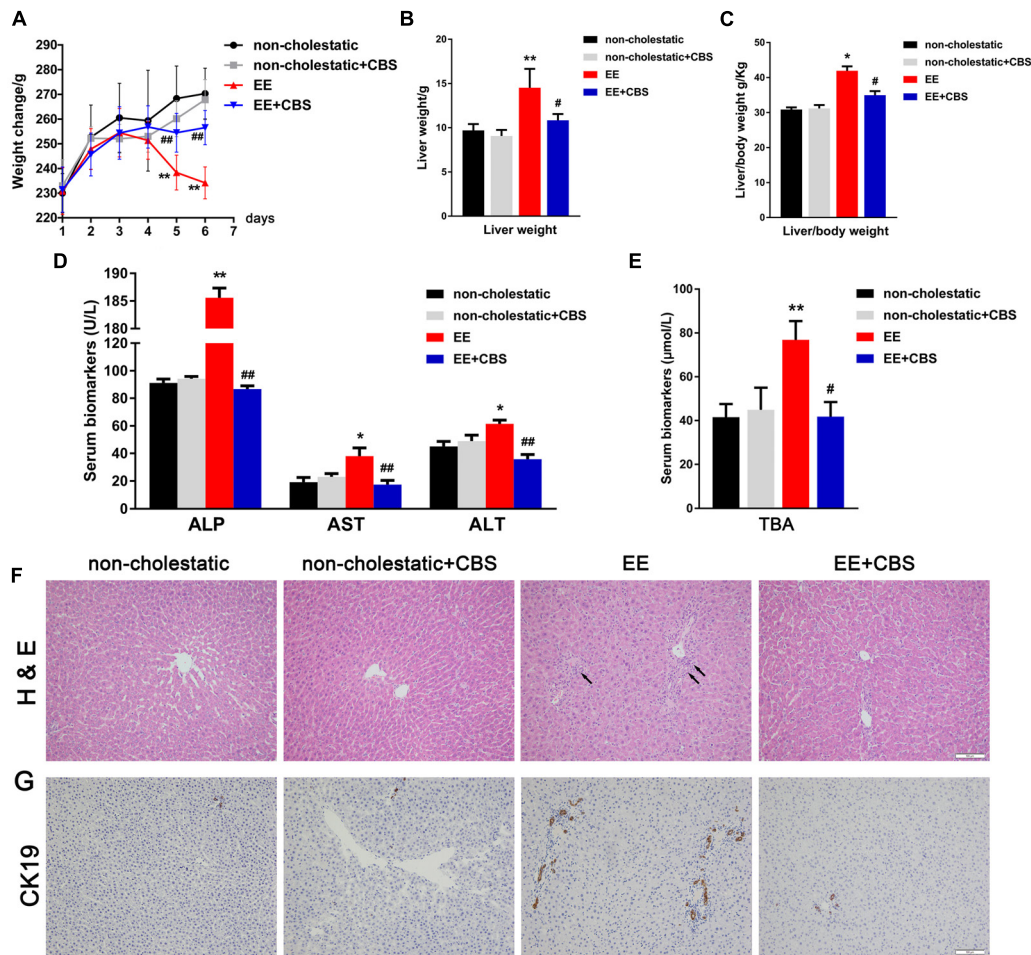
FIGURE 1 | CBS alleviates liver injury and reduces serum bile acid levels in rats with 17α-ethinylestradiol-induced cholestasis. **(A)** Changes in body weight in each group during the six experimental days. Determination of **(B)** liver weight, **(C)** liver/body weight, and **(D)** serum alanine aminotransferase (ALT), aspartate aminotransferase (AST), alkaline phosphatase (ALP), and **(E)** total bile acid (BA) levels. **(F)** Hematoxylin and eosin (H&E) staining was used to investigate hepatic structural changes under non-cholestatic and cholestatic conditions in rats. **(G)** Immunohistochemistry of CK19 was performed to evaluate proliferation of the bile duct. Data are presented as the mean ± SD ($n = 6$). Significant differences compared with the non-cholestatic group, $*p < 0.05$; $**p < 0.01$; compared with the 17α-ethinylestradiol (EE) group, $\#p < 0.05$; $\#\#p < 0.01$.

for 1 h at room temperature at a 1:2500 dilution. Protein expression was evaluated by an enhanced chemiluminescence (ECL) approach and membranes were imaged with a BOX Chemi XRQ imaging system (SynGene, Cambridge, United Kingdom).

Immunohistochemistry

Immunohistochemical analysis for CK19, FXR, and CYP7A1 was performed as previously described (Liu et al., 2014). In brief, hepatic or intestinal tissues sections were incubated with antibodies directed against CK19, FXR, or CYP7A1 for 5 h at 37°C, then treated with corresponding secondary antibodies. Images were taken using an Olympus microscope (Tokyo, Japan), and analyzed by Image-Pro Plus 6.0 software (Media Cybernetics, Silver Spring, MD, United States). Positive staining was quantified by counting three different fields per section (200×).

Statistical Analysis

Data are expressed as the mean ± SE. Significance was determined by one-way analysis of variance (ANOVA) followed by Tukey's test using GraphPad Prism 7 software. $P < 0.05$ was considered statistically significant.

RESULTS

CBS Alleviates Liver Injury and Reduces Serum Bile Acid Levels

In our preliminary study, we found the best hepatoprotective effects of CBS in the high dose group. Therefore, in the present study, 150 mg/kg of CBS was chosen. At the first 4 days, the body weight of the animals in the four groups was not significantly changed. However, at days 5 and 6, the body weight
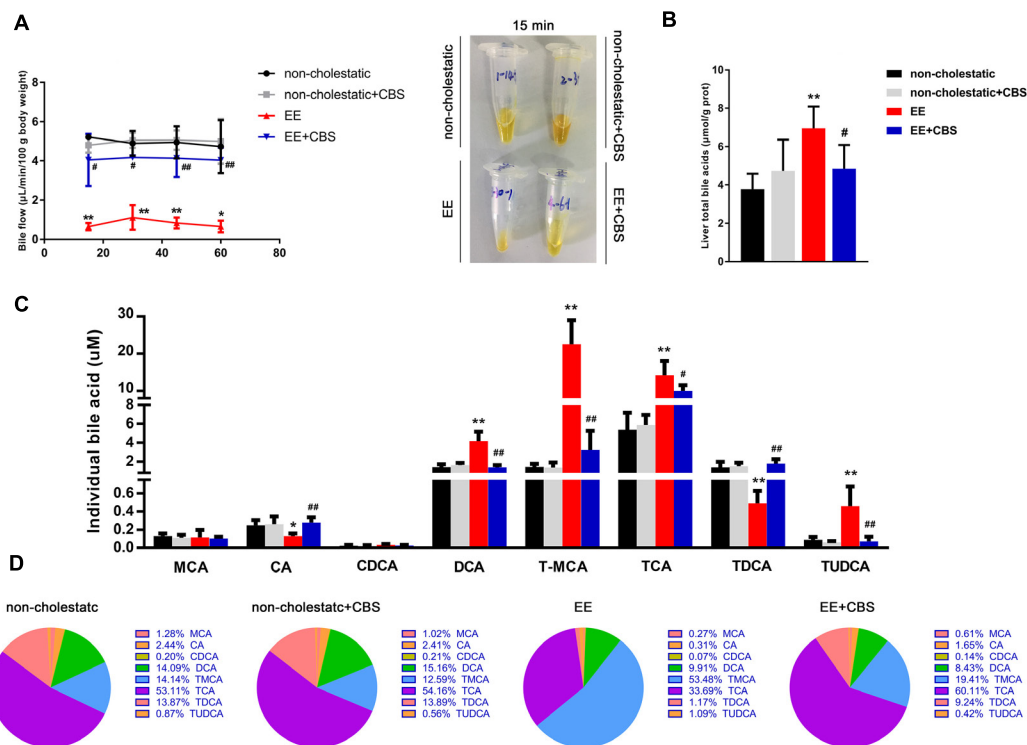
FIGURE 2 | CBS improves intrahepatic bile acid accumulation and composition. **(A)** Bile was collected for four 15-min periods over 60 min under basal, non-stimulated conditions. The bile flow rate was calculated by gravimetry, assuming the density of the bile of 1.0 g/mL. Representative collection tubes are shown here. **(B)** Liver total bile acids (BAs). **(C)** Hepatic individual BAs were assessed by liquid chromatography-tandem mass spectrometry (LC-MS/MS). **(D)** Analysis of BA composition. Data are presented as the mean ± SD (n = 6). Significant differences when compared with the non-cholestatic group, *p < 0.05; **p < 0.01; compared with the 17α-ethinylestradiol (EE) group, #p < 0.05; ##p < 0.01. Abbreviations: MCA, muricholic acid; CA, cholic acid; CDCA, chenodeoxycholic acid; DCA, deoxycholic acid; TMCA, tauromuricholic acid; TCA, taurocholic acid; TDCA, taurodeoxycholic acid; TUDCA, tauroursodeoxycholic acid.

of EE cholestatic rats was markedly reduced when compared to that of non-cholestatic rats. In contrast, the body weight of cholestatic rats treated with CBS was slightly reduced but not significantly different from the body weight of non-cholestatic rats (**Figure 1A**). This suggested that CBS treatment improved the overall condition of cholestatic animals. This beneficial effect was also noted in the liver weight and liver/body weight: the weight or relative weight of livers of rats in the EE+CBS group was markedly lower when compared to that of rats in the EE group (**Figures 1B,C**).

As previously reported (Liu et al., 2014; Meng et al., 2015), serum ALT, AST, and ALP levels were significantly higher in EE cholestatic rats when compared to that of non-cholestatic rats. These biochemical indicators of hepatotoxicity were reduced by CBS treatment (**Figure 1D**). Serum TBA levels were markedly higher in EE cholestatic rats, whereas CBS administration resulted in a striking reduction in serum TBA levels in cholestatic rats (**Figure 1E**).

Histological assessments of the liver further indicated EE-induced hepatotoxicity. EE groups associated with significant increases in inflammatory cell infiltration, edema, bile duct proliferation, and severe hepatic necrosis (**Figure 1F**). Immunohistochemistry of CK19 further confirmed the bile duct proliferation in EE groups. These pathological changes

were markedly reduced by CBS treatment (**Figure 1G** and **Supplementary Figure 1**). CBS administration in non-cholestatic rats did not cause significant changes in body weight, liver weight, liver/body weight, serum biomarkers, or liver histology.

CBS Improves Intrahepatic Bile Acid Accumulation and Composition

Figure 2 shows the basal bile flow, liver total BAs as well as hepatic BA composition in EE cholestatic and non-cholestatic rats treated with CBS or vehicle. As expected, remarkable bile flow obstruction (approximately down to 16.3%) and hepatic BA accumulation (up to 183.7%) were observed in EE-induced cholestasis when compared with non-cholestatic rats. However, CBS administration significantly increased bile flow 5.0-fold and decreased liver total BAs 1.4-fold in EE cholestatic rats (**Figures 2A,B**). Individual BA levels and BA composition was performed in liver tissues using an LC-MS/MS method. Representative chromatograms are shown in **Supplementary Figure 2** and the method details are provided in **Supplementary Tables 2**, **3**. Together, these results suggested that EE-induced rats increased hepatic DCA, TMCA, TCA, and TUDCA levels, and decreased CA and TDCA levels, as well as impaired
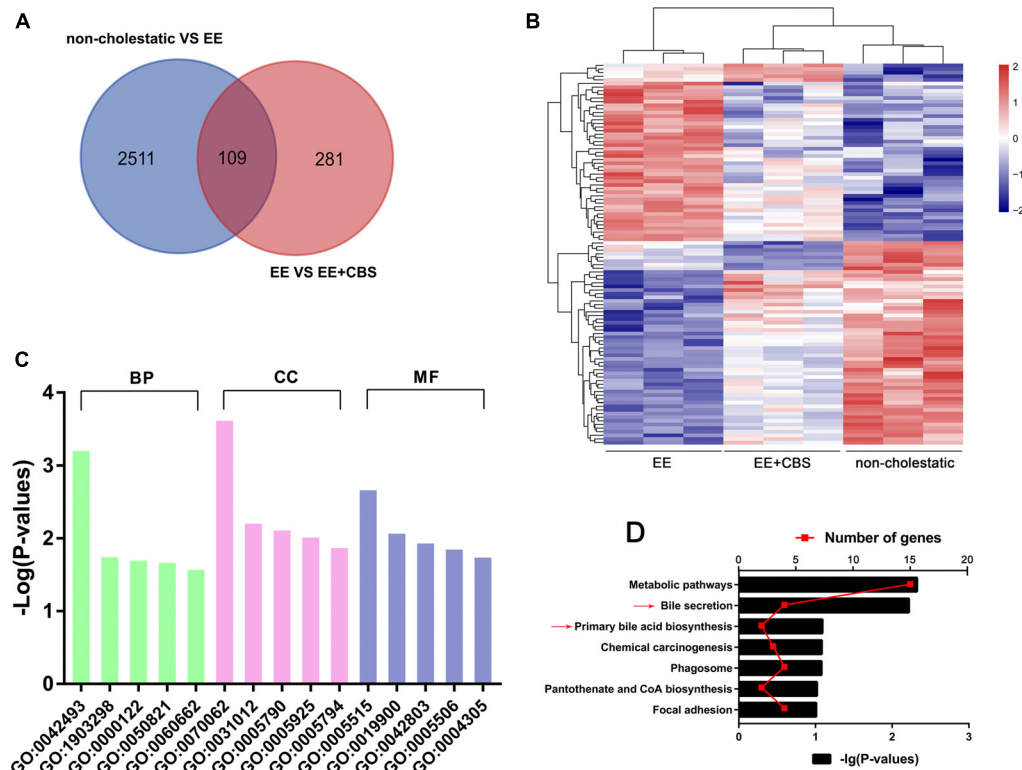
FIGURE 3 | DNA microarray analysis of non-cholestatic, 17α-ethinylestradiol (EE) and EE+CBS rat livers. **(A)** Venn diagram analysis of differentially expressed genes of non-cholestatic, EE and EE+CBS groups. **(B)** Heat map of differentially expressed genes in non-cholestatic, EE and EE+CBS groups **(C)** gene ontology (GO) analysis of differentially expressed genes **(D)** Kyoto encyclopedia of genes and genomes (KEGG) pathway analysis of differentially expressed genes. Arrows point to the pathways related to bile acid (BA) homeostasis; ($n = 3$). Abbreviations: BP, biological process; CC, cellular component; MF, molecular function. Interpretation: GO:0042493, response to drug; GO:1903298, negative regulation of hypoxia-induced intrinsic apoptotic signaling pathway; GO:0000122, negative regulation of transcription from RNA polymerase II promoter; GO:0050821, protein stabilization; GO:0060662, salivary gland cavitation; GO:0070062, extracellular exosome; GO:0031012, extracellular matrix; GO:0005790, smooth endoplasmic reticulum; GO:0005925, focal adhesion; GO:0005794, Golgi apparatus; GO:0005515, protein binding; GO:0019900, kinase binding; GO:0042803, protein homodimerization activity; GO:0005506, iron ion binding; and GO:0004305, ethanolamine kinase activity.

BA composition (**Figures 2C,D**). However, CBS administration reversed individual BA levels (**Figure 2C**) and nearly shifted the abnormal BA composition to non-cholestatic level (**Figure 2D**).

Gene Expression Profile of CBS on EE-Induced Cholestasis

To systematically investigate the molecular mechanisms underlying the hepatoprotective effects of CBS on EE-induced cholestasis, we first performed DNA microarray analysis. The results of the significant difference ($p < 0.05$ and fold change >1.2) gene showed that: compared with non-cholestatic rats, there were 2511 differentially expressed genes in EE cholestatic rats. In addition, compared with EE cholestatic rats, there were 281 differentially expressed genes in CBS-treated cholestatic rats. When comparing all three groups, a total of 109 genes overlapped (**Figure 3A**). The heatmap of 109 differentially expressed genes is presented in **Figure 3B**. GO analysis suggested that the main biological process involved a response to drugs (GO: 0042493), the molecular function primary involved protein binding (GO: 0070062), and the main cellular component was

associated with extracellular exosome (GO: 0005515) (**Figure 3C** and **Supplementary Table 4**). The KEGG pathways were mainly enriched in metabolic pathways, bile secretion, primary BA biosynthesis, and chemical carcinogenesis (**Figure 3D** and **Supplementary Table 5**). In conclusion, CBS improved intrahepatic BA accumulation involved in regulating multiple pathways.

CBS Promotes Bile Acid Efflux and Reduces Bile Acid Influx

Because CBS improved hepatic BA accumulation, and the gene expression profile of CBS treatment was enriched in bile secretion and primary BA biosynthesis (**Figure 3D**), we hypothesized that CBS alleviating EE-induced cholestasis might be involved in the modulation of BA homeostasis, including BA transport, metabolism, and synthesis. Therefore, we first evaluated changes in expression of various BA transporters after CBS administration.

The basolateral uptake transporter Ntcp showed a significant decrease in CBS administration when compared to EE cholestatic
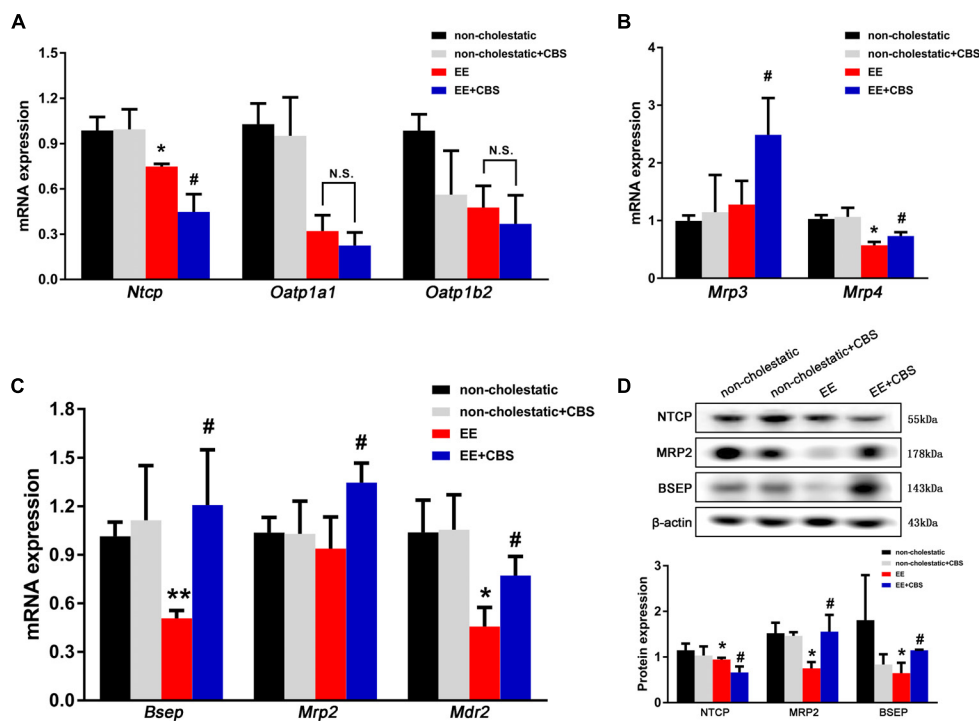
FIGURE 4 | CBS promotes bile acid efflux and reduces bile acid influx in cholestatic rats. mRNA expression of **(A)** basolateral uptake transporters, *Ntcp*, *Oatp1a1*, and *Oatp1b2*, as well as **(B)** basolateral efflux transporters, *Mrp3* and *Mrp4*, and **(C)** canalicular efflux transporters, *Bsep*, *Mrp2*, and *Mdr2*, was determined by real-time PCR and normalized to β-actin. **(D)** Protein levels of NTCP, BSEP, and MRP2 were determined by Western blot analysis and normalized with β-actin. Data are presented as the mean ± SD ($n = 6$). Significant differences compared to the non-cholestatic group, *$p < 0.05$; **$p < 0.01$; compared with the 17α-ethinylestradiol (EE) group, #$p < 0.05$; ## $p < 0.01$. N.S., no significance.

rats, whereas Oatp1a1 and Oatp1b2 were unaffected (**Figure 4A**). In addition, CBS administration in EE-treated rats significantly induced mRNA expression of *Mrp3* and *Mrp4* in the liver, which predominantly secreted BAs into the circulation (**Figure 4B**). However, apical transporters such as *Bsep*, *Mrp2,* and *Mdr2* decreased in rats after EE treatment but increased after CBS administration when compared to EE cholestatic rats (**Figure 4C**). Western blot results for the main efflux and influx transporters corresponded with real-time PCR findings. The protein expression of BSEP, MRP2, and NTCP was decreased in EE cholestatic rats, whereas NTCP levels further reduced, and MRP2 and BSEP levels markedly increased with CBS treatment (**Figure 4D**). Thus, CBS protected the liver from toxic BA accumulation involved in decreasing BA uptake from the portal circulation and increased the excretion of BA from hepatocytes.

CBS Reduces Bile Acid Synthesis and Promotes Bile Acid Metabolism

Next, we investigated BA synthesis and metabolism. As shown in **Figure 5A**, mRNA levels of *Cyp7a1* and *Cyp8b1*, two enzymes involved in the classic pathway of BA synthesis, were significantly reduced by 50 and 90%, respectively, in EE-induced cholestatic rats when compared to non-cholestatic rats. In addition, CBS administration further inhibited the transcription of *Cyp7a1*, and completely abolished *Cyp8b1* expression. Western blot

analysis showed that CYP7A1 was modestly but markedly decreased in CBS-treated livers when compared to the EE group (**Figure 5B**). Moreover, immunohistochemical staining of CYP7A1 further confirmed these results (**Figure 5C** and **Supplementary Figure 3**).

It has been shown that phase I (CYP3A2 and CYP2B10) and phase II (SULT2A1, BAL and BAAT) metabolic enzymes mainly mediate BAs detoxification in the liver (Li and Chiang, 2013). In our study, we showed that expression levels of *Cyp3a2* and *Cyp2b10* mRNA were dramatically decreased in EE-induced cholestatic rats, which were mildly, but markedly increased by CBS treatment (**Figure 5D**). EE decreased mRNA expression of *Sult2a1*, *Bal*, and *Baat*, whereas CBS administration significantly enhanced *Sult2a1* expression level but did not affect *Bal* and *Baat* (**Figure 5E**). Taken together, CBS not only improved BA transport but CBS also decreased BA synthesis and increased BA phase I and phase II metabolism in the liver, with the net result being decreased accumulation of toxic BAs.

CBS Activates Protein Expression and Nuclear Translocation of FXR in the Liver and Intestine

Numerous studies have demonstrated that liver nuclear receptors including FXR, PXR, CAR, VDR, LXR, and PPARα, play important roles in BA homeostasis through controlling BA
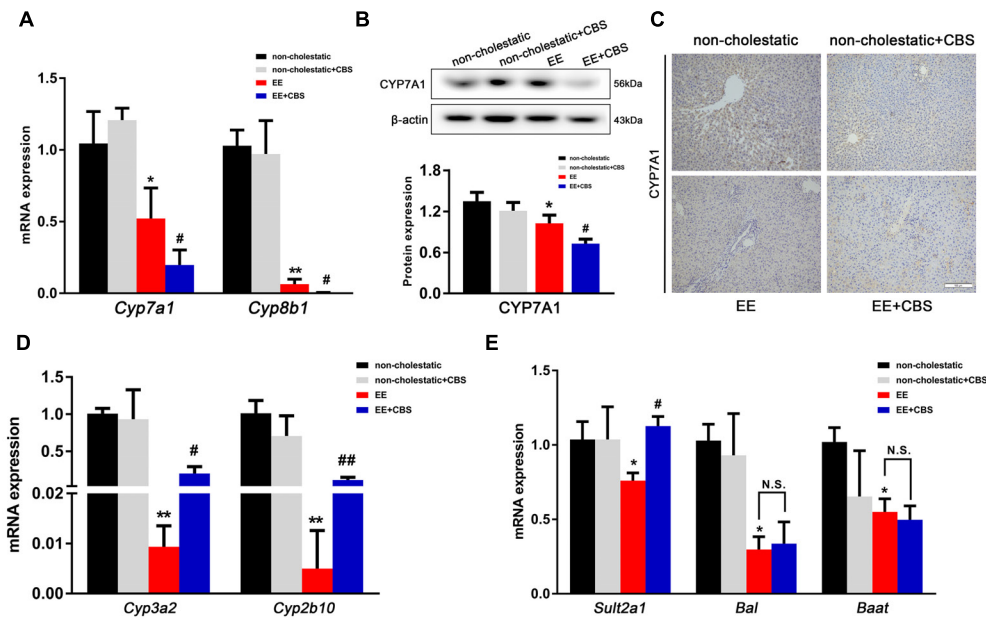
FIGURE 5 | CBS reduces bile acid synthesis and promotes bile acid metabolism in cholestatic rats. **(A)** mRNA expression of bile acid (BA) synthetic enzymes, *Cyp7a1* and *Cyp8b1*, was determined by real-time PCR and normalized to β-actin. **(B)** Protein expression of hepatic CYP7A1 was determined by Western blot analysis and normalized to β-actin. **(C)** Representative images of immunohistochemical staining of hepatic CYP7A1. mRNA expression of **(D)** *Cyp3a2*, *Cyp2b10* and **(E)** *Sult2a1*, *Bal*, and *Baat* was evaluated by real-time PCR and normalized to β-actin. Data are presented as the mean ± SD ($n = 6$). Significant differences compared with the non-cholestatic group, $*p < 0.05$; $**p < 0.01$; compared with the 17α-ethinylestradiol (EE) group, $^{\#}p < 0.05$; $^{\#\#}p < 0.01$. N.S., no significance.

synthesis, metabolism, and transport (Li and Chiang, 2013). CBS alleviated EE-induced cholestasis, which was associated with mediating hepatic BA transporters and enzymes, therefore we next examined whether those nuclear receptors were involved in this regulatory progress. Unexpectedly, microarray analysis showed that there was no significant alteration between the EE+CBS group and EE group among these nuclear receptors (**Supplementary Figure 4**), which was consistent the real-time PCR results (**Figure 6A**). Interestingly, Western blot analysis showed that FXR was dramatically decreased by 50% in EE cholestatic rats, but was totally reversed to the non-cholestatic level after CBS treatment (**Figures 6B,C**). Furthermore, CBS administration significantly increased FXR nuclear translocation in cholestatic rats (**Figures 6D,E**). However, protein levels and nuclear translocation of other nuclear receptors did not change in CBS-treated cholestatic rats when compared with EE cholestatic rats (**Figures 6B–E**). Moreover, hepatic small heterodimer partner (SHP), a direct target gene of FXR, was markedly increased (**Figure 6G**). These results may indicate that FXR-mediated signaling, but not PXR, CAR, VDR, LXR, and PPARα, play a critical role in CBS administration in EE-induced cholestatic rats.

In our study, CYP7A1 was severely inhibited in the rat liver. Recent studies have shown that hepatic CYP7A1 is down-regulated by both hepatic FXR-SHP and intestinal FXR-fibroblast growth factor 15 (FGF15)-mediated pathways (Kong et al., 2012). Therefore, we investigated if intestinal FXR participated in CBS treatment in EE cholestatic rats. Consistent with the liver observations, CBS administration did not alter

mRNA expression of intestinal *Fxr*, but dramatically increased protein expression and nuclear translocation of intestinal FXR (**Figure 6F**), and increased mRNA expression of its target gene *Fgf15* (**Figure 6G**). In addition, immunohistochemical staining showed increased expression of hepatic and intestinal FXR after CBS treatment (**Figures 6H,I** and **Supplementary Figure 5**). Thus, CBS administration activated both hepatic and intestinal FXR and increased their nuclear translocation to regulate the expression of BA transporters and enzymes.

CBS Improved Hepatic Bile Acid Homeostasis Is Abrogated by FXR Antagonist GS

To further confirm that CBS activated FXR to regulate BA homeostasis, the FXR antagonist GS was used in rats. Because of abrogation of the FXR after GS treatment, there was a significant serum elevation of ALP, AST, and TBA levels, whereas serum ALT levels were unchanged (**Figures 7A,B**). In the liver, GS directly decreased protein expression and nuclear translocation of CBS-activated FXR (**Figure 7C**). Similarly, GS decreased the expression of *Shp* and *Bsep*, classical FXR target genes, and enhanced the expression of *Cyp7a1* in CBS-treated cholestatic rats (**Figure 7D**). In the intestine, GS decreased protein expression and nuclear translocation of CBS-induced FXR (**Figure 7E**). *Fgf15*, a direct target gene of FXR in the intestine, was reduced by GS treatment (**Figure 7F**). Because FGF15 and SHP were both decreased, the reduced expression of *Cyp7a1* by CBS was abrogated by GS administration
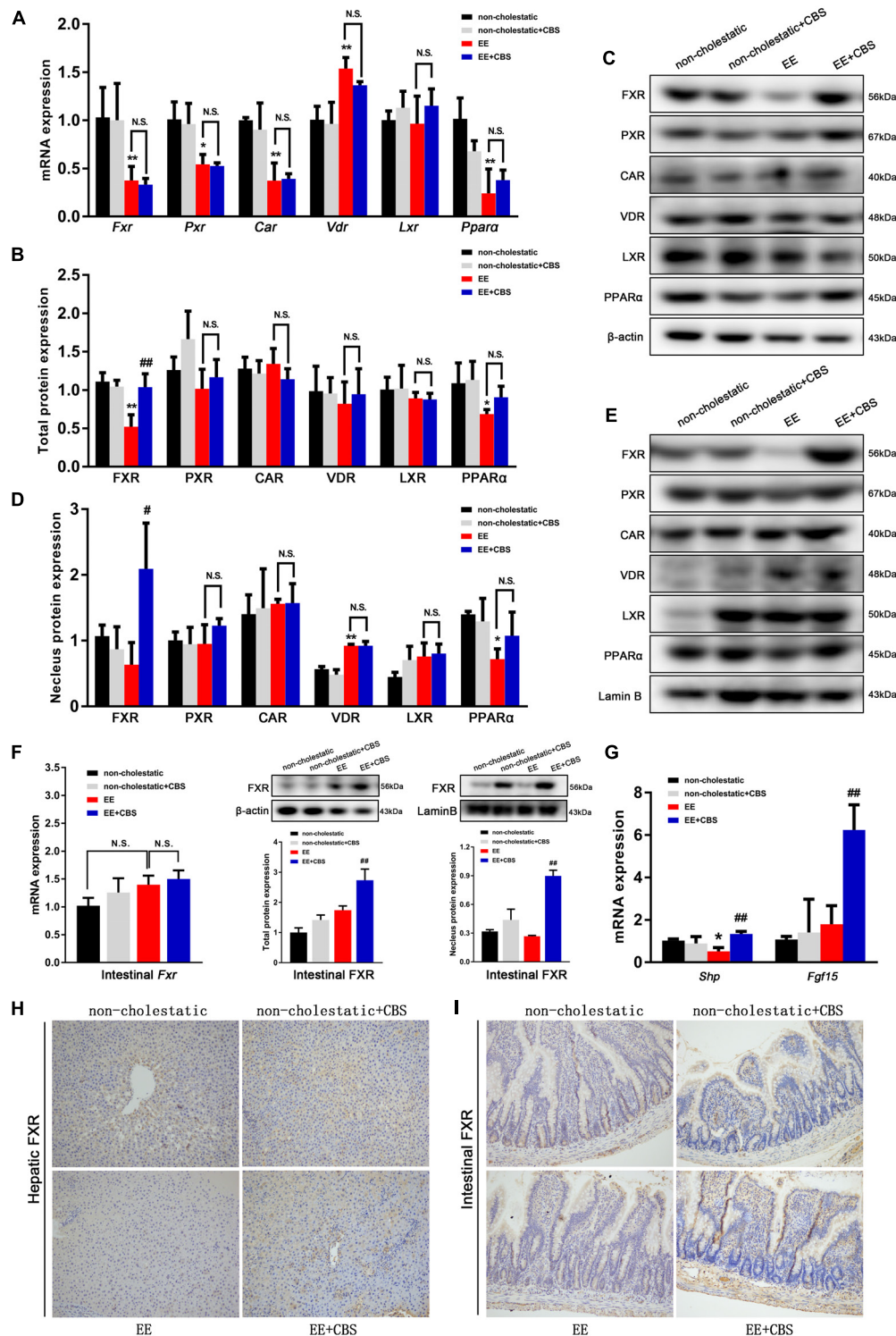
FIGURE 6 | CBS activates the protein expression and nuclear translocation of FXR in liver and intestine. **(A)** mRNA expression of hepatic nuclear receptors *Fxr*, *Pxr*, *Car*, *Vdr*, *Lxr*, and *Pparα* was determined by real-time PCR and normalized to β-actin. **(B,C)** Total protein levels and **(D,E)** nuclear protein levels of hepatic FXR, PXR, CAR, VDR, LXR, and PPARα were determined by Western blot analysis and normalized to β-actin and Lamin B. Representative immunoblot images are shown. **(F)** mRNA, total protein and nuclear protein levels of intestinal FXR were determined using real-time PCR and Western blot analysis and normalized to β-actin and Lamin B. **(G)** mRNA levels of *Shp* in liver and *Fgf15* in intestine were evaluated by real-time PCR and normalized to β-actin. Representative images of immunohistochemical staining of **(H)** hepatic FXR and **(I)** intestinal FXR. Data are presented as the mean ± SD (*n* = 6). Significant differences compared with the non-cholestatic group, *p < 0.05; **p < 0.01; compared with the 17α-ethinylestradiol (EE) group, #p < 0.05; ##p < 0.01. N.S., no significance.
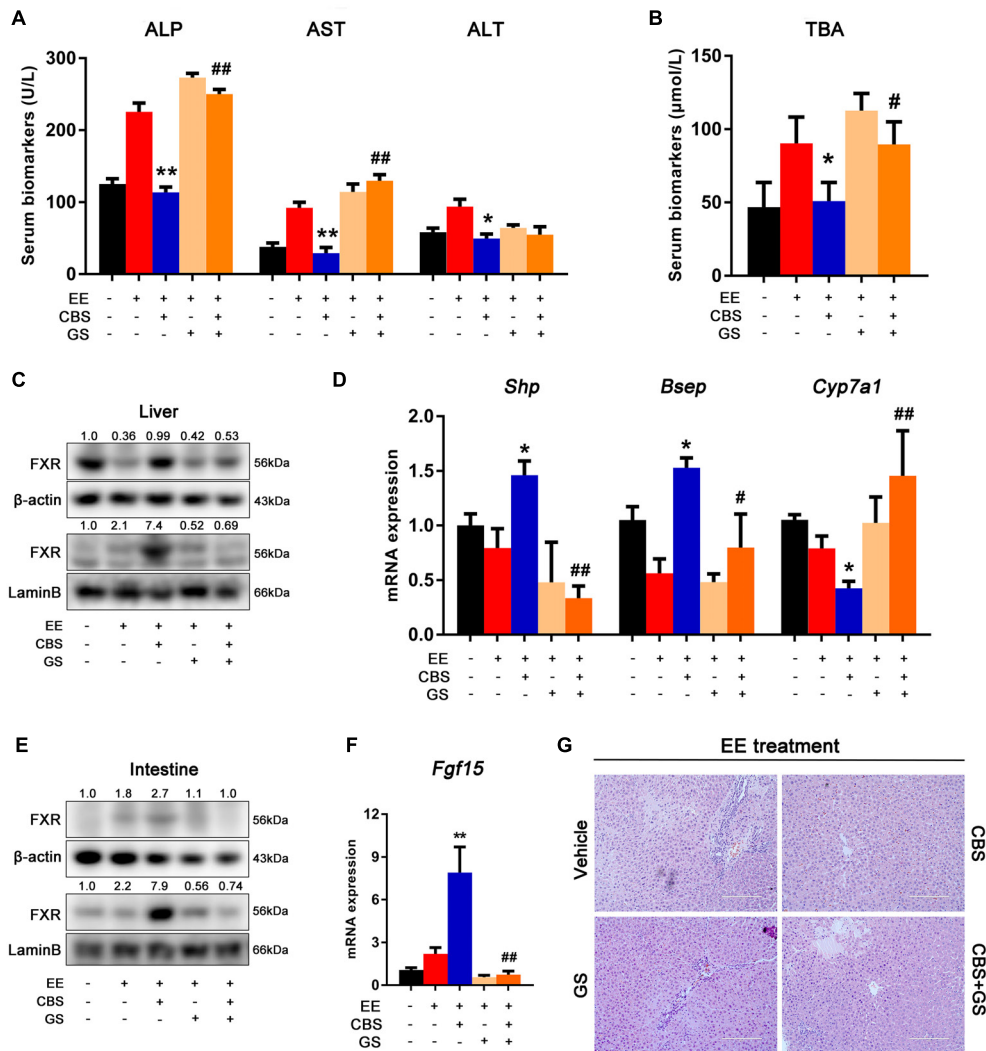
FIGURE 7 | CBS improved hepatic bile acid homeostasis is abrogated by FXR antagonist GS. **(A)** Serum levels of alanine aminotransferase (ALT), aspartate aminotransferase (AST), and alkaline phosphatase (ALP). **(B)** Serum levels of liver total bile acids (TBA). **(C)** Total and nuclear protein levels of hepatic FXR were determined by Western blot analysis and normalized to β-actin and Lamin B. **(D)** mRNA expression of hepatic *Shp*, *Bsep* and *Cyp7a1* were evaluated by real-time PCR and normalized to β-actin. **(E)** Total and nuclear protein levels of intestinal FXR were determined by Western blot analysis and normalized to β-actin and Lamin B. **(F)** mRNA expression of intestinal *Fgf15* was determined by real-time PCR and normalized to β-actin. **(G)** Representative images of hematoxylin and eosin straining. Data are presented as the mean ± SD (n = 6). Significant differences compared with the non-cholestatic group, *$p < 0.05$; **$p < 0.01$; compared with the 17α-ethinylestradiol (EE) group, #$p < 0.05$; ##$p < 0.01$.

(**Figure 7D**). Furthermore, liver histology showed that GS blocked the hepatoprotective effect of CBS, with markedly increased inflammatory cell infiltration, necrosis, and bile duct proliferation observed (**Figure 7G**). Taken together, these results demonstrated that in rats CBS protected against EE-induced liver injury and dysfunction of BA homeostasis primarily through activating FXR signaling.

DISCUSSION

Estrogen-induced cholestasis is characterized by impairment of BA uptake and secretion, resulting in the accumulation of toxic

BAs and alteration of BA composition, subsequently leading to liver injury (Marrone et al., 2016). In the present study, CBS played a role in protecting against estrogen-induced cholestasis as evidenced by ameliorative liver histology and significant decreases in serum levels of AST, ALT, ALP, and TBA, as well as increases in bile flow and decreases in hepatic BA accumulation. Our data suggested that CBS exhibited hepatoprotective effects and predominantly improved BA homeostasis through FXR-mediated regulation of BA transporters and enzymes (**Figure 8**). First, CBS decreased hepatic BA uptake and increased BA efflux through downregulation of uptake transporter (NTCP) and upregulation of efflux transporters (BSEP, MRP2, MRP3, and MRP4). In addition, CBS reduced BA biosynthesis in

FIGURE 8 | Schematic diagram of potential mechanisms that CBS improves liver injury and hepatic bile acid accumulation in estrogen-induced cholestasis. In liver and intestine, CBS activates protein expression and nuclear translocation of FXR, and then alters the expression of downstream genes. Regarding transporters, CBS decreases NTCP levels to reduce hepatic bile acid (BA) uptake and increases BSEP, MRP2, MRP3, and MRP4 levels to augment BA efflux. Moreover, CBS reduces BA biosynthesis in the liver by repressing BA synthetic enzymes, CYP7A1 and CYP8B1, via hepatic FXR-SHP and intestinal FXR-FGF15 axes. Lastly, CBS increases BA metabolism by increasing the expression of CYP3A2, CYP2B10, and SULT2A1.

the liver via repressing BA synthetic enzymes (CYP7A1 and CYP8B1) through both hepatic FXR-SHP and intestinal FXR-FGF15 axes. Finally, CBS increased BA metabolism by inducing phase I enzyme (CYP3A2 and CYP2B10) and phase II enzyme (SULT2A1).

Bile acids are not only detergents for lipid absorption, but also signaling molecules, which play essential roles in regulating lipid, glucose, and energy homeostasis (Chiang, 2013). In many livers, the synthesis and clearance of BAs in diseases can be disturbed, thereby potentially leading to alterations in the concentration and composition of BAs in the liver (Liu et al., 2018). The consequential BA accumulation can result in hepatotoxicity and even hepatic necrosis (Woolbright et al., 2015). Therefore, BAs have been considered biomarkers of hepatic diseases and therapeutic efficacy of several drugs (Han et al., 2015; Woolbright et al., 2015; Marrone et al., 2016; Yang et al., 2016; Liu et al., 2018). In this study, the analysis of hepatic BAs showed that major endogenous BAs, such as DCA, TMCA, TCA, and TUDCA, were significantly

increased, leading to an abnormal BA composition in EE-induced cholestasis. CBS effectively reversed EE-induced changes in individual BAs and abnormal BA composition in cholestatic rats (**Figure 2**).

Presently, genomics is widely used in identifying key targets or pivotal pathways for traditional Chinese medicine in treating diseases (Wen et al., 2011). In our study, differentially expressed genes were screened among non-cholestatic, EE, and EE+CBS liver tissues through DNA microarray analysis. We focused on two top enriched pathways, bile secretion, and primary BA synthesis, which are involved in BA homeostasis (**Figure 3**). In addition, analysis of individual BAs in the liver suggested that anti-cholestatic effects of CBS markedly correlated with mediating BA homeostasis (**Figure 2**). Therefore, in this study, we focused on the effects of CBS on regulating BA homeostasis, including BA transport, synthesis, and metabolism.

Bile acid transporters and metabolic enzymes play crucial roles in the maintenance of BA homeostasis (Staudinger et al., 2013). BSEP and MRP2 are two main transporters in the canalicular membranes of hepatocytes that are involved in transporting conjugated and unconjugated BAs into bile in human and rodents. This process constitutes the rate-limiting step in hepatic BA excretion (Kast et al., 2002; Plass et al., 2002). Our data showed that EE reduced BSEP and MRP2 protein expression, leading to a decrease in bile flow and hepatic BA accumulation. Moreover, EE decreased the expression of MDR2 to efflux phosphatidylcholine, which is an important ingredient for bile formation (Ghonem et al., 2014). However, CBS administration upregulated the expression of BSEP, MRP2, and MDR2 and recovered the impairment of bile flow and hepatic retention of toxic BAs. In addition, CBS increased the expression of basolateral transporters, MRP3 and MRP4, to increase BAs efflux into the systemic circulation. Hepatic uptake of BAs from the circulation takes place at the basolateral membrane of hepatocytes, and is mediated by NTCP and OATPs (Slijepcevic and van de Graaf, 2017). NTCP takes up most of the reabsorbed BAs in their conjugated form and OATPs mainly uptake some unconjugated BAs into hepatocytes (Slijepcevic and van de Graaf, 2017; Slijepcevic et al., 2018). Combined, previous publications as well as the current study showed that NTCP, OATP1A1, and OTAP1B2 were markedly inhibited by EE to defense against excessive BAs entering hepatocytes (Muchova et al., 2015; Yu et al., 2016), whereas CBS reduced the mRNA and protein expression of NTCP for further inhibition of BA reabsorption. In addition, BA synthetic and metabolic enzymes also play important roles in mediating BA homeostasis. CBS treatment reduced CYP7A1 and CYP8B1 expression leading to suppression of BA synthesis. CBS treatment further increased CYP3A2, CYP2B10, and SULT2A1 expression, which had been shown to contribute to BA detoxification.

In previous studies, it has been shown that several hepatic nuclear receptors, including FXR, PXR, CAR, VDR, LXR, and PPARα participate in regulating BA homeostasis. It has been suggested that PXR and CAR activation results in coordinated stimulation of major hepatic BA metabolizing and detoxifying

enzymes (CYP3A, CYP2 isoforms, SULT2A1, CYP7A1) and hepatic key alternative efflux systems (MRP2, MRP3, and MRP4) (Li and Chiang, 2013, 2014). In both mouse and primary human hepatocytes, activation of VDR induced CYP3A and CYP2B expression and repressed CYP7A1 gene expression (Drocourt et al., 2002; Han and Chiang, 2009). LXR, a sterol sensor, affected sensitivity to BA toxicity and cholestasis (Uppal et al., 2007). Cholestatic resistance in LXR transgenic mice was associated with enhancing expression of SULT2A, BSEP, MRP4, and repressing CYP7B1 expression (Uppal et al., 2007). Activation of PPARα had a beneficial effect on cholestatic liver diseases, and was mainly involved in the inhibition of CYP7A1 and upregulation of CYP3A4, UGT1A, and SULT2A1, and induction of MDR2 to increase biliary phospholipids secretion (Ghonem et al., 2015). In previous studies, it was shown that FXR is an extremely important upstream nuclear receptor in the regulation of BA signaling (Massafra et al., 2018). In the liver, FXR directly activated BSEP and SHP, whereas SHP was determined as the upstream gene of NTCP, CYP7A1, and CYP8B1, which can be suppressed by activating FXR–SHP axis (Li and Chiang, 2014). In addition, activation of FXR enhanced CYP3A, CYP2B as well as SULT2A1, BAL, and BAAT expression to increase BA metabolism (Li and Chiang, 2013). In the intestine, FXR activates FGF15, which encodes a hormone that travels to the liver where it interacts with its receptor fibroblast growth factor receptor 4 (Fgfr4), and activates the ERK or JNK signaling cascade to decrease Cyp7a1 and Cyp8b1 expression and inhibit BA synthesis (Zhou et al., 2016). Above all, BA transporters, synthetic and metabolic enzymes may be synergetically controlled by these nuclear receptors.

In the present study, we demonstrated that mRNA and protein levels of hepatic nuclear receptors, including PXR, CAR, VDR, LXR, and PPARα were not significantly different between cholestatic rats or CBS-treated cholestatic rats (**Figure 6**). In contrast, although the FXR mRNA level was similar between EE and CBS-treated cholestatic rats, FXR protein levels were markedly different in CBS-treated cholestatic rats. CBS administration in cholestatic rats significantly increased FXR protein levels and their nuclear translocation in liver and intestine, and then enhanced the expression of downstream genes (**Figure 6**). These studies suggest that CBS alleviated EE-induced cholestasis through activating FXR in a posttranscriptional regulation manner. Furthermore, we used FXR antagonist GS to confirm if CBS activated FXR that contributed to recovering BA homeostasis. As expected, GS blocked CBS-induced FXR upregulation and nuclear translocation in liver and intestine, and consequently blocked FXR direct target genes, *Shp* and *Fgf15*. In addition, the beneficial changes in hepatic BA transporters and enzymes, as well as ameliorative serum biomarkers, and liver histology in CBS-treated rats were abrogated by GS (**Figure 7**).

Farnesoid X receptor is a ligand-activated nuclear receptor that can be activated by free and conjugated-BAs (Ding et al., 2015). The most efficacious BA ligand of FXR is CDCA, followed by LCA, DCA, and CA (Ding et al., 2015). The main constituents of CBS as published in the 2015 edition of the Chinese Pharmacopoeia are BAs and bilirubin. In our

previous study, we successfully identified twelve main BAs including CDCA, DCA, and CA as well as their glycine-conjugated and taurine-conjugated derivatives in CBS (Feng et al., 2015). These BAs may be partial bioactive constituents for CBS activating FXR to treat cholestasis. With in-depth research, targeting FXR signaling has been considered to have potential for cholestatic diseases (Fiorucci et al., 2014). In recent years, many FXR agonists have been studied in animal experiments and clinical trials (Fiorucci et al., 2012; Sepe et al., 2015), among which obeticholic acid (OCA) has been successfully approved by U S Food and Drug Administration (FDA) to treat patients with PBC (Kowdley et al., 2018). Thus, there is a great prospect for the development of CBS as an anti-cholestatic drug.

CBS is composed of multiple ingredients, including at least 26 types of BAs (Kai et al., 2018). Future studies are needed to identify the effective substances in CBS and the role of these ingredients on activating FXR in cholestatic animals. Except for dysfunction in BA homeostasis, estrogen cholestasis-induced inflammation, and oxidative stress *in vivo* are also important factors to promote tissue injury (Ozler et al., 2014). Our unpublished studies indicated that CBS markedly alleviated hepatic inflammation and oxidative stress in estrogen-induced cholestatic animals. In this study, even though the effects of CBS on regulating BA homeostasis were suggested, other pathways analyzed by DNA microarray may also play important roles in alleviating cholestasis. Thus, the anti-cholestatic role of CBS needs further investigation, and we will continue to focus on this matter in our future studies.

In summary, CBS improved BA homeostasis in EE-induced cholestatic rats through activating hepatic and intestinal FXR signaling pathways to up-regulate hepatic efflux and metabolism of BAs, and decreased hepatic uptake and synthesis of BAs. Our data suggested that CBS may have considerable potential as a therapeutic in cholestatic liver diseases.

AUTHOR CONTRIBUTIONS

DX designated the study, collected and analyzed the data, and wrote the manuscript. JY and YL contributed to data collection. SZ and WH partly performed the experiments. XL analyzed the data. CZ and DL supervised the study. All authors reviewed and approved the manuscript.

FUNDING

SUPPLEMENTARY MATERIAL

The Supplementary Material for this article can be found online at: https://www.frontiersin.org/articles/10.3389/fphar. 2019.00048/full#supplementary-material

REFERENCES

Bai, S. L., and Zhao, Y. Q. (2011). Progress research on pharmacology of *Calculus bovis* and its role on anti-hepatic injury. *Hubei J. Tradit. Chin. Med.* 33, 65–67.

Beuers, U., Trauner, M., Jansen, P., and Poupon, R. (2015). New paradigms in the treatment of hepatic cholestasis: from UDCA to FXR, PXR and beyond. *J. Hepatol.* 62, S25–S37. doi: 10.1016/j.jhep.2015.02.023

Chen, S. P. (1987). Research on *Calculus bovis*. *Zhong Yao Tong Bao* 12:59.

Cheng, L., Zheng, Y., Zhan, L., Wang, J., and Li, H. (2014). Clinical observation of bezoar cultivated in vitro for treating chronic hepatitis B with syndrome of damp and heat retention. *Chin. J. Integr. Tradit. West. Med. Liver Dis.* 24, 273–275.

Chiang, J. Y. (2013). Bile acid metabolism and signaling. *Compr. Physiol.* 3, 1191–1212. doi: 10.1002/cphy.c120023

Ding, L., Yang, L., Wang, Z., and Huang, W. (2015). Bile acid nuclear receptor FXR and digestive system diseases. *Acta Pharm. Sin. B* 5, 135–144. doi: 10.1016/j.apsb.2015.01.004

Drocourt, L., Ourlin, J. C., Pascussi, J. M., Maurel, P., and Vilarem, M. J. (2002). Expression of CYP3A4, CYP2B6, and CYP2C9 is regulated by the vitamin D receptor pathway in primary human hepatocytes. *J. Biol. Chem.* 277, 25125–25132. doi: 10.1074/jbc.M201323200

Feng, C., Li, X., Zhang, C., He, G., Xu, Y., Li, W., et al. (2015). Development of a rapid and simple LC-MS/MS method for identification and quality control of natural *Calculus bovis* and *Calculus bovis* sativus. *Anal. Methods* 7, 7606–7617. doi: 10.1039/c5ay01288k

Fiorucci, S., Distrutti, E., Ricci, P., Giuliano, V., Donini, A., and Baldelli, F. (2014). Targeting FXR in cholestasis: hype or hope. *Expert Opin. Ther. Targets* 18, 1449–1459. doi: 10.1517/14728222.2014.956087

Fiorucci, S., Mencarelli, A., Distrutti, E., and Zampella, A. (2012). Farnesoid X receptor: from medicinal chemistry to clinical applications. *Future Med. Chem.* 4, 877–891. doi: 10.4155/FMC.12.41

Fischer, S., Beuers, U., Spengler, U., Zwiebel, F. M., and Koebe, H. G. (1996). Hepatic levels of bile acids in end-stage chronic cholestatic liver disease. *Clin. Chim. Acta* 251, 173–186. doi: 10.1016/0009-8981(96)06305-X

Ghonem, N. S., Ananthanarayanan, M., Soroka, C. J., and Boyer, J. L. (2014). Peroxisome proliferator-activated receptor alpha activates human multidrug resistance transporter 3/ATP-binding cassette protein subfamily B4 transcription and increases rat biliary phosphatidylcholine secretion. *Hepatology* 59, 1030–1042. doi: 10.1002/hep. 26894

Ghonem, N. S., Assis, D. N., and Boyer, J. L. (2015). Fibrates and cholestasis. *Hepatology* 62, 635–643. doi: 10.1002/hep.27744

Halilbasic, E., Claudel, T., and Trauner, M. (2013). Bile acid transporters and regulatory nuclear receptors in the liver and beyond. *J. Hepatol.* 58, 155–168. doi: 10.1016/j.jhep.2012.08.002

Han, J., Liu, Y., Wang, R., Yang, J., Ling, V., and Borchers, C. H. (2015). Metabolic profiling of bile acids in human and mouse blood by LC-MS/MS in combination with phospholipid-depletion solid-phase extraction. *Anal. Chem.* 87, 1127–1136. doi: 10.1021/ac503816u

Han, S., and Chiang, J. Y. (2009). Mechanism of vitamin D receptor inhibition of cholesterol 7alpha-hydroxylase gene transcription in human hepatocytes. *Drug Metab. Dispos.* 37, 469–478. doi: 10.1124/dmd.108.025155

He, W., Xu, Y., Zhang, C., Lu, J., Li, J., Xiang, D., et al. (2017). Hepatoprotective effect of *Calculus bovis* sativus on nonalcoholic fatty liver disease in mice by inhibiting oxidative stress and apoptosis of hepatocytes. *Drug Des. Dev. Ther.* 11, 3449–3460. doi: 10.2147/DDDT.S150187

Jansen, P. L. M., Ghallab, A., Vartak, N., Reif, R., Schaap, F. G., Hampe, J., et al. (2017). The ascending pathophysiology of cholestatic liver disease. *Hepatology* 65, 722–738. doi: 10.1002/hep.28965

Kai, L., Ya-nan, L., Cheng-liang, Z., Dong, X., and Xi-ping, L. I. (2018). Simultaneous quantification of 26 bile acids in *Calculus bovis* sativus and *Calculus bovis* by HPLC-MS/MS. *Chin. Trad. Herbal Drugs* 49, 2447–2453. doi: 10.7501/j.issn.0253-2670.2018.10.029

Kast, H. R., Goodwin, B., Tarr, P. T., Jones, S. A., Anisfeld, A. M., Stoltz, C. M., et al. (2002). Regulation of multidrug resistance-associated protein 2 (ABCC2) by the nuclear receptors pregnane X receptor, farnesoid X-activated receptor, and constitutive androstane receptor. *J. Biol. Chem.* 277, 2908–2915. doi: 10. 1074/jbc.M109326200

Kong, B., Wang, L., Chiang, J. Y., Zhang, Y., Klaassen, C. D., and Guo, G. L. (2012). Mechanism of tissue-specific farnesoid X receptor in suppressing the expression of genes in bile-acid synthesis in mice. *Hepatology* 56, 1034–1043. doi: 10.1002/hep.25740

Kowdley, K. V., Luketic, V., Chapman, R., Hirschfield, G. M., and Poupon, R. (2018). A randomized trial of obeticholic acid monotherapy in patients with primary biliary cholangitis. *Hepatology* 67, 1890–1902. doi: 10.1002/hep. 29569

Li, T., and Chiang, J. Y. L. (2013). Nuclear receptors in bile acid metabolism. *Drug Metab. Rev.* 45, 145–155. doi: 10.3109/03602532.2012.740048

Li, T., and Chiang, J. Y. L. (2014). Bile acid signaling in metabolic disease and drug therapy. *Pharmacol. Rev.* 66, 948–983. doi: 10.1124/pr.113.008201

Li, X., Liu, R., Luo, L., Yu, L., and Chen, X. (2017). Role of AMP-activated protein kinase α1 in 17α-ethinylestradiol-induced cholestasis in rats. *Arch. Toxicol.* 91, 481–494. doi: 10.1007/s00204-016-1697-8

Liu, B., Yu, S., Xing, L., Zhao, X., Lv, Y., and Gao, Q. (2010). Analysis of therapeutical effects of Xihuang Pills with intraarterial intervention chemotherapy on 80 cases of advanced primary hepatic carcinoma. *Chin. J. Tradit. Chin. Med. Pharm.* 25, 947–948.

Liu, D., Wu, T., Zhang, C., Xu, Y., and Chang, M. (2014). Beneficial effect of *Calculus bovis* Sativus on 17α-ethynylestradiol-induced cholestasis in the rat. *Life Sci.* 113, 22–30. doi: 10.1016/j.lfs.2014.07.024

Liu, Y., Rong, Z., Xiang, D., Zhang, C., and Liu, D. (2018). Detection technologies and metabolic profiling of bile acids: a comprehensive review. *Lipids Health Dis.* 17:121. doi: 10.1186/s12944-018-0774-9

Marrone, J., Soria, L. R., Danielli, M., Lehmann, G. L., Larocca, M. C., and Marinelli, R. A. (2016). Hepatic gene transfer of human aquaporin-1 improves bile salt secretory failure in rats with estrogen-induced cholestasis. *Hepatology* 64, 535–548. doi: 10.1002/hep.28564

Massafra, V., Pellicciari, R., Gioiello, A., and van Mil, S. (2018). Progress and challenges of selective farnesoid x receptor modulation. *Pharmacol. Ther.* 191, 162–177. doi: 10.1016/j.pharmthera.2018.06.009

Meng, Q., Chen, X., Wang, C., Liu, Q., and Sun, H. (2015). Protective effects of Alisol B 23-Acetate via farnesoid X receptor-mediated regulation of transporters and enzymes in estrogen-induced cholestatic liver injury in mice. *Pharm. Res.* 32, 3688–3698. doi: 10.1007/s11095-015-1727-x

Muchova, L., Vanova, K., Suk, J., Micuda, S., Dolezelova, E., Fuksa, L., et al. (2015). Protective effect of heme oxygenase induction in ethinylestradiol-induced cholestasis. *J. Cell. Mol. Med.* 19, 924–933. doi: 10.1111/jcmm. 12401

Muhler, M. R., Clement, O., Salomon, L. J., Balvay, D., and Autret, G. (2011). Maternofetal pharmacokinetics of a gadolinium chelate contrast agent in mice. *Radiology* 258, 455–460. doi: 10.1148/radiol.10100652

Ozler, A., Ucmak, D., Evsen, M. S., Kaplan, I., and Elbe, B. (2014). Clinical immunology Immune mechanisms and the role of oxidative stress in intrahepatic cholestasis of pregnancy. *Cent. Eur. J. Immunol.* 2, 198–202. doi: 10.5114/ceji.2014.43723

Plass, J. R., Mol, O., Heegsma, J., Geuken, M., and Faber, K. N. (2002). Farnesoid X receptor and bile salts are involved in transcriptional regulation of the gene encoding the human bile salt export pump. *Hepatology* 35, 589–596. doi: 10. 1053/jhep.2002.31724

Sepe, V., Distrutti, E., Fiorucci, S., and Zampella, A. (2015). Farnesoid X receptor modulators (2011 – 2014): a patent review. *Expert Opin. Ther. Pat.* 25, 885–896. doi: 10.1517/13543776.2015.1045413

Slijepcevic, D., Roscam, A. R., Fuchs, C. D., Haazen, L., and Beuers, U. (2018). Na(+) -taurocholate cotransporting polypeptide inhibition has hepatoprotective effects in cholestasis in mice. *Hepatology* doi: 10.1002/hep. 29888 [Epub ahead of print]. doi: 10.1002/hep.29888

Slijepcevic, D., and van de Graaf, S. F. J. (2017). Bile acid uptake transporters as targets for therapy. *Dig. Dis.* 35, 251–258. doi: 10.1159/000450983

Staudinger, J. L., Woody, S., Sun, M., and Cui, W. (2013). Nuclear-receptor–mediated regulation of drug–and bile-acid–transporter proteins in gut and liver. *Drug Metab. Rev.* 45, 48–59. doi: 10.3109/03602532.2012. 748793

Trauner, M., Fuchs, C. D., Halilbasic, E., and Paumgartner, G. (2017). New therapeutic concepts in bile acid transport and signaling for management of cholestasis. *Hepatology* 65, 1393–1404. doi: 10.1002/hep. 28991

Uppal, H., Saini, S. P. S., Moschetta, A., Mu, Y., and Zhou, J. (2007). Activation of LXRs prevents bile acid toxicity and cholestasis in female mice. *Hepatology* 45, 422–432. doi: 10.1002/hep.21494

Wang, Y., Aoki, H., Yang, J., Peng, K., and Liu, R. (2017). The role of sphingosine 1-phosphate receptor 2 in bile-acid-induced cholangiocyte proliferation and cholestasis-induced liver injury in mice. *Hepatology* 65, 2005–2018. doi: 10.1002/hep.29076

Wen, Z., Wang, Z., Wang, S., Ravula, R., and Yang, L. (2011). Discovery of molecular mechanisms of traditional Chinese medicinal formula Si-Wu-Tang using gene expression microarray and connectivity map. *PLoS One* 6:e18278. doi: 10.1371/journal.pone.0018278

Woolbright, B. L., Dorko, K., Antoine, D. J., Clarke, J. I., and Gholami, P. (2015). Bile acid-induced necrosis in primary human hepatocytes and in patients with obstructive cholestasis. *Toxicol. Appl. Pharmacol.* 283, 168–177. doi: 10.1016/j.taap.2015.01.015

Yang, F., Tang, X., Ding, L., Zhou, Y., and Yang, Q. (2016). Curcumin protects ANIT-induced cholestasis through signaling pathway of FXR-regulated bile acid and inflammation. *Sci. Rep.* 6:33052. doi: 10.1038/srep33052

Yu, L., Liu, X., Li, X., Yuan, Z., and Yang, H. (2016). Protective effects of SRT1720 via the HNF1α/FXR signalling pathway and anti-inflammatory mechanisms in mice with estrogen-induced cholestatic liver injury. *Toxicol. Lett.* 264, 1–11. doi: 10.1016/j.toxlet.2016.10.016

Zhang, C. L., Xu, Y. J., Xiang, D., Yang, J. Y., Lei, K., and Liu, D. (2018). Pharmacokinetic characteristics of baicalin in rats with 17alpha-ethynyl-estradiol-induced intrahepatic cholestasis. *Curr. Med. Sci.* 38, 167–173. doi: 10.1007/s11596-018-1861-x

Zhou, M., Learned, R. M., Rossi, S. J., Depaoli, A. M., Tian, H., and Lei, L. (2016). Engineered fibroblast growth factor 19 reduces liver injury and resolves sclerosing cholangitis in Mdr2-deficient mice. *Hepatology* 63, 914–929. doi: 10.1002/hep.28257

Zollner, G., and Trauner, M. (2009). Nuclear receptors as therapeutic targets in cholestatic liver diseases. *Br. J. Pharmacol.* 156, 7–27. doi: 10.1111/j.1476-5381.2008.00030.x

Chinese Herbal Medicine for Wilson's Disease: A Systematic Review and Meta-Analysis

Meng-Bei Xu[†], Pei-Qing Rong[†], Ting-Yu Jin[†], Pei-Pei Zhang, Hai-Yong Liang and Guo-Qing Zheng*

Department of Neurology, The Second Affiliated Hospital and Yuying Children's Hospital of Wenzhou Medical University, Wenzhou, China

Wilson's disease (WD) is a rare autosomal recessive inherited disorder of chronic copper toxicosis. Currently, Chinese herbal medicines (CHM) is widely used for WD. Here, we conducted an updated systematic review to investigate the efficacy and safety of CHM for WD and its possible mechanisms. Randomized-controlled clinical trials (RCTs), which compared CHM with Western conventional medicine or placebo for WD, were searched in six databases from inception to July 2017. The methodological quality was assessed using 7-item criteria from the Cochrane's collaboration tool. All the data were analyzed using Rev-Man 5.3 software. Eighteen studies involving 1,220 patients were identified for the final analyses. A score of study quality ranged from 2/7 to 4/7 points. Meta-analyses showed that CHM could significantly increase 24-h urinary copper excretion and improve liver function and the total clinical efficacy rate for WD compared with control ($p < 0.05$). Additionally, CHM was well tolerated in patients with WD. The underlying mechanisms of CHM for WD are associated with reversing the ATP7B mutants, exerting anti-oxidation, anti-inflammation, and anti-hepatic fibrosis effects. In conclusion, despite the apparent positive results, the present evidence supports, to a limited extent because of the methodological flaws and CHM heterogeneity, that CHM paratherapy can be used for patients with WD but could not be recommended as monotherapy in WD. Further rigorous RCTs focusing on individual CHM formula for WD are warranted.

Keywords: Wilson's disease, Chinese herbal medicine, ATP7B, anti-oxidation, systematic review

INTRODUCTION

Wilson's disease (WD) is a rare autosomal recessive inherited disorder that causes copper poisoning in the body, predominantly in the liver and the brain (Walshe, 2009). The global prevalence of WD is between 1 in 5,000 and 1 in 30,000 (Gomes and Dedoussis, 2015). Epidemiological studies have shown a higher incidence and prevalence of WD in China than in western countries (Hu et al., 2011). The WD gene was identified as the trans-membrane copper transporter ATP7B in hepatocytes (Bull et al., 1993; Petrukhin et al., 1993). An absent or reduced function of ATP7B protein causes decreased hepatocellular excretion of copper into bile. In WD, the ever-increasing positive copper balance overwhelms the copper chaperones (copper-binding proteins), causing elevated levels of free copper and copper-induced tissue injury (Patil et al., 2013). Copper metabolism disorder results in multifaceted neurological, hepatic and psychiatric symptoms (Brewer, 2009). When left untreated, WD is fatal. With early diagnosis and appropriate treatment,

patients can obtain excellent prognosis (Roberts and Schilsky, 2008; Coffey et al., 2013). Currently, medical treatments and liver transplantation are two main therapeutic approaches that can achieve the generation of a negative copper balance (Hedera, 2017). The EASL Clinical Practice Guidelines of Wilson's disease by European Association for Study of Liver recommended D-penicillamine, trientine, zinc, tetrathiomolybdate, and dimercaprol as medications. However, many side effects such as nephrotoxicity, dermatological toxicity, bone marrow toxicity, severe thrombocytopenia, and total aplasia have been observed in patients with lifelong pharmacological therapy (European Association for Study of Liver, 2012). Liver transplantation is an effective treatment for patients of WD with acute liver failure but it is used only in particular scenarios because of the risks including relatively low engrafting efficiency and lifelong immunosuppression (Filippi and Dhawan, 2014). Thus, an alternative and/or complementary strategy for WD is increasingly sought.

Chinese herbal medicine (CHM) is widely used for WD in the clinic (Ren et al., 1997; Han et al., 1999, 2014; Hong et al., 2000; Cui and Zhao, 2001; Xiao, 2003; Xue et al., 2007; Zhang, 2007; Chen and Wang, 2008, 2010; Wang et al., 2010; Xu et al., 2012a,b; Hu, 2014; Zhang et al., 2014a,b; Fang, 2015; Jiang, 2016; Li et al., 2016), and has been extensively tested by experimental research (Zhang et al., 2011; Lin et al., 2015). Pharmacological studies have shown that CHM can improve the urinary copper excretion and hepatic fibrosis, and protect the brain, liver and kidney (Lutsenko et al., 2007). These beneficial effects are associated with ATP7B gene reversing, anti-oxidant functions, anti-inflammatory actions and suppression of apoptosis (Rosencrantz and Schilsky, 2011). Our group has demonstrated that CHM brings benefits to some patients with WD (Wang et al., 2012). In addition, emerging randomized-controlled clinical trials (RCTs) continuously report the effectiveness and safety of CHM for WD. Therefore, in the present study we aimed to conduct an updated systematic review of CHM for WD focusing on the clinical evidence and possible mechanisms.

METHODS

Database and Search Strategies

Two trained researchers systematically searched the following databases from their inception to July 2017: PubMed, Cochrane Central Register of Controlled Trials, Chinese National Knowledge Infrastructure, Chinese VIP information and WanFang database. The search strategy of PubMed was as follows, and it was modified to suit other English or Chinese databases.

PubMed search strategy:
#1. Wilson's disease [mh]
#2. Hepatolenticular degeneration [mh]
#3. Copper storage disease [tiab]
#4. Progressive lenticular degeneration [tiab]
#5. or/1-4
#6. Medicine, Chinese Traditional [mh]
#7. Herbal Medicine [mh]
#8. Integrative Medicine [mh]
#9. Traditional Chinese medicine [tiab]#10. herb*[tiab]
#11. or/6-10
#12. #5 and #11
#13. Randomized controlled trial [pt]
#14. Controlled clinical trial [pt]
#15. Randomized [tiab]
#16. placebo [tiab]
#17. drug therapy [sh]
#18. randomly [tub]
#19. groups [tub]
#20. or/13–19
#21. animals [mph] not (humans [min] and animals [min])
#22. 20 not 21
#23. #12 and #22

Eligibility Criteria

Types of Studies

Only RCTs were included, irrespective of population characteristics, blinding, publication status, and language. Quasi-RCTs, such as those in which patients were allocated according to date of birth and order of admission number, were excluded.

Types of Participants

We included participants with a diagnosis of WD, according to Chinese Yang Renmin criteria (1995) (Yang, 1995), Chinese Medical Association of Neurology Guidelines for the diagnosis and treatment of hepatolenticular degeneration (2008) (Chinese Medical Association of Neurology, 2008), American Association for the Study of Liver Diseases practice guidelines of Wilson Disease (2008) (Roberts and Schilsky, 2008), and European Association for the Study of the Liver clinical practice guidelines: Wilson's disease (2012) (European Association for Study of Liver, 2012), regardless of age, gender, disease course and severity. The other diagnostic criteria with comparable definitions were also used.

Types of Interventions

Analyzed interventions were CHM monotheism or adjunct therapy using any form, any dose or any administrated methods. Comparator treatments were placebo or Western conventional medication (WCM) (Chinese Medical Association of Neurology, 2008; European Association for Study of Liver, 2012). WCM refers to the combination of needed therapies of the following aspects according to the EASL clinical practice guidelines of WD (European Association for Study of Liver, 2012): (1) General supportive care and low copper diet; (2) Medical therapy: D-penicillamine, trientine, zinc, tetrathiomolybdate, or dimercaprol; (3) Liver transplantation. Chinese guideline for diagnoses and treatment of WD (Chinese Medical Association of Neurology, 2008) is similar to the EASL guideline; however, some recommended drugs such as Trientine are not accessible in China, whereby Dimercaprol, including dimercaptosuccinicacid (DMSA) or sodium dimercaptosulphonate (DMPS), are recommended and commonly used for patients with WD. Thus, DMSA or DMPS used as control is also included.

Studies comparing one kind of CHM therapy to another CHM were excluded.

Types of Outcome Measures

The primary outcome measures were: (1) the amount of copper excreted in the urine in a 24 h period, liver function, and the indicator of hepatic fibrosis; (2) clinical deficit score: the Unified Wilson's Disease Rating Scale (Leinweber et al., 2008) or the Novel Global Assessment Scale (GAS) for Wilson's Disease

(Aggarwal et al., 2009); (3) imaging: Brain MRI and functional neuroimaging. The secondary outcome measures were: the total clinical effective rate, laboratory values and adverse events.

Selection and Data Extraction

The data were extracted using a standardized data extraction form, including study design, eligibility criteria, characteristics of the sample, the course of treatment, interventions, outcomes, the constituent of CHM and pharmaceutical quality control. Reasons
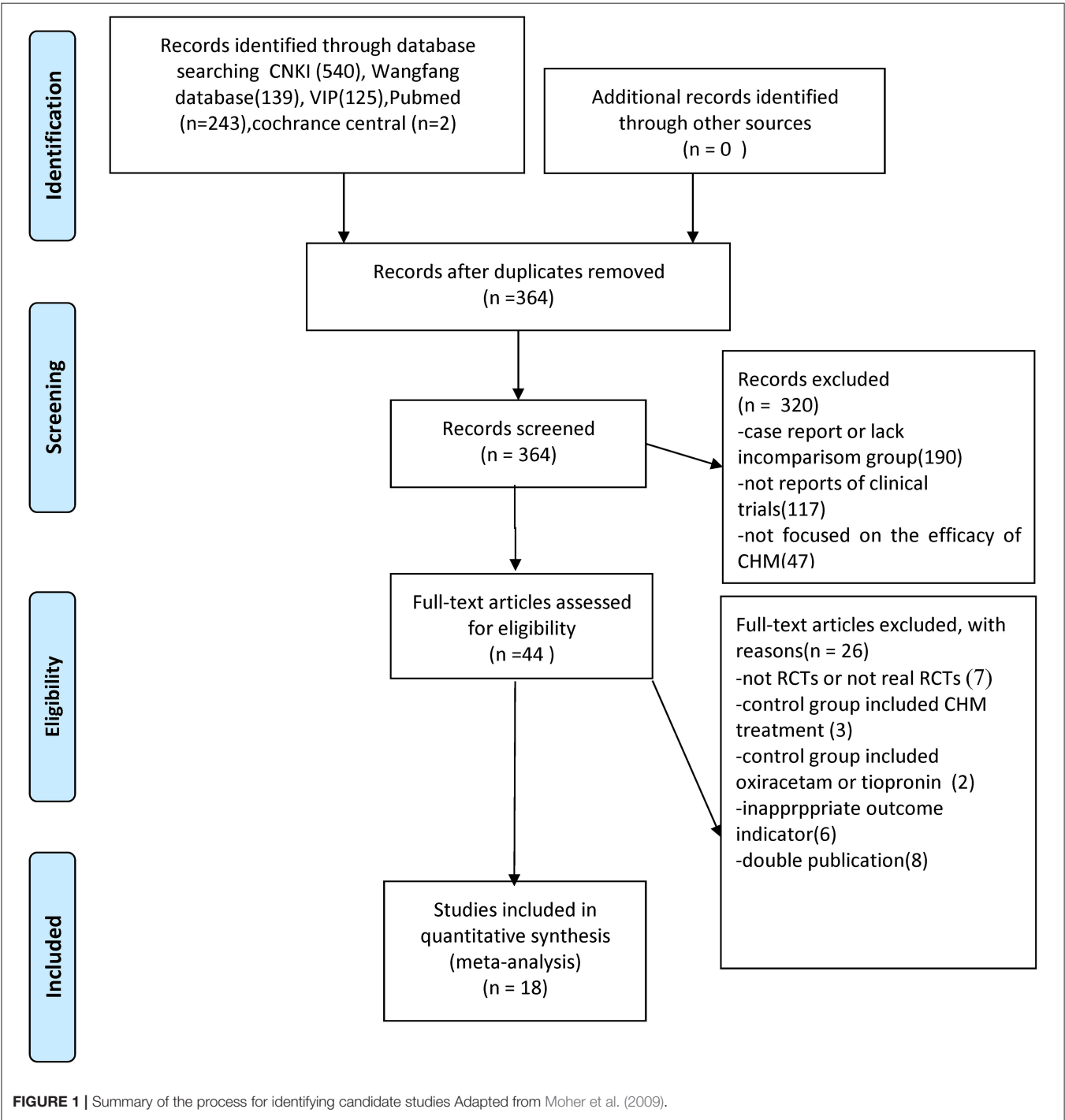
FIGURE 1 | Summary of the process for identifying candidate studies Adapted from Moher et al. (2009).

for the exclusion of studies were recorded. Any disagreements were resolved by discussion with or by involving a third author.

Assessment of Risk of Bias

The RoB of included articles was assessed using the 7-item criteria from the Cochrane's collaboration tool (Higgins et al., 2011). Two authors independently evaluated the study quality, and the final result was identified by discussion when countering the disagreement.

CHM Composition

The frequency of use of the particular herb was calculated and those used at a high frequency were described in detail.

The Reporting Completeness of the Clinical Studies

In order to assess the reporting completeness with a rating system quality of the clinical studies, we used a rating system according to our previous articles (Wang et al., 2019) as follows: (1) high quality: full information about the botanical material is provided, including a voucher specimen; (2) moderate quality: only partial information about the botanical material is provided and a voucher specimen is missing; there are taxonomic inaccuracies; (3) low quality: inadequate information and overall taxonomically is inadequate.

Statistical Analysis

The pooled analyses were carried out with RevMan 5.3 software. Heterogeneity was assessed using the Cochrane Q-statistic test ($p < 0.05$ was considered statistically significant) and the I^2-statistic test. A fixed effects model ($I^2 < 50\%$) or a random effects model ($I^2 > 50\%$) was used depending on the value of I^2. Funnel plots were used to visually estimate publication bias. We calculated the standard mean difference (SMD) with 95% Confidence Intervals (CIs). Sensitivity analyses omitting everyone, which study at a time from the original analysis were conducted to demonstrate our main results to be robust.

RESULTS

Description of Studies

We identified 1,049 hints, of which 364 articles remained after removal of duplicates. Through screening titles and abstracts, 320 studies were excluded because they were case reports, they lacked a comparison group, they were not CHM studies or reports of clinical trials. After full-text evaluation of the remaining 44 articles, 26 studies were excluded for the following reasons: (1) 7 articles were not RCTs; (2) 3 articles included CHM treatment in control groups; (3) 2 articles included oxiracetam or tiopronin in control group; (4) 6 articles have inappropriate outcome measures; (5) 8 articles were suspected of being published more than once. Eventually, 18 eligible studies were identified (**Figure 1**).

Study Characteristics

Eighteen studies with 1,220 participants were included from 1997 to 2016. The sample size ranged from 33 to 146 with an age of 3 to 59 years. The duration of diseases lasted from 1 month to 31 years. The course of treatment ranged from 28 to 90 days. Five studies (Han et al., 2014; Hu, 2014; Zhang et al., 2014a; Fang, 2015; Jiang, 2016) were diagnosed according to Chinese Medical Association of Neurology (2008), 9 studies (Han et al., 1999; Hong et al., 2000; Xue et al., 2007; Zhang, 2007; Chen and Wang, 2010; Wang et al., 2010; Xu et al., 2012a,b; Zhang et al., 2014b) were diagnosed according to Yang criteria (1995) and 4 studies used comparable definitions (Ren et al., 1997; Cui and Zhao, 2001; Xiao, 2003; Chen and Wang, 2008). Three studies (Han et al., 1999; Chen and Wang, 2008, 2010) used CHM monotherapy, and the others used CHM paratherapy. The control group used penicillamine (Xiao, 2003; Zhang, 2007; Chen and Wang, 2008, 2010), DMSA (Ren et al., 1997; Xiao, 2003; Zhang et al., 2014a; Fang, 2015), DMPS (Hong et al., 2000; Xue et al., 2007; Wang et al., 2010; Xu et al., 2012a,b; Han et al., 2014; Hu, 2014; Zhang et al., 2014b; Jiang, 2016), Zinc sulfate (Cui and Zhao, 2001; Xiao, 2003). The characteristics of the 18 trials are summarized in **Table 1**. In four studies (Han et al., 1999; Hong et al., 2000; Xiao, 2003; Chen and Wang, 2010), the preparations were made in hospitals including the associated pharmaceutical quality control. Six studies (Wang et al., 2010; Xu et al., 2012b; Han et al., 2014; Zhang et al., 2014a; Fang, 2015; Jiang, 2016) used a commercial preparation and in 8 studies (Ren et al., 1997; Cui and Zhao, 2001; Xue et al., 2007; Zhang, 2007; Chen and Wang, 2008; Xu et al., 2012a; Hu, 2014; Zhang et al., 2014b) no data on quality control were reported. The constituent of CHM and pharmaceutical quality control in each included study was listed in detail in **Table 2**.

The Reporting Completeness of the Clinical Studies

We accessed the reporting completeness of the material in each study with a rating system, which is related to the information about the botanical material and voucher specimens. Only two studies (Han et al., 2014; Zhang et al., 2014a) are of high quality, which provided the full information about the botanical material and included voucher specimens. Twelve studies (Ren et al., 1997; Han et al., 1999; Hong et al., 2000; Cui and Zhao, 2001; Xiao, 2003; Xue et al., 2007; Zhang, 2007; Chen and Wang, 2008, 2010; Xu et al., 2012a; Hu, 2014; Zhang et al., 2014b) are of moderate quality, which provided partial information about the botanical material and did not provide voucher specimens. Four studies (Wang et al., 2010; Xu et al., 2012b; Fang, 2015; Jiang, 2016) are of low quality with inadequate information and were overall taxonomically inadequate. The quality of each included clinical study is summarized in **Table 3**.

Risk of Bias in Included Studies

The score of RoB ranged from 2/7 to 4/7. Of which, 10 studies got two points (Ren et al., 1997; Cui and Zhao, 2001; Xiao, 2003; Xue et al., 2007; Zhang, 2007; Chen and Wang, 2008, 2010; Xu et al., 2012b; Fang, 2015; Jiang, 2016); 7 studies got three points (Han et al., 1999; Hong et al., 2000; Wang et al., 2010; Xu et al., 2012a; Hu, 2014; Zhang et al., 2014a,b); and 1 study got four points (Han et al., 2014). Two studies (Xu et al., 2012a; Han et al., 2014) described the detailed methods for random sequence generation

TABLE 1 | Characteristics of the included studies.

References	Eligibility criteria	Study design	Interventions(n) drug Trial	Interventions(n) drug Control	Sample size	Sample and characteristics (male/female), age, duration Trial	Sample and characteristics (male/female), age, duration Control	Course of treatment	Course of treatment Outcomes	Intergroup differences
Jiang, 2016	CMAN Standard	RCT	GDL+DMPS	DMPS	60	16/14 25.67 ± 4.82	15/15 25.10 ± 4.63	32 d	1. Vascular injury factor 1.1 Homocysteine 1.2 Von Willebrand Factor 1.3 Thrombomodulin 1.4 Endothelial cell protein C receptor 2. Ultrasound cerebral vessels function 3. Transcranial doppler 4. Perfusion-weighted imaging	1.1 $p > 0.05$ 1.2 $p < 0.01$ 1.3 $p < 0.05$ 1.4 $p < 0.01$ 2. $p > 0.05$ 3. $p < 0.05$ 4. $p < 0.05$
Fang, 2015	CMAN Standard	RCT	GDL+DMSA	DMSA	60	16/14 21.53 ± 8.35 –	15/15 22.03 ± 9.01 –	30 d	1. Cardiac function 1.1 Electrocardiogram ECG 1.2 Cardiacultrasound:EF 1.3 Myocardial enzyme spectrum (CK,CK-MBL,DH) 2. Blood trace of Ceruloplasmin, Cu2+,copper oxidase 3.24 h excretion of urinary copper 4. Clinical symptoms 5. Adverse effect	1.1 $p < 0.05$ 1.2 $p < 0.05$ 1.3 $p < 0.05$ 2. $p > 0.05$ 3. $p < 0.05$
Zhang et al., 2014a	CMAN Standard	RCT	GDL+DMSA	DMSA	70	20/15 19.36 ± 4.85 10 mo to 20 y	19/16 18.16 ± 4.02 2 m to 18 y	30 d	1.urinary microalbumin	1. $p < 0.05$
Zhang et al., 2014b	YanRenMing Standard	RCT	A:GDT + DMPS B:GDT	C:DMPS	61	38/23a 17.64 ± 6.28 6 m–19y		46 d	1. The indicator of portal circulation PVFV, SVFV 2. 24 h excretion of urinary copper	1. $p > 0.05$ 2. $p < 0.01$
Hu, 2014	CMAN Standard	RCT	GDT+DMPS	DMPS	67	16/19 22.66 ± 8.17 5 mo–30 y	15/17 21.97 ± 8.42 3 m–27 y	30 d	1. Pulmonary ventilation function 1.1 FVC % 1.2 FEV1.0/FVC% 2.blood trace of Ceruloplasmin, Cu2+,copper oxidase 3. 24 h excretion of urinary copper 4. adverse effect	1.1 $p < 0.05$ 1.2 $p < 0.05$ 2. $p > 0.05$ 3. $p < 0.05$
Han et al., 2014	CMAN Standard	RCT	GDL+DMPS	DMPS	52	12/19 22.31 ± 4.62 –	11/10 20.63 ± 5.79 –	84 d	1. MMSE 2. MoCA	1. $p < 0.01$ 2. $p < 0.01$
Xu et al., 2012a	YanRenMing Standard	RCT	GDT+DMPS +GSH	DMPS+GSH	56	25/11 21.0 6.6	14/6 22.5 6.3	62 d	1. Clinical symptoms, 2. 24 h excretion of urinary copper 3. Liver function 4. Adverse effect	1. $p < 0.05$ 2. $p < 0.01$ 3. $p > 0.05$

(Continued)

TABLE 1 | Continued

References	Eligibility criteria	Study design	Interventions(n) drug		Sample size	Sample and characteristics (male/female), age, duration		Course of treatment	Course of treatment Outcomes	Intergroup differences
			Trial	Control		Trial	Control			
Xu et al., 2012b	YanRenMing Standard	RCT	GDL+DMPS	DMPS	41	29/12a 17.64 ± 6.28 5.56 ± 4.55y		64 d	1. The indicator of portal circulation PVF,SVFV 2. 24 h excretion of urinary copper 3. Adverse effect	1. $p < 0.05$ 2. $p < 0.01$
Wang et al., 2010	YanRenMing Standard	RCT	GDL+DMPS	DMPS	112	32/26 21.6 ± 9.17 3 mo to 31 y	36/18 2.16 ± 10.79 5 mo to 29 y	6 mo	1. Clinical symptoms 2. T cell,CD3+,CD4+, CD8+, 3. NK cell	1. $p > 0.05$ 2. $p > 0.05$ 3. $p < 0.05$
Chen and Wang, 2010	YanRenMing Standard	RCT	CHGD	Penicillamine	88	32/27; 21.24 ± 11.32; 6−34 mo	16/13; 20.98 ± 10.75; 7−33 mo	90 d	1.Clinical symptoms 2.24 h excretion of urinary copper 3.Blood Cu2+ and CP 4.Liver function 5.Adverse effect	1.$p > 0.05$ 2. $p < 0.05$ 3. $p > 0.05$ 4. $p > 0.05$
Chen and Wang, 2008	Sternlieb standard	RCT	SGLDPD	Penicillamine	61	29/11; 21.12 ± 10.96; 8−35 mo	14/7; 20.81 ± 10.46; 8−34 mo	90 d	1. Hepaticul trasonography 2. Liver function 3. 24 h excretion of urinary copper 4. Cornea Kayser−Fleischer rings 5. Adverse effect	1. $p < 0.05$ 2. $p < 0.05$ 3. $p < 0.01$ 4. $p > 0.05$
Zhang, 2007	YanRenMing Standard	RCT	DHGD + Penicillamine	Penicillamine	40	12/8;− 3mo−2.18y	11/9;- 5 mo to 2.25 y	30 d	1.Clinical symptoms 2. 24 h excretion of urinary copper	1. $p < 0.05$ 2. $p < 0.05$
Xue et al., 2007	Yang RenMin Standard	RCT	GDT No. 2 +DMPS	DMPS	61	17/14 23.1 ± 7.8 9 mo-3.5 y	17/13 22.3 ± 8.5 6 mo to 4 y	62 d	1. Liver function 2.The indicator of hepatic fibrosis	1. $p < 0.05$ 2. $p > 0.05$,
Xiao, 2003	Homemade standard	RCT	RJ+penicillamine and Zincsulfate	Penicillamine and Zinc sulfate	38	22/16a 5−13 y		3 mo	1.Clinical symptoms 2.Liver function 3.Index of hepatic fibrosis	1. $p < 0.05$ 2,$p < 0.05$ 3,$p < 0.05$
Cui and Zhao, 2001	Shi Yuquan standard	RCT	GDT +Zincsulfate	Zincsulfate	33	10/7 19.8 ± 2.93y 4 mo to 6 y	11/5 20.14 ± 2.6y 6 mo to 7y	4 w	1. Clinical symptoms 2. 24 hexcretion ofurinary copper	1. $p > 0.05$ 2. $p < 0.05$
Hong et al., 2000	Yang RenMing Standard	RCT	GDP +DMPS	DMPS	146	31/19 18.6 ± 2.7y 2.6 ± 0.8y	26/24 18.9 ± 6.8y 3.1 ± 1.2y	8 w	1.Hepatic ultrasonography 2.Electrophoresis of serumprotein 3.24 hexcretion ofurinary copper	1. $p < 0.01$ 2. $p > 0.05$ 3. $p < 0.05$
Han et al., 1999	Yang RenMing Standard	RCT	GDP	DMSA	94	21/11; 17.6 ± 7.2; 3 mo to 7 y	38/24; 19.0 ± 4.1; 2 mo to 14 y	4 w	1. Clinical symptoms 2. 24hexcretion ofurinary copper 3. Adverse effect	1. $p > 0.05$ 2. $p < 0.01$
Ren et al., 1997	Shi Yuquan standard	RCT	GDT+DMSA	DMSA	80	21/19; 20.48 ± 10.90; 4 mo to 6 y	22/18; 19.65 ± 7.18; 6 mo to 5 y	4 w	1. Clinical symptoms 2. 24hexcretion ofurinary copper 3. Adverse effect	1. $p < 0.05$ 2. $p > 0.05$

GDL, Gandouling Tablet; SGLDPD, Shugan Lidan Paidu Decoction; CHGD, Chaihuang Gandou Powder; GDT, Gandou Tang; GDP, Gandou Pian; RJ, Ruanjian Syrup; GDT No. 2, Gandou Tang No. 2; DHGD, Dahuang Gandou Decoction; CMAN, Chinese medical association of neurology; CP, copper-protein; d, day; DMPS, sodium dimercaptopropanesulfonate; DMSA, dimercaptosuccinate acid; EDTA, calcium disodium ethylene diaminotetraacetate; EF, ejection fraction; FEV1, forcedexpiratory volume at 1 sec; FVC, forced vital capacity; h, hour; mo, month; MMSE, Mini-mental State Examination; MoCA, Montreal Cognitive Assessment; PVF, portal venous flow; RCT, randomized controlled trial; SVF, splenic vein flow; TECT, tiopronin enteric-coated tablet; w, week.

TABLE 2 | Ingredients, usage and quality control of CHM.

References	Prescription name	Ingredients of herb prescription	Usage of prescription	Preparations	Quality control
Jiang, 2016	GDL	Radix Curcumae, Radix Salviae Miltiorrhizae, Caulis Spatholobi, Rhizoma Acori Tatarinowii, Rhizoma Curcumae Longae, Rhizoma Curcumae, Rhizoma Coptidis, Radix et Rhizoma Rhei, Herba Scutellariae Barbatae, Herba Andrographis	5#tid	Tablet	Traditional Chinese patented medicine WY:Z20050071
Fang, 2015	GDL	Radix Curcumae, Radix Salviae Miltiorrhizae, Caulis Spatholobi, Rhizoma Acori Tatarinowii, Rhizoma Curcumae Longae, Rhizoma Curcumae, Rhizoma Coptidis, Radix et Rhizoma Rhei, Herba Scutellariae Barbatae, Herba Andrographis	5# tid	Tablet	Traditional Chinese patented medicine WY:Z20050071
Zhang et al., 2014a	GDL	Radix Curcumae, Radix Salviae Miltiorrhizae, Caulis Spatholobi, Rhizoma Acori Tatarinowii, Rhizoma Curcumae Longae, Rhizoma Curcumae, Rhizoma Coptidis, Radix et Rhizoma Rhei, Herba Scutellariae Barbatae, Herba Andrographis	5#tid	Tablet	Traditional Chinese patented medicine WY:Z20050071
Zhang et al., 2014b	GDT	Radix et Rhizoma Rhei, Rhizoma Coptidis, Radix Scutellariae, Herba Andrographis, Herba Scutellariae Barbatae, Rhizoma Dioscoreae Hypoglaucae, Cortex Phellodendri, Rhizoma Alismatis, Herba Houttuyniae	200 mL qd po	Decoction	UR
Hu, 2014	GDT	Radix et Rhizoma Rhei, Rhizoma Coptidis, Radix Scutellariae, Herba Andrographis, Herba Scutellariae Barbatae, Rhizoma Dioscoreae Hypoglaucae, Cortex Phellodendri, Rhizoma Alismatis, Herba Houttuyniae	1# bid po	Decoction	UR
Han et al., 2014	GDL	Radix Curcumae, Radix Salviae Miltiorrhizae, Caulis Spatholobi, Rhizoma Acori Tatarinowii, Rhizoma Curcumae Longae, Rhizoma Curcumae, Rhizoma Coptidis, Radix et Rhizoma Rhei, Herba Scutellariae Barbatae, Herba Andrographis	3–5g (80 mg/kg) tid po	Tablet	Traditional Chinese patented medicine WY:Z20050071
Xu et al., 2012a	GDT	Radix et Rhizoma Rhei, Rhizoma Coptidis, Radix Scutellariae, Herba Andrographis, Herba Scutellariae Barbatae, Rhizoma Dioscoreae Hypoglaucae, Cortex Phellodendri, Rhizoma Alismatis, Herba Houttuyniae	1# bid po	Decoction	UR
Xu et al., 2012b	GDL	Radix Curcumae, Radix Salviae Miltiorrhizae, Caulis Spatholobi, Rhizoma Acori Tatarinowii, Rhizoma Curcumae Longae, Rhizoma Curcumae, Rhizoma Coptidis, Radix et Rhizoma Rhei, Herba Scutellariae Barbatae, Herba Andrographis	UR	Tablet	Traditional Chinese patented medicine WY:Z20050071
Wang et al., 2010	GDL	Radix Curcumae, Radix Salviae Miltiorrhizae, Caulis Spatholobi, Rhizoma Acori Tatarinowii, Rhizoma Curcumae Longae, Rhizoma Curcumae, Rhizoma Coptidis, Radix et Rhizoma Rhei, Herba Scutellariae Barbatae, Herba Andrographis	5#tid	Tablet	Traditional Chinese patented medicine WY:Z20050071
Chen and Wang, 2010	CHGD	Radix Bupleuri, Radix et Rhizoma Rhei, Herba Lysimachiae, Herba Artemisiae Scopariae, Radix Aucklandiae, Pericarpium Citri Reticulatae Viride, Rhizoma Alismatis, Rhizoma Dioscoreae Hypoglaucae, Caulis Spatholobi, Radix Salviae Miltiorrhizae	5 g tid po	powder	Hospital Preparation
Chen and Wang, 2008	SGLDPD	Herba Lysimachiae 30 g, Radix Bupleuri 15 g, Radix Curcumae 15 g, Herba Artemisiae Scopariae 15 g, Rhizoma Alismatis15 g, Pericarpium Citri Reticulatae Viride 20 g, Pericarpium Citri Reticulatae 20 g, Rhizoma Dioscoreae Hypoglaucae 12 g, Radix Clematidis 18 g, Caulis Spatholobi 18 g, Rhizoma Ligustici Chuanxiong 9 g, Radix et Rhizoma Rhei 9 g	196 g qd po	Decoction	UR
Zhang, 2007	DHGD	Rhizoma Polygonati 20 g, Radix et Rhizoma Rhei 10 g, Herba Lysimachiae 20 g, Gypsum Fibrosum 9 g, Radix Curcumae 9 g, Radix Angelicae Sinensis 20 g, Radix Salviae Miltiorrhizae 15 g, Radix Asparagi 15 g, Poria 20 g, Flos Chrysanthemi 9 g, Radix Paeoniae Alba 15 g, Pericarpium Citri Reticulatae 9 g, Rhizoma Atractylodis 9 g, Rhizoma Acori Tatarinowii 6 g	250 ml# bid po	Decoction	UR
Xue et al., 2007	GDT No. 2	Radix et Rhizoma Rhei, Radix Salviae Miltiorrhizae, Radix Sophorae Flavescenti, Radix Astragali seu Hedysari, Rhizoma Alismatis	1# qd po	Decoction	UR
Xiao, 2003	RJ	Radix Codonopsis, Radix Bupleuri, Radix Paeoniae Rubra, Radix Paeoniae Alba, Rhizoma Sparganii, Rhizoma Curcumae, Radix Curcumae, Concha Ostreae, Fructus Lycii	15–30 ml tid po	syrup	Hospital Preparation

(Continued)

TABLE 2 | Continued

References	Prescription name	Ingredients of herb prescription	Usage of prescription	Preparations	Quality control
Cui and Zhao, 2001	GDT	Radix et Rhizoma Rhei 6–9 g, Rhizoma Coptidis 20 g, Radix Scutellariae 20 g, Herba Scutellariae Barbatae 20 g, Herba Andrographis 20 g, Rhizoma Dioscoreae Hypoglaucae 20 g	250 ml bid po	Decoction	UR
Hong et al., 2000	GDP	Radix et Rhizoma Rhei 0.25 g, Rhizoma Coptidis 0.25 g, Rhizoma Curcumae Longae 0.25 g, Herba Lysimachiae 0.625 g, Rhizoma Alismatis 0.625 g, Radix Notoginseng 0.042 g	<15 years old: 6# tid po ≥15 years old: 8# tid po	Tablet	Hefei Chinese Medicine Factory
Han et al., 1999	GDP	Radix et Rhizoma Rhei 0.25 g, Rhizoma Coptidis 0.25 g, Rhizoma Curcumae Longae 0.25 g, Herba Lysimachiae 0.625 g, Rhizoma Alismatis 0.625 g, Radix Notoginseng 0.042 g	<15 years old: 6# tid po ≥15 years old: 8# tid po	Tablet	Hefei Chinese Medicine Factory
Ren et al., 1997	GDT	Radix et Rhizoma Rhei, Rhizoma Coptidis, Radix Scutellariae, Herba Andrographis, Herba Scutellariae Barbatae, Rhizoma Dioscoreae Hypoglaucae, Cortex Phellodendri, Rhizoma Alismatis, Herba Houttuyniae	1# bid po	Decoction	UR

GDL, Gandouling Tablet; SGLDPD, Shugan Lidan Paidu Decoction; CHGD, Chaihuang Gandou Powder; GDT, Gandou Tang; GDP, Gandou Pian; RJ, Ruanjian Syrup; GDT No. 2, Gandou Tang No. 2; DHGD, Dahuang Gandou Decoction; UR, Unreported.bid, bis in die; d:day; po, peros; qd, quaquedie; tid, ter in die;#, tablet.

and no studies described allocation concealment. No blinding on patients or personnel was applied. All studies reported drop-out data. Ten studies (Cui and Zhao, 2001; Xiao, 2003; Xue et al., 2007; Zhang, 2007; Chen and Wang, 2008, 2010; Xu et al., 2012a,b; Fang, 2015; Jiang, 2016) were judged as unclear risk of bias for selective reporting. There were baseline comparisons and patients' consent were well reported, and other biases were not found in all included studies. The RoB in each included study is concluded in **Table 4**.

Effectiveness
CHM vs. Placebo
None of RCTs used a specific comparison between CHM and placebo.

CHM vs. WCM
Two studies (Chen and Wang, 2008, 2010) showed that CHM monotherapy had no significance for increasing the amount of copper excreted in the urine in a 24 h period ($n = 149$, SMD-1.32, 95% CI [-1.70 to -0.95], $p < 0.01$; heterogeneity: $\chi^2 = 0.02$, df = 1 ($p = 0.88$); $I^2 = 0$%) (**Figure 2**).

CHM Plus WCM vs. WCM
24 h excretion of urinary copper
Nine studies were included. Meta-analysis of 5 studies (Xu et al., 2012a,b; Hu, 2014; Zhang et al., 2014b; Fang, 2015) reported a significant effect of CHM on increasing the amount of 24 h excretion of urinary copper in patients with WD compared to the control ($n = 228$, SMD 0.93, 95% CI [0.65 to 1.21], $p < 0.01$; heterogeneity: $\chi^2 = 4.01$, df = 4 ($p = 0.40$); $I^2 = 0$%) (**Figure 3**). Four studies (Ren et al., 1997; Hong et al., 2000; Cui and Zhao, 2001; Zhang, 2007) failed for pool analysis because the

measurement unit of 24 h excretion of urinary copper was different from the remaining. However, they all got the significant effects of improving the 24 h excretion of urinary copper on patients ($p < 0.05$).

Liver function and the indicator of hepatic fibrosis
Two studies (Xue et al., 2007; Xu et al., 2012a) used the value of serum alanine aminotransferase (ALT) as the indicator of liver function. Pooled data showed that CHM was significantly better at decreasing the ALT compared with control group [$n = 117$, SMD-0.62, 95% CI [-1.00 to -0.24], $p < 0.01$; heterogeneity: $\chi^2 = 1.40$, df = 1 ($p = 0.24$); $I^2 = 29$%], (**Figure 4**). One study (Xiao, 2003) used ALT recovery rate as the indicator of liver function, and it demonstrated significant effects on decreasing the ALT ($p < 0.05$). One study (Xiao, 2003) showed that CHM had significant effects on reducing HA, PCIII, and LN ($p < 0.05$), however, another study (Xue et al., 2007) showed that CHM had no effect on reducing HA, PCIII and LN in short time ($p > 0.05$).

The total clinical effective rate
Data on the rate of total clinical effectiveness were available from eight studies with 487 participants included. Meta-analysis of 8 studies showed a significant effect of CHM on increasing the total clinical effective rate compared with control group ($n = 487$, RR 1.27, 95% CI [1.15 to 1.39], $p < 0.01$; heterogeneity: $\chi^2 = 6.56$, df = 7 ($p = 0.48$), $I^2 = 0$%) (**Figure 5**).

Laboratory values or imaging indices
One study (Xu et al., 2012b) showed that CHM paratherapy is significant for increasing portal venous flow (PVF) and splenic vein flow (SVF) ($p < 0.05$) compared with WCM, whereas another study (Zhang et al., 2014b) showed no difference. One

TABLE 3 | The quality of the clinical studies.

References	Botanical material information	Voucher specimen	Quality
Zhang et al., 2014a	P	+	High
Han et al., 2014	P	+	High
Zhang et al., 2014b	P	−	Moderate
Hu, 2014	P	−	Moderate
Xu et al., 2012a	P	−	Moderate
Chen and Wang, 2010	P	−	Moderate
Chen and Wang, 2008	P	−	Moderate
Zhang, 2007	P	−	Moderate
Xue et al., 2007	P	−	Moderate
Xiao, 2003	P	−	Moderate
Cui and Zhao, 2001	P	−	Moderate
Hong et al., 2000	P	−	Moderate
Han et al., 1999	P	−	Moderate
Ren et al., 1997	P	−	Moderate
Jiang, 2016	I	+	Low
Fang, 2015	I	+	Low
Xu et al., 2012b	I	+	Low
Wang et al., 2010	I	+	Low

F, Full information about the botanical material is provided; P, Partial information about the botanical material is provided; I, Inadequate information about the botanical material is provided; +, includes a voucher specimen; −, a voucher specimen is missing.

TABLE 4 | Risk of bias of the included studies.

Included studies	A	B	C	D	E	F	G	Total
Jiang, 2016	?	0	0	0	1	?	1	2
Filippi and Dhawan, 2014	?	0	0	0	1	?	1	2
Zhang et al., 2014a	?	0	0	0	1	1	1	3
Zhang et al., 2014b	?	0	0	0	1	1	1	3
Hu, 2014	?	0	0	0	1	1	1	3
Han et al., 2014	1	0	0	0	1	1	1	4
Xu et al., 2012a	1	0	0	0	1	?	1	3
Xu et al., 2012b	?	0	0	0	1	?	1	2
Wang et al., 2010	?	0	0	0	1	1	1	3
Chen and Wang, 2010	?	0	0	0	1	?	1	2
Chen and Wang, 2008	?	0	0	0	1	?	1	2
Zhang, 2007	?	0	0	0	1	?	1	2
Xue et al., 2007	?	0	0	0	1	?	1	2
Xiao, 2003	?	0	0	0	1	?	1	2
Cui and Zhao, 2001	?	0	0	0	1	?	1	2
Hong et al., 2000	?	0	0	0	1	1	1	3
Han et al., 1999	?	0	0	0	1	1	1	3
Ren et al., 1997	?	0	0	0	1	1	1	2

Cochrane Collaboration's tool: A, Random sequence generation; B, Allocation concealment; C, Blinding of participants or personnel; D, Blinding of outcome assessment; E, Incomplete outcome data; F, Selective reporting; G, Anything else; 1, Low risk of bias; 0, High risk of bias; ?, Uncertain risk of bias.

study (Fang, 2015) showed that CHM could significantly improve the cardiac function according to electrocardiogram, ejection fraction, and myocardial enzyme spectrum relative to WCM ($p < 0.05$). One study (Han et al., 2014) showed that CHM is significant for improving the Mini-mental State Examination (MMSE) and Montreal Cognitive Assessment (MoCA) ($p < 0.05$) compared with WCM.

Adverse Events

Adverse effects were reported in 8 studies (Ren et al., 1997; Han et al., 1999; Chen and Wang, 2008, 2010; Xu et al., 2012a,b; Hu, 2014; Fang, 2015). There were no significant differences in routine blood, routine urine, routine stool, and osteoporosis after CHM treatment in three studies (Ren et al., 1997; Xu et al., 2012a,b). Five studies (Han et al., 1999; Chen and Wang, 2008, 2010; Hu, 2014; Fang, 2015) reported that CHM could significantly reduce the adverse events of acne, gastrointestinal reaction, joint pain, and blood reduction compared with WCM. However, life-threatening adverse effects were not mentioned in all of these studies.

Description of the CHM

Twenty-five herbs were included in the 18 studies. The top 13 most frequently used herbs were *Radix et Rhizoma Rhei, Rhizoma Coptidis, Rhizoma Curcumae Longae, Rhizoma Curcumae, Radix Salviae Miltiorrhizae, Herba Andrographis, Herba Lysimachiae, Herba Scutellariae Barbatae, Caulis Spatholobi, Rhizoma Alismatis, Radix Curcumae, Radix Scutellariae* and *Rhizoma Acori Tatarinowii,* and all of them were used more than 5 times.

The full and validated botanical names of herbs were generalized in **Table 5**.

The Possible Mechanisms of CHM for WD

The possible mechanisms of the most frequently used herbs and the main active ingredients are as follows: (1) *Curcumin*: an active ingredient from commonly used herbs like *Rhizoma Curcumae Longae, Rhizoma Curcumae, Radix Curcumae* and *Radix Curcumae* can partially restore protein expression of most ATP7B mutants to restore functional copper export (van den Berghe et al., 2000; Zhang et al., 2011; European Association for Study of Liver, 2012). Furthermore, curcumin is an ideal antioxidant, an effective scavenger of reactive oxygen species (Samarghandian et al., 2017), and it exerts anti-fibrotic effect through regulating hepatic stellate cells (HSCs) function (Jin et al., 2016; Liu et al., 2016; Mustafa, 2016). (2) *Radix et Rhizoma Rhei*: Rhubarb root and its active components have anti-oxidation (Shia et al., 2009), anti-fibrotic (Jin et al., 2005), and anti-inflammation effects (Hwang et al., 2013). (3) *Rhizoma Coptidis*: Berberine from *Rhizoma Coptidis* exerted anti-fibrotic and anti-oxidation effects (Zhang et al., 2008). (4) *Herba Scutellariae Barbatae*: P-coumaric acid from *Herba Scutellariae Barbatae* possess anti-oxidative activities (Ibrahim et al., 2007) and reverse the ATP7B function defect via regulating pre-mRNA splicing (Lin et al., 2015). (5) *Herba Andrographis*: Andrographolide from *Herba Andrographis* displayed anti-inflammatory activity through reducing the expression of pro-inflammatory mediators (Panossian et al., 2002) and exhibited hepatoprotective effects through anti-oxidative effect (Vetriselvan et al., 2011).

FIGURE 2 | The forest plot: The 24 h excretion of urinary copper of CHM vs. WCM.

FIGURE 3 | The forest plot: The 24 h excretion of urinary copper of CHM plus WCM vs. WCM.

FIGURE 4 | The forest plot: The liver function of CHM plus WCM vs. WCM.

FIGURE 5 | The forest plot: the total clinical effective rate of CHM plus WCM vs. WCM.
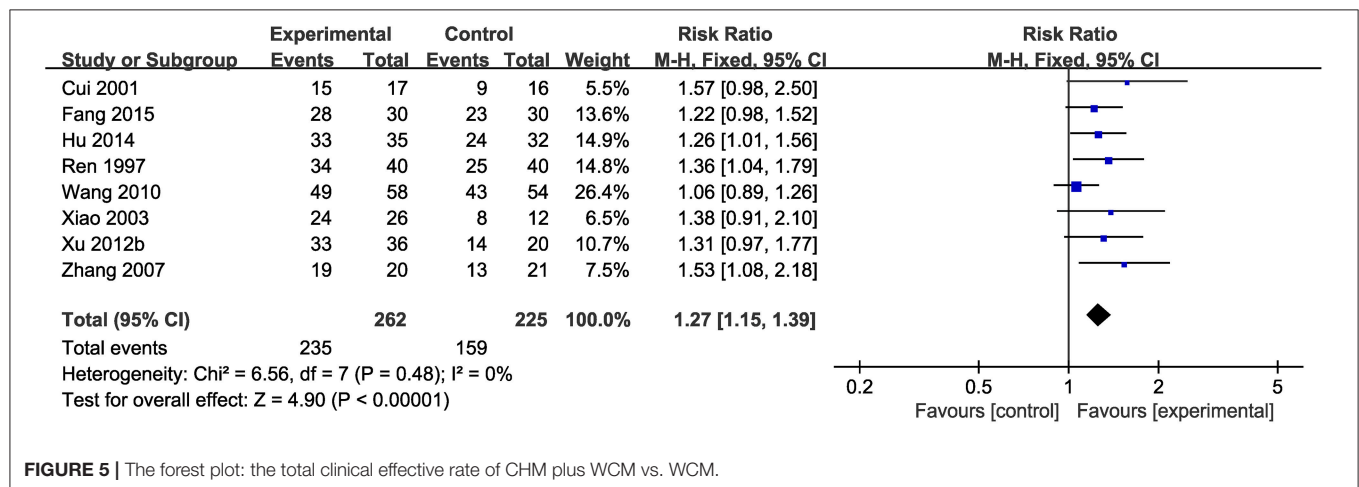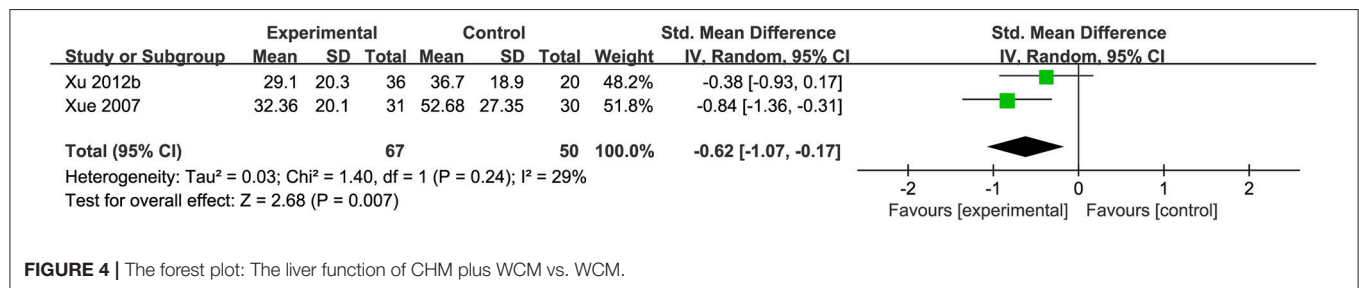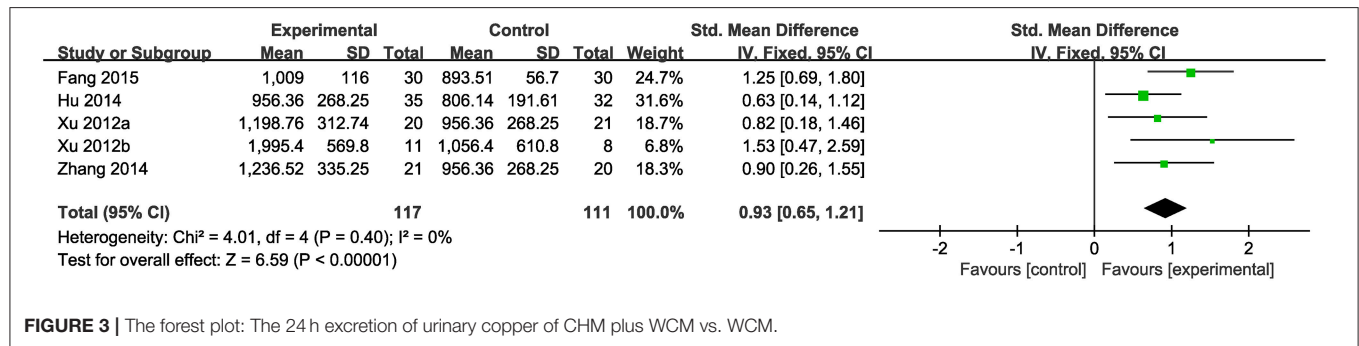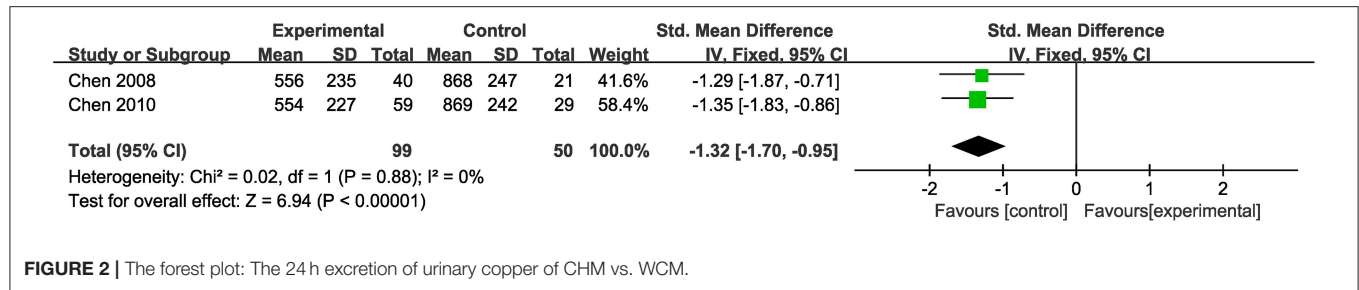
DISCUSSION

Summary of Evidence

Eighteen RCTs involving 1,220 patients suffering from WD were identified. The main findings of this study were that CHM adjuvant therapy could increase 24 h urinary copper excretion, and improve liver function and the total clinical efficacy rate for WD. Two trails (Chen and Wang, 2008, 2010) indicated that CHM monotherapy was not superior to the WCM. Eight out of eighteen studies reported no serious adverse events relevant to

TABLE 5 | Details of the most commonly used herbs for WD.

Chinese name	Pharmaceutical name	Species	Family	Record	N/18 (%)
Dahuang	*Radix et Rhizoma Rhei*	*Rheum officinale* Baill.	*Polygonaceae*	–	17(94%)
Huanglian	*Rhizoma Coptidis*	*Coptis chinensis* Franch.	*Ranunculaceae*	–	13(72%)
Banzhilian	*Herba Scutellariae Barbatae*	*Scutellaria barbata* D.Don	*Lamiaceae*	188943	11(61%)
Chuanxinlian	*Herba Andrographis*	*Andrographis paniculata* (Burm.f.) Nees	*Acanthaceae*	–	11(61%)
Danshen	*Radix Salviae Miltiorrhizae*	*Salvia miltiorrhiza* Bunge	*Lamiaceae*	183206	9(50%)
Zexie	*Rhizoma Alismatis*	*Alisma orientale* (Sam.) Juz.	*Alismataceae*	294832	9(50%)
Ezhu	*Rhizoma Curcumae*	*Curcuma phaeocaulis* Valeton	*Zingiberaceae*	235270	9(50%)
Yujin	*Radix Curcumae*	*Curcuma wenyujin* Y.H.Chen & C.Ling	*Zingiberaceae*	235308	9(50%)
Jianghuang	*Rhizoma Curcumae Longae*	*Curcuma longa* L.	*Zingiberaceae*	235249	8(44%)
Shichangpu	*Rhizoma Acori Tatarinowii*	*Acorus tatarinowii* Schott	*Acoraceae*	2337	7(39%)
Jixueteng	*Caulis Spatholobi*	*Spatholobus suberectus* Dunn	*Leguminosae*	32974	8(44%)
Huangqin	*Radix Scutellariae*	*Scutellaria baicalensis* Georgi	*Lamiaceae*	188938	5(28%)
Jinqiancao	*Herba Lysimachiae*	*Lysimachia christinae* Hance	*Primulaceae*	–	5(28%)

CHM formulas, indicating that CHM formulas were generally safe and well tolerated for patients with WD. The possible mechanisms are associated with reversing the ATP7B mutants, and exerting anti-oxidation, anti-inflammation and anti-fibrotic effects. Thus, the findings of the present study suggested, to a limited extent, that CHM paratherapy can be used for WD according to the methodological flaws, whereas the beneficial use of CHM monotherapy for WD still lacks evidence.

Limitations

There are several limitations in the primary studies. Firstly, although we included RCTs, some inherent and methodological weaknesses still existed in the primary studies: only 2 trials provided sufficient information on how the random allocation was generated, while none of the other trials included reported the allocation concealment. No study employed the blinding procedure, making it difficult to bias results intentionally or unintentionally and to help ensure the credibility of study conclusions. A placebo effect is conceptually defined as the beneficial effect associated with an intervention that does not include the presumed active ingredients; however, CHM placebo are hard to mimic identical interventional herbal prescription due to the fact that CHM is special in color, smell and taste. Thus, placebo-controlled randomized trials are well-recognized method when evaluating the efficacy of CHM treatment. In addition, most trials are without calculating the formal pretrial sample size. The trials with inadequate sample sizes seem to be one risk in exaggerating intervention benefits. Secondly, WD is a chronic disease, which needs life-long treatments. Long-term efficacy and safety are important assessments to determine the clinical effectiveness of an agent in treatment. However, in the present study, treatment duration ranged from 28 to 90 days. Long-term safety of CHM for WD could not be determined because duration of treatment is short and dropouts were only reported in one study. According to other clinical trials for WD (Brewer et al., 2009; Weiss et al., 2015; Nicholl et al., 2017), it is recommended that the treatment duration of further trials must not be >60 days, and must last more than 1 year. Thirdly, clinical heterogeneity would be very significant due to the

variations in study quality, intervention of CHM prescriptions, comparators, and outcome measures. Owing to being highly variable in composition and dosage of CHMs, it is difficult to assess the efficacy of a specific CHM by performing pooling analysis. Fourthly, all trials were conducted in China, which may limit the generalizability. Further international multicenter RCTs of CHM for WD are needed, in order to generalize the results worldwide.

Implications for Practice

Use of CHM for WD patients has increased in the past decades. However, the choice of CHM is mainly empirical and lacking consensus among clinical doctors. The available evidence from the present study supported, to a limited extent, that CHM paratherapy can be used for patients with WD but should not be recommended as monotherapy in WD. In addition, the most frequently used herbs selected by the present study should be considered as herbal prescription for WD and as a candidate for further clinical trials.

Implications for Research

In the present study, we identified an area that is worthy of further study. Firstly, the potential benefit of CHM as an adjunct treatment for WD still needs to be further confirmed by high-quality RCTs. Thus, we recommend that CONSORT 2010 statement (Schulz et al., 2010), CONSORT for CHM Formulas (Cheng et al., 2017), and RCTs investigating CHM (Flower et al., 2011) should be used as the guidelines when the designing, registering and reporting of further RCTs. Secondly, WD was thought of as a "rare" autosomal disorder by neurologists, and it proved difficult to conduct large sample RCT. However, this review identified 1,220 subjects with WD from 1997 to 2016. If the primary clinical data of all RCTs were recorded in standard, the evidence would be more reliable. Thus, it is necessary to promote clinical data sharing, as has been suggested by the International Committee of Medical Journal Editors (ICMJE) (Taichman et al., 2017).

WD is caused by ATP7B mutations, resulting in copper accumulation and toxicity. The possible mechanisms of CHM for

WD not only involve the targets of the ATP7B gene, but also the multiple targets of copper accumulation in various tissues and organs. Curcumin and P-coumaric acid were reported to reverse the ATP7B function defect. Curcumin could partially restore protein expression by directly enhancing the protein expression of mutant ATP7B with residual copper export activity (van den Berghe et al., 2000; Zhang et al., 2011; European Association for Study of Liver, 2012). The EASL Guidelines recommended that treatment with curcumin might be a novel therapeutic strategy in WD (European Association for Study of Liver, 2012). P-coumaric acid, another ingredient of herbs, can also reverse the ATP7B function defect via a different mechanism by regulating pre-mRNA splicing (Lin et al., 2015).

Copper accumulates in hepatocytes where it induces damage through oxidative stress due to its highly reactive redox capacity (Rosencrantz and Schilsky, 2011). In addition, necrosis and apoptosis triggered immune reaction and inflammation to activate the quiescent HSCs, causing hepatic fibrosis (Jin et al., 2016). The possible pharmacological mechanisms of CHM for copper accumulations of WD are as follows: (1) Antioxidant effects: Curcumin, Anthraquinone (from *Radix et Rhizoma Rhei*), Danshensu and Salvianolic acid B (from *Radix Salviae Miltiorrhizae*), were shown to ameliorate the oxidative stress by reducing oxidative stress parameters malondialdehyde, thereby improving the hepatic glutathione content and hepatic superoxide dismutase (SOD) (Liu et al., 2016; Samarghandian et al., 2017), inhibiting the formation of superoxide anions (Shia et al., 2009), and exerting a low level of lipid peroxidase (Mishra et al., 2014; Lee et al., 2016, 2017), leading to maintenance of mitochondrial activity (Zhou et al., 2015). *Radix*

Scutellariae improved the antioxidant capacity by induction of the antioxidative enzymes and removal of reactive oxygen species (ROS) (Pan et al., 2015). P-coumaric acid (Ibrahim et al., 2007), Andrographolideand (Vetriselvan et al., 2011), *Caulis Spatholobi* (Jeon et al., 2008) and Tanshinone IIA, (Shu et al., 2016) have also been shown to exhibit antioxidant effects; (2) Anti-inflammatory effects: Emodin (from *Radix et Rhizoma Rhei*), Andrographolide (from *Herba Andrographis*), *Radix Salviae Miltiorrhizae* and Curcumin analog demonstrated anti-inflammatory properties by reducing the expression of pro-inflammatory mediators via the NF-kB activation pathway (Lee et al., 2003; Hwang et al., 2013; Yue et al., 2014) and MAPK/AP-1 pathway (Choi et al., 2013), and by inhibiting iNOS and COX-2 expression (Paulino et al., 2016). The bioactive components from *Radix Scutellariae* (Liu et al., 2016) and Quercetin from *Herba Lysimachiae* (Wang et al., 2015) have been reported to exhibit anti-inflammatory activity; (3) Anti-fibrotic effects: activation of quiescent HSCs is the major event in hepatic fibrosis (Jin et al., 2016). Skullcapflavone I (from *Radix Scutellariae*) (Park et al., 2005) and Curcumin (Jin et al., 2016) exerted anti-fibrotic effects by inducing apoptosis or senescence in activated HSCs. Furthermore, Curcumin was found to be an anti-fibrotic mediator that inhibits HSCs activation and the transition to myofibroblast-like cells (Mustafa, 2016). In contrast, *Radix et Rhizoma Rhei* exerted anti-fibrotic effects by the direct inhibition of stellate cell activation without reducing hepatocyte cell death (Jin et al., 2005). Salvianolic acid A and B from Danshen (Tsai et al., 2011), Berberine (Zhang et al., 2008), *Radix Scutellariae* (Chen et al., 2013) and *Radix et Rhizoma Rhei* (Pan et al., 2015) have been reported to prevent hepatic fibrosis in different aspects,

FIGURE 6 | Simplified model of copper toxicity and disease progression and potential targets for CHM intervention.
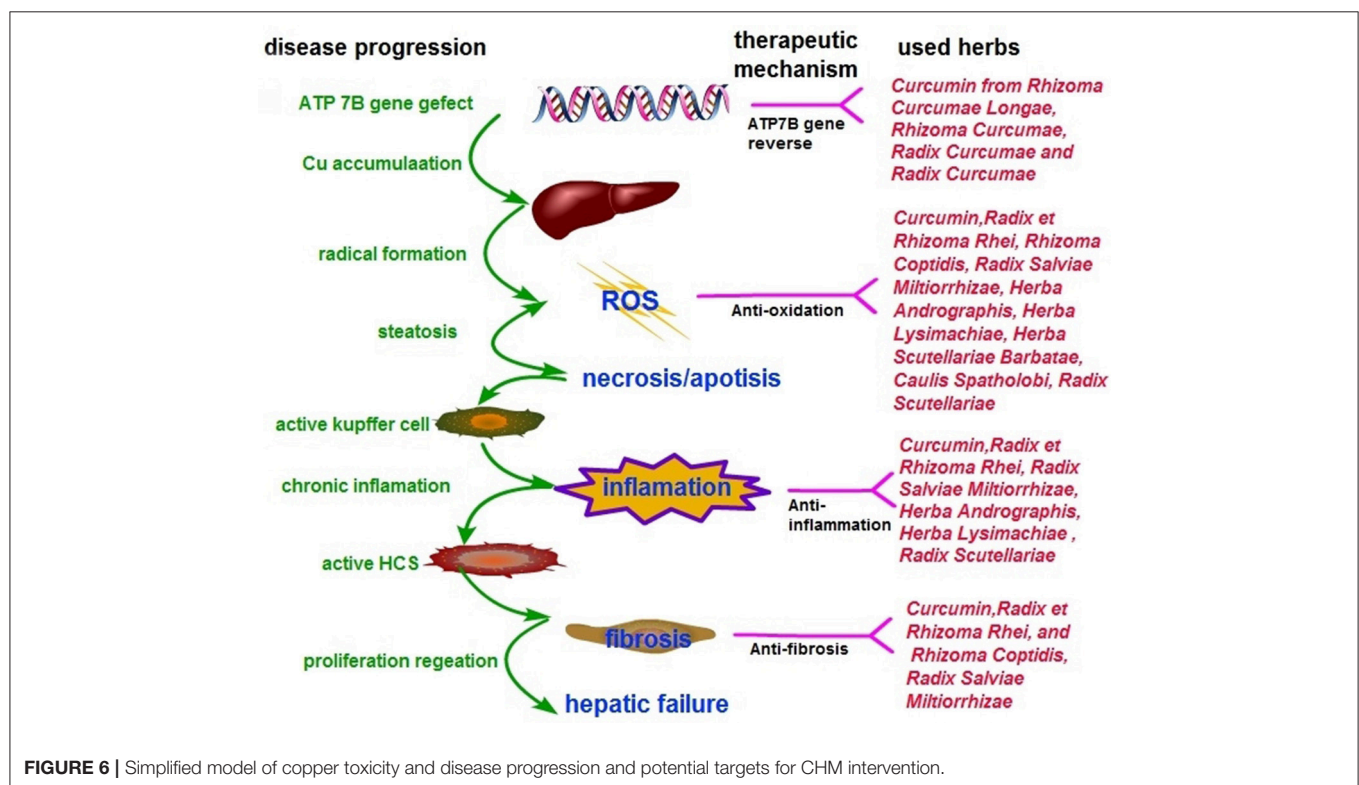
including inhibition of proliferation and fibrogenesis of HSCs, and regulation of the antioxidant system and lipid peroxidation. Thus, CHM is likely to be useful as a multi-targeting therapy for WD pathogenesis (**Figure 6**).

CONCLUSION

Despite the apparent positive results, the present evidence supports, to a limited extent because of the methodological flaws and CHM heterogeneity, that CHM paratherapy can be used for patients with WD but should not be recommended as monotherapy in WD. The possible mechanisms involved are associated with reversing the ATP7B mutants, and exerting anti-oxidation, anti-inflammation and anti-hepatic fibrosis effects. Further rigorous RCTs, focusing on an individual CHM formula for WD, are warranted.

AUTHOR CONTRIBUTIONS

G-QZ contribute as the senior authors and the principal investigator (PI) of this study. M-BX, P-QR, and T-YJ wrote the first draft of the manuscript and contributed to the overall design. G-QZ refined the study. P-PZ and H-YL identified reviewed studies for eligibility and performed the meta-analysis of data. All authors read, critically reviewed and approved the final manuscript.

FUNDING

REFERENCES

Aggarwal, A., Aggarwal, N., Nagral, A., Jankharia, G., and Bhatt, M. (2009). A novel Global Assessment Scale for Wilson's Disease (GAS for WD). *Mov. Disord.* 24, 509–518. doi: 10.1002/mds.22231

Brewer, G. J. (2009). Zinc and tetrathiomolybdate for the treatment of Wilson's disease and the potential efficacy of anticopper therapy in a wide variety of diseases. *Metallomics* 1, 199–206. doi: 10.1039/b901614g

Brewer, G. J., Askari, F., Dick, R. B., Sitterly, J., Fink, J. K., Carlson,. M., et al. (2009). Treatment of Wilson's disease with tetrathiomolybdate: V. Control of free copper by tetrathiomolybdate and a comparison with trientine. *Transl. Res.* 154, 70–77. doi: 10.1016/j.trsl.2009.05.002

Bull, P. C., Thomas, G. R., Rommens, J. M., Forbes, J. R., and Cox, D. W. (1993). The Wilson disease gene is a putative copper transporting Ptype ATPase similar to the Menkes gene. *Nat. Genet.* 5, 327–337. doi: 10.1038/ng1293-327

Chen, H. J., Liang, T. M., Lee, I. J., Huang, Y. T., and Lin, Y. L. (2013). Scutellariae radix suppresses LPS-induced liver endothelial cell activation and inhibits hepatic stellate cell migration. *J. Ethnopharmacol.* 150, 835–842. doi: 10.1016/j.jep.2013.08.049

Chen, J. L., and Wang, D. H. (2008). Observation of liver function and cirrhosis on patients with Wilson's disease treated by Shuganlidanpaidu Decoction (Chinese). *J. N. Chin. Med.* 38, 28–29. doi: 10.13457/j.cnki.jncm.2008.12.026

Chen, J. L., and Wang, D. H. (2010). Clinical observation on 59 cases of Wilson's disease treated by chaihuang gandou pulvis (Chinese). *Sichuan Trad. Chin. Med.* 1, 72–74.

Cheng, C. W., Wu, T. X., Shang, H. C., Li, Y. P., Altman, D. G., Moher,. D., et al. (2017). CONSORT extension for chinese herbal medicine Formulas2017:recommendations, explanation, and elaboration (Traditional Chinese Version). *Ann. Intern. Med.* 167, W7–W20. doi: 10.7326/IsTranslatedFrom_M17-2977_1

Chinese Medical Association of Neurology (2008). Guidelines for the diagnosis and treatment of hepatolenticular degeneration (Chinese). *Chin. J. Neurol.* 8, 566–569. doi: 10.3321/j.issn:1006-7876.2008.08.022

Choi, R. J., Ngoc, T. M., Bae, K., Cho, H. J., Kim, D. D., Chun, J., et al. (2013). Anti-inflammatory properties of anthraquinones and their relationship with the regulation of P-glycoprotein function and expression. *Eur. J. Pharm. Sci.* 48, 272–281. doi: 10.1016/j.ejps.2012.10.027

Coffey, A. J., Durkie, M., Hague, S., McLay, K., Emmerson, J., and Lo, C. (2013). A genetic study of Wilson's disease in the United Kingdom. *Brain* 136:1476–1487. doi: 10.1093/brain/awt035

Cui, G. X., and Zhao, Q. W. (2001). Clinical observation on 33 cases of patients with Wilson's disease treated by traditional Chinese and western medicine (Chinese). *Shandong, J. Trad. Chin. Med.* 20, 353–355. doi: 10.16295/j.cnki.0257-358x.2001.05.023

European Association for Study of Liver (2012). EASL clinical practice guidelines: Wilson's disease. *J. Hepatol.* 56, 671–685. doi: 10.1016/j.jhep.2011.11.007

Fang, S. Z. (2015). *Effect of Gandouling Tablet on Index of Cardiac Function in Patients With Wilson's Disease and Cardiac Ultrastructure of Copper-Loaded Rats (Chinese)*. Hefei: Master's thesis, Anhui university of Chinese medicine.

Filippi, C., and Dhawan, A. (2014). Current status of human hepatocyte transplantation and its potential for Wilson's disease. *Ann. N. Y. Acad. Sci.*1315,50–55. doi: 10.1111/nyas.12386

Flower, A., Witt,. C., Liu, J. P., Ulrich-Merzenich, G., Yu, H., and Lewith, G. (2011). Guidelines for randomised controlled trials investigating Chinese herbal medicine. *J. Ethnopharmacol.* 140,550–554. doi: 10.1016/j.jep.2011.12.017

Gomes, A., and Dedoussis, G. V. (2015). Geographic distribution of ATP7B mutations in Wilson disease. *Ann. Hum. Biol.* 43, 1–8. doi: 10.3109/03014460.2015.1051492

Han, H., Fang, X., Wu, L. M., Zhang, J., Fang, S. Z., He, W. S., et al. (2014). Observation of 21 cases of cognitive impairment of Wilson's disease treated by huatanquyu method (Chinese). *J. Anhui Univ. Trad. Chin. Med.* 33, 21–23. doi: 10.3969/j.issn.2095-7246.2014.01.009

Han, Y. Z., He, G. Y., Wang, X., Le, K., Wang, G. Q., and Yang, R. M. (1999). Comparison of therapeutic effects of gandouling tablet I and dimercaptosuccinate acid on hepatolenticular degeneration (Chinese). *Chin. J. Integr. Trad. West. Med.* 19, 69–70.

Hedera, P. (2017). Update on the clinical management of Wilson's disease. *Appl. Clin. Genet.* 10, 9–19. doi: 10.2147/TACG.S79121

Higgins, J., Altman, D., and Sterne, J. (eds.). (2011). "Chapter 8: Assessing risk of bias in included studies," in *Cochrane Handbook for Systematic Reviews of Interventions*. Version 5.1.0. (London: The Cochrane Collaboration). Available online at: http://handbook-5-1.cochrane.org/

Hong, M. F., Wang, G. Q., Yang, R. M., Hu, J. Y., Wang, X. P., and Lv, D. P. (2000). Effect of integrated traditional Chinese and western medicine on liver cirrhosis and liver function in patients with hepatolenticular degeneration (Chinese). *Chin. J. Integr. Trad. West. Med.* 20, 890–892. doi: 10.3321/j.issn:1003-5370.2000.12.003

Hu, W. B., Han, Y. Z., Xue, B. C., Cheng, N., Sun, D. Y., Ye, D. Q., et al. (2011). Epidemiological investigation of Wilson disease in Hanshan county, Anhui Province. *Chin. Med. J.* 91, 894–897.doi: 10.3760/cma.j.issn.0376-2491.2011.13.008

Hu, Y. X. (2014). *Effect of Doudou Decoction on Pulmonary Ventilation Function and Immunologic Index in Patients With Wilson's Disease and Pneumonic Ultrastructure of Model Rats (Chinese)*. Hefei: Master's thesis, Anhui university of Chinese medicine.

Hwang, J. K., Noh, E. M., Moon, S. J., Kim, J. M., Kwon, K. B., Park, B. H., et al. (2013). Emodin suppresses inflammatory responses and joint destruction in collagen-induced arthritic mice. *Rheumatology* 52, 1583–1591. doi: 10.1093/rheumatology/ket178

Ibrahim, N. A., El-Seedi, H. R., and Mohammed, M. M. (2007). Phytochemical investigation and hepatoprotective activity of *Cupressus*

sempervirens L.leaves growing in Egypt. *Nat. Prod. Res.* 21, 857–866. doi: 10.1080/14786410601132477

Jeon, H., Cha, D. S., Ko, S. H., Park, H. J., Lee, Y. J., Lim, J. P., et al. (2008). Radical scavenging effects and protective effect of Spatholobus suberectus against CCl4 induced liver damage in rats. *Nat. Prod. Sci.* 14, 127–130. Available online at: http://www.koreascience.or.kr/article/JAKO200824067121771.page

Jiang, H. L. (2016). *Effect of Gandouling Tablet on Indexes of Cerebral Hemodynamics and Vascular Injury Factor in Patients With Wilson's Disease and the Mechanism of Vascular Injury in TX Mice (Chinese).* Hefei: Master's thesis, Anhui University of Chinese Medicine.

Jin, H., Lian, N., Zhang, F., Chen, L., Chen, Q., Lu, C., et al. (2016). Activation of PPARγ/P53 signaling is required for curcumin to induce hepatic stellate cell senescence. *Cell. Death. Dis.* 7:e2189. doi: 10.1038/cddis.2016.92

Jin, H., Sakaida, I., Tsuchiya, M., and Okita, K. (2005). Herbal medicine Rhei rhizome prevents liver fibrosis in rat liver cirrhosis induced by a choline-deficient L-amino acid-defined diet. *Life Sci.* 76, 2805–2816. doi: 10.1016/j.lfs.2004.09.041

Lee, G. H., Lee, H. Y., Choi, M. K., Chung, H. W., Kim, S. W., and Chae, H. J. (2017). Protective effect of *Curcuma longa* L. extract on CCl(4)-induced acute hepatic stress. *BMC Res. Notes* 10:77. doi: 10.1186/s13104-017-2409-z

Lee, H., Kim, Y. O., Kim, H., Kim, S. Y., Noh, H. S., Kang, S. S., et al. (2003). Flavonoid wogonin from medicinal herb is neuroprotective by inhibiting inflammatory activation of microglia. *FASEB J.* 17, 1943–1944. doi: 10.1096/fj.03-0057fje

Lee, H. Y., Kim, S. W., Lee, G. H., Choi, M. K., Jung, H. W., Kim, Y. J., et al. (2016). Turmeric extract and its active compound, curcumin, protect against chronic CCl4-induced liver damage by enhancing antioxidation. *BMC Complement. Altern. Med.* 16:316. doi: 10.1186/s12906-016-1307-6

Leinweber, B., Möller, J. C., Scherag, A., Reuner, U., Günther, P., Lang, C. J., et al. (2008). Evaluation of the Unified Wilson's Disease Rating Scale (UWDRS) in German patients with treated Wilson's disease. *Mov. Disord.* 23, 54–62. doi: 10.1002/mds.21761

Li, W. J., Chen, C., You, Z. F., Yang, R. M., and Wang, X. P. (2016). Current drug managements of Wilson's disease: from west to east. *Curr. Neuropharmacol.* 14, 322–325 doi: 10.2174/1570159X14666151130222427

Lin, Y. J., Ho, T. J., Lin, T. H., Hsu, W. Y., Huang, S. M., Liao, C. C., et al. (2015). P-coumaric acid regulates exon 12 splicing of the ATP7B gene by modulating hnRNP A1 protein expressions. *Biomed* 5:10. doi: 10.7603/s40681-015-0010-0

Liu, Z., Dou, W., Zheng, Y., Wen, Q., Qin, M., Wang, X., et al. (2016). Curcumin upregulates Nrf2 nuclear translocation and protects rat hepatic stellate cells against oxidative stress. *Mol. Med. Rep.* 13, 1717–1724. doi: 10.3892/mmr.2015.4690

Lutsenko, S., Barnes, N., Bartee, M., and Dmitriev, O.Y. (2007). Function and regulation of human copper-transporting ATPases. *Physiol. Rev.* 87, 1011–1046. doi: 10.1152/physrev.00004.2006

Mishra, S. K., Tiwari, S., Shrivastava, A., Srivastava, S., Boudh, G. K., Chourasia, S. K., et al. (2014). Antidyslipidemic effect and antioxidant activity of anthraquinone derivatives from Rheum emodi rhizomes in dyslipidemic rats. *J. Nat. Med.* 68, 363–371. doi: 10.1007/s11418-013-0810-z

Moher, D., Liberati, A., Tetzlaff, J., Altman, D. G., and The PRISMA Group. (2009). Preferred reporting items for systematic reviews and meta-analyses: the PRISMA statement. PLoS Med. 6: e1000097. doi: 10.1371/journal.pmed.1000097

Mustafa, H. (2016). The role of curcumin in streptozotocin-induced hepatic damage and the trans-differentiation of hepatic stellate cells. *Tissue Cell* 48, 81–88. doi: 10.1016/j.tice.2016.02.003

Nicholl, D., Flint, S., Olsson, L., Plitz, T., Bjartmar, C., and Schilsky, M. L. (2017). Bis-choline tetrathiomolybdate in patients with Wilson's disease: an open-label, multicentre, phase 2 study. *Lancet Gastroenterol. Hepatol.* 2, 869–876. doi: 10.1016/S2468-1253(17)30293-5

Pan, T. L., Wang, P. W., Huang, C. H., Leu, Y. L., Wu, T. H., Wu, Y. R., et al. (2015). Herbal formula,Scutellariae radix and Rhei rhizoma attenuate dimethylnitrosamine-induced liver fibrosis in a rat model. *Sci. Rep.* 5:11734. doi: 10.1038/srep11734

Panossian, A., Davtyan, T., Gukassyan, N., Gukasova, G., Mamikonyan, G., Gabrielian, E., et al. (2002). Effect of andrographolide and Kan Jang—Fixed combination of extract SHA-10 and extract SHE-3—On proliferation of human lymphocytes, production of cytokines and immune activation

markers in the whole blood cells culture. *Phytomedicine* 9, 598–605. doi: 10.1078/094471102321616409

Park, E. J., Zhao, Y. Z., Lian, L., Kim, Y. C., and Sohn, D. H. (2005). Skullcapflavone I from Scutellaria baicalensis induces apoptosis in activated rat hepatic stellate cells. *Planta Med.* 71, 885–887. doi: 10.1055/s-2005-871280

Patil, M., Sheth, K. A., Krishnamurthy, A. C., and Devarbhavi, H. (2013). A review and current perspective on Wilson disease. *J. Clin. Exp. Hepatol.* 3, 321–336. doi: 10.1016/j.jceh.2013.06.002

Paulino, N., Paulino, A. S., Diniz, S. N., de Mendonça, S., Gonçalves, I. D., Faião Flores, F., et al. (2016). Evaluation of the anti-inflammatory action of curcumin analog (DM1): Effect on iNOS and COX-2 gene expression and autophagy pathways. *Bioorg. Med. Chem.* 24, 1927–1935. doi: 10.1016/j.bmc.2016.03.024

Petrukhin, K., Fischer, S. G., Pirastu, M., Tanzi, R. E., Chernov, I., Devoto, M., et al. (1993). Mapping,cloning and genetic characterization of the region containing the Wilson disease gene. *Nat. Genet.* 5, 338–343. doi: 10.1038/ng1293-338

Ren, M. S., Zhang, B., Yang, R. M., Han, Y. Z., and Wang, X. (1997). Clinical study on treatment of hepatolenticular degeneration with integrated traditional Chinese and western Medicine (Chinese). *Chin. J. Integr. Trad. West. Med.* 6, 136–138.

Roberts, E. A., and Schilsky, M. L., American Association for Study of Liver Diseases. (2008). Diagnosis and treatment of Wilson disease: an update. *Hepatology* 47, 2089–2111. doi: 10.1002/hep.22261

Rosencrantz, R., and Schilsky, M. (2011). Wilson disease: pathogenesis and clinical considerations in diagnosis and treatment. *Semin. Liver Dis.* 31, 245–259. doi: 10.1055/s-0031-1286056

Samarghandian, S., Azimi-Nezhad, M., Farkhondeh, T., and Samini, F. (2017). Anti-oxidative effects of curcumin on immobilization-induced oxidative stress in rat brain, liver and kidney. *Biomed. Pharmacother.* 87, 223–229. doi: 10.1016/j.biopha.2016.12.105

Schulz, K., Altman, D., Moher, D., and CONSORT Group. (2010). Consort 2010 statement: updated guidelines for reporting parallel group randomised trials. *PLoS Med.* 7:e1000251. doi: 10.1371/journal.pmed.1000251

Shia, C. S., Juang, S. H., Tsai, S. Y., Chang, P. H., Kuo, S. C., Hou, Y. C., et al. (2009). Metabolism and pharmacokinetics of anthraquinones in Rheum palmatum in rats and *ex vivo* antioxidant activity. *Planta Med.* 75, 1386–1392. doi: 10.1055/s-0029-1185725

Shu, M., Hu, X., Hung, Z., Huang, D., and Zhang, S. (2016). Effects of tanshinone IIA on fibrosis in a rat model of cirrhosis through heme oxygenase-1, inflammation, oxidative stress and apoptosis. *Mol. Med. Rep.* 13, 3036–3042. doi: 10.3892/mmr.2016.4886

Taichman, D. B., Sahni, P., Pinborg, A., Peiperl, L., Laine, C., James, A., et al. (2017). Data sharing statements for clinical trials. *BMJ* 357:j2372. doi: 10.1136/bmj.j2372

Tsai, M., Lin, Y., and Huang, Y. (2011). Differential inhibitory effects of salvianolic acids on activation of rat hepatic stellate cells by platelet-derived growth factor. *Planta. Med.* 77, 1495–1503. doi: 10.1055/s-0030-1270783

van den Berghe, P. V., Stapelbroek, J. M., Krieger, E., de Bie, P., van de Graaf, S. F., de Groot, R. E., et al. (2000). Reduced expression of ATP7B affected by Wilson disease-causing mutations is rescued by pharmacological folding chaperones 4-phenylbutyrate and curcumin. *Hepatology* 50, 1783–1795. doi: 10.1002/hep.23209

Vetriselvan, S., Subasini, U., Rajamanickam, C., and Thirumurugu, S. (2011). Hepatoprotective activity of Andrographis paniculata in ethanol induced hepatotoxicity in albino wistar rats. *Pharmacie Glob.* 2, 1–4. Available online at: journaldatabase.info/articles/research_hepatoprotective_activity_andrographis.html

Walshe, J. M. (2009). The conquest of Wilson's disease. *Brain* 132, 2289–2295. doi: 10.1093/brain/awp149

Wang, H., Yang, W. M., Bao, Y. C., Wang, M. X., Han, H., Wang, X. Y., et al. (2010). Effects of ganodu ling tablet on T cells and NK cells in 58 cases of patients with Wilson's disease (Chinese). *Clin. J. Trad. Chin. Med.* 22, 963–964. doi: 10.16448/j.cjtcm.2010.11.007

Wang, J., Miao, M., Zhang, Y., Liu, R., Li, X., Cui, Y., et al. (2015). Quercetin ameliorates liver injury induced with Tripterygium glycosides by reducing oxidative stress and inflammation *Can. J. Physiol. Pharmacol.* 93, 427–433. doi: 10.1139/cjpp-2015-0038

Wang, Y., Lou, X. T., Shi, Y. H., Tong, Q., and Zheng, G. Q. (2019).Erxian decoction, a Chinese herbalformula, for menopausal syndrome: an updated

systematic review. *J. Ethnopharmacol.* 15, 8–20. doi: 10.1016/j.jep.2019.01.010

Wang, Y., Xie, C. L., Fu, D. L., Lu, L., Lin, Y., Dong, Q. Q., et al. (2012). Clinical efficacy and safety of Chinese herbal medicine for Wilson's disease: a systematic review of 9 randomized controlled trials. *Complement. Ther. Med.* 20, 143–154. doi: 10.1016/j.ctim.2011.12.004

Weiss, K. H., Askari, F. K., Czlonkowska, A., Ferenci, P., Bronstein, J. M., Bega, D., et al. (2015). Prospective pilot study of a single daily dosage of trientine for the treatment of Wilson disease. *Dig. Dis. Sci.* 60,1433–1439. doi: 10.1007/s10620-014-3495-6

Xiao, L. M. (2003). Clinical observation on treatment of hepatic fibrosis in patients with Wilson's disease by integrated traditional Chinese and western medicine (Chinese). *Hubei J. Trad. Chin. Med.* 25, 9–10. doi: 10.3969/j.issn.1000-0704.2003.12.004

Xu, G. C., Chen, H. Z., Zhang, J., Fang, X., Li, J., Ge, Q., et al. (2012a). Observation on improvement of 24-hour urinary excretion of copper and improvement effect in treatment of hepatolenticular degeneration by gandou decoction (Chinese). *Clin. J. Trad. Chin. Med.* 24, 1055–1057. doi: 10.16448/j.cjtcm.2012.11.041

Xu, G. C., Zhang, J., and Chen, H. Z. (2012b). Effect of gandouling tablet on portal hemodynamics in patients with Wilson's disease (Chinese). *Clin. J. Trad. Chin. Med.* 24, 204–205. doi: 10.16448/j.cjtcm.2012.03.027

Xue, B. C., Yang, R. M., Hu, J. Y., Han, Y. Z., and Wang, J. H. (2007). Study on the mechanism of liver fibrosis in patients with Wilson's disease treated by gandou decoction No.2 (Chinese). *Anhui Med. J.* 28, 296–299. doi: 10.3969/j.issn.1000-0399.2007.04.005

Yang, R. M. (1995). *Hepatolenticular Degeneration.* Hefei: Science and Technology Publishing House of Anhui.

Yue, S., Hu, B., Wang, Z., Yue, Z., Wang, F., Zhao, Y., et al. (2014). Salvia miltiorrhiza compounds protect the liver from acute injury by regulation of p38 and NFκB signaling in Kupffer cells. *Pharm. Biol.* 52, 1–8. doi: 10.3109/13880209.2014.889720

Zhang, B. J., Xu, D., Guo, Y., Ping, J., Chen, L. B., and Wang, H. (2008). Protection by and anti-oxidant mechanism of berberine against rat liver fibrosis induced by multiple hepatotoxic factors. *Clin. Exp. Pharmacol. Physiol.* 35, 303–309. doi: 10.1111/j.1440-1681.2007.04819.x

Zhang, H. B. (2007). Effect of dahuang gandou decoction combined with penicillamine on Wilson's disease (Chinese). *Int. J. Trad. Chin. Med.* 29, 141–143.

Zhang, J., Bao, Y. C., Xie, D. J., Tong, J. B., Zhou, L., Ding, W. J., et al. (2014a). Effect of gandouling tablet on indexes of urinary microprotein in patients with Wilson's disease (Chinese). *J. Anhui Univ. Trad. Chin. Med.* 33, 22–25. doi: 10.3969/j.issn.2095-7246.2014.03.008

Zhang, J., Chen, H. Z., Li, L. Y., and Fang, X. (2014b). Effect of gandou decoction combined with sodium dimercaptopropanesulfonate on the indicator of portal circulation in patients with Wilson's disease(Chinese). *J. N. Chin. Med.* 24, 57–59. doi: 10.13457/j.cnki.jncm.2014.01.076

Zhang, S., Chen, S., Li, W., Guo, X., Zhao, P., Xu, J., et al. (2011). Rescue of ATP7B function in hepatocyte-like cells from Wilson's disease induced pluripotent stem cells using gene therapy or the chaperone drug curcumin. *Hum. Mol. Genet.* 20, 3176–3187. doi: 10.1093/hmg/ddr223

Zhou, X., Cheung, C. M., Yang, J. M., Or, P. M., Lee, W. Y., and Yeung, J. H. (2015). Danshen (Salvia miltiorrhiza) water extract inhibits paracetamol-induced toxicity in primary rat hepatocytes via reducing CYP2E1 activity and oxidative stress. *J. Pharm. Pharmacol.* 67, 980–989. doi: 10.1111/jphp.12381

Baishouwu Extract Suppresses the Development of Hepatocellular Carcinoma via TLR4/MyD88/ NF-κB Pathway

Yong-fang Ding[1], Zi-xuan Peng[2], Lan Ding[3] and Yun-ru Peng[1]*

[1] Department of Pharmacology and Toxicology, Jiangsu Province Academy of Traditional Chinese Medicine, Nanjing, China,
[2] Third College of Clinical Medicine, Xinjiang Medical University, Ürümqi, China, [3] Department of Nephrology, Suzhou
Wuzhong People's Hospital, Suzhou, China

Purpose: The root of *Cynanchum auriculatum* Royle ex Wight, known as Baishouwu, has been widely used for a tonic supplement since ancient times. The current study was performed to explore the effect of Baishouwu extract on the development of experimental hepatocellular carcinoma (HCC) and the potential mechanism involved.

Methods: Rats were injected diethylnitrosamine (DEN) to initiate the multistep hepatocarcinogenesis. Animals were treated concurrently with Baishouwu extract given daily by oral gavage for 20 weeks to evaluate its protective effects. Time series sera and organ samples from each group were collected to evaluate the effect of Baishouwu extract on hepatic carcinogenesis.

Results: It was found that Baishouwu extract pretreatment successfully attenuated liver injury induced by DEN, as shown by decreased levels of serum biochemical indicators (AST, ALT, ALP, TP, and T-BIL). Administration of Baishouwu extract inhibited the fibrosis-related index in serum and live tissue, respectively from inflammation stage to HCC stage after DEN treatment. It significantly reduced the incidence and multiplicity of DEN-induced HCC development in a dose-dependent manner. Macroscopic and microscopic features suggested that pretreatment with Baishouwu extract for 20 weeks was effective in inhibiting DEN-induced inflammation, liver fibrosis, and HCC. Furthermore, TLR4 overexpression induced by DEN was decreased by Baishouwu extract, leading to the markedly down-regulated levels of MyD88, TRAF6, NF-κB p65, TGF-β1 and α-SMA in hepatitis, cirrhosis, and hepatocarcinoma.

Conclusion: In conclusion, Baishouwu extract exhibited potent effect on the development of HCC by altering TLR4/MyD88/ NF-κB signaling pathway in the sequence of hepatic inflammation-fibrosis-cancer, which provided novel insights into the mechanism of Baishouwu extract as a candidate for the pretreatment of HCC in the future.

Keywords: Baishouwu extract, pretreatment, hepatocellular carcinoma, TLR4, inflammation-fibrosis-cancer axis

INTRODUCTION

Hepatocellular carcinoma (HCC) is the fifth most common cancer in the world and the third cause of cancer-related deaths (Jemal et al., 2011). Chronic inflammation, caused by chemical, biological and physical factors, is found to be related to certain human cancers. The effect of inflammation-fibrosis-cancer (IFC) axis acts as a bridge from inflammation to cancer, and therefore promotes inflamed liver evolving to fibrosis/cirrhosis and HCC (Lam et al., 2016; Ding et al., 2017). Upon exposure to risk factors like alcohol, viruses, parasitesand toxic substances, hepatic injury resulted in the degeneration and inflammation, leading to chronic liver diseases, which may further progress to different stages of fibrosis, cirrhosis, and HCC. HCC is the final stage of this process.

Traditional Chinese medicines contain natural active constituents, which demonstrate remarkable antitumor effect with little untoward effects. *Cynanchum auriculatum* Royle ex Wight is widely distributed in China. The root of this plant, known as "Baishouwu," has been used for thousands of years as a tonic supplement. It is wildly used to replenish the liver and kidney, enrich vital essence and blood, strengthen the bones and muscles, clear away toxins, and prolong life (Liu and Ma, Song Dynasty). Modern studies indicated that the extract of this herb possessed various pharmacological activities, such as hepatoprotection, immune enhancement, antiaging, and antitumor (Zhang et al., 2015). Phytochemical and pharmacological studies have demonstrated that C-21 steroidal glycosides are the major active components of *Baishouwu* (Zhang et al., 2000; Wang et al., 2007; Peng et al., 2008a). Recently, C-21 steroidal glycosides are of considerable interest because of their bioactivities, including prevention and therapy of chronic hepatitis (Yin et al., 2007), hepatic fibrosis (Lv et al., 2009), and liver cancer (Wang et al., 2007, 2014). And our early studies showed that C-21 steroidal glycosides inhibited the growth of human hepatoma cell lines SMMC7721 and HepG2 (Peng et al., 2011; Peng and Ding, 2015]. Based on the literature and our studies, the C-21 steroidal glycosides were commonly accepted as the most important active ingredients of *Baishouwu* and could be considered as markers for the quality control. Hence, the C-21 steroidal glycosides constituents of Baishouwu extract have been identified and characterized in our following studies (Wang et al., 2017).

However, to date, limited information is known regarding the therapeutic effects of C-21 steroidal glycosides on HCC as well as their underlying mechanisms about IFC axis. In the present study, we aim to reveal the prevention of Baishouwu on diethylnitrosamine (DEN) -induced HCC model in rats at various stages of the disease's progression, from hepatic inflammation to cancer.

MATERIALS AND METHODS

Experimental Animals

Male Sprague-Dawley rats, weighing 150–180 g, were purchased from S.L.A.C. Laboratory Animal Co., Ltd. (Shanghai, China). Care of the animals used in this study was conducted according to the *Guide for the care and Use of Laboratory Animals* published by the U.S. National Institutes of Health (publication no. 85-23, revised 1996). Rats were housed under controlled temperature (22 ± 2°C) and relative humidity (40–70%) with a 12 h light/dark cycle, and allowed free access to standard rat-chow diet and tap water. All the experimental protocols were approved by our Academy Animal Experimental Ethical Committee.

Extract Preparation

The root tubers of *C. auriculatum* Royle ex Wight were collected from Binhai County, Jiangsu Province, China. The plant was authenticated by Prof. Shi-Hui Qian (Jiangsu Province Academy of Traditional Chinese Medicine). The voucher specimen (No. WFC-20151225) was deposited in the herbarium of this academy. The root tubers were cut into small pieces and extracted with boiling 95% ethanol (1:10) two times, each for 2 h. The ethanol extract was evaporated in *vacuo* and further extracted by chloroform and ethyl acetate. The two fractions were merged together and analyzed for major components. As detected according to the vanillin-vitriol colorimetric method, C-21 steroidal glycosides were the main components of Baishouwu extract and the total glycosides content was 52.89% (Wang et al., 2017). In order to identify the main chemical components of Baishouwu extract, an Ultra High-Performance Liquid Chromatography/Quadrupole-Time-of-Flight-Mass Spectrometry (UHPLC-Q-TOF-MS) method was developed. An Acquity UHPLC BEH C_{18} column (2.1 mm × 100 mm, 1.7 μm) was used for separations. The mobile phase was composed of (A) water (0.1% (v/v) formic acid) and (B) acetonitrile, and a linear gradient elution was used. It was revealed that Baishouwu extract mainly contained eight C-21 steroidal glycoside components including caudatin 2,6-dideoxy-3-O-methy-β-D-cymaroseglycoside, wilfoside C1N, caudatin, wilfoside K1N, wilfoside C1G, cynauricuoside A, cynauricuoside C, and auriculoside IV. The chemical structures were presented in our previous studies (Wang et al., 2017). The total ion chromatograms of the eight compounds are presented in **Figure 1**.

Experimental Design

Treatment schedules are illustrated in **Figure 2**. The rats were randomly divided into 4 groups. Control group was intraperitoneally injected with 0.9% normal saline solution twice a week. Rats in model group (DEN-bearing non-treated group) were given intraperitoneal injection of DEN (Sigma Aldrich, St. Louis, MO, United States) at a dose of 30 mg/kg body weight (b.w.) on the same day as control group for 11 weeks (Peng and Ding, 2015; Zeng et al., 2015; Ding et al., 2017). Rats in Baishouwu-H and Baishouwu-L groups were treated with DEN as in model group and daily orally fed with Baishouwu extract (4 g/kg b.w and 2 g/kg b.w, respectively) until 20 weeks.

Body weight of the animals was recorded once every 2 weeks throughout the study. To monitor the progress of stepwise hepatocarcinogenesis, according to our previous study,

FIGURE 1 | Total ion chromatograms in the negative mode of the reference compounds and the sample of Baishouwu extract. **(A)** Reference compounds and **(B)** Sample of Baishouwu extract. M1, caudatin 2,6-dideoxy-3-O-methy-β-D-cymaroseglycoside; M2, wilfoside C1N; M4, caudatin; M5, wilfoside K1N; M6, wilfoside C1G; M7, cynauricuoside A; M8, cynauricuoside C; M9, auriculoside IV.

FIGURE 2 | Experimental schedule.

a time-serial sera set was collected at the end of 6th week (inflammation stage), 10th week (fibrosis stage), and 20th week (HCC stage). To examine the preventive effects of Baishouwu extract on HCC about IFC axis, 8 rats from every group were sacrificed by diethyl ether at 6th week, 10th week, and 20th week. Livers were removed and weighed. The tissues were cut and fixed in 10% formalin for histopathology and immunohistochemiacal examinations. The remaining portions were frozen and stored at −80°C until analysis.

Serum Biochemical Indicators Levels and Hydroxyproline Contents Measurement

Serum aspartate transaminase (AST), alanine aminotransferase (ALT), alkaline phosphatase (ALP), total protein (TP), albumin (ALB), and total bilirubin (T-BIL) levels were measured using an automatic analyzer (C8000 Roche; Hoffmann-La Roche Inc., Switzerland). Serum levels of tumor necrosis factor-α (TNF-α)

and interleukin 6 (IL-6) were measured using ELISA kits (R&D Systems, Inc.), according to the manufacturer's instructions.

The hydroxyproline (Hyp) contents in whole liver specimens were quantified using ultraviolet spectrophotometry as previously reported (Ding et al., 2013). Hyp contents were expressed as μg/gram of livers wet weights.

Morphometric Evaluation

Hepatic tissues of experimental groups of rats were examined morphologically for visible neoplastic nodules when the rats were sacrificed at the end of the study. The nodules were easily recognized and distinguished from the surrounding reddish-brown liver parenchyma. The nodules with a diameter of 2 mm or more in each rat were counted by two independent investigators. The incidence was expressed as percentage of rats with tumors. The multiplicity as average hepatocellular neoplasm number per rat was calculated (Ansil et al., 2014; Rui et al., 2014).

Histologic Examination

Maximum sagittal section of each liver lobe was used for histopathological examination. Tissues were fixed in formaldehyde neutral buffer solution and embedded in paraffin blocks. 4 μm-thick sections were stained with hematoxylin-eosin (HE) for cell morphometry and with collagen-specific Masson's trichrome for detection of fibrosis.

The degrees of liver necroinflammation were assessed against the METAVIR necroinflammatory activity score from A0–A3 (A0, no activity; A1, mild activity; A2, moderate activity; and A3, severe activity). The degrees of liver fibrosis were assessed using the METAVIR fibrosis score range F0-F4 (F0, no fibrosis; F1, portal fibrosis without septa; F2, portal fibrosis with rare septa; F3, numerous septa without cirrhosis; and F4, cirrhosis) (Bedossa and Poynard, 1996; Praneenararat et al., 2014). All sections were examined microscopically (200 × magnification) on an Axioskop 2 microscope (Carl Zeiss, Germany) by two blinded independent investigators.

Immunohistochemical Analyses

Immunohistochemistry was employed to assess NF-κB expression in the rat liver tissue. The detection of NF-κB p65 was performed using paraffin-embedded sections. After deparaffinization and rehydration, sections were soaked in 3% H_2O_2 and skim milk to block endogenous peroxidase activity and non-specific protein binding, respectively. Samples were then incubated with anti-NF-κB p65 antibody (1:500, ab16502, Abcam) to detect bound antibodies. After staining, the sections were counterstained with hematoxylin for microscopy analyses. All sections were examined by light microscopy (Axioskop 2 microscope, Carl Zeiss, Germany). Five fields (200 × magnification) were randomly selected in each sample for analysis. Positive NF-κB signals appeared brown. The percentage of positive area was determined using Image-Pro Plus software 6.0 (Media Cybernetics Inc., Baltimore, MD, United States). The image analysis was conducted by pathologists blinded to the treatments.

Western Blotting Analysis

Proteins were extracted from liver tissues randomly from three individual rats in each group using RIPA. Samples were separated by SDS-PAGE and transferred to PVDF membrane. Subsequently, membranes were blocked and probed with primary antibodies followed by secondary horseradish peroxidase-conjugated antibody. Immunolabeled proteins were detected by incubation with ECL substrate and the gray density was measured. Target proteins levels were normalized against the level of β-actin or Lamin B1. The following antibodies were used: TLR4 (1:1000, ab22048, Abcam, United Kingdom), MyD88 (1:1000, #4283, Cell Signaling Technology, United States), TRAF6 (1:800, sc-7221, Santa Cruz, CA, United States), NF-κB p65 (1:2000, ab16502, Abcam, United Kingdom), TGF-β1 (1:2000, ab25121, Abcam, United Kingdom), α-SMA (1:1000, ab5694, Abcam, United Kingdom), β-actin (1:1000, sc-47778, Santa Cruz, CA, United States), and Lamin B1 (1:10000, ab16048, Abcam, United Kingdom).

RNA Extraction and Quantitative Real-Time PCR Detection

Total RNA was extracted from frozen liver tissues randomly from three individual rats in each group using Trizol reagent. Gene-specific prime sequences were designed using Primer 5.0 software and custom-synthesized by GenScript Inc., Nanjing, China. Real-time PCR samples were prepared using the SYBR premix EX Taq Kit (TaKaRs, Dalian, China) and amplification was performed on a LightCycler 480 SYBR Green I Master device (Roche Applied Science, Basel, Switzerland). GAPDH gene was used as an internal control. The relative expression levels of the target genes were calculated by the $2^{-\Delta\Delta Ct}$ method. The primer sequences utilized are shown in **Table 1**.

Statistical Analysis

Data were expressed as mean ± standard deviation (SD). All statistical analyses were performed using the statistical package for social science (SPSS, Version 11.5, SPSS Inc., Chicago, IL, United States). Experimental and control groups were compared by one-way ANOVA. The incidences of hepatocellular neoplasm were analyzed by Chi-square test. The Kruskal-Wallist test was used to compare the METAVIR score. Statistical significance was set at p-value < 0.05.

RESULTS

Effect of Baishouwu Extract on Body and Liver Weights

Average body weights of different groups at various time points are shown in **Figure 3**. Animals in model group receiving 30 mg/kg of DEN exhibited slowly increased weight and the body weights were lower compared to control group. Body weights in Baishouwu-H and Baishouwu-L groups were higher than that in model group after the 20-week experimental period.

Relative liver weights of various groups are presented in **Table 2**. Relative liver weight were increased in model group

Gene	Forward primer	Reverse primer
Collagen I	5-CTGCTGGTCCTAAGGGAGAG-3	5-GACAGCACCATCGTTACCAC-3
Collagen III	5-TCCTGGATACCAAGGTCCTC-3	5-GACCAATAGCACCAGGAGGT-3
TLR4	5-GATTGCTCAGACATGGCAGT-3	5-CCCACTCGAGGTAGGTGTTT-3
MyD88	5-TGGTGGTTGTTTCTGACGAT-3	5-GATCAGTCGCTTCTGTTGGA-3
TRAF6	5-GACATTCATGCACCTGGAAG-3	5-CATGTCAAAGCGGGTAGAGA-3
GAPDH	5-GGCCTTCCGTGTTCCTACC-3	5-CGCCTGCTTCACCACCTTC-3
α-SMA	5-CACGCGAAGCTCGTTATAGA-3	5-GGGATCCTGACCCTGAAGTA-3
TGF-β$_1$	5-CTTGCCCTCTACAACCAACA-3	5-CTTGCGACCCACGTAGTAGA-3
NF-κB p65	5-GGTTTGAGACATCCCTGCTT-3	5-TATGGCTGAGGTCTGGTCTG-3

induced by DEN than that in control group ($P < 0.01$). Liver to body weight ratios were significantly or tended to be lower in Baishouwu extract pretreated groups compared to the model group ($P < 0.05\sim0.01$), respectively.

Baishouwu Extract Improves Liver Functions

As shown in **Figures 4A–F**, serum biochemical analyses were performed to determine hepatic function. Both serum levels of ALT and AST were significantly increased in DEN-treated group which were prevented by Baishouwu extract from inflammation stage (week 6) to HCC stage (week 20). In parallel, there was a decrease in serum concentration of TP in Baishouwu extract group at week 10 and week 20 ($P < 0.05\sim0.01$, compared to the model group). But no significant changes of serum ALB levels were found between all groups. Serum level of ALP was higher in the DEN-treated group compared to the control group. Baishouwu extract pre-administration resulted in suppression of ALP levels in the blood serum in a dose-dependent manner as compared with the model group. Serum T-BIL level was also significantly higher in the model group than that in the control. Pretreatment with Baishouwu extract dramatically reduced the

T-BIL levels from week 6 to week 20 ($P < 0.05\sim0.01$, compared to the model group).

The serum levels of inflammatory factors, such as IL-6 and TNF-α, were analyzed subsequently. Serum IL-6 levels in the model group were obviously increased in inflammation, liver fibrosis and HCC and they were suppressed by pre-administration of Baishouwu extract at week 12 and week 20 (**Figure 4G**). Serum TNF-α levels were higher in the model group than in control group from week 6 to week 20 ($P < 0.01$). Baishouwu extract pretreated group with high dose displayed a decrease in comparison to that from the model group ($P < 0.05$; **Figure 4H**).

Baishouwu Extract Inhibits the Expression of Collagen

As a biomarker of total collagen content, Hyp was detected. Data was showed in **Figure 5A**. DEN administration markedly increased the liver Hyp content in rats. Compared with the model group, the elevated Hyp contents were significantly suppressed by the pretreatment of Baishouwu extract at both dose levels throughout the experiment period ($P < 0.05\sim0.01$).

A gradual increase in mRNA expression of Collagen I and Collagen III was observed after administration of DEN compared with the control group ($P < 0.01$ **Figures 5B,C**). Prereatment with Baishouwu extract prevented the increase in Collagen I and Collagen III mRNA levels in inflammation, fibrosis, and HCC stages. This result was consistent with the observation in Hyp.

FIGURE 3 | Effect of Baishouwu extract on growth curve of rats treated with DEN. Results are expressed as mean ± SD (1st~6th week $n = 24$, 7th~10th week $n = 16$, 11th~20th $n = 8$, respectively). $^{\triangle\triangle}P < 0.01$ vs. control group, $^{**}P < 0.01$ vs. model group.
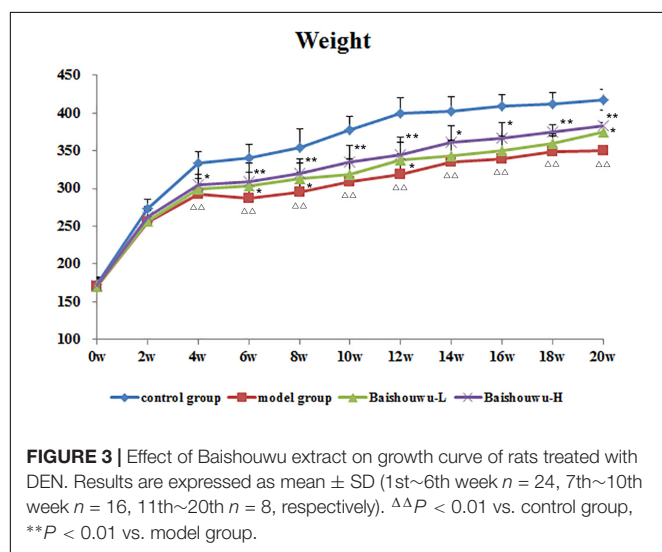
TABLE 2 | Effect of Baishouwu extract on liver weights of rats treated with diethylnitrosamine.

Group	n	6th week	10th week	20th week
		Relative (/100 g b.w.)	Relative (/100 g b.w.)	Relative (/100 g b.w.)
Control group	8	1.972 ± 0.221	2.388 ± 0.2424	2.515 ± 0.280
Model group	8	4.224 ± 0.663$^{\triangle\triangle}$	6.621 ± 1.25$^{\triangle\triangle}$	8.430 ± 0.773$^{\triangle\triangle}$
Baishouwu-L	8	3.707 ± 0.566	5.464 ± 0.74*	6.612 ± 0.524**
Baishouwu-H	8	3.405 ± 0.230**	4.284 ± 0.332**	4.568 ± 0.615**

*Relative liver weight = [Liver weight (g)/Body weight (b.w., g) *100]. Values are expressed as the mean ± SD. $^{\triangle\triangle}P < 0.01$ vs. control group, *P < 0.05 vs. model group, **P < 0.01 vs. model group.*
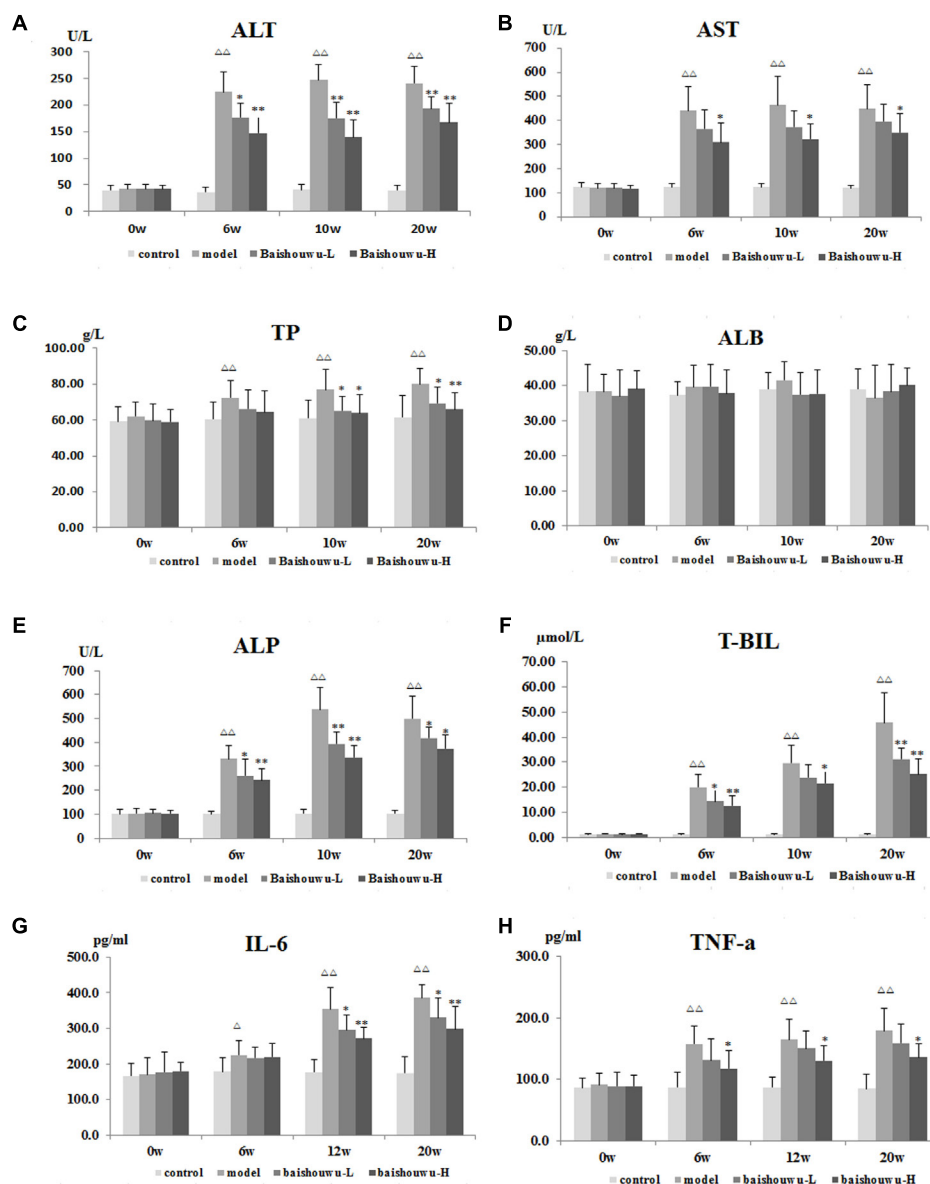
FIGURE 4 | Effect of Baishouwu extract on serum biochemical indicators induced by DEN. Serum levels of **(A)** ALT, **(B)** AST, **(C)** TP, **(D)** ALB, **(E)** ALP, **(F)** T-BIL, **(G)** IL-6, and **(H)** TNF-α. Results are expressed as mean ± SD ($n = 8$). $^{\triangle\triangle}P < 0.01$ vs. control group, $*P < 0.05$, $**P < 0.01$ vs. model group.

Baishouwu Extract Reduces the Hepatoma Incidence and Multiplicity Induced by DEN

Morphological changes were observed in the livers of different groups at different stages (inflammation, fibrosis, and HCC stages). As expected, livers from the control group of rats were normal in appearance, without any morphological changes. The surface of the liver of the control group was brown, soft in texture and smooth, with an evident gloss. Macroscopically, the appearance of the liver was not evidently abnormal in the model group in the inflammation stage at 1–6 weeks (**Figure 6**). Following DEN exposure, the livers with dark color

and granulose appearance in the model group were slightly bigger and harder than those of control-rats in fibrosis stage (**Figure 6**). The livers of rats treated with Baishouwu extract showed decreased hepatic fibrosis progression. As shown in **Figure 6**, the rats at week 20 post-DEN exposure were observed white nodules, indicating that HCC had developed by this stage. Nodules were easily recognized and distinguished from the surrounding non-nodular reddish-brown liver parenchyma at the end of week 20. The livers in the model group were rough and nodular, with uniform micronodules (<2 mm) and macronodules (≥2 mm) throughout. Pretreatment with Baishouwu extract remarkably enhanced the recovery of DEN-induced liver structure damage (**Figure 6**). The nodule
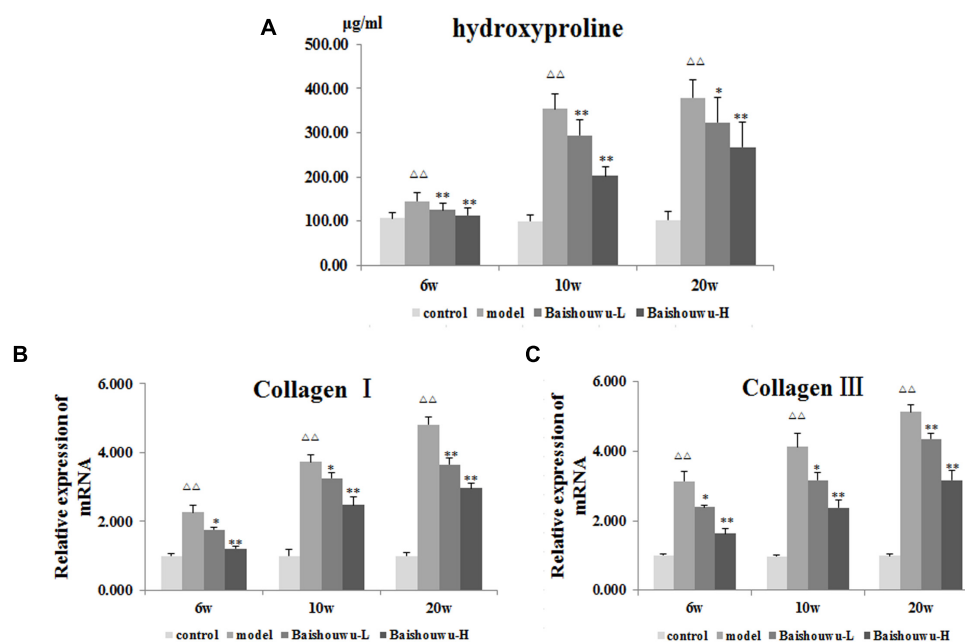
FIGURE 5 | Effect of Baishouwu extract on fibrosis related indicators induced by DEN. Tissue levels of (A) hydroxyproline, (B) Collagen I, and (C) Collagen III. Results are expressed as mean ± SD ($n = 8$). $^{\triangle\triangle}P < 0.01$ vs. control group, $^*P < 0.05$, $^{**}P < 0.01$ vs. model group.
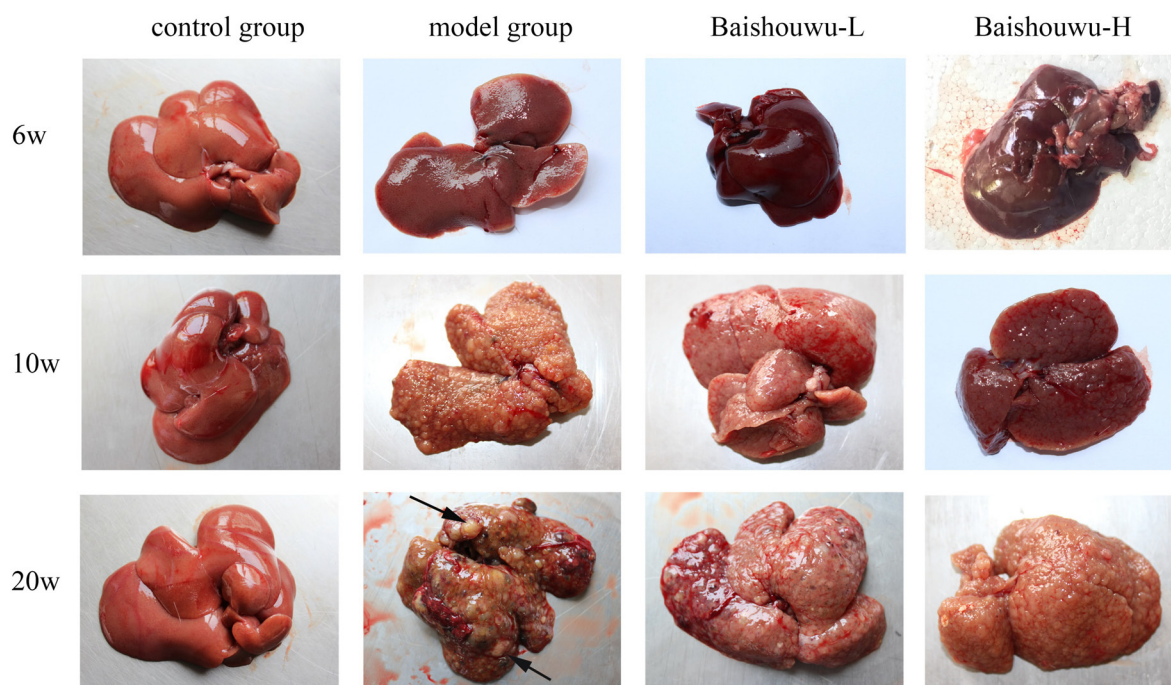
FIGURE 6 | Effect of Baishouwu extract on macroscopic features of livers in DEN-treated rats. Representative photographs of the livers from each group at the stages of inflammation (6 weeks), fibrosis (10 weeks), and HCC (20 weeks). Arrows indicate the representative tumors.

incidence was 100% in model rats, while the incidence decreased to 87.5% in Baishouwu extract group (4 g/kg). Furthermore, the number of liver nodules in Baishouwu-pretreated rats was less as compared to the model rats, with

a significant difference at week 20 ($p < 0.01$; **Table 3**). So the incidence and multiplicity of HCC development in Baishouwu-pretreated rats were significantly lower than that in the model rats.

TABLE 3 | Effect of Baishouwu extract on incidence and multiplicity of tumor in diethylnitrosamine induced hepatoma rats.

Group	n	Incidence	Multiplicity
Control group	8	0	0 ± 0
Model group	8	8/8	$155.4 \pm 34.2^{\Delta\Delta}$
Baishouwu-L	8	8/8	$70.8 \pm 12.5^{**}$
Baishouwu-H	8	7/8	$50.1 \pm 17.4^{**}$

Values are expressed as the mean $\pm$ S.D. $^{\Delta\Delta}P < 0.01$ vs. control group, $^{**}P < 0.01$ vs. model group.

Baishouwu Extract Alleviates Hepatic Pathological Changes

The histopathological changes observed in the livers of control and experimental animals are represented in **Figure 7**. Livers from control rats showed normal liver histology with no signs of liver injury manifested as normal hepatic lobules and central vein (**Figure 7**). Exposure to DEN resulted in a sequence of lesions that evolved over time, from inflammation observed at 6th week, fibrosis observed at 10th week, to the HCC observed at 20th week. Six weeks after DEN injection (inflammation stage), liver sections

FIGURE 7 | Effect of Baishouwu extract on the liver histological changes in the DEN-treated rats. Representative photomicrographs of HE **(A)** and Masson **(B)** staining of the livers in the DEN-treated rats from each group at the stages of inflammation (6 weeks), fibrosis (10 weeks), and HCC (20 weeks). Arrows indicate the representative tumors. Original magnification: 200×.

TABLE 4 | Effect of Baishouwu extract on the distribution of inflammatory features in the diethylnitrosamine treated rats assessed by METAVIR score.

Time	Group	A0	A1	A2	A3	*P* value (vs. model)
Inflammation stage (6 weeks)	Control	8 (100%)	0 (0%)	0 (0%)	0 (0%)	0.001
	Model	0 (0%)	0 (0%)	0 (0%)	8 (100%)	
	Baishouwu-L	0 (0%)	3 (37.5%)	3 (37.5%)	2 (25.0%)	0.001
	Baishouwu-H	0 (0%)	4 (50.0%)	4 (50.0%)	0 (0%)	0.001
Fibrosis stage (10 weeks)	Control	8 (100%)	0 (0%)	0 (0%)	0 (0%)	0.001
	Model	0 (0%)	0 (0%)	0 (0%)	8 (100%)	
	Baishouwu-L	0 (0%)	2 (25.0%)	2 (25.0%)	4 (50.0%)	0.001
	Baishouwu-H	0 (0%)	3 (37.5%)	3 (37.5%)	2 (25.0%)	0.001
HCC stage (20 weeks)	Control	8 (100%)	0 (0%)	0 (0%)	0 (0%)	0.001
	Model	0 (0%)	0 (0%)	0 (0%)	8 (100%)	
	Baishouwu-L	0 (0%)	0 (0%)	3 (37.5%)	5 (62.5%)	0.001
	Baishouwu-H	0 (0%)	1 (12.5%)	4 (50.0%)	3 (37.5%)	0.001

Compared to model group; calculated using the Chi-Square test. METAVIR inflammation stages: A0, no activity; A1, mild activity; A2, moderate activity; A3, severe activity.

TABLE 5 | Effect of Baishouwu extract on the distribution of fibrosis features in the diethylnitrosamine treated rats assessed by METAVIR score.

Time	Group	F0	F1	F2	F3	F4	*P* value (vs. model)
Inflammation stage (6 weeks)	Control	8 (100%)	0 (0%)	0 (0%)	0 (0%)	0 (0%)	0.001
	Model	0 (0%)	(0%)	8 (100%)	0 (0%)	0 (0%)	
	Baishouwu-L	0 (0%)	6 (75.0%)	2 (25.0%)	0 (0%)	0 (0%)	0.001
	Baishouwu-H	0 (0%)	8 (100%)	0 (0%)	0 (0%)	0 (0%)	0.001
Fibrosis stage (10 weeks)	Control	8 (100%)	0 (0%)	0 (0%)	0 (0%)	0 (0%)	0.001
	Model	0 (0%)	0 (0%)	0 (0%)	2 (25.0%)	6 (75.0%)	
	Baishouwu-L	0 (0%)	2 (25.0%)	2 (25.0%)	2 (25.0%)	2 (25.0%)	0.001
	Baishouwu-H	0 (0%)	4 (50.0%)	2 (25.0%)	1 (12.5%)	1 (12.5%)	0.001
HCC stage (20 weeks)	Control	8 (100%)	0 (0%)	0 (0%)	0 (0%)	0 (0%)	0.001
	Model	0 (0%)	0 (0%)	0 (0%)	0 (0%)	8 (100%)	
	Baishouwu-L	0 (0%)	0 (0%)	1 (12.5%)	3 (37.5%)	4 (50.0%)	0.001
	Baishouwu-H	0 (0%)	1 (12.5%)	2 (25.0%)	3 (37.5%)	2 (25.0%)	0.001

Compared to model group; calculated using the Chi-Square test. METAVIR fibrosis stages: F0, no fibrosis; F1, portal fibrosis without septa; F2, portal fibrosis with rare septa; F3, numerous septa without cirrhosis; F4, cirrhosis.

showed evidence features of chronic inflammatory infiltrates with diffuse ballooning degeneration, dilated lymph vessels, and proliferating bile ducts in the portal area (**Figure 7**). Liver from rats pretreated with Baishouwu extract showed no significant hepatic injury manifested as minimal vascular congestion and focal lymphoplasmacytic infiltrates (**Figure 7**), which correspond to the METAVIR score (**Table 4**).

After 10 weeks of DEN injury (fibrosis stage), the animals exhibited fibrosis, and many also had cirrhosis. As **Figure 7** shown, lobules of livers in model group exhibited a disordered arrangement of hepatocytes and a pile of deposition of fibrous tissue. Lipid droplets, hydropic degeneration, necrosis, and regeneration of hepatocytes were found. According to the METAVIR liver fibrosis assessment scales, Baishouwu extract preadministration decreased the extent of liver fibrosis induced by DEN (**Table 5**). By preadministration of Baishouwu extract, the animal models had successfully developed the different stages of early liver fibrosis.

After 20 weeks of DEN injection (HCC stage), the liver lesions of model group were classified as the high or middle differentiation of HCC. DEN alone (model group) showed loss of architecture, hepatic parenchyma with granular cytoplasm and cancerous focus with patchy necrosis (**Figure 7**). Liver nodules consisted of relatively giant hepatocytes with large nuclei and eosinophilic cytoplasm surrounded by fibrotic stroma. HCC features appeared as malignant hepatocytes, multinodular areas of necrosis, and nodules of necrotic malignant hepatocytes. DEN-bearing Baishouwu extract-pretreated groups showed moderately malignant with focal necrosis and less mitotic count (**Figure 7**).

Baishouwu Extract Down-Regulates the Expression of NF-κB p65 by Immunohistochemistry

NF-κB p65 positive staining was mainly located in the nucleus of the hepatic cells, stained as brown granules or dots. Its expression was estimated as the percentage of cells positively stained by the antibody. In normal control liver section there was a limited number of NF-κB p65 positive cells as shown in **Figure 8A**. Rats which received DEN showed a significant increase compared
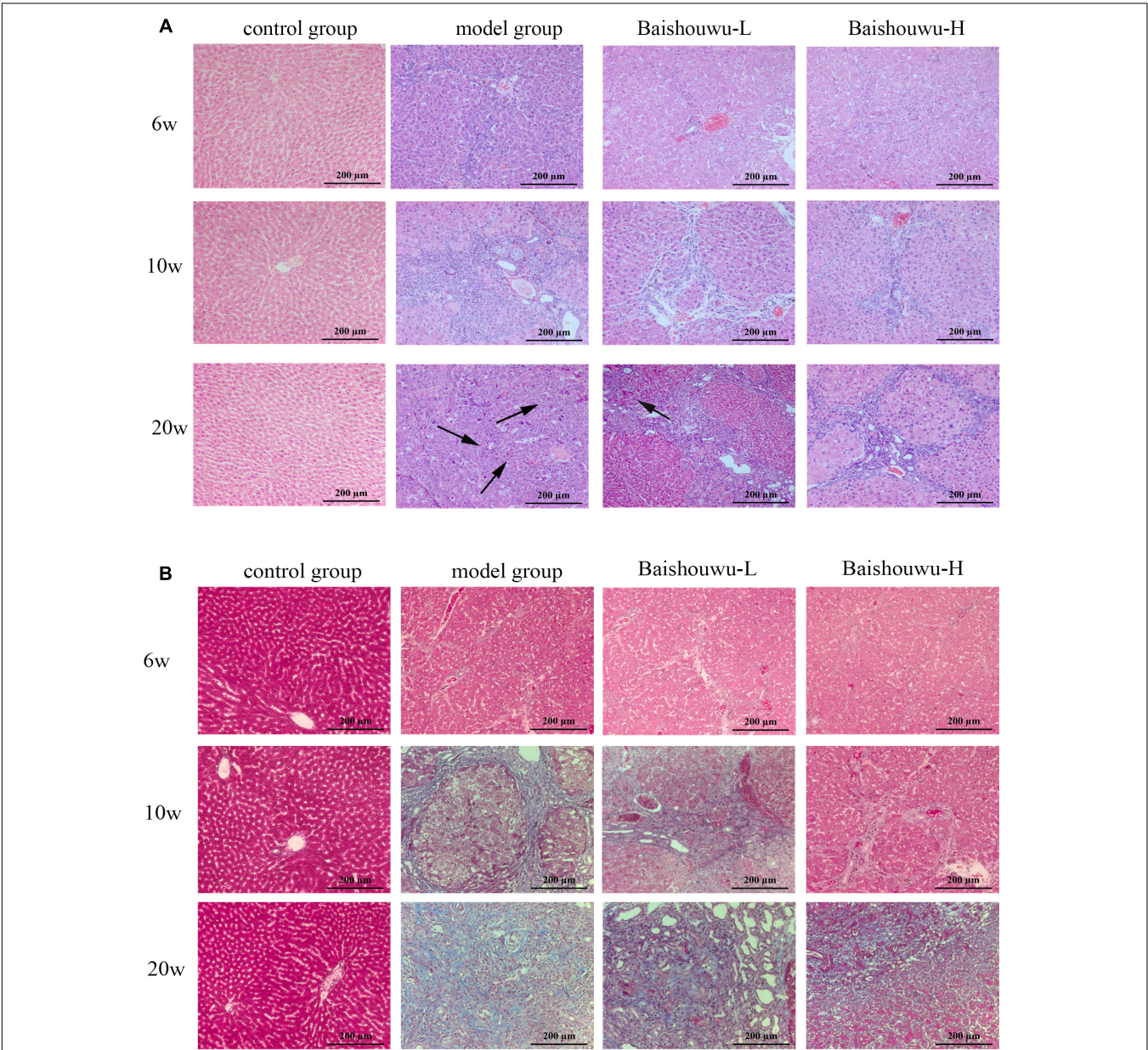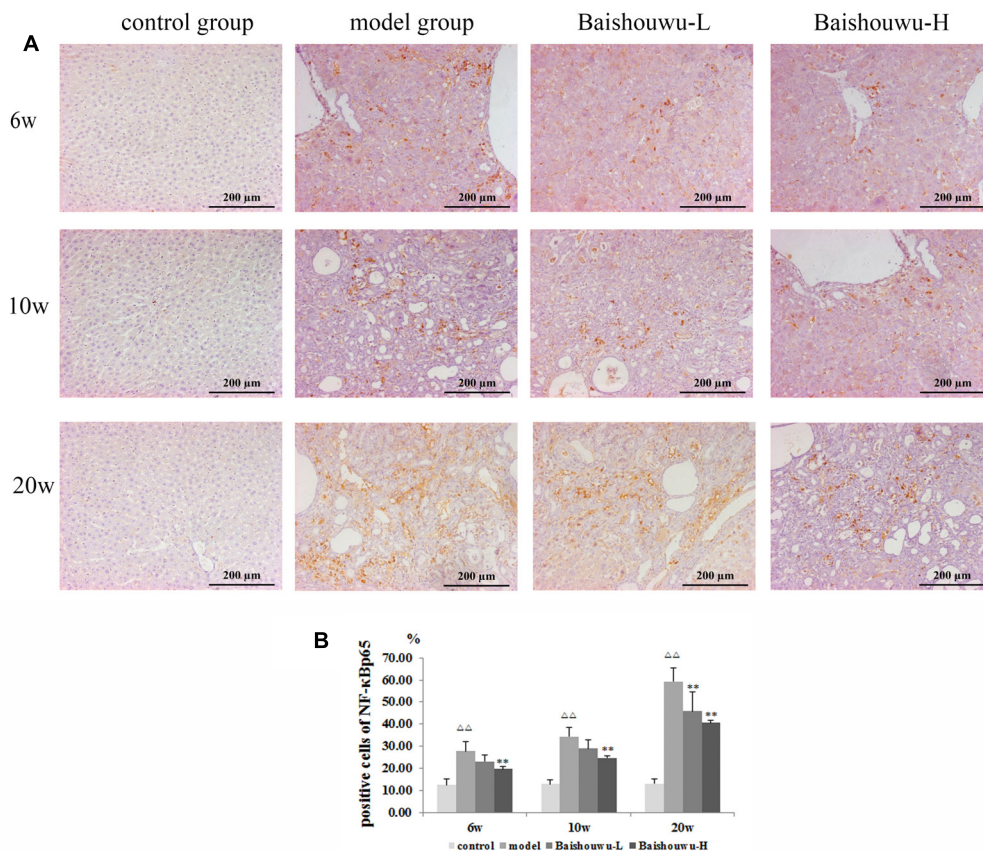
FIGURE 8 | Effect of Baishouwu extract on the expression of NF-κB p65 in the livers of the DEN-treated rats. Representative photomicrographs of immunohistochemical analysis of NF-κB p65 in the livers developed in DEN-treated rats. **(A)** Representative liver tissues immunostained with anti- NF-κB p65 antibody in hepatitis, cirrhosis and hepatocarcinoma control at 6th week, 10th week, and 20th week (magnification: 200×). **(B)** The percentage of NF-κB p65 positive cells in control and experimental groups. Results are expressed as mean ± SD ($n = 3$). $^{\triangle\triangle}P < 0.01$ vs. control group, $^{**}P < 0.01$ vs. model group.

with the control group. The positive expression rates of the NF-κB p65 protein in the inflammation, fibrosis and HCC tissues were 27.9, 34.5, and 59.4%, respectively. The expression of the NF-κB p65 protein in HCC stage was significantly higher than those in the inflammation and fibrosis. On the other hand, Baishouwu extract-pretreated rats showed considerable reduction compared with the model group ($p < 0.05\sim0.01$; **Figure 8B**) in inflammation, fibrosis and HCC stages.

Baishouwu Extract Pretreatment Is Associated With Down-Regulated TLR4/MyD88/NF-κB Signaling Pathway

TLR4 is an important mediator of the inflammatory response to infection and plays a role in the development and progression of HCC (Wang et al., 2015). TLR4 drives myofibroblast activation and fibrogenesis in HCC and TLR4-dependent modulation of TGF-β signaling provides a link between proinflammatory and profibrogenic signals through the MyD88- NF-κB pathway (Seki et al., 2007). TLR signaling involves the recruitment of MyD88 adapter protein and final activation of NF-κB. To confirm the hepatoprotective effect of Baishouwu extract, the protein and

mRNA expression levels of TLR4, MyD88, TRAF6, NF-κBp65, TGF-β$_1$, and α-SMA in the livers were examined at inflammation, fibrosis and HCC stages in DEN-induced HCC model. After DEN treatment, the mRNA levels of TLR4, MyD88, TRAF6, and NF-κB p65 were significantly increased compared to the control group from week 6 to week 20 (**Figure 9A**), which were demonstrated by western blotting (**Figure 9B**). All of these results suggested that TLR4/MyD88/NF-κB signaling pathway was activated in the liver of DEN-treated rats (**Figure 9**). However, these elevations were reversed by the pretreatment with Baishouwu extract (**Figure 9**). At the same time, the changes of TGF-β$_1$ and α-SMA after Baishouwu extract pretreatment for 6 weeks, 10 weeks, and 20 weeks were consistent with the changes of TLR4 (**Figure 9**). The results indicated that Baishouwu extract may inhibit hepatic inflammation, fibrosis, and HCC by inhibiting TLR4/MyD88/NF-κB signaling pathway.

DISCUSSION

As the main active components of Baishouwu, C-21 steroidal glycosides have shown to possess anticancer activity including
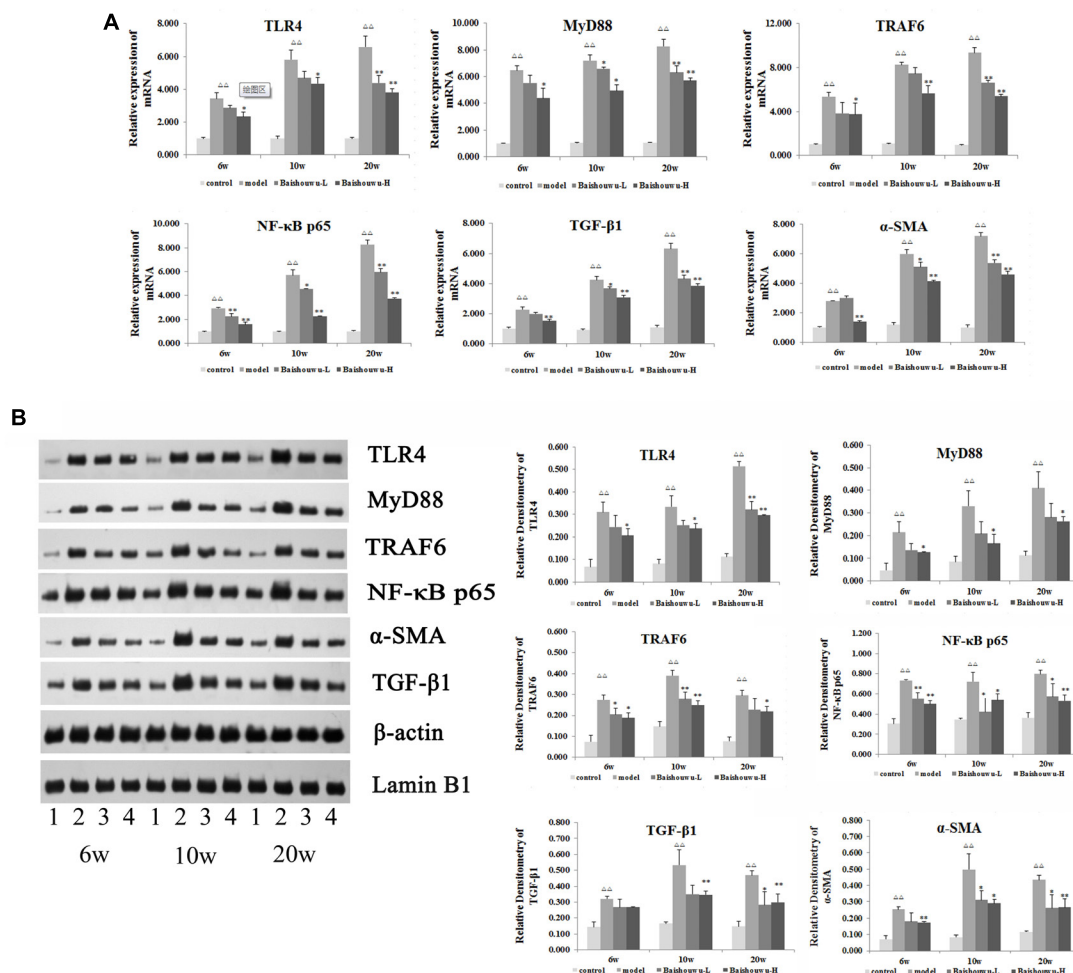
FIGURE 9 | Effect of Baishouwu extract on the TLR4/MyD88/NF-κB signaling pathway. The expression levels of TLR4, MyD88, TRAF6, NF-κB p65, TGF-β₁, and α-SMA were detected by Real-time PCR **(A)** and western blot **(B)**: (1) control group, (2) model group, (3) Baishouwu extract-L group, and (4) Baishouwu extract-H group. Results are expressed as mean ± SD ($n = 3$). $^{\triangle\triangle}P < 0.01$ vs. control group, $^*P < 0.05$, $^{**}P < 0.01$ vs. model group.

modulating cell cycle and apoptotic signaling, inhibiting invasion, and metastatic potential in cancer cells (Shan et al., 2005; Fei et al., 2012; Wang et al., 2017). Our previous studies found that C-21 steroidal glycosides could inhibit the proliferation of human hepatoma cell by inducing cell apoptosis through caspase-3 activation (Peng et al., 2008b, Peng et al., 2011). It was also reported that a C-21 steroidal glycoside from Baishouwu exhibited anti-tumor activity against human gastric cancer cells by inducing G1 phase cell cycle arrest and capase-dependent apoptosis cascades (Wang et al., 2013). Recent studies have demonstrated that ERK/JNK/MAPK pathways were involved in C-21 steroidal glycosides induced tumor cells apoptosis (Fei et al., 2012; Fu et al., 2015). It has been widely accepted that Baishouwu extract, especially the C-21 steroidal glycosides, is effective in anticancer, but the potential molecular mechanism

remains largely unknown. In the present study, a rat model with HCC was developed to evaluate the effect of Baishouwu extract on different stages of DEN-induced hepatic IFC sequence by influencing the inflammatory signaling pathway.

Chronic inflammation of the liver is a well-recognized risk factor for carcinogenesis, the molecular link between inflammation, hepatic fibrogenesis, and HCC remains elusive. The liver is the main site of inflammatory response to intestine-derived bacterial products crossing the intestinal barrier. Recently, several studies implicated that toll-like receptors (TLRs) and their proinflammatory mediators may be of the host inflammatory response to infection and plays a role in the human hepatic IFC axis (Abastado, 2012; Soares et al., 2012; Li W. et al., 2015). TLRs represent one important receptor family which enables the innate

immune system to immediately react to infections. They contribute to adaptive immune reactions and the regulation of sterile inflammation and tissue regeneration as well as carcinogenesis (O'Neill et al., 2013; Roh and Seki, 2013). Of the TLRs, TLR4 responsibles for detecting Gram-negative bacteria including lipopolysaccharide (LPS), whereas TLR2 identifies components of Gram-positive bacteria such as peptidoglycan (Kawai and Akira, 2010). There are several types of TLR-expressing cells in the liver, including hepatocytes, Kupffer cells (Mcdonald et al., 2013), stellate cells (Zhu et al., 2012), sinusoidal endothelial cells (Suzuki et al., 2016), and biliary epithelial cells (Kim et al., 2016). Of these cells, the role of hepatic stellate cells (HSC) has been extensively investigated in the development of liver inflammation, fibrosis and subsequent tumor via TLR4 (Dapito et al., 2012). TLR4-mediated inflammation is critical in both host defenses against invading pathogens and for physiological responses to inflammatory stimuli. Ligation of TLR4 also markedly promotes liver fibrosis (Aoyama et al., 2010). Similarly, TLR4 ligation by LPS derived from selected intestinal microbiota promotes hepatocellular carcinogenesis (Dapito et al., 2012). Overall, hepatic expression of TLR4 is increased in chronic hepatitis and cirrhosis and is maintained in hepatocarcinoma.

It had been suggested that DEN-induced liver injury was accompanied by elevation of plasma LPS level, and then LPS can transiently exaggerated DEN-induced liver damage (Yu et al., 2010). After binding to TLR4, two critical intracellular signaling pathways are triggered, including the myeloid differentiation primary response 88 (MyD88) dependent and MyD88-independent signaling cascades (Pang et al., 2018). The MyD88-dependent signal transduction activates NF-κB through activation of its inhibitory protein IκBα, which allows NF-κB nuclear translocation and controls the expression of a multitude of proinflammatory cytokines and other immune-related genes, such as TNF-α, IL-1, IL-1β, IL-6, and IL-12 (Shi et al., 2013; Li X. et al., 2015). In the parallel MyD88-independent, TIR-domain-containing adaptor-inducing interferon-β (TRIF) pathway, TRIF associates with TRAF3 and TRAF6 to activate tank-binding kinase-1 (TBK1) and I-kappa-B kinase epsilon (IKKi), which results in the activation of interferon regulatory transcription factor 3 (IRF3) and IRF7 (Bagchi et al., 2007; Yu et al., 2010). Activated IRF3 and IRF7 drive transcription of interferon-α (IFN-α), IFN-β and IFN-responsive genes. It is reasonable that both of TLR4 signals can induce liver inflammation, promote fibrosis, and aggravate progression toward malignancies in TLR4-dependent cancers such as HCC (Demaria et al., 2010; Szabo and Petrasek, 2015). In the present work, the antinflammatory capability of Baishouwu extract mainly resulted in decreased levels of MyD88, TRAF6, NF-κB, IL-6 and TNF-α via the reduction of TLR4 expression in hepatitis, cirrhosis, and hepatocarcinoma stages of the HCC models induced by DEN. Thus, TLR4 signaling pathway was involved in the inhibition of proinflammatory cytokines expression by Baishouwu extract rich in C-21 steroidal glycosides. Therefore, these results supported a novel effect of C-21 steroidal glycosides on the antinflammatory ability, which suggested C-21 steroidal

glycosides as a promising pretreatment agent for ameliorating the development of HCC.

We and others have previously shown that chronic hepatic inflammation was tightly linked to fibrosis and hepatocarcinogenesis (Wai et al., 2015; Ding et al., 2017), but the molecular link remains elusive. Our study has identified TLR4 signaling as a central mediator in liver tumor via TLR4-MyD88-NF-κB pathway. On the other hand, it is well-known that TGF-β pathway caused by activation of at least one of the TGF-β signaling components is an important risk factor for fibrogenesis and HCC in man and animal models (Yang et al., 1999; Kitisin et al., 2007). Activation of TLR4 enhances TGF-β signaling in the development of hepatic fibrosis. The lack of functional type I and type II TGF-β receptors and Smad3 results in extensive inflammation due to increased TLR4 expression (Yang et al., 1999; Lucas et al., 2000; Mccartneyfrancis et al., 2004). Studies on TLR4-deficient mice uncovered that TLR4 mediated the regulation of the TGF-β1 pseudoreceptor BAMBI (bone morphogenic protein and active membrane bound inhibitor) by TLR4-MyD88-NF-κB-dependent pathway, thus sensitizing HSCs to TGF-β1 signaling. HSCs were being activated and consequently increased proliferation and caused overexpression of α-SMA. The enhanced expression of α-SMA indicated that the invasion of numerous fibroblasts (Friedman, 2007; Seki et al., 2007). The cross talk between TLR4 and TGF-β pathway provides a link between proinflammatory and profibrogenic signals in HCC. Here, we demonstrated that TLR4, MyD88, TGF-β1 expressions, and NF-κB p65 nuclear translocation increased in model rats at 6th, 10th and 20th week, but Baishouwu extract pretreatment downregulated TLR4, MyD88, and TGF-β1 expressions and even suppressed downstream signaling through NF-κB p65 nuclear translocation. Moreover, the expression of α-SMA and collagen I and II, the marker of HSCs activation and the major components of extracellular matrix in fibrotic liver, were significantly elevated in the DEN-treated rats and were inhibited by Baishouwu extract. Taken together, our results suggest that Baishouwu extract maybe contribute to modulation of TGF-β signaling by TLR4-MyD88-NF-κB-dependent pathway in HCC, but the precise molecule mechanism of Baishouwu extract on the crosstalk between TLR4 and TGF-β pathway requires further investigation.

In conclusion, based on IFC axis, Baishouwu extract exhibited potent effect on the development of HCC, and their underlying mechanism might by associate with altering TLR4/MyD88/NF-κB signaling pathway in the sequence of hepatic IFC. Our study provided novel insights into the mechanism of Baishouwu extract as a candidate for the pretreatment of HCC in the future.

ETHICS STATEMENT

This study was carried out in accordance to the recommendation of *Guide for the Care and Use of Laboratory Animals* published by the US National Institutes of Health (Publication No. 85-23,

revised 1996). The protocol was approved by the Animal Experimental Ethical Committee of Jiangsu Province Academy of Traditional Chinese Medicine.

AUTHOR CONTRIBUTIONS

All authors designed and carried out the experimental work, read, and approved the final manuscript. Z-xP analyzed the statistical data and interpretation the results. Y-fD and LD drafted and critically evaluated the manuscript.

FUNDING

REFERENCES

Abastado, J. P. (2012). The next challenge in cancer immunotherapy: controlling T-cell traffic to the tumor. *Cancer Res.* 72, 2159–2161. doi: 10.1158/0008-5472. CAN-11-3538

Ansil, P. N., Nitha, A., Prabha, S. P., and Latha, M. S. (2014). Curative effect of *Amorphophallus campanulatus* (Roxb.) Blume. tuber on N-nitrosodiethylamine-induced hepatocellular carcinoma in rats. *J. Environ. Pathol. Toxicol. Oncol.* 33, 205–218. doi: 10.1615/JEnvironPatholToxicolOncol. 2014011320

Aoyama, T., Paik, Y. H., and Seki, E. (2010). Toll-like receptor signaling and liver fibrosis. *Gastroenterol. Res. Pract.* 2010, 1–8. doi: 10.1155/2010/192543

Bagchi, A., Herrup, E. A., Warren, H. S., Trigilio, J., Shin, H. S., Valentine, C., et al. (2007). MyD88-dependent and MyD88-independent pathways in synergy, priming, and tolerance between TLR agonists. *J. Immunol.* 178, 1164–1171. doi: 10.4049/jimmunol.178.2.1164

Bedossa, P., and Poynard, T. (1996). An algorithm for the grading of activity in chronic hepatitis C. The METAVIR cooperative Study Group. *Hepatology* 24, 289–293. doi: 10.1002/hep.510240201

Dapito, D. H., Mencin, A., Gwak, G. Y., Pradere, J. P., Jang, M. K., Mederacke, I., et al. (2012). Promotion of hepatocellular carcinoma by the intestinal microbiota and TLR4. *Cancer Cell* 21, 504–516. doi: 10.1016/j.ccr.2012.02.007

Demaria, S., Pikarsky, E., Karin, M., Coussens, L. M., Chen, Y. C., Ei-Omar, E. M., et al. (2010). Cancer and inflammation: promise for biological therapy. *J. Immunother.* 33, 335–351. doi: 10.1097/CJI.0b013e3181d32e74

Ding, Y. F., Peng, Y. R., Li, J., Shen, H., Shen, M. Q., and Fang, T. H. (2013). Gualou Xiebai decoction prevents myocardial fibrosis by blocking TGF-beta/Smad signalling. *J. Pharm. Pharmacol.* 65, 1373–1381. doi: 10.1111/jphp.12102

Ding, Y. F., Wu, Z. H., Wei, Y. J., Shu, L., and Peng, Y. R. (2017). Hepatic inflammation-fibrosis-cancer axis in the rat hepatocellular carcinoma induced by diethylnitrosamine. *J. Cancer Res. Clin. Oncol.* 143, 821–834. doi: 10.1007/s00432-017-2364-z

Fei, H. R., Chen, H. L., Xiao, T., Chen, G., and Wang, F. Z. (2012). Caudatin induces cell cycle arrest and caspase-dependent apoptosis in HepG2 cell. *Mol. Biol. Rep.* 39, 131–138. doi: 10.1007/s11033-011-0721-6

Friedman, S. L. (2007). A deer in the headlights: BAMBI meets liver fibrosis. *Nat. Med.* 13, 1281–1283. doi: 10.1038/nm1107-1281

Fu, X. Y., Zhang, S., Wang, K., Yang, M. F., Fan, C. D., and Sun, B. L. (2015). Caudatin inhibits human glioma cells growth through triggering DNA damage-mediated cell cycle arrest. *Cell Mol. Neurobiol.* 35, 953–959. doi: 10.1007/s10571-015-0190-x

Jemal, A., Bray, F., Center, M. M., Ferlay, J., Ward, E., and Foman, D. (2011). Global cancer statistics. *CA Cancer J. Clin.* 61, 69–90. doi: 10.3322/caac.20107

Kawai, T., and Akira, S. (2010). The role of pattern-recognition receptors in innate immunity: update on toll-like receptors. *Nat. Immunol.* 11, 373–384. doi: 10.1038/ni.1863

Kim, Y., Lee, E. J., Jang, H. K., Kim, C. H., Kim, D. G., Han, J. H., et al. (2016). Statin pretreatment inhibits the LPS-induced EMT via the downregulation of TLR4 and NF-κB in human biliary epithelial cells. *J. Gastroenterol. Hepatol.* 31, 1220–1228. doi: 10.1111/jgh.13230

Kitisin, K., Ganesan, N., Tang, Y., Jogunoori, W., Volpe, E. A., Kim, S. S., et al. (2007). Disruption of transforming growth factor-beta signaling through beta-spectrin ELF leads to hepatocellular cancer through cyclin D1 activation. *Oncogene* 26, 7103–7110. doi: 10.1038/sj.onc.1210513

Lam, P., Cheung, F., Tan, H. Y., Wang, N., Yuen, M. F., and Feng, Y. (2016). Hepatoprotective effects of Chinese medicinal herbs: a focus on anti-inflammatory and anti-oxidative activities. *Int. J. Mol. Sci.* 17:465. doi: 10.3390/ijms17040465

Li, W., Xiao, J., Zhou, X., Xu, M., Hu, C., Xu, X., et al. (2015). STK4 regulates TLR pathways and protects against chronic inflammation–related hepatocellular carcinoma. *J. Clin. Invest.* 125, 4239–4254. doi: 10.1172/JCI81203

Li, X., Wang, Z., Zou, Y., Lu, E., Duan, J., Yang, H., et al. (2015). Pretreatment with lipopolysaccharide attenuates diethylnitrosamine-caused liver injury in mice via TLR4-dependent induction of Kupffer cell M2 polarization. *Immunol. Res.* 62, 137–145. doi: 10.1007/s12026-015-8644-2

Liu, H., and Ma, Z. (Song Dynasty). *Kaibao Materia Medica.* China.

Lucas, P. J., Kim, S. J., Melby, S. J., and Gress, R. E. (2000). Disruption of T Cell homeostasis in mice expressing a T cell–specific dominant negative transforming growth factor β II receptor. *J. Exp. Med.* 191, 1187–1196. doi: 10.1084/jem.191.7.1187

Lv, W., Zhang, A., Xu, S., and Zhang, H. Q. (2009). Effects of general glycosides in *Cynanchum auriculatum* of Jiangsu province on liver fibrosis of rats. *Chin. J. Chin. Mater. Med.* 34, 2508–2511.

Mccartneyfrancis, N., Jin, W., and Wahl, S. M. (2004). Aberrant toll receptor expression and endotoxin hypersensitivity in mice lacking a functional TGF-β1 signaling pathway. *J. Immunol.* 172, 3814–3821. doi: 10.4049/jimmunol.172. 6.3814

Mcdonald, B., Jenne, C. N., Zhuo, L., Kimata, K., and Kubes, P. (2013). Kupffer cells and activation of endothelial TLR4 coordinate neutrophil adhesion within liver sinusoids during endotoxemia. *Am. J. Physiol. Gastrointest. Liver Physiol.* 305, G797–G806. doi: 10.1152/ajpgi.00058.2013

O'Neill, L. A. J., Golenbock, D., and Bowie, A. G. (2013). The history of toll-like receptors — redefining innate immunity. *Nat. Rev. Immunol.* 13, 453–460. doi: 10.1038/nri3446

Pang, Z., Junkins, R. D., Raudonis, R., MacNeil, A. J., McCormick, C., Cheng, Z., et al. (2018). Regulator of calcineurin 1 differentially regulates TLR-dependent MyD88 and TRIF signaling pathways. *PLoS One* 13:e0197491. doi: 10.1371/journal.pone.0197491

Peng, Y., and Ding, Y. (2015). Pharmacokinetics and tissue distribution study of caudatin in normal and diethylnitrosamine-induced hepatocellular carcinoma model rats. *Molecules* 20, 4225–4237. doi: 10.3390/molecules20034225

Peng, Y., Ding, Y., Wei, Y., Shu, L., Li, Y. B., and Liu, X. D. (2011). Caudatin-2, 6-dideoxy-3-O-methy-β-d-cymaropyranoside 1 induced apoptosis through caspase 3-dependent pathway in human hepatoma cell line SMMC7721. *Phytother. Res.* 25, 631–637. doi: 10.1002/ptr.3312

Peng, Y. R., Li, Y. B., Liu, X. D., Zhang, J. F., and Duan, J. A. (2008a). Antitumor activity of C-21 steroidal glycosides from *Cynanchum auriculatum* Royle ex Wight. *Phytomedicine* 15, 1016–1020.

Peng, Y. R., Li, Y. B., Liu, X. D., Zhang, J. F., and Duan, J. A. (2008b). Apoptosis induced by caudatin in human hepatoma cell line SMMC7721. *Chin. J. Nat. Med.* 6, 210–213. doi: 10.1002/ptr.3312

Praneenararat, S., Chamroonkul, N., Sripongpun, P., Kanngurn, S., Jarumanokul, R., and Piratvisuth, T. (2014). HBV DNA level could predict significant liver fibrosis in HBeAg negative chronic hepatitis B patients with biopsy indication. *BMC Gastroenterol.* 14:218. doi: 10.1186/s12876-014-0218-6

Roh, Y. S., and Seki, E. (2013). Toll-like receptors in alcoholic liver disease, non-alcoholic steatohepatitis and carcinogenesis. *J. Gastroenterol. Hepatol.* 28, 38–42. doi: 10.1111/jgh.12019

Rui, W., Xie, L., Liu, X., He, S., Wu, C., Zhang, X., et al. (2014). Compound *Astragalus* and *Salvia miltiorrhiza* extract suppresses hepatocellular carcinoma progression by inhibiting fibrosis and PAI-1 mRNA transcription. *J. Ethnopharmacol.* 151, 198–209. doi: 10.1016/j.jep.2013.10.022

Seki, E., De Minicis, S., Österreicher, C. H., Kluwe, J., Osawa, Y., Brenner, D. A., et al. (2007). TLR4 enhances TGF-beta signaling and hepatic fibrosis. *Nat. Med.* 13, 1324–1332. doi: 10.1038/nm1663

Shan, L., Zhang, W. D., Zhang, C., Liu, R. H., Su, J., and Zhou, Y. (2005). Antitumor activity of crude extract and fractions from root tuber of *Cynanchum auriculatum* Royle ex Wight. *Phytother. Res.* 19, 259–261. doi: 10.1002/ptr.1678

Shi, H., Dong, L., Jiang, J., Zhao, J., Zhao, G., Dang, X., et al. (2013). Chlorogenic acid reduces liver inflammation and fibrosis through inhibition of toll-like receptor 4 signaling pathway. *Toxicology* 303, 107–114. doi: 10.1016/j.tox.2012.10.025

Soares, J. B., Pimentel-Nunes, P., Afonso, L., Rolanda, C., Lopes, P., Roncon-Albuquerque, R. Jr., et al. (2012). Increased hepatic expression of TLR2 and TLR4 in the hepatic inflammation-fibrosis-carcinoma sequence. *Innate Immun.* 18, 700–708. doi: 10.1177/1753425912436762

Suzuki, K., Murakami, T., Hu, Z., Tamura, H., Kuwahara-Arai, K., Iba, T., et al. (2016). Human host defense cathelicidin peptide LL-37 enhances the lipopolysaccharide uptake by liver sinusoidal endothelial cells without cell activation. *J. Immunol.* 196, 1338–1347. doi: 10.4049/jimmunol.1403203

Szabo, G., and Petrasek, J. (2015). Inflammasome activation and function in liver disease. *Nat. Rev. Gastroenterol. Hepatol.* 12, 387–400. doi: 10.1038/nrgastro.2015.94

Wai, K. K., Liang, Y., Zhou, L., Cai, L., Liang, C., Liu, L., et al. (2015). The protective effects of *Acanthus ilicifolius* alkaloid A and its derivatives on pro- and anti-inflammatory cytokines in rats with hepatic fibrosis. *Biotechnol. Appl. Biochem.* 62, 537–546. doi: 10.1002/bab.1292

Wang, D. Y., Hua, X., Ye, J. L., Li, J. J., Li, Q., and Yan, H. S. (2014). Antitumor effect of C21 steroidal glycosides in radix cynanchi bungei on heps rats and its influence on hematopoiesis. *J. Clin. Med. Pract.* 18, 6–8.

Wang, D. Y., Zhang, H. Q., and Li, X. (2007). Apoptosis induced by the C-21 sterols in Baishouwu and its mechanism of action in hepatoma. *Acta. Pharmacol. Sin.* 42, 366–370.

Wang, X., Li, Z., Lv, X., Zuo, Q. Y., Zhao, Y. M., Ding, Y. F., et al. (2017). Antitumor evaluation and multiple analysis on different extracted fractions of the root of *Cynanchum auriculatum* Royle ex Wight. *J. Sep. Sci.* 40, 3054–3063. doi: 10.1002/jssc.201601415

Wang, Y., Tu, Q., Yan, W., Xiao, D., Zeng, Z., Ouyang, Y., et al. (2015). CXC195 suppresses proliferation and inflammatory response in LPS-induced human hepatocellular carcinoma cells via regulating TLR4-MyD88-TAK1-mediated NF-κB and MAPK pathway. *Biochem. Biophys. Res. Commun.* 456, 373–379. doi: 10.1016/j.bbrc.2014.11.090

Wang, Y. Q., Zhang, S. J., Lu, H., Yang, B., Ye, L. F., and Zhang, R. S. (2013). A C21 -Steroidal glycoside isolated from the roots of *Cynanchum auriculatum* Induces cell cycle arrest and apoptosis in human gastric cancer SGC-7901 Cells. *Evid. Based Complement. Alternat. Med.* 2013:180839. doi: 10.1155/2013/180839

Yang, X., Letterio, J. J., Lechleider, R. J., Chen, L., Hayman, R., Gu, H., et al. (1999). Targeted disruption of SMAD3 results in impaired mucosal immunity and diminished T cell responsiveness to TGF-β. *EMBO J.* 18, 1280–1291. doi: 10.1093/emboj/18.5.1280

Yin, J. L., Li, X., Zhang, S. X., and Zhang, H. Q. (2007). Protective effect of C21 steroidal ester saponin of *Cynanchum auriculatum* royle ex wight on acute CCL4-induced liver injury in mice. *Anhui Med. Pharmaceut. J.* 11, 198–200.

Yu, L. X., Yan, H. X., Liu, Q., Yang, W., Wu, H. P., Dong, W., et al. (2010). Endotoxin accumulation prevents carcinogen-induced apoptosis and promotes liver tumorigenesis in rodents. *Hepatology* 52, 1322–1333. doi: 10.1002/hep.23845

Zeng, J., Huang, X., Zhou, L., Tan, Y., Hu, C., Wang, X., et al. (2015). Metaboomics identifies biomarker pattern for early diagnosis of hepatocellular carcinoma: from diethylnitrosamine treated rats to patients. *Sci. Rep.* 5:16101. doi: 10.1038/srep16101

Zhang, R. S., Ye, Y. P., and Liu, X. L. (2000). Studies on in vitro antitumor activity of total steroidal glycoside from the root of *Cynanchum auriculatum*. *Chin. Tradit. Herb. Drugs* 31, 599–602.

Zhang, W., Peng, Y. R., and Ding, Y. F. (2015). Biotransformation and metabolic profile of caudatin-2,6-dideoxy-3-O-methy-β-d-cymaropyranoside with human intestinal microflora by liquid chromatography quadrupole time-of-flight mass spectrometry. *Biomed. Chromatogr.* 29, 1715–1723. doi: 10.1002/bmc.3484

Zhu, Q., Zou, L., Jagavelu, K., Simonetto, D. A., Huebert, R. C., Jiang, Z. D., et al. (2012). Intestinal decontamination inhibits TLR4 dependent fibronectin-mediated cross-talk between stellate cells and endothelial cells in liver fibrosis in mice. *J. Hepatol.* 56, 893–899. doi: 10.1016/j.jhep.2011.11.013

The Protective Effect of Magnesium Lithospermate B on Hepatic Ischemia/Reperfusion *via* Inhibiting the Jak2/Stat3 Signaling Pathway

Ning Zhang[1], Li Han[2,3], Yaru Xue[2,3], Qiangqiang Deng[2], Zhitao Wu[2], Huige Peng[2], Yiting Zhang[2,3], Lijiang Xuan[2,3], Guoyu Pan[2,3]* and Qiang Fu[1]*

[1] Department of Pharmacology of Chinese Materia Medica, China Pharmaceutical University, Nanjing, China, [2] Shanghai Institute of Materia Medica, Chinese Academy of Sciences, Shanghai, China, [3] University of Chinese Academy of Sciences, Beijing, China

Acute inflammation is an important component of the pathogenesis of hepatic ischemia/reperfusion injury (HIRI). Magnesium lithospermate B (MLB) has strong neuroprotective and cardioprotective effects. The purpose of this study was to determine whether MLB had underlying protective effects against hepatic I/R injury and to reveal the potential mechanisms related to the hepatoprotective effects. In this study, we first examined the protective effect of MLB on HIRI in mice that underwent 1 h ischemia followed by 6 h reperfusion. MLB pretreatment alleviated the abnormal liver function and hepatocyte damage induced by I/R injury. We found that serum inflammatory cytokines, including IL-6, IL-1β, and TNF-α, were significantly decreased by MLB during hepatic ischemia/reperfusion (I/R) injury, suggesting that MLB may alleviate hepatic I/R injury *via* inhibiting inflammatory signaling pathways. Second, we investigated the protein level of p-Jak2/Jak2 and p-Stat3/Stat3 using Western blotting and found that MLB could significantly inhibit the activation of the Jak2/Stat3 signaling pathway, which was further verified by AG490 in a mouse model. Finally, the effect of MLB on the Jak2/Stat3 pathway was further assessed in an *in vitro* model of RAW 264.7 cells; 1 µg/ml LPS induced the secretion of inflammatory mediators, including IL-6, TNF-α, and activation of the Jak2/Stat3 signaling pathway. MLB significantly inhibited the abnormal secretion of inflammatory factors and the activation of the Jak2/Stat3 signaling pathway in RAW264.7 cells. In conclusion, MLB was found for the first time to reduce inflammation induced by hepatic I/R *via* suppressing the Jak2/Stat3 pathway.

Keywords: magnesium lithospermate B, hepatic ischemia/reperfusion, acute injury, anti-inflammation, Jak2/Stat3 signaling pathway

INTRODUCTION

Hepatic ischemia/reperfusion injury (HIRI) is a major complication during various diseases and liver surgery procedures, such as hemorrhagic shock, trauma, liver transplantation, and hepatectomy (Arkadopoulos et al., 2011; Douzinas et al., 2012; Lu et al., 2018). HIRI is characterized by high morbidity and mortality, which is attributed to the fact that oxidative stress, immune responses,

and cell apoptosis are activated by ischemia/reperfusion (I/R) (Bzeizi et al., 1997; Van Golen et al., 2012; Van Golen et al., 2013). Currently, ischemic preconditioning and pharmacological agents are employed in clinics to prevent and mitigate I/R injury (Li et al., 2015). However, ischemic preconditioning is effective only in some young patients (Clavien et al., 2003), and the efficacy of available drugs is limited. There is no well-established method to prevent and mitigate I/R injury, which will improve the safety of major liver surgery and liver transplantation (Robertson et al., 2017). Thus, there is an urgent need to find effective methods/drugs for the treatment of hepatic I/R injury.

The dominant pathogenesis for HIRI involves two phases: the early process of ischemia-induced hepatocyte injury and the successive process of reperfusion-induced immune response (Ju et al., 2016; Zhang et al., 2018). During the ischemic process, damage-associated molecular patterns (DAMPs), such as reactive oxygen species (ROS), DNA fragments, nuclear factors, cytosolic proteins, and others, are released from the dead cells (Lu et al., 2018; Mihm, 2018). DAMPs will be recognized by Toll-like receptors (TLRs) on the cell membrane and then activate hepatic resident macrophages, Kupffer cells (KCs) (Chang and Toledo-Pereyra, 2012). KCs will secrete excessive proinflammatory cytokines to cause high levels of hepatocyte death, exacerbate liver damage, and even lead to systemic inflammatory response syndrome and multiple-organ failure (Guo, 2013; Triantafyllou et al., 2018). Suppression of the inflammatory response may be a powerful way to reduce I/R-induced hepatic injury.

According to previous studies, in addition to TLR recognition of DAMPS, the Janus kinase/signal transducers and activators of the transcription (Jak/Stat) signaling pathway plays a vital role in the inflammatory responses (Wang et al., 2015a; Roskoski, 2016; Rahimifard et al., 2017; Bousoik and Montazeri Aliabadi, 2018); Jak2 and Stat3 are the most important family members of the Jak and Stat proteins. Mutations in the Jak and Stat genes lead to multiple immune syndromes (Banerjee et al., 2017). The expression of cytokines is impacted due to the change in the Jak/Stat signaling pathway (Gurzov et al., 2016). In addition, the Jak2/Stat3 signaling pathway participates in the multiple-organ damage caused by I/R, such as brain (Hu et al., 2017), myocardial (Chen et al., 2019), and renal I/R injury (Luo et al., 2016). Organ damage was alleviated by changing Jak2/Stat3 activation or phosphorylation.

Magnesium lithospermate B (MLB, **Figure 1**) is a water-soluble component and is extracted from the traditional Chinese medicine *Salvia miltiorrhiza Bunge*, known as DanShen, which has been used to cure cardiac–cerebral vascular disease and chronic renal failure (Zhou et al., 2005; Bu et al., 2013; Huang et al., 2018). In past studies, substantial scientific evidence has suggested that MLB could protect against stroke (Cao et al., 2015), myocardial infarction (Du et al., 2010), and depression (Quan et al., 2015). Meanwhile, MLB could protect against neuroinflammation induced by lipopolysaccharide (LPS) in BV2 microglial cells and inhibit the inflammatory response *via* inhibiting the nuclear factor-kappa B signaling pathway in activation T cells (Cheng et al., 2012; Tai et al., 2018). It is unclear whether the anti-neuroinflammatory efficacy of MLB could help alleviate hepatic I/R damage.

In this study, we established HIRI in mice to investigate whether MLB could ameliorate this condition. The potential mechanisms of MLB anti-I/R in the liver were investigated, especially from inflammatory response perspectives.

MATERIALS AND METHODS

In Vivo Experiment
Animals
The animals used in our study were obtained from the Shanghai Laboratory Animal Co. (Shanghai, China). Male C57BL/6 mice weighing 22–24 g and aged 6–8 weeks were housed in a specific pathogen-free environment with air-conditioned animal quarters at a controlled temperature of 23 ± 1.5°C and a relative humidity of 70 ± 20%. The mice were fed *ad libitum* with laboratory chow.

All animal experiments were approved by the Institutional Animal Care and Use Committee of Shanghai Institute of Materia Medica, Chinese Academy of Sciences.

Animal Surgery
All animals underwent sham operations or hepatic I/R surgery. A warm partial (~70%) hepatic I/R model was conducted as previously described (Castellaneta et al., 2014). In brief, mice were anesthetized by injection intraperitoneally (i.p.) with pentobarbital sodium (50 mg/kg). The animals were laparotomized, and the portal vein, hepatic artery, and bile duct were clamped with an atraumatic vascular clip blocking blood supply to the median and left lateral lobes of the liver. The sham mice were only laparotomized without hepatic ischemia. After
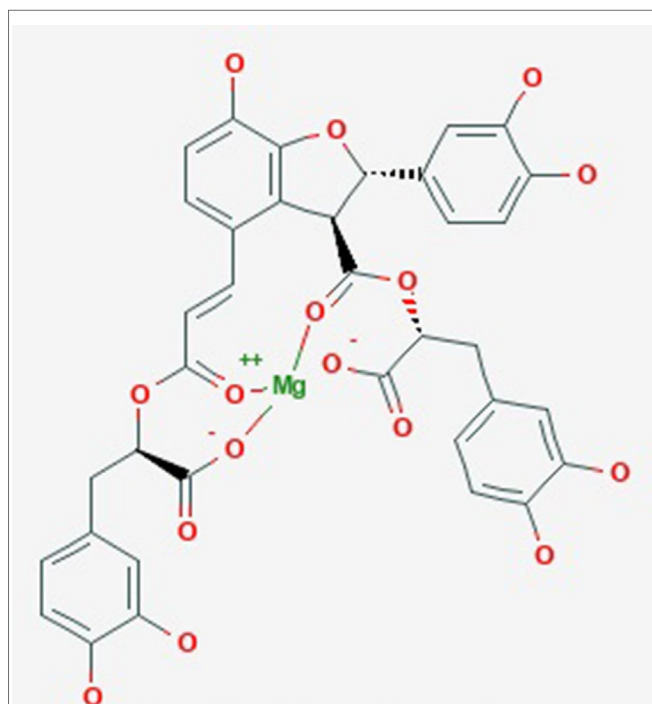

FIGURE 1 | The molecular structure of magnesium lithospermate B obtained from PubChem substance SID: 135075733.

60 min of hepatic ischemia, the clip was removed, and the blood supply was restored. After 6 h of reperfusion, blood was drawn from the hearts of mice under isoflurane anesthesia, and liver tissues were collected.

Drug Treatment

MLB (purity ≥ 99%) was kindly provided by Professor Lijiang Xuan (Shanghai Institute of Materia Medica, Chinese Academy of Sciences). It was administered by the intravenous route (30 mg/kg body weight, dissolved in sterile physiological saline solution) 24 h, 12 h, and 1 h before surgery. The Jak2 inhibitor AG490 (12 mg/kg body weight) was obtained from Selleck Chemical (Houston, TX, USA) and dissolved in 5% DMSO and 95% PBS. AG490 was administered i.p. as a positive control.

Blood and Tissue Samples

All blood samples were centrifuged (3,000 rpm, 4°C) for 15 min to obtain serum stored at −80°C for biochemistry analyses. The liver tissues were collected, and parts were stored at −80°C for Western blot analysis, while others were immediately fixed in 10% formalin for hematoxylin-and-eosin staining.

Blood Biochemical Analyses

Alanine aminotransferase (ALT), aspartate aminotransferase (AST), and lactate dehydrogenase (LDH) levels in serum were measured by a standard clinical automatic analyzer (SYSMEX JCA-BM6010C) in the laboratory of the Chinese National Compound Library.

Hematoxylin–Eosin Staining

Three or four liver tissues were randomly selected for pathology analysis. Briefly, the fixed liver tissues were embedded in paraffin wax, and then, 4-μm-thick liver sections were cut for the next experiment. The prepared sections were stained with hematoxylin and eosin (H&E). The morphology results were assessed by a pathologist who was blinded to the experimental groups. The liver injury score was determined according to Suzuki's method (Ge et al., 2017).

Detection of Superoxide Dismutase Activity and Malondialdehyde Production

Appropriate liver tissues were lysed using the specific lysate, and the supernatants were separated from the homogenization by centrifugation (12,000×*g*, 10 min, 4°C) to detect superoxide dismutase (SOD) activity and MDA content. SOD activity and malondialdehyde (MDA) content were detected using the SOD and MDA assay kit (Beyotime Biotechnology, Jiangsu, China) according to the manufacturer's instructions.

In Vitro Experiment
Cell Culture
RAW264.7 macrophage cells were kindly provided by Professor Likun Gong, Shanghai Institute of Materia Medica, Chinese

Academy of Sciences. Cells were cultured with DMEM containing 10% (v/v) FBS at 37°C in an atmosphere of 5% CO_2.

Cell Viability Assays

Cells were seeded into 96-well plates (3×10^5 cells/ml) for 12 h prior to the experiment. After incubation with different concentrations of MLB (0.1–500 μg/ml) for 24 h, Cell Counting Kit-8 (CCK-8, Yeasen Biotech Co. Ltd., Shanghai, China) was used to determine the cell viability according to the manufacturer's instructions. Briefly, 10 μL CCK-8 was added to each well and incubated for 1–4 h at 37°C, and then, the absorbance of each well was measured at 450 nm using a microplate reader (BioTek, USA).

Measurement of Nitric Oxide in Culture Medium

Cells were seeded into six-well plates (3×10^5 cells/ml) for 12 h before the experiment. After incubation with or without AG490 (75 μM) or different concentrations of MLB for 2 h, RAW264.7 cells were stimulated with 1 μg/ml LPS (Sigma Aldrich, USA) for 8 h. The nitric oxide (NO) content was investigated by Griess reagent according to the manufacturer's instructions on the NO assay kit (Beyotime Biotechnology, Jiangsu, China). In brief, cell media were mixed with an equal volume of Griess reagent, and the absorbance of the mixture was measured using a microplate reader (BioTek, USA) at 540 nm. All experimental results were repeated at least five times independently. The concentrations of nitrite can be relatively calculated to use the content of NO in cell media.

Enzyme Linked Immunosorbent Assays (ELISAs)

ELISA kits, obtained from R&D and Multi Science, were used to detect the concentrations of proinflammatory factors, including interleukin-6 (IL-6), interleukin-1β (IL-1β), and tumor necrosis factor-α (TNF-α), in the serum and culture medium, respectively. All the studies were conducted according to the specific manufacturer's instructions. The absorbance was tested using a microplate reader (BioTek, USA) at 450 nm. All data are shown as pictograms per milliliter serum (pg/ml).

Western Blot Assay

For protein extraction, the frozen liver tissues or cell samples were lysed using cold RIPA lysis buffer (Beyotime Biotechnology, Jiangsu, China) with 1% protease inhibitor cocktail (Bimake, Shanghai, China), and the supernatants of liver tissue homogenates or cell lysis solutions were obtained by centrifugation at 12,000 rpm for 10 min. The protein concentrations were quantified using a BCA assay kit (Thermo, USA) according to the manufacturer's instructions. Equal amounts of protein samples were intermixed with sodium dodecyl sulfate (SDS)–loading buffer (Yeasen Biotech Co. Ltd, Shanghai, China) and then boiled for 10 min at 100°C. Subsequently, protein samples were separated by 10% SDS–polyacrylamide gel electrophoresis and then transferred onto polyvinylidene difluoride (PVDF) membranes (Millipore,

USA) with Trans-Blot system (Bio-Rad, Hercules, CA). The membrane was blocked for 1 h with 3% bovine serum albumin (BSA) in Tris-buffered saline (TBS) containing 0.1% Tween 20 (TBST) at room temperature and then incubated overnight at 4°C with the primary antibodies. The membranes, washed with TBST three times, were treated with horseradish peroxidase (HRP)– labeled secondary antibody for 1 h at room temperature. Finally, the bands were identified using chemiluminescence (ECL) kits (Yeasen Biotech Co. Ltd, Shanghai, China). The signal intensity of the target bands was determined with Image-Pro Plus (IPP).

Statistical Analysis

GraphPad Prism 5.0 software was used for statistical analyses, and all data are expressed as mean ± SD. The results were obtained by one-way analysis of variance (ANOVA) followed by Tukey's multiple-comparison tests. There was a statistically significant difference when the P value was less than 0.05.

RESULTS

Effect of MLB on Liver Damage Induced by I/R

ALT, AST, and LDH in mouse serum were examined using a standard clinical automatic analyzer. The ALT, AST, and LDH

levels (**Figure 2A–C**) were not significantly different in the sham+MLB group compared to the sham group, suggesting that MLB has no adverse effect on the function of the mouse liver. The animals in the I/R group had significantly elevated ALT, AST, and LDH contents in the serum. MLB pretreatment significantly reduced the serum ALT, AST, and LDH levels in the mice after I/R surgery. Liver pathological changes were mainly revealed as varying degrees of hepatocellular swelling/ necrosis, sinusoidal/vascular congestion, and inflammatory cell infiltration. The changes were more severe in the I/R group than in the sham group (**Figure 2D**) and were reversed in the MLB pretreatment group. The pathological score of the MLB group was significantly lower than that of the I/R-alone group (**Figure 2E**). These results suggest that MLB could protect against I/R-induced hepatic injury.

Effect of MLB on Oxidative Stress in Liver and Proinflammatory Mediators in Serum

To evaluate the effects of MLB on oxidative stress, the concentrations of SOD and MDA in liver tissue were measured. SOD and MDA concentrations did not change significantly in the sham+MLB group (**Figure 3A**, **B**). The concentrations of SOD and MDA were significantly changed due to I/R. MLB pretreatment could alleviate these changes and reduce oxidative stress. Serum IL-6, IL-1β, and TNF-α in the sham+MLB group were not significantly

FIGURE 2 | MLB pretreatment attenuates liver injury caused by ischemia–reperfusion. **(A–C)** The levels of ALT, AST, and LDH in sham, I/R, and MLB pretreatment groups. **(D, E)** Classical images of sham, I/R, and MLB treatment groups were examined by H&E staining, and histopathological score was calculated by Suzuki's scoring standard, magnification x200, scale bar 50μm. Data shown are mean ± SD; ns: no statistical significance; ###P < 0.001 versus sham group; **P < 0.01, and ***P < 0.001 versus I/R group; n = 5 for each group.

FIGURE 3 | MLB pretreatment affected oxidative stress in liver and inhibited inflammatory factors' expression. **(A**, **B)** The levels of SOD and MDA in liver tissue of sham, I/R, and MLB pretreatment groups. **(C–E)** Serum IL-6, IL-1β, and TNF-α were detected by ELISA in sham, I/R, and MLB group. The data are expressed as mean ± SD; ns: no statistical significance; ##P < 0.01, and ###P < 0.001 versus sham group; **P < 0.01, and ***P < 0.001 versus I/R group; n = 5 for each group.

altered compared with the sham group (**Figure 3C–E**). However, serum IL-6, IL-1β, and TNF-α concentrations were abnormally elevated in the I/R group, and MLB pretreatment significantly decreased the concentrations of serum IL-6, IL-1β, and TNF-α throughout the observation period.

Effect of MLB on Jak2/Stat3 Signaling Pathway

To explore the underlying mechanism of MLB on HIRI, we detected the ratio of p-Jak2/Jak2 and p-Stat3/Stat3 in the liver tissue of I/R animals. As described in **Figure 4A–D**, p-Jak2 and p-Stat3 levels were significantly higher in the I/R group versus the sham group. After MLB pretreatment, there was a significant decrease in the levels of p-Jak2 and p-Stat3.

Effect of AG490 or MLB on Hepatic Injury Induced by I/R

In addition, to further explore whether the mechanism of MLB alleviation of hepatic I/R is related to the inhibition of Jak2 signaling pathway, we selected AG490, a specific inhibitor of Jak2, as a positive control or in combination with MLB. The contents of ALT, AST, and LDH (**Figure 5A–C**) were significantly reduced by AG490 pretreatment after I/R surgery, but there was no significant difference compared to the MLB pretreatment group. Thus, we combined MLB with AG490 to further investigate the

protective mechanism of MLB. AG490 was given i.p. 1 h prior to MLB treatment. As shown in **Figure 5D–F**, serum ALT, AST and LDH levels were also reduced by MLB+AG490, but there was also no significant difference between the MLB+AG490 group and the MLB group.

Subsequently, we found that liver pathological changes were also significantly reversed in the AG490 pretreatment group compared to the I/R group, and the serious liver pathological changes were also reversed by MLB+AG490, but all the pathological scores in the AG490 or MLB+AG490 group were not significantly different compared to the group with MLB pretreatment alone (**Figure 5G–J**).

Effect of AG490 or MLB on Oxidative Stress in Liver and Proinflammatory Mediator in Serum

Next, we repeated assays to detect oxidative stress–related enzymes and proinflammation factors. As shown in **Figure 6A** and **B**, oxidative stress–related enzymes such as SOD and MDA were altered by Jak2 inhibitor AG490 pretreatment versus those of the I/R group (**Figure 6A** and **B**). However, AG490 pretreatment did not significantly improve the expression of SOD and MDA in liver tissues compared with the MLB group. Analogously, proinflammatory cytokines including IL-6, IL-1β, and TNF-α were observably decreased by AG490 in serum, as shown in **Figure 6C–E**.

FIGURE 4 | MLB pretreatment inhibited Jak2/Stat3 signal pathway in the liver tissue of I/R. (A) Western blot was utilized to detect the level of p-Jak2. (B) The quantification of p-Jak2/Jak2 was statistically analyzed. (C) Western blot was utilized to detect the level of p-Stat3. (D) The quantification of p-Stat3/Stat3 was statistically analyzed. The data are expressed as mean ± SD; n = 5 for each group; ns: no statistical significance; ###P < 0.001 versus sham group; ***P < 0.001 versus I/R group.
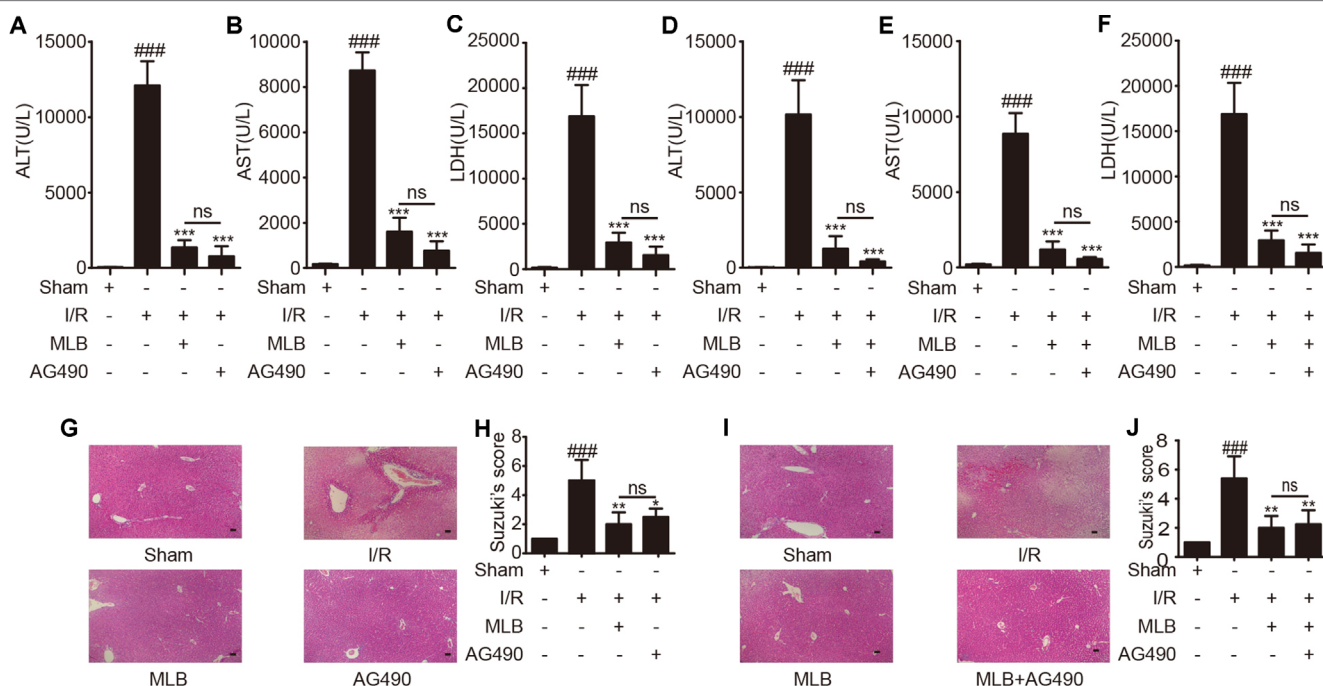
FIGURE 5 | AG490 or MLB+AG490 pretreatment attenuates liver injury caused by ischemia–reperfusion. (A–F) The levels of ALT, AST, and LDH in sham, I/R, MLB, and AG490 or MLB+AG490 groups. (G–J) Classical images of sham, I/R, MLB, and AG490 or MLB+AG490 pretreatment groups were examined by H&E staining, and histopathological score was calculated by Suzuki's scoring standard, magnification x200, scale bar 50μm. Data shown are mean ± SD; n = 3–5 for each group; ns: no statistical significance; ###P < 0.001 versus sham group; *P < 0.05, **P < 0.01, and ***P < 0.001 versus I/R group.
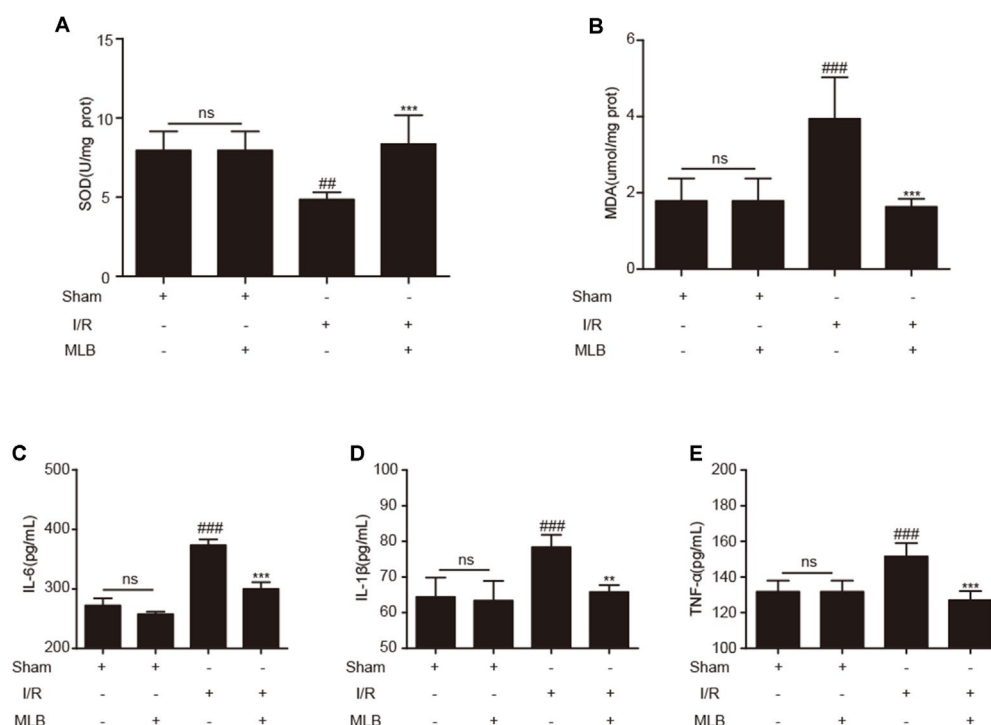
FIGURE 6 | AG490 or MLB+AG490 pretreatment affected oxidative stress in liver and inhibited inflammatory factors' expression. **(A, B)** The expression of SOD and MDA in liver tissue of sham, I/R, MLB, and AG490 groups. **(C–E)** Serum IL-6, IL-1β, and TNF-α were detected by ELISA in sham, I/R, MLB, and AG490 groups. **(F–G)** The expression of SOD and MDA in liver tissue of sham, I/R, MLB, and MLB+AG490 groups. **(H–J)** Serum IL-6, IL-1β, and TNF-α were detected by ELISA in sham, I/R, MLB, and MLB+AG490 groups. The data are expressed as mean ± SD; n = 5 for each group; ns: no statistical significance; $^{###}P < 0.001$ versus sham group; $^{*}P < 0.05$, $^{**}P < 0.01$, and $^{***}P < 0.001$ versus I/R group; $^{\&\&\&}P < 0.001$ versus MLB group.

Subsequently, we also investigated the oxidative-stress markers, including SOD and MDA, in the MLB+AG490 pretreatment group compared to the MLB pretreatment group. As shown in **Figure 6F**, **G**, the expression of SOD and MDA were also altered by MLB+AG490 pretreatment versus the I/R group, while their expression also had no significant difference between the two groups. The levels of proinflammatory mediators were also significantly decreased by MLB+AG490 pretreatment versus MLB pretreatment (**Figure 6H–J**). In this study, we also found that the levels of IL-1β and TNF-α had no significantly difference in the MLB group compared with the AG490 group or MLB+AG490 group, expect for the expression of IL-6 in serum.

Effect of MLB+AG490 on Jak2/Stat3 Signaling Pathway

Moreover, to confirm the effect of MLB on Jak2/Stat3, we investigated the levels of proteins such as p-Jak2/Jak2 and p-Stat3/Stat3. As shown in **Figure 7A–D**, the expression levels of p-Jak2/Jak2 and p-Stat3/Stat3 were significantly decreased in the MLB+AG490 group versus the I/R group. However, the levels of these proteins were not significantly different between the MLB group and the MLB+AG490 group. These results suggested that

MLB could inhibit the Jak2/Stat3 signaling pathway in the liver, which prevented the liver from the injury by I/R.

Effect of MLB on Macrophage RAW264.7 Cells

To further clarify the anti-inflammatory mechanism of MLB, we verified it in macrophage RAW264.7 cells. First, the cytotoxicity of MLB on RAW264.7 was investigated using a CCK-8 kit. As shown in **Figure 8A**, there was no cytotoxicity at concentrations of 0–100 μg/ml of MLB. The cell viability was increased at concentrations of 25–50 μg/ml of MLB. As shown in **Figure 8B**, the NO content was significantly increased after LPS stimulation compared to that of the native control (NC) group.

Proinflammatory factors such as IL-6 and TNF-α were also investigated by ELISAs in cell media. The levels of IL-6 (**Figure 8C**) and TNF-α (**Figure 8D**) were significantly elevated after 8-h treatment with LPS compared to NC. MLB dose-dependently reduced the concentrations of IL-6 and TNF-α.

To further analyze the effect of MLB on Jak2/Stat3, we performed Western blotting to measure the levels of characteristic proteins in the Jak2/Stat3 pathway, including p-Jak2, Jak2, p-Stat3, and Stat3. As shown in **Figure 8E–G**, LPS stimulation observably may increase the ratio of p-Jak2/Jak2 and p-Stat3/
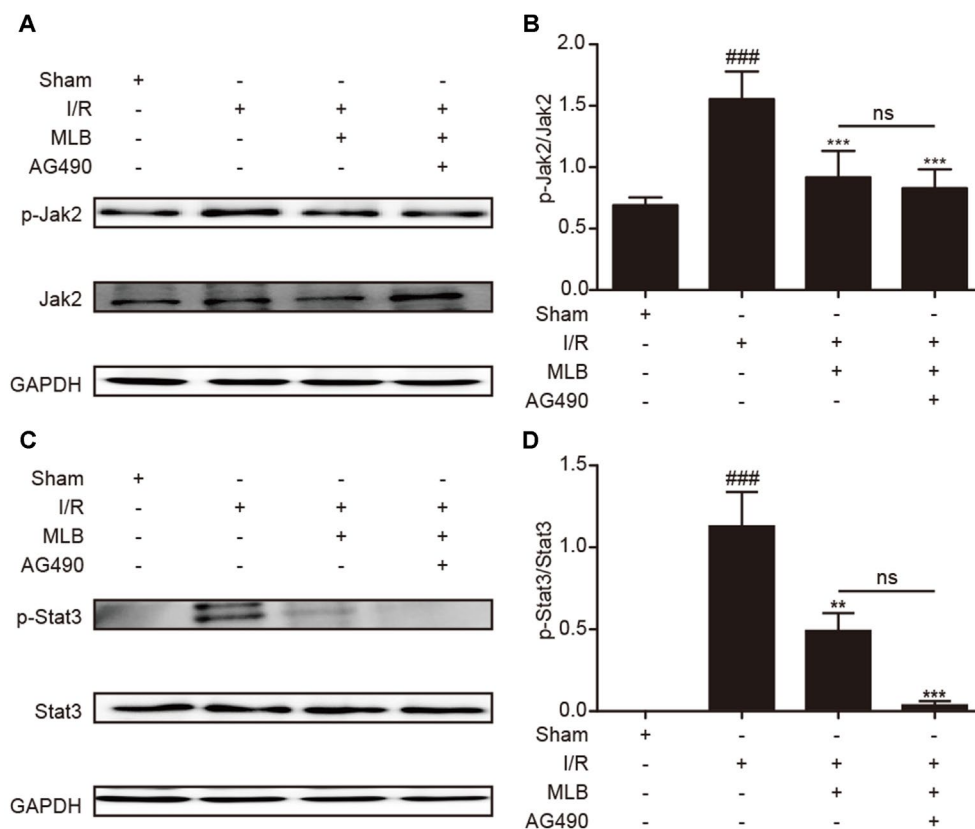
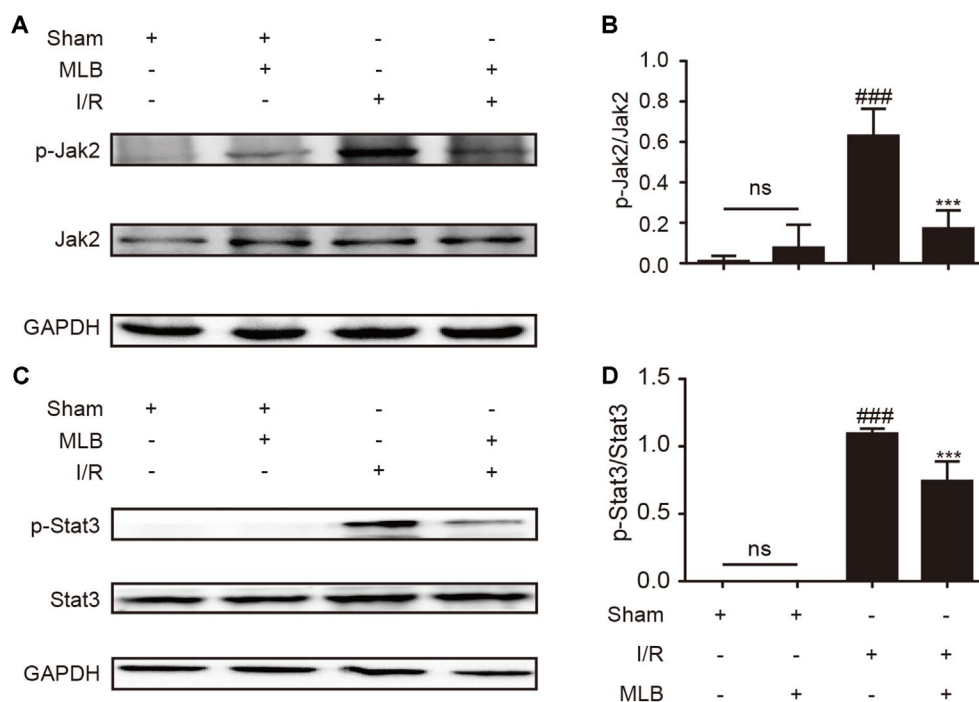**FIGURE 7** | MLB+AG490 pretreatment inhibited Jak2/Stat3 signal pathway in the liver tissue of I/R. **(A)** Western blot was utilized to detect the level of p-Jak2. **(B)** The quantification of p-Jak2/Jak2 was statistically analyzed. **(C)** Western blot was utilized to detect the level of p-Stat3; **(D)** The quantification of p-Stat3/Stat3 was statistically analyzed. The data are expressed as mean ± SD; n = 5 for each group; ns: no statistical significance; ###P < 0.001 versus sham group; **P < 0.01, and ***P < 0.001 versus I/R group.
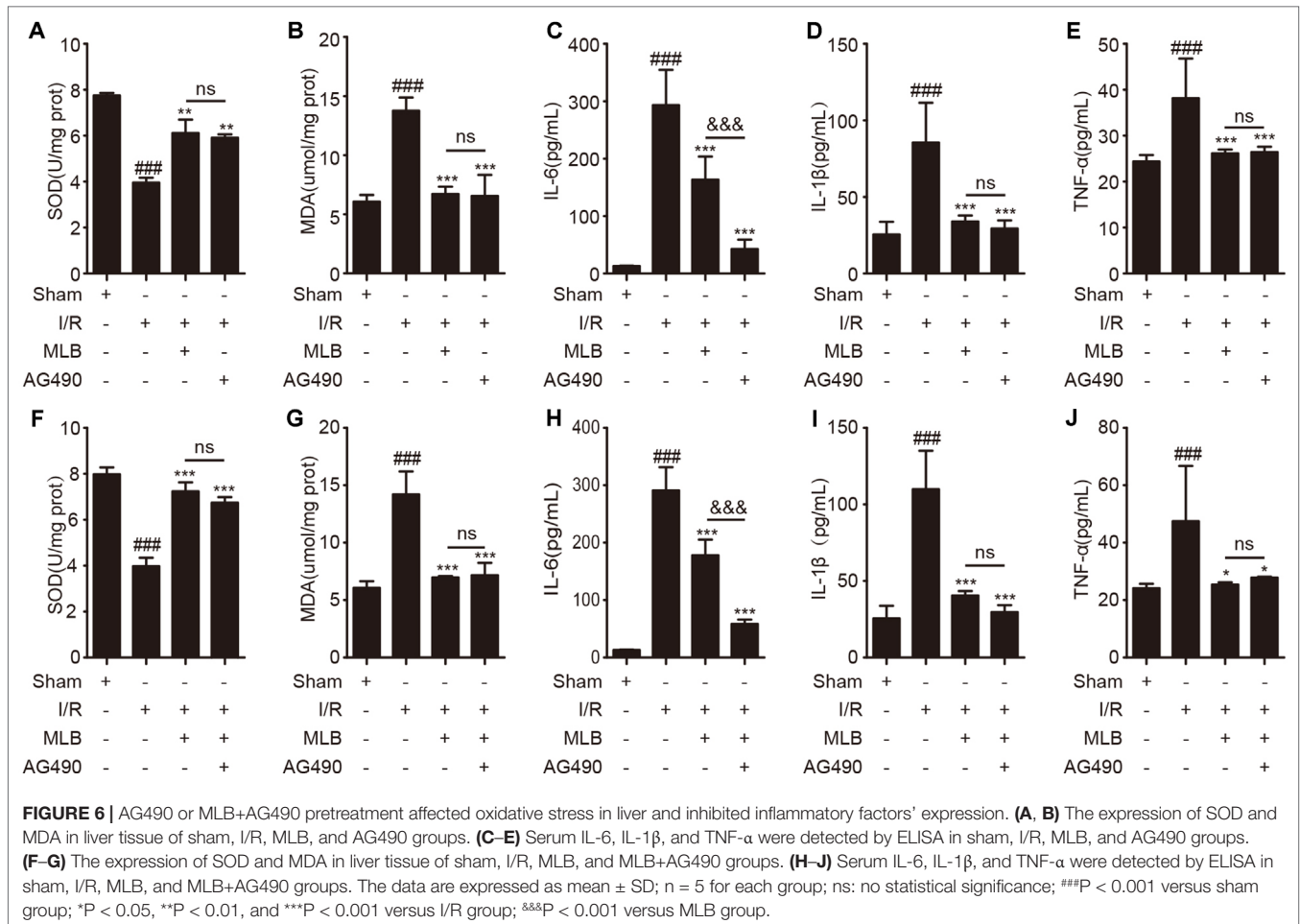
Stat3 in RAW264.7 cells. However, MLB pretreatment strikingly inhibited the expressions of p-Jak2/Jak2 and p-Stat3/Stat3 due to LPS-induced elevation. These results also suggest that the anti-inflammatory effect of MLB is closely related to the inhibition of the Jak2/Stat3 signaling pathway.

DISCUSSION

MLB is a hydrophilic constituent of *Salvia miltiorrhiza*, which was widely used for the treatment of cardiovascular and cerebrovascular disease (Zhu Jinqiang, 2010). As the natural existing form in the herb, MLB is different from its free acid form, salvianolic acid B (or lithospermic acid B) in its physicochemical properties and its bioacticity because the chelating magnesium stabilizes the molecule and makes its conformation different. MLB possesses multitudinous pharmacological properties, including antioxidative, anti-inflammatory, and antiapoptotic effects, in various experimental disease models (Wu and Wang, 2012). MLB was shown to inhibit inflammatory mediator production *via* regulation of nuclear factor-kappa B signaling pathways in activated T cells (Cheng et al., 2012). Moreover, MLB was shown to protect against stroke by upregulating p-Akt (Cao et al., 2015). The reports about MLB in liver diseases

are limited. Paik et al. (2011) found that MLB had an antifibrotic effect in thioacetamide (TAA)-induced cirrhotic rats *via* inhibiting fibrogenic responses. However, the protective effect of MLB on hepatic I/R needs more research. In this study, we found that MLB can protect the liver from HIRI by inhibiting the Jak2/Stat3 signaling pathway. To our knowledge, this is the first report demonstrating that MLB attenuates liver I/R injury through Jak2 inhibition.

HIRI is a common pathological phenomenon and an acute injury with high morbidity and mortality during liver surgery, liver transplantation, and hepatectomy (Arkadopoulos et al., 2011; Douzinas et al., 2012; Lu et al., 2018). Liver function was impacted after I/R surgery (Nakazato et al., 2018). The drug could not get into the ischemic liver to reduce injury during the ischemia period. Therefore, the present study assessed the impact of MLB pretreatment on hepatic function and its therapeutic efficacy against liver I/R injury. The data showed that hepatic I/R aggravated the contents of ALT, AST, and LDH and increased histopathological features compared to the sham group, indicating liver dysfunction and hepatocyte damage induced by I/R in mice. We also found that MLB had no adverse effect on liver function (ALT, AST, and LDH) compared with the sham treatment. MLB pretreatment significantly protected the mice against liver I/R injury, as confirmed by alterations in abnormal liver function and histopathology.

FIGURE 8 | MLB inhibited inflammation *via* Jak2/Stat3 in RAW264.7. **(A)** Cell viability was examined using CCK-8. **(B)** The NO production was measured by Griess assays in cell media, and the levels of IL-6 **(C)** and TNF-α **(D)** were ascertained by ELISA. **(E–G)** The levels of the Jak2/Stat3 signaling pathway were measured by Western blotting. All samples were from 5 independent experiments. Each value is expressed as mean ± SD; n = 5 for each group; ns: no statistical significance; #$P < 0.05$, and ###$P < 0.001$ versus NC group; *$P < 0.05$, **$P < 0.01$, and ***$P < 0.001$ versus LPS group.

In the process of ischemia, some parenchymal hepatic cells are killed because of metabolic dysfunction due to hypoxia and innutrition (Zhai et al., 2013). Oxidative stress plays an important role during I/R (Ma and Jin, 2019; Yao et al., 2019). SOD activity is closely related to oxygen free radical clearance and lipid oxidation resistance, and all of these indicators are also important markers of I/R injury (Okado-Matsumoto and Fridovich, 2001). If the SOD activity is inhibited during I/R, MDA will be produced due to lipid oxidation in cells, and the balance of antioxidants and oxidants will also be disturbed (Demiryilmaz et al., 2014; Wang et al., 2015b). The present experiment showed that MLB pretreatment could increase SOD activity and decrease MDA production in the process of hepatic I/R.

When the blood supply is restored, there is a shift from metabolic dysfunction caused by ischemia to an excessive innate immune response caused by reperfusion. After DAMP recognition by the TLRs on the membrane of the KCs, excessive proinflammatory mediators are secreted during the I/R injury (Langdale et al., 2008; Harari and Liao, 2010; Zhao et al., 2018). Our data showed that the proinflammatory cytokines, including IL-6, IL-1β, and TNF-α, were abnormally elevated in the serum during liver I/R. Our results are consistent with numerous research reports showing that increased contents of inflammatory factors induced by the I/R injury (Walsh et al., 2009; Van Golen et al., 2012; Gendy et al., 2017; Rong et al., 2017). A clinical study found that KC activation was inhibited using glycine in human liver transplantation and that the damage caused by I/R was also reduced (Schemmer et al., 2001). Meanwhile, John D. et al. (Lang et al., 2014) found that preemptive inhaled nitric oxide could protect against I/R injury and reduce the inflammatory effects during human liver transplantation. Therefore, controlling the inflammatory response may be helpful for the prevention and treatment of HIRI. Our data indicated that the production of inflammatory mediators was significantly reduced by MLB pretreatment after I/R surgery.
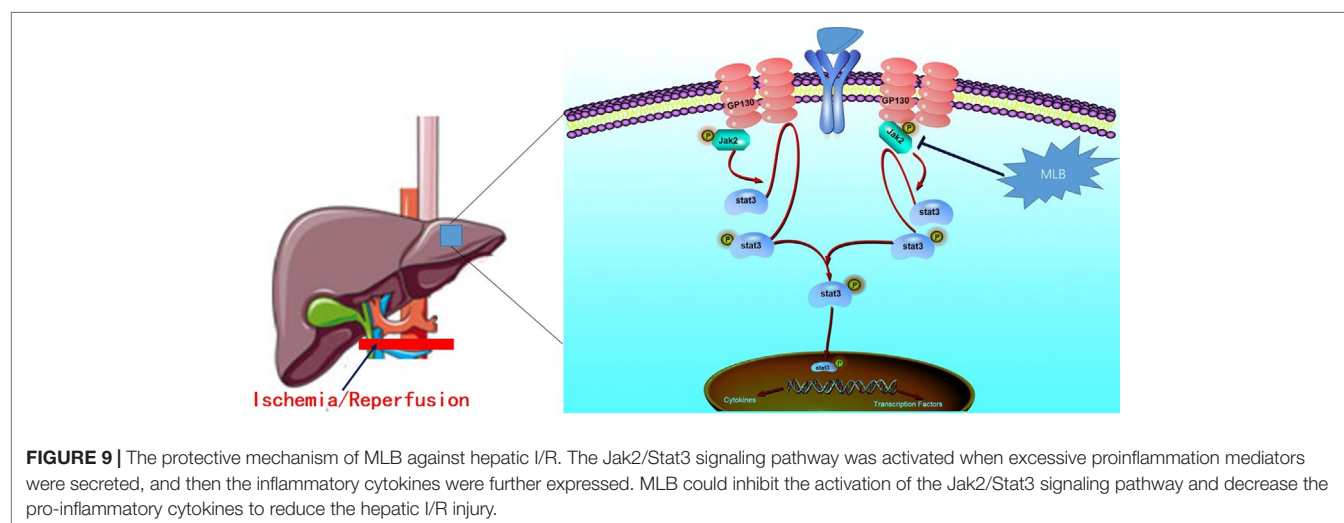
According to a previous report, the Jak2/Stat3 pathway is an important signaling pathway that has been confirmed to regulate the inflammatory response during I/R injury (Si et al., 2014; Luo et al., 2016). The Jak/Stat signaling pathway is activated by proinflammatory cytokines when excessive proinflammatory cytokines such as interleukin and interferon are secreted (Aaronson and Horvath, 2002; Banerjee et al., 2017; Li et al., 2018). The expression of inflammatory cytokines could also be regulated by the Jak2/Stat3 signal pathway (Zhou et al., 2016; Kim et al., 2017; Zhang et al., 2017; Li et al., 2018). Therefore, the efficacy of MLB on Jak2/Stat3 signaling was investigated in a mouse hepatic I/R model. Jak2 was activated *via* phosphorylation during I/R injury (Freitas et al., 2010; Luo et al., 2016; Zhao et al., 2016; Hu et al., 2017). The data showed that I/R significantly increased the level of p-Jak2 compared to that of the sham group. We found that Jak2 activation was significantly suppressed by pretreatment of mice with MLB, and the level of p-Jak2 was significantly reduced in the MLB pretreatment group compared with the I/R group. Stat3 is the most widely studied member of the Stat family of proteins, which is closely related to the Jak family of proteins, and cytosolic Stat3 undergoes phosphorylation following Jak2 activation (Banerjee et al., 2017; Bousoik and Montazeri Aliabadi, 2018). Xiong et al. (2018) also found that when the Stat3 activation was depressed in hepatic I/R injury, hepatic injury was alleviated. Han et al. (2018) reported that Stat3 upregulation or activation is one critical molecular mechanism of hepatic I/R injury. The level of p-Stat3 was detected in the ischemic liver, and p-Stat3 level was abnormally elevated in the I/R group versus the sham group. And p-Stat3 was significantly lower in mice pretreated with MLB than mice in the I/R group.

To further clarify the anti-inflammatory mechanism of MLB, we selected Jak2 inhibitor AG490 as a positive control. Mascareno et al. (2001) found that interfering with activation of the Jak/Stat pathway promotes recovery in cardiac function. Freitas et al. (2010) also showed that the blockade of the Jak2 signaling pathway ameliorates mouse liver injury induced by I/R. In this study, we found that the liver I/R injury was reduced by blockade of Jak2 activation using AG490, while all results of the AG490 pretreatment group showed no significant difference from those

of the MLB pretreatment group, expect for IL-6. To confirm the correlation between the anti-inflammatory effect of MLB and Jak2, mice were pretreated using MLB+AG490. Compared with the I/R group, MLB+AG490 pretreatment could recover abnormal liver function and reduce the degree of liver tissue damage, inflammatory response, and oxidative stress caused by I/R, but there was no significant difference between the MLB group and the I/R group. Moreover, MLB+AG490 significantly inhibited the Jak2 and Stat3 activation. These results suggest that the anti-inflammatory mechanism of MLB was related to the inhibition of Jak2.

RAW264.7 cells, as murine macrophages, were selected for this study. According to a previous report, macrophages or immune systems are activated by some toxicant, such as LPS (Hsu and Wen, 2002; Lawrence et al., 2002; Pestka and Zhou, 2006). Therefore, we established an *in vitro* model in RAW264.7 cells with LPS stimulation. After the LPS stimulation, the inflammatory mediators, including NO, IL-6, IL-1β, and TNF-α, were secreted from the macrophage (Yun et al., 2008; Ham et al., 2015). MLB pretreatment could reverse these abnormal phenomena. Research also finds that Jak2 and Stat3 are specifically activated by IL-6 or INF-γ (Ivashkiv and Hu, 2003; Murray, 2007). We also observed that IFN-γ reversed the MLB's inhibition effect on content of NO and IL-6 after LPS stimulation (**Figure S2A** and **B**). LPS provoked various signal pathways including Jak/Stat (Okugawa et al., 2003; Li et al., 2019). In this study, we also observed that the levels of p-Jak2 and p-Stat3 were abnormally elevated after the LPS stimulation. MLB pretreatment significantly decreased these effects in a dose-dependent manner. The *in vivo* results were confirmed by these *in vitro* findings.

In conclusion, we identified the protective effect of MLB in hepatic I/R injury and a key mechanism underlying the hepatoprotective properties of MLB (**Figure 9**). Mechanistic studies suggested that MLB pretreatment could inhibit Jak2/Stat3 signaling pathway activation, which contributes to its liver-protective role in liver I/R injury. Collectively, these data support the conclusion that MLB pretreatment may be used as an alternative therapy for the prevention of liver I/R injury in clinical practice.

FIGURE 9 | The protective mechanism of MLB against hepatic I/R. The Jak2/Stat3 signaling pathway was activated when excessive proinflammation mediators were secreted, and then the inflammatory cytokines were further expressed. MLB could inhibit the activation of the Jak2/Stat3 signaling pathway and decrease the pro-inflammatory cytokines to reduce the hepatic I/R injury.

DATA AVAILABILITY STATEMENT

All datasets generated for this study are included in the manuscript and/or the supplementary files.

ETHICS STATEMENT

This study was carried out in accordance with the recommendations of Institutional Animal Care and Use Committee (IACUC), Shanghai Institute of Materia Medica (SIMM). The protocol was approved by the Institutional Animal Care and Use Committee (IACUC), Shanghai Institute of Materia Medica (SIMM).

AUTHOR CONTRIBUTIONS

NZ, LH, YX, GP, and QF conceived and designed the experiments. QD, ZW, HP, YZ, and LX assisted with the experiments. NZ wrote the paper. LH, YX, ZW, HP, LX, YZ, and GP critically revised the manuscript. All the authors read and reviewed the final manuscript.

SUPPLEMENTARY MATERIAL

The Supplementary Material for this article can be found online at: https://www.frontiersin.org/articles/10.3389/fphar.2019.00620/full#supplementary-material

REFERENCES

Aaronson, D. S., and Horvath, C. M. (2002). A road map for those who don't know JAK–STAT. *Science* 296 (5573), 1653–1655. doi: 10.1126/science.1071545

Arkadopoulos, N., Defterevos, G., Nastos, C., Papalois, A., Kalimeris, K., Papoutsidakis, N., et al. (2011). Development of a porcine model of post-hepatectomy liver failure. *J. Surg. Res.* 170 (2), e233–e242. doi: 10.1016/j.jss.2011.06.006

Banerjee, S., Biehl, A., Gadina, M., Hasni, S., and Schwartz, D. M. (2017). JAK–STAT signaling as a target for inflammatory and autoimmune diseases: current and future prospects. *Drugs* 77 (5), 521–546. doi: 10.1007/s40265-017-0701-9

Bousoik, E., and Montazeri Aliabadi, H. (2018). "Do we know jack" about JAK? A closer look at JAK/STAT signaling pathway. *Front. Oncol.* 8, 287. doi: 10.3389/fonc.2018.00287

Bu, Y., Lee, K., Jung, H. S., and Moon, S. K. (2013). Therapeutic effects of traditional herbal medicine on cerebral ischemia: a perspective of vascular protection. *Chin. J. Integr. Med.* 19 (11), 804–814. doi: 10.1007/s11655-013-1341-2

Bzeizi, K. I., Jalan, R., Plevris, J. N., and Hayes, P. C. (1997). Primary graft dysfunction after liver transplantation: from pathogenesis to prevention. *Liver Transpl. Surg.* 3 (2), 137–148. doi: 10.1002/lt.500030206

Cao, Z. Q., Quan, W., Hou, S. X., Guo, C., Ma, S. B., Zhang, W., et al. (2015). The natural therapeutic magnesium lithospermate B potently provides neuroprotective effects on cerebral ischemia/reperfusion injury in rats. *J. Ethnopharmacol.* 162, 191–198. doi: 10.1016/j.jep.2014.12.048

Castellaneta, A., Yoshida, O., Kimura, S., Yokota, S., Geller, D. A., Murase, N., et al. (2014). Plasmacytoid dendritic cell–derived IFN-alpha promotes murine liver ischemia/reperfusion injury by induction of hepatocyte IRF-1. *Hepatology* 60 (1), 267–277. doi: 10.1002/hep.27037

Chang, W. J., and Toledo-Pereyra, L. H. (2012). Toll-like receptor signaling in liver ischemia and reperfusion. *J. Invest. Surg.* 25 (4), 271–277. doi: 10.3109/08941939.2012.687802

Chen, P. J., Shang, A. Q., Yang, J. P., and Wang, W. W. (2019). microRNA-874 inhibition targeting STAT3 protects the heart from ischemia–reperfusion injury by attenuating cardiomyocyte apoptosis in a mouse model. *J. Cell. Physiol.* 234 (5), 6182–6193. doi: 10.1002/jcp.27398

Cheng, C. C., Yang, S. P., Lin, W. S., Ho, L. J., Lai, J. H., Cheng, S. M., et al. (2012). Magnesium lithospermate B mediates anti-inflammation targeting activator protein-1 and nuclear factor-kappa B signaling pathways in human peripheral T lymphocytes. *Int. Immunopharmacol.* 13 (3), 354–361. doi: 10.1016/j.intimp.2012.04.011

Clavien, P. A., Selzner, M., Rudiger, H. A., Graf, R., Kadry, Z., Rousson, V., et al. (2003). A prospective randomized study in 100 consecutive patients undergoing major liver resection with versus without ischemic preconditioning. *Ann. Surg.* 238 (6), 843–850; discussion 851-842. doi: 10.1097/01.sla.0000098620.27623.7d

Demiryilmaz, I., Turan, M. I., Kisaoglu, A., Gulapoglu, M., Yilmaz, I., and Suleyman, H. (2014). Protective effect of nimesulide against hepatic ischemia/reperfusion injury in rats: effects on oxidant/antioxidants, DNA mutation and COX-1/COX-2 levels. *Pharmacol. Rep.* 66 (4), 647–652. doi: 10.1016/j.pharep.2014.02.015

Douzinas, E. E., Livaditi, O., Tasoulis, M. K., Prigouris, P., Bakos, D., Goutas, N., et al. (2012). Nitrosative and oxidative stresses contribute to post-ischemic liver injury following severe hemorrhagic shock: the role of hypoxemic resuscitation. *PLoS One* 7 (3), e32968. doi: 10.1371/journal.pone.0032968

Du, C. S., Yang, R. F., Song, S. W., Wang, Y. P., Kang, J. H., Zhang, R., et al. (2010). Magnesium lithospermate B protects cardiomyocytes from ischemic injury *via* inhibition of TAB1-p38 apoptosis signaling. *Front. Pharmacol.* 1, 111. doi: 10.3389/fphar.2010.00111

Freitas, M. C., Uchida, Y., Zhao, D., Ke, B., Busuttil, R. W., and Kupiec-Weglinski, J. W. (2010). Blockade of Janus kinase-2 signaling ameliorates mouse liver damage due to ischemia and reperfusion. *Liver Transpl.* 16 (5), 600–610. doi: 10.1002/lt.22036

Ge, M., Yao, W., Yuan, D., Zhou, S., Chen, X., Zhang, Y., et al. (2017). Brg1-mediated Nrf2/HO-1 pathway activation alleviates hepatic ischemia–reperfusion injury. *Cell Death Dis.* 8 (6), e2841. doi: 10.1038/cddis.2017.236

Gendy, A. M., Abdallah, D. M., and El-Abhar, H. S. (2017). The potential curative effect of rebamipide in hepatic ischemia/reperfusion injury. *Naunyn. Schmiedebergs. Arch. Pharmacol.* 390 (7), 691–700. doi: 10.1007/s00210-017-1370-7

Guo, W. A. (2013). The search for a magic bullet to fight multiple organ failure secondary to ischemia/reperfusion injury and abdominal compartment syndrome. *J. Surg. Res.* 184 (2), 792–793. doi: 10.1016/j.jss.2012.06.024

Gurzov, E. N., Stanley, W. J., Pappas, E. G., Thomas, H. E., and Gough, D. J. (2016). The JAK/STAT pathway in obesity and diabetes. *FEBS J.* 283 (16), 3002–3015. doi: 10.1111/febs.13709

Ham, Y.-M., Ko, Y.-J., Song, S.-M., Kim, J., Kim, K.-N., Yun, J.-H., et al. (2015). Anti-inflammatory effect of litsenolide B2 isolated from *Litsea japonica* fruit *via* suppressing NF-κB and MAPK pathways in LPS-induced RAW264.7 cells. *J. Funct. Foods.* 13, 80–88. doi: 10.1016/j.jff.2014.12.031

Han, Y. F., Zhao, Y. B., Li, J., Li, L., Li, Y. G., Li, S. P., et al. (2018). Stat3–Atg5 signal axis inducing autophagy to alleviate hepatic ischemia–reperfusion injury. *J. Cell Biochem.* 119 (4), 3440–3450. doi: 10.1002/jcb.26516

Harari, O. A., and Liao, J. K. (2010). NF-kappaB and innate immunity in ischemic stroke. *Ann. N. Y. Acad. Sci.* 1207, 32–40. doi: 10.1111/j.1749-6632.2010.05735.x

Hsu, H. Y., and Wen, M. H. (2002). Lipopolysaccharide-mediated reactive oxygen species and signal transduction in the regulation of interleukin-1 gene expression. *J. Biol. Chem.* 277 (25), 22131–22139. doi: 10.1074/jbc.M111883200

Hu, G. Q., Du, X., Li, Y. J., Gao, X. Q., Chen, B. Q., and Yu, L. (2017). Inhibition of cerebral ischemia/reperfusion injury–induced apoptosis: nicotiflorin and JAK2/STAT3 pathway. *Neural Regen. Res.* 12 (1), 96–102. doi: 10.4103/1673-5374.198992

Huang, C., Wu, X., Wang, S., Wang, W., Guo, F., Chen, Y., et al. (2018). Combination of *Salvia miltiorrhiza* and ligustrazine attenuates bleomycin-induced pulmonary fibrosis in rats *via* modulating TNF-alpha and TGF-beta. *Chin. Med.* 13, 36. doi: 10.1186/s13020-018-0194-9

Ivashkiv, L. B., and Hu, X. (2003). The JAK/STAT pathway in rheumatoid arthritis: pathogenic or protective? *Arthritis Rheum.* 48 (8), 2092–2096. doi: 10.1002/art.11095

Ju, C., Colgan, S. P., and Eltzschig, H. K. (2016). Hypoxia-inducible factors as molecular targets for liver diseases. *J. Mol. Med. (Berl.)* 94 (6), 613–627. doi: 10.1007/s00109-016-1408-1

Kim, H. C., Kim, E., Bae, J. I., Lee, K. H., Jeon, Y. T., Hwang, J. W., et al. (2017). Sevoflurane postconditioning reduces apoptosis by activating the JAK–STAT pathway after transient global cerebral ischemia in rats. *J. Neurosurg. Anesthesiol.* 29 (1), 37–45. doi: 10.1097/ANA.0000000000000331

Lang, J. D., Jr., Smith, A. B., Brandon, A., Bradley, K. M., Liu, Y., Li, W., et al. (2014). A randomized clinical trial testing the anti-inflammatory effects of preemptive inhaled nitric oxide in human liver transplantation. *PLoS One* 9 (2), e86053. doi: 10.1371/journal.pone.0086053

Langdale, L. A., Hoagland, V., Benz, W., Riehle, K. J., Campbell, J. S., Liggitt, D. H., et al. (2008). Suppressor of cytokine signaling expression with increasing severity of murine hepatic ischemia–reperfusion injury. *J. Hepatol.* 49 (2), 198–206. doi: 10.1016/j.jhep.2008.03.014

Lawrence, T., Willoughby, D. A., and Gilroy, D. W. (2002). Anti-inflammatory lipid mediators and insights into the resolution of inflammation. *Nat. Rev. Immunol.* 2 (10), 787–795. doi: 10.1038/nri915

Li, J., Li, R. J., Lv, G. Y., and Liu, H. Q. (2015). The mechanisms and strategies to protect from hepatic ischemia–reperfusion injury. *Eur. Rev. Med. Pharmacol. Sci.* 19 (11), 2036–2047.

Li, M., Zhang, X., Wang, B., Xu, X., Wu, X., Guo, M., et al. (2018). Effect of JAK2/STAT3 signaling pathway on liver injury associated with severe acute pancreatitis in rats. *Exp. Ther. Med.* 16 (3), 2013–2021. doi: 10.3892/etm.2018.6433

Li, R., Hong, P., and Zheng, X. (2019). Beta-carotene attenuates lipopolysaccharide-induced inflammation *via* inhibition of the NF-kappaB, JAK2/STAT3 and JNK/p38 MAPK signaling pathways in macrophages. *Anim. Sci. J.* 90 (1), 140–148. doi: 10.1111/asj.13108

Lu, T. F., Yang, T. H., Zhong, C. P., Shen, C., Lin, W. W., Gu, G. X., et al. (2018). Dual effect of hepatic macrophages on liver ischemia and reperfusion injury during liver transplantation. *Immune Netw.* 18 (3), e24. doi: 10.4110/in.2018.18.e24

Luo, L. N., Xie, Q., Zhang, X. G., and Jiang, R. (2016). Osthole decreases renal ischemia–reperfusion injury by suppressing JAK2/STAT3 signaling activation. *Exp. Ther. Med.* 12 (4), 2009–2014. doi: 10.3892/etm.2016.3603

Ma, J., and Jin, G. (2019). Epidermal growth factor protects against myocardial ischemia reperfusion injury through activating Nrf2 signaling pathway. *Free Radic. Res.* 53(3), 313–323. doi: 10.1080/10715762.2019.1584399

Mascareno, E., El-Shafei, M., Maulik, N., Sato, M., Guo, Y., Das, D. K., et al. (2001). JAK/STAT signaling is associated with cardiac dysfunction during ischemia and reperfusion. *Circulation* 104 (3), 325–329. doi: 10.1161/01.CIR.104.3.325

Mihm, S. (2018). Danger-Associated Molecular Patterns (DAMPs): molecular triggers for sterile inflammation in the liver. *Int. J. Mol. Sci.* 19 (10), 3104. doi: 10.3390/ijms19103104

Murray, P. J. (2007). The JAK–STAT signaling pathway: input and output integration. *J. Immunol.* 178 (5), 2623–2629. doi: 10.4049/jimmunol.178.5.2623

Nakazato, P. C. G., Victorino, J. P., Fina, C. F., Mendes, K. D. S., Gomes, M. C. J., Evora, P. R. B., et al. (2018). Liver ischemia and reperfusion injury. Pathophysiology and new horizons in preconditioning and therapy. *Acta Cir. Bras.* 33 (8), 723–735. doi: 10.1590/s0102-865020180080000008

Okado-Matsumoto, A., and Fridovich, I. (2001). Subcellular distribution of superoxide dismutases (SOD) in rat liver: Cu,Zn–SOD in mitochondria. *J. Biol. Chem.* 276 (42), 38388–38393. doi: 10.1074/jbc.M105395200

Okugawa, S., Ota, Y., Kitazawa, T., Nakayama, K., Yanagimoto, S., Tsukada, K., et al. (2003). Janus kinase 2 is involved in lipopolysaccharide-induced activation of macrophages. *Am. J. Physiol. Cell Physiol.* 285 (2), C399–C408. doi: 10.1152/ajpcell.00026.2003

Paik, Y. H., Yoon, Y. J., Lee, H. C., Jung, M. K., Kang, S. H., Chung, S. I., et al. (2011). Antifibrotic effects of magnesium lithospermate B on hepatic stellate cells and thioacetamide-induced cirrhotic rats. *Exp. Mol. Med.* 43 (6), 341–349. doi: 10.3858/emm.2011.43.6.037

Pestka, J., and Zhou, H. R. (2006). Toll-like receptor priming sensitizes macrophages to proinflammatory cytokine gene induction by deoxynivalenol and other toxicants. *Toxicol. Sci.* 92 (2), 445–455. doi: 10.1093/toxsci/kfl012

Quan, W., Liu, F., Zhang, Y., Xie, C., Wu, B., Yin, J., et al. (2015). Antidepressant-like effects of magnesium lithospermate B in a rat model of chronic unpredictable stress. *Pharm. Biol.* 53 (8), 1168–1175. doi: 10.3109/13880209.2014.967783

Rahimifard, M., Maqbool, F., Moeini-Nodeh, S., Niaz, K., Abdollahi, M., Braidy, N., et al. (2017). Targeting the TLR4 signaling pathway by polyphenols: a novel therapeutic strategy for neuroinflammation. *Ageing Res. Rev.* 36, 11–19. doi: 10.1016/j.arr.2017.02.004

Robertson, F. P., Fuller, B. J., and Davidson, B. R. (2017). An evaluation of ischaemic preconditioning as a method of reducing ischaemia reperfusion injury in liver surgery and transplantation. *J. Clin. Med.* 6 (7), 69. doi: 10.3390/jcm6070069

Rong, Y. P., Huang, H. T., Liu, J. S., and Wei, L. (2017). Protective effects of geniposide on hepatic ischemia/reperfusion injury. *Transplant. Proc.* 49 (6), 1455–1460. doi: 10.1016/j.transproceed.2017.02.063

Roskoski, R., Jr. (2016). Janus kinase (JAK) inhibitors in the treatment of inflammatory and neoplastic diseases. *Pharmacol. Res.* 111, 784–803. doi: 10.1016/j.phrs.2016.07.038

Schemmer, P., Golling, M., Kraus, T., Mayatepek, E., Herfarth, C., and Klar, E. (2001). Glycine reduces reperfusion injury in human liver transplantation: our first patients. *Transplant. Proc.* 33 (7–8), 3750–3752. doi: 10.1016/S0041-1345(01)02588-X

Si, Y. N., Bao, H. G., Xu, L., Wang, X. L., Shen, Y., Wang, J. S., et al. (2014). Dexmedetomidine protects against ischemia/reperfusion injury in rat kidney. *Eur. Rev. Med. Pharmacol. Sci.* 18 (13), 1843–1851. doi: 10.4314/tjpr.v13i7.24

Tai, Y., Qiu, Y., and Bao, Z. (2018). Magnesium lithospermate B suppresses lipopolysaccharide-induced neuroinflammation in BV2 microglial cells and attenuates neurodegeneration in lipopolysaccharide-injected mice. *J. Mol. Neurosci.* 64 (1), 80–92. doi: 10.1007/s12031-017-1007-9

Triantafyllou, E., Woollard, K. J., Mcphail, M. J. W., Antoniades, C. G., and Possamai, L. A. (2018). The role of monocytes and macrophages in acute and acute-on-chronic liver failure. *Front. Immunol.* 9, 2948. doi: 10.3389/fimmu.2018.02948

Van Golen, R. F., Reiniers, M. J., Olthof, P. B., Van Gulik, T. M., and Heger, M. (2013). Sterile inflammation in hepatic ischemia/reperfusion injury: present concepts and potential therapeutics. *J. Gastroenterol. Hepatol.* 28 (3), 394–400. doi: 10.1111/jgh.12072

Van Golen, R. F., Van Gulik, T. M., and Heger, M. (2012). The sterile immune response during hepatic ischemia/reperfusion. *Cytokine Growth Factor Rev.* 23 (3), 69–84. doi: 10.1016/j.cytogfr.2012.04.006

Walsh, K. B., Toledo, A. H., Rivera-Chavez, F. A., Lopez-Neblina, F., and Toledo-Pereyra, L. H. (2009). Inflammatory mediators of liver ischemia–reperfusion injury. *Exp. Clin. Transplant.* 7 (2), 78–93. doi: 10.1097/MOT.0b013e32832b2f6c

Wang, P. F., Xiong, X. Y., Chen, J., Wang, Y. C., Duan, W., and Yang, Q. W. (2015a). Function and mechanism of toll-like receptors in cerebral ischemic tolerance: from preconditioning to treatment. *J. Neuroinflamm.* 12, 80. doi: 10.1186/s12974-015-0301-0

Wang, Y., Liu, Z. S., Zhang, S. L., Diao, Q. X., and Ge, Y. J. (2015b). Effect and mechanism of portal blood stasis removal on intestinal endotoxemia and hepatic ischemia reperfusion injury. *Transplant. Proc.* 47 (9), 2752–2756. doi: 10.1016/j.transproceed.2015.09.039

Wu, W. Y., and Wang, Y. P. (2012). Pharmacological actions and therapeutic applications of *Salvia miltiorrhiza* depside salt and its active components. *Acta Pharmacol. Sin.* 33 (9), 1119–1130. doi: 10.1038/aps.2012.126

Xiong, L., Yu, K. H., and Zhen, S. Q. (2018). MiR-93 blocks STAT3 to alleviate hepatic injury after ischemia–reperfusion. *Eur. Rev. Med. Pharmacol. Sci.* 22 (16), 5295–5304. doi: 10.26355/eurrev_201808_15729

Yao, J., Zheng, J., Cai, J., Zeng, K., Zhou, C., Zhang, J., et al. (2019). Extracellular vesicles derived from human umbilical cord mesenchymal stem cells alleviate rat hepatic ischemia–reperfusion injury by suppressing oxidative stress and

neutrophil inflammatory response. *FASEB J.* 33 (2), 1695–1710. doi: 10.1096/fj.201800131RR

Yun, K. J., Kim, J. Y., Kim, J. B., Lee, K. W., Jeong, S. Y., Park, H. J., et al. (2008). Inhibition of LPS-induced NO and PGE2 production by asiatic acid *via* NF-kappa B inactivation in RAW 264.7 macrophages: possible involvement of the IKK and MAPK pathways. *Int. Immunopharmacol.* 8 (3), 431–441. doi: 10.1016/j.intimp.2007.11.003

Zhai, Y., Petrowsky, H., Hong, J. C., Busuttil, R. W., and Kupiec-Weglinski, J. W. (2013). Ischaemia–reperfusion injury in liver transplantation—from bench to bedside. *Nat. Rev. Gastroenterol. Hepatol.* 10 (2), 79–89. doi: 10.1038/nrgastro.2012.225

Zhang, H., Liu, Y., Wang, L. K., and Wei, N. (2017). Pyrrolidine dithiocarbamate alleviates the anti-tuberculosis drug–induced liver injury through JAK2/STAT3 signaling pathway: an experimental study. *Asian Pac. J. Trop. Med.* 10 (5), 520–523. doi: 10.1016/j.apjtm.2017.05.010

Zhang, X. J., Cheng, X., Yan, Z. Z., Fang, J., Wang, X., Wang, W., et al. (2018). An ALOX12–12-HETE–GPR31 signaling axis is a key mediator of hepatic ischemia–reperfusion injury. *Nat. Med.* 24 (1), 73–83. doi: 10.1038/nm.4451

Zhao, H., Chen, Z., Xie, L. J., and Liu, G. F. (2018). Suppression of TLR4/NF-kappaB signaling pathway improves cerebral ischemia–reperfusion injury in rats. *Mol. Neurobiol.* 55 (5), 4311–4319. doi: 10.1007/s12035-017-0552-0

Zhao, Y. R., Wang, D., Liu, Y., Shan, L., and Zhou, J. L. (2016). The PI3K/Akt, p38MAPK, and JAK2/STAT3 signaling pathways mediate the protection of

SO2 against acute lung injury induced by limb ischemia/reperfusion in rats. *J. Physiol. Sci.* 66 (3), 229–239. doi: 10.1007/s12576-015-0418-z

Zhou, G. Y., Yi, Y. X., Jin, L. X., Lin, W., Fang, P. P., Lin, X. Z., et al. (2016). The protective effect of juglanin on fructose-induced hepatitis by inhibiting inflammation and apoptosis through TLR4 and JAK2/STAT3 signaling pathways in fructose-fed rats. *Biomed. Pharmacother.* 81, 318–328. doi: 10.1016/j.biopha.2016.04.013

Zhou, L., Zuo, Z., and Chow, M. S. (2005). Danshen: an overview of its chemistry, pharmacology, pharmacokinetics, and clinical use. *J. Clin. Pharmacol.* 45 (12), 1345–1359. doi: 10.1177/0091270005282630

Zhu Jinqiang, Y. C., and Kang, L. (2010). Research progress on the stability and degradation mechanism of salvianolic acid B. *Chin. J. Tradit. Chin. Med.* 17 (12), 113–115. doi: 10.3969/j.issn.1005-5304.2010.12.060

Check for
updates

Emodin Induced SREBP1-Dependent and SREBP1-Independent Apoptosis in Hepatocellular Carcinoma Cells

Nian Yang[1,2,3], Chen Li[1,2], Hongliang Li[1,2], Ming Liu[1,2], Xiaojun Cai[1], Fengjun Cao[1]*, Yibin Feng[4], Minglun Li[5] and Xuanbin Wang[1,2]*

[1] Laboratory of Chinese Herbal Pharmacology, Oncology Center, Renmin Hospital, Hubei University of Medicine, Shiyan, China, [2] Hubei Key Laboratory of Wudang Local Chinese Medicine Research, Biomedical Research Institute, Hubei University of Medicine, Shiyan, China, [3] Department of Pharmacy, Jurong Hospital Affiliated to Jiangsu University, Zhenjiang, China, [4] School of Chinese Medicine, The University of Hong Kong, Hong Kong, China, [5] Department of Radiation Oncology, University Hospital, LMU, Munich, Germany

Reynoutria multiflora (Thunb.) Moldenke (He Shou Wu) has been used for about 20 centuries as a Chinese medicinal herb for its activities of anticancer, anti-hyperlipidemia, and anti-aging. Previously, we found that He Shou Wu ethanol extract could induce apoptosis in hepatocellular carcinoma cells, and we also screened its active components. In this study, we investigated whether lowering lipid metabolism of emodin, a main active component in He Shou Wu, was associated with inhibitory effects in hepatocellular carcinoma cells. The correlation of apoptosis induction and lipid metabolism was investigated. The intrinsic apoptotic cell death, lipid production, and their signaling pathways were investigated in emodin-treated human hepatocellular carcinoma cells Bel-7402. The data showed that emodin triggered apoptosis in Bel-7402 cells. The mitochondrial membrane potential ($\Delta\Psi$m) was reduced in emodin-treated Bel-7402 cells. We also found that emodin activated the expression of intrinsic apoptosis signaling pathway-related proteins, cleaved-caspase 9 and 3, Apaf 1, cytochrome c (CYTC), apoptosis-inducing factor, endonuclease G, Bax, and Bcl-2. Furthermore, the level of triglycerides and desaturation of fatty acids was reduced in Bel-7402 cells when exposed to emodin. Furthermore, the expression level of messenger RNA (mRNA) and protein of sterol regulatory element binding protein 1 (SREBP1) as well as its downstream signaling pathway and the synthesis and the desaturation of fatty acid metabolism-associated proteins (adenosine triphosphate citrate lyase, acetyl-CoA carboxylase alpha, fatty acid synthase (FASN), and stearoyl-CoA desaturase D) were also decreased. Notably, knock-out of *SREBP1* in Bel-7402 cells was also found to induce less intrinsic apoptosis than did emodin. In conclusion, these results indicated that emodin could induce apoptosis in an SREBP1-dependent and SREBP1-independent manner in hepatocellular carcinoma cells.

Keywords: emodin, lipid metabolism, SREBP1, intrinsic apoptosis, hepatocellular carcinoma cells

INTRODUCTION

Reynoutria multiflora (Thunb.) Moldenke, a type of Chinese medicine and a Taoist medicine, was named as Maganshi (马肝石) in the era of Eastern Han Dynasty (25–220 AD) and after a long-lived man in Tang Dynasty (618–907 AD), He Shou Wu (何首乌), in the legend of Chinese Medical Work, Compendium of Materia Medica (本草纲目) (Li, 2016). In Chinese folk medicine philosophy, the root of He Shou Wu tonifies the liver and kidney, boosts essence blood, blackens the beard and hair, strengthens sinew and bone, transforms turbidity, and reduces lipid levels, which acts to protect the liver, bone, sexual and reproductive functions, improve memory and intelligence, and promote antiaging, lipid lowering, and anticancer qualities (Chen, 2017). Taoists preferred it because of its antiaging effects (Shang, 2004). He Shou Wu consisted of 2,3,5,4'-tetrahydroxystilbene-2-O-β-D-glucoside, anthraquinones (Lin et al., 2015; Li H. et al., 2016) and other active compounds. We previously found that the ethanol extract of processed He Shou Wu (HSWE) induces apoptosis and inhibits lipogenesis in human hepatocellular carcinoma (HCC) cells by inhibiting sterol regulatory element binding protein 1 (SREBP1).

A growing body of evidence suggested that many human cancers emerge as alterations in lipid metabolism and *de novo* lipogenesis was essential for tumor growth, survival, and resistance to therapies. Increased SREBP-1 and lipogenic enzymes transcriptionally activated by SREBP1 have been found in tumor patients (Huang et al., 2012; Pandey et al., 2013; Li et al., 2014). SREBP1 regulates the expression of genes associated with fatty acid synthesis (Edwards et al., 2000; Moon et al., 2001). When intracellular unsaturated fatty acids or sterols are depleted, concomitant cleavage in the Golgi bodies by two site-specific proteases occurs, and the mature form of the N-terminal protein (mSREBP1) is released and enters the nucleus to activate transcription of target genes such as ACLY, ACACA, FASN, and SCD (Zhao et al., 2014) with sterol regulatory element sequences in their promoters (Horton, 2002). In the pathway of fatty acid metabolism, ACLY, ACACA, and FASN are the key enzymes in the synthesis of fatty acids. ACLY converts mitochondrial citric acid to oxaloacetate and acetyl-CoA, the precursor for fatty acid synthesis. Next, ACACA carboxylates acetyl-CoA to form malonyl-CoA, a substrate for fatty acid synthesis. In turn, FASN catalyzes successive condensation polymerizations to form a fatty acid from malonyl-CoA and acetyl-CoA substrates, generating mainly long-chain fatty acid palmitic acid (Currie et al., 2013). It has been reported that specific blocking of the FASN expression led to an accumulation of malonyl-CoA, resulting in apoptosis induction (Bandyopadhyay et al., 2006). Regarding fatty acid desaturation, SCD is a subtype of the Δ9 fatty acid desaturation-limiting enzyme family that can catalyze saturated fatty acids (SFAs, including palmitic acid and stearic acid) to form monounsaturated fatty acids (MUFAs, including palmitoleic acid and oleic acid) (Mele et al., 2007; Angelucci et al., 2015). SFAs and MUFAs are the basic elements of membrane phospholipids (Evans et al., 2009). Once the expression of SCD is inhibited, it can result in the imbalance between mitochondrial SFAs and MUFAs, leading to apoptosis (Lewis et al., 2015). Therefore, SREBP1-targeted therapy is expected to be an effective strategy for the treatment of metabolic syndrome

and cancer (Guo et al., 2014; Soyal et al., 2015). HSWE inhibited mRNA and protein expression of stearoyl-CoA desaturase (SCD) by blocking its upstream factor SREBP1, inducing a decrease of ratio of SFA and MUFAs, which led to an increased level of reactive oxygen species (ROS), alanine aminotransferase (ALT), and aspartate aminotransferase (AST)and apoptosis, finally (Li J. et al., 2016; Li et al., 2018). We then screened the bioactive components in HSWE and found that emodin (1,3,8-trihydroxy-6-methyl-anthraquinone), a natural anthraquinone derivative, was the major bioactive component (Yang et al., 2018). Studies showed that emodin possessed numerous functions that included arresting cell cycle by blocking cyclin D, cyclin E (Wang et al., 2015), and CDK2 (Zhang et al., 2015); inducing apoptosis by upregulating extrinsic apoptotic fas ligand (FASL) signaling (Li et al., 2014); activating intrinsic apoptotic factors, Cyto c, Caspase-9, and apoptosis-inducing factor (AIF) (Ma et al., 2012); declining the mitochondrial membrane potential (ΔΨm) (Liu et al., 2012); inhibiting migration and invasion by downregulating transforming growth factor-β (TGF-β) (Thacker and Karunagaran, 2015) and Wnt/beta-Catenin signaling pathway (Gu et al., 2019); reversing multidrug resistance by downregulating multidrug resistance-associated protein 1 (MRP1) (Ma et al., 2014), and restricting energy metabolism by inhibiting fatty acid synthase (Lee et al., 2017) in cancers. Moreover, emodin induces both extrinsic and intrinsic apoptosis (Cui et al., 2016). However, it remains unclear whether a decrease in lipids is associated with cancer treatment. However, the underlying mechanism of lipid metabolism regulation and apoptosis induction *via* emodin in HCC cells remains unknown.

In this study, we concentrated on the capacities of emodin on restricting lipid metabolism and inducing apoptosis in HCC cells to broaden insight in the mechanisms of He Shou Wu in preventing and treating cancer.

MATERIALS AND METHODS

Chemicals and Reagents

Emodin (purity: 95.0%) was purchased from Topscience (Shanghai, China). RPMI-1640 was used as the culture medium and was purchased from Gibco (Gaithersburg, MD, USA). Neonatal bovine serum (NBS) was obtained from Tianhang (Hangzhou, China). PE Annexin V-7AAD apoptosis detection kit was supplied by BD Biosciences (San Jose, CA, USA). JC-10 mitochondrial membrane potential kit was purchased from Solarbio (Beijing, China). Triglyceride (TG) Assay Kit was supplied by Jiancheng Bioengineering Institute (Nanjing, China). Oleic acid, stearic acid, palmitoleic acid, and palmitic acid were obtained from Sigma-Aldrich (St. Louis, MO, USA). Primary antibodies glyceraldehyde 3-phosphate dehydrogenase (GAPDH, 60004-1-Ig, mouse monoclonal, 1:10,000), adenosine triphosphate citrate lyase (ACLY, 15421-1-AP, rabbit polycolonal, 1:1,000), acetyl-CoA carboxylase alpha (ACACA, 21923-1-AP, rabbit polycolonal, 1:500), fatty acid synthase (FASN, 10624-2-AP, rabbit polycolonal, 1:500), SCD (23393-1-AP, rabbit polycolonal, 1:500), B-cell lymphoma-2 (Bcl-2, 60178-1-Ig, mouse monoclonal, 1:1,000), Bcl-2-associated X (Bax, 50599-2-Ig, rabbit polycolonal, 1:2,000), AIF (17984-1-AP, rabbit

polocolonal, 1:4,000), endonuclease G (ENDOG) (22148-1-AP, rabbit polocolonal, 1:1,000), Cytochrome c (CYTC, 66264-1-Ig, mouse monoclonal, 1:5,000), and APAF1 (21710-1-AP, rabbit polocolonal, 1:500) were purchased from Proteintech Group (Wuhan, China). Primary antibodies SREBP1 (NB600-582, mouse monoclonal, 1:1,000) were obtained from Novus (Littleton, CO, USA). Primary antibodies for caspase-3 (9662, rabbit polocolonal, 1:1,000), cleaved-caspase-3 (9661, rabbit polocolonal, 1:1,000), caspase-9 (9502, rabbit polocolonal, 1:1,000) and cleaved-caspase-9 (9501, rabbit polocolonal, 1:1,000) as well as secondary antibodies were supplied by Cell Signaling Technology (Danvers, MA, USA).

Establishment of SREBP1 Overexpression and Knockout HCC Cell Lines

To construct lentiCRISPRv2/SREBP1-knockout (KO) recombinant plasmid, the sgRNAs targeting SREBP1 were designed according to CRISPR DESIGN (http://crispr.mit.edu/), and the CRISPR KO plasmids were constructed according to ZhangLab' instructions (Sanjana et al., 2014; Shalem et al., 2014). To generate the SREBP1 overexpression (OE) vector, a fragment containing the complete SREBP1 open reading frame was released from the recombinant plasmid pHAGE-CMV-MCS-IZsGreen/SREBP1 OE by digestion with restriction enzymes XhoI and BamHI. Next, the two recombinant plasmids were confirmed by enzyme analysis and DNA sequencing. To obtain the single cell of SREBP1 KO and SREBP1 OE clones, Bel-7402 cells were respectively transfected with two recombinant plasmid according to Lipofectamine™ 3000 (Invitrogen, Carlsbad, CA, USA) instructions. Stable transfectants of SREBP1 KO were screened using puromycin (5.5 μg/mL) for a 3- to 4-day period of selection, and SREBP1 OE was screened by green fluorescence of recombinant plasmid. Next, the two stable transfected cell lines were confirmed by polymerase chain reaction (PCR) and Western blotting analysis. T7 endonuclease 1 (T7E1) assayed SREBP1 KO cell lines additionally (**Figure 1**).

Cell Culture and Drug Treatment

The HCC cells Bel-7402 (stored in our laboratory) were cultured in RPMI-1640 supplemented with 10% NBS in a humidified incubator (5% CO_2 and 37°C). The stock solutions of emodin (100 mmol/L) dissolved in dimethyl sulfoxide (DMSO) were diluted to different concentrations as needed.

MTT Assay

To assess the inhibitory effects of emodin on Bel-7402 cells, cell viability was evaluated by MTT (3-(4,5-dimethylthiazol-2-yl)-2,5 diphenyltetrazolium bromide) assay. Briefly, exponentially growing cells (7 × 10³ cells per well) were seeded 24 h prior to treatment into 96-well plates. After treatment with emodin (0, 25, 50, 100, 200, 400, and 600 μmol/L) for 12, 24, and 48 h, cell proliferation was performed by adding 10 μL of MTT solution (5 mg/mL) to each well, and plates were then incubated for 4 h. After dissolving the purple formazan crystals, 150 μL DMSO was added to each well at 37°C for 5 min. The absorbance values at

490 nm were read using a Microplate Reader (BioTek, Winooski, VT, USA).

PE Annexin V-7AAD Assay

To investigate the apoptosis in emodin-treated Bel-7402 cells, PE Annexin V-7AAD double staining was used, and the apoptosis was assessed using flow cytometry. Briefly, cells (1 × 10⁶ cells per well) were seeded into six-well plates, incubated at 37°C overnight. After treatments with emodin for 24 h, the cells were harvested and washed twice with cold phosphate buffered saline (PBS). Then, the cells were resuspended in Annexin-V binding buffer and stained with PE Annexin V and 7-AAD according to the manufacturer's protocol. The fluorescence intensity was examined using a flow cytometer (Beckman, Brea, CA, USA). Onset of early and late apoptosis was determined using Annexin-V, whereas 7AAD was used for testing necrosis and late apoptosis.

JC-10 Assay

JC-10 is a fluorescent probe, and it exists as a red fluorescent dimer under a high mitochondrial potential (ΔΨm). However, under a low ΔΨm, e.g., a condition of mitochondrial injury, it converts into monomeric form and stains cells green. Thus a ratio of red/green JC-10 fluorescence can be used to indicate the change of ΔΨm. A high ratio of red/green JC-10 fluorescence indicates a higher ΔΨm, whereas a low ratio of red/green JC-10 fluorescence means a lower ΔΨm. To analyze the mitochondrial injury by emodin, the ΔΨm was detected using JC-10 assay. Briefly, cells were cultured in 6-well plates at a density of 4 × 10⁵/well and incubated at 37°C overnight. After treatments with emodin for 24 h, the culture medium was removed and the cells were washed twice with PBS. Then, cells were loaded with 1 mL JC-10 water solution (0.5%, v/v) according to the manufacturer's protocol. JC-10 fluorescence was measured *via* fluorescent microscopy (Olympus, Tokyo, Japan).

TG Assay

To analyze the alterations of fatty acids contents by emodin, the level of TG was measured. Briefly, cells (1 × 10⁶ cells per well) were seeded 24 h prior to treatment into 6-well plates. After treatments with emodin for 24 h, the cells were collected and washed twice with PBS. Then, resuspended cells were lysed using 100 μL Triton X-100 (2%). The samples were measured according to the manufacturer's protocol. Results were normalized to total protein content as determined by the bicinchoninic acid (BCA) assay.

Fatty Acids Assay

To evaluate the lipid metabolism changes, the production ratio of oleic acid/stearic acid and palmitoleic acid/palmitic acid was measured using ultra-performance liquid chromatography-mass spectrometry (UPLC-MS) assay (Waters Corporation, Milford, MA, USA). Briefly, cells (1 × 10⁶ cells per well) were seeded 24 h prior to treatment into six-well plates. After treatment with emodin for 24 h, the cells were harvested and washed twice with PBS. Then, fatty acids were extracted and measured
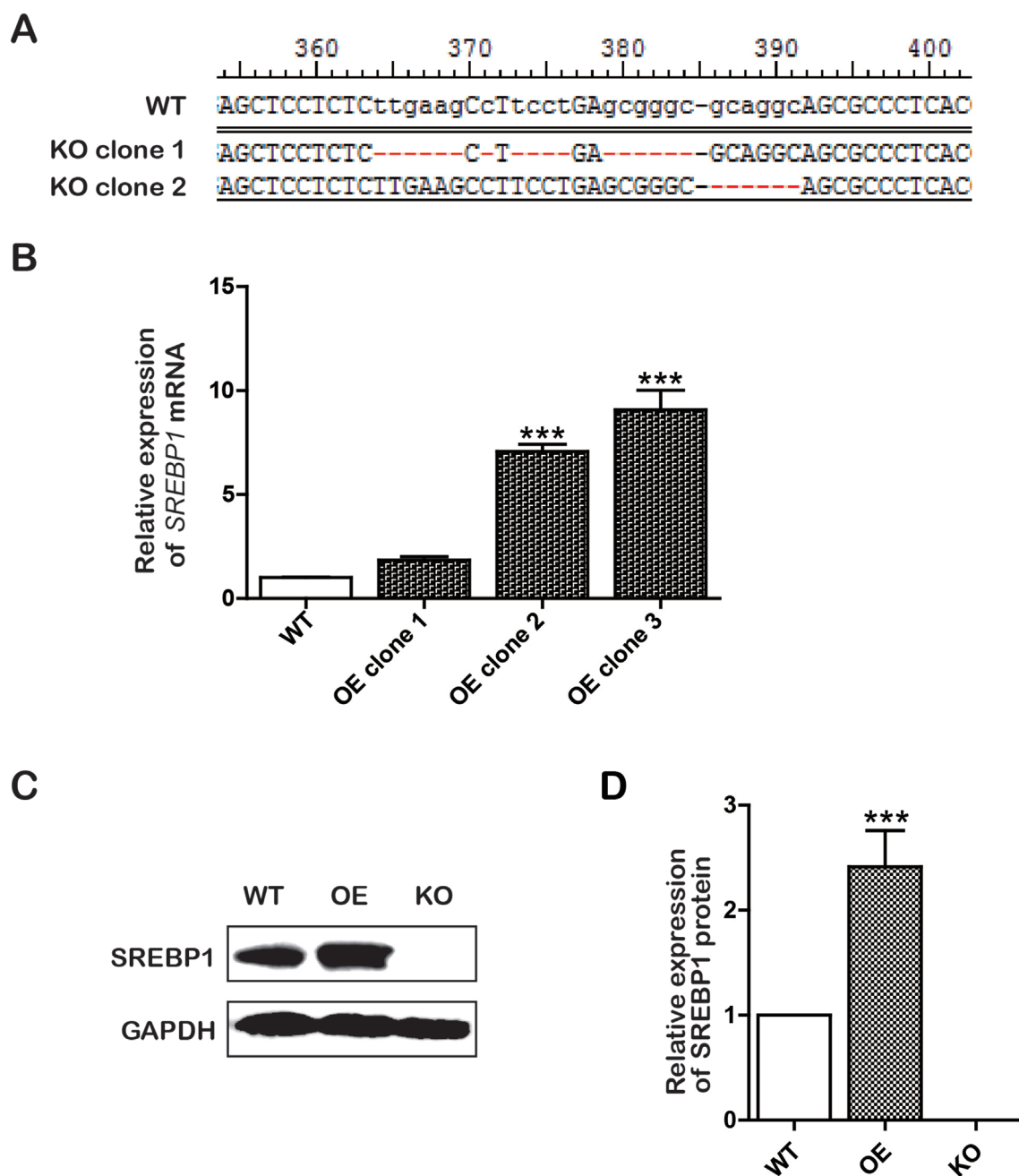
FIGURE 1 | Construction of knockout (KO) and overexpression (OE) cell lines. **(A)** The sequencing results of KO positive clone cells; **(B)** The messenger RNA (mRNA) level of *SREBP1* in wild type (WT) and OE Bel-7402 cells. Data were expressed as mean ± standard error of the mean. ***$P < 0.001$ vs. WT group; **(C** and **D)** The protein level of SREBP1 in WT, OE, and KO Bel-7402 cells. Data were expressed as mean ± standard error of the mean. ***$P < 0.001$ vs. WT group.

using UPLC-MS assay as mentioned in the previous report (Li et al., 2018). Results were normalized to total protein content as determined using the BCA assay.

Real-Time Quantitative Polymerase Chain Reaction

To observe the inhibitory effects of emodin on the lipid metabolism-associated genes, the mRNA expressions were detected by the

real-time quantitative polymerase chain reaction (RT-qPCR) assay. Total RNA from the cells was isolated using Trizol Reagent (Invitrogen, Carlsbad, CA, USA) and converted into complementary DNA (cDNA) *via* reverse transcription using the ReverTra Ace qPCR RT Kit (TOYOBO, Osaka, Japan) as instructed in the supplier's protocol. Then, RT-qPCR analysis was performed using SYBR™ Green qPCR supermix-UDG with ROX in a Quantitative PCR System (Applied Biosystems, Foster, CA, USA). Primers used in the RT-qPCR assay are listed in **Table 1**. The following cycling

TABLE 1 | List of primers used in the study.

Gene	Primer sequence (5'→3')	Product (bp)
SREBP1	Forward 5'-ACACAGCAACCAGAAACTCAAG-3'	153
	Reverse 5'-AGTGTGTCCTCCACCTCAGTCT-3'	
ACLY	Forward 5'-GACCTATGACTATGCCAAGACTAT-3'	88
	Reverse 5'-GATGCTGCCTCCAATGATGA-3'	
ACACA	Forward 5'-AATAGCGTCTCTAACTTCCTTCAC-3'	200
	Reverse 5'-CCGTCACTCAGCCGATGTA-3'	
FASN	Forward 5'-GGACATGGCTTAGAAGTGGAA-3'	164
	Reverse 5'-TTGGTGTTGCTGGTGAGTG-3'	
SCD	Forward 5'-GCGATATGCTGTGGTGCTTA-3'	153
	Reverse 5'-GAGTGGTGGTAGTTGTGGAAG-3'	
β-actin	Forward 5'-TCGTGCGTGACATTAAGGAG-3'	176
	Reverse 5'-GAAGGAAGGCTGGAAGAGTG-3'	

SREBP1, sterol regulatory element binding protein 1; ACACA, acetyl-CoA carboxylase alpha; ACLY, ATP citrate lyase; FASN, fatty acid synthase; SCD, stearoyl-coenzyme A desaturase.

conditions were used: 10 min at 95°C, and 40 cycles of 15 s at 95°C and 1 min at 60°C. Relative expression was statistically evaluated by the $2^{-\Delta\Delta Ct}$ method with normalization against β-actin.

Western Blotting Assay

To assess the effects of lipid metabolism and apoptosis-associated proteins by emodin, the expression of proteins was detected by Western blotting. After planned treatments, cells were collected and lysed in radio immunoprecipitation assay (RIPA) buffer [1% Triton X-100, 1% deoxycholate, 0.1% sodium dodecyl sulfate (SDS)]. Equal amounts of total proteins were separated by appropriate SDS-polyacrylamide gel electrophoresis (SDS-PAGE) followed by transferring to polyvinylidene difluoride (PVDF) membranes. After blocking with 5% bovine serum albumin, the membrane was incubated with specific primary antibodies and the corresponding second antibodies, respectively. The specific protein bands were visualized with Millipore enhanced chemiluminescence kit and imaged using ChemiDocTM XRS+ Molecular Imager (Bio-Rad, Hercules, CA, USA).

Statistical Analysis

All experiments were performed separately at least three times. The significance of intergroup differences was evaluated by one-way analysis of variance using the GraphPad Prism 5.0 software (GraphPad Software, La Jolla, CA, USA). Values of $P < 0.05$ were considered as significant.

RESULTS

Emodin Inhibited Cell Proliferation and Induced Intrinsic Apoptosis in Bel-7402 Cells

Emodin is a natural anthraquinone derivative ($C_{15}H_{10}O_5$). Its chemical structure is shown in **Figure 2A**. To determine the antiproliferative effect of emodin in HCC cells, the HCC cells Bel-7402 were incubated with emodin in different concentrations for 12, 24, and 48 h, and cell viabilities were then examined using

the MTT assay. We found that emodin profoundly reduced cell viability in a dose-dependent and time-dependent manner in Bel-7402 cells (**Figure 2B**). Thus, we selected the concentration of 100 μmol/L and 24-h incubation for further experiments.

We further investigated the emodin-induced apoptosis using PE Annexin V-7AAD apoptosis detection kit. The results of flow cytometric analysis showed that 24 h treatment with emodin (100 μmol/L) significantly increased the apoptosis as compared to the control group (72.72% *vs,* 11.84% (**Figure 2C**). Previous studies have shown that apoptosis induced by anticancer drugs involved two major signal pathways: the mitochondria-mediated intrinsic apoptosis pathway and the death receptor-mediated extrinsic apoptosis pathway (Galluzzi et al., 2012). Thus, we speculated that emodin had induced apoptosis *via* the intrinsic pathway. For validation, we investigated the alterations of ΔΨm in emodin-treated Bel-7402 cells. We found that ΔΨm was diminished in Bel-7402 cells when exposed to emodin (**Figure 2D**). Furthermore, we found that emodin upregulated the expressions of Bax and downregulated the expression of Bcl-2 (**Figure 2F** and **G**). These results also approved the intrinsic pathway of emodin-induced apoptosis in Bel-7402 cells.

Because the intrinsic apoptotic pathway is divided into caspase-dependent and caspase-independent pathways (Galluzzi et al., 2012), we performed Western blotting to further clarify the apoptotic pathway induced by emodin and found an upregulation of caspase-independent-associated proteins (AIF and ENDOG). Interestingly, emodin also increased the expression of caspase-dependent-associated proteins (CYTC, APAF1, cleaved-caspase-9, and cleaved-caspase-3) (**Figure 2F** and **G**). Our results suggested that emodin induced both caspase-dependent and caspase-independent intrinsic apoptosis in Bel-7402 cells.

Emodin Decreased Lipid Metabolism in Bel-7402 Cells

It has been reported that intrinsic apoptosis results from a bioenergetics and metabolic catastrophe coupled to multiple active executioner mechanisms. We then attempted to observe the effects of emodin on fatty acid metabolism. To determine the effect of emodin on *de novo* lipogenesis in Bel-7402 cells, we first examined the level of TG in Bel-7402 cells. Our data indicated that emodin decreased production of TG (**Figure 3A**). However, fatty acid metabolism includes the synthesis and desaturation of fatty acid. We presumed that emodin could alter the cellular lipid composition by restricting lipid desaturation. We therefore assessed the effect of emodin on cellular lipid composition by UPLC-MS. It should be mentioned that the UPLC-MS method employed here does not permit the definition of positional isomers. By doing so, we observed marked augments in the percentage of SFAs within MUFAs in emodin-treated cells. Likewise, we also found that the corresponding increase in palmitic acid and stearic acid and the reductions in palmitoleic acid and oleic acid (**Figure 3B**). These results emerged as alterations of cellular lipid composition by blocking lipid desaturation in emodin-treated Bel-7402 cells. To illuminate the molecular mechanisms by which emodin regulated the synthesis and desaturation of fatty acids, we assessed the expression of some lipid metabolism associated-genes involved in this process. Data showed that the mRNA expression of *SREBP1*
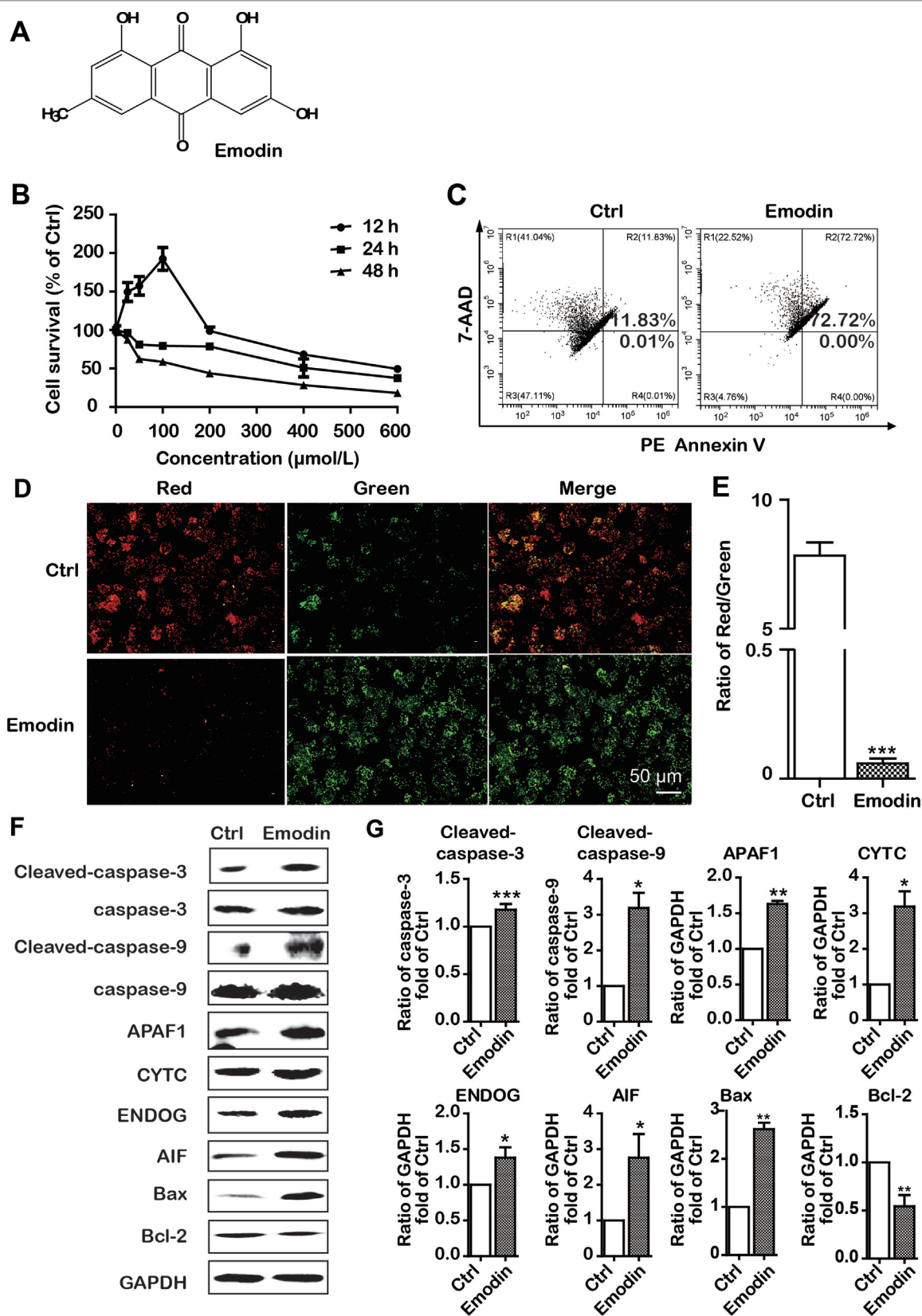
FIGURE 2 | Continued

FIGURE 2 | Emodin inhibited cell proliferation and induced intrinsic apoptosis in Bel-7402 cells. **(A)** The chemical structure of emodin. **(B)** Bel-7402 cell viability after treatment with emodin determined by the MTT assay. **(C)** Apoptosis in emodin-treated Bel-7402 cells as assessed by flow cytometry. **(D** and **E)** The fluorescence images with JC-10 staining in Bel-7402 cells. Bel-7402 cells were exposed to emodin (100 µmol/L) for 24 h followed by 30-min incubation with JC-10. When the mitochondrial membrane potential (ΔΨm) was higher, the JC-10 accumulated in the mitochondria matrix to form the polymer producing red fluorescence; otherwise, the green fluorescence from the JC-10 monomers was used to represent the cells that lost ΔΨm. Quantitative data of the ratio of red and green fluorescence intensity were measured. **(F** and **G)** Expression level of intrinsic apoptosis-associated proteins was measured after emodin treatment by Western blotting analysis. Data were expressed as mean ± standard error of the mean. $*P < 0.05$, $**P < 0.01$, and $***P < 0.001$ *vs.* ctrl group (0 µmol/L), respectively.

was significantly downregulated in Bel-7402 cells after treatment with emodin (**Figure 3C**). To strengthen this evidence, we analyzed the expression of the key enzymes of fatty acid synthesis and desaturation that are regulated by SREBP1, including ACLY, ACACA, FASN, and SCD. Emodin dramatically attenuated the mRNA expression of *ACLY, ACACA, FASN,* and *SCD* in Bel-7402 cells (**Figure 3C**). These results were concordant with that of decreased protein levels of SREBP1, ACLY, ACACA FASN, and SCD in emodin-treated Bel-7402 cells (**Figure 3D**), indicating that emodin decreased lipid metabolism in Bel-7402 cells.

SREBP1 Played a Pivotal Role in Maintaining Lipid Metabolism and Partially Avoiding Intrinsic Apoptosis in Bel-7402 Cells

Based on the aforementioned results, we assumed that the effects of emodin on lowering lipid metabolism and inducing intrinsic apoptosis would involve interaction with SREBP1. To further support this assumption, we subsequently constructed stable OE/KO *SREBP1* Bel-7402 cell lines (**Figure 1**). Compared with the wild type (WT) control group, the synthesis of TG was decreased (**Figure 4A**), and the ratio of SFAs to MUFAs was decreased in SREBP1-KO (**Figure 4B**). Furthermore, the mRNA and protein expression of fatty acid synthesis genes (ACLY, ACACA, and FASN) and fatty acid desaturation gene SCD was downregulated (**Figure 4C** and **D**).

Similarly, to explore the role of SREBP1 in apoptosis induction, we examined the apoptosis in stable SREBP1-KO, SREBP1-OE, and WT Bel-7402 cell lines. Our data clearly indicated that KO of SREBP1 induced apoptosis (**Figure 5A**) and caused ΔΨm decline (**Figure 5B**) compared with that of WT Bel-7402 cells. Furthermore, compared with WT cells, the results of Western blot analysis indicated that the expression of intrinsic apoptosis-associated proteins (cleaved-caspase-3, cleaved-caspase-9, APAF1, CYTC, ENDOG, and AIF) was activated, and Bcl-2 was repressed in SREBP1-KO cell lines (**Figure 5D** and **E**). Interestingly, the apoptosis rate in SREBP1-KO cells (**Figure 5A**) was significantly less than that in emodin-treated cells (18.11% *vs.* 72.72%) (**Figure 2C** and **5A**), indicating SREBP1 was not the unique signaling pathway for cell survival and emodin may also induce cell apoptosis through other SREBP1-independent pathways.

Emodin Decreased Lipid Metabolism and Induced Apoptosis by SREBP1-Dependent and -Independent Ways

To examine whether emodin induced apoptosis in an SBREP1-dependent manner, we investigated apoptosis induction in

emodin-treated *SREBP1*-KO cell lines. As shown in **Figure 6**, compared with SREBP1-KO cells, emodin combined with SREBP1-KO induced more apoptosis and decreased more mitochondrial membrane potential. In addition, the activation of caspase-dependent and caspase-independent intrinsic apoptosis-associated proteins was enhanced in emodin-treated SREBP1-KO cell lines (**Figure 7**). These results indicated that emodin induced apoptosis through both SREBP1-dependent and SREBP1-independent pathways in Bel-7402 cells.

DISCUSSION AND CONCLUSION

According to statistical data from 2018, liver cancer is universally diagnosed and identified as a leading cause of cancer death, it is ranked fourth among common malignant tumors in global cancer mortality in which HCC accounted for 70% to 90% of mortality cases (Torre et al., 2015; Bray et al., 2018). The dysregulation of energy metabolism and resistance to cell death have recently been recognized as one of the most important hallmarks of HCC (Hanahan and Weinberg, 2011). The coordinated synthesis of macromolecules, including proteins and lipids, are the requirements for cell growth and survival (Griffiths et al., 2013). As compared with cells in most other normal tissues in humans, solid tumors, including HCC cells, can be exposed to low concentrations of nutrients and oxygen due to the ineffective vascular network (Lewis et al., 2015). Interestingly, the normal cells generally rely on the uptake of lipids from the circulation, whereas tumors often obtain the ability to make their own lipids (Menendez and Lupu, 2007). In additions, alteration in cellular metabolism constantly noted in cancer is the enhanced capacity of *de novo* lipid synthesis (Ricoult et al., 2016). Recent studies have drawn significant attention to metabolic reprogramming, especially lipid metabolism alteration, which is regarded as the initiating factor of tumor pathogenesis and progression. Continuous *de novo* lipogenesis is frequently activated in cancers, thereby providing extra lipids and lipid precursors during rapid cell proliferation (Martinez-Outschoorn et al., 2017). In the vital role of lipid metabolic reprogramming in cancer cell biology, the molecular programs and pathways that support the cancer metabolic process remain elusive; therefore, it is crucial to identify molecular mechanisms of lipid metabolism in tumorigenesis and tumor progression in HCC cells.

Because of the high recurrence of HCC after surgery and resistance to chemotherapy, traditional Chinese medicines used for cancer treatment have gained increasing attention, including He Shou Wu (Lin et al., 2015). As the main component of He Shou Wu, emodin induces both extrinsic and intrinsic
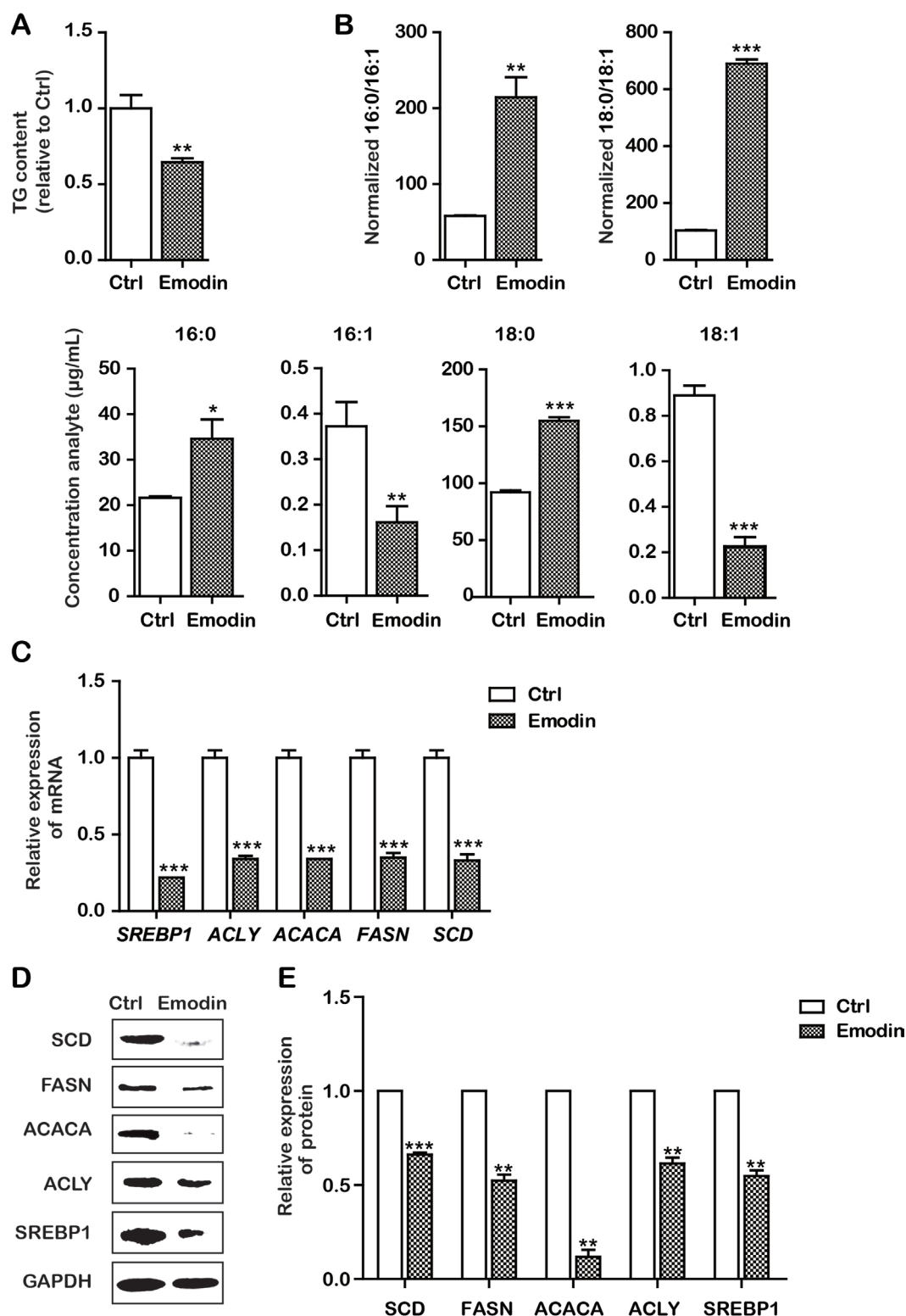
FIGURE 3 | Emodin decreased lipid metabolism in Bel-7402 cells. **(A)** Total cellular TG content of Bel-7402 cells treated with emodin. **(B)** High-performance liquid chromatography-mass spectrometry (HPLC-MS) determination of the saturated fatty acids (SFAs) to monounsaturated fatty acids (MUFAs) ratios (palmitic acid to palmitoleic acid, 16:0 to 16:1) (stearic acid to oleic acid, 18:0 to 18:1) as well as the content of 16:0, 16:1, 18:0, and 18:1 in Bel-7402 cells treated with emodin. **(C)** The transcript level of lipid-associated genes in Bel-7402 cells when exposed to emodin. **(D** and **E)** The protein level of lipid-associated genes in Bel-7402 cells when exposed to emodin. Data were expressed as mean ± standard error of the mean. *$P < 0.05$, **$P < 0.01$, and ***$P < 0.001$ *vs.* ctrl group, respectively.
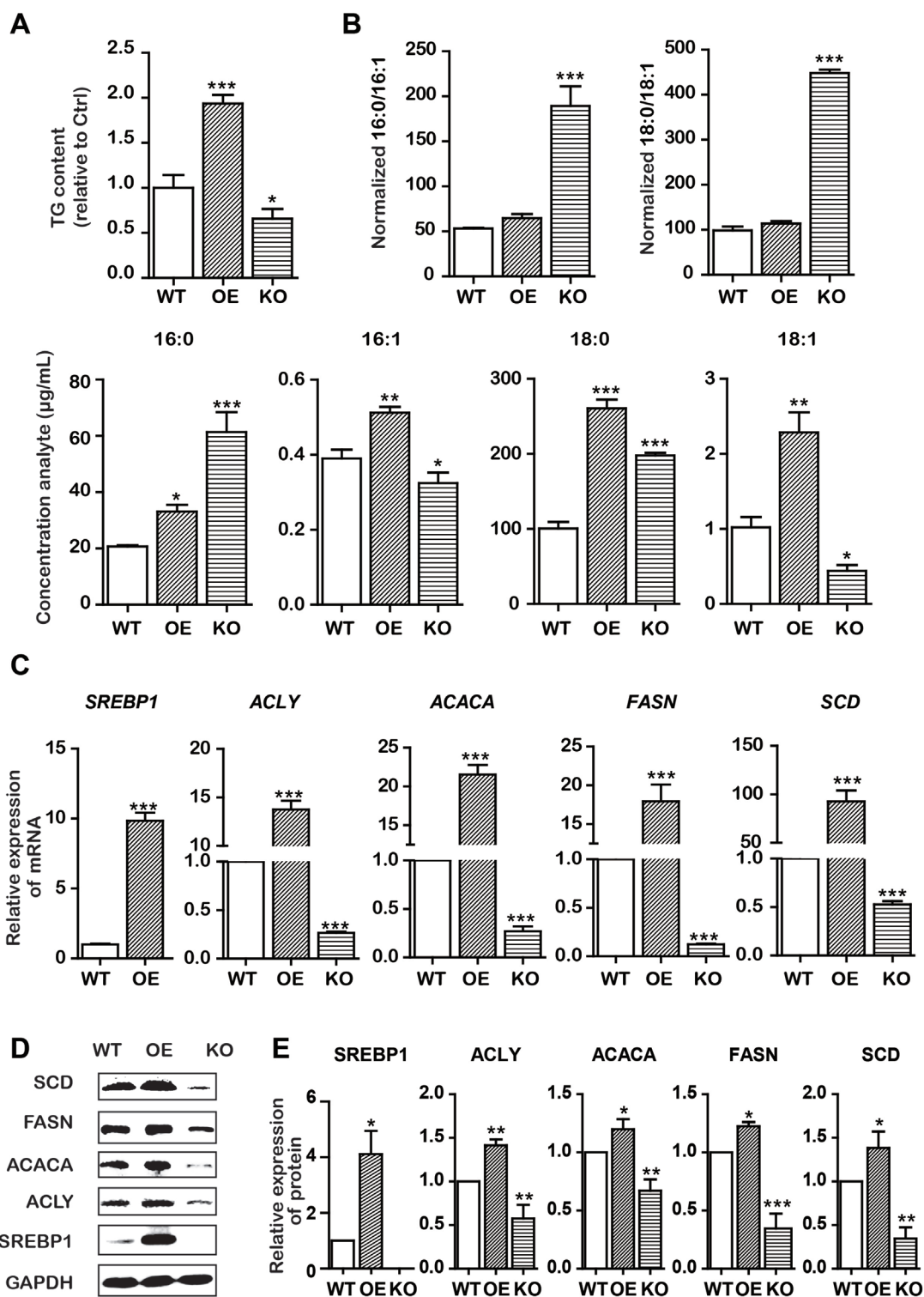
FIGURE 4 | KO and OE of SREBP1 influenced lipid metabolism in Bel-7402 cells. **(A)** Total cellular TG content of SREBP1-KO, SREBP1-OE, and WT Bel-7402 cells. **(B)** HPLC-MS determination of the SFAs to MUFAs ratios (palmitic acid to palmitoleic acid, 16:0 to 16:1) (stearic acid to oleic acid, 18:0 to 18:1) as well as the content of 16:0, 16:1, 18:0, and 18:1 in SREBP1-KO, SREBP1-OE, and WT Bel-7402 cells. **(C)** The transcript level of lipid-associated genes in SREBP1-KO, SREBP1-OE, and WT Bel-7402 cells. **(D** and **E)** The protein level of lipid-associated genes in SREBP1-KO, SREBP1-OE, and WT Bel-7402 cells. Data were expressed as mean ± standard error of the mean. *$P < 0.05$, **$P < 0.01$, and ***$P < 0.001$ vs. WT group, respectively.
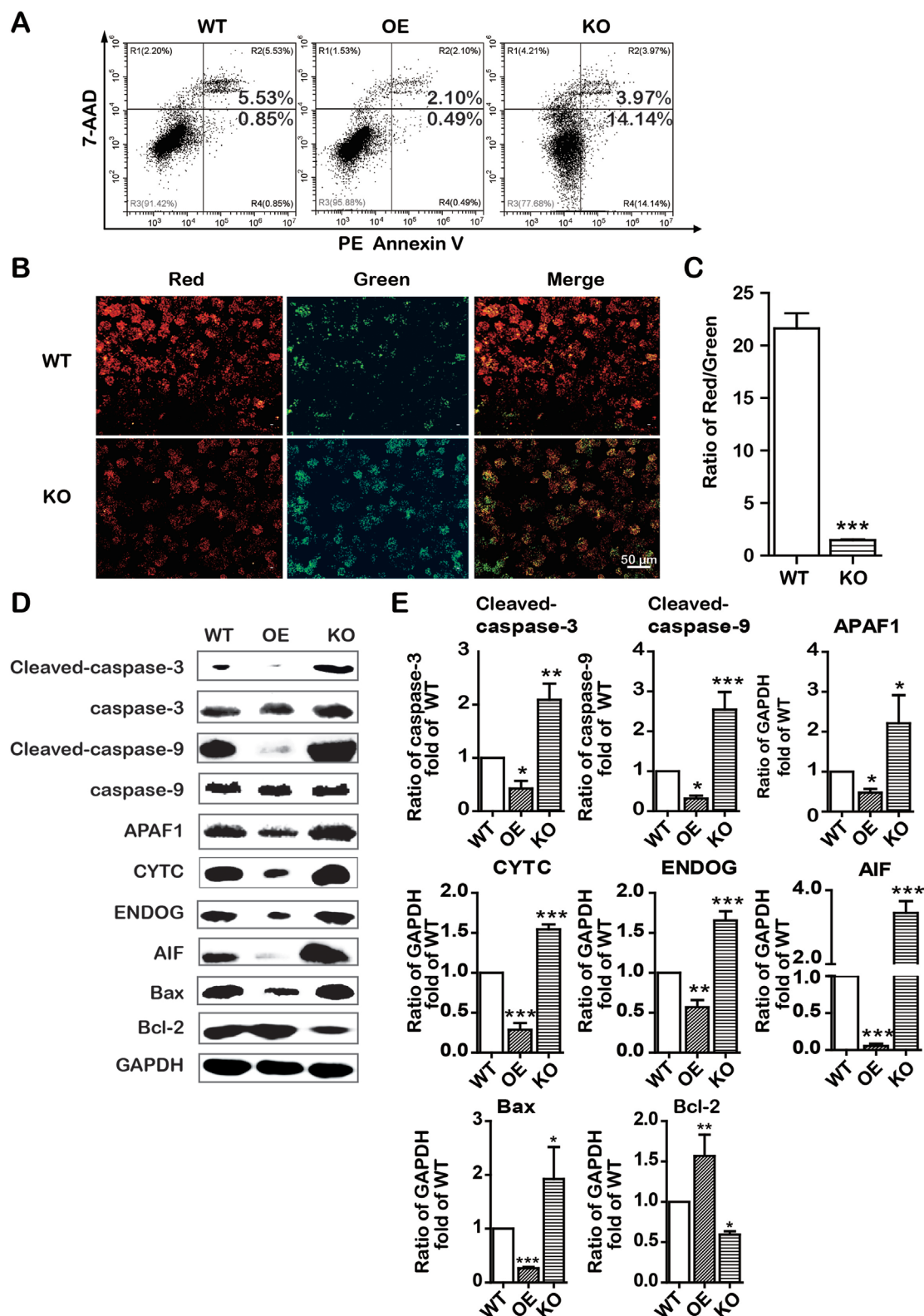
FIGURE 5 | KO and OE of SREBP1 influenced intrinsic apoptosis in Bel-7402 cells. **(A)** Apoptotic cells were detected by the PE Annexin V-7AAD double staining assay in SREBP1-KO, SREBP1-OE, and WT Bel-7402 cells. **(B** and **C)** The ΔΨm was detected by JC-10 assay in SREBP1-KO, SREBP1-OE, and WT Bel-7402 cells. **(D** and **E)** The expression of intrinsic apoptosis associated-proteins in SREBP1-KO, SREBP1-OE, and WT Bel-7402 cells. Data were expressed as mean ± standard error of the mean. $^*P < 0.05$, $^{**}P < 0.01$, and $^{***}P < 0.001$ vs. WT group, respectively.
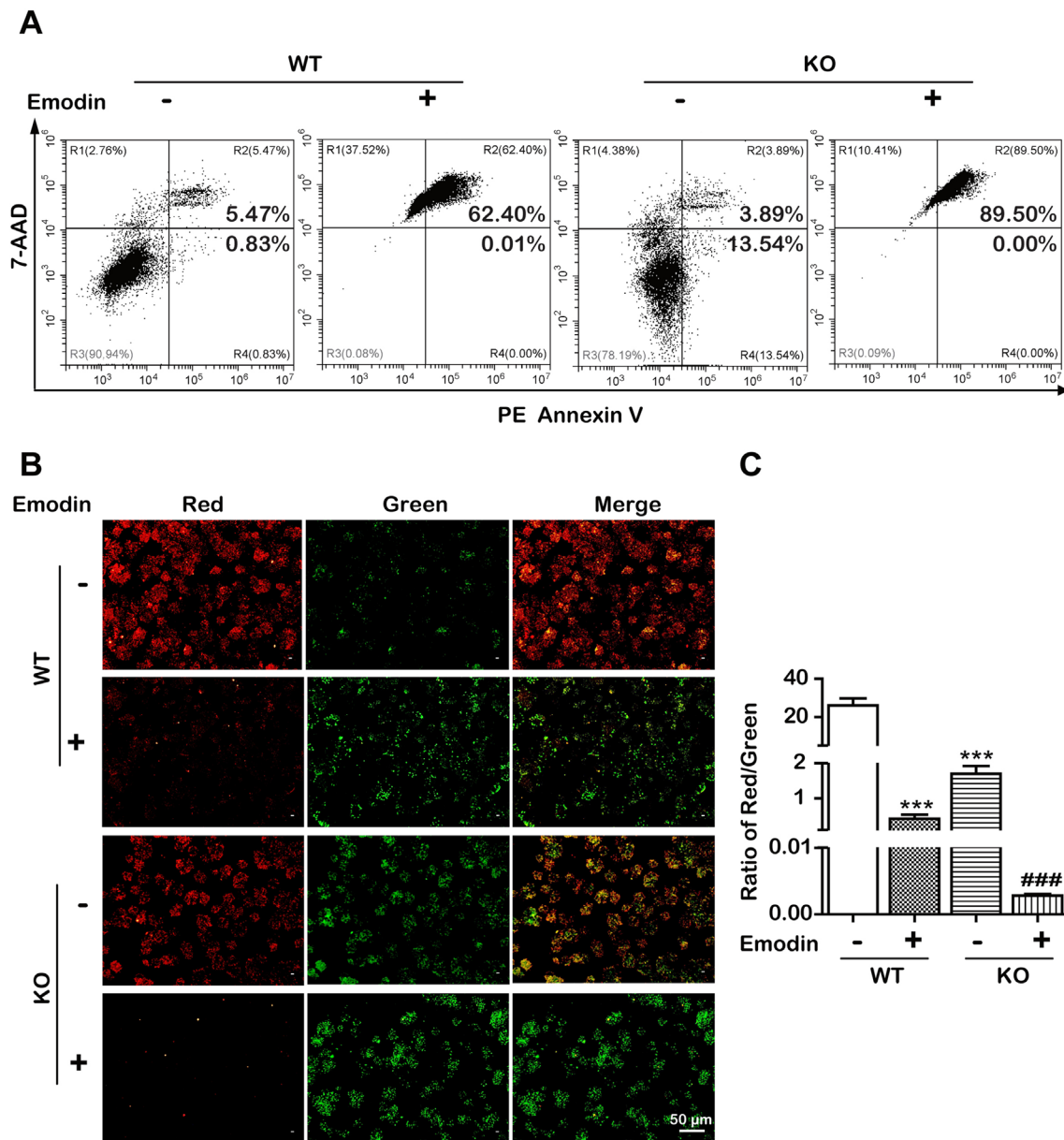
FIGURE 6 | Emodin induced SREBP1-dependent and -independent apoptosis. **(A)** Apoptotic cells were detected using the PE Annexin V-7AAD double staining assay in SREBP1-KO and WT Bel-7402 cells after treatment with emodin. **(B** and **C)** The ΔΨm was detected using JC-10 assay in SREBP1-KO and WT Bel-7402 cells. Data were expressed as mean ± standard error of the mean. ***$P < 0.001$ *vs.* WT group, respectively. ###$P < 0.001$ *vs.* SREBP1-KO group, respectively.

apoptosis (Cui et al., 2016). However, it remains unclear whether a decrease in lipids is associated with cancer treatment. In this study, we found that emodin has significant antitumor activity as it suppressed cell viability and triggered apoptosis in Bel-7402 cells (**Figure 2B** and **C**). Based on the latest definition of cell death by the Nomenclature Committee on Cell Death (NCCD), the apoptosis is divided into intrinsic apoptosis and extrinsic apoptosis. The intrinsic apoptosis is mainly relevant to a mitochondrion-centered control mechanism (Galluzzi et al., 2012). After the ΔΨm dissipates, the apoptosis will be

nonreversible. Our data showed that emodin distinctly decreased mitochondrial membrane potential, indicating a functional injury of mitochondria (**Figures 2D** and **E**). Furthermore, our data showed that the ratio of the protein expression of Bax/Bcl-2 was decreased, and caspase-9, APAF1, and CYTC were increased in emodin-treated Bel-7402 cells, this suggested that emodin induced intrinsic apoptosis. In addition, the intrinsic apoptosis has two pathways: one is caspase-dependent through releasing CYTC along with APAF1, triggering the caspase-9 to caspase-3 proteolytic cascade. The other is a caspase-independent pathway
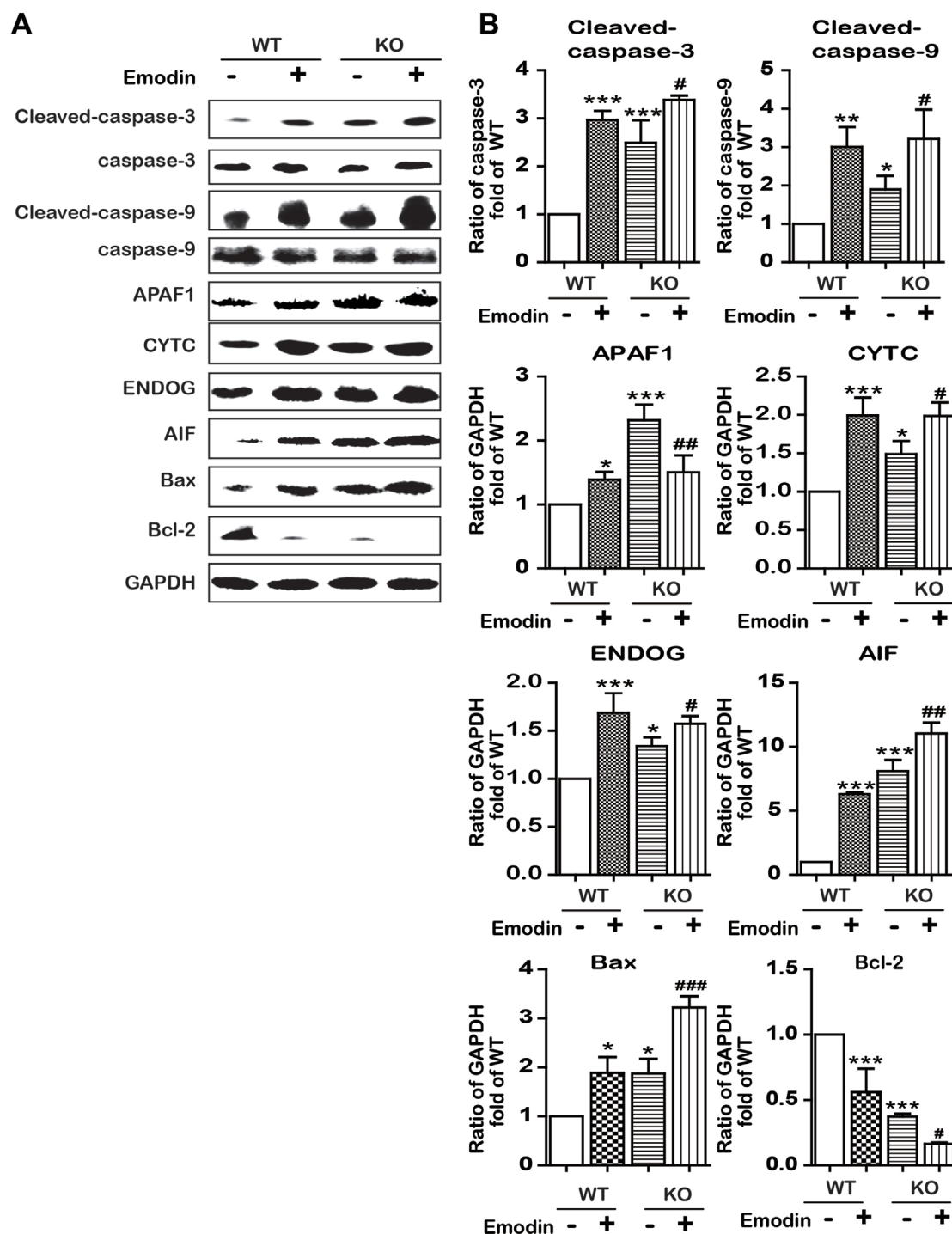
FIGURE 7 | Emodin activated apoptosis-associated proteins by blocking in a SREBP1-dependent and SREBP1-independent manner. **(A** and **B)** The expression of intrinsic apoptosis-associated proteins in SREBP1-KO and WT Bel-7402 cells. Data were expressed as mean ± standard error of the mean. *$P < 0.05$, **$P < 0.01$, and ***$P < 0.001$ vs. WT group, respectively. #$P < 0.05$, ##$P < 0.01$, and ###$P < 0.001$ vs. KO group, respectively.

with AIF and ENDOG functions (Galluzzi et al., 2012). In this study, emodin also activated AIF and ENDOG, indicating that emodin induced apoptosis in both caspase-dependent and caspase-independent pathways.

Subsequently, we explored the underlying mechanisms of induction of intrinsic apoptosis by emodin. Here, we found that emodin acted as a potent inhibitor of SREBP1 and the downstream genes including *ACLY, ACACA,* and *FASN*. We

observed substantial reduction in ACLY, ACACA, FASN, and SCD mRNA and protein expression in emodin-treated Bel-7402 cells, finally leading to the decrease in fatty acid biosynthesis (**Figure 3**). Furthermore, KO SREBP1 induced apoptosis and OE SREBP1 reversed this apoptotic process (**Figures 4** and **5**). These results strongly suggested that emodin induced intrinsic apoptosis in a SREBP1-dependent manner. In addition, interestingly, we observed that emodin alone and, combined with SREBP1-KO, induced more apoptosis than SREBP1-KO alone (**Figures 2C**, **5A**, **6A**, and **7**). Based on the evidence that emodin induced apoptosis in previous studies (Wang et al., 2013; Yu et al., 2013; Cui et al., 2016), this suggested that emodin may also induce apoptosis through a SREBP1-independent pathway in Bel-7402 cells. With regard to the effects of emodin on lipid metabolism in other types of cancer cells, Lee et al. reported that emodin inhibited proliferation and induced apoptosis by blocking FASN at a concentration of 10 to 50 μmol/L in colon cancer HCT116 cells (Lee et al., 2017), and Dong found that emodin could reduce FASN in a dose-dependent manner (20, 40, and 80 μmol/L) in liver cancer HCCLM3 cells (Dong, 2007). Li et al. reported chrysophanol, an analogue of emodin, inhibited liver cancer Huh-7 cells by suppressing expression of SREBPs and the downstream genes, FASN, ACACA, ACLY, SCD, and HMGCR at a concentration of 40 μmol/L (Li et al., 2015). In this study, the IC_{50} value for emodin on HCC Bel-7402 cells was around 80 μmol/L, indicating that different types of cancer cells require different inhibitory concentrations. Our data were consistent with the previous studies on emodin against other types of cancer cells.

Regarding the toxicity of emodin on normal human liver cells, Cui found that emodin at a concentration of 80 μmol/L could inhibit liver cancer HepG2 cells with a cell viability of 45.07% in 24 h; however, 100 μmol/L of emodin had no toxicity on human normal HL-7702 cells (Cui, 2016). Zhang reported 6.25 and 12.5 μg/L (about 23.15 and 46.30 μmol/L, respectively) of emodin showed no toxicity on L02 cells in 24 and 48 h, whereas 25 and 50 μg/L (about 92.59 and 185.18 μmol/L, respectively) of emodin

induced S phase arrest and apoptosis in HL-7702 cells (Zhang et al., 2010). Our previous study also found that IC_{50} value for emodin on L02 cells was 36.69 μg/L (about 135 μmol/L) (Li et al., 2017). Compared with the aforementioned IC_{50} value (10 to 80 μmol/L) for emodin on cancer cells, the toxicity of emodin on human normal cells (with a IC_{50} value from 92.59 to 185.18 μmol/L) was slightly less.

In summary, our study demonstrated that emodin inhibited SREBP1-dependent and SREBP1-independent cell proliferation and resulted in caspase-dependent and caspase-independent intrinsic apoptosis induction in HCCs. Emodin might have a high potential for targeting SREBP1 in HCC.

AUTHOR CONTRIBUTIONS

XW and FC designed the study; NY, HL, and ML conducted the experiments; NY, CL, XW, and XC analyzed the data; NY, CL, XW, and ML wrote the manuscript; NY, YF, XW and ML revised manuscript. All authors read and approved the final manuscript.

FUNDING

REFERENCES

Angelucci, C., Maulucci, G., Colabianchi, A., Iacopino, F., D'Alessio, A., Maiorana, A., et al. (2015). Stearoyl-CoA desaturase 1 and paracrine diffusible signals have a major role in the promotion of breast cancer cell migration induced by cancer-associated fibroblasts. *Br. J. Cancer* 112, 1675–1686. doi: 10.1038/bjc.2015.135

Bandyopadhyay, S., Zhan, R., Wang, Y., Pai, S. K., Hirota, S., Hosobe, S., et al. (2006). Mechanism of apoptosis induced by the inhibition of fatty acid synthase in breast cancer cells. *Cancer Res.* 66, 5934–5940. doi: 10.1158/0008-5472.CAN-05-3197

Bray, F., Ferlay, J., Soerjomataram, I., Siegel, R. L., Torre, L. A., Jemal, A., et al. (2018). Global cancer statistics 2018: GLOBOCAN estimates of incidence and mortality worldwide for 36 cancers in 185 countries. *CA Cancer J. Clin.* 68, 394–424. doi: 10.3322/caac.21492

Chen, C. X. (2017). *Pharmacology of Chinese Materia Medica. 1st Edn.* Beijing: Zhong Guo Zhong Yi Chu Ban She, 235–237.

Cui, Y. (2016). Effect and mechanism of emodin on apoptosis in human hepatoma cells. Master. Yangling: Master, Northwest A&F University.

Cui, Y. T., Lu, P. R., Song, G., Liu, Q., Zhu, D., and Liu, X. B. (2016). Involvement of PI3K/Akt, ERK and p38 signaling pathways in emodin-mediated extrinsic and

intrinsic human hepatoblastoma cell apoptosis. *Food Chem. Toxicol.* 92, 26–37. doi: 10.1016/j.fct.2016.03.013

Currie, E., Schulze, A., Zechner, R., Walther, T. C., and Farese, R. V., Jr. (2013). Cellular fatty acid metabolism and cancer. *Cell Metab.* 18, 153–161. doi: 10.1016/j.cmet.2013.05.017

Dong, L. (2007). Mechanistic study of emodin's anti-cancer effects on human liver cancer HCCLM3 cell line. Ph.D. Chengdu: Sichuan University.

Edwards, P. A., Tabor, D., Kast, H. R., and Venkateswaran, A. (2000). Regulation of gene expression by SREBP and SCAP. *Biochim. Biophys. Acta* 1529, 103–113. doi: 10.1016/S1388-1981(00)00140-2

Evans, L. M., Cowey, S. L., Siegal, G. P., and Hardy, R. W. (2009). Stearate preferentially induces apoptosis in human breast cancer cells. *Nutr. Cancer* 61, 746–753. doi: 10.1080/01635580902825597

Galluzzi, L., Vitale, I., Abrams, J. M., Alnemri, E. S., Baehrecke, E. H., Blagosklonny, M. V., et al. (2012). Molecular definitions of cell death subroutines: recommendations of the Nomenclature Committee on Cell Death 2012. *Cell Death Differ.* 19, 107–120. doi: 10.1038/cdd.2011.96

Griffiths, B., Lewis, C. A., Bensaad, K., Ros, S., Zhang, Q., Ferber, E. C., et al. (2013). Sterol regulatory element binding protein-dependent regulation of lipid synthesis supports cell survival and tumor growth. *Cancer Metab.* 1, 3. doi: 10.1186/2049-3002-1-3

Gu, J., Cui, C. F., Yang, L., Wang, L., and Jiang, X. H. (2019). Emodin inhibits colon cancer cell invasion and migration by suppressing epithelial-mesenchymal transition via the Wnt/beta-catenin pathway. *Oncol. Res.* 27, 193–202. doi: 10.3727/096504018X15150662230295

Guo, D., Bell, E. H., Mischel, P., and Chakravarti, A. (2014). Targeting SREBP-1-driven lipid metabolism to treat cancer. *Curr. Pharm. Des.* 20, 2619–2626. doi: 10.2174/13816128113199990486

Hanahan, D., and Weinberg, R. A. (2011). Hallmarks of cancer: the next generation. *Cell* 144, 646–674. doi: 10.1016/j.cell.2011.02.013

Horton, J. D. (2002). Sterol regulatory element-binding proteins: transcriptional activators of lipid synthesis. *Biochem. Soc.* 30, 1091–1095. doi: 10.1042/bst0301091

Huang, W. C., Li, X., Liu, J., Lin, J., and Chung, L. W. (2012). Activation of androgen receptor, lipogenesis, and oxidative stress converged by SREBP-1 is responsible for regulating growth and progression of prostate cancer cells. *Mol. Cancer Res.* 10, 133–142. doi: 10.1158/1541-7786.MCR-11-0206

Lee, K. H., Lee, M. S., Cha, E. Y., Sul, J. Y., Lee, J. S., Kim, J. S., et al. (2017). Inhibitory effect of emodin on fatty acid synthase, colon cancer proliferation and apoptosis. *Mol. Med. Rep.* 15, 2163–2173. doi: 10.3892/mmr.2017.6254

Lewis, C. A., Brault, C., Peck, B., Bensaad, K., Griffiths, B., Mitter, R., et al. (2015). SREBP maintains lipid biosynthesis and viability of cancer cells under lipid- and oxygen-deprived conditions and defines a gene signature associated with poor survival in glioblastoma multiforme. *Oncogene* 34, 5128–5140. doi: 10.1038/onc.2014.439

Li, W. Y., Ng, Y. F., Zhang, H., Guo, Z. D., Guo, D. J., Kwan, Y. W., et al. (2014). Emodin elicits cytotoxicity in human lung adenocarcinoma A549 cells through inducing apoptosis. *Inflammopharmacology* 22, 127–134. doi: 10.1007/s10787-013-0186-4

Li, C., Yang, W., Zhang, J., Zheng, X., Yao, Y., Tu, K., et al. (2014). SREBP-1 has a prognostic role and contributes to invasion and metastasis in human hepatocellular carcinoma. *Int. J. Mol. Sci.* 15, 7124–7138. doi: 10.3390/ijms15057124

Li, J., Ding, L., Song, B., Yang, L., and Wang, Z. (2015). Effects of chrysophanol on expression of SREBPs and lipid metabolism in Huh-7 cells. *Yao Xue Xue Bao* 50, 174–179. doi: 10.16438/j.0513-4870.2015.02.007.

Li, S. Z. (2016). *Compendium of Materia Medica. 2nd Edn.* Beijing: Ren Min Wei Sheng Chu Ban She, 1054–1058.

Li, H., Cao, S., Wang, X., Zuo, Q., Chen, P., Liu, Y., et al. (2016). Quality evaluation of Heshouwu, a Taoist medicine in Wudang, China. *Exp. Ther. Med.* 12, 2317–2323. doi: 10.3892/etm.2016.3580

Li, J., Ding, L., Song, B., Xiao, X., Qi, M., Yang, Q., et al. (2016). Emodin improves lipid and glucose metabolism in high fat diet-induced obese mice through regulating SREBP pathway. *Eur. J. Pharmacol.* 770, 99–109. doi: 10.1016/j.ejphar.2015.11.045

Li, H., Wang, X., Liu, Y., Pan, D., Wang, Y., Yang, N., et al. (2017). Hepatoprotection and hepatotoxicity of Heshouwu, a Chinese medicinal herb: context of the paradoxical effect. *Food Chem. Toxicol.* 108, 407–418. doi: 10.1016/j.fct.2016.07.035

Li, H., Xiang, L., Yang, N., Cao, F., Li, C., Chen, P., et al. (2018). Zhiheshouwu ethanol extract induces intrinsic apoptosis and reduces unsaturated fatty acids via SREBP1 pathway in hepatocellular carcinoma cells. *Food Chem. Toxicol.* 119, 169–175. doi: 10.1016/j.fct.2018.04.054

Lin, L., Ni, B., Lin, H., Zhang, M., Li, X., Yin, X., et al. (2015). Traditional usages, botany, phytochemistry, pharmacology and toxicology of Polygonum multiflorum Thunb.: a review. *J. Ethnopharmacol.* 159, 158–183. doi: 10.1016/j.jep.2014.11.009

Liu, J. X., Zhang, J. H., Li, H. H., Lai, F. J., Chen, K. J., Chen, H., et al. (2012). Emodin induces Panc-1 cell apoptosis via declining the mitochondrial membrane potential. *Oncol. Rep.* 28, 1991–1996. doi: 10.3892/or.2012.2042

Ma, Y. S., Weng, S. W., Lin, M. W., Lu, C. C., Chiang, J. H., Yang, J. S., et al. (2012). Antitumor effects of emodin on LS1034 human colon cancer cells *in vitro* and *in vivo*: roles of apoptotic cell death and LS1034 tumor xenografts model. *Food Chem. Toxicol.* 50, 1271–1278. doi: 10.1016/j.fct.2012.01.033

Ma, J., Yang, J., Wang, C., Zhang, N., Dong, Y., Wang, Y., et al. (2014). Emodin augments cisplatin cytotoxicity in platinum-resistant ovarian cancer cells via ROS-dependent MRP1 downregulation. *Biomed Res. Int.* 2014, 107671. doi: 10.1155/2014/107671

Martinez-Outschoorn, U. E., Peiris-Pages, M., Pestell, R. G., Sotgia, F. and Lisanti, M. P. (2017). Cancer metabolism: a therapeutic perspective. *Nat. Rev. Clin. Oncol.* 14, 11–31. doi: 10.1038/nrclinonc.2016.60

Mele, M., Conte, G., Castiglioni, B., Chessa, S., Macciotta, N. P., Serra, A., et al. (2007). Stearoyl-coenzyme A desaturase gene polymorphism and milk fatty acid composition in Italian Holsteins. *J. Dairy Sci.* 90, 4458–4465. doi: 10.3168/jds.2006-617

Menendez, J. A. and Lupu, R. (2007). Fatty acid synthase and the lipogenic phenotype in cancer pathogenesis. *Nat. Rev. Cancer* 7, 763–777. doi: 10.1038/nrc2222

Moon, Y. A., Shah, N. A., Mohapatra, S., Warrington, J. A., and Horton, J. D. (2001). Identification of a mammalian long chain fatty acyl elongase regulated by sterol regulatory element-binding proteins. *J. Biol. Chem.* 276, 45358–45366. doi: 10.1074/jbc.M108413200

Pandey, P. R., Xing, F., Sharma, S., Watabe, M., Pai, S. K., Iiizumi-Gairani, M., et al. (2013). Elevated lipogenesis in epithelial stem-like cell confers survival advantage in ductal carcinoma in situ of breast cancer. *Oncogene* 32, 5111–5122. doi: 10.1038/onc.2012.519

Ricoult, S. J., Yecies, J. L., Ben-Sahra, I., and Manning, B. D. (2016). Oncogenic PI3K and K-Ras stimulate de novo lipid synthesis through mTORC1 and SREBP. *Oncogene* 35, 1250–1260. doi: 10.1038/onc.2015.179

Sanjana, N. E., Shalem, O., and Zhang, F. (2014). Improved vectors and genome-wide libraries for CRISPR screening. *Nat. Methods* 11, 783–784. doi: 10.1038/nmeth.3047

Shalem, O., Sanjana, N. E., Hartenian, E., Shi, X., Scott, D. A., Mikkelson, T., et al. (2014). Genome-scale CRISPR-Cas9 knockout screening in human cells. *Science* 343, 84–87. doi: 10.1126/science.1247005

Shang, R. B. (2004). "Kan"formulae in Taoist medicine. *Wudang* 161, 55–56.

Soyal, S. M., Nofziger, C., Dossena, S., Paulmichl, M., and Patsch, W. (2015). Targeting SREBPs for treatment of the metabolic syndrome. *Trends Pharmacol. Sci.* 36, 406–416. doi: 10.1016/j.tips.2015.04.010

Thacker, P. C., and Karunagaran, D. (2015). Curcumin and emodin down-regulate TGF-beta signaling pathway in human cervical cancer cells. *PLoS One* 10, e0120045. doi: 10.1371/journal.pone.0120045

Torre, L. A., Bray, F., Siegel, R. L., Ferlay, J., Lortet-Tieulent, J., and Jemal, A. (2015). Global cancer statistics, 2012. *CA Cancer J. Clin.* 65, 87–108. doi: 10.3322/caac.21262

Wang, Y. X., Yu, H., Zhang, Y., Liu, Y. Q., Ge, X., and Wu, X. K. (2013). Emodin induces apoptosis of human cervical cancer hela cells *via* intrinsic mitochondrial and extrinsic death receptor pathway. *Cancer Cell Int.* 13, 71. doi: 10.1186/1475-2867-13-71

Wang, Y., Yu, H., Zhang, J., Ge, X., Gao, J., Zhang, Y., et al. (2015). Anti-tumor effect of emodin on gynecological cancer cells. *Cell. Oncol. (Dordr.)* 38, 353–363. doi: 10.1007/s13402-015-0234-8

Yang, N., Cao, F. J., Huo, J. W., Li, H. L., Li, C., Wang, Q., et al. (2018). SREBP1-based active component screening of anthraquinones radix polygoni multiflori preparata for lowering lipid metabolism in hepatocellular carcinoma cells. *J. Hubei Univ. Med.* 37, 156–160. doi: 10.13819/j.issn.1006-9674.2018.02.014

Yu, J. Q., Bao, W., and Lei, J. C. (2013). Emodin regulates apoptotic pathway in human liver cancer cells. *Phytother. Res.* 27, 251–257. doi: 10.1002/ptr.4703

Zhang, K., Jiao, K., Zhu, Y., Wu, F., Li, J., and Yu, Z. (2015). Effect of emodin on proliferation and cell cycle of human oral squamous carcinoma Tca8113 cells *in vitro*. *Nan Fang Yi Ke Da Xue Xue Bao* 35, 665–670. doi: 10.3969/j.issn.1673-4254.2015.05.08

Zhang, R. C., Liu, B., Sun, Z. X., and Xu, D. Y. (2010). Effects of extract of Polygonum multiflorum on cell cycle arrest and apoptosis of human liver cell line L02. *Zhong Xi Yi Jie He Xue Bao* 8, 554–561. doi: 10.3736/jcim20100608

Zhao, X., Xiaoli, Zong, H., Abdulla, A., Yang, E. S., Wang, Q., et al. (2014). Inhibition of SREBP transcriptional activity by a boron-containing compound improves lipid homeostasis in diet-induced obesity. *Diabetes* 63, 2464–2473. doi: 10.2337/db13-0835

The Essential Oils and Eucalyptol From *Artemisia vulgaris* L. Prevent Acetaminophen-Induced Liver Injury by Activating Nrf2–Keap1 and Enhancing APAP Clearance Through Non-Toxic Metabolic Pathway

OPEN ACCESS

Zhihui Jiang[1], Xiao Guo[1]*, Kunpeng Zhang[1], Ganesh Sekaran[2,3], Baorui Cao[1], Qingqing Zhao[1], Shouquan Zhang[4], Gordon M. Kirby[5], Xiaoying Zhang[1,2,5]*

[1] Henan Joint International Research Laboratory of Veterinary Biologics Research and Application, Anyang Institute of Technology, Anyang, China, [2] College of Veterinary Medicine, Northwest A&F University, Xianyang, China, [3] Department of Biotechnology, Nehru Arts and Science College, Coimbatore, India, [4] Tangyin Administrative Office of Pharmaceutical Industry, Anyang, China, [5] Department of Biomedical Sciences, Ontario Veterinary College, University of Guelph, Guelph, ON, Canada

Artemisia has long been used in traditional medicine and as a food source for different functions in eastern Asia. *Artemisia vulgaris* L. (AV) is a species of the genus Artemisia. Essential oils (EOs) were extracted from AV by subcritical butane extraction. EO contents were detected by electronic nose and headspace solid-phase microextraction coupled with gas chromatography (HS-SPME-GC-MS). To investigate the hepatoprotective effects, mice subjected to liver injury were treated intragastrically with EOs or eucalyptol for 3 days. Acetaminophen (APAP) alone caused severe liver injury characterized by significantly increased serum AST and ALT levels, ROS and hepatic malondialdehyde (MDA), as well as liver superoxide dismutase (SOD) and catalase (CAT) depletions. EOs significantly attenuated APAP-induced liver damages. Further study confirmed that eucalyptol is an inhibitor of Keap1, the affinity K_D of eucalyptol and Keap1 was 1.42×10^{-5}, which increased the Nrf2 translocation from the cytoplasm into the mitochondria. The activated Nrf2 increased the mRNA expression of uridine diphosphate glucuronosyltransferases (UGTs) and sulfotransferases (SULTs), also inhibiting CYP2E1 activities. Thus, the activated Nrf2 suppressed toxic intermediate formation, promoting APAP hepatic non-toxicity, whereby APAP was metabolized into APAP-gluc and APAP-sulf. Collectively, APAP non-toxic metabolism was accelerated by eucalyptol in protecting the liver against APAP-induced injury, indicating eucalyptol or EOs from AV potentials as a natural source of hepatoprotective agent.

Keywords: *Artemisia vulgaris*, essential oil, eucalyptol, acetaminophen, Nrf2-Keap1, liver

GRAPHICAL ABSTRACT
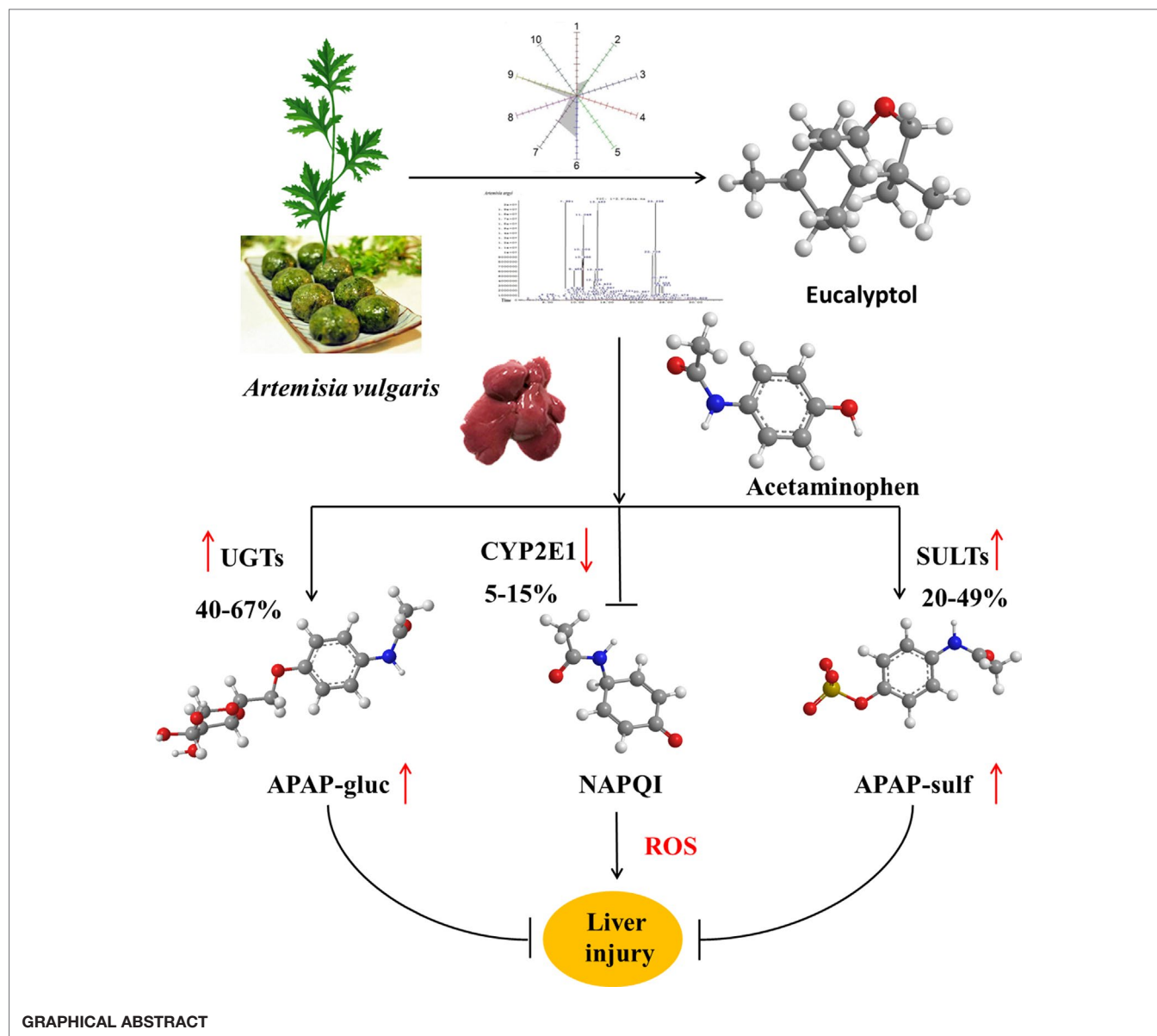
INTRODUCTION

Artemisia is a class of fragrant annual herb species of the composite family, distributed widely in Asia, Europe, and North America. It has a long history of traditional and popular use as both medicine and food with medicinal literature documentation since the Eastern Han Dynasty in 1st-century China (Song et al., 2016). *Artemisia* leaves have been considered to have a broad range of functions including anti-diarrhea, anti-inflammation, cough relief, antioxidant, and hepatoprotection (Giangaspero et al., 2009; Ferreira and Luthria, 2010; Obolskiy et al., 2011; Meng et al., 2018). The search for active compounds from Artemisia has led to the discovery and isolation of many phytochemicals and essential oils (EOs) with interesting activity. Artemisinin, a sesquiterpene lactone with antimalarial properties, is a prominent

example (Gaur et al., 2014). EOs from other plants have been used in the treatment of inflammation, against free radicals, and for their hepatoprotective effect (Yoon et al., 2010; Younsi et al., 2017). *Artemisia vulgaris* L. (AV) is a major and common *Artemisia* plant that was first recorded by Ben-Cao-Gang-Mu (Ming Dynasty, 16th century by Shizhen Li), who stated that the leaves should be collected and dried in summer for medical uses, including improving Yang-qi and decreasing skeleton raw.

Eucalyptol (1,8-cineole) is one of the major essential oils in AV. Eucalyptol has been used as a percutaneous penetration enhancer (Levison et al., 1994), an antibacterial and expectorant (Giamakis et al., 2001), and as an anti-inflammatory (Juergens et al., 1998) or antihypertensive agent (Lahlou et al., 2002). Eucalyptol acted as a strong inhibitor of proinflammatory cytokines such as tumor necrosis factor (TNF)-α and interleukin (IL)-1β and showed an

analgesic effect in an inflammatory model. Even though there is a report about eucalyptol acting against fatty liver in mammals and zebrafish (Cho, 2012; Murata et al., 2015), the effect and mechanism of eucalyptol against drug-induced liver injury remain unclear.

Drug-induced liver injury has become a major public health concern (Asrani et al., 2018; Real et al., 2019). Acetaminophen (APAP) overdose is the leading cause of drug-induced acute liver failure. Oxidative stress is considered to be the primary cellular event in APAP-induced liver injury (Nikravesh et al., 2018; Zhao et al., 2018). Under overdose conditions, most APAP is metabolized by phase II conjugating enzymes, mainly sulfotransferase (SULT) and UDP-glucuronosyltransferase (UGT), converting it to nontoxic compounds, which are then excreted with the urine. The remaining APAP, approximately 5–9%, is metabolized by the cytochrome P450 enzymes (CYPs), mainly CYP2E1, into the highly reactive intermediate metabolite N-acetyl-p-benzoquinone imine (NAPQI). NAPQI is usually rapidly detoxified by conjugating it with glutathione (GSH). However, when phase II metabolizing enzymes are saturated after APAP overdose, excessive NAPQ1 can deplete GSH, leading to covalent binding of sulfhydryl groups in cellular proteins and resulting in liver oxidative stress (Lancaster et al., 2015; Du et al., 2016). Nuclear factor erythroid 2-related factor 2 (Nrf2) is likely activated by redox status changes induced by NAPQI. Nrf2 dissociates from Keap1 and translocates into the nucleus to stimulate transcription of target genes with the help of small Maf proteins. These preceding processes led to the transcriptional activation of antioxidant enzymes, such as NAD(P)H, quinone oxidoreductase 1 (NQO1), heme oxygense-1 (HO-1), glutamate cysteine ligase (GCL), and glutathione S-transferase A (GSTA), increasing the expression of SOD and CAT (Loboda et al., 2016). In this study, the common reagent APAP that induced drug liver injury was chosen to explain the mechanism of AV and eucalyptol hepatoprotection.

MATERIALS AND METHODS

Phylogenetic Analysis

The plant sample 2 (*Artemisia vulgaris*) was collected in Tangyin, Henan province (N 38°39′27.97″, E 104°04′58.66″) with monsoon climate of medium latitudes and cinnamon soil. According to plant morphological analysis, the collected sample had nine vein stem leaves compared with sample 1, *Artemisia argyi* (five vein stem) cultivated in Hubei province (N30°13′39.89″, E115°26′10.36″). For both samples, single leaves were collected. Genomic DNA was extracted using the modified hexadecyl trimethyl ammonium Bromide (CTAB) method and diluted to a concentration of 20 ng/µl in ddH$_2$O. The PCR primers ITS2 are S2F: ATGCGATACTTGGTGTGAAT, S3R: GACGCTTCTCCAGACTACAAT. PCR reactions (25 µl) were composed of 4 µl genomic DNA (20 ng/µl), 2.5 µl PCR buffer (10×), 2.0 µl dNTPs (2 mmol), 2.0 µl MgSO$_4$ (25 mmol), primers (2 µmol), 0.4 U Kod-Plus-Neo DNA polymerase (TOYOBO, Osaka, Japan), and sterile water.

PCR amplification started with the denaturing step at 94°C for 3 min, followed by 36 cycles of denaturation at 98°C for 20 s,

annealing at 58–60°C for 20 s, extension at 68°C for 50 s, and a final extension at 68°C for 6–8 min before cooling to 10°C.

The original sequences were assembled using CodonCode Aligner V3.0 (CodonCode Co., Centerville, MA, USA). The ITS2 sequences were subjected to Hidden Markov Model (HMM) (Keller et al., 2009) model analysis to remove the conserved 5.8S and 28S DNA sequences (Koetschan et al., 2012). The ITS2 sequences were aligned using Clustal W (Thompson et al., 2002), and the genetic distances were computed using MEGA 6.0 according to the Kimura 2-Parameter (K2P) model (Tamura et al., 2011). Subsequently, MEGA6.0 software 20 was employed to construct an unrooted phylogenetic tree based on alignments using the neighbor-joining (NJ) method with the following parameters: JTT model, pairwise gap deletion, and 1,000 bootstraps. Furthermore, maximum likelihood, minimal evolution, and PhyML methods were also applied in the tree construction to validate the results from the NJ method. Annotated ITS2 sequences of Sample 1, Sample 2, Artemisia vulgaris, Artemisia lavandulifolia, Artemisia argyi, and Artemisia annua were folded by energy minimization using the ITS2 database web server (http://its2.bioapps.biozentrum. uni-wuerzburg.de/) for secondary structure analysis.

Subcritical Butane Extraction of AV-EOs and Purification

The EOs were obtained by subcritical butane extraction apparatus (Henan Subcritical Biological Technology Co., Ltd., Anyang, China). The liquid/solid ratio was 30:1, the temperature was 45°C, extraction time was 34 min, and the particle size was 0.26 mm. The extract was subjected to hydrodistillation in Clevenger-type apparatus for 2 h. The oil/water emulsion produced was collected and stored at 4°C overnight to separate the essential oil from the residual water. The essential oil was then removed and stored in an amber glass bottle at room temperature until further use.

Electronic Nose Analysis

The constituent of EOs from AV was captured by measuring the headspace PEN3 (Airsense Analytics system GmbH, Schwerin, Germany). The e-nose system consisted of a fully automated Headspace-Sampler, an array of ten sensors (Alpha MOS company, France), and an electronic unit for data acquisition. The MOS sensors consisted of W1C (aromatic), W5S (broadrange), W3C (aromatic), W6S (hydrogen), W5C (arom-aliph), W1S (broad-methane), W1W (sulphur-organic), W2S (broad-alcohol), W2W (sulph-chlor), and W3S (methane-aliph). Volatile organic compounds (VOCs) were injected into the Portable Electronic Nose PEN3 system using an auto-sampler at a low rate of 60 ml/min from 10 ml sealed glass vials containing 1 ml of oil sample. The VOCs were carried by pure gas (carrier gas) at 5 psi and exposed to the sensor chambers. The relative change in the resistance (G0/G) value determines the response of sensors for oil samples. The $\Delta R/R$ value was monitored precisely for 130 s. The data were analyzed using Loading (Lo) and principal component analysis (PCA). The PCA values were determined using Eq 1

$$r_{ij} = \frac{\sum_{k=1}^{n}(x_{ki} - \bar{x}_j)}{\sqrt{\sum_{k=1}^{n}(x_{ki} - \bar{x}_j)^2} \times \sqrt{\sum_{k=1}^{n}(x_{kj} - \bar{x}_j)}} \quad (ij) = 1, 2, \cdots, p)$$

(Eq 1)

Determination of Essential Oil Ingredients by Headspace Solid-Phase Microextraction Coupled to Gas Chromatography (HS-SPME-GC-MS)

The EOs were analyzed on an HS-SPME-GC-MS system consisting of commercial manual sampling SPME devices (Supelco, Inc. Bellefonte, PA, USA). SPME fibers with 100 μm polydimethylsiloxane (PDMS), 65 μm PDMS/divinylbenzene (PDMS/DVB), 85 μm polyacrylate (PA), 85 μm carboxen/PDMS (CAR/PDMS), and 70 μm carbowax/DVB (CW/DVB) were used. The analysis was carried out on a GC system (GC-2010, Shimadzu Tokyo, Japan) coupled with a flame ionization detector (FID). All the fibers were conditioned before use in the GC injector, according to the instructions provided by the manufacturer. Separation was performed using a DB-5 capillary column (30 m × 0.25 mm I.D. and 0.25 μm, J&W Scientific, CA, USA).

The instrument parameters for the analysis were as follows: N2 flow: 1.47 ml/min; column temperature program: held at 40°C for 3 min, then increased from 40 to 70°C at 15°C/min and maintained for 1 min, and then increased to 250°C at 30°C/min and held for 1 min. The detector temperature was held at 280°C. In optimized conditions, the temperature of the injector was set at 250°C, and the desorption process was performed in the splitless mode for 2 min.

For the HS-SPME experiments, EOs (3 ml) were placed in a 10 ml glass vial. The vial was closed with Teflon-lined septa (Supelco, Pennsylvania, USA). The standard solutions and EOs samples were stored at room temperature. Afterwards, a fiber was introduced into the headspace of the vial for 10 min at the same extraction temperature. After extraction, the fiber was removed from the vial, inserted into the inlet of the GC, and desorbed at 250°C for 2 min.

Compounds, Targets, and Pathway Analysis

AV compounds (85) were used to analyze the ADME properties using SwissADME (swissadme.ch/index.php). Based on the Lipinski rule, a total of 31 compounds were finalized for target fishing and pathway analysis. All selected compounds from SN structural data were retrieved from Pubchem (https://pubchem.ncbi.nlm.nih.gov/). Active components were identified and compared with Similarity Ensemble Approach (SEA) (http://sea.bkslab.org/) (Keiser et al., 2007) and Drug Repositioning and Adverse Reaction *via* Chemical-Protein Interactome (DRAR-CPI) (http://cpi.bio-x.cn/drar/) (Luo et al., 2011). Furthermore, Comparative Toxicogenomics Database (CTD) (http://ctdbase.org/) was applied for the target mining process. The target genes of AV were applied for pathway analysis using The Database for Annotation, Visualization and Integrated Discovery 6.8 server (DAVID) (http://

david.abcc.ncifcrf.gov): analytical tools used to identify the gene or proteins systematically. KEGG pathway information was retrieved (**Supplementary Table 1**) (Dennis et al., 2003).

Experimental Animals

The experimental protocol was reviewed and approved by the Ethics Committee of the Institute of Modern Biotechnology for the Use of Laboratory Animals. A total of 42 (15 male and 15 female) inbred Kunming mice (18–20 g) aged 4 weeks and 12 inbred SD rats (200–220 g) were obtained from the animal center of Zhengzhou University (Zhengzhou, China). The animals were kept under controlled conditions at temperature 22 ± 2°C, humidity 70% ± 4% with 12 h light–dark cycling.

Animal Treatments

Experiment 1: Mice were randomly divided into five groups with six mice in each group (n = 6, three males and three females). Control group: Tween-80 (100 ml/kg); APAP group: 300 mg/kg; APAP-Essential oil (APAP-EO) group: essential oil was emulsified in Tween-80 (95 %), essential oil (100 ml/kg) with oral administration after APAP (300 mg/kg) treatment for 1 h; APAP-eucalyptol (APAP-EU) group: eucalyptol (5 ml/kg) with oral administration after APAP (300 mg/kg) treatment for 1 h; Essential oil group (EO): 5% essential oil (100 ml/kg); eucalyptol (EU) group: 5 ml/kg; Positive group: NAC (100 mg/kg) with oral administration after APAP treatment for 1 h.

Experiment 2: Rats were randomly divided into two groups of five each. APAP group: 300 mg/kg; eucalyptol-APAP group: 5 ml/kg eucalyptol with oral administration after APAP (300 mg/kg) treatment for 1 h. After eucalyptol treatment for 0.2, 0.5, 0.75, 1, 1.5, 2, 4, and 6 h, the plasma was collected for high performance liquid chromatography (HPLC) or high performance liquid chromatography-tandem mass spectrometry (HPLC-MS/MS) analysis. The plasma samples were mixed with acetonitrile and centrifuged at 13,000 g for 15 min at 4°C.

Determination of Serum ALT and AST Levels

Enzymatic activities of aspartate aminotransferase (AST) and alanine aminotransferase (ALT) in serum were evaluated by spectrophotometer using commercial diagnostic kits (Nanjing Jiancheng Institute of Biotechnology, Nanjing, China).

Determination of Histology

Liver tissues were fixed in 10% formalin and embedded in paraffin for histological assessment. Samples were sectioned 5 μm and stained with hematoxylin and eosin. The slides were examined under a light microscope with photo-micrographic attachment.

Determination of Hepatic ROS, SOD, CAT, and MDA Levels

Frozen liver tissues were homogenized in ice-cold PBS. The supernatants were collected after the homogenate was centrifuged at 3000 g, 4°C for 10 min. Superoxide dismutase (SOD), catalase (CAT), and malondialdehyde (MDA) levels were measured with a

spectrophotometer using the commercially available assay kits as per the manufacturer's instructions (Nanjing Jiancheng Bioengineering Institute, Nanjing, China). The reactive oxygen species (ROS) levels were assayed with a fluorescence detector using commercial kits (Jiancheng Bioengineering Institute, Nanjing, China). The protein concentrations in tissue homogenates were measured with Bradford protein assay using bovine serum albumin as the standard (Jiancheng Bioengineering Institute, Nanjing, China).

Determination of Drug Metabolism-Related Gene Expressions

Total mRNA was isolated from frozen liver tissues using a Total RNA kit (Tiangen, Beijing, China). Quantitative real-time PCR (qPCR) was carried out for the amplification of cDNA using 2×SYBR Green I PCR Master Mix (Vazyme, Nanjing, China). The PCR procedure consisted of 95°C for 30 s followed by 35 cycles of 95°C for 15 s, 58°C for 30 s, and 72°C for 30 s. The PCR primers were used as shown in **Table 1**. The melting curve and dissociation curve were extrapolated to confirm primer specificity and product purity. The relative abundance of each mRNA was calculated with the formula $2^{-(\Delta\Delta Ct)}$, where $\Delta\Delta Ct = (Ct_{Target} - Ct_{GAPDH})$ treatment $-$ $(Ct_{Target} - Ct_{GAPDH})$ control.

Determination of CYP2E1 and Nrf2 Protein Expression

For Nrf2 expression analysis, the extraction and isolation of cytoplasmic and nuclear proteins were performed using a Cytoplasmic and Nuclear Protein Extraction Kit (Beyotime, Nanjing, China), according to the manufacturer's instructions. For CYP2E1 expression analysis, the extraction and isolation of microsomal proteins were carried out as described previously (Jiang et al., 2016; Chen et al., 2019). The protein concentration was determined by BCA assay kit (Beyotime, Nanjing, China). Equal amounts of protein extracts were subjected to SDS–polyacrylamide gel electrophoresis under reducing conditions in concentrate protein gel 5% (pH = 6.8) and separating protein gel 12% (pH = 8.8). The separated proteins were transferred to PVDF membranes using tank transfer for 2 h at 200 mA in Tris–glycine buffer with 15% methanol. Membranes were blocked with 5% skimmed milk for 3 h and incubated for 12 h with anti-CYP2E1 (1:1500, Boster, Wuhan, China), anti-Nrf-2 (1:500, Bioss, Beijing, China), anti-GAPDH

(1:1000, Boster, Wuhan, China), and anti-Lamin B (1:500, Bioss, Beijing, China) for 2 h at 37°C. The secondary antibodies (IgG/HRP) were incubated for 2 h at 37°C. The images of the blots were visualized by ECL (Genshare, Xi'an, China).

Molecular Docking

Molecular docking was employed to study the interactions between the eucalyptol and the Keap1 using Autodock vina version 1.1.2 package. The three-dimensional (3D) structure of the Keap1 (PDB ID: 3WN7) was retrieved from the RCSB Protein Data Bank (http://www.rcsb.org). The 2D structure of the eucalyptol was drawn by ChemBioDraw Ultra 14.0 and converted to the 3D structure by ChemBio3D Ultra 14.0 package. The AutoDockTools version 1.5.6 was used to obtain the docking input files. The binding site of the Keap1 was identified as center_x: 3.766, center_y: 1.122, and center_z: 19.296 with dimensions size_x: 15, size_y: 15, and size_z: 15. To increase the accuracy of the calculation, the value of exhaustiveness was set to 20. In addition, the default parameters were used, if it was not mentioned. The best docking pose as judged by the Vina score was chosen and further analyzed using PyMoL 1.7.6 software (http://www.pymol.org/).

SPR Interaction and Affinity Analysis

To understand the interactions between eucalyptol and the Keap1 protein, we performed an affinity measurement using surface plasmon resonance (SPR) technology. The SPR validation experiment was performed with the bScreen LB 991 Label-free Microarray System (Berthold Technologies, Germany). To validate detection of the eucalyptol–Keap1 interactions, the photo-cross-linker sensor chip was used. Rapamycin and DMSO were selected as system positive control and negative control, respectively. We arranged kinetic constant tests with FKBP12 immediately after the sample tests. During the SPR test, the Keap1 protein (MyBioSource, Vancouver, Canada) was diluted separately with running buffer to 200, 400, 800, 1600, and 3200 nM and injected for 600 s at a flow rate of 0.5 μl s⁻¹ at associating stage, followed by running buffer for 360 s at a flow rate of 0.5 μl s⁻¹ at each dissociating stage. At the end of each associating–dissociating cycle, the surface was regenerated to remove any remaining bound material with a pulse of 10 mM glycine–HCl (pH 2.0) at 20 μl min⁻¹ for 30 s.

TABLE 1 | Primers used for quantitative real-time PCR.

Target gene	Sense 5'-3'	Antisense 5'-3'
Nrf2	GCTGATGGAGTACCCTGAGGCTAT	ATGTCCGCAATGGAGGAGAAGTCT
HO-1	TGCCAGTGCCACCAAGTTCAAG	TGTTGAGCAGGAACGCAGTCTTG
NQO1	GGAGACAGCCTCTTACTTGCCAAG	CCAGCCGTCAGCTATTGTGGATAC
GCLC	TGAGATTTAAGC CCCCTCCT	TTGGGATCAGTCCAGGAAAC
GSTA2	TCAGTAACCTGCCCACAGTGAAG	GCATGTTCTTGACCTCTATGGCTGG
UGT1A1	CACGCTGGGAGGCTGTTAGT	CACAGTGGGCACAGTCAGGTA
UGT1A6	CACGTGCTACCTAGAGGCACAG	GACCACCAGCAGCTTGTCAC
UGT1A9	GAAGAACATGCATTTTGCTCCT	CTGGGCTAAAGAGGTCTGTCATAGTC
SULT1A1	CCCGTCTATGCCCGGATAC	GGGCTGGTGTCTCTTTCAGAGT
SULT2A1	TAGGGAAAAATTTAGGGCCAGAT	TTGTTTTCTTTCATGGCTTGGA
CYP2E1	CACCGTTGCCTTGCTTGTCTG	CTCATGAGCTCCAGACACTTC
GAPDH	ACATGGCCTCCAAGGAGTAAGA	GATCGAGT TGGGGCTGTGACT

The raw sensorgrams and measurements of the binding process of ligands and proteins were recorded in real time. The response unit (RU) of surface resonance was compared to determine the different binding affinities between each sample dot. The response unit data collected on the SPR biosensor was further processed to eliminate any artifacts such as non-specific binding and differences in buffer composition. The process and analysis of association and dissociation rate constants (K_a/K_{on} and K_d/K_{off} respectively) and the equilibrium dissociation constant (K_D, K_d/K_a) were performed using the data analysis software of the bScreen LB 991 unlabeled microarray system according to a single-site binding model (1:1 Langmuir binding) with mass transfer limitations for binding kinetics determination.

LC-MS/MS Analysis of APAP and its Metabolites

Plasma samples were obtained 0.2, 0.5, 0.75, 1, 1.5, 2, 4, and 6 h after different treatments. The concentrations of APAP and its conjugated metabolites were analyzed using modified LC-MS/MS. Briefly, plasma samples were centrifuged at 13,000g for 15 min at 4°C. The supernatants were diluted with ultrapure water. Reversed phase chromatography of APAP, APAP-glucuronide (APAP-gluc), and APAP-sulfate (APAP-sulf) was carried out using an ACE AQ C18 column (Advanced Chromatography Technologies, UK; 2.1×100 mm, 3 μm) at 50°C at a flow rate 0.3 ml/min. Mobile phase A was 0.2% formic acid in acetonitrile, while mobile phase B was 0.1% formic acid in methanol. The condition of chromatographic separation was 2% B from 0 to 0.5 min, held at 95% B for 0.8 min and then to 2% B at 3.31 min, followed by 5 min of column equilibration using 2% B.

The mass spectrometer was operated in ESI+Agilent Jet Stream mode with multiple reaction monitoring (MRM). The target compounds were detected by monitoring the m/z transition: m/z 150.0→107.0 for APAP, m/z 326.0→150.0 for APAP-gluc, and m/z 230.0→150.0 for APAP-sulf, with a dwell time of 100 ms for each mass transition. TIS temperature was 500°C, and TIS voltage was 3.5 kV. Curtain gas, nebulizing gas, TIS gas, and collision gas was 25, 90, 80, and 10 units, respectively. Collision energy and collision cell exit potential are 14 and 80 V for APAP, 5 V and 100 V for APAP-gluc, and 30 and 110 V for APAP-sulf, respectively. The mass spectrometer was operated at unit mass resolution for both Q1 and Q3 quadruples.

The standard curve consisted of samples containing 0, 20, 40, 80, 160, and 320 μg/ml of APAP, APAP-gluc, and APAP-sulf.

Statistical Analysis

The results were presented by means of, at least, five measurements, duplicated for each set, having a coefficient of variation less than 5%. One-way ANOVA followed by Duncan's multiple range test ($p < 0.05$) with SPSS 20.0 (SPSS Inc., Chicago, IL, USA) was applied for the mean values compared.

RESULTS

Phylogenetic Relationships

DNA barcode analysis with ITS2 sequence was used to investigate the evolutionary history and phylogenetic relationships of sample 1. A phylogenetic tree based on NJ cluster algorithm was constructed in **Figure 1A**. NJ sequence similarity analysis discovered that sample 1 was close to its close species from Artemisia (*Artemisia vulgaris*, *Artemisia lavandulifolia* and *Artemisia annua*). The branches indicate the bootstrap values for 1000 replicates. Furthermore, inter-species variations were also calculated and the results showed that Sample 1 and Artemisia argyi showed the highest similarity (0.005), while Sample 2 and Artemisia vulgaris showed the highest similarity (0.003) as presented in **S. Table 2**. The secondary structure of ITS2 of Sample 1 is similar to *Artemisia argyi*, while Sample 2 is similar to *Artemisia vulgaris* (**Figure 1B**). Compared with multiple analysis
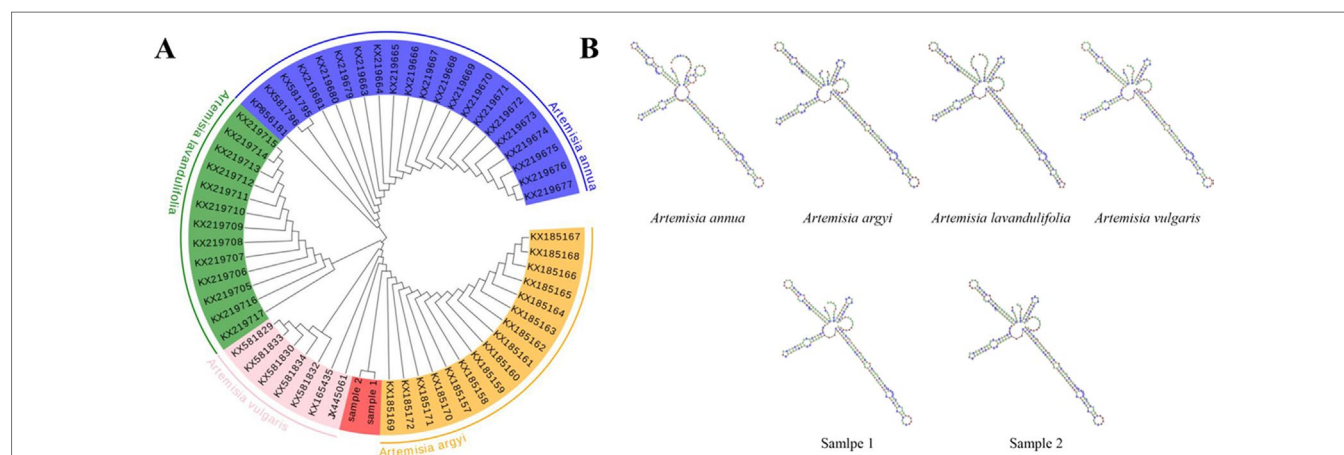
FIGURE 1 | Species identification of sample 2 by phylogenetic tree and ITS2 secondary structure. **(A)** Phylogenetic tree of the four Artemisia species constructed with the ITS2 sequences using the neighbor-joining (NJ) method; **(B)** ITS2 secondary structure.

methods, the results show that Sample 1 was *Artemisia argyi* L, and Sample 2 was *Artemisia vulgaris* L.

E-Nose Analysis

To analyze the volatile organic compounds from AV, the e-nose was used. The polar plot display of sensor values of EOs from AV at 57s was given by the cursor in the measurement window. The sensor of W2W, W1W, and W1S was highly sensitive to the EOs of AV **(Figure 2A)**, indicating that the collected EOs contained sulph-chlor, sulphur-organic and broad-methane. The flying data were examined with PCA to visualize the response patterns in the feature space of principal components (PC). Two PCs, namely, PC1 and PC2, which explained 80.4% and 16.4%, respectively, of the data variance, were chosen based on the Eigen values ($p > 0.5$). Using PCA, the three main odors of AV were sulph-chlor, sulphur-organic, and broadrange **(Figure 2B)**. The Lo analysis revealed that W5S and W1W have higher response to the compounds of AV, indicating that the broad range and sulphur-organic were present in EOs of AV. W6S, W5C, W2S, and W3S were not sensitive to the EOs of AV **(Figure 2C)**.

Phytochemical Analysis of AV-EOs

Eighty components were identified from EOs of AV by HS-SPME-GC-MS analysis **(Table 2, Figure 2D)**. The three highest components of AV were eucalyptol (28.07%), Cis-β-Terpineol (16.44%), Byciclo [3.1.0] hex-2-ene, 4-methyl-1-(1-methylethyl) (8.89%), Benzene,1-methyl-4-(1-methylethyl) (7.38%), 1,4-Cyclohexadiene,1-methyl-4-(1-methylethyl)(4.88%),1S-a-Pinene (4.16%), and 3-Cyclohexen-1-ol, 4-methyl-1-(1-methylethyl) (3.35%).

Effect of EOs and Eucalyptol on APAP-Induced Hepatotoxicity

APAP-treated mice exhibited hepatocellular injury **(Figure 3B)** compared with control group **(Figure 1A)**. More than half of the centrilobular hepatocytes were swollen with marked cytoplasmic vacuolation and condensed nuclei. The white spots were on the liver, while the EO and eucalyptol group did not show hepatotoxic effects **(Figures 3C–G)**. ALT and AST levels were significantly increased by 2.67-fold and 2.06-fold in the APAP group, respectively, as compared to the control group **(Figure 3F)**. APAP-EO and APAP-EU decreased the ALT and AST activities compared with

FIGURE 2 | Component analysis of *Artemisia vulgaris* L. essential oils (AV-EOs). **(A)** Polar plot display of sensor values of EOs from AV at 57 s given by the cursor in the measurement window; **(B)** principal component analysis (PCA); **(C)** loading (Lo) analysis; W1C (aromatic), W5S (broadrange), W3C (aromatic), W6S (hydrogen), W5C (arom-aliph), W1S (broad-methane), W1W (sulphur-organic), W2S (broad-alcohol), W2W (sulph-chlor), W3S (methane-aliph); **(D)** the headspace solid-phase microextraction coupled with gas chromatography (HS-SPME-GC-MS) diagram of AV.

FIGURE 3 | Effect of essential oil and eucalyptol on the acetaminophen (APAP)-induced liver changes and serum biomarkers of liver toxicity in mice. **(A–E)** The liver changes in mice. **(A)** Control group; **(B)** APAP treatment group, circle means cytoplasmic vacuolation; **(C)** APAP-EO treatment group; **(D)** APAP-EU treatment group; **(E)** APAP-NAC treatment group; **(F)** EO treatment group; **(G)** EU treatment group; **(H)** the activity of ALT and AST. $n = 6$, bars that do not share a common letter (a, b, c) were considered significantly different from each other ($p < 0.05$).

APAP-treated liver. The liver indexes were 4.43, 4.98, 4.48, 4.46, 4.42, 4.41, and 4.42 in the control-, APAP-, APAP-EO-, APAP-EU-, APAP-NAC-, EO, and EU group, respectively.

Hepatic Antioxidant Effects of AV-EOs and EU on Oxidative Stress Biomarkers

To investigate the antioxidant effect of AV-EOs and EU, the levels of oxidative stress biomarkers were examined in mice **(Figure 4)**. APAP treatment significantly increased the content of MDA and ROS by 2.38- and 1.92-fold, respectively. APAP administration resulted in a significant decrease in the activities of SOD and CAT to 0.72- and 0.44-fold.

APAP-EO or EU co-administration reversed the decrease in OD and CAT and reduced the levels of ROS and MDA. Meanwhile, EOs and eucalyptol could eliminate ROS ($p < 0.05$).

Effect of AV-EU on Oxidative Stress-Related Gene Expression

qPCR analysis indicated that APAP-EU co-treatment alleviated APAP-induced reduction of GCLC and GSTA. EU treatment significantly increased the levels of HO-1, NQO1, GCLC, and GSTA2, suggesting EU's activities in antioxidant mediation **(Figure 5)**.

Effect of AV-EU on APAP Metabolism

APAP and its major conjugates in plasma were analyzed using HPLC-MS/MS. The AUC of APAP in the APAP group was significantly higher (1.65 fold) than in APAP-EU treatment group, and APAP-EU significantly increased the levels of AUC of APAP-gulc and APAP-sulf in plasma **(Figure 6A)**.

The hepatic mRNA expressions of UGT1A1, UGT1A6, and UGT1A9 in the eucalyptol-treated group were 2.3-, 1.95-, and 2.07-fold higher than the control group **(Figure 6B)**, respectively. Compared with the control group, the mRNA expression of UGT1A6 significantly decreased 0.45-fold after APAP treatment. AV-EU post-treatment increased the mRNA levels of UGT1A6. Likewise, eucalyptol increased SULT1A1 and SULT2A1 mRNA levels by 2.5- and 2.0-fold, respectively **(Figure 6C)**. The expression of CYP2E1 was significantly increased (2.8-fold) after APAP treatment; the mRNA levels of CYP2E1 significantly increased after eucalyptol treatment **(Figure 6D)**.
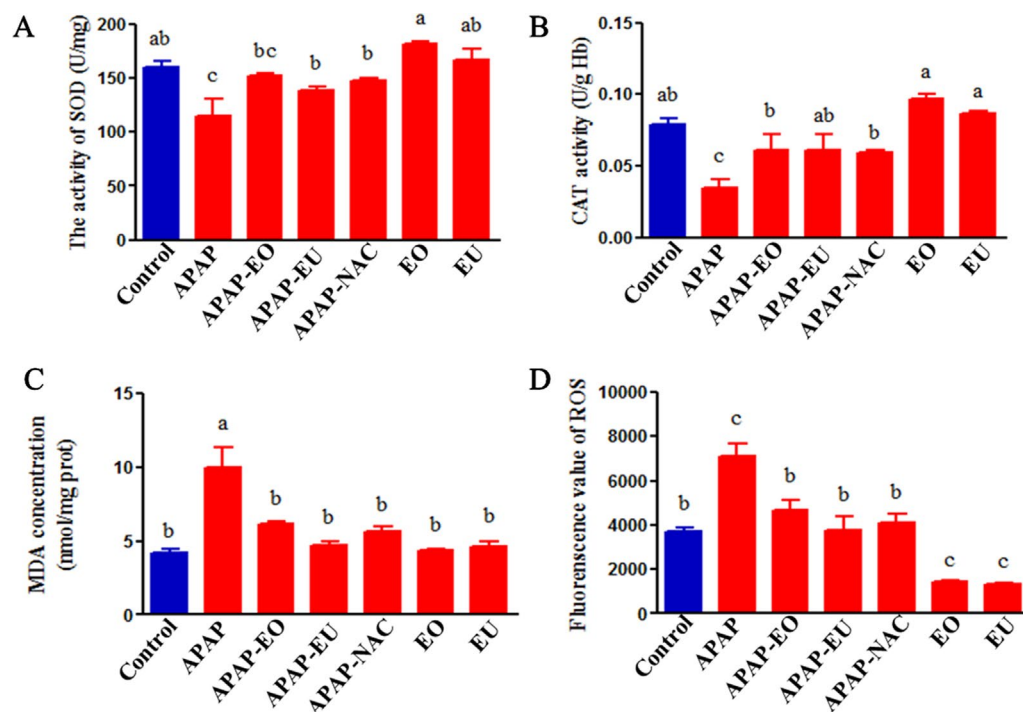
FIGURE 4 | Effects of essential oil and eucalyptol on the APAP-induced oxidative stress parameters. [a, b, c] different letters indicate statistically different groups ($p < 0.05$).
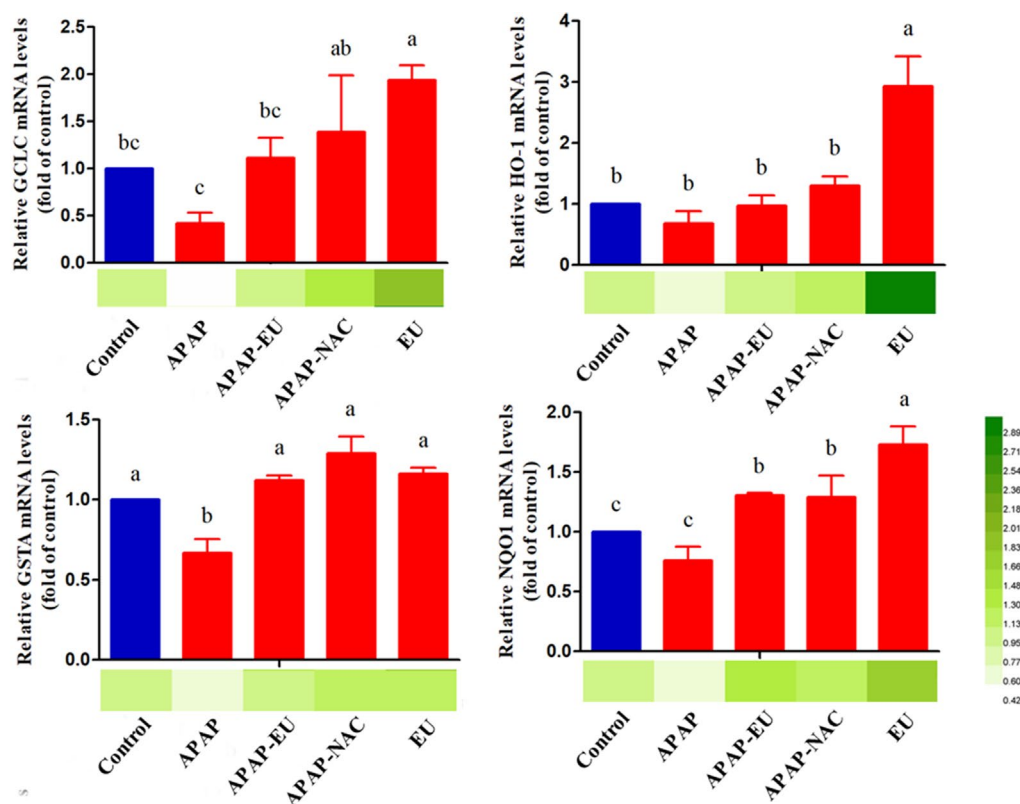
FIGURE 5 | mRNA expression levels of oxidative stress-related genes . [a, b, c, d] different letters indicate statistically different groups ($p < 0.05$).
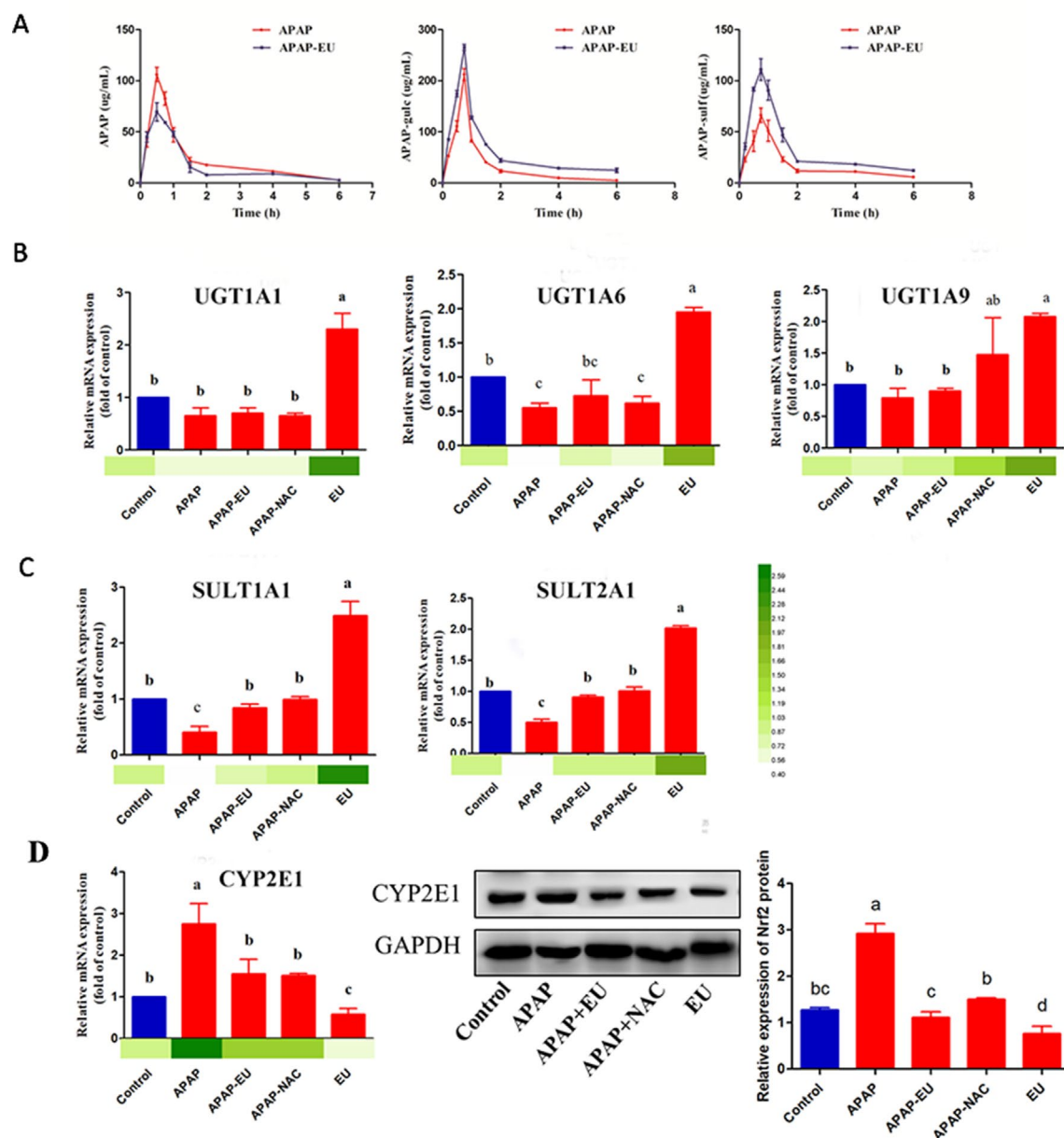
FIGURE 6 | Effects of eucalyptol on the APAP metabolic disposition. APAP: APAP treatment group; APAP+EU: EU was intragastrically administrated after APAP treatment group; APAP+NAC: NAC was oral administration after APAP treatment group. EU: EU was intragastrically administrated. [a, b, c] different letters indicate statistically different groups ($p < 0.05$).

Effect of AV-EU on Nrf2 Expression

The theoretical binding mode of the eucalyptol in the Nrf2 binding site of the Keap1 was illustrated in **Figure 7A**. Detailed analysis showed that the compound eucalyptol was positioned at the hydrophobic pocket, surrounded by the residues Tyr-525, Ala-556, Tyr-572, and Phe-577, forming a stable hydrophobic binding. Importantly, the "O" atom of eucalyptol formed the key hydrogen-bond interaction with the residue Arg-415, with a bond length of 2.9 Å. The hydrogen bond was the main interaction between eucalyptol and Keap1. According to the affinity measurement, eucalyptol showed a strong affinity ($K_D = 1.42 \times 10^{-5}$) for Keap1 protein. The association rate constants k_{on} and k_{off} were 1.75×10^3 and 2.49×10^{-2}, respectively. Their binding curves during the test are shown in **Figure 7B**. These interactions helped to anchor eucalyptol in the Nrf2 binding site of Keap1. In addition, the estimated binding energy of eucalyptol is -5.5 kcal•mol^{-1}, suggesting that eucalyptol is an inhibitor of the Keap1.

qPCR and WB analysis show that eucalyptol treatment increased Nrf2 mRNA **(Figures 7B, C)** and stimulated the nuclear translocation of Nrf-2 transcription factor. The ratio of protein
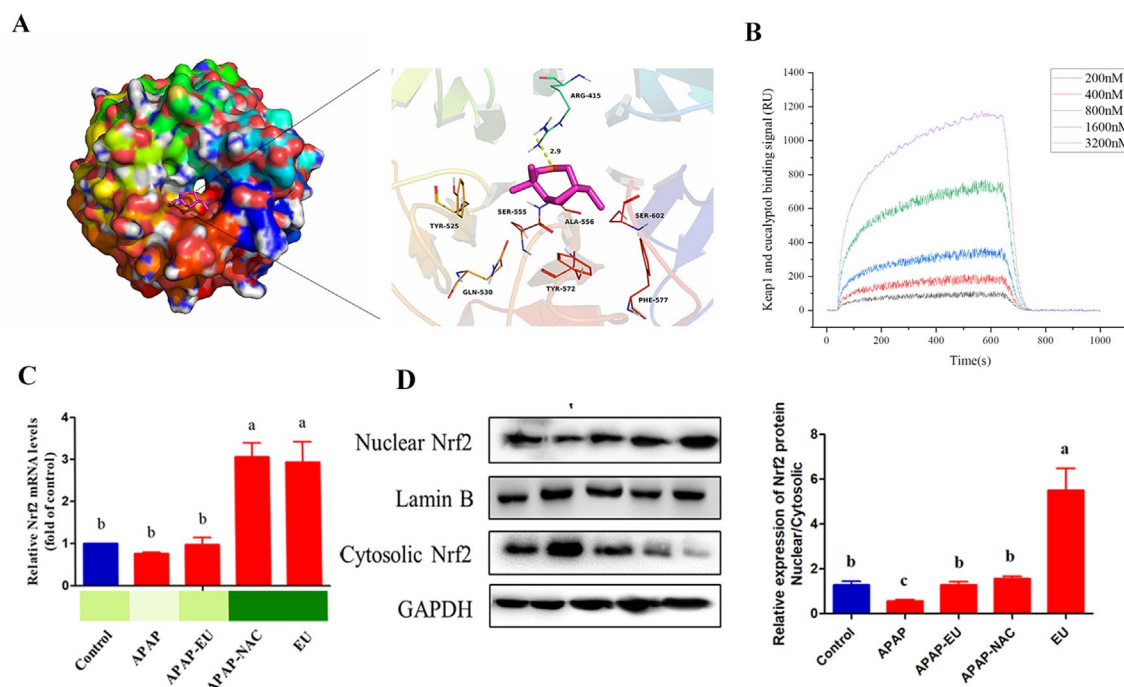
FIGURE 7 | Effect of eucalyptol on nuclear factor erythroid 2-related factor 2 (Nrf2) expression. **(A)** eucalyptol docking with Keap1; **(B)** binding signal of Keap1 and eucalyptol (RU); **(C)** mRNA levels of Nrf2; **(D)** protein levels of Nrf2 in nuclear and cytosolic. [a, b, c] different letters indicate statistically different groups ($p < 0.05$).

expression of nuclear Nrf-2 and cytoplasmic Nrf-2 in eucalyptol was 5.8-fold higher than that of the control group **(Figure 7C)**.

DISCUSSION

AV is one of the famous *Artemisia* species compared to others such as *A. absinthium*, *A. nilagirica*, and *A. deserti*, (Kazemi et al., 2013; Pelkonen et al., 2013; Sati et al., 2013). AV-EOs have a high content of eucalyptol and Cis-β-Terpineol, which shown anti-inflammatory and antioxidant effects against various diseases, including respiratory disease, pancreatitis, colon damage, and non-alcoholic steatohepatitis (Murata et al., 2015; Seol and Kim, 2016). In our present study, treatment with AV-EOs and eucalyptol significantly attenuated APAP overdose (300 mg/kg) and induced the increase of serum aminotransferase and hepatic histopathological lesions **(Figure 3)**, suggesting that AV-EOs possess the ability to prevent APAP-induced hepatotoxicity.

Many studies on *Artemisia* did not result in any significant adverse effects in food/water consumption, body weight, mortality, hematology, serum biochemistry, organ weight, and histopathology (Wan et al., 2017; Yun et al., 2017); high-dose (752 mg/kg) usage of *Artemisia* may pose health based on mutagenesis and hepatotoxicity, suggesting that high-dose application of the extract in the treatment of serious disease is not recommended (Kalantari et al., 2013). *Artemisia abstinthium* may have neurotoxic; because of the major activity of thujone, it can inhibit the gammaaminobutyric acid A (GABAA) receptor causing excitation and convulsions in a dose-dependent manner (Pelkonen et al., 2013). In our study, AV-EOs

do not contain thujone **(Table 2)**, and the dose of essential oil from *Artemisia vulgaris* was lower than the toxic dose. Our data show that dose of essential oil from Artemisia vulgaris (5%, 100 ml/kg) did not induce the liver injury. The liver index in the APAP group was significantly higher than that of the control group, while no significant difference was observed among APAP-EO $_{(AV)}$, EO, and control group. Compared with compounds of EOs and the liver function indicators after EO treatment, we speculate that low dose of AV is safe.

APAP has non-toxic and toxic metabolic pathways in the liver. In the non-toxic pathway, APAP was glucuronidated and sulfated into APAP-gluc and APAP-sulf and excreted into blood and bile with the involvement of UGT and SULT family (Cao et al., 2017). In this study, the levels of UGT1A1, UGT1A6, UGT1A9, SULT1A1, and SULT2A1 were significantly increased after eucalyptol treatments, suggesting eucalyptol-enhanced APAP metabolism by the non-toxic pathway. The Nrf2 gene, with the consensus of TGAG/CNNNGC (N represents any base), is essential for inducing an increase in UGT and SULT family's expression (Hayes and Dinkova-Kostova, 2014). Eucalyptol significantly increased the mRNA expression of Nrf2 **(Figure 7B)**. Eucalyptol can directly combine with Keap1 at site Arg-415, which was Nrf2-Keap1 binding site. Eucalyptol showed a strong affinity for Keap1 protein. The activated Nrf2 was transferred from cytoplasmic into nuclear. The expression of Nrf2 mRNA was also increased, resulting in an increase in nuclear/cytosolic relative expression under EO treatment **(Figure 7C)**. In addition, Nrf2 is a transcription factor that modulates endogenous antioxidant enzymes (Hou et al., 2018; Liu et al., 2018; Mahmoud et al., 2018). EOs stimulate Nrf2 activation. The activated Nrf2

TABLE 2 | The compositions of *Artemisia vulgaris* L. (AV).

		Artemisia vulgaris			
Rank	Time (min)	Compound	CAS#	Matching rate	Relative amount
1	1.423	1,3-Dioxolane-4-methanol	005464-28-8	64	0.03%
2	1.623	Oxirane,(propoxymethyl)-	003126-95-2	64	0.02%
3	1.805	3(2H)-Furanone,dihydor-2-methyl-	003188-00-9	42	0.00%
4	1.846	Methacrolein	000078-85-3	72	0.01%
5	2.382	2-Butanone,3-methyl-	000563-80-4	49	0.02%
6	2.452	Oxirane,tirmethyl-	005076-19-7	43	0.00%
7	2.799	1,3-Dioxolane,4-methyl-	001072-47-5	47	0.01%
8	3.346	1-Butanol,3-methyl-	000123-51-3	59	0.02%
9	3.393	1-Heptene	000592-76-7	50	0.04%
10	3.846	Toluene	000108-88-3	70	0.02%
11	4.276	1-Octene	000111-66-0	94	0.07%
12	4.481	Hexanal	000066-25-1	90	0.07%
13	5.74	2-Hexanal	000505-57-7	96	0.42%
14	6.74	1-Nonene	000124-11-8	95	0.05%
15	7.622	Tircyclo[2.2.1.0(2,6)]heptane,1,7,7-trimethyl-	000508-32-7	96	0.07%
16	7.74	Bicyclo[3.1.0]hexane,4-methyl-1-(1-methylethyl)-,didehydro derive.	058037-87-9	94	2.01%
17	7.964	1S-.alpha.-Pinene	007785-26-4	96	4.16%
18	8.264	Bicyclo[3.1.0]hex-2-ene,4-methylene-1-(1-methylethyl)-	036262-09-6	91	0.13%
19	8.466	Camphene	000079-92-5	97	1.74%
20	8.558	1-Butanol,4-(phenylmethoxy)-	004541-14-4	47	0.03%
21	8.852	Benzaldehyde	000100-52-7	97	0.11%
22	9.046	Benzaldehyde	000100-52-7	42	0.02%
23	9.175	Byciclo[3.1.0]hex-2-ene,4-methyl-1-(1-methylethyl)-	028634-89-1	91	8.89%
24	9.305	.beta.-Pinene	000127-91-3	97	1.54%
25	9.487	1-Octen-3-ol	003391-86-4	90	2.65%
26	9.675	1-Octen-3-ol	003391-86-4	43	0.10%
27	9.734	2-Propyl-1-pentanol	058175-57-8	50	0.23%
28	10.122	Octanal	000124-13-0	80	0.10%
29	10.205	.alpha.-Phellandrene	000099-83-2	90	0.75%
30	10.546	(+)-4-Carene	029050-33-7	98	2.92%
31	10.84	Benzene,1-methyl-4-(1-methylethyl)-	000099-87-6	97	7.38%
32	11.11	Eucalyptol	000470-82-6	97	28.07%
33	11.775	1,4-Cyclohexadiene,1-methyl-4-(1-methylethyl)-	000099-85-4	94	4.88%
34	12.175	Cis-.beta.-Terpineol	007299-40-3	96	16.44%
35	12.469	(+)-4-Carene	029050-33-7	98	1.04%
36	12.599	Benzene,1-methyl-4-(1-methylethenyl)-	001195-32-0	94	0.16%
37	12.805	Acetoacetic acid isoamyl ester	002308-18-1	43	0.03%
38	13.116	Terpineol, Cis-.beta.-	007299-41-4	90	0.06%
39	13.246	1-Methoxy-1,3-cyclohexadiene	002161-90-2	60	0.03%
40	13.328	1,6-Dimethylhepta-1,3,5-triene	1000196-61-0	94	0.16%
41	13.446	2-Cyclohexen-1-ol,1-methyl-4-(1-methylethyl)-,trans-	029803-81-4	96	0.30%
42	13.522	Cyclohexanone,5-methyl-2-(1-methylethenyl)-,trans-	029606-79-9	78	0.07%
43	13.599	Cyclopentasiloxane,decamethyl-	000541-02-6	80	0.02%
44	13.904	2-Cyclohexen-1-ol,1-methyl-4-(1-methylethyl)-,cis-	029803-82-5	46	0.14%
45	14.01	Camphor	000076-22-2	98	3.02%
46	14.193	Benzyl alcohol	000100-51-6	55	0.15%
47	14.275	2,6-Dimethylbicyclo[3.2.1]octane	000215-28-2	72	0.13%
48	14.404	Bicyclo[2.2.1]heptan-3-one,6,6-dimethyl-2-methylene-	1016812-40-1	97	0.16%
49	14.687	3-Cyclohexene-1-methanol,.alpha.,.alpha.,4-trimethyl-,(S)-	010482-56-1	72	0.39%
50	14.757	Borneol	010385-78-1	97	1.87%
51	14.981	3-Cyclohexen-1-ol,4-methyl-1-(1-methylethyl)-	000562-74-3	93	3.35%
52	15.44	3-Cyclohexene-1-methanol,.alpha.,.alpha.,4-trimethyl-,(S)-	010482-56-1	87	2.97%
53	16.504	Bicyclo[2.2.1]heptan-2-ol,1,7,7-trimethyl-,acetate,(1S-endo)-	005655-61-8	72	0.11%
54	16.934	Cyclohexene,1-methyl-3-(1-methylethenyl)-,(.+/-.)-	000499-03-6	91	0.06%
55	17.087	2-Cyclohexen-1-one,2-methyl-5-(1-methylethyl)-,(S)-	002244-16-8	38	0.06%
56	18.428	1-Cyclohexene-1-carboxaldehyde,4-(1-methylethyl)-	002111-75-3	98	0.25%
57	18.751	Bornyl acetate	000076-49-3	99	0.15%
58	19.604	Cyclohexasiloxane,dodecamethyl-	000540-97-6	91	0.02%
59	19.781	Triallylmethylsilane	001112-91-0	38	0.07%
60	21.557	Phenol,2-methoxy-3-(2-propenyl)	001941-12-4	98	0.45%
61	22.145	Copaene	003856-25-5	98	0.12%

(Continued)

TABLE 2 | Continued

Rank	Time (min)	Compound	CAS#	Matching rate	Relative amount
62	22.351	.alpha.-Bourbonene	1000293-01-9	87	0.04%
63	22.574	Benzenepropanoic aid,10-undecenyl	000281-79-0	43	0.03%
64	22.645	Phenol,4-methyl-	1000106-44-5	64	0.04%
65	22.757	Tetradecane	000629-59-4	97	0.04%
66	23.027	3-Carene	013466-78-9	81	0.04%
67	23.157	Caryophyllene	000087-44-5	99	0.48%
68	23.421	Bicyclo[3.1.1]hept-2-ene,2,6-dimethyl-6-(4-methyl-3-pentenyl)-	017699-05-7	98	0.04%
69	23.786	1,6,10-Dodecatriene,7,11-dimethyl- 3-methylene-,(Z)-	028973-97-9	93	0.11%
70	23.863	.alpha.-Caryophyllene	006753-98-6	97	0.05%
71	23.986	1H-Benzocycloheptene,2,4a,5,6,7,8,9 ,9a,-octahydro-3,5,5-trimethyl-9-methylene-,(4aS-cis)-	003853-83-6	70	0.03%
72	24.168	Naphthalene,decahydro-4a-methyl-1-methylene-7-(1-methylethylidene)-,(4aR-trans)-	000515-17-3	98	0.05%
73	24.333	1,6,10-Dodecatriene,7,11-dimethyl- 3-methylene-,(Z)-	028973-97-9	95	0.22%
74	24.333	Decahydro-4a-methyl-methylene-7-(1-methylethenyl)-,[4aR-(4a. alpha.,7.alpha.,8a.beta.)]-	017066-67-0	99	0.15%
75	24.533	1H-Cycloprop[e]azulene,1a,2,3,4,4a,5,6,7b-octahydro-1,1,4,7-tetramethyl-,[1aR-(1a.alpha.,4.alpha.,4a.beta.,7b.alpha.)]-	000489-40-7	86	0.04%
76	24.688	Isobornyl propinonate	002756-56-1	38	0.05%
77	24.792	Naphthalene,1,2,4a,5,6,8a-hexahydro-4,7-dimethyl-1-(1-methylethyl)-	000483-75-0	97	0.01%
78	24.851	Naphthalene,1,2,3,,5,6,8a-hexahydro-4,7-dimethyl-1-(1-methylethyl)-,(1S-cis)-	000483-76-1	99	0.01%
79	24.904	Naphthalene,1,2,3,4-tetrahydro-1,6-dimethyl-4-(1-methylethyl)- ,(1S-cis)-	000483-77-2	96	0.02%
80	25.715	Caryophyllene oxide	001139-30-6	90	0.05%
81	25.845	Hentriacontane	000630-04-6	38	0.01%
82	26.592	5.beta.,7.beta.H,10.alpha.-Eudesm-11-en-1.alpha.-ol	025826-85-1	52	0.02%
83	26.768	1-Propene,2-(3-methylphenyl)-1-phenyl-,(Z)-	000138-72-6	70	0.01%
84	28.239	Phthalic acid,2-ethoxyethyl octyl ester	1000322-87-6	50	0.01%
85	31.539	1,1,1,5,7,7,7-Heptamethyl-3,3-bis (trimethylsiloxy)tetrasiloxane	038147-00-1	32	0.04%

FIGURE 8 | Mechanism by which eucalyptol protects APAP induced liver injury.
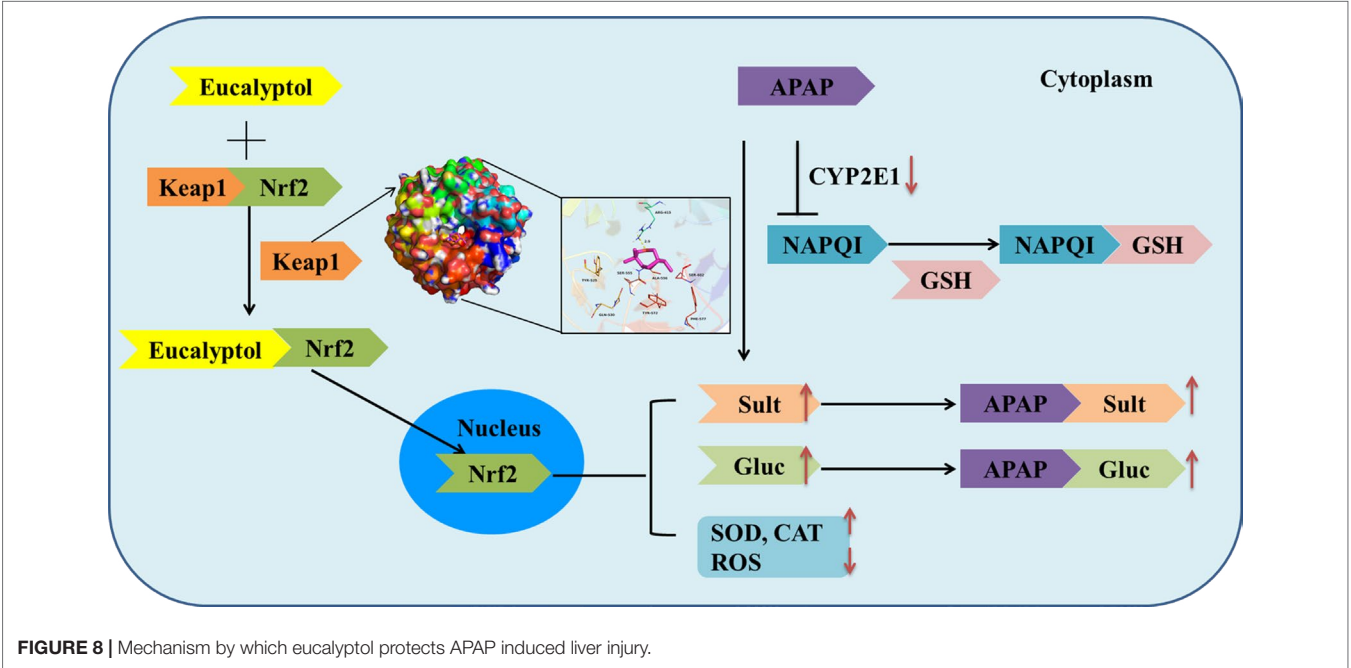
binds to the antioxidant response element and further activates the transcription of gene encoding for antioxidants and detoxifications including heme oxygenase-1 (HO-1), NAD(P)H: quinone oxidoreductase-1 (NQO-1), and glutathione-synthesizing enzymes [glutamate-cysteine ligase catalytic subunit (GCLC)] (Hu et al., 2018). Our results suggest that EOs increased Nrf2 transfer from the cytoplasm to the nucleus, thereby leading to the transcriptional activation of antioxidant enzymes (HO-1, SOD, and CAT; Figs. 4 and 5) and phase II metabolic enzymes (UGT and SULT, **Figure 6**).

The second metabolism pathway of APAP was a toxic reaction. Overdosed APAP was transferred into NAPQI by CYP2E1 (Ganetsky et al., 2018), which undergoes chemical and enzymatic conjugation to GSH. The toxic pathway could lead to lipid peroxidation; antioxidant enzyme activities were reduced, and the levels of ROS were increased. Here, APAP increased MDA and ROS levels and decreased the activities of SOD and CAT, suggesting that APAP-induced hepatic dysfunction is caused by oxidative stress. The expression of CYP2E1 was significantly increased by APAP and decreased by eucalyptol treatment **(Figure 6)**. CYP2E1-deficient mice were resistant to the liver injury-induced APAP, while the transgenic mouse expressing human CYP2E1 was susceptible to the conversion of APAP to NAPQI. Our results show that eucalyptol inhibits CYP2E1 expression and attenuates liver injury. The pathway analysis study also reported the following active compounds: 2-Butanone,3-methyl-, 1-Octene, Benzaldehyde, Phenol,4-methyl-, Octanal, 1-Nonene, and Hexanal. These compounds represent the effective targets such as Aldo-keto reductase family 1 member C1, Alcohol dehydrogenase 1B, Cytochrome P450 2A6, and Cytochrome P450 1A2, which are involved in the metabolism of xenobiotics by cytochrome P450 and drug metabolism–cytochrome P450 pathway, respectively, which is related to CYP2E1 expression.

Collectively, AV-EOs can prevent APAP-induced liver injury through two pathways: down-regulation of CYP2E1 expression, which decreases plasma concentration of APAP into NAPQI, and the up-regulation of the expression of the detoxification pathway. The up-regulation pathway includes inhibitory binding with Keap1, which stimulates Nrf2 translocation from cytoplasm into mitochondria, activates Nrf2, and thus increases the activity of antioxidant enzymes (SOD, GSH, CAT, and GPx) and phase II enzymes (SULTs and UGTs) **(Figure 8)**, thereby decreasing APAP plasma concentration and accelerating APAP harmless metabolism.

DATA AVAILABILITY

All datasets generated for this study are included in the manuscript and the supplementary files.

ETHICS STATEMENT

The mice were obtained from the animal center of Zhengzhou University (Zhengzhou, China). The experimental protocol was reviewed and approved by the Ethics Committee of the Institute of Modern Biotechnology for the Use of Laboratory Animals.

AUTHOR CONTRIBUTIONS

ZJ and XG designed the study, performed the research, analyzed data, and wrote the paper; KZ, GS, BC, QZ, and SZ performed animal research and analyzed data. GK and XZ designed research and organized the discussion.

FUNDING

SUPPLEMENTARY MATERIAL

The Supplementary Material for this article can be found online at: https://www.frontiersin.org/articles/10.3389/fphar.2019.00782/full#supplementary-material

REFERENCES

Asrani, S. K., Devarbhavi, H., Eaton, J., and Kamath, P. S. (2018). Burden of liver diseases in the world. *J. Hepatol.* 70, 151–171. doi: 10.1016/j.jhep.2018.09.014

Cao, L., Kwara, A., and Greenblatt, D. J. (2017). Metabolic interactions between acetaminophen (paracetamol) and two flavonoids, luteolin and quercetin, through in-vitro inhibition studies. *Int. J. Clin. Pharm-Net.* 69, 12, 1762–1772. doi: 10.1111/jphp.12812

Chen, M., Li, X., Shi, Q., Zhang, Z., and Xu, S. (2019). Hydrogen sulfide exposure triggers chicken trachea inflammatory injury through oxidative stress-mediated FOS/IL8 signaling. *J. Hazard. Mater.* 368, 243–254. doi: 10.1016/j.jhazmat.2019.01.054

Cho, K. H. (2012). 1,8-cineole protected human lipoproteins from modification by oxidation and glycation and exhibited serum lipid-lowering and anti-inflammatory activity in zebrafish. *BMB Rep.* 45 (10), 565–570. doi: 10.5483/BMBRep.2012.45.10.044

Dennis, G., Jr., Sherman, B. T., Hosack, D. A., Yang, J., Gao, W., Lane, H. C., et al. (2003). DAVID: Database for Annotation, Visualization, and Integrated Discovery. *Genome Biol.* 4 (5), P3. doi: 10.1186/gb-2003-4-9-r60

Du, K., Ramachandran, A., and Jaeschke, H. (2016). Oxidative stress during acetaminophen hepatotoxicity: sources, pathophysiological role and therapeutic potential. *Redox. Biol.* 10, 148–156. doi: 10.1016/j.redox.2016.10.001

Ferreira, J. F., and Luthria, D. L. (2010). Drying affects artemisinin, dihydroartemisinic acid, artemisinic acid, and the antioxidant capacity of Artemisia annua L. leaves. *J. Agric Food Chem.* 58 (3), 1691–1698. doi: 10.1021/jf903222j

Ganetsky, M., Berg, A. H., Solano, J. J., and Salhanick, S. (2018). Inhibition of CYP2E1 with propylene glycol does not protect against hepatocellular injury in human acetaminophen daily-dosing model. *J. Clin. Pharmacol.* 00 (0), 1–8. doi: 10.1002/jcph.1299

Gaur, R., Darokar, M. P., Ajayakumar, P. V., Shukla, R. S., and Bhakuni, R. S. (2014). In vitro antimalarial studies of novel artemisinin biotransformed products and its derivatives. *Phytochemistry* 107, 135–140. doi: 10.1016/j.phytochem.2014.08.004

Giamakis, A., Kretsi, O., Chinou, I., and Spyropoulos, C. G. (2001). Eucalyptus camaldulensis: volatiles from immature flowers and high production of 1,8-cineole and beta-pinene by in vitro cultures. *Phytochemistry* 58 (2), 351–355. doi: 10.1016/S0031-9422(01)00193-5

Giangaspero, A., Ponti, C., Pollastro, F., Del Favero, G., Della Loggia, R., Tubaro, A., et al. (2009). Topical anti-inflammatory activity of Eupatilin, a lipophilic flavonoid from mountain wormwood (Artemisia umbelliformis Lam.). *J. Agric Food Chem.* 57 (17), 7726–7730. doi: 10.1021/jf901725p

Hayes, J. D., and Dinkova-Kostova, A. T. (2014). The Nrf2 regulatory network provides an interface between redox and intermediary metabolism. *Trends Biochem. Sci.* 39 (4), 199–218. doi: 10.1016/j.tibs.2014.02.002

Hou, Y., Peng, S., Li, X., Yao, J., Xu, J., and Fang, J. (2018). Honokiol alleviates oxidative stress-induced neurotoxicity via activation of Nrf2. *ACS Chem. Neurosci.* 9, 12, 3108-3116. doi: 10.1021/acschemneuro.8b00290

Hu, Y., Yu, C., Yao, M., Wang, L., Liang, B., Zhang, B., et al. (2018). The PKCdelta-Nrf2-ARE signalling pathway may be involved in oxidative stress in arsenic-induced liver damage in rats. *Environ. Toxicol. Pharmacol.* 62, 79–87. doi: 10.1016/j.etap.2018.05.012

Jiang, Z., Chen, C., Wang, J., Xie, W., Wang, M., Li, X., et al. (2016). Purple potato (Solanum tuberosum L.) anthocyanins attenuate alcohol-induced hepatic injury by enhancing antioxidant defense. *J. Nat. Med.* 70 (1), 45–53. doi: 10.1007/s11418-015-0935-3

Juergens, U. R., Stober, M., Schmidt-Schilling, L., Kleuver, T., and Vetter, H. (1998). Antiinflammatory effects of euclyptol (1.8-cineole) in bronchial asthma: inhibition of arachidonic acid metabolism in human blood monocytes ex vivo. *Eur. J. Med. Res.* 3 (9), 407–412.

Kalantari, H., Galehdari, H., Zaree, Z., Gesztelyi, R., Varga, B., Haines, D., et al. (2013). Toxicological and mutagenic analysis of Artemisia dracunculus (tarragon) extract. *Food Chem. Toxicol.* 51, 26–32. doi: 10.1016/j.fct.2012.07.052

Kazemi, M., Dakhili, M., Dadkhah, A., Fadaeian, M., and Shafizadeh, S. (2013). Composition, antimicrobial and antioxidant activities of Artemisia deserti Kracsh essential oil from Iran. *Asian. J. Chem.* 25 (1), 47–51. doi: 10.14233/ajchem.2013.12409

Keiser, M. J., Roth, B. L., Armbruster, B. N., Ernsberger, P., Irwin, J. J., and Shoichet, B. K. (2007). Relating protein pharmacology by ligand chemistry. *Nat. Biotechnol.* 25 (2), 197–206. doi: 10.1038/nbt1284

Keller, A., Schleicher, T., Schultz, J., Muller, T., Dandekar, T., and Wolf, M. (2009). 5.8S-28S rRNA interaction and HMM-based ITS2 annotation. *Gene* 430 (1–2), 50–57. doi: 10.1016/j.gene.2008.10.012

Koetschan, C., Hackl, T., Muller, T., Wolf, M., Forster, F., and Schultz, J. (2012). ITS2 database IV: interactive taxon sampling for internal transcribed spacer 2 based phylogenies. *Mol. Phylogenet. Evol.* 63 (3), 585–588. doi: 10.1016/j.ympev.2012.01.026

Lahlou, S., Figueiredo, A. F., Magalhaes, P. J., and Leal-Cardoso, J. H. (2002). Cardiovascular effects of 1,8-cineole, a terpenoid oxide present in many plant essential oils, in normotensive rats. *Can. J. Physiol. Pharmacol.* 80 (12), 1125–1131. doi: 10.1139/y02-142

Lancaster, E. M., Hiatt, J. R., and Zarrinpar, A. (2015). Acetaminophen hepatotoxicity: an updated review. *Arch. Toxicol.* 89 (2), 193–199. doi: 10.1007/s00204-014-1432-2

Levison, K. K., Takayama, K., Isowa, K., Okabe, K., and Nagai, T. (1994). Formulation optimization of indomethacin gels containing a combination of three kinds of cyclic monoterpenes as percutaneous penetration enhancers. *J. Pharm. Sci.* 83 (9), 1367–1372. doi: 10.1002/jps.2600830932

Liu, X. F., Zhou, D. D., Xie, T., Hao, J. L., Malik, T. H., Lu, C. B., et al. (2018). The Nrf2 signaling in retinal ganglion cells under oxidative stress in ocular neurodegenerative diseases. *Int. J. Biol. Sci.* 14 (9), 1090–1098. doi: 10.7150/ijbs.25996

Loboda, A., Damulewicz, M., Pyza, E., Jozkowicz, A., and Dulak, J. (2016). Role of Nrf2/HO-1 system in development, oxidative stress response and diseases: an evolutionarily conserved mechanism. *Cell. Mol. Life Sci.* 73 (17), 3221–3247. doi: 10.1007/s00018-016-2223-0

Luo, H., Chen, J., Shi, L., Mikailov, M., Zhu, H., Wang, K., et al. (2011). DRAR-CPI: a server for identifying drug repositioning potential and adverse drug reactions via the chemical–protein interactome. *Nucleic Acids Res.* 39 (suppl_2), W492–W498. doi: 10.1093/nar/gkr299

Mahmoud, A. M., Germoush, M. O., Al-Anazi, K. M., Mahmoud, A. H., Farah, M. A., and Allam, A. A. (2018). Commiphora molmol protects against methotrexate-induced nephrotoxicity by up-regulating Nrf2/ARE/HO-1 signaling. *Biomed. Pharmacother.* 106, 499–509. doi: 10.1016/j.biopha.2018.06.171

Meng, X., Li, Y., Li, S., Gan, R.-Y., and Li, H.-B. (2018). Natural products for prevention and treatment of chemical-induced liver injuries. *Compr. Rev. Food Sci. Food Saf.* 17 (2), 472–495. doi: 10.1111/1541-4337.12335

Murata, S., Ogawa, K., Matsuzaka, T., Chiba, M., Nakayama, K., Iwasaki, K., et al. (2015). 1,8-Cineole ameliorates steatosis of Pten liver specific KO mice via Akt inactivation. *Int. J. Mol. Sci.* 16 (6), 12051–12063. doi: 10.3390/ijms160612051

Nikravesh, H., Khodayar, M. J., Mahdavinia, M., Mansouri, E., Zeidooni, L., and Dehbashi, F. (2018). Protective effect of gemfibrozil on hepatotoxicity induced by acetaminophen in mice: the importance of oxidative stress suppression. *Adv. Pharm. Bull.* 8 (2), 331–339. doi: 10.15171/apb.2018.038

Obolskiy, D., Pischel, I., Feistel, B., Glotov, N., and Heinrich, M. (2011). Artemisia dracunculus L. (tarragon): a critical review of its traditional use, chemical composition, pharmacology, and safety. *J. Agric Food Chem.* 59 (21), 11367–11384. doi: 10.1021/jf202277w

Pelkonen, O., Abass, K., and Wiesner, J. (2013). Thujone and thujone-containing herbal medicinal and botanical products: toxicological assessment. *Regul. Toxicol. Pharmacol.* 65 (1), 100–107. doi: 10.1016/j.yrtph.2012.11.002

Real, M., Barnhill, M. S., Higley, C., Rosenberg, J., and Lewis, J. H. (2019). Drug-induced liver injury: highlights of the recent literature. *Drug Saf.* 42 (3), 365–387. doi: 10.1007/s40264-018-0743-2

Sati, S. C., Sati, N., Ahluwalia, V., Walia, S., and Sati, O. P. (2013). Chemical composition and antifungal activity of Artemisia nilagirica essential oil growing in northern hilly areas of India. *Nat. Prod. Res.* 27 (1), 45–48. doi: 10.1080/14786419.2011.650636

Seol, G. H., and Kim, K. Y. (2016). Eucalyptol and its role in chronic diseases. *Adv. Exp. Med. Biol.* 929, 389–398. doi: 10.1007/978-3-319-41342-6_18

Song, M., Li, J., Xiong, C., Liu, H., and Liang, J. (2016). Applying high-resolution melting (HRM) technology to identify five commonly used Artemisia species. *Sci. Rep.* 6, 34133. doi: 10.1038/srep34133

Tamura, K., Peterson, D., Peterson, N., Stecher, G., Nei, M., and Kumar, S. (2011). MEGA5: molecular evolutionary genetics analysis using maximum likelihood, evolutionary distance, and maximum parsimony methods. *Mol. Biol. Evol.* 28 (10), 2731–2739. doi: 10.1093/molbev/msr121

Thompson, J. D., Gibson, T. J., and Higgins, D. G. (2002). Multiple sequence alignment using ClustalW and ClustalX. *Curr. Protoc. Bioinf.* 00 (1), 2.3.1–2.3.22. doi: 10.1002/0471250953.bi0203s00 Chapter 2, Unit 2.3.

Wan, X., Zhang, J., He, J., Bai, K., Zhang, L., and Wang, T. (2017). Dietary enzymatically treated Artemisia annua L. supplementation alleviates liver oxidative injury of broilers reared under high ambient temperature. *Int. J. Biometeorol.* 61 (9), 1629–1636. doi: 10.1007/s00484-017-1341-1

Yoon, W. J., Moon, J. Y., Song, G., Lee, Y. K., Han, M. S., Lee, J. S., et al. (2010). Artemisia fukudo essential oil attenuates LPS-induced inflammation by suppressing NF-kappaB and MAPK activation in RAW 264.7 macrophages. *Food Chem. Toxicol.* 48 (5), 1222–1229. doi: 10.1016/j.fct.2010.02.014

Younsi, F., Mehdi, S., Aissi, O., Rahali, N., Jaouadi, R., Boussaid, M., et al. (2017). Essential oil variability in natural populations of Artemisia campestris (L.) and Artemisia herba-alba (Asso) and incidence on antiacetylcholinesterase and antioxidant activities. *Chem. Biodivers.* 14 (7), 24–28. doi: 10.1002/cbdv.201700017

Yun, J. W., Kim, S. H., Kim, Y. S., You, J. R., Cho, E. Y., Yoon, J. H., et al. (2017). A comprehensive study on in vitro and in vivo toxicological evaluation of Artemisia capillaris. *Regul. Toxicol. Pharmacol.* 88, 87–95. doi: 10.1016/j.yrtph.2017.05.010

Zhao, H., Jiang, Z., Chang, X., Xue, H., Yahefu, W., and Zhang, X. (2018). 4-Hydroxyphenylacetic acid prevents acute APAP-induced liver injury by increasing phase II and antioxidant enzymes in mice. *Front. Pharmacol.* 9, 653. doi: 10.3389/fphar.2018.00653

Protective Effect of Patchouli Alcohol Against High-Fat Diet Induced Hepatic Steatosis by Alleviating Endoplasmic Reticulum Stress and Regulating VLDL Metabolism in Rats

Xue Wu[1], Nan Xu[1], Minyao Li[1], Qionghui Huang[1], Jiazhen Wu[1,2], Yuxuan Gan[1], Liping Chen[3], Huijuan Luo[1], Yucui Li[1], Xiaoqi Huang[1], Ziren Su[1]* and Yuhong Liu[1]*

[1] Guangdong Provincial Key Laboratory of New Drug Development and Research of Chinese Medicine, Mathematical Engineering Academy of Chinese Medicine, Guangzhou University of Chinese Medicine, Guangzhou, China, [2] The First Affiliated Hospital of Chinese Medicine, Guangzhou University of Chinese Medicine, Guangzhou, China, [3] Sun Yat-Sen Memorial Hospital, Sun Yat-Sen University, Guangzhou, China

Nonalcoholic fatty liver disease (NAFLD) is currently the most common chronic hepatic disorder worldwide. The earliest stage of NAFLD is simple steatosis, which is characterized by the accumulation of triglycerides in hepatocytes. Inhibition of steatosis is a potential treatment for NAFLD. Patchouli alcohol (PA) is an active component of *Pogostemon cablin* (Blanco) Benth. (Labiatae), which is a medicinal food in Asia countries and proved to possess hepatoprotective effect. This research aimed to investigate the effectiveness of PA against high fat diet (HFD)-induced hepatic steatosis in rats. In this study, male Sprague Dawley rats were fed a HFD for 4 weeks to induce NAFLD. Oral administration with PA significantly reduced pathological severity of steatosis in HFD-fed rats. It was associated with suppressing endoplasmic reticulum (ER) stress and regulating very low-density lipoprotein (VLDL) metabolism. Our data showed that PA treatment effectively attenuated ER stress by inhibiting the activation of protein kinase-like ER kinase (PERK), inositol-requiring transmembrane kinase/endoribonuclease 1 (IRE1), and activating transcription factor 6 (ATF6). Moreover, PA decreased hepatic VLDL uptake by suppressing very low-density lipoprotein receptor (VLDLR) expression. It also restored VLDL synthesis and export by increasing apolipoprotein B100 (apoB 100) secretion and microsomal triglyceride-transfer protein (MTP) activity. Taken together, PA exerted a protective effect on the treatment of NAFLD in HFD-fed rats and may be potential therapeutic agent acting on hepatic steatosis.

Keywords: patchouli alcohol, nonalcoholic fatty liver disease, hepatic steatosis, very low-density lipoprotein, endoplasmic reticulum stress

GRAPHICAL ABSTRACT | This study demonstrated that supplementation of PA attenuated HFD-induced hepatic steatosis by suppressing ER stress and regulating VLDL metabolism in rats.
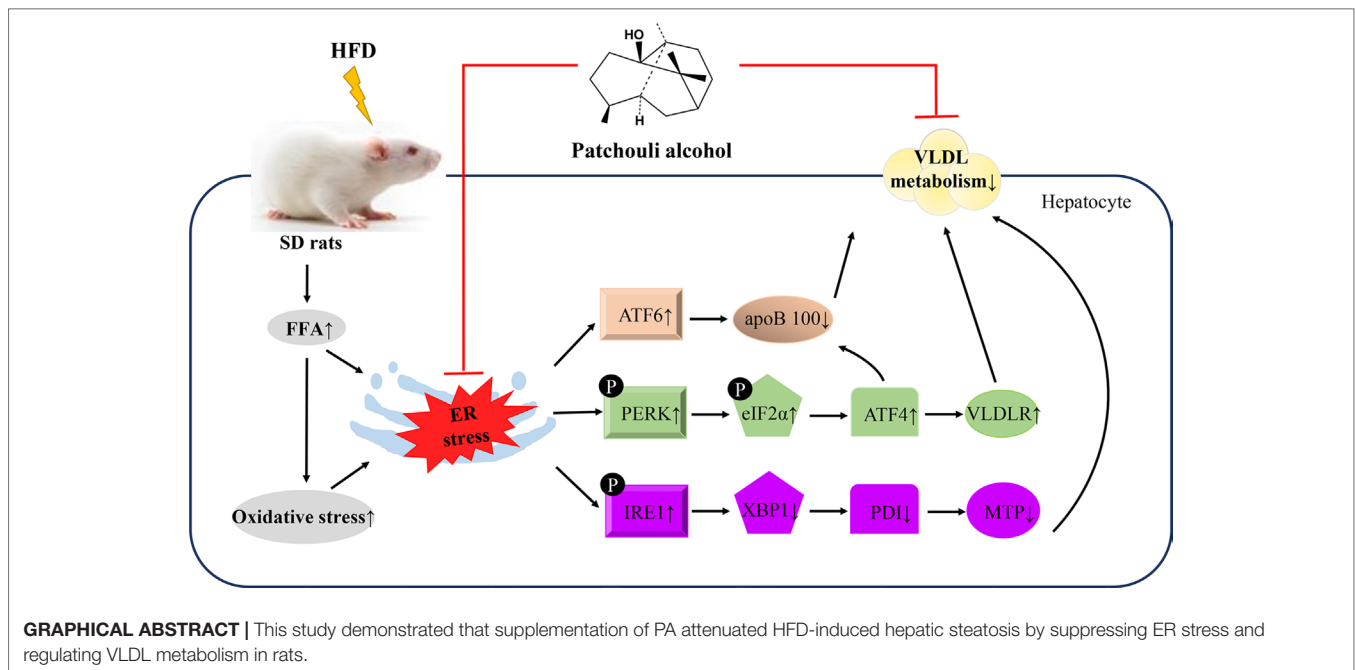
INTRODUCTION

Nonalcoholic fatty liver disease (NAFLD), a result of the pandemic of obesity and diabetes, has become a leading cause of liver disease and emerged a major challenge in modern society. It affects 6–45% of the general population worldwide with highly prevalence and incidence (Fazel et al., 2016). NAFLD is one of the most common chronic liver diseases, ranging from simple steatosis to nonalcoholic steatohepatitis (NASH), and eventually to hepatocellular carcinoma (HCC) (Younossi et al., 2019). Hepatic steatosis occurs in the early stages of NAFLD, which is defined as abnormal lipid deposition in the liver. When the rate of hepatic lipid uptake exceeds the rate of lipid disposal, lipid accumulates in the liver and results in steatosis (Ipsen et al., 2018). Very low-density lipoprotein (VLDL) metabolism is considered as a beneficial factor in overcoming the excess formation of triglyceride (TG) and regulating intrahepatic and plasma lipid homeostasis. A dysregulation in VLDL uptake, export, or synthesis is one of the major causes of hepatic steatosis (As, 2018). Current studies have demonstrated that endoplasmic reticulum (ER) stress is implicated in the inhibition of VLDL

metabolism. ER stress interferes with VLDL metabolism in several manners, including enhancing VLDL delivery to hepatocytes and inhibiting VLDL synthesis and export from these cells. Free fatty acids (FFAs) from diet are thought to be crucial for the onset of hepatic steatosis. Elevated level of FFAs results in disruption of ER homeostasis and VLDL metabolism, bringing about TG accumulation in the liver and finally leading to hepatic steatosis (Wei et al., 2007; Ghemrawi et al., 2018).

To date, there are no effective medical intervention strategies for NAFLD. Natural compounds are deemed as viable treatment regimens to inhibit the progress of NAFLD because of the beneficial effects they have shown (Li et al., 2018; Zhu et al., 2018). *Pogostemon cablin* (Blanco) Benth. (Labiatae) is a widely used traditional healthy food and medicinal herb in Asian countries such as China, Malaysia, and India. Its fresh leaves and dried powder are used in the form of food flavour supplements, tea, beverages, candy, baked products, and common botanical ingredients in functional foods and dietary supplements (Hou and Jiang, 2013; Preedy, 2016). It has been reported to display excellent anti-inflammatory, anti-oxidative, and multiple-organ protective activities (Zhang et al., 2016; Chen et al., 2017). Our previous study also confirmed the protective effect of patchouli oil (the extractive from the dry leaves of *Pogostemon cablin*) against lipid accumulation in a rat model of alcoholic liver injury (ALI) (Huang et al., 2018). Patchouli alcohol (PA, **Figure 1A**), as the phytochemical marker determining the quality of *Pogostemon cablin* and patchouli oil, has been demonstrated to possess various medicinal activities (Yu et al., 2015; Liu et al., 2017). However, the mechanism of PA action in NAFLD by reducing hepatic steatosis still remains uncertain. Therefore, this study aimed to evaluate if PA supplementation to a HFD would reduce hepatic steatosis by alleviating ER stress and regulating VLDL metabolism in rats.

Abbreviations: apoB 100, apolipoprotein B100; ALT, alanine aminotransferase; AST, aspartate transaminase; ATF4, activating transcription factor 4; ATF6, activating transcription factor 6; CAT, catalase; eIF2α, eukaryotic translation initiation factor 2α; ER, endoplasmic reticulum; FFA, free fatty acid; GRP78, glucose-regulated protein 78 kDa; GSH, glutathione; HFD, high fat diet; IRE1α, inositol-requiring transmembrane kinase/endoribonuclease 1α; MDA, malondialdehyde; MTP, microsomal triglyceride-transfer protein; NAFLD, nonalcoholic fatty liver disease; ND, normal diet; PA, patchouli alcohol; PDI, protein disulfide isomerase; p-eIF2α, phospho-eIF2α; PERK, protein kinase-like ER kinase; p-IRE1α, phospho-IRE1α; p-PERK, phosphor-PERK; ROS, reactive oxygen species; SOD, superoxide dismutase; TC, Total Cholesterol; TG, triglyceride; VE, vitamin E; VLDL, very low-density lipoprotein; VLDLR, very low-density lipoprotein receptor; XBP1, X box binding protein 1.
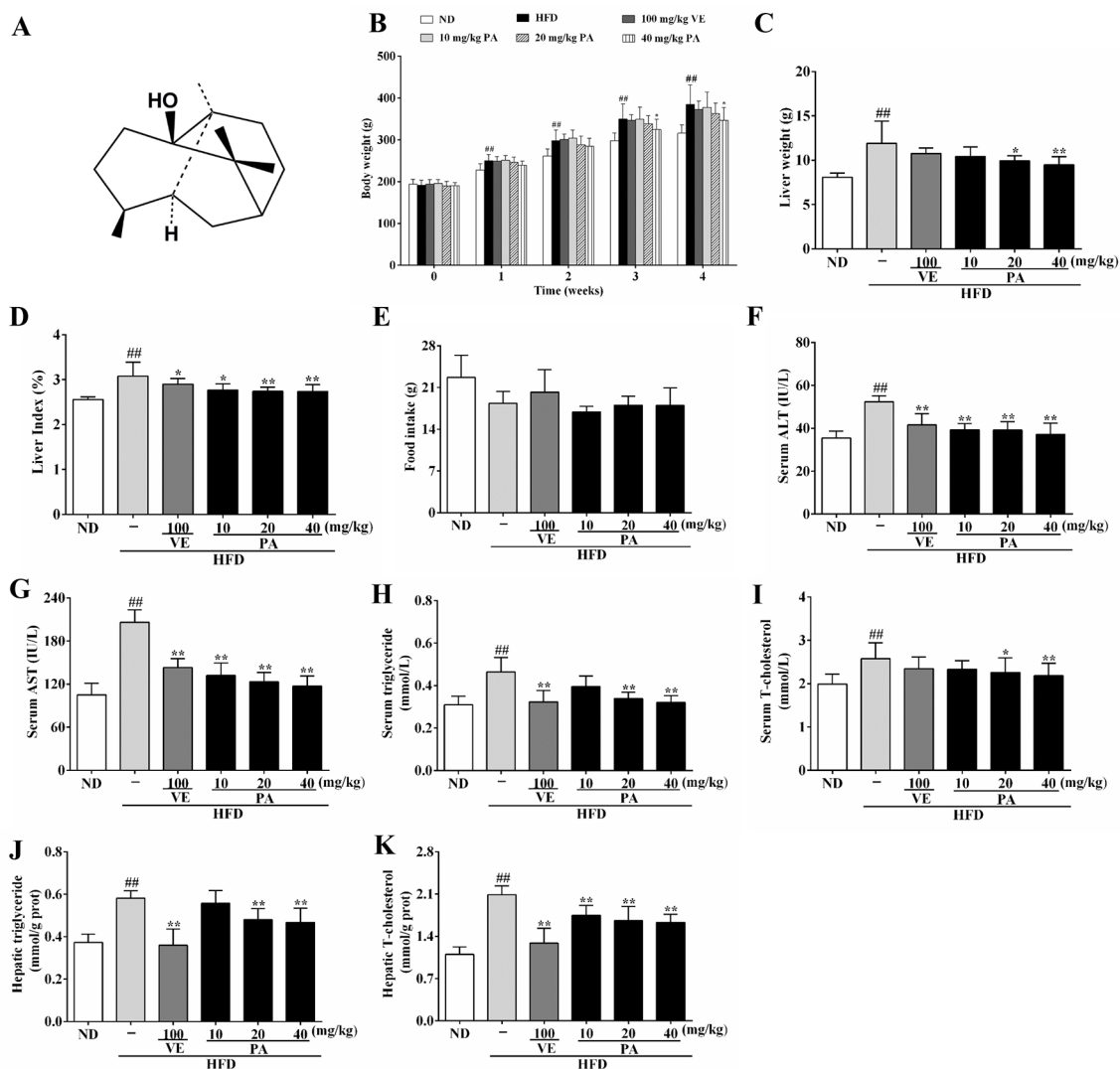
FIGURE 1 | Chemical structure of patchouli alcohol (PA) and PA treatment attenuated HFD-induced lipid accumulation in rats. **(A)** Chemical structure of PA; **(B)** Body weight; **(C)** Liver weight; **(D)** Liver index; **(E)** Food intake; **(F)** Serum levels of ALT, **(G)** AST, **(H)** TG and **(I)** TC; **(J)** Hepatic levels of TG and **(K)** TC. Values were presented as mean ± SD (n = 8 per group). ##p < 0.01 vs. ND group; *p < 0.05,**p < 0.01 vs. HFD group.

MATERIALS AND METHODS

Drugs and Chemicals

PA was isolated from patchouli oil according to published article at purity of 99.0% (Su et al., 2014). Vitamin E (VE; purity ≥ 98%) was purchased from Dalian Meilun Biological Technology Co. Ltd (Dalian, Liaoning, China). Normal diet (ND; ≥ 4% energy as fat) was purchased from the Medical Experiment Animal Center of Guangzhou University of Chinese Medicine, and high fat diet (HFD, D12492, 60% energy as fat) was purchased from Guangdong Medical Lab Animal Center (Guangzhou, Guangdong, China). The kits for biochemical analysis of aspartate transaminase (AST), alanine aminotransferase (ALT), triglyceride (TG), total cholesterol (TC), superoxide dismutase (SOD), glutathione (GSH) catalase (CAT), and malondialdehyde

(MDA) were obtained from Nanjing Jiancheng Bioengineering Institute (Nanjing, Jiangsu, China). ELISA kits for free fatty acid (FFA), reactive oxygen species (ROS), apolipoprotein B100 (apoB 100), and VLDL measurement were purchased from Shanghai Enzyme-linked Biotechnology Co. Ltd (Shanghai, China). Primers for determination of mRNA expressions of glucose-regulated protein 78 kDa (GRP78), protein kinase-like ER kinase (PERK), inositol-requiring transmembrane kinase/endoribonuclease 1 (IRE1), eukaryotic translation initiation factor 2α (eIF2α), activating transcription factor 4 (ATF4), very low-density lipoprotein receptor (VLDLR), X box binding protein 1 (XBP1), protein disulfide isomerase (PDI), microsomal triglyceride-transfer protein (MTP), activating transcription factor 6 (ATF6), apoB 100, and glyceraldehyde-3-phosphate dehydrogenase (GAPDH) were provided by Sangon Biotech

Co., Ltd (Shanghai, China). Primary antibodies against GRP78 (AF5366), PERK (AF5304), p-PERK (DF7576), eIF2α (AF6087), p-eIF2α (AF3087), IRE1 (DF7709), p-IRE1 (DF8322), ATF4 (DF6008), XBP1 (AF5110), MTP (DF6591), ATF6 (DF6009), β-actin (AF7018), and goat anti-rabbit IgG (H+L) HRP (S0001) secondary antibody were obtained from Affinity Biosciences Inc. (USA). Primary antibody against VLDLR (19493-1-AP) was purchased from Proteintech Group Inc. (USA). Primary antibody against PDI (CY6636) was purchased from Abways Technology Inc. Primary antibody against apoB 100 (A1330) was purchased from ABclonal Technology Inc. (USA). All reagents were of analytical grade.

Animals and Treatments

Animal experiment procedures were approved by the Ethics Committee for the Welfare of Experimental Animals of Guangzhou University of Chinese Medicine (No. 20181015002). Male Sprague Dawley rats were purchased from the Medical Experiment Animal Center of Guangzhou University of Chinese Medicine (SYXK (YUE) 2018-0085). After 7 days acclimation, rats were randomly divided into six experimental groups ($n = 8$): ND, HFD, HFD supplemented with VE (100 mg/kg), and HFD supplemented with different doses of PA (10, 20, and 40 mg/kg), respectively. VE was used as positive control. PA and VE were dissolved in 0.5% tween 80 solution. Except the ND group (fed with normal diet), all rats were fed with HFD and water *ad libitum* for a period of 4 weeks to induce NAFLD. Meanwhile, rats received intragastric administration once daily. The body weights of rats were recorded daily, and food intake were recorded every week throughout the study. At the last day, all rats were weighted and anesthetized with sodium pentobarbital after fasting overnight. Blood samples from each rat were collected for biochemical analysis and their livers were rapidly dissected for histological evaluation and further analysis.

Serum Biochemistry

Blood samples were centrifuged at 3000 rpm at 4°C for 10 min, and the supernatants were collected for serum biochemistry examination. The serum levels of ALT, AST, TG, and TC were measured with commercial assay kits according to manufacturer's instructions by microplate reader.

Histopathological Analysis

After fixed with 4% paraformaldehyde, liver segments were dehydrated, cleaned, and embedded in paraffin. Then, the liver slices of 5 μm thickness were stained with hematoxylin and eosin (H&E) and 5-μm-thick frozen sections were stained with Oil red O. Analysis were performed under a light microscope according to the method previously reported (Ding et al., 2017; Huang et al., 2017).

Hepatic Biochemical Analysis

The liver tissues were homogenized in ice-physiological saline or absolute ethanol, and centrifuged at 4000 rpm and 4°C for 10 min to obtain supernatant for further analysis. Liver SOD, GSH, CAT, MDA, TG, and TC levels were determined using commercial assay kits according to corresponding product specifications and analyzed by microplate reader.

Enzyme Linked Immunosorbent Assay (ELISA)

Liver tissues were homogenized in phosphate buffer saline (pH 7.2–7.4) and then centrifuged at 4000 rpm at 4°C for 10 min to obtain supernatants for hepatic FFA, ROS, and VLDL examination. Blood samples were centrifuged at 3000 rpm at 4°C for 10 min, and the supernatants were collected for serum VLDL and apoB 100 examination. Hepatic levels of FFA, ROS, and VLDL as well as serum levels of VLDL and apoB 100 were measured by ELISA kits using a microplate reader.

Western Blot Analysis

Hepatic proteins were extracted using a commercial protein extraction kit (Servicebio, Wuhan, Hubei, China). After denaturation, proteins were separated by electrophoresis on SDS-PAGE gels and transferred to PVDF membranes. Membranes were blocked for 1 h with 5% (w/v) skim milk in Tris-buffered saline-tween 20 (TBST) and incubated with 1: 1000 dilution of primary antibodies and 1:3000 dilution of HRP-conjugated secondary antibody. Protein bands were visualized with ECL reagents (AmershamBiosciences, Buckinghamshire, UK), and densitometry analysis was performed using Quantity One 4.6.2 software. All blots were quantified and normalized against β-actin to adjust for the amount of proteins loaded.

Reverse Transcription-Quantitative Polymerase Chain Reaction (RT-qPCR)

Total RNA was extracted from liver tissue using TRI-zol® reagent and further synthesized as cDNA. The cDNA was used as the template for real-time PCR. The mRNA expressions of GRP78, PERK, eIF2α, IRE1, ATF4, VLDLR, XBP1, PDI, MTP, ATF6, and apoB 100 (the primers of PCR are listed in **Table 1**) were measured by HiScript® II Q RT SuperMix (+gDNA wiper) and ChamQ™ SYBR® qPCR Master Mix Kit according to manufacturer's instruction (Vazyme Biotech, China). Each reaction was conducted in triplicate under the following cycling conditions: 10 min at 95°C, followed by 40 cycles at 95°C for 15 s and then 60°C for 1 min. The relative expression levels of target genes were normalized by GAPDH. The relative quantification of gene expression was calculated using the $2^{-\Delta\Delta Ct}$ method.

Statistical Analyses

Data were presented as mean ± SD. Statistical analyses were performed using Statistical Product and Service Solutions (SPSS) software (version 20.0). Group differences were assessed by one-way analysis of variance (ANOVA) followed by an LSD test for multiple comparisons. $P < 0.05$ was considered statistical significant.

TABLE 1 | Primer sequences.

Gene	Forward primer (5'-3')	Reverse primer (5'-3')
GRP78	CGGAGGAGGAGGACAAGAAGGAG	ATACGACGGTGTGATGCGGTTG
PERK	CGCTGCTGCTGCTGTTCCTG	GCAATGCCTCGGCGTCTTCC
IRE1	GACGAGCATCCGAATGTGATCCG	GAGGTGGTCTGATGAAGCAAGGTG
ATF6	GGCTTCCTCCAGTTGTTCTGTCTC	GCTTCTCTTCCTTCAGTGGCTCTG
eIF2α	GCCGATAAGGTTACGATGCTGTGG	GTAGGAAGCGCCTGTCTTGTCAAC
ATF4	GACCGAGATGAGCTTCCTGAACAG	CCGCCTTGTCGCTGGAGAAC
VLDLR	GACGCAGACTGTTCCGACCAATC	GCAGGTTCGAGAAGGACAGTTGAC
apoB 100	TCTGACTGGTGGACTCTGACTGC	TCTTGGAGAGCGTGGAGACTGAC
XBP1	AGGTCTCAGAGGCAGAGTCCAAG	AAGAGGCAACAGCGTCAGAATCC
PDI	CAACGTCCTGGTGCTGAAGAAGAG	TGCTAGTCGGATCTCAGAGCCTTC
MTP	TTCATTCAGCACCTCCGCACTTC	AGTCCAGGATGGCTTCCAGTGAG
GAPDH	ACGGCAAGTTCAACGGCACAG	CGACATACTCAGCACCAGCATCAC

RESULTS

Effect of PA on Body Weight, Liver Weight, Liver Index, and Lipid Accumulation in HFD-Fed Rats

Chronic exposure to HFD disturbed lipid homeostasis in a time-dependent manner leading to development of NAFLD. Data in **Figures 1B–D** showed that a profound increase in body weight, liver weight, and liver index was observed in the HFD group. VE treatment did not alter the increase of body weight and liver weight, but significantly decreased liver index in rats. Furthermore, PA treatment dramatically reduced body weight, liver weight, and liver index in HFD-fed rats. Data in **Figure 1E** showed that there was no significant difference in the food intake among all groups. As shown in **Figures 1F–K**, compared to the rats only fed with ND, the serum levels of AST, ALT, TG, and TC along with hepatic levels of TG and TC were significantly increased in the HFD-fed rats. These lipid parameters in VE and PA treated groups were lower than the HFD group. Moreover, rats with 40 mg/kg PA treatment exhibited superior effect in the reduction of serum ASL, ALT, TG, and TC among all treated groups. Histological assessments of liver tissue in **Figure 2** showed presence of NAFLD, characterized by increased vesicular lipid droplets, hepatic vacuoles, and slight inflammatory infiltrate in HFD-fed rats. VE and PA supplementation for 4 weeks markedly decreased vacuoles, lipid droplets area, and inflammation in the liver of HFD-fed rats. These results indicated that PA was effective in reducing HFD-induced body weight gain and preventing hepatic steatosis in rats.

Effect of PA on FFA and Oxidative Stress in HFD-Fed Rats

ER stress is often associated with FFA and oxidative stress. To explore the role of PA against elevated FFA and oxidative stress, we examined the hepatic levels of FFA and the oxidative stress indicators: ROS and MDA. As shown in **Figures 3A–C**, higher levels of FFA, ROS, and MDA were presented in the HFD-fed rats when compared to the ND-fed rats. However, the PA or VE groups showed similar hepatic levels of FFA, ROS, and MDA to ND group when compared to the HFD group. Data in **Figures 3D–F** showed that the hepatic levels of GSH, SOD, and CAT

were lower in the HFD-fed rats than ND-fed rats. Conversely, VE or PA supplementation dramatically increased the activities of SOD and CAT in HFD-fed rats. Moreover, the level of GSH was normalized in VE or PA treated rats, whereas there was no significant difference between HFD-fed rats and VE treated rats. Collectively, these results indicated that PA exerted a protective effect against elevated FFA and oxidative stress in HFD-fed rats.

Effect of PA on ER Stress and VLDL Secretion in HFD-Fed Rats

The enhanced FFA and oxidative stress induced by HFD-fed resulted in aggravating ER stress and decreasing VLDL secretion. As shown in **Figures 3G** and H, HFD feeding decreased the hepatic and serum levels of VLDL; however, VE or PA treated rats exhibited higher hepatic and serum levels of VLDL than HFD-fed rats. Data in **Figure 4** indicated that HFD-induced ER stress markers, including GRP78, PERK, IRE1, and ATF6, were inhibited by VE or PA supplementation. Data in **Figures 4A–E** showed that HFD-fed rats significantly increased hepatic protein expressions of GRP78 and ATF6. These ER markers were down regulated by VE or PA treatment, whereas VE-treated rats had no significant change on GRP78 expression. In addition, VE or PA treatment decreased the ratios of p-PERK/PERK and p-IRE1α/IRE1α in HFD-fed rats, whereas there was no significant difference in the ratio of p-IRE1α/IRE1α between HFD and the treated groups. Data in **Figures 4F–I** showed that the hepatic mRNA expressions of GRP78, PERK, IRE1, and ATF6 were dramatically decreased after administration with PA and VE. These results indicated that PA was a regulator for ER homeostasis and VLDL secretion.

Effect of PA on VLDLR Expression in HFD-Fed Rats

VLDLR plays a vital role in modulating VLDL-TG metabolism. To investigate the impact of PA on VLDLR expression, we measured the VLDLR and VLDLR-related indicators. Data in **Figures 5A–D** showed that the hepatic protein expressions of ATF4, VLDLR, and the ratio of p-eIF2α/eIF2α were promoted in HFD-fed rats. In contrast, VE and PA treatment dramatically demoted the expressions of these proteins, while there was no
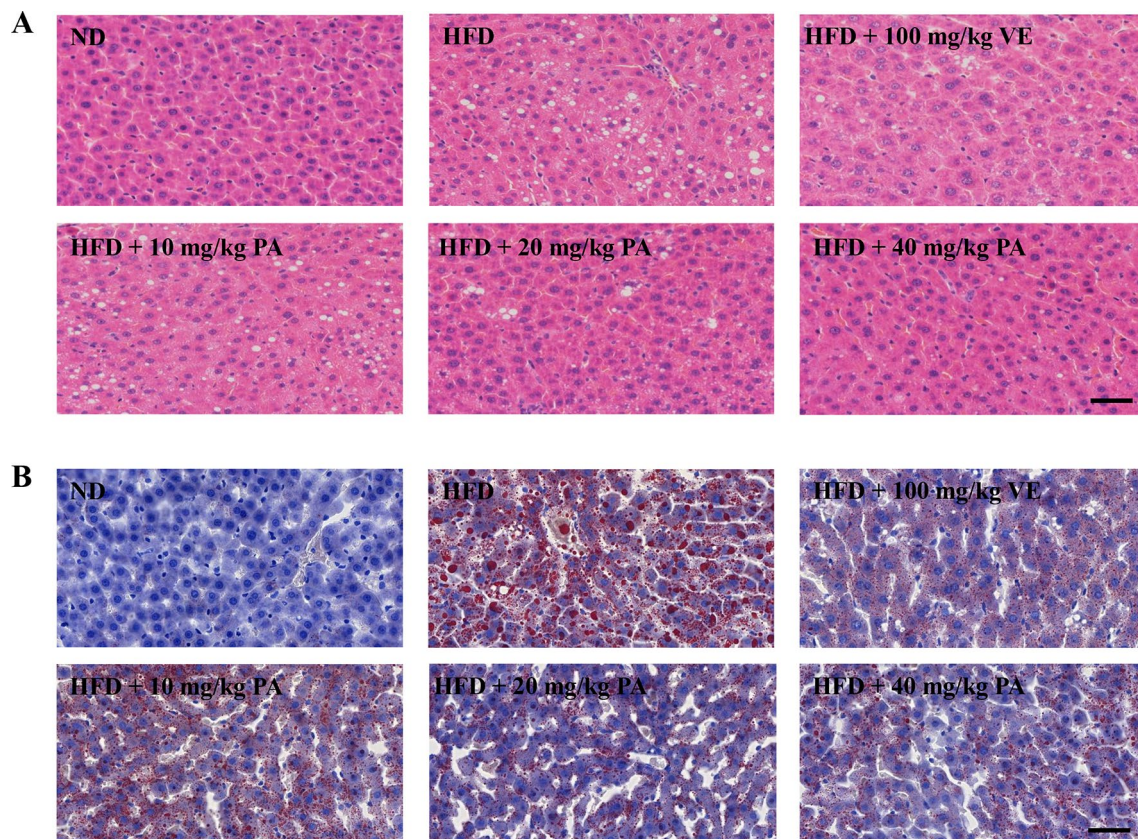
FIGURE 2 | PA treatment attenuated HFD-induced hepatic steatosis in rats. **(A)** Representative photomicrographs of H&E staining (400×) and **(B)** Oil Red O staining (400×) of livers.

significant difference in VLDLR and ATF4 expression between HFD and VE treated groups. Data in **Figures 5E–G** showed that the hepatic mRNA expressions of ATF4, VLDLR, and eIF2α were significantly increased in HFD-fed rats, whereas these trends were completely inhibited by VE and PA treatment. These results suggested that PA may prevent hepatic steatosis by decreasing VLDLR expression and regulating VLDL metabolism.

Effect of PA on ApoB100 Secretion in HFD-Fed Rats

Serum and hepatic levels of apoB 100 were assessed to evaluate the effect of PA on apoB secretion. Data in **Figure 6** showed that the serum level as well as the hepatic mRNA and protein expressions of apoB 100 were markedly reduced after exposure to HFD. When rats were supplemented with VE and PA, the reduced serum level of apoB 100 as well as the protein and mRNA expressions in liver tissue of apoB 100 were enhanced. In addition, 40 mg/kg PA exhibited prominent effect comparable to other treated groups. No significant difference of the protein and mRNA expressions of apoB 100 was observed between the HFD and VE-treated groups. This suggested that under condition of PA treatment, serum and hepatic apoB 100 secretion was normalized and further beneficial for VLDL secretion.

Effect of PA on MTP Level in HFD-Fed Rats

To further understand the role of PA on MTP expression, we analyzed the MTP and related genes and proteins expressions in this study. Data in **Figure 7** showed that the chronic stimulation with HFD caused decreases of hepatic protein and mRNA expressions of XBP1, PDI, and MTP. However, these trends were dramatically attenuated by VE and PA administration. These results indicated that PA supplementation increased MTP level and restored VLDL secretion in HFD-fed rats.

DISCUSSION

The increasing intake of dietary lipid makes the occurrence of NAFLD widespread. *Pogostemon cablin*, a traditional healthy food and medicinal herb, was proved to possess hepatoprotective activity against lipid accumulation in rats. PA is a main effective component of *Pogostemon cablin*. However, its protective effect for the treatment of lipid deposition still remains elusive. In this study, it is firstly provided evidence that PA could alleviate HFD-induced hepatic steatosis by inhibiting lipid droplet formation and lipid accumulation in liver accompanied with reduced levels of TG, TC, FFA, AST, and ALT.
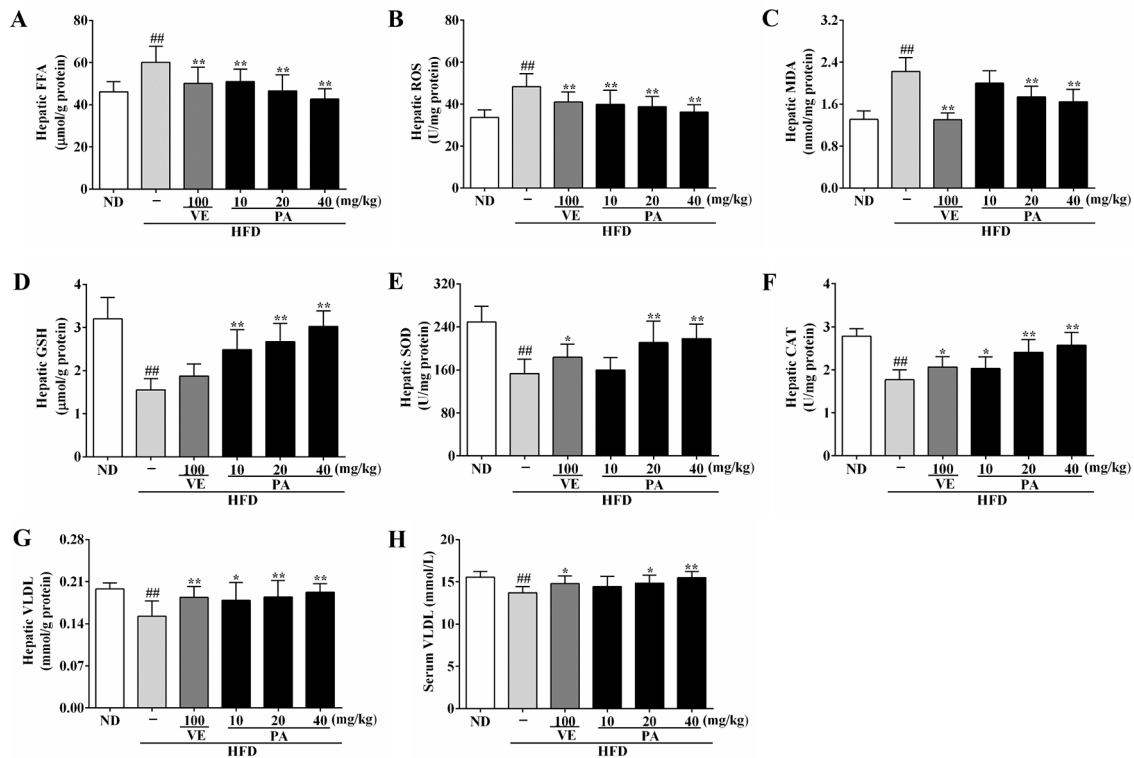
FIGURE 3 | PA treatment reduced HFD-induced elevated FFA level, oxidative stress, and decreased VLDL levels in rats. **(A)** Hepatic levels of FFA, **(B)** ROS, **(C)** MDA, **(D)** GSH, **(E)** SOD, **(F)** CAT, and **(G)**VLDL; **(H)** Serum level of VLDL. Values were presented as mean ± SD (n = 8 per group). $^{\#\#}p < 0.01$ vs. ND group; $^{*}p < 0.05, ^{**}p < 0.01$ vs. HFD group.

Its key mechanism may be involved in suppressing ER stress and regulating VLDL metabolism.

ER is served as a main site of lipid synthesis and VLDL assembly. Previous studies have demonstrated hepatic ER stress in several animal models of steatosis, suggesting that ER stress may contribute to the induction of NAFLD (Ghemrawi et al., 2018). Elevation of FFA concentration and oxidative stress are common feature of NAFLD and proved to be tightly associated with ER stress. Excessive FFA not only activates cellular ER stress, but also causes oxidative stress by enhancing mitochondria-associated membranes (MAM) and increasing ROS production (Hager et al., 2012; Ghemrawi et al., 2018). Oxidative stress could perturb the redox status of ER lumen and inhibit protein folding, then acts as a trigger to ER stress (Ashraf and Sheikh, 2015). In response to ER stress, normal ER function in maintaining protein homeostasis becomes compromised, resulting in accumulation of unfolded or misfolded proteins and triggering unfolded protein response (UPR). During the response to ER stress, all three main brunches of UPR including PERK, IRE1, and ATF6 pathways are activated and mediates hepatic steatosis. GRP78 is an ER stress marker in liver. Under unstressed conditions, IRE1, PERK, and ATF6 are associated with GRP78 and remain inactive. Upon ER stress, GRP78 dissociates from these sensor proteins, and further actives PERK and IRE1, and regulates intramembrane proteolysis of ATF6 (As, 2018). In this study,

after 4 weeks of PA administration, the increased levels of ROS and MDA were markedly decreased in HFD-fed rats. PA also increased the GSH, SOD, CAT, and VLDL levels in HFD-fed rats. Moreover, PA treatment decreased the protein and mRNA expressions of ER stress markers including GRP78, IRE1, PERK, and ATF6. This indicated that PA may restore VLDL secretion and attenuate hepatic steatosis by alleviating ER stress in HFD-induced NAFLD rats.

Recent data has revealed that the activated PERK–eIF2α–ATF4 pathway during ER stress induces hepatic steatosis *via* increase VLDLR by enhancing intracellular TG accumulation with VLDL uptake (Jo et al., 2013). VLDLR is a member of low-density lipoprotein receptor (LDLR) superfamily. It binds APOE-containing VLDL, which then converts into TG, leading to decrease lipid secretion and increase lipid accumulation (Kim et al., 2014). Previous study has demonstrated that inhibition of VLDLR upregulation can protect mice against hepatic steatosis induced by HFD feeding (Zaire et al., 2018). Upon dissociation from GRP78, PERK is activated by dimerization and autophosphorylation, triggering phosphorylation of the eIF2α. Furthermore, promotion of eIF2α halts global protein translation and selectively translates ATF4 mRNA (Lebeaupin et al., 2018). ATF4 is a well-known transcription factor that mediates PERK downstream pathway and functions to increase hepatic VLDLR expression (Jo et al., 2013). In our work, PA treatment significantly
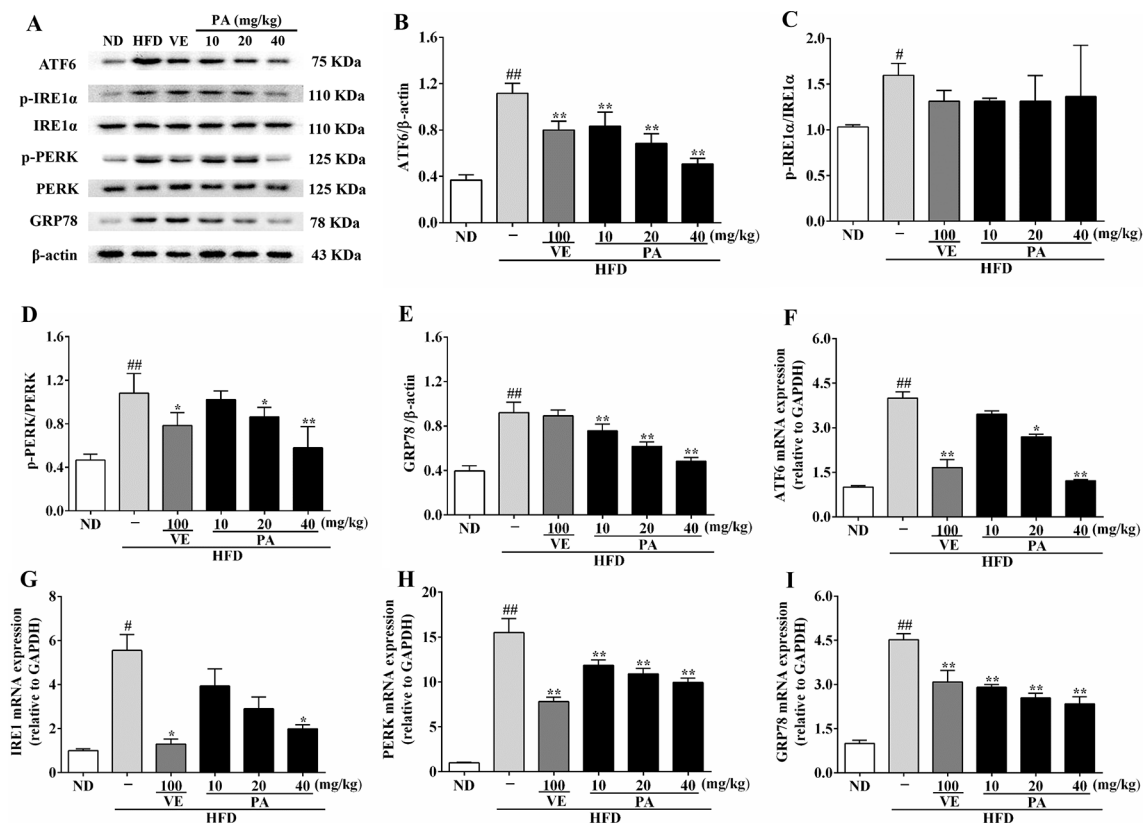
FIGURE 4 | PA treatment attenuated HFD-induced ER stress in rats. **(A)** Representative immunoreactive bands of GRP78, PERK, p-PERK, IRE1α, p-IRE1α, and ATF6; **(B)** Ratios of ATF6/β-actin, **(C)** p-IRE1α/IRE1α, **(D)** p-PERK/PERK, and **(E)** GRP78/β-actin; the relative expression levels of target proteins were normalized by β-actin; **(F)** mRNA expressions of ATF6, **(G)** IRE1, **(H)** PERK, and **(I)** GRP78; the relative expression levels of target genes were normalized by GAPDH. Values were presented as mean ± SD ($n = 3$ per group). $^{\#}p < 0.05$, $^{\#\#}p < 0.01$ vs. ND group; $^{*}p < 0.05$, $^{**}p < 0.01$ vs. HFD group.

reduced the mRNA and protein expressions of eIF2α, ATF4, and VLDLR. These results demonstrated that PA is able to lower VLDL uptake by down-regulating VLDLR.

ER stress not only impacts the hepatocytes uptake of VLDL but also impairs VLDL secretion. VLDL synthesis is a two-stage process. The first step in VLDL assembly is the apoB synthesis within the ER lumen following by its lipidation by MTP and the inclusion of TGs into a lipid droplet. In the second step, bulk neutral lipid, especially TGs, are added to the VLDL precursors and form lipid-rich VLDL. ApoB100 is a major protein component of VLDL, accounting for approximately one third of total lipoproteins present in VLDL. Impaired apoB 100 synthesis results in reduced VLDL synthesis, which inhibits the transport of endogenous TG from the liver to the extrahepatic, leading to TG deposition in hepatocytes (Watts et al., 2017). Hepatic apoB100 synthesis and secretion is a complex process involving ER stress. Under conditions of ER stress, hepatic lipid synthesis and secretion are affected, making a significant proportion of newly synthesized apoB100 degraded *via* the ubiquitin-proteasome-dependent degradative pathway (Suzuki et al., 2012). Evidences showed that ER chaperone protein such as GRP78 increased accompanied by decreasing apoB100 secretion, suggesting that there is an inverse relationship between ER stress and apoB100 secretion (Ota et al., 2008).

In addition, apoB100 secretion appears to be regulated by PERK and ATF6 pathways. Activated PERK pathway is found to impair apoB100 synthesis in glucosamine-treated cells (Qiu et al., 2009). Recent study has pointed out that ATF6α-knockout mice show enhanced hepatic steatosis caused by impaired formation of VLDL due to destabilized apoB100, whereas the exact mechanism of ATF6 in regulating apoB100 formation still remains unclear (Yamamoto et al., 2010). Following exposed to HFD, the serum level as well as the protein and mRNA expressions of apoB100 were decreased in rats. However, PA treatment altered apoB100 secretion in HFD-fed rats. This alteration of apoB100 secretion was proved to beneficial for VLDL assembly.

MTP is an ER-localized lipid transfer protein, plays a crucial role in lipoprotein assembly, and acts as a cofactor to apoB100 at both stages of VLDL synthesis. It is responsible for the lipidation of the nascent apoB protein and the transfer of neutral lipids between vesicles (Yao et al., 2013). PDI is a subunit of MTP necessary for normal MTP activity. Previous studies demonstrated that MTP activity is highly dependent on PDI expression and related to IRE1α- XBP1-PDI pathway (Wang et al., 2012). IRE1α-XBP1 induce PDI expression to increase MTP activity for VLDL assembly and secretion. IRE1 appears in mammal with two isoforms: IRE1α and IRE1β. IRE1α is a transmembrane protein
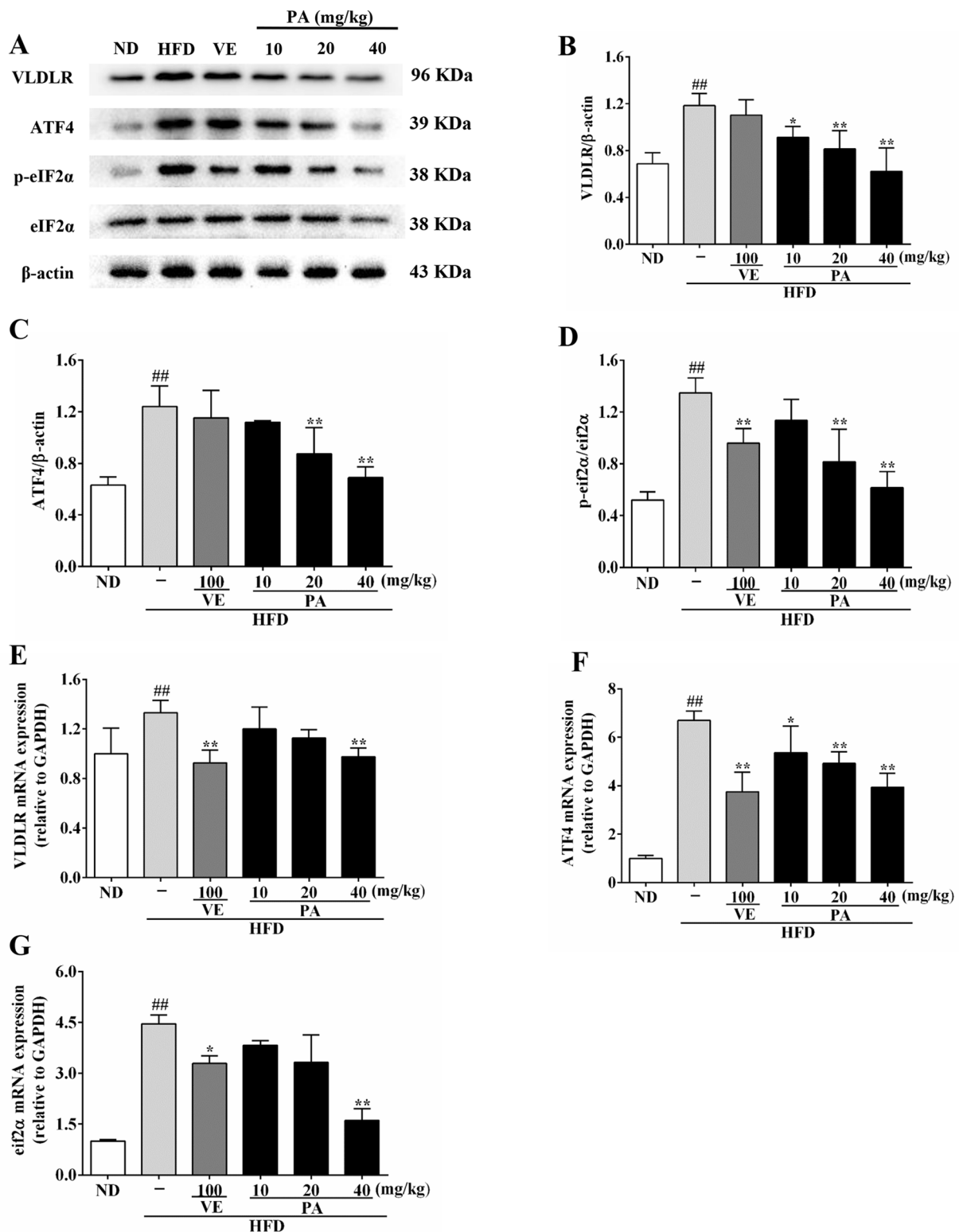
FIGURE 5 | PA treatment attenuated HFD-induced VLDLR expression in rats. (A) Representative immunoreactive bands of eIF2α, p-eIF2α, ATF4, and VLDLR; (B) Ratios of VLDLR/β-actin, (C) ATF4/β-actin and (D) p-eIF2α/eIF2α; the relative expression levels of target proteins were normalized by β-actin; (E) mRNA expressions of VLDLR, (F) ATF4, and (G) eIF2α; the relative expression levels of target genes were normalized by GAPDH. Values were presented as mean ± SD (n = 3 per group). $^{\#\#}p < 0.01$ vs. ND group; $^{*}p < 0.05$,$^{**}p < 0.01$ vs. HFD group.
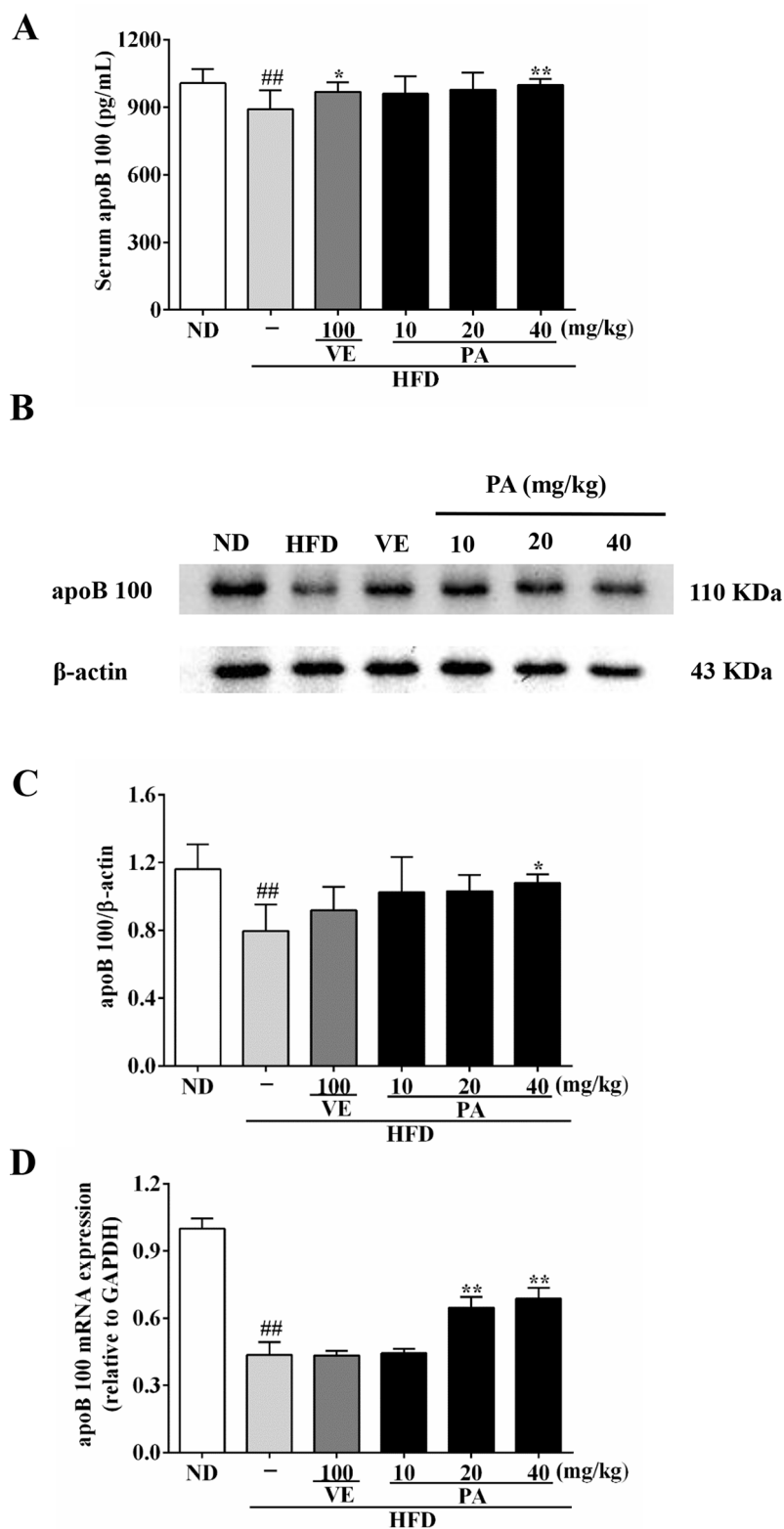
FIGURE 6 | PA treatment attenuated HFD-induced apoB 100 reduction in rats. **(A)** Serum level of apoB 100 (n = 8 per group); **(B)** Representative immunoreactive band of apoB 100; **(C)** Ratio of apoB 100/β-actin; the relative expression level of target protein was normalized by β-actin (n = 3 per group); **(D)** mRNA expression of apoB 100; the relative expression level of target gene was normalized by GAPDH (n = 3 per group). Values were presented as mean ± SD. $^{\#\#}p < 0.01$ vs. ND group; $^{*}p < 0.05$, $^{**}p < 0.01$ vs. HFD group.
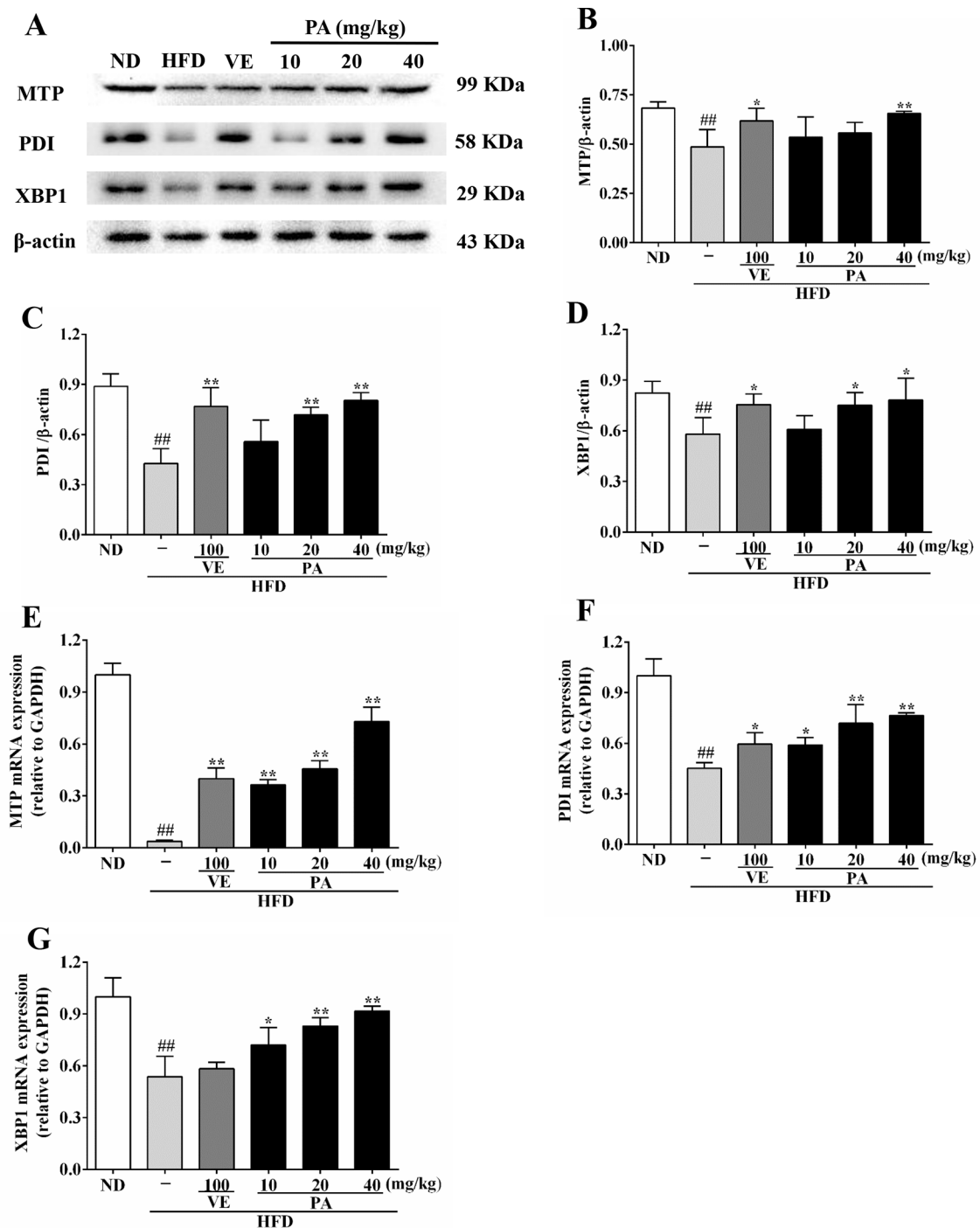
FIGURE 7 | PA treatment attenuated HFD-induced MTP reduction in rats. **(A)** Representative immunoreactive bands of XBP1, PDI, and MTP; **(B)** Ratios of MTP/β-actin, **(C)** PDI/β-actin, and **(D)** XBP1/β-actin; the relative expression levels of target proteins were normalized by β-actin; **(E)** mRNA expressions of MTP, **(F)** PDI, and **(G)** XBP1; the relative expression levels of target genes were normalized by GAPDH. Values were presented as mean ± SD (n = 3 per group). ##p < 0.01 vs. ND group; *p < 0.05, **p < 0.01 vs. HFD group.

that possesses endoribonuclease (RNase) activity, which is responsible for production spliced XBP1 (XBP1s). After activated by ER stress, IRE1α initiates unconventional splicing of XBP1 mRNA and translates it into a potent transcription factor (XBP1s)

(Wang et al., 2018). In turn, XBP1s drives a large transcriptional program to adjust the ER's protein-folding capacity according to the protein folding load in the ER lumen (Li et al., 2018). Our data showed that HFD-induced ER stress led to defective XBP1,

MTP, and PDI expressions in rats. PA administration not only improved XBP1, PDI, and MTP expressions but also decreased IRE1α expression from ER stress. These results indicated that PA may be able to reduce steatosis by attenuating MTP down-regulation and restoring VLDL secretion.

In conclusion, this study provides compelling evidence to support that PA is effective in ameliorating hepatic steatosis caused by HFD through suppressing ER stress and regulating VLDL uptake, assembly, and secretion, which is associated with the regulation of VLDLR, apoB100, and MTP expression. Given the promising preclinical findings presented in this study, we suggest that PA might play a protective role as possible therapeutic agents acting on hepatic steatosis.

DATA AVAILABILITY STATEMENT

The datasets analyzed in this manuscript are not publicly available. Requests to access the datasets should be directed to liuyuhong@gzucm.edu.cn.

ETHICS STATEMENT

The animal study was reviewed and approved by Animal experiment procedures were approved by the Ethics Committee for the Welfare of Experimental Animals of Guangzhou University of Chinese Medicine (No. 20181015002).

AUTHOR CONTRIBUTIONS

XW and YhL drafted and prepared the article. YhL and ZS conceived and designed the experiments; XW, NX, ML, QH, and JW performed experiments; YG, HL, and LC analyzed the data; YcL and XH prepared figures and tables.

FUNDING

REFERENCES

As, H. (2018). Unfolded protein response sensors in hepatic lipid metabolism and nonalcoholic fatty liver disease. *Semin. Liver Dis.* 38, 320–332. doi: 10.1055/s-0038-1670677

Ashraf, N. U., and Sheikh, T. A. (2015). Endoplasmic reticulum stress and Oxidative stress in the pathogenesis of Non-alcoholic fatty liver disease. *Free Radical Res.* 49, 1405–1418. doi: 10.3109/10715762.2015.1078461

Chen, X.-Y., Dou, Y.-X., Luo, D.-D., Zhang, Z.-B., Li, C.-L., Zeng, H.-F., et al. (2017). beta-Patchoulene from patchouli oil protects against LPS-induced acute lung injury *via* suppressing NF-kappa B and activating Nrf2 pathways. *Int. Immunopharmacol.* 50, 270–278. doi: 10.1016/j.intimp.2017.07.001

Ding, S., Jiang, J., Zhang, G., Bu, Y., Zhang, G., and Zhao, X. (2017). Resveratrol and caloric restriction prevent hepatic steatosis by regulating SIRT1-autophagy pathway and alleviating endoplasmic reticulum stress in high-fat diet-fed rats. *PloS ONE* 12 (8). doi: 10.1371/journal.pone.0183541

Fazel, Y., Koenig, A. B., Sayiner, M., Goodman, Z. D., and Younossi, Z. M. (2016). Epidemiology and natural history of non-alcoholic fatty liver disease. *Metab. Clin. Exp.* 65, 1017–1025. doi: 10.1016/j.metabol.2016.01.012

Ghemrawi, R., Battaglia-Hsu, S. F., and Arnold, C. (2018). Endoplasmic reticulum stress in metabolic disorders. *Cells* 7, 35. doi: 10.3390/cells7060063

Hager, L., Li, L., Pun, H., Liu, L., Hossain, M. A., Maguire, G. F., et al. (2012). Lecithin: cholesterol acyltransferase deficiency protects against cholesterol-induced hepatic endoplasmic reticulum stress in mice. *J. Biol. Chem.* 287, 20755–20768. doi: 10.1074/jbc.M112.340919

Hou, Y., and Jiang, J.-G. (2013). Origin and concept of medicine food homology and its application in modern functional foods. *Food Funct.* 4, 1727–1741. doi: 10.1039/c3fo60295h

Huang, C. Z., Tung, Y. T., Hsia, S. M., Wu, C. H., and Yen, G. C. (2017). The hepatoprotective effect of Phyllanthus emblica L. fruit on high fat diet-induced non-alcoholic fatty liver disease (NAFLD) in SD rats. *Food Funct.* 8, 842–850. doi: 10.1039/C6FO01585A

Huang, Q. H., Wu, X., Chen, X. H., Wu, J. Z., Su, Z. R., Liang, J. L., et al. (2018). Patchouli oil isolated from the leaves of Pogostemon cablin ameliorates ethanol-induced acute liver injury in rats *via* inhibition of oxidative stress and lipid accumulation. *Rsc Adv.* 8, 24399–24410. doi: 10.1039/C8RA02422G

Ipsen, D. H., Lykkesfeldt, J., and Tveden-Nyborg, P. (2018). Molecular mechanisms of hepatic lipid accumulation in non-alcoholic fatty liver disease. *Cell. Mol. Life Sci.* 75, 3313–3327. doi: 10.1007/s00018-018-2860-6

Jo, H., Choe, S. S., Shin, K. C., Jang, H., Lee, J. H., Seong, J. K., et al. (2013). Endoplasmic reticulum stress induces hepatic steatosis *via* increased expression of the hepatic very low-density lipoprotein receptor. *Hepatology* 57, 1366–1377. doi: 10.1002/hep.26126

Kim, Y., Yoon, S., Lee, S. B., Han, H. W., Oh, H., Lee, W. J., et al. (2014). Fermentation of soy milk *via* Lactobacillus plantarum improves dysregulated lipid metabolism in rats on a high cholesterol Diet. *PloS ONE* 9, 8. doi: 10.1371/journal.pone.0088231

Lebeaupin, C., Vallée, D., Hazari, Y., Hetz, C., Chevet, E., and Bailly-Maitre, B. (2018). Endoplasmic reticulum stress signalling and the pathogenesis of non-alcoholic fatty liver disease. *J. Hepatol.* 69, 927–947. doi: 10.1016/j.jhep.2018.06.008

Li, D., Ikaga, R., and Yamazaki, T. (2018). Soya protein beta-conglycinin ameliorates fatty liver and obesity in diet-induced obese mice through the down-regulation of PPAR gamma. *Br. J. Nutr.* 119, 1220–1232. doi: 10.1017/S0007114518000739

Liu, Y., Liang, J., Wu, J., Chen, H., Zhang, Z., Yang, H., et al. (2017). Transformation of patchouli alcohol to beta-patchoulene by gastric juice: beta-patchoulene is more effective in preventing ethanol-induced gastric injury. *Sci. Rep.* 7, 1–13. doi: 10.1038/s41598-017-05996-5

Ota, T., Gayet, C., and Ginsberg, H. N. (2008). Inhibition of apolipoprotein B100 secretion by lipid-induced hepatic endoplasmic reticulum stress in rodents. *J. Clin. Invest.* 118, 316–332. doi: 10.1172/JCI32752

Qiu, W., Su, Q., Rutledge, A. C., Zhang, J., and Adeli, K. (2009). Glucosamine-induced endoplasmic reticulum stress attenuates apolipoprotein B100 synthesis *via* PERK signaling. *J. Lipid Res.* 50, 1814–1823. doi: 10.1194/jlr.M800343-JLR200

Preedy, V. R. (2016). *Essential Oils in Food Preservation, Flavor and Safety* (Elsevier 2016).

Su, Z. Q., Wu, X. L., Bao, M. J., Li, C. W., Kong, S. Z., Su, Z. R., et al. (2014). Isolation of (−)-patchouli alcohol from patchouli oil by fractional distillation and crystallization. *Trop. J. Pharm. Res.* 13, 359–363. doi: 10.4314/tjpr.v13i3.7

Suzuki, M., Otsuka, T., Ohsaki, Y., Cheng, J. L., Taniguchi, T., Hashimoto, H., et al. (2012). Derlin-1 and UBXD8 are engaged in dislocation and degradation of

lipidated ApoB-100 at lipid droplets. *Mol. Biol. Cell* 23, 800–810. doi: 10.1091/mbc.e11-11-0950

Wang, J. M., Qiu, Y. N., Yang, Z., Kim, H., Qian, Q. W., Sun, Q. H., et al. (2018). IRE1 alpha prevents hepatic steatosis by processing and promoting the degradation of select microRNAs. *Sci. Signal.* 11, 13. doi: 10.1126/scisignal.aao4617

Wang, S., Chen, Z., Lam, V., Han, J., Hassler, J., Finck, B. N., et al. (2012). IRE1 alpha-XBP1s induces PDI expression to increase MTP activity for hepatic VLDL assembly and lipid homeostasis. *Cell Metab.* 16, 473–486. doi: 10.1016/j.cmet.2012.09.003

Watts, G. F., Chan, D. C., Dent, R., Somaratne, R., Wasserman, S. M., Scott, R., et al. (2017). Factorial effects of evolocumab and atorvastatin on lipoprotein metabolism. *Circulation* 135, 338–33+. doi: 10.1161/CIRCULATIONAHA.116.025080

Wei, Y., Wang, D., and Pagliassotti, M. J. (2007). Saturated fatty acid-mediated endoplasmic reticulum stress and apoptosis are augmented by trans-10, cis-12-conjugated linoleic acid in liver cells. *Mol. Cell. Biochem.* 303, 105–113. doi: 10.1007/s11010-007-9461-2

Yamamoto, K., Takahara, K., Oyadomari, S., Okada, T., Sato, T., Harada, A., et al. (2010). Induction of liver steatosis and lipid droplet formation in ATF6 alpha-knockout mice burdened with pharmacological endoplasmic reticulum stress. *Mol. Biol. Cell* 21, 2975–2986. doi: 10.1091/mbc.e09-02-0133

Yao, Z. M., Zhou, H., Figeys, D., Wang, Y. W., and Sundaram, M. (2013). Microsome-associated lumenal lipid droplets in the regulation of lipoprotein secretion. *Curr. Opin. Lipidol.* 24, 160–170. doi: 10.1097/MOL.0b013e32835aebe7

Yu, J.-L., Zhang, X.-S., Xue, X., and Wang, R.-M. (2015). Patchouli alcohol protects against lipopolysaccharide-induced acute lung injury in mice. *J. Surg. Res.* 194, 537–543. doi: 10.1016/j.jss.2014.10.026

Younossi, Z., Tacke, F., Arrese, M., Chander Sharma, B., Mostafa, I., Bugianesi, E., et al. (2019). Global perspectives on nonalcoholic fatty liver disease and nonalcoholic steatohepatitis. *Hepatology (Baltimore, Md.)* 69, 2672–2682. doi: 10.1002/hep.30251

Zaire, M., Barroso, E., Palomer, X., Dai, J., Rada, P., Quesada-López, T., et al. (2018). Hepatic regulation of VLDL receptor by PPARβ/δ and FGF21 modulates non-alcoholic fatty liver disease. *Mol. Metab.* 8, 117–131. doi: 10.1016/j.molmet.2017.12.008

Zhang, Z., Chen, X., Chen, H., Wang, L., Liang, J., Luo, D., et al. (2016). Anti-inflammatory activity of beta-patchoulene isolated from patchouli oil in mice. *Eur. J. Pharmacol.* 781, 229–238. doi: 10.1016/j.ejphar.2016.04.028

Zhu, X., Xiong, T., Liu, P., Guo, X., Xiao, L., Zhou, F., et al. (2018). Quercetin ameliorates HFD-induced NAFLD by promoting hepatic VLDL assembly and lipophagy *via* the IRE1a/XBP1s pathway. *Food Chem. Toxicol.* 114, 52–60. doi: 10.1016/j.fct.2018.02.019

Integrating Network Pharmacology and Pharmacological Evaluation for Deciphering the Action Mechanism of Herbal Formula Zuojin Pill in Suppressing Hepatocellular Carcinoma

Wei Guo[1†], Jihan Huang[1,2†], Ning Wang[1], Hor-Yue Tan[1], Fan Cheung[1], Feiyu Chen[1] and Yibin Feng[1*]

[1] School of Chinese Medicine, Li Ka Shing Faculty of Medicine, The University of Hong Kong, Hong Kong, China, [2] Center for Drug Clinical Research, Shanghai University of Traditional Chinese Medicine, Shanghai, China

Hepatocellular carcinoma (HCC) is a kind of complicated disease with an increasing incidence all over the world. A classic Chinese medicine formula, Zuojin pill (ZJP), was shown to exert therapeutic effects on HCC. However, its chemical and pharmacological profiles remain to be elucidated. In the current study, network pharmacology approach was applied to characterize the action mechanism of ZJP on HCC. All compounds were obtained from the corresponding databases, and active compounds were selected according to their oral bioavailability and drug-likeness index. The potential proteins of ZJP were obtained from the traditional Chinese medicine systems pharmacology (TCMSP) database and the traditional Chinese medicine integrated database (TCMID), whereas the potential genes of HCC were obtained from OncoDB.HCC and Liverome databases. The potential pathways related to genes were determined by gene ontology (GO) and pathway enrichment analyses. The compound-target and target-pathway networks were constructed. Subsequently, the potential underlying action mechanisms of ZJP on HCC predicted by the network pharmacology analyses were experimentally validated in HCC cellular and orthotopic HCC implantation murine models. A total of 224 components in ZJP were obtained, among which, 42 were chosen as bioactive components. The compound-target network included 32 compounds and 86 targets, whereas the target-pathway network included 70 proteins and 75 pathways. The *in vitro* and *in vivo* experiments validated that ZJP exhibited its prominent therapeutic effects on HCC mainly *via* the regulation of cell proliferation and survival though the EGFR/MAPK, PI3K/NF-κB, and CCND1 signaling pathways. In conclusion, our study suggested combination of network pharmacology prediction with experimental validation may offer a useful tool to characterize the molecular mechanism of traditional Chinese medicine (TCM) ZJP on HCC.

Keywords: Zuojin pill, hepatocellular carcinoma, network pharmacology, pharmacological evaluation, cell proliferation and survival

INTRODUCTION

As the third predominant cause of cancer-related death in the world, hepatocellular carcinoma (HCC) is a kind of complicated disease with various risk factors, such as hepatitis B viral or hepatitis C viral infection, obesity, and alcohol abuse (Ferlay et al., 2015). The incidence of HCC is mounting all over the world, whereas the prognosis of this disease is still far from satisfactory (Sherman, 2008). There are five commonly used treatments for HCC currently, namely, liver transplantation, transcatheter arterial chemoembolization, surgical resection, radiofrequency ablation, and sorafenib (Llovet et al., 2015). However, as most HCC patients are diagnosed at middle or later disease stages, only sorafenib treatment is still feasible for these patients. What is worse, fewer than 20% patients are able to respond to sorafenib, whereas moderate or severe side effects are frequently caused by sorafenib. There is an essential need to develop more effective and less toxic therapies for HCC (Zhu et al., 2016). Traditional Chinese medicine (TCM) has been used clinically in Asia for more than 2,000 years. As one of the most popular complementary and alternative medicine modalities in China, TCM has been gradually accepted by non-Chinese due to its prominent efficacy, rich resource, and less toxicity. There have been many TCM formulas used alone or as an adjuvant to conventional chemotherapy in the clinical treatment of cancers (Kim et al., 2012; Xu et al., 2012a; Gavaraskar et al., 2015).

Zuojin pill (ZJP) is a drug pair commonly used in TCM. It consists of only two herbs, namely, Coptidis Rhizoma (CR, Huang-lian in Chinese) and Evodiae Fructus (EF, Wu-chu-yu in Chinese). The ratio of CR and EF is 6:1 (w/w). CR is obtained from the dried rhizome of *Coptis chinensis* Franch and widely applied for the treatment of various diseases, such as gastrointestinal disorders, hepatic damages, and diabetes (Wang et al., 2015a; Lam et al., 2016). EF is obtained from the immature fruit of *Evodia rutaecarpa* Benth and widely applied for the treatment of headache, inflammation, and hypertension (Xu et al., 2012b). Alkaloids are proved to be the primary compounds of both CR and EF. Previous studies revealed that ZJP, its comprising herbs CR and EF, as well as the active compounds exhibited multiple pharmacological effects against cancer *via* various mechanisms of action (Wang et al., 2009; Wang et al., 2010a; Chou et al., 2017; Pan et al., 2017). ZJP extracts exerted its anticancer activity on colorectal cancer cells through the attenuation of the 5-HTR1D-Wnt/β-catenin signaling pathway (Pan et al., 2017). ZJP showed anticancer activity against sarcoma cancer *via* its effects on gene expression and activities of serum tumor markers (Wang

---

Abbreviations: ATCC, American type culture collection; ADME, absorption, distribution, metabolism, and excretion; BP, biological process; BSA, bovine serum albumin; CC, cellular component; CCND1, cyclin D1; CR, coptidis Rhizoma; CTD, comparative toxicogenomics database; CULATR, committee on the use of live animals in teaching and research; DL, drug-likeness; EASE, expression analysis systematic explorer; EF, evodiae fructus; GO, gene ontology; HCC, hepatocellular carcinoma; MF, molecular function; OB, oral bioavailability; PVDF, polyvinylidene fluoride; SDS-PAGE, sodium dodecyl sulfate-polyacrylamide gel electrophoresis; TBST, tris buffered saline-tween 20; TCM, traditional Chinese medicine; TCMID, traditional Chinese medicine integrated database; TCMSP, traditional Chinese medicine systems pharmacology; TTD, therapeutic target database; ZJP, Zuojin pill.

et al., 2009). Notably, ZJP markedly inhibited tumor growth in orthotopic HepG2 xenograft-bearing immunocompetent mice model (Chou et al., 2017). However, the chemical and pharmacological foundations of ZJP in inhibiting human cancers, especially HCC, was not globally evaluated with appropriate approaches.

TCM is a complex system with multiple targets and synergistic or antagonistic interactions among its components (Ma et al., 2015). Unlike western medicine of "one target, one drug," the concept of the integrity of the whole human body is emphasized in the theory of TCM. Because of its complexity in composition, conventional pharmacological approaches to experimentally identify the unique action of mechanism may not be applicable to TCM research. Along with the rapid development of bioinformatics, the newly emerging network pharmacology is based on big databases and has become a useful tool to characterize the action mechanisms of complicated drug system in detail, from the molecular level to the pathway level (Chen et al., 2016). Network pharmacology meets the key ideas of the holistic philosophy of TCM (Li and Zhang, 2013). As a state-of-the-art technique, this method updates the research paradigm from the current "one target, one drug" mode to a new "network target, multicomponents" mode. It helps to evaluate the rationality and compatibility of TCM by providing the detailed compound-target and target-pathway networks. It has been widely applied in the mechanism study of TCM for the treatment of complex diseases, such as cancer, asthma, and cardiovascular disorders. Successful attempts to apply this method to investigate complex TCM have been achieved in our laboratory (Hong et al., 2017a; Hong et al., 2017b; Huang et al., 2017a; Huang et al., 2017b; Huang et al., 2017c) and other researchers (Liang et al., 2014; Chen et al., 2018; Wang et al., 2018; Zheng et al., 2018; Zuo et al., 2018).

In the current study, we used computational tools and resources to investigate the pharmacological network of ZJP on HCC to predict the active compounds and potential protein targets and pathways. In addition, *in vitro* and *in vivo* experiments were also conducted to validate the potential underlying mechanism of ZJP on HCC, as predicted by network pharmacology approach. The detailed technical strategy of the current study was shown in **Figure 1**.

MATERIALS AND METHODS

Network Pharmacology-Based Analysis
Identification of Candidate Components in ZJP

All components of the two Chinese medicinal herbs in ZJP (Huang-lian and Wu-chu-yu) were retrieved from the traditional Chinese medicine systems pharmacology (TCMSP) database (http://tcmspw.com/) (Ru et al., 2014).

Screening Strategy for Bioactive Components in ZJP

The oral TCM must overcome the barriers posed by absorption, distribution, metabolism, and excretion (ADME) processes to be active. In ADME processes, oral bioavailability (OB) is one of the most significant pharmacokinetic parameters (Xu et al., 2012c).

FIGURE 1 | The technical strategy of the current study.

High OB is usually an essential indicator to determine the drug-likeness (DL) index of active substances. The substances with OB ≥ 30% were regarded to have high OB.

As a qualitative concept applied in drug design to estimate the druggability of a molecule (Tao et al., 2013), the DL index is useful for rapid screening of active substances. In the DrugBank database, the average DL index is 0.18. The substances with DL index ≥0.18 were regarded to have high druggability.

Therefore, the compounds in ZJP with OB ≥ 30% and DL index ≥0.18 were selected as active substances in the current study.

Prediction of Drug Targets for ZJP
The protein targets of the active substances in ZJP were retrieved from the TCMSP database and the traditional Chinese medicine integrated database (TCMID, http://www.megabionet.org/tcmid/).

Collection of Gene Targets for HCC
HCC-related human genes were collected from two databases, namely, OncoDB.HCC (http://oncodb.hcc.ibms.sinica.edu.tw/index.htm) (Su et al., 2007) and Liverome (http://liverome.kobic.re.kr/index.php) (Lee et al., 2011). Then, the protein targets of ZJP were mapped with HCC using the therapeutic target database (TTD, http://bidd.nus.edu.sg/group/cjttd/TTD_HOME.asp), the comparative toxicogenomics database (CTD, http://ctdbase.org/), and PharmGKB (https://www.pharmgkb.org/).

Gene Ontology and Pathway Enrichment Analysis for HCC-Related Targets of ZJP
The gene ontology (GO) and pathway enrichment analyses were conducted using the functional annotation tool of DAVID

Bioinformatics Resources 6.7 (http://david.abcc.ncifcrf.gov/) (Huang da et al., 2009). Terms with thresholds of Count ≥ 2 and Expression Analysis Systematic Explorer (EASE) scores ≤ 0.05 were chosen in functional annotation clustering.

Construction of Networks and Analysis
To further characterize the molecular mechanism of ZJP on HCC, the compound-target and target-pathway networks were generated using Cytoscape 3.3.0 (Smoot et al., 2011). In these graphical networks, the compounds, proteins, or pathways were expressed as nodes, whereas the compound-target or target-pathway interactions were expressed as edges.

Experimental Validation
Preparation of ZJP Aqueous Extract
Coptidis Rhizoma (voucher No. 44-1) and Evodiae Fructus (voucher No. 0018) were obtained and authenticated by the executive manager of dispensary of School of Chinese Medicine, The University of Hong Kong under the guidance of Chinese Pharmacopeia 2015 edition. The herbs were vouched and stored in specimen room of School of Chinese Medicine, The University of Hong Kong. To prepare the aqueous extract of ZJP, 60 g Coptidis Rhizoma and 10 g Evodiae Fructus were soaked in 700 ml distilled water for 30 min, and then were decocted for 1 h. The solvent was centrifuged at 10,000 rpm for 30 min, and the supernatant was collected. This extraction step was repeated twice, and the supernatants were merged and then evaporated to dryness. The dried powder was redissolved in distilled water to 10 mg/ml and filtered with a 0.22 μm pore-size filter and stored at -20°C for further use.

Phytochemical Analysis of ZJP

Fingerprinting analysis was conducted by UPLC to identify the chemical profile of ZJP. In detail, 5 µl of ZJP aqueous extract (1 mg/ml) and standards were respectively injected into the UPLC system (Thermo Fisher Scientific, USA) and separated on C18 ODS column (250×4.6 mm id, ACE, Scotland) with gradient elution. 0.085% H_3PO_4 (A) and acetonitrile (B) was used as mobile phase and the gradient elution procedure was as follows: 0 min, A:B = 97:3; 3 min, A:B = 97:3; 16 min, A:B = 80:20; 50 min, A:B = 76:24; 55 min, A:B = 65:35; 65 min, A:B = 50:50; and 70 min, A:B = 35:75. The flow rate was 1.0 ml/min and the detection was under the absorption wavelength of 280 nm.

Cell Culture

Human HCC HepG2, MHCC97L, PLC/PRF/5, and HLE cells were chosen for the following experiments. HepG2 and PLC/PRF/5 cells were commercially obtained from American Type Culture Collection (ATCC; Manassa, VA, USA); HLE cells were purchased from JCRB (Japan); and MHCC97L cells were kindly gifted by Professor Man Kwan from Department of Surgery, The University of Hong Kong. Cells were cultured in DMEM medium supplemented with 10% FBS, 100 U/ml penicillin, and 100 mg/ml streptomycin and maintained at 37°C in a humidified chamber with 5% CO_2.

Cell Viability Assay

HCC cells (5,000 cells/well) were seeded in 96-well plates and incubated for 24 h. After pretreatment with different concentrations of ZJP (0, 7.8125, 15.625, 31.25, 62.5, 125, 250, 500, and 1,000 µg/ml) for 24, 48, and 72h, 10 µl of 3-(4,5-Dimethylthiazol-2-yl)-2,5-diphenyltetrazolium bromide solution (MTT, 5 mg/ml; Sigma, USA) was added to each well and then cells were cultured at 37°C for another 4 h. Then, the supernatants were discarded and 100 µl of DMSO was added to each well. The absorbance was measured at 595 nm using Multiskan MS microplate reader (Labsystems, Finland).

Colony Formation Assay

MHCC97L and PLC/PRF/5 cells were seeded in 6-well plates at 5000 cells per well and incubated for 24 h. Then, cells were treated with or without ZJP (150 and 300 µg/ml for MHCC97L, 50 and 100 µg/ml for PLC/PRF/5) for continuous 10 days. After fixation with 4% paraformaldehyde for 30 min, the cells were stained with crystal violet solution for 2 h. The photographs of the colonies were taken manually after washed with water.

Flow Cytometry for Cell Cycle Analysis

MHCC97L and PLC/PRF/5 cells (5 × 10^5 cells/well) were seeded in 6-well plates. After incubation for 12 h, the medium was changed to serum-free DMEM for another 12 h and then cells were treated with or without ZJP (150 and 300 µg/ml for MHCC97L, 50 and 100 µg/ml for PLC/PRF/5) for 24 h. Cells were collected and fixed with 70% ethanol at 4°C overnight. After fixation, the cells were stained with propidium iodide (PI, 50 µg/ml, Sigma-aldrich, USA) for 45 min in dark. The cell samples were tested with Canto II flow cytometer (BD Bioscience, USA) for cell cycle analysis.

Wound-Healing and Transwell Invasion Assay

For wound-healing assay, MHCC97L and PLC/PRF/5 cells were incubated in 6-well plates with 100% confluence. A denuded area was scrapped using a plastic pipette tip on the cell monolayer. Medium was removed and the monolayer was washed 3 times with PBS. Then, medium containing different concentrations of ZJP (150 and 300 µg/ml for MHCC97L, 50 and 100 µg/ml for PLC/PRF/5) was added to each well and cell movements into the wound area were obtained after 0, 24, and 48 h incubation with a microscope. For transwell invasion assay, millicell cell culture inserts in 24-well plates were pretreated with 100 µl of cold Matrigel (BD Biosciences, USA, diluted 1:4 with cold PBS) for 2 h at 37°C. MHCC97L and PLC/PRF/5 cells (1 × 10^5 cells/well) were seeded to the chamber with 200 µl of serum-free DMEM and then incubated with or without ZJP (150 and 300 µg/ml for MHCC97L, 50 and 100 µg/ml for PLC/PRF/5) at 37°C for 24 h. The invaded cells are fixed with 4% paraformaldehyde for 30 min and stained with crystal violet solution for 2 h and then counted with a light microscope.

Orthotopic HCC Implantation Murine Model

All animals received human care throughout the experiments and the study protocols were approved by the Committee on the Use of Live Animals in Teaching and Research (CULATR). In brief, 5×10^6 luciferase-tagged MHCC97L cells were subcutaneously injected into the left waist of 5-week-old male BALB/c nu/nu athymic nude mice to establish xenografted tumor. When the subcutaneous tumor reached 1 cm in diameter, it was dissected and cut into small cubes (approximately 1 mm^3). The small tumor cube was orthotopically implanted into the left liver lobe of 5-week-old male BALB/c nu/nu athymic nude mice to establish orthotopic HCC implantation murine model. One week after implantation, the growth of liver tumor was checked under *in vivo* live imaging system (IVIS Spectrum, Perkin-Elmer, USA) by injecting luciferin (i.p., 150 mg/kg) into the mice. All tumor-presenting mice were then randomized into model and ZJP treatment groups (n = 5) receiving gavage of PBS and ZJP (400 mg powder/kg/2 day) respectively for 4 weeks. Liver tumor growth was monitored weekly. At the end of treatment, the nude mice were humanely sacrificed to collect tissues.

Western Blotting

For cell samples, HCC cells (5 × 10^5 cells/well) were seeded in 6-well plates. After incubation overnight, the cells were treated with or without ZJP for 24 h (50 and 100 µg/ml for HepG2 and PLC/PRF/5, 150 and 300 µg/ml for MHCC97L, 25 and 50 µg/ml for HLE). The cells were harvested using a microscraper (Corning). For tissue samples, the tumor tissues were collected after 4 weeks' treatment of ZJP. The expression levels of PIK3CA, EGFR, NFKIBA, CCND1, and pMAPK1 were examined by western blotting. In brief, the whole-cell extracts and tumor homogenates were lysed with RIPA buffer supplemented with proteinase inhibitor (1% PMSF, 0.5% aprotinin, and 0.5% leupeptin) and phosphatase inhibitor (1 mM Na_3VO_4 and 1 mM NaF) on ice for 30 min. Subsequently, the lysates were centrifuged at 14,000 rpm for 10 min at 4°C. The protein concentration was detected using bovine serum albumin (BSA; Sigma, MO, USA) as

a standard. Equal amount of protein in each sample was resolved by sodium dodecyl sulfate-polyacrylamide gel electrophoresis (SDS-PAGE) and transferred onto a polyvinylidene fluoride membrane (PVDF; Biorad, USA). Next, the membrane was blocked with 5% BSA in Tris buffered saline-Tween 20 (TBST) buffer (10 mmol/L Tris, 150 mmol/L NaCl, 1% Tween 20, pH 7.4) for 2 h at room temperature. The blots were then incubated with primary antibodies (anti-PIK3CA, anti-EGFR, anti-NFKIBA, anti-CCND1, and anti-pMAPK1 antibody at 1:1000; Abcam, UK) at 4°C overnight. After washed with TBST buffer for three times, the blots were incubated with the secondary antibody (Abcam, UK) for 2 h at room temperature. Immunoreactivity was determined using an advanced ECL kit (GE Healthcare, UK) and visualized using a chemiluminescence imaging system (Biorad).

Histopathological Examination
Livers from the orthotopic implanted mice were dissected and fixed in 4% formalin buffer. Paraffin-embedded blocks were prepared and sections at 5 μm thickness were cut and stained with hematoxylin and eosin for histological examination.

Statistical Analysis
Statistical analysis was processed with Prism 6 software. Data were expressed as the mean ± SD and analyzed using Student's t-test. Differences between groups were considered to be statistically significant if values of $P < 0.05$.

RESULTS

Network Pharmacology-Based Analysis
Identification of Bioactive Components in ZJP
The fingerprinting analysis of ZJP aqueous extract were conducted by the UPLC. As shown in **Supplement 1**, approximately 14 chromatographic peaks were identified as the phytochemical profile of ZJP. Among them, two compounds of main peaks of UPLC chromatogram were identified as berberine and palmatine based on their retention time and UV spectrum.

A total of 224 components in ZJP were obtained from TCMSP database, 48 of which belong to CR and 176 to EF (**Supplement 2**). Of note, there were eight common components shared in these two herbs, namely, berberine, isovanillin, heriguard, obacunoic acid, obamegine, obacunone, limonin, and quercetin. Among the 48 components in Coptidis Rhizoma, 26 (54.2%) met the requirement of OB ≥30% and 14 (29.2%) met the requirements of OB ≥30% and DL index ≥0.18. Among the 176 components in Evodiae Fructus, 106 (60.2%) met the requirement of OB ≥30% and 31 (29.2%) met the requirements of OB ≥30% and DL index ≥0.18 (**Table 1**). After eliminating the overlaps, 42 components were chosen as candidate bioactive components for further analyses and the detailed information was shown in **Table 2**.

Targets Identification of ZJP on HCC
Among the 42 candidate bioactive components, 1,092 protein targets were retrieved from TCMSP database and TCMID. The detailed information was shown in **Supplement 3**. After eliminating the overlaps, 517 protein targets were obtained for

TABLE 1 | Number of components in ZJP with OB ≥ 30% and DL index ≥ 0.18.

Herbs	Total	OB ≥ 30%	OB ≥ 30% and DL ≥ 0.18
Coptidis Rhizoma	48	26 (54.2)	14 (29.2)
Evodiae Fructus	176	106 (60.2)	31 (17.6)

further analyses. 566 HCC-related human genes were collected from OncoDB.HCC and Liverome databases. The detailed information was shown in **Supplement 4**. Then, these protein targets of ZJP were mapped with HCC using TTD, CTD, and PharmGKB. As a result, 86 targets of 32 components in ZJP were associated with HCC and the detailed information of the 86 targets of ZJP on HCC was shown in **Table 3**.
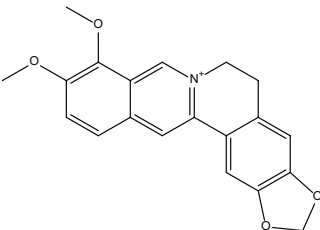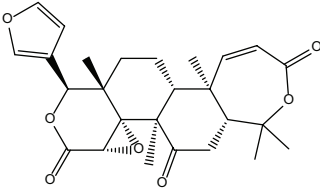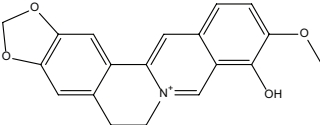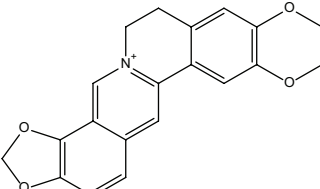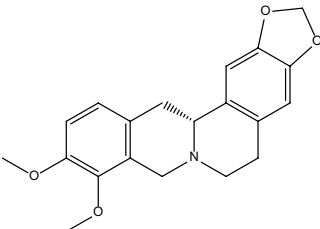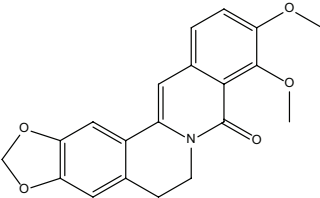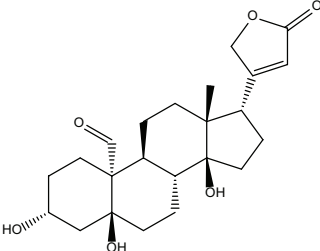
Compound-Target Network and Analysis
As TCM formulas exhibited multiple pharmacological activities *via* multiple targets, it was constructive for us to investigate the underlying mechanisms of TCM formulas on complex diseases by network analysis. In the current study, the compound-target network of ZJP on HCC was constructed (**Figure 2**), which included 118 nodes (32 for candidate bioactive components and 86 for potential protein targets). Among these bioactive components, there were six high-degree components associated with multiple HCC targets, namely, quercetin (MOL034, degree = 74), berberine (MOL001, degree = 31), evodiamine (MOL133, degree = 16), isorhamnetin (MOL104, degree = 9), rutaecarpine (MOL095, degree = 9), and gossypetin (MOL193, degree = 6). Among these potential protein targets, there were seven high-degree targets associated with multiple compounds, namely, AR (degree = 27), PTDG2 (degree = 26), HSP90AA1 (degree = 16), ERS1 (degree = 10), PIK3CA (degree = 7), CA2 (degree = 5), and PARP1 (degree = 5). These high-degree protein targets in the network may account for the essential therapeutic effects of ZJP on HCC.
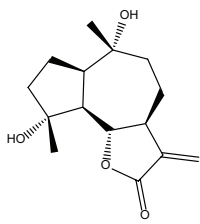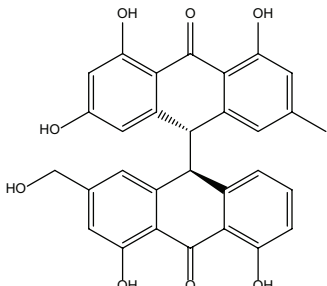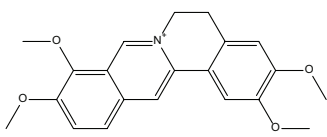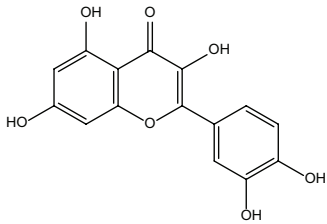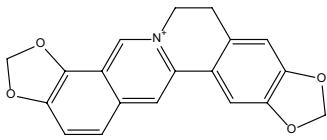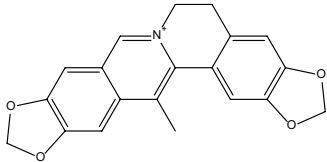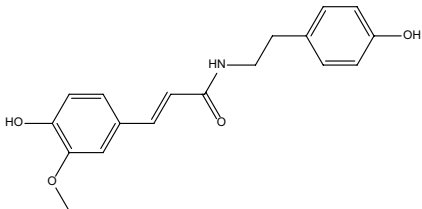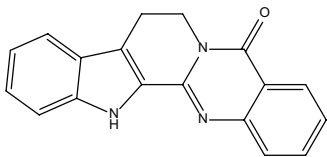
GO and Pathway Enrichment Analysis
To identify the biological characteristics of putative targets of ZJP on HCC in detail, the GO and pathway enrichment analyses of involved targets were conducted *via* the functional annotation tool of DAVID Bioinformatics Resources 6.7. There were respectively 90 biological process (BP), 36 cellular component (CC), and 63 molecular function (MF) terms in total, which met the requirements of Count ≥ 2 and EASE scores ≤ 0.05. The detailed GO information was shown in **Supplement 5**. The top 15 significantly enriched terms in BP, CC, and MF categories were shown in **Figure 3A**, which indicated that ZJP may regulate cancer cell proliferation *via* enzyme binding, protein binding, and transcription factor binding in cytosol, plasma membrane, and extracellular space to exert its therapeutic effects on HCC. To explore the underlying involved pathways of ZJP on HCC, KEGG pathway analysis of involved targets was conducted. The detailed pathway information of ZJP on HCC was shown in **Supplement 6**. The top 15 significantly enriched pathways of ZJP on HCC were shown in **Figure 3B**. The pathways in cancer exhibited the largest number of involved targets (31 counts).

TABLE 2 | Information for candidate bioactive components of ZJP.

Number	Molecule Name	OB (%)	DL	Molecules structure	Herb
MOL001	Berberine	36.86	0.78		Coptidis Rhizoma/Evodiae Fructus
MOL011	Obacunone	43.29	0.77		Coptidis Rhizoma/Evodiae Fructus
MOL013	Berberrubine	35.74	0.73		Coptidis Rhizoma
MOL016	Epiberberine	43.09	0.78		Coptidis Rhizoma
MOL022	(R)-Canadine	55.37	0.77		Coptidis Rhizoma
MOL023	Berlambine	36.68	0.82		Coptidis Rhizoma
MOL026	Corchoroside A_qt	104.95	0.78		Coptidis Rhizoma
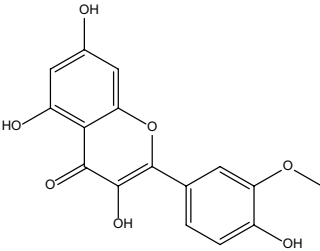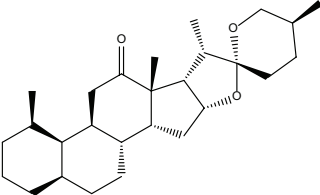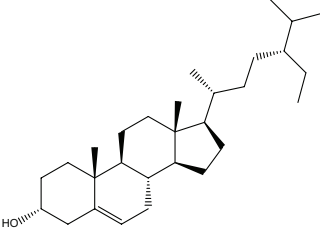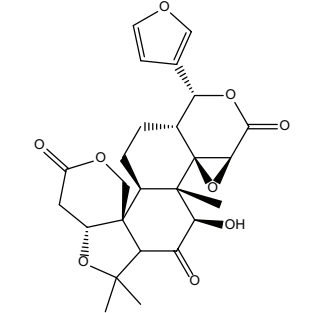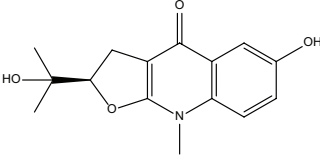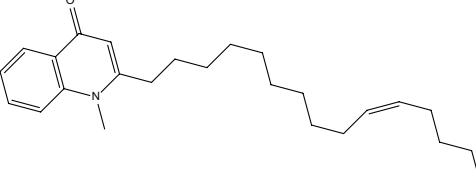
(*Continued*)

TABLE 2 | Continued.

Number	Molecule Name	OB (%)	DL	Molecules structure	Herb
MOL028	Magnograndiolide	63.71	0.19		Coptidis Rhizoma
MOL029	Palmidin A	35.36	0.65		Coptidis Rhizoma
MOL032	Palmatine	64.6	0.65		Coptidis Rhizoma
MOL034	Quercetin	46.43	0.28		Coptidis Rhizoma/Evodiae Fructus
MOL038	Coptisine	30.67	0.86		Coptidis Rhizoma
MOL041	Worenine	45.83	0.87		Coptidis Rhizoma
MOL047	Moupinamide	86.71	0.26		Coptidis Rhizoma
MOL095	Rutaecarpine	40.3	0.6		Evodiae Fructus

(*Continued*)

TABLE 2 | Continued.

Number	Molecule Name	OB (%)	DL	Molecules structure	Herb
MOL104	Isorhamnetin	49.6	0.31		Evodiae Fructus
MOL106	Beta-sitosterol	36.91	0.75		Evodiae Fructus
MOL107	Sitosterol	36.91	0.75		Evodiae Fructus
MOL117	Rutaevine	66.05	0.58		Evodiae Fructus
MOL118	Rutalinidine	40.89	0.22		Evodiae Fructus
MOL122	1-Methyl-2-[(Z)-pentadec-10-enyl]-4-quinolone	48.45	0.46		Evodiae Fructus
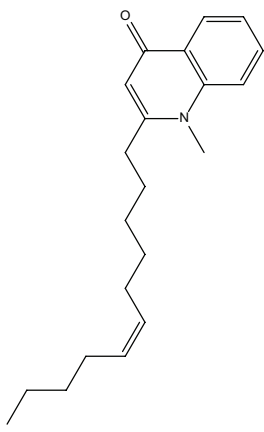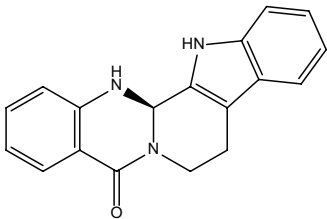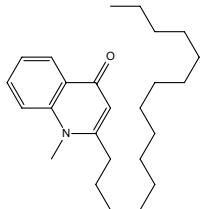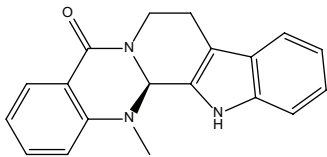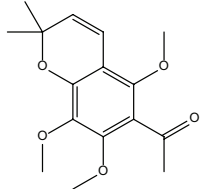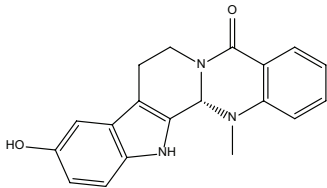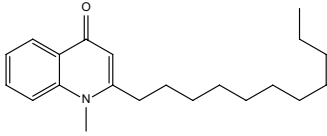
(Continued)

Target-Pathway Network and Analysis

It has been suggested that genes and proteins do not exhibit their biological and pharmacological activities independently. Actually, they function in interactive and dynamics pathways and networks at the cell and molecular levels (Kumar et al., 2015). To further characterize the molecular mechanism by which ZJP alleviated HCC, a target-pathway network was performed based on all involved proteins and their corresponding significant signalling pathways (**Figure 4**). This network included 145 nodes (70 for proteins and 75 for
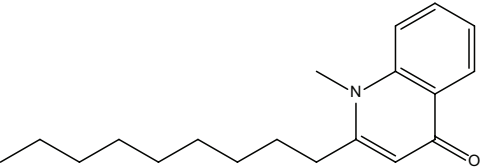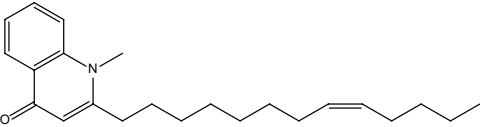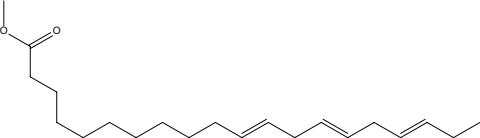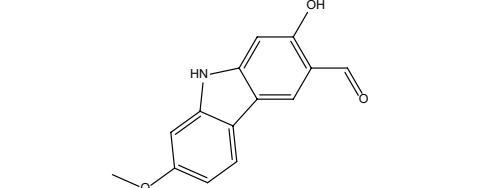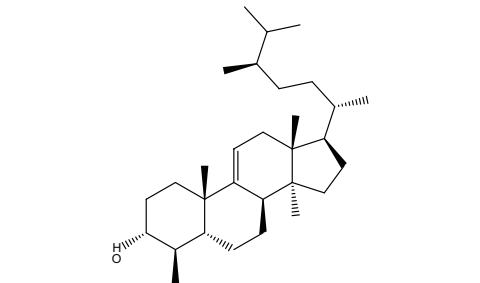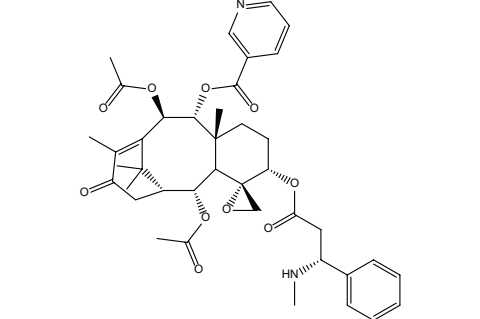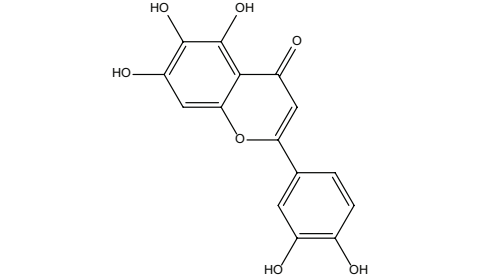
TABLE 2 | Continued.

Number	Molecule Name	OB (%)	DL	Molecules structure	Herb
MOL125	1-Methyl-2-[(Z)-undec-6-enyl]-4-quinolone	48.48	0.27		Evodiae Fructus
MOL131	Dihydrorutaecarpine	42.27	0.6		Evodiae Fructus
MOL132	1-Methyl-2-pentadecyl-4-quinolone	44.52	0.46		Evodiae Fructus
MOL133	Evodiamine	86.02	0.64		Evodiae Fructus
MOL134	1-(5,7,8-Trimethoxy-2,2-dimethylchromen-6-yl)ethanone	30.39	0.18		Evodiae Fructus
MOL137	Hydroxyevodiamine	72.11	0.71		Evodiae Fructus
MOL138	1-Methyl-2-undecyl-4-quinolone	47.59	0.27		Evodiae Fructus
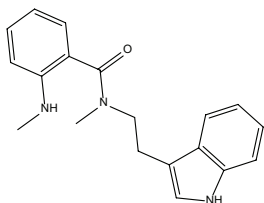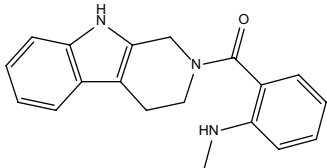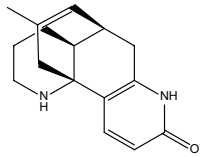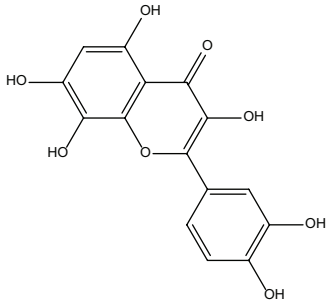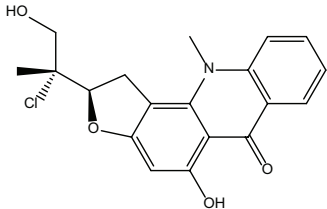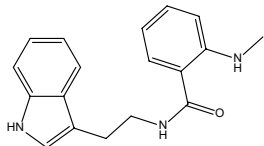
(Continued)

TABLE 2 | Continued.

Number	Molecule Name	OB (%)	DL	Molecules structure	Herb
MOL145	1-Methyl-2-nonyl-4-quinolone	48.42	0.2		Evodiae Fructus
MOL147	Evocarpine	48.66	0.36		Evodiae Fructus
MOL148	Icosa-11,14,17-trienoic acid methyl ester	44.81	0.23		Evodiae Fructus
MOL161	2-Hydroxy-3-formyl-7-methoxycarbazole	83.08	0.18		Evodiae Fructus
MOL167	24-Methyl-31-norlanost-9(11)-enol	38	0.75		Evodiae Fructus
MOL175	5alpha-O-(3'-Methylamino-3'-phenylpropionyl) nicotaxine	30.86	0.49		Evodiae Fructus
MOL177	6-OH-Luteolin	46.93	0.28		Evodiae Fructus

(Continued)

TABLE 2 | Continued.

Number	Molecule Name	OB (%)	DL	Molecules structure	Herb
MOL187	Evodiamide	73.77	0.28		Evodiae Fructus
MOL190	Fordimine	55.11	0.26		Evodiae Fructus
MOL191	Goshuyuamide I	83.19	0.39		Evodiae Fructus
MOL192	Goshuyuamidell	69.11	0.43		Evodiae Fructus
MOL193	Gossypetin	35	0.31		Evodiae Fructus
MOL194	Gravacridoneshlirine	63.73	0.54		Evodiae Fructus
MOL198	N-(2-Methylaminobenzoyl) tryptamine	56.96	0.26		Evodiae Fructus

pathways). Among these potential pathways, pathway in cancer was consider the most significant one with the highest degree value. Among these potential targets, MAPK1, PIK3CA, EGFR, CCND1, and NFKBIA were identified as relatively high-degree targets, which played an essential role in cell proliferation and survival and were considered as the key markers of ZJP treatment on HCC. From the integrated drug target prediction, GO, and pathway enrichment as well as network analyses, we speculated that the antitumor effects of ZJP on HCC might be associated with the roles of its key targets including MAPK1,

PIK3CA, EGFR, CCND1, and NFKBIA in regulating HCC cell proliferation and survival.

Experimental Validation
ZJP-Inhibited HCC Cell Growth *in Vitro*

To validate the antiproliferative effect of ZJP on HCC as postulated from network pharmacology analysis, various cell function assays were conducted. When exposed to increasing concentrations (7.8125-1000 μg/ml) of ZJP, a dose- and time-dependent decrease in HCC cell viability at different time

TABLE 3 | Targets of ZJP on HCC.

Number	Protein name	Gene name	Score	Degree
1	Mitogen-activated protein kinase 1	MAPK1	3	52
2	Phosphatidylinositol 4,5-bisphosphate 3-kinase catalytic subunit gamma isoform	PIK3CA	7	51
3	RAF proto-oncogene serine/threonine-protein kinase	RAF1	1	42
4	Cellular tumor antigen p53	TP53	3	31
5	G1/S-specific cyclin-D1	CCND1	4	28
6	Epidermal growth factor receptor	EGFR	2	28
7	NF-kappa-B inhibitor alpha	NFKBIA	3	24
8	Cyclin-dependent kinase inhibitor 1	CDKN1A	2	21
9	Pro-epidermal growth factor	EGF	2	21
10	Myc proto-oncogene protein	MYC	2	21
11	Proto-oncogene tyrosine-protein kinase Src	SRC	1	19
12	Proto-oncogene c-Fos	FOS	2	17
13	Caspase-3	CASP3	4	16
14	Cyclin-dependent kinase 4	CDK4	1	16
15	Catenin beta-1	CTNNB1	1	14
16	Retinoblastoma-associated protein	RB1	1	14
17	Signal transducer and activator of transcription 1-alpha/beta	STAT1	1	14
18	Vascular endothelial growth factor A	VEGFA	3	14
19	Transcription factor E2F1	E2F1	1	13
20	Receptor tyrosine-protein kinase erbB-2	ERBB2	1	13
21	Focal adhesion kinase 1	PTK2	1	13
22	Apoptosis regulator BAX	BAX	4	12
23	SHC-transforming protein 1	SHC1	1	12
24	Matrix metalloproteinase-9	MMP9	4	9
25	Prostaglandin G/H synthase 2	PTGS2	26	9
26	Fibronectin	FN1	2	8
27	Intercellular adhesion molecule 1	ICAM1	2	8
28	Heat shock cognate 71 kDa protein	HSPA8	1	7
29	Protransforming growth factor alpha	TGFA	1	7
30	Stromal cell-derived factor 1	CXCL12	1	6
31	Interleukin-2	IL2	2	6
32	72 kDa type IV collagenase	MMP2	2	6
33	Ras association domain-containing protein 1	RASSF1	1	6
34	Tumor necrosis factor ligand superfamily member 10	TNFSF10	1	6
35	Cyclin-A2	CCNA2	4	5
36	Heat shock protein HSP 90	HSP90AA1	17	5
37	Tumor necrosis factor ligand superfamily member 11	TNFSF11	2	5
38	Baculoviral IAP repeat-containing protein 5	BIRC5	2	4
39	Cytochrome P450 1A2	CYP1A2	3	4
40	Cytochrome P450 2E1	CYP2E1	1	4
41	Estrogen receptor	ESR1	10	4
42	Heat shock protein beta-1	HSPB1	1	4
43	Proliferating cell nuclear antigen	PCNA	2	4
44	Urokinase-type plasminogen activator	PLAU	2	4
45	Plasminogen activator inhibitor 1	SERPINE1	1	4
46	Collagen alpha-1(I) chain	COL1A1	1	3
47	C-X-C motif chemokine 2	Cxcl2	1	3
48	Receptor tyrosine-protein kinase erbB-3	ERBB3	1	3
49	Glutathione S-transferase P	GSTP1	1	3
50	Stromelysin-1	MMP3	1	3
51	Osteopontin	SPP1	1	3
52	Androgen receptor	AR	27	2
53	Catalase	CAT	1	2
54	Claudin-4	CLDN4	1	2
55	Cytochrome P450 2B6	CYP2B6	1	2
56	Cytochrome P450 3A4	CYP3A4	3	2
57	Insulin-like growth factor-binding protein 3	IGFBP3	1	2
58	Interferon regulatory factor 1	IRF1	1	2
59	Solute carrier family 2, facilitated glucose transporter member 2	SLC2A2	1	2
60	Superoxide dismutase [Cu-Zn]	SOD1	1	2
61	Vimentin	VIM	1	2
62	Multidrug resistance protein 1	ABCB1	4	1
63	Catechol O-methyltransferase	COMT	1	1

(Continued)

TABLE 3 | Continued.

Number	Protein name	Gene name	Score	Degree
64	Flap endonuclease 1	FEN1	1	1
65	Glycogen synthase kinase-3 alpha	GSK3A	1	1
66	78 kDa glucose-regulated protein	HSPA5	1	1
67	Insulin-like growth factor II	IGF2	1	1
68	Poly [ADP-ribose] polymerase 1	PARP1	5	1
69	Plasminogen	PLG	1	1
70	Superoxide dismutase [Mn], mitochondrial	SOD2	2	1
71	ATP-binding cassette sub-family G member 2	ABCG2	2	0
72	Apolipoprotein E	APOE	2	0
73	Carbonic anhydrase 1	CA1	1	0
74	Carbonic anhydrase 2	CA2	5	0
75	CD9 antigen	CD9	1	0
76	Sterol 26-hydroxylase, mitochondrial	CYP27A1	2	0
77	Cytochrome P450 2C8	CYP2C8	1	0
78	Cytochrome P450 2C9	CYP2C9	1	0
79	DNA excision repair protein ERCC-1	ERCC1	1	0
80	Hyaluronan synthase 2	HAS2	1	0
81	Heat shock 70 kDa protein 4	HSPA4	1	0
82	Keratin, type I cytoskeletal 19	KRT19	1	0
83	Methylated-DNA–protein-cysteine methyltransferase	MGMT	1	0
84	Metallothionein-1F	MT1F	1	0
85	DNA topoisomerase 2-alpha	TOP2A	2	0
86	DNA repair protein complementing XP-C cells	XPC	1	0

points (24 h, 48 h, 72 h) was observed (**Figure 5A**). The IC50 values of ZJP in different kinds of HCC cell lines were shown in **Supplement 7**. Then, MHCC97L and PLC/PRF/5 cells were chosen for other cell function assays. As shown in **Figure 5B**, a dose-reduced colony formation was observed in MHCC97L and PLC/PRF/5 cells after treatment with increasing ZJP for 10 days. The delay of the G1/S transition in HCC cells after treatment with ZJP was further confirmed by cell cycle analysis (**Figure 5C**). Interestingly, a dose-reduced migratory and invasive property was also observed in MHCC97L and PLC/PRF/5 cells after treatment with increasing ZJP, as shown in **Figures 5D**, **E**. In summary, these data conformed that ZJP may inhibit HCC cell growth *in vitro* in various aspects.

ZJP Inhibited Tumor Growth of Orthotopic HCC Implantation Murine Model *in Vivo*

To further verify the antiproliferative effect of ZJP on HCC, an orthotopic HCC implantation murine model was established. The tumors in the model group continued to grow into large tumors, giving out very strong luminescence signals. In contrast, there was no remarkable enhancement of the luminescence signals in the ZJP-treated group during the treatment time (**Figure 6A**). By the end of the treatment course (week 4), the size of dissected tumor in the ZJP group was significantly decreased when compared with the model group (**Figure 6B**). These observations indicated that the growth rate of orthotopically implanted HCC was significantly inhibited with the treatment of ZJP. On the other hand, the model and ZJP-treated group had comparable body weight, suggesting that there was no severe toxicity in the presence of ZJP (**Figure 6C**).

Histological examination showed an irregular and invasive edge at the growth front of the tumors in the model group, revealing significant local invasion of orthotopically implanted

HCC cells into the normal liver tissue (**Figure 6D**). In contrast, there was a regular and well-defined tumor growth front of the tumors in the ZJP-treated group. In addition, there was a significant inhibition of mitotic events in the ZJP-treated group when compared with the model group (**Figure 6E**), demonstrating a significant antiproliferative property of ZJP on *in vivo* growth of HCC.

ZJP Attenuated HCC Partially by Regulating Cell Proliferation and Cell Survival

Network pharmacology analysis predicted that the molecular targets highly associated with the common signaling pathways including MAPK1, PIK3CA, EGFR, CCND1, and NFKBIA may be related with the antitumor effects of ZJP on HCC in regulating HCC cell proliferation and survival. We further validated the antitumor properties of ZJP on the expressions of the potential targets identified *via* network pharmacology. As shown in **Figure 7A**, pretreatment of MHCC97L cells with ZJP (150 and 300 µg/ml) and Hep G2 cells with ZJP (50 and 100 µg/ml) led to apparent repression of pMAPK1, PIK3CA, and EGFR. Pretreatment of PLC/PRF/5 cells with ZJP (50 and 100 µg/ml) led to apparent enrichment of NFKBIA and repression of pMAPK1, PIK3CA, and CCND1. Likewise, pretreatment of HLE cells with ZJP (25 and 50 µg/ml) led to apparent enrichment of NFKBIA and repression of pMAPK1, PIK3CA, and EGFR. In addition, the expressions of the potential targets obtained from the tumors of orthotopic HCC implantation murine model were also examined. As shown in **Figure 7B**, the oral treatment of ZJP led to apparent enrichment of NFKBIA and repression of pMAPK1, EGFR, PIK3CA, and CCND1. These results validated that ZJP may regulate the cell proliferation and cell survival mainly through PI3K-NF-κB, EGFR-MAPK, and CCND1 pathways.

FIGURE 2 | The compound-target network for ZJP on HCC. The purple nodes represent candidate active compounds and the green nodes represent potential protein targets. The edges represent the interactions between them and nodes size are proportional to their degree.

DISCUSSION
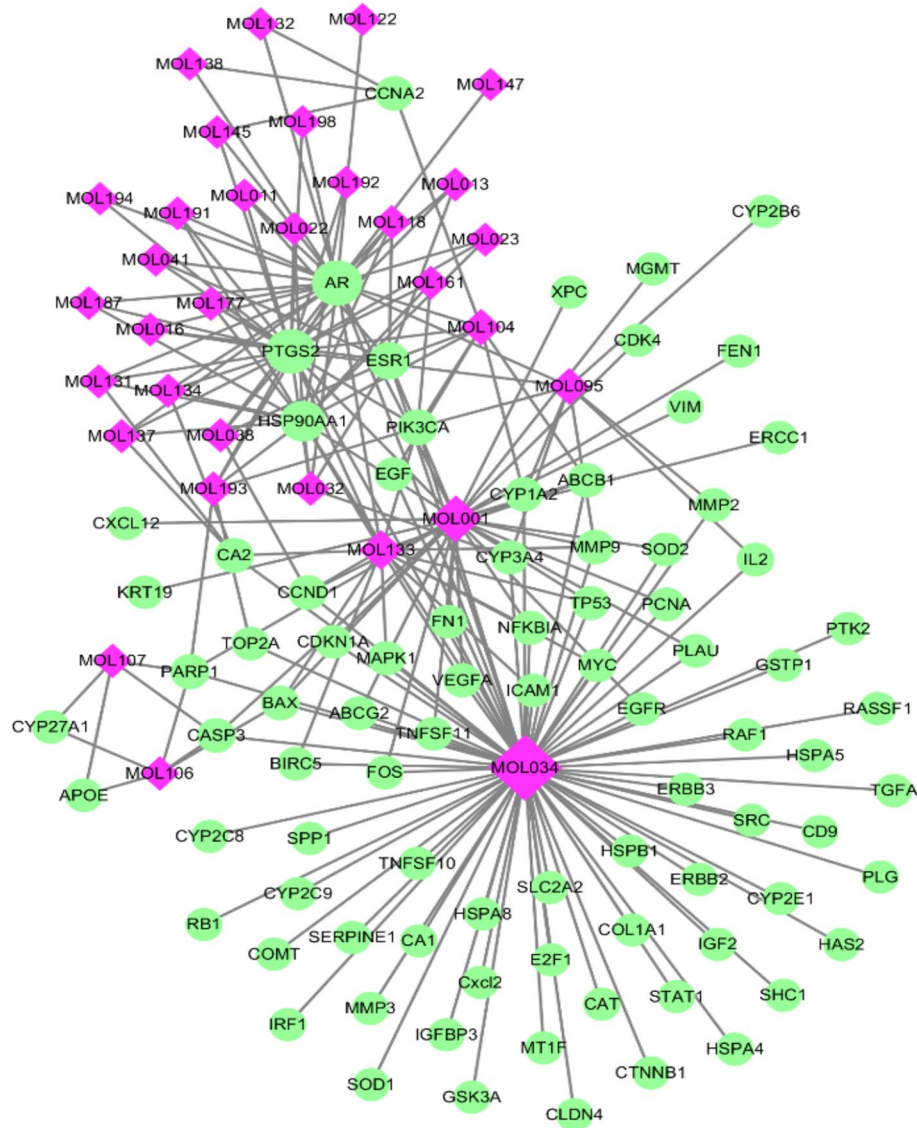
HCC is a complex disease with a stepwise sequence of events, which are related to multiple proteins or pathways during the development and progression (Feitelson et al., 2002). Being composed of multiple compounds, TCM may exhibit extensive pharmacological activities with multiple targets and pathways (Zhou et al., 2014), which may benefit the treatment of HCC. On the other hand, this property of TCM may bring difficulty towards the in-depth study of the underlying mechanisms. Network pharmacology approach, which integrates the systems biology and in silico technologies, may offer a direction for the mechanistic study of complicated TCM. In the current study, we used this approach to clarify the pharmacological mechanism by which ZJP alleviated HCC.

In the system of TCM, compounds lacking proper pharmacokinetical properties could not reach the target organs to deliver the biological activities. In the current study, the compounds in ZJP with OB ≥ 30% and DL index ≥ v0.18 were considered pharmacokinetically active as they are possibly absorbed and distributed in human body. In the compound-target network, compounds with high-degree may account for the major therapeutic effects of ZJP on HCC. In this study, quercetin was the most significant compound, followed by berberine, evodiamine, isorhamnetin, rutaecarpine, and gossypetin. Quercetin, a natural flavonoid, was shown an anticarcinogenic action *via* inhibiting PI3K pathway (Maurya and Vinayak, 2015). Berberine and evodiamine are the primary bioactive compound in CR and EF, respectively. The most significantly bioactive compound berberine from CR could

FIGURE 3 | The 15 most significance of gene ontology **(A)** and pathway enrichment **(B)** analysis of therapy target genes of ZJP on HCC.
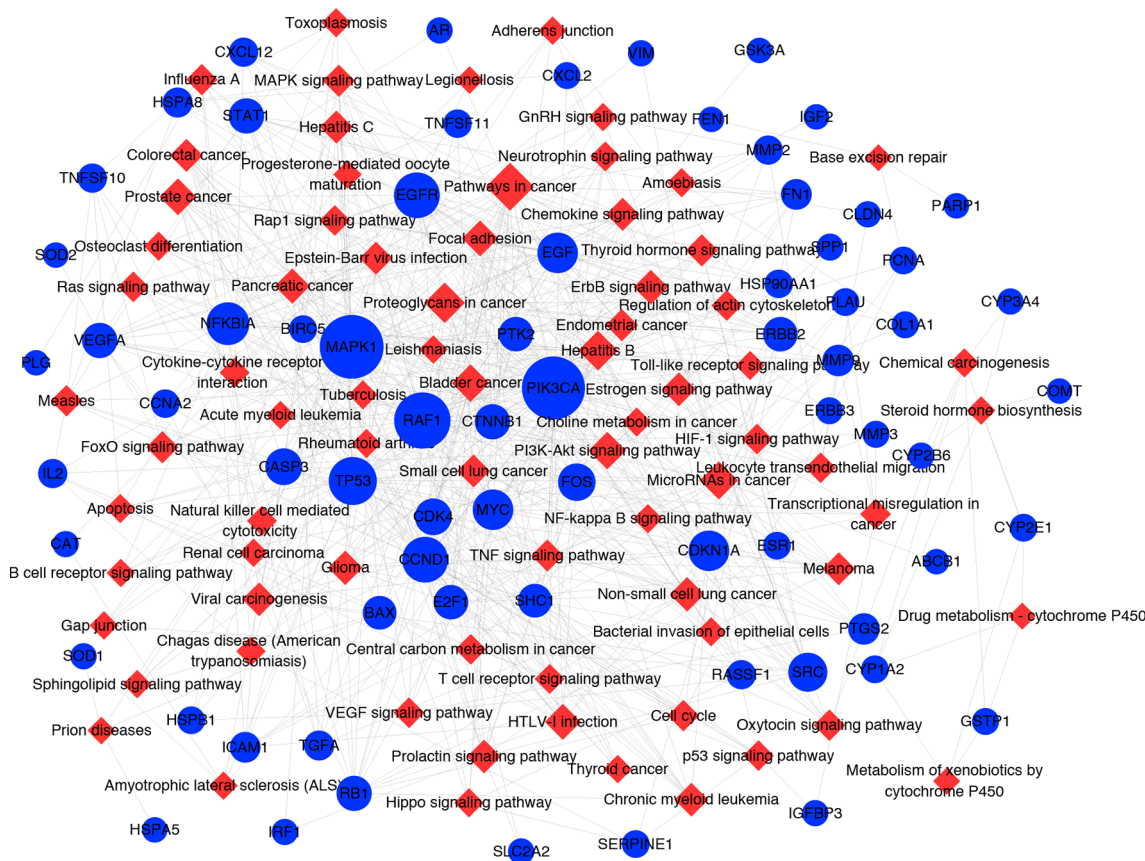
FIGURE 4 | The target-pathway network for ZJP on HCC. The blue nodes represent targets and the red nodes represent pathways. The edges represent the interactions between them and node size is proportional to their degree.

suppress Cyclin D1 expression *via* proteasomal degradation in human hepatoma cells (Wang et al., 2016). In addition, berberine could also induce autophagic cell death and mitochondrial apoptosis in liver cancer cells (Wang et al., 2010b). The bioactive compound evodiamine from EF was shown to exert its antitumor effect on HCC *via* inducing Akt-mediated apoptosis (Yang et al.,

2017). Isorhamnetin, a flavonol aglycone, obtained from the TCM *Hippophae rhamnoides L.*, was shown to exhibit *in vitro* antitumor activity against HCC cells (Teng et al., 2006). Although there was no literature relating rutaecarpine with HCC, it was reported to ameliorate the hyperlipidemia and hyperglycemia, which were the risk factors of HCC (Nie et al., 2016). Gossypetin,
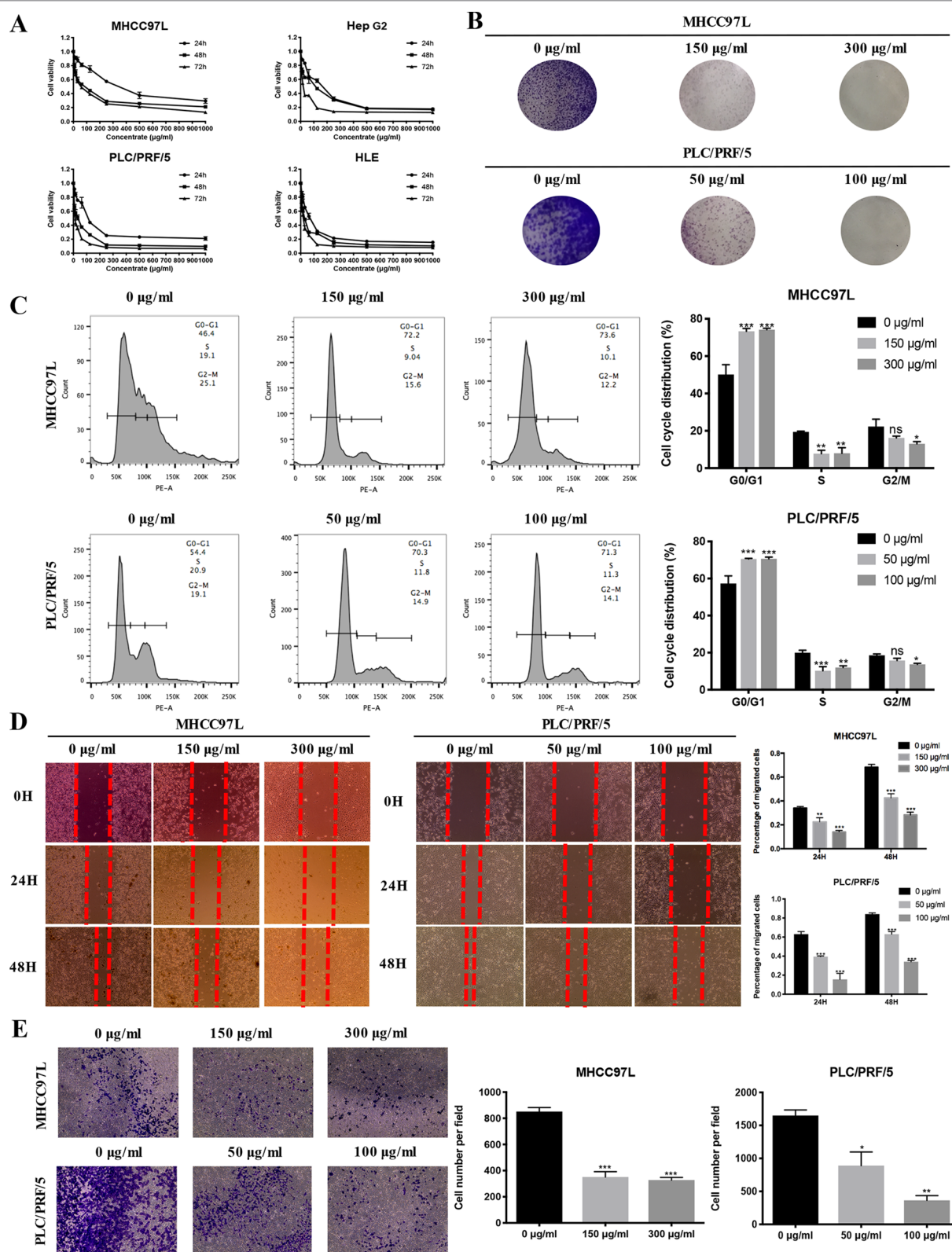
FIGURE 5 | ZJP inhibited HCC cell growth *in Vitro*. **(A)** Time- and dose-dependent effects of ZJP treatment on the viability of HCC cells. **(B)** Representatives images of colony formation of MHCC97L and PLC/PRF/5 cells. **(C)** The representative images and statistical graphs of MHCC97L and PLC/PRF/5 cell cycle analysis. **(D)** The representative images and statistical graphs of migration assay of MHCC97L and PLC/PRF/5 cells. **(E)** The representative images and statistical graphs of transwell chambers of MHCC97L and PLC/PRF/5 cells. *P < 0.05, **P < 0.01, ***P < 0.001 versus the nontreated group.
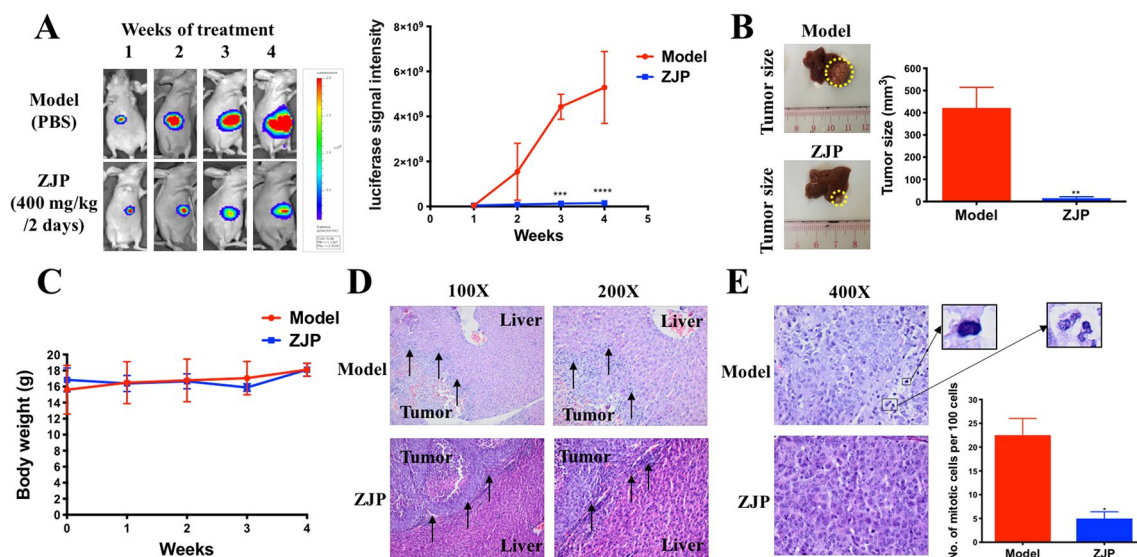
FIGURE 6 | ZJP-inhibited tumor growth of orthotopic HCC implantation murine model *in vivo*. **(A)** The representative images and statistical graph of luciferase signal of animals throughout the oral treatment. **(B)** The representative images and statistical graph of tumor size at the end of experiment. **(C)** The body weight of animals throughout the experiment. **(D)** ZJP suppressed the invasion of the orthotopic tumor cells into the livers. **(E)** ZJP suppressed the mitotic events in tumors. *P < 0.05, **P < 0.01, ***P < 0.001 versus the nontreated group.
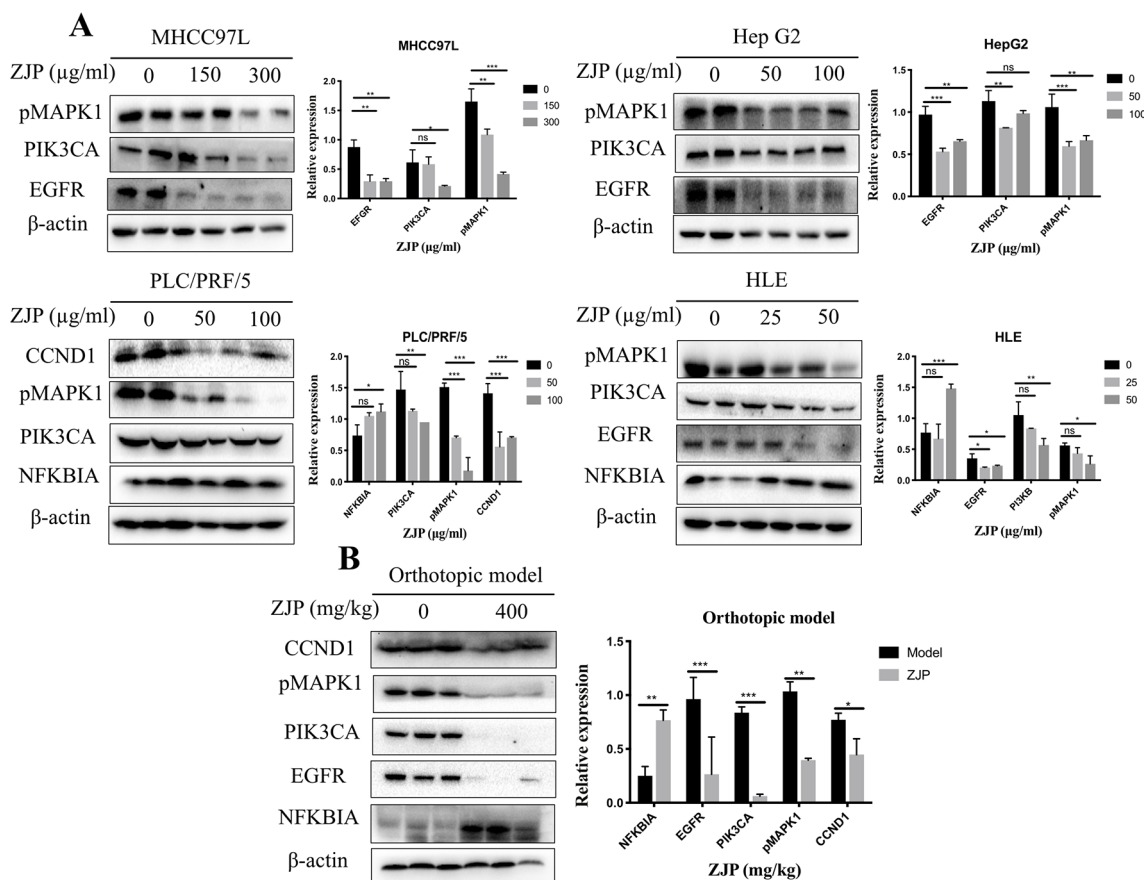
FIGURE 7 | The relative expressions of related proteins with ZJP treatment on HCC cells **(A)** and orthotopic HCC implantation murine model **(B)** *P < 0.05, **P < 0.01, *** P< 0.001 versus the nontreated group.

a naturally occurring hexahydroxy flavone, has been shown to exert anticancer potential *via* inducing apoptotic and autophagic cell death (Lee et al., 2017). All these literatures together with our experimental studies supported the conclusion of network prediction and demonstrated a successful practice of network pharmacology approach in identification of action mechanism of TCM.

From the integrated drug target prediction and pathway analysis, ZJP may exert its antitumor effects on HCC *via* the regulation of cell proliferation and survival, which was characterized as the important mechanism of liver cancer progression (Llovet and Bruix, 2008). Signaling pathways that control multiple processes, such as cell proliferation, invasion, metastasis, and angiogenesis, are commonly dysregulated in the pathological progression of HCC, which have become an important source of targets from a therapeutic perspective in HCC treatment (Moeini et al., 2012). As predicted by network pharmacology approach, ZJP may exert therapeutic effects on HCC primarily by regulating HCC cell proliferation and cell survival *via* PI3K-NF-κB, EGFR-MAPK, and CCND1 signaling pathways. To further validate the postulation, we investigated the curative effects of ZJP on different kinds of HCC cells *in vitro* and orthotopic HCC implantation murine model *in vivo*. The *in vitro* results showed that ZJP treatment significantly decreased HCC cell viability and colony formation ability, halted the cells in G0/G1 phase, and inhibited the cell migration and invasion activities in a dose-dependent manner. The *in vivo* results revealed that oral treatment of ZJP significantly decreased tumor growth and invasion. Especially, the expression levels of PIK3CA, EGFR, pMAPK1, and CCND1 were significantly decreased, whereas NFKBIA was significantly increased. NFKBIA is a member of the NF-κB inhibitor family. It could inhibit NF-κB, which has an essential role in promoting cell survival *via* immune, inflammatory, and stress responses. The aberrant regulation of

NF-κB and the signaling pathways that control its activity are related to cancer development and progression (Baud and Karin, 2009). PIK3CA has been shown to be mutated in multiple tumors and considered as a potential therapeutic target (Hanker et al., 2013). The PI3K signaling pathway has an essential role in regulating the proliferation, apoptosis, and metastasis of tumor cells, which could be hyperactivated *via* activating mutations in PIK3CA. It is a key juncture in signaling communication network and it makes crosstalk between several important pathways, including NF-κB (Engelman, 2009). EGFR is a transmembrane glycoprotein, which is a member of the protein kinase superfamily. As a receptor for members of the epidermal growth factor family, binding this protein with ligand would trigger tyrosine kinase activity and lead to cell proliferation. EGFR was usually overexpressed at both mRNA and protein levels in HCC (Villanueva et al., 2008). Specifically, the EGFR signaling pathway has a pivotal role in regulating the multiple processes of HCC, such as cell proliferation, angiogenesis, invasion, and metastasis (Wang et al., 2015b). Therefore, when HCC cells were pretreated with ZJP, the decreased expression of EGFR may partially contribute to its curative effects. MAPK1 is one of the members of the MAP kinase family. MAP kinases, also known as extracellular signal-regulated kinases, are associated with a wide variety of biochemical processes, including proliferation and differentiation. In HCC, the activation of MAPK pathway might result from aberrant upstream signals, such as aberrant EGFR signaling (Calvisi et al., 2006). After phosphorylation, it could translocate to the nucleus and phosphorylate the nuclear targets. From the experimental validation, effective blockade of EGFR and pMAPK1 in HCC cells after pretreatment with ZJP may contribute to its curative effects. Cyclin D1 (CCND1) is a member of D-type cyclin family, which also includes cyclin D2 and D3. CCND1 could promote the transition from the G1 to S phase of the cell cycle (Fu et al., 2004). It has been shown that overexpression
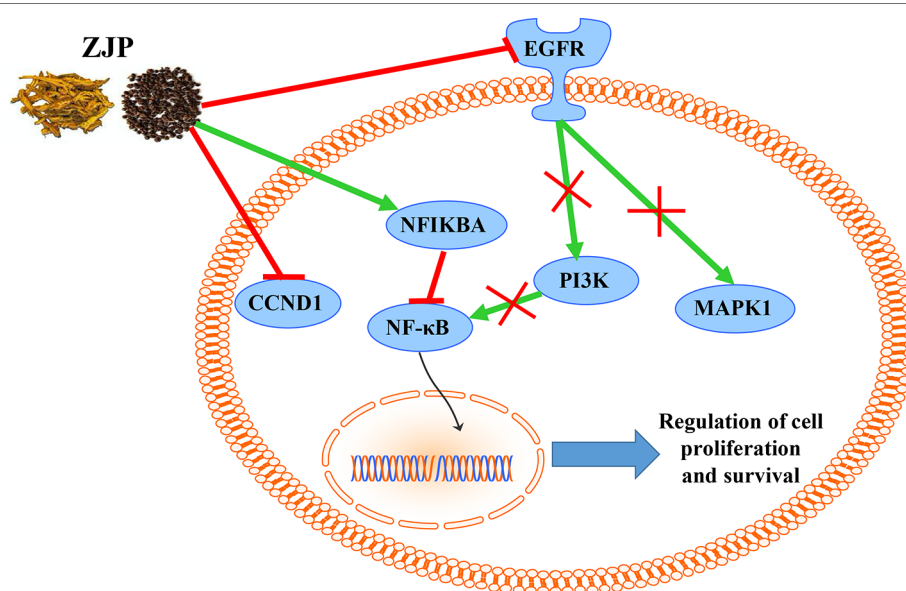
FIGURE 8 | The overall regulatory network involved in the inhibitory effect of ZJP on HCC.

of CCND1 in liver can induce HCC in a transgenic mice model (Deane et al., 2001). Taken together, our findings suggested that ZJP may inhibit HCC progression mainly *via* the regulation of cell proliferation and survival through the EGFR-MAPK, PI3K-NF-κB, and CCND1 signaling pathways (**Figure 8**). Furthermore detailed pharmacological mechanisms by which ZJP ameliorates HCC will be investigated in our future study.

CONCLUSION

In conclusion, the pharmacological mechanism by which ZJP inhibited HCC was investigated with the combination of network pharmacology prediction and experimental validation. We demonstrated that ZJP may inhibit the proliferation and survival of HCC mainly *via* the regulation of EGFR/MAPK, PI3K/NF-κB, and CCND1 signaling pathways. Our study further suggested combined network pharmacology prediction and experimental validation study may offer a useful tool to characterize the action mechanism of TCM in detail. The potential therapeutic effects of ZJP on HCC may benefit from the further studies on clinical trials of HCC patients with ZJP treatment.

DATA AVAILABILITY STATEMENT

The raw data supporting the conclusions of this manuscript will be made available by the authors, without undue reservation, to any qualified researcher.

ETHICS STATEMENT

All animals received human care throughout the experiments and the study protocols were approved by the Committee on the Use of Live Animals in Teaching and Research (CULATR).

AUTHOR CONTRIBUTIONS

YF designed the experiments, analyzed the data, and prepared the manuscript. WG and JH conducted the experiments, analyzed data, and prepared the manuscript. NW and H-YT conducted the experiments, and FC and FYC revised the manuscript. All authors confirmed the final manuscript.

FUNDING

SUPPLEMENTARY MATERIAL

The Supplementary Material for this article can be found at: https://www.frontiersin.org/articles/10.3389/fphar.2019.01185/full#supplementary-material

SUPPLEMENT 1 | The chromatographic fingerprinting of ZJP and standards.

SUPPLEMENT 2 | The summary of total components in ZJP.

SUPPLEMENT 3 | The summary of protein targets from the candidate bioactive components in ZJP.

SUPPLEMENT 4 | The detailed information of 566 HCC-related human genes.

SUPPLEMENT 5 | The detailed GO information of terms which met the requirements of Count ≥2 and EASE scores ≤0.05.

SUPPLEMENT 6 | The detailed pathway information of ZJP on HCC.

SUPPLEMENT 7 | The IC50 of ZJP in different kinds of HCC cell lines.

REFERENCES

Baud, V., and Karin, M. (2009). Is NF-kappaB a good target for cancer therapy? Hopes and pitfalls. *Nat. Rev. Drug Discov.* 8 (1), 33–40. doi: 10.1038/nrd2781

Calvisi, D. F., Ladu, S., Gorden, A., Farina, M., Conner, E. A., Lee, J. S., et al. (2006). Ubiquitous activation of ras and jak/stat pathways in human HCC. *Gastroenterology* 130 (4), 1117–1128. doi: 10.1053/j.gastro.2006.01.006

Chen, Y., Kern, T. S., Kiser, P. D., and Palczewski, K. (2016). Eyes on systems pharmacology. *Pharmacol. Res.* 114, 39–41. doi: 10.1016/j.phrs.2016.09.026

Chen, Y., Wei, J., Zhang, Y., Sun, W., Li, Z., Wang, Q., et al. (2018). Anti-endometriosis mechanism of jiawei foshou san based on network pharmacology. *Front. Pharmacol.* 9, 811. doi: 10.3389/fphar.2018.00811

Chou, S. T., Hsiang, C. Y., Lo, H. Y., Huang, H. F., Lai, M. T., Hsieh, C. L., et al. (2017). Exploration of anti-cancer effects and mechanisms of Zuo-Jin-Wan and its alkaloid components *in vitro* and in orthotopic HepG2 xenograft immunocompetent mice. *BMC Complement Altern. Med.* 17 (1), 121. doi: 10.1186/s12906-017-1586-6

Deane, N. G., Parker, M. A., Aramandla, R., Diehl, L., Lee, W. J., Washington, M. K., et al. (2001). Hepatocellular carcinoma results from chronic cyclin D1 overexpression in transgenic mice. *Cancer Res.* 61 (14), 5389–5395.

Engelman, J. A. (2009). Targeting PI3K signalling in cancer: opportunities, challenges and limitations. *Nat. Rev. Cancer* 9 (8), 550–562. doi: 10.1038/nrc2664

Feitelson, M. A., Sun, B., Satiroglu Tufan, N. L., Liu, J., Pan, J., and Lian, Z. (2002). Genetic mechanisms of hepatocarcinogenesis. *Oncogene* 21 (16), 2593–2604. doi: 10.1038/sj.onc.1205434

Ferlay, J., Soerjomataram, I., Dikshit, R., Eser, S., Mathers, C., Rebelo, M., et al. (2015). Cancer incidence and mortality worldwide: sources, methods and major patterns in GLOBOCAN 2012. *Int. J. Cancer* 136 (5), E359–E386. doi: 10.1002/ijc.29210

Fu, M., Wang, C., Li, Z., Sakamaki, T., and Pestell, R. G. (2004). Minireview: cyclin D1: normal and abnormal functions. *Endocrinology* 145 (12), 5439–5447. doi: 10.1210/en.2004-0959

Gavaraskar, K., Dhulap, S., and Hirwani, R. R. (2015). Therapeutic and cosmetic applications of evodiamine and its derivatives–a patent review. *Fitoterapia* 106, 22–35. doi: 10.1016/j.fitote.2015.07.019

Hanker, A. B., Pfefferle, A. D., Balko, J. M., Kuba, M. G., Young, C. D., Sanchez, V., et al. (2013). Mutant PIK3CA accelerates HER2-driven transgenic mammary tumors and induces resistance to combinations of anti-HER2 therapies. *Proc. Natl. Acad. Sci. U. S. A.* 110 (35), 14372–14377. doi: 10.1073/pnas.1303204110

Hong, M., Li, S., Tan, H. Y., Cheung, F., Wang, N., Huang, J., et al. (2017a). A network-based pharmacology study of the herb-induced liver injury potential of traditional hepatoprotective chinese herbal medicines. *Molecules* 22 (4), 632. doi: 10.3390/molecules22040632

Hong, M., Li, S., Wang, N., Tan, H. Y., Cheung, F., and Feng, Y. (2017b). A biomedical investigation of the hepatoprotective effect of radix salviae miltiorrhizae and network pharmacology-based prediction of the active compounds and molecular targets. *Int. J. Mol. Sci.* 18 (3), 620. doi: 10.3390/ijms18030620

Huang da, W., Sherman, B. T., and Lempicki, R. A. (2009). Systematic and integrative analysis of large gene lists using DAVID bioinformatics resources. *Nat. Protoc.* 4 (1), 44–57. doi: 10.1038/nprot.2008.211

Huang, J., Cheung, F., Tan, H. Y., Hong, M., Wang, N., Yang, J., et al. (2017a). Identification of the active compounds and significant pathways of yinchenhao decoction based on network pharmacology. *Mol. Med. Rep.* 16 (4), 4583–4592. doi: 10.3892/mmr.2017.7149

Huang, J., Li, L., Cheung, F., Wang, N., Li, Y., Fan, Z., et al. (2017b). Network pharmacology-based approach to investigate the analgesic efficacy and molecular targets of xuangui dropping pill for treating primary dysmenorrhea. *Evid. Based Complement Altern. Med.* 2017, 7525179. doi: 10.1155/2017/7525179

Huang, J., Tang, H., Cao, S., He, Y., Feng, Y., Wang, K., et al. (2017c). Molecular targets and associated potential pathways of danlu capsules in hyperplasia of mammary glands based on systems pharmacology. *Evid. Based Complement Altern. Med.* 2017, 1930598. doi: 10.1155/2017/1930598

Kim, K. C., Yook, J. H., Eisenbraun, J., Kim, B. S., and Huber, R. (2012). Quality of life, immunomodulation and safety of adjuvant mistletoe treatment in patients with gastric carcinoma - a randomized, controlled pilot study. *BMC Complement Altern. Med.* 12, 172. doi: 10.1186/1472-6882-12-172

Kumar, A., Butler, B. M., Kumar, S., and Ozkan, S. B. (2015). Integration of structural dynamics and molecular evolution *via* protein interaction networks: a new era in genomic medicine. *Curr. Opin. Struct. Biol.* 35, 135–142. doi: 10.1016/j.sbi.2015.11.002

Lam, P., Cheung, F., Tan, H. Y., Wang, N., Yuen, M. F., and Feng, Y. (2016). Hepatoprotective effects of chinese medicinal herbs: a focus on anti-inflammatory and anti-oxidative activities. *Int. J. Mol. Sci.* 17 (4), 465. doi: 10.3390/ijms17040465

Lee, L., Wang, K., Li, G., Xie, Z., Wang, Y., Xu, J., et al. (2011). Liverome: a curated database of liver cancer-related gene signatures with self-contained context information. *BMC Genomics* (12 Suppl 3, S3). doi: 10.1186/1471-2164-12-S3-S3

Lee, M. S., Tsai, C. W., Wang, C. P., Chen, J. H., and Lin, H. H. (2017). Anti-prostate cancer potential of gossypetin *via* inducing apoptotic and autophagic cell death. *Mol. Carcinog.* 56 (12), 2578–2592. doi: 10.1002/mc.22702

Li, S., and Zhang, B. (2013). Traditional Chinese medicine network pharmacology: theory, methodology and application. *Chin. J. Nat. Med.* 11 (2), 110–120. doi: 10.1016/S1875-5364(13)60037-0

Liang, X., Li, H., and Li, S. (2014). A novel network pharmacology approach to analyse traditional herbal formulae: the Liu-Wei-Di-Huang pill as a case study. *Mol. Biosyst.* 10 (5), 1014–1022. doi: 10.1039/C3MB70507B

Llovet, J. M., and Bruix, J. (2008). Molecular targeted therapies in hepatocellular carcinoma. *Hepatology* 48 (4), 1312–1327. doi: 10.1002/hep.22506

Llovet, J. M., Villanueva, A., Lachenmayer, A., and Finn, R. S. (2015). Advances in targeted therapies for hepatocellular carcinoma in the genomic era. *Nat. Rev. Clin. Oncol.* 12 (7), 408–424. doi: 10.1038/nrclinonc.2015.103

Ma, Y. M., Zhang, X. Z., Su, Z. Z., Li, N., Cao, L., Ding, G., et al. (2015). Insight into the molecular mechanism of a herbal injection by integrating network pharmacology and *in vitro*. *J. Ethnopharmacol.* 173, 91–99. doi: 10.1016/j.jep.2015.07.016

Maurya, A. K., and Vinayak, M. (2015). Anticarcinogenic action of quercetin by downregulation of phosphatidylinositol 3-kinase (PI3K) and protein kinase C (PKC) *via* induction of p53 in hepatocellular carcinoma (HepG2) cell line. *Mol. Biol. Rep.* 42 (9), 1419–1429. doi: 10.1007/s11033-015-3921-7

Moeini, A., Cornella, H., and Villanueva, A. (2012). Emerging signaling pathways in hepatocellular carcinoma. *Liver Cancer* 1 (2), 83–93. doi: 10.1159/000342405

Nie, X. Q., Chen, H. H., Zhang, J. Y., Zhang, Y. J., Yang, J. W., Pan, H. J., et al. (2016). Rutaecarpine ameliorates hyperlipidemia and hyperglycemia in fat-fed, streptozotocin-treated rats *via* regulating the IRS-1/PI3K/Akt and AMPK/ACC2 signaling pathways. *Acta Pharmacol. Sin.* 37 (4), 483–496. doi: 10.1038/aps.2015.167

Pan, J., Xu, Y., Song, H., Zhou, X., Yao, Z., and Ji, G. (2017). Extracts of Zuo Jin Wan, a traditional chinese medicine, phenocopies 5-HTR1D antagonist

in attenuating Wnt/beta-catenin signaling in colorectal cancer cells. *BMC Complement Altern. Med.* 17 (1), 506. doi: 10.1186/s12906-017-2006-7

Ru, J., Li, P., Wang, J., Zhou, W., Li, B., Huang, C., et al. (2014). TCMSP: a database of systems pharmacology for drug discovery from herbal medicines. *J. Cheminf.* 6, 13. doi: 10.1186/1758-2946-6-13

Sherman, M. (2008). Recurrence of hepatocellular carcinoma. *N. Engl. J. Med.* 359 (19), 2045–2047. doi: 10.1056/NEJMe0807581

Smoot, M. E., Ono, K., Ruscheinski, J., Wang, P. L., and Ideker, T. (2011). Cytoscape 2.8: new features for data integration and network visualization. *Bioinformatics* 27 (3), 431–432. doi: 10.1093/bioinformatics/btq675

Su, W. H., Chao, C. C., Yeh, S. H., Chen, D. S., Chen, P. J., and Jou, Y. S. (2007). OncoDB.HCC: an integrated oncogenomic database of hepatocellular carcinoma revealed aberrant cancer target genes and loci. *Nucleic Acids Res.* 35 (Database issue), D727–D731. doi: 10.1093/nar/gkl845

Tao, W., Xu, X., Wang, X., Li, B., Wang, Y., Li, Y., et al. (2013). Network pharmacology-based prediction of the active ingredients and potential targets of Chinese herbal Radix Curcumae formula for application to cardiovascular disease. *J. Ethnopharmacol.* 145 (1), 1–10. doi: 10.1016/j.jep.2012.09.051

Teng, B. S., Lu, Y. H., Wang, Z. T., Tao, X. Y., and Wei, D. Z. (2006). *In vitro* anti-tumor activity of isorhamnetin isolated from Hippophae rhamnoides L. against BEL-7402 cells. *Pharmacol. Res.* 54 (3), 186–194. doi: 10.1016/j.phrs.2006.04.007

Villanueva, A., Chiang, D. Y., Newell, P., Peix, J., Thung, S., Alsinet, C., et al. (2008). Pivotal role of mTOR signaling in hepatocellular carcinoma. *Gastroenterology* 135 (6), 1972–1983, 1983 e1971-1911. doi: 10.1053/j.gastro.2008.08.008

Wang, N., Feng, Y., Lau, E. P., Tsang, C., Ching, Y., Man, K., et al. (2010a). F-actin reorganization and inactivation of rho signaling pathway involved in the inhibitory effect of coptidis rhizoma on hepatoma cell migration. *Integr. Cancer Ther.* 9 (4), 354–364. doi: 10.1177/1534735410379121

Wang, N., Feng, Y., Zhu, M., Tsang, C. M., Man, K., Tong, Y., et al. (2010b). Berberine induces autophagic cell death and mitochondrial apoptosis in liver cancer cells: the cellular mechanism. *J. Cell Biochem.* 111 (6), 1426–1436. doi: 10.1002/jcb.22869

Wang, N., Tan, H. Y., Li, L., Yuen, M. F., and Feng, Y. (2015a). Berberine and coptidis rhizoma as potential anticancer agents: recent updates and future perspectives. *J. Ethnopharmacol.* 176, 35–48. doi: 10.1016/j.jep.2015.10.028

Wang, N., Wang, X., Tan, H. Y., Li, S., Tsang, C. M., Tsao, S. W., et al. (2016). Berberine suppresses cyclin D1 expression through proteasomal degradation in human hepatoma cells. *Int. J. Mol. Sci.* 17 (11), 1899. doi: 10.3390/ijms17111899

Wang, N., Yang, B., Zhang, X., Wang, S., Zheng, Y., Li, X., et al. (2018). Network pharmacology-based validation of caveolin-1 as a key mediator of Ai Du Qing inhibition of drug Resistance in breast cancer. *Front. Pharmacol.* 9, 1106. doi: 10.3389/fphar.2018.01106

Wang, N., Ma, X. P., Shi, Z., Zhang, P., Ding, D. L., Huang, H. X., et al. (2015b). Epidermal growth factor receptor pathway polymorphisms and the prognosis of hepatocellular carcinoma. *Am. J. Cancer Res.* 5 (1), 396–410.

Wang, X. N., Xu, L. N., Peng, J. Y., Liu, K. X., Zhang, L. H., and Zhang, Y. K. (2009). *In vivo* inhibition of S180 tumors by the synergistic effect of the Chinese medicinal herbs Coptis chinensis and Evodia rutaecarpa. *Planta Med.* 75 (11), 1215–1220. doi: 10.1055/s-0029-1185538

Xu, L., Li, H., Xu, Z., Wang, Z., Liu, L., Tian, J., et al. (2012a). Multi-center randomized double-blind controlled clinical study of chemotherapy combined with or without traditional Chinese medicine on quality of life of postoperative non-small cell lung cancer patients. *BMC Complement Altern. Med.* 12, 112. doi: 10.1186/1472-6882-12-112

Xu, S., Peng, J., Li, Y., He, L., Chen, F., Zhang, J., et al. (2012b). Pharmacokinetic comparisons of rutaecarpine and evodiamine after oral administration of Wu-Chu-Yu extracts with different purities to rats. *J. Ethnopharmacol.* 139 (2), 395–400. doi: 10.1016/j.jep.2011.11.023

Xu, X., Zhang, W., Huang, C., Li, Y., Yu, H., Wang, Y., et al. (2012c). A novel chemometric method for the prediction of human oral bioavailability. *Int. J. Mol. Sci.* 13 (6), 6964–6982. doi: 10.3390/ijms13066964

Yang, F., Shi, L., Liang, T., Ji, L., Zhang, G., Shen, Y., et al. (2017). Anti-tumor effect of evodiamine by inducing Akt-mediated apoptosis in hepatocellular carcinoma. *Biochem. Biophys. Res. Commun.* 485 (1), 54–61. doi: 10.1016/j.bbrc.2017.02.017

Zheng, J., Wu, M., Wang, H., Li, S., Wang, X., Li, Y., et al. (2018). Network pharmacology to unveil the biological basis of health-strengthening herbal

medicine in cancer treatment. *Cancers (Basel)* 10 (11), 461. doi: 10.3390/cancers10110461

Zhou, X., Menche, J., Barabasi, A. L., and Sharma, A. (2014). Human symptoms-disease network. *Nat. Commun.* 5, 4212. doi: 10.1038/ncomms5212

Zhu, R. X., Seto, W. K., Lai, C. L., and Yuen, M. F. (2016). Epidemiology of hepatocellular carcinoma in the asia-pacific region. *Gut. Liver* 10 (3), 332–339. doi: 10.5009/gnl15257

Zuo, J., Wang, X., Liu, Y., Ye, J., Liu, Q., Li, Y., et al. (2018). Integrating network pharmacology and metabolomics study on anti-rheumatic mechanisms and antagonistic effects against methotrexate-induced toxicity of Qing-Luo-Yin. *Front. Pharmacol.* 9, 1472. doi: 10.3389/fphar.2018.01472

2′-Hydroxychalcone Induced Cytotoxicity *via* Oxidative Stress in the Lipid-Loaded Hepg2 Cells

Yun Qian[1,2†], Yang Yang[2†], Kai Wang[2], Wenjun Zhou[1], Yanqi Dang[1], Mingzhe Zhu[3], Fenghua Li[2*] and Guang Ji[1*]

[1] Institute of Digestive Diseases, Longhua Hospital, China-Canada Center of Research for Digestive Diseases (ccCRDD), Shanghai University of Traditional Chinese Medicine, Shanghai, China, [2] Experiment Center for Science and Technology, Shanghai University of Traditional Chinese Medicine, Shanghai, China, [3] School of Public Health, Shanghai University of Traditional Chinese Medicine, Shanghai, China

Licorice is a common herb used in traditional Chinese medicine, and has been widely used clinically. Physiologically, although it is relatively safe, licorice-induced hepatotoxicity in the presence of other diseases needs to be evaluated. The present study was conducted to investigate the toxicological effects of the bioactive components of licorice in HepG2 cells cultured with or without free fatty acid (FFA). The compounds, isoliquiritigenin, licorice chalcone A, bavachalcone, and 2′-hydroxy chalcone (2′-HC) inhibited cell proliferation at certain concentrations in lipid loaded cells with limited effects on the normal cells. The representative compound 2′-HC (at a concentration of $\geq$ 20μM) increased the oxygen consumption rate, ATP production, mitochondrial membrane potential, generation of total and mitochondrial reactive oxygen species (ROS) production, and expression of inflammatory cytokines (TNF-α, IL-6, and IL-8) and Caspase-9 protein; and reduced the expression of SOD1. In addition, we found exaggerated lipid accumulation in HepG2 cells treated with FFA. Our results suggest that 2′-HC at a concentration of $\geq$ 20μM might cause damage to the hepatocytes. The toxicity may be related to excess ROS production and inadequate SOD1 expression, leading to apoptosis, inflammation, and cellular dysfunctions.

Keywords: licorice, 2′-hydroxychalcone, cytotoxicity, reactive oxygen species, hepatocyte

INTRODUCTION

Licorice or liquorice is the root of *Glycyrrhiza glabra* L., which is an herbaceous perennial legume. In some European and Middle-east countries, licorice flavor is used as a sweeteners and food additive, and has been approved by the United States Food and Drug Administration as a food supplement (Michielsen et al., 2018; Alagawany et al., 2019). In China, after extraction and processing, licorice is used in herbalism. It is one of the oldest medicinal herbs, and has been included in the pharmacopoeia of the Asian and European countries (Substances et al., 1974). As a widely used herb, licorice is considered to have the effect of reconciling the medicinal properties of other herbs, and is often included as an auxiliary drug in clinical practice (Li et al., 2019).

In the past few decades, pharmacological studies have suggested that licorice and its bioactive components have the therapeutic effects against inflammation, ulcer, chronic viral infection, hyperlipidemia, and immune dysregulation (Yang et al., 2015). In addition, its major constituent

glycyrrhizic acid has been widely used for the treatment of various liver diseases, including hepatitis B, chronic hepatitis, cholestasis, liver fibrosis, liver cancer, etc. (Li et al., 2014). An animal study has shown that glycyrrhizin has a significant protective effects against the development of nonalcoholic steatohepatitis in mice treated with methionine and choline deficiency diet (Yan et al., 2018). Glycyrrhizin can also ameliorate acute liver injury induced by acetaminophen. Besides, it is also suggested that glycyrrhetinic acid has hepatoprotective effects (Jeong et al., 2002; Ji et al., 2016) and has been used for the treatment of liver fibrosis (Moro et al., 2008).

The liver is the main metabolic organ and is also the main site of drug metabolism. It is suggested that stressed hepatocytes are more sensitive to the toxic side effects of drugs (Almazroo et al., 2017). Nonalcoholic fatty liver disease (NAFLD) has become a common disease due to the increased global prevalence of obesity. The typical feature of NAFLD is the accumulated lipids in hepatocytes. Licorice is a frequently used agent as a component of formula such as Sinisan and Ling-gui-zhu-gan decoctionon in preventing and treating NAFLD (Cheng et al., 2017; Dang et al., 2019). While the lipid-loaded hepatocytes are susceptible to chemical toxicity, their resistance to drug toxicity is still unknown.

The main bioactive components of licorice include triterpenoids (glycyrrhizic acid, glycyrrhetinic acid, etc.), flavonoids (isoglycin, isoliquiritn, etc.), alkaloids, polysaccharides, and free phenols (Yang et al., 2015; Li et al., 2019). More than 300 flavonoids have been isolated from licorice including dihydroflavones, dihydroflavonols, chalcone, isoflavones, isoflavones, flavonoids, flavonols, isoflavones, and isoflavones with hydroflavonoids and chalcones as the main types. In the present study, we evaluated the effects of the representative chalcones of licorice on HepG2 cells cultured with or without free fatty acid (FFA), and explored the potential mechanisms of a licorice monomer compound (2′-HC) in the presence of cellular damage.

MATERIALS AND METHODS

Reagents

2′-hydroxychalcone (2′-HC, purity > 95%) (**Figure 1D**) and bavachalcone (BC, purity > 98%) (**Figure 1C**) were purchased from Shanghai Yuanye Biological Technology Co, Ltd. Isoliquiritigenin (LSL, purity ≥ 98%) (**Figure 1A**) and licorice chalcone A (LCA, purity ≥ 98%) (**Figure 1B**) were purchased from Dalian Meilun Biological Technology Co, Ltd. Oleic acid (OA) and Palmitic acid (PA) were purchased from Sinopharm Chemical Reagent Co, Ltd. (Shanghai, China).

Cell Culture and Treatment

The HepG2 human hepatocytes were grown in Dulbecco's modified Eagle's medium (DMEM) containing 10% fetal bovine serum (FBS, Gibco) and 1% antibiotic (100 U/ml penicillin and 100 ug/ml streptomycin, Gibco, USA) at 37°C in a humid atmosphere of 5% CO_2. The cells were harvested and seeded at an initial density of 1×10^5 cells/ml onto the bottom of 96-well plates for experimental use. The cell density of a 6-well culture plate was 1.5×10^5 cells/ml. A special 96-well culture plate

(Seahorse Bioscience) with a cell density of 8×10^4 cells/mL was used to detect the cellular respiratory function. A combination of OA and PA (2:1) was dissolved in DMEM medium (Gibco, USA) to induce NAFLD in HepG2 cells.

MTT [3-(4,5-Dimethylthiazol-2-Yl)-2,5-Diphenyltetrazolium Bromide] (MTT) Assay

MTT (Sangon Biotech, Shanghai, China; 20 μL; 0.25 mg/ml) was added to each well and the cells were incubated for 4 h. The supernatants were removed and 100 μL DMSO was added to each well, and the plates were shaken for 5 min. The absorbance was measured at 570 nm by a microplate reader (Molecular Devices, USA).

Crystal Violet Assay

After removing the supernatants, the cells were washed twice and stained by 50 μL/well crystal violet solution for 15 min. Each well was rinsed with running water and dried. Crystal violet (100 μL) solution was added to each well, and the plates were shaken for 5 min. The absorbance was measured at 540 nm and 630 nm by a microplate reader (molecular Devices, USA).

Microplate Detection Analysis

The HepG2 cells in the logarithmic growth phase were adjusted to 1.5×10^5 cells/ml and inoculated in 6-well plates. After adhering for 24 h, 0.3 mM free fatty acid was added for modeling, and the same amount was added to the control group. DMEM was added to 2′-HC at a final concentration of 10, 20, and 40 μM, and the supernatant and the cells were collected after 24 h of culture. After the treatments, the triglyceride (TG) content, lactate dehydrogenase (LDH) activity, adenine nucleotide triphosphate (ATP) content, malondialdehyde (MDA) activity and nicotinamide adenine dinucleotide (NADH) activity were estimated according to the kit instructions (Jiancheng, Nanjing, China).

Estimation of Lipid Accumulation Within Cells

Oil red O staining is commonly used to stain lipids and demonstrate hepatic steatosis. The cells were cultured with FFA along with various concentrations of 2′-HC overnight. The cells were then fixed with 10% neutral formaldehyde for 1 h, and stained with oil red O for 20 min followed by hematoxylin for 3 min. After washing with PBS, the cellular morphology and lipid accumulation were observed under the microscope (Advanced Microscopy Group, USA).

Detection of Intracellular ROS Detection

Dichlorodihydrofluorescein diacetate(DCFH-DA) probe and MitoSOX™ Red Mitochondrial Superoxide Indicator were used to detect the total and mitochondria-derived ROS. The cells were seeded in 6-well plates with various concentrations of 2′-HC and FFA and washed once with PBS. The cells were incubated with either DCFH-DA probe (10 μM, Dalian Meilun Biological

Technology Co, Ltd. China) or MitoSOX™ reagent (5 μM, Thermo Fisher Scientific, USA) and Hoechst 33342 (0.5 μg/mL, Invitrogen, USA) at 37°C for 30 min. After the staining, the excess dye was washed away and the analysis was carried out using Image Xpress Micro 4 (Molecular Devices, USA).

Flow Cytometry Analysis

Apoptosis and mitochondrial membrane potential changes were analyzed by flow cytometry. The cells were collected by trypsinization (250 g, 4°C, and 5 min) and washed twice with cold PBS. Apoptosis analysis was performed using the BD FACSCalibur™ flow cytometer (BD Biosciences, USA) according to the instructions of FITC Annexin V Apoptosis Detection Kit I (BD Biosciences, USA). The experimental procedure for the detection of membrane potential was the same as that of detecting apoptosis and the cells were stained with JC-10 (Dalian Meilun Biological Technology Co, Ltd. China). The results were analyzed by FlowJo software.

Cellular Oxygen Consumption Rate (OCR) and Extracellular Acidification Rate (ECAR) Assay

The cellular respiratory function promoted by 2′-HC was measured using an XF96 Extracellular Flux analyzer (Seahorse Bioscience, North Billerica, MA). After the cells were treated with FFA (0.3 mM) and 2′-HC with different concentrations overnight, the medium was discarded, replaced with a dedicated medium for detection, and incubated for 1 h at 37°C in a carbon dioxide-free environment. The OCR and ECAR assays were performed in real-time by injecting oligomycin (0.5 μM), carbonyl cyanide-4 (trifluoromethoxy) phenylhydrazone (FCCP, 0.5 μM), and rotenone + antimycin A (0.5 μM) at indicated time points according to the instructions of XF Cell Mito Stress Test Kit (Seahorse Bioscience, USA).

Real-Time Quantitative Reverse Transcription Polymerase Chain Reaction (Rt-Pcr)

Real-time quantitative RT-PCR was used to determine the relative expression of mRNAs. According to the manufacturer's instruction, the total RNA was isolated from the cells using RNAiso Plus (Takara, Japan), and cDNA was synthesized using PrimeScript™ RT Master Mix (Takara, Japan) by Biometra Tone Cycler (Analytixjena, German). Real-time quantitative PCR was performed using TB Green™ *Premix Ex Taq*™ (Takara, Japan) and the 7500 fast Real-Time PCR Systems (Applied Biosystems, USA). The primer sequences were obtained from Invitrogen (Shanghai, China) and listed in **Table 1**. The gene expression was normalized by β-actin.

Western Blotting Analysis

The hepatocytes were lysed with ice-cold RIPA buffer and the protein extraction was immunoblotted to analyze the protein expression. The protein lysates were separated by SDS-PAGE

TABLE 1 | Primer sequence.

Primer name	Primer sequence (5′-3′)
β-actin	F: CATGTACGTTGCTATCCAGGC
	R: CTCCTTAATGTCACGCACGAT
CYCs	R: TTATTGGCGGCTGTGTAAGAG
IL-8	R: AACCCTCTGCACCCAGTTTTC
IL-6	R: CCATCTTTGGAAGGTTCAGGTTG
TNF-α	R: CGGGCCGATTGATCTCAGC
IL-Iβ	R: TTTTTGCTGTGAGTCCCGGAG
BAX	R: CCAGCCCATGATGGTTCTGAT
BCL-2	R: CGGTTCAGGTACTCAGTCATCC
Caspase-3	R: CTACAACGATCCCCTCTGAAAAA
Caspase-9	R: GCATTTCCCCTCAAACTCTCAA
Caspase-7	R: CGGCATTTGTATGGTCCTCTT
Caspase-6	R: AGGAGGAGCCATATTTTCCCA

and transferred onto polyvinylidene fluoride membranes (Merck Millipore Co, Ltd. USA). Immunoblotting was performed according to the standard procedures with the following primary antibodies: β-actin (4,970, 1:1,000), BAX (5,023, 1:1,000), BCL-2 (2,870, 1:1,000), Caspase-3 (9,665,1:1,000), SOD2 (13,141,1:1,000), and Cytochrome C (11,940, 1:1,000) antibodies [Cell Signaling Technology (Beverly, MA, USA)], antibodies for SOD1 (ab13,498,1:5,000) and Caspase-9 (ab219590, 1:1,000) [obtained from Abcam (Cambridge, MA, USA)], and goat anti-rabbit IgG (H + L) HRP (BS13278, 1:5,000) [obtained from Bioworld Technology (St. Paul, MN, USA)]. The membranes were exposed and visualized using the ECL immobilon western chemiluminescent HRP substrate (WBKLS0500, Millipore, USA). Quantitative analysis was performed using Quantity One software (Bio-Rad Laboratories).

Statistical Analyses

The results are expressed as the mean ± SD. The data were compared using one-way ANOVA followed by Tukey's test. GraphPad Prism 6.0 was used for the statistical analyses. A p-value of < 0.05 indicated statistical significance.

RESULTS

Lipid-Loaded Hepatocytes Were More Sensitive to 2′-HC and Its Derivatives

Hepatic steatosis was characterized by the accumulation of lipids within the hepatocytes and is thought to be in a reversible stage. FFA is commonly used to induce steatosis *in vitro*. As
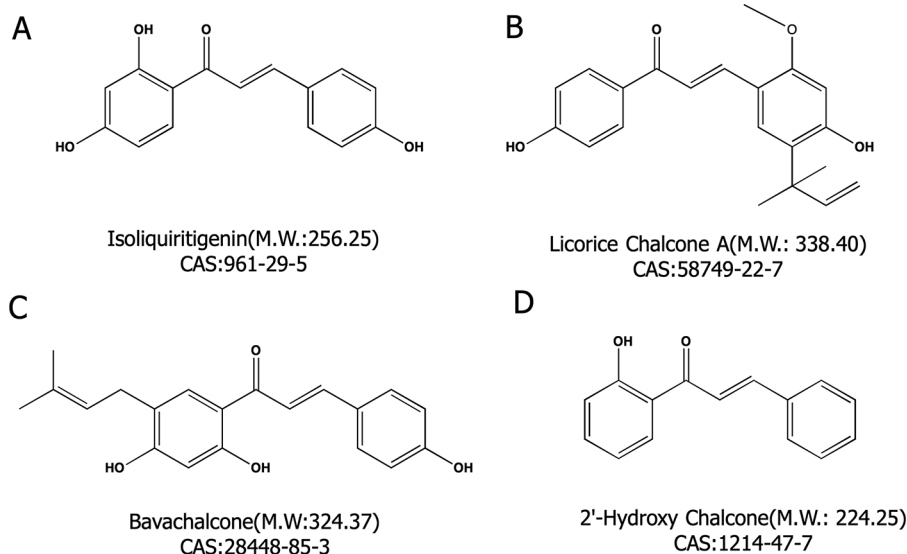
FIGURE 1 | Four chalcone compounds. (A) Isoliquiritigenin (2′,4′,4-trihydroxychalcone; ISL) is a flavonoid found in licorice. (B) Licochalcone A (LCA) is a characteristic chalcone that is found in licorice. (C) Bavachalcone (BC) is a substance with a 2′-HC core structure. (D) 2′-HC is the monomeric compound discussed in this paper.

shown in **Figure 2A**, low concentrations (0.1-0.4 mM) of FFA had no significantly effects on cell viability. Morphologically, lipid droplets could be found within the HepG2 cells when cultured with 0.3 mM of FFA (**Figure 2B**). The toxicity of chalcones, including LSL, LCA, BC, and 2′-HC, was evaluated

in the HepG2 cells cultured with and without FFA. The chalcones had no or limited effects on the viability of HepG2 cells cultured in the common medium. When the HepG2 cells were treated with FFA, chalcones could reduce the IC_{50} value (**Figure 2C**). Of the four chalcone compounds, the IC_{50} value
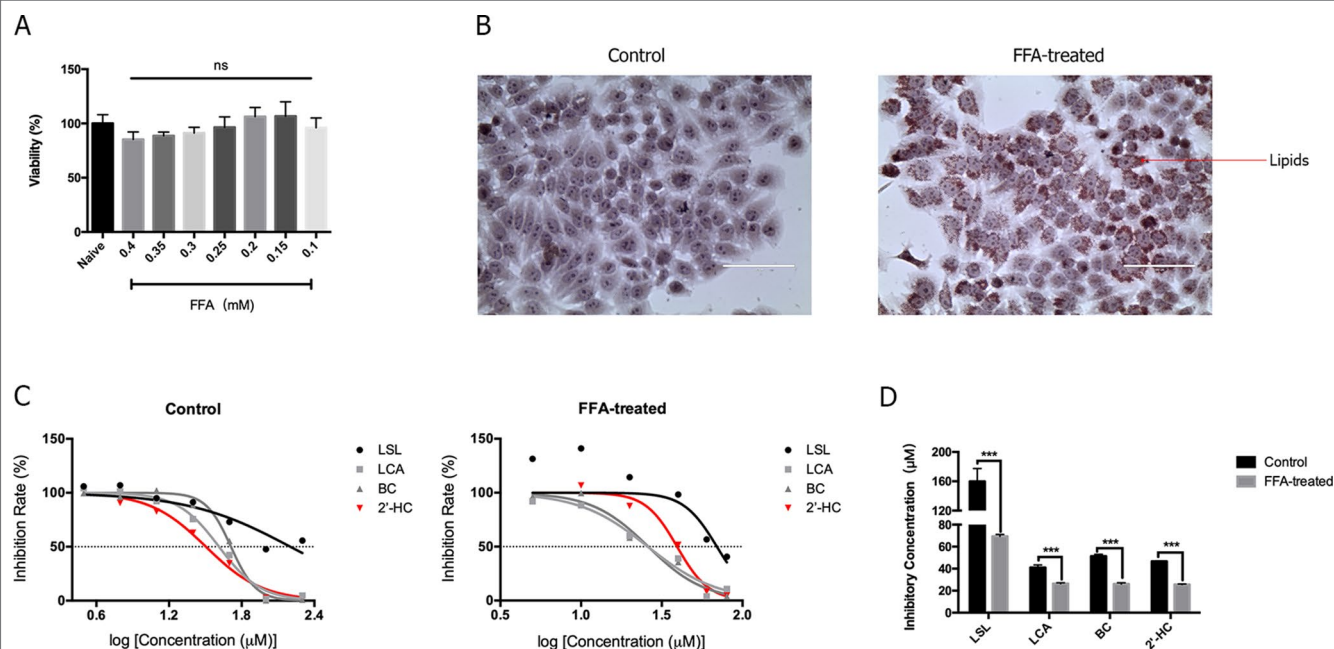
FIGURE 2 | The lipid-loaded hepatocytes were more sensitive following treatment with 2′-HC and its derivatives. (A) Effects of different concentrations of FFA on cell viability. (B) Effects of FFA (0.3mM) on lipid droplet formation by Oil Red O staining. (C) Effects of different chalcone compounds on cell viability. (D) IC_{50} of the chalcone compounds. The data are shown as the mean ± SD, ***$p < 0.001$. ns, no statistical difference.

was significantly reduced in HepG2 cells co-cultured with FFA in comparison to common the medium culture (**Figure 2D**). It is worth noting that 2′-HC is the parental structure and an intermediate metabolite of other chalcone compounds, and hence, we selected 2′-HC as the representative compound for the following experiment.

2′-HC Induced Cytotoxicity in the Lipid-Loaded Hepatocytes

As shown in **Figure 3A**, the HepG2 cells were treated with FFA and the effects of different concentrations of 2′-HC were assessed. The rate of inhibition of 2′-HC was increased with an increased FFA concentration. As previously indicated, 0.3 mM of FFA was a proper concentration to induce lipid accumulation within the HeG2 cells. Under this condition, the cell viability was significantly inhibited with 2′-HC (20 μM, 40 μM, and 60 μM) treatment (**Figure 3B**). The effect was further validated during LDH detection (**Figure 3C**), and both 20 μM and 40 μM 2′-HC increased the LDH level in the lipid-loaded cells, indicating potential cell damage. We compared MTT and crystal violet assays in evaluating cell viability, and confirmed the toxicity of 2′-HC and its concentrations (**Figure 3D**).

2′-HC Promoted Cell Respiration in the Lipid-Loaded Hepatocytes

Since cell viability is closely associated with cellular respiratory function, we studied the effect of 2′-HC on the cellular respiratory function. Seahorse XF analyzer was used to detect OCR (an indicator of monitoring oxidative respiration) and ECAR (an indicator of monitoring glycolysis). As shown in **Figure 4A**, the respiratory function of the FFA-treated cells did not change significantly as compared to that of the negative control cells cultured without FFA. 2′-HC increased OCR and ECAR of the cells, indicating that 2′-HC can promote respiratory function in the FFA-treated cells. As a metabolic substrate of the cellular respiratory chain, FFA significantly increased ATP production, which can be further promoted by 2′-HC treatment in the FFA-treated cells (**Figure 4B**). NADH dehydrogenase is closely associated with the mitochondrial function and oxidative stress. However, the NADH value did not change upon 2′-HC treatment (**Figure 4C**). The mitochondrial membrane potential is a prerequisite for the production of ATP, which can adequately reflect the activity of the entire mitochondrial function. Thus, changes in mitochondrial membrane potential in cells

FIGURE 3 | 2′-HC exacerbated damage in the lipid-loaded hepatocytes. **(A)** Inhibitory effects of different concentrations of 2′-HC treated with FFA. **(B)** Effects of different concentrations of 2′-HC on cell viability. **(C)** Effects of different concentrations of 2′-HC on the LDH level. **(D)** Different methods for detecting cell viability. The data are shown as the mean ± SD, *$p < 0.05$, **$p < 0.01$, ***$p < 0.001$.

FIGURE 4 | 2′-HC promoted cell respiration within the lipid-loaded hepatocytes. **(A)** Effects of different concentrations of 2′-HC on cell oxygen consumption and extracellular acidification rate. **(B)** Effects of different concentrations of 2′-HC on ATP production. **(C)** Effects of different concentrations of 2′-HC on NADH. **(D)** Effects of different concentrations of 2′-HC on mitochondrial membrane potential. The data are shown as the mean ± SD, *$p < 0.05$, **$p < 0.01$, ***$p < 0.001$.

were detected, which also suggests the enhancing effects of 2′-HC on the cellular respiratory function (**Figure 4D**). FFA increased the mitochondrial membrane potential in the cells while 2′-HC showed a dose-dependent effects on the FFA-treated cells. These results indicate that 2′-HC may promote cellular respiratory metabolisms, such as oxygen consumption in aerobic respiration and stimulate the release of H+ during glycolysis.

2′-HC Promoted Oxidative Stress in the Lipid-Loaded Hepatocytes

The production of ROS may increase when the cellular respiratory function and energy metabolism increases. The oxidative stress response is further induced when there is an imbalance between the production and elimination of ROS. The total ROS in the cells was detected by specific fluorescent markers, and high-content analysis revealed that 2′-HC (20 μM and 40 μM) significantly increased the relative fluorescence intensity of ROS in the FFA-treated cells (**Figure 5A**). Through MitoSOX™ assay, we also found that 2′-HC dose-dependently increased mitochondrial-specific ROS production (**Figure 5B**). MDA is one of the most important products of membrane lipid peroxidation, and an indicator of cell damage. We noticed that 2′-HC (10 μM and 20 μM) increased the MDA level in the FFA treated hepatocytes (**Figure 5C**). SOD is an important antioxidant enzyme. By detecting the relevant protein expression, we found that 2′-HC reduced the SOD1 and SOD2 expression in the FFA-treated

HepG2 cells, especially at a concentration of 40 μM (**Figure 5D**). The above data showed that 2′-HC deranged the oxidant and anti-oxidant balance.

2′-HC Caused Apoptosis of the Lipid-Loaded Hepatocytes

Abnormal cell metabolism leads to ROS production and resulting in the changes in apoptosis-related gene targets and activation of apoptosis programs. Therefore, flow cytometry was used to detect the effects of different concentrations of 2′-HC on apoptosis of the FFA-treated cells (**Figure 6A**). The proportion of apoptosis of the FFA-treated cells was higher as compared to the control, and the apoptosis rate was directly proportional to the concentration of 2′-HC. To assess the effect of 2′-HC on apoptotic pathways, several relevant mRNA levels were investigated. Cytochrome C (CYC) is an important carrier of neutrons in the mitochondrial respiratory chain. When CYC is released from the mitochondria into the cytosol, the caspase family and other pathways can be triggered to induce apoptosis. As shown in **Figure 6B**, 20 μM of 2′-HC significantly increased the mRNA expression of the total CYC in the FFA-treated HepG2 cells. 2′-HC significantly increased the mRNA expression of BAX and BCL-2 in the FFA-treated HepG2 cells. In addition, The BAX/BCL-2 expression ratio increased as the drug concentration was reduced (**Figure 6C**). As shown in **Figure 6D**, 20 μM and 40 μM of 2′-HC increased the mRNA expression of Caspase-7 and Caspase-9 in the FFA-treated HepG2 cells. Moreover, the protein expression of
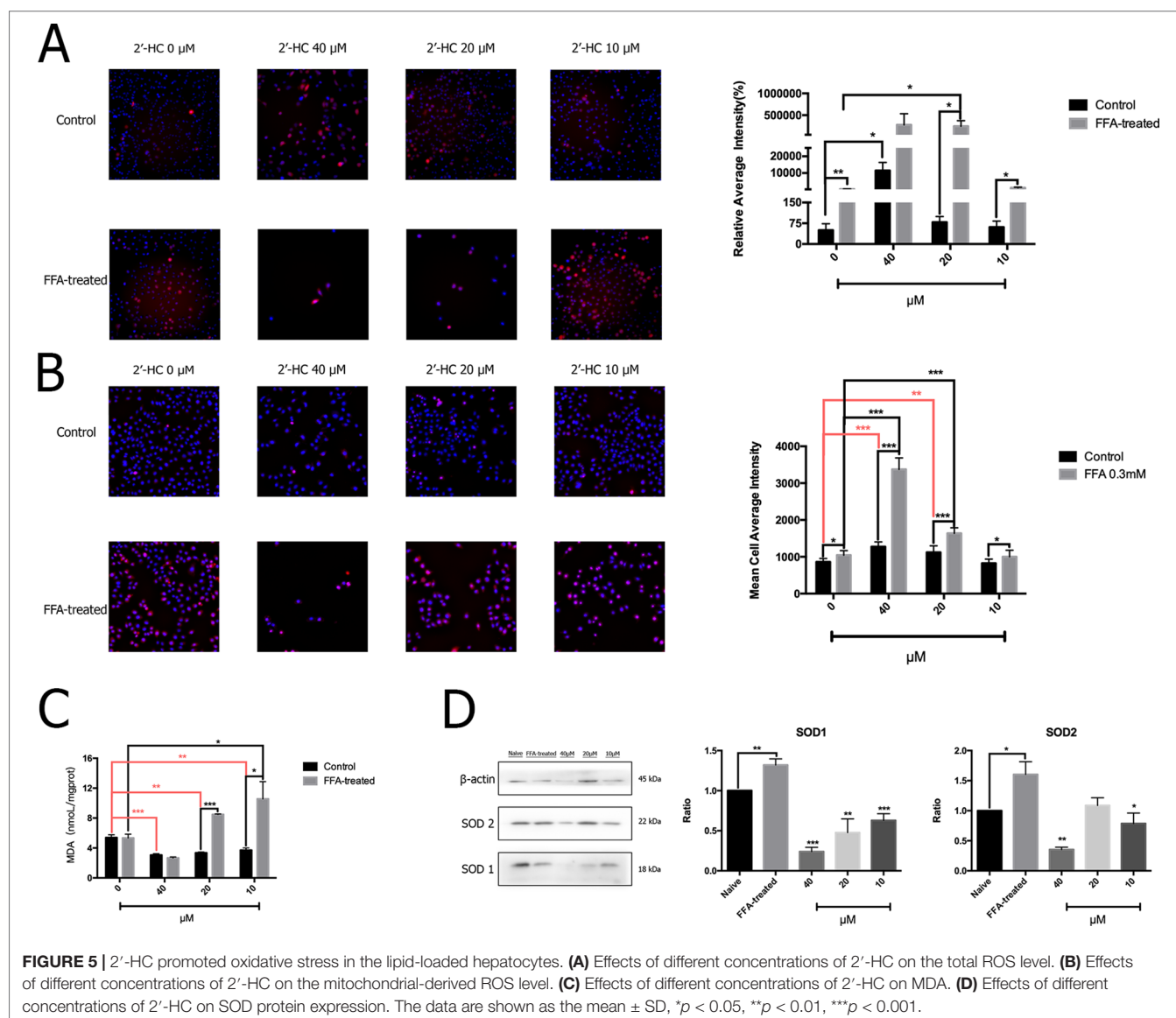
FIGURE 5 | 2′-HC promoted oxidative stress in the lipid-loaded hepatocytes. **(A)** Effects of different concentrations of 2′-HC on the total ROS level. **(B)** Effects of different concentrations of 2′-HC on the mitochondrial-derived ROS level. **(C)** Effects of different concentrations of 2′-HC on MDA. **(D)** Effects of different concentrations of 2′-HC on SOD protein expression. The data are shown as the mean ± SD, *$p < 0.05$, **$p < 0.01$, ***$p < 0.001$.

Caspase-9 upon 2′-HC treatment was increased (**Figure 6E**), confirming the role of 2′-HC in regulating apoptosis of the lipid-loaded hepatocytes.

2′-HC Aggravated Inflammation and Lipid Stress in the Lipid-Loaded Hepatocytes

Oxidative stress is a key inducer of inflammation. Therefore, the expression of the relevant inflammatory cytokines transcription was evaluated. After co-culturing with 2′-HC, the mRNA expression of IL-1β, TNF-α, IL-6, and IL-8 significantly increased in the FFA treated HepG2 cells in comparison to those cultured in the common medium (**Figure 7A**). Besides, 2′-HC promoted lipid accumulation in the FFA-treated hepatocytes. As shown in **Figure 7B**, 2′-HC at concentrations of 20 and 40 μM increased TG in the FFA-treated cells. Oil red O staining also showed an obviously increased in the lipid

droplets in the 2′-HC treated cells as compared to the controls (**Figure 7C**).

DISCUSSION

Drugs are an important cause of hepatotoxicity. A multi-center retrospective survey of the European and Brazilian poison center revealed that licorice was one of the most ten frequently reported plants causing adverse effects (LüDe et al., 2016). In the present study, we found that chalcone, the main ingredient of licorice, was toxic to the lipid-loaded hepatocytes, and the toxicity might be related to the active cell respiration and oxidative stress, leading to cellular apoptosis and inflammation.

We found that chalcone compounds (LSL, LCA, BC, and 2′-HC) in licorice dose-dependently reduced the viability

FIGURE 6 | 2′-HC caused apoptosis of lipid-loaded hepatocytes. **(A)** Effects of different concentrations of 2′-HC on apoptosis by flow cytometry. **(B)** Effects of different concentrations of 2′-HC on the total Cytochrome C mRNA expression. **(C)** Effects of different concentrations of 2′-HC on BAX and BCL-2 mRNA expression. **(D)** Effects of different concentrations of 2′-HC on mRNA expression of Caspase-3, 6, 7, and 9. **(E)** Effects of different concentrations of 2′-HC on total Cytochrome C, BAX, BCL-2, Caspase-3 and 9 protein expression. The data are shown as the mean ± SD, $*p < 0.05$, $**p < 0.01$, $***p < 0.001$.

of the cells and increased the level of LDH released from the lipid-loaded hepatocytes, suggesting the hepatoxic potential of the compounds. Studies have demonstrated that the mechanisms of hepatoxicity are various, including the

formation of enzyme-drug adducts that may cause immune response and damage to the cells (Beaune et al., 1987; Robin et al., 1997), inhibition of hepatic drug transformation and metabolism (Honig et al., 1992; Yun et al., 1993), prevention

FIGURE 7 | 2′-HC aggravated inflammation and lipid stress in the lipid-loaded hepatocytes. **(A)** Effects of different concentrations of 2′-HC on the cytokines. **(B)** Effects of different concentrations of 2′-HC on TG. **(C)** Effects of different concentrations of 2′-HC on lipid droplet formation by Oil Red O staining. The data are shown as the mean ± SD, *$p < 0.05$, **$p < 0.01$, ***$p < 0.001$. ns, no statistical difference.

of bilirubin secretion, etc. Dysfunctions of the mitochondria and apoptosis are also frequently reported mechanisms responsible for drug-induced hepatoxicity (Pessayre et al., 2001). Here we observed that 2′-HC significantly promoted OCR and EACR in the lipid-loaded hepatocytes, suggesting that the respiration of the cells was active upon 2′-HC treatment. The liver is the main organ metabolizing drugs, and the transformational and metabolic process requires a large amount of energy (Almazroo et al., 2017). Consistent with active respiration, the ATP production was also increased in the lipid-loaded HepG2 cells treated with 2′-HC. However, we are uncertain whether the number of mitochondria plays a role in this process.

ROS are derived from the metabolism of oxygen as by-products of cellular respiration (Imen Belhadj et al., 2014). Physiologically, anti-oxidants, such as SOD could combat the oxidative agent to maintain the dynamic balance. Once the balance is destroyed, excess ROS might cause damage to the cells (Lobo et al., 2010). It is reported that the cytotoxicity of acetaminophen and ethanol was associated with ROS overproduction and mitochondrial Hsp70, which might be mediated through CYP2E1 (Laetitia et al., 2011). Non-steroidal anti-inflammatiory drugs (NSAIDs), especially diclofenac, are often found to induce cytotoxicity to multiple organs. The dysfunction of the mitochondria and the increased production of ROS are the main causes of the hepatoxicity (Han et al., 2019). In our study, both total mitochondrial ROS and MDA were increased in the lipid-loaded HepG2 cells treated with 2′-HC, while the expression of SOD1 was decreased, indicating the imbalance between the two systems along with possible oxidative stress due to 2′-HC treatment.

ROS, especially mitochondrial ROS, is actively involved in regulating immune response and inflammasome activation. It is revealed that mitochondrial ROS can directly activate NACHT, LRR, and PYD domain-containing protein 3 (NLRP3) inflammasome; promote caspase 1 activation and maturation; and subsequently lead to the release of the proinflammatory mediators, such IL-1β (Fumitake et al., 2015). Our results indicate that 2′-HC promoted ROS production and stimulated the release of inflammatory factors, such as TNF-α, IL-6, IL-1β, and IL-8. These data suggest that 2′-HC had toxic effects on the FFA-treated HepG2 cell model which is associated with the inflammation.

Licorice is widely used as the most commonly traditional Chinese medicine, and many health products contain licorice or its ingredients. A report of the European Union indicates a series of symptoms, such as hypertension, muscle weakness, and headache which may appear upon licorice overdose. The herb is also being used in TCM prescriptions for treating various diseases, including NAFLD. Chalcone compound is a major component of the active components of licorice, and has a potential risk of causing cell damage and lipid accumulation within the hepatocytes. Therefore, the licorice should to be cautiously used in the clinics, and the dosage needs to be comprehensively considered. Our data provided a preliminary idea of the safety profile of licorice for the suitable medical use in the future.

In summary, the present study evaluated the toxicological effects of the bioactive components of licorice, and focused on the toxic effects of 2′-HC on the lipid-loaded HepG2 cells. We demonstrated that 2′-HC promoted cellular respiration, ROS production, oxidative stress, inflammation and apoptosis. However, our experiments were limited to *in vitro* cells.

The hepatotoxicity of licorice *in vivo* may also be affected by the interactions of various compounds, absorption and metabolism of the compound, tissue distribution, physiological and pathological states, etc. (Luís et al., 2018). Concurrent administration of licorice with NSAIDs, insulin, aspirin, etc. should be paid special attention. Notably, future studies are necessary to further evaluate the adverse effects of licorice, especially in the presence of pathological conditons.

DATA AVAILABILITY STATEMENT

The raw data supporting the conclusions of this manuscript will be made available by the authors, without undue reservation, to any qualified researcher.

AUTHOR CONTRIBUTIONS

FL and GJ designed experiments. YQ, YY, and KW performed the experiment. WZ and YD analyzed data. YQ and MZ drafted the manuscript along with the figures and tables.

REFERENCES

Alagawany, M., Elnesr, S. S., Farag, M. R, Abd El-Hack, M. E., Khafaga, A. F., Taha, A. E., et al. (2019). Use of Licorice (Glycyrrhiza glabra) Herb as a Feed Additive in Poultry: Current Knowledge and Prospects. *Anim.* 9 (8), 536. doi: 10.3390/ani9080536

Almazroo, O. A., Mohammad, K. M., and Raman, V. (2017). Drug Metabolism in the Liver. *Clinics In Liver Dis.* 21 (1), 1–20. doi: 10.1016/j.cld.2016.08.001

Beaune, P., Dansette, P. M., Mansuy, D., Kiffel, L., Finck, M., Amar, C., et al. (1987). Human anti-endoplasmic reticulum autoantibodies appearing in a drug-induced hepatitis are directed against a human liver cytochrome P-450 that hydroxylates the drug. *Proc. of the Natl. Acad. of Sci. U. S. A.* 84 (2), 551–555. doi: 10.1073/pnas.84.2.551

Cheng, F., Ma, C., Wang, X., Zhai, C., Wang, G., Xu, X., et al. (2017). Effect of traditional Chinese medicine formula Sinisan on chronic restraint stress-induced nonalcoholic fatty liver disease: a rat study. *BMC Complement. Altern. Med.* 17 (1), 203. doi: 10.1186/s12906-017-1707-2

Dang, Y., Hao, S., Zhou, W., Zhang, L., and Ji, G. (2019). The traditional Chinese formulae Ling-gui-zhu-gan decoction alleviated non-alcoholic fatty liver disease via inhibiting PPP1R3C mediated molecules. *BMC Complement. Altern. Med.* 19 (1), 8. doi: 10.1186/s12906-018-2424-1

Fumitake, U., Koumei, S., Hiroaki, K., Kazuki, T., Akira, K., Tadayoshi, K., et al. (2015). Inflammasome activation by mitochondrial oxidative stress in macrophages leads to the development of angiotensin II-induced aortic aneurysm. *Arterioscler. Thromb. & Vasc. Biol.* 35 (1), 127. doi: 10.1161/ATVBAHA.114.303763

Han, W., Ding, M., Liu, S., Chen, Y., and Duan, Z., (2019). Evaluation of 3D re-cellularized tissue engineering: a drug-induced hepatotoxicity model for hepatoprotectant research. *Toxicol. Mech. Methods.* 29 (9), 654–664. doi: 10.1080/15376516.2019.1646371

Honig, PK., Woosley, R. L., Zamani, K., Conner, D. P., and Cantilena, L. R. (1992). Changes in the pharmacokinetics and electrocardiographic pharmacodynamics of terfenadine with concomitant administration of erythromycin. *Clin. Pharmacol. Ther.* 52 (3), 231. doi: 10.1038/clpt.1992.135

Imen Belhadj, S., Taha, N., Abdeljelil, G,. Hajer, D., Moncef, B. M., and Manef, A. (2014). Reactive oxygen species, heat stress and oxidative-induced mitochondrial damage. A review. *Int. J. Hyperthermia Off. J. Eur. Soc. for Hyperthermic Oncol. North Am. Hyperthermia Group* 30 (7), 513. doi: 10.3109/02656736.2014.971446

Jeong, H. G., You, H. J., Park, S. J., Moon, A. R., Chung, Y. C., Kang, S. K., et al. (2002). Hepatoprotective effects of 18beta-glycyrrhetinic acid on carbon tetrachloride-induced liver injury: inhibition of cytochrome P450 2E1 expression. *Pharmacol. Res.* 46 (3), 221–227. doi: 10.1016/s1043-6618(02)00121-4

Ji, S., et al. (2016). Bioactive constituents of glycyrrhiza uralensis (Licorice): discovery of the effective components of a traditional herbal medicine. *J. Natural Prod.* 79 (2), 281. doi: 10.1021/acs.jnatprod.5b00877

Laetitia, K., Véronique, D., Nathalie, V., Bernard, F.,and Marie-Anne, R. (2011). Mitochondrial CYP2E1 is sufficient to mediate oxidative stress and cytotoxicity induced by ethanol and acetaminophen. *Toxicol. In Vitro An Int. J. Published in Assoc. Bibra* 25 (2), 475–484. doi: 10.1016/j.tiv.2010.11.019

Li, J. Y., Cao, H. Y., Liu, P., Cheng, G. H., and Sun, M. Y. (2014). Glycyrrhizic acid in the treatment of liver diseases: literature review. *Biomed. Res. Int.* 2014, 872139. doi: 10.1155/2014/872139

Li, X., Sun, R., and Liu, R. (2019). Natural products in Licorice for the therapy of liver diseases: Progress and future opportunities. *Pharmacol. Res.* 144, 210–226. doi: 10.1016/j.phrs.2019.04.025

Lobo, V., Patil, A., Phatak, A., and Chandra, N. (2010). Free radicals, antioxidants and functional foods: Impact on human health. *Pharmacogn. Rev.* 4 (8), 118–126. doi: 10.4103/0973-7847.70902

LüDe, S., Vecchio, S., Sinno-Tellier, S., Dopter, A., Mustonen, H., Vucinic, S., et al. (2016). Adverse Effects of Plant Food Supplements and Plants Consumed as Food: Results from the Poisons Centres-Based PlantLIBRA Study. *Phytotherapy Research* 30 (6), 988–996. doi: 10.1002/ptr.5604

Luís, Â, Fernanda, D., and Luísa, P. (2018). Metabolic changes after licorice consumption: a systematic review with meta-analysis and trial sequential analysis of clinical trials. *Phytomed.* 39, 17–24. doi: 10.1016/j.phymed.2017.12.010

Michielsen, C. C. J. R., Almanza-Aguilera, E., Brouwer-Brolsma, E. M., Urpi-Sarda, M., and Afman, L. A., (2018). Biomarkers of food intake for cocoa and liquorice (products): a systematic review. *Genes Nutr.* 13 (1), 22. doi: 10.1186/s12263-018-0610-x

Moro, T., Shimoyama, Y., Kushida, M., Hong, Y. Y., Nakao, S., Higashiyama, R., et al. (2008). Glycyrrhizin and its metabolite inhibit Smad3-mediated type I collagen gene transcription and suppress experimental murine liver fibrosis. *Life Sci.* 83 (15-16), 531–539. doi: 10.1016/j.lfs.2008.07.023

Pessayre, D., Berson, A., Fromenty, B., and Mansouri, A. (2001). Mitochondria in steatohepatitis. *Semin. Liver Dis.* 21 (1), 57–69. doi: 10.1055/s-2001-12929.

Robin, M. A., Roy, M. L., Descatoire, V., and Pessayre, D. (1997). Plasma membrane cytochromes P450 as neoantigens and autoimmune targets in drug-induced hepatitis. *J. Hepatol.* 26 Suppl 1, 23–30. doi: 10.1016/s0168-8278(97)82329-x

Substances, Federation of American Societies for Experimental Biology. Life Sciences Research Office. Select Committee on GRAS, United States. Food, and Drug Administration. Bureau of Foods 1974 Evaluation of the health aspects of licorice, glycyrrhiza and ammoniated glycyrrhizin as food ingredients: Life Sciences Research Office, Federation of American Societies of Experimental Biology.

Yan, T., Wang, H., Cao, L., Wang, Q., Takahashi, S., Yagai, T., et al. (2018). Glycyrrhizin Alleviates Nonalcoholic Steatohepatitis via Modulating Bile Acids and Meta-Inflammation. *Drug Metab. Dispos.* 46 (9), 1310–1319. doi: 10.1124/dmd.118.082008

Yang, R., Wang, L. Q., Yuan, B. C., and Liu, Y. (2015). The Pharmacological Activities of Licorice. *Planta Med.* 81 (18), 1654–1669. doi: 10.1055/s-0035-1557893

Yun, C. H., Okerholm, R. A., and Guengerich, F. P. (1993). Oxidation of the antihistaminic drug terfenadine in human liver microsomes. Role of

cytochrome P-450 3A(4) in N-dealkylation and C-hydroxylation. *Drug Metab. Dispos.* 21, 403-409. doi: 10.1002/app.1965.070090112

Conflict of Interest: The authors declare that the research was conducted in the absence of any commercial or financial relationships that could be construed as a potential conflict of interest.

Xiaozhang Tie Improves Intestinal Motility in Rats With Cirrhotic Ascites by Regulating the Stem Cell Factor/ c-kit Pathway in Interstitial Cells of Cajal

Qiang Zhao[1†‡], Feng Xing[1†], Yanyan Tao[1], Hongliang Liu[1], Kai Huang[2], Yuan Peng[1], Nianping Feng[3*] and Chenghai Liu[1,2,4,5*]

[1] Institute of Liver Diseases, Shuguang Hospital Affiliated to Shanghai University of Traditional Chinese Medicine, Shanghai, China, [2] Shanghai Key Laboratory of Traditional Chinese Clinical Medicine, Shanghai, China, [3] Department of Pharmaceutical Sciences, School of Pharmacy, Shanghai University of Traditional Chinese Medicine, Shanghai, China, [4] Key Laboratory of Liver and Kidney Diseases, Ministry of Education, Shanghai, China, [5] Shanghai Innovation Center of TCM Health Service, Shanghai, China

We previously discovered that Xiaozhang Tie (XZT) was helpful for cirrhotic ascites, with obvious abdominal distention relief, suggesting that it may improve gastrointestinal (GI) motility. However, the underlying mechanisms of GI motility in cirrhotic ascites are unclear. Here, we aimed to discover explored the effect of XZT on GI motility in animal cirrhotic ascites and probed the action mechanism affecting GI motility by regulating the stem cell factor (SCF)/c-kit pathway in interstitial cells of Cajal (ICCs) and GI hormones. First, rat models of cirrhotic ascites were developed and then divided randomly into the following three subgroups: model control, XZT group, and mosapride group. The efficacy of XZT on treating cirrhotic ascites was evaluated on the basis of ascites weight and volume, 24 h urine volume, and feces water content. GI motility of the cirrhotic model, intestine propulsion, and gastric residue were detected using the migration distance of ink *in vivo*, and the frequency of contraction and tension of isolated gastric and jejunal muscle strips were measured after incubation with XZT extracts. Serum GI hormone content, including motilin (MTL), substance P (SP), somatostatin (SS), and vasoactive intestinal polypeptide were assayed. Subsequently, ICCs were isolated from jejunum, and primarily cultured ICCs were incubated with and without XZT and SCF. The cell vitality of the ICCs was measured. A whole-cell patch recording technique was used to record the current of K^+ and Na^+ channels in the ICC membrane. Expressions of c-kit/p-c-kit, p-Akt, p-STAT3, and p-Erk1/2 were detected *in vivo* and *in vitro*. The results revealed that XZT significantly reduced ascites weight and increased urine volume and fecal water content in model rats. XZT promoted intestinal motility and increased MTL level but reduced SP and SS levels. It enhanced the current of Na^+ and K^+ in ICCs and improved c-kit expression and signaling mediator phosphorylation in SCF/c-kit, which was inhibited by imatinib *in vitro* and downregulated in model rats *in vivo*. Our study concluded that XZT reduced the

amount of ascites and improved intestinal motility in cirrhotic rats, which may be associated with its effect on ascites and was involved in the mechanisms regulating the SCF/c-kit signaling pathway in ICCs and improving gastrointestinal hormone secretion.

Keywords: Xiaozhang Tie (XZT), cirrhotic ascites, intestinal motility, interstitial cells of Cajal, stem cell factor (SCF)/c-kit.

INTRODUCTION

Ascites is the most common clinical manifestation of cirrhosis (Runyon and Committee, 2009) and is an indicator that cirrhosis has developed from the compensation stage to the decompensation stage. It not only affects the quality of life of patients but is also closely related to other complications of cirrhosis, such as endotoxemia, spontaneous bacterial peritonitis, hepatorenal syndrome, and gastrointestinal dysfunction. Over half of compensated cirrhosis cases develop ascites within 10 years, with 1- and 5-year mortality rates of approximately 15% and 50%, respectively, for patients with cirrhotic ascites (Planas et al., 2006; Hsu and Huang, 2013). Thus, methods of managing cirrhotic ascites have great clinical significance.

Two therapeutic strategies for cirrhotic ascites are currently used. One is drug therapy, including diuretics and human serum albumin. Another is invasive therapy, such as peritoneal paracentesis and autoinfusion of concentrated ascites. However, the use of diuretics and large-volume paracentesis are likely to cause electrolyte disturbances and circulatory dysfunction, and are less effective for treating refractory ascites. Thus, a suitable method for the management of cirrhotic ascites, refractory ascites in particular, remains to be identified, and new treatments are required.

In Chinese medicine, external patching therapy for cirrhosis and ascites through application of a patch with drugs such as euphorbia gansui, mirabilite, and euphorbia on the body has a history extending thousands of years. This external patching therapy usually involved mixing drug powder with vinegar and pasting the mixture onto the patient's navel. In our previous work, we designed a new formula named Xiaozhang Tie (XZT), composed of dahuang (*Rheum palmatum L.*), laifuzi (*Raphanus sativus L.*), gansui (*Euphorbia kansui T.N. Liou ex T.P. Wang*), chenxiang [*Aquilaria sinensis (Lour.) Gilg*], dingxiang (*Eugenia caryophyllata Thunb.*), bingpian (*borneolum syntheticum*), and shexiang (*artificial Moschus*), and developed a modern pharmaceutical dose. Our clinical trials indicated that XZT increased urine output and reduced the amount of ascites in patients with cirrhotic ascites without obvious side effects. In particular, after the initial application, it increased exhaust and defecation, improved appetite, and alleviated abdominal distention (Xing et al., 2012), suggesting that it could improve patients' gastrointestinal motility by acting on ascites.

Studies have demonstrated that patients with cirrhotic ascites often have prolonged gastrointestinal transit time and gastrointestinal motility disorders, such as indigestion and flatulence. In addition, bacterial proliferation and translocation may occur in the intestinal tract of patients with cirrhotic ascites as a result of gastrointestinal motility dysfunction and portal hypertension, thereby increasing the amount of ascites and leading to higher susceptibility to other complications such as endotoxemia, spontaneous bacterial peritonitis, and hepatorenal syndrome (Chander Roland et al., 2013). Therefore, the discovery of gastrointestinal motility disorder has key clinical implications for patients with cirrhotic ascites; it can not only improve quality of life by alleviating abdominal distention, constipation, and other symptoms but also reduce the amount of ascites by promoting urinary and fecal excretion (Zhang et al., 2017). The relationship between gastrointestinal motility and cirrhotic ascites is not fully understood, however, and the action mechanism of effective agents on ascites with respect to gastrointestinal motility remains unclear.

In the current study, we attempted to answer the following two questions through *in vivo* and *in vitro* experiments: (1) whether the XZT effect on reducing the amount of cirrhotic ascites is associated with improved gastrointestinal motility and (2) if so, what the action mechanism of XZT is in regulating gastrointestinal motility in cirrhotic ascites.

MATERIALS AND METHODS

Drugs

Mosapride citrate (License No. H19990317) was provided by Lunan-beite Pharmaceutical Co., Ltd. (Shandong, China). Imatinib Mesylate (Art. No. T1621) was purchased from TargetMol (Boston, MA, USA). XZT, and blank poultices were provided by Changshu Leiyunshang Pharmaceutical Co., Ltd. (Jiangsu, China).

Compositional Analysis of XZT

The formula for XZT (one dose): 1.0 g of dahuang, 1.0 g of laifuzi, 1.0 g of gansui, 0.2 g of chenxiang, 1.0 g of dingxiang, 0.04 g of borneolum syntheticum, and 0.004 g of artificial Moschus.

The manufacturing procedures for the XZT and blank poultices were detailed by Xing et al. (2012). XZT was extracted through ultrasonication in an aqueous solution of methanol, and essential oils were obtained using a hydrodistillation method. Subsequently, the XZT extract was characterized using a Waters Acquity Ultra-Performance LC-Synapt G2 Q/TOF system (Waters Corporation, Milford, MA, USA). The composition of XZT extract includes more than 50 ingredients, such as gallic acid, desulfo-glucoraphanin, and glucoraphenin. Additional details regarding the extraction and **Supplementary Methods** were provided by Zhang et al. (2019).

Reagents

In vivo, a cirrhotic rat model complicated with ascites was established with CCl$_4$ (Cat. No. 10006428) and olive oil (Cat. No. 69018028) obtained from Sinopharm Group Co., Ltd. (Shanghai, China). Enzyme-Linked Immunosorbent Assay (ELISA) kits of stem cell factor (SCF) (Art. No. YX-190306R), p-Akt (Art. No. 011120R), p-c-kit (Art. No. 110920R), p-STAT3 (Art. No. YX-012003R), and p-ERK1/2 (Art. No. 181102R) were purchased from Pepro Tech Inc. (Su Zhou, China), and the kits of substance P (SP) (Art. No. 10171), somatostatin (SS) (Art. No. XF-100), motilin (MTL) (Art. No. XF-094), and vasoactive intestinal polypeptide (VIP) (Art. No. XF-10162) were offered and their indexes tested by Shanghai Xinfan Biotechnology Co., Ltd. (Shanghai, China). The rabbit antihuman polyclonal c-kit primary antibody (Art. No. SC-365504) was purchased from CST Inc. (Shanghai, China). The rabbit SABC immune-histochemical kit (Art. No. SA1022) and DAB color development kit (Art. No. AR1022) were purchased from Boster Bio-Engineering Limited Company (Wuhan, China).

In vitro, polyclonal primary antibodies of akt (Art. No. 4691), stat3 (Art. No. 12640), erk1/2 (Art. No. 4695), p-Akt (Art. No. 4060), p-STAT3 (Art. No. 98543), and p-ERK1/2 (Art. No. 9101) were purchased from Abcam (Cambridge, UK) to determine the expression levels of the related proteins in interstitial cells of Cajal (ICCs) through western blotting.

Animals and Experimental Design

In this experiment, 80 male Sprague-Dawley (SD) rats weighing 170±10 g were purchased from Shanghai SLAC Laboratory Co. Ltd. (Shanghai, China). All rats were housed in an animal room under standard conditions, with a temperature of 22°C, humidity of 55%, 12 h light dark cycle, and free access to food and water. The study was carried out in accordance with the Committee on the Care and Use of Live Animals for Teaching and Research of the Shanghai University of Traditional Chinese Medicine, and the procedures were performed according to the guidelines of the committee.

First, 80 male SD rats were randomly divided into two groups, a normal control group (n = 10) and a model group (n = 70). To make rats cirrhotic with ascites, rats were injected intraperitoneally with 20% CCl$_4$ for the first week, 30% CCl$_4$ for the second week, and then 40% CCl$_4$ at a dose of 2 ml·kg^{-1} twice a week until the cirrhotic model was successfully established. The rats in the control group were injected with the same volume of pure olive oil. Eventually, the ascites model of cirrhosis was established successfully in 29 rats, and these rats were randomly divided into three groups as follows: a model group (*n* = 9), an XZT group (*n* = 8), and a mosapride group (*n* = 8). The remaining four mice were used for *in vitro* gastrointestinal electrophysiological testing. The body weight and urine output volume in each group were measured and recorded on a daily basis for treatment assessment. Subsequently, rats in the test group were administered an umbilical compress with XZT at a daily dose of 2.25 cm^2 for 1 week, while those in positive control group were treated with mosapride citrate orally at dose of 2 mg·kg^{-1} for 1 week. On their last day in metabolic

cages, all rats were deprived of food for 12 h, but water was allowed. The feces were collected and measured. The wet feces were dried in an oven at 60°C for 24 h. The fecal water content was calculated using the following calculation formula: [wet weight (g) − dry weight (g)]/wet weight (g) × 100%. After a 7-day intervention and observation period in metabolic cages, all rats were intragastrically administered nutritious semisolid paste containing ink to determine the propulsive rate of the small intestine. After 30 min, the rats were subjected to anesthesia and laparotomy, and serum and liver samples were harvested. The small intestinal tract from the pylorus to the ileocecal valve was removed, and the distance from the pylorus to the front of the ink was measured as the migration distance of the ink. The following formula was used to calculate the ink propulsion rate: ink propulsion rate (%) = migration distance of ink/whole length of the small intestine × 100%.

Immunohistological Analysis of c-kit in Jejunum Sections

A 1 cm segment of jejunum at a distance of 1 cm from the duodenum was taken for immunohistochemical analysis. Jejunum tissues were fixed with 10% formalin, embedded in paraffin, cut into 4 μm sections for staining with rabbit antihuman polyclonal c-kit primary antibody (Art. No. SC-365504), and visualized with the rabbit SABC immunohistochemical kit (Art. No. SA1022) and DAB color development kit (Art. No. AR1022). An Olympus DP71 digital charge-coupled microscope device was used to collect positive images, and Image-Pro Plus 6.0 software was used for semiquantitative analysis of the c-kit positive expression area of jejunum tissue.

Measurements of Gut Hormones in Serum

Serum levels of gut hormones such as MTL, SP, SS, and VIP were detected through radioimmunoassay with commercial kits purchased from Shanghai Xin Fan Biotechnology Co., Ltd. (Shanghai, China).

ELISA

Levels of SCF (Art. No. YX-190306R), p-c-kit (Art. No. 110920R), p-STAT3 (Art. No. YX-012003R), p-Akt (Art. No. 011120R), and p-ERK1/2 (Art. No. 181102R) in serum were detected according to instructions provided by SCIGE Biotechnology Co., Ltd. (Shanghai, China) for using commercial ELISA kits.

Isolation and Identification of ICCs

In this experiment, 10 g of germ-free 3-day-old C57/BL6 neonatal mice were decapitated, and their jejunum was separated and cut into 1 mm^3 sections. The tissue fragments of intestine were washed with phosphate-buffered saline (PBS) and digested with a trypsin–EDTA solution (sterile PBS containing 0.25% trypsin and 0.02% EDTA under pH 8.0) at 37 °C for 1 h. After a series of filtration, centrifugation, and precipitation, the cells were seeded in culture flasks and cultured in an incubator at 37 °C in a 5% CO$_2$ atmosphere. After 24 h, the medium was

carefully changed. The cells were incubated with c-kit antibody ($1\,\mu g/1 \times 10^{6}$ cells) for 30 min. After PBS resuspension and centrifugation for 5 min, the cells were incubated with goat antirabbit IgG H & L for 30 min at 22°C. Cell purity was detected using a flow cytometer.

Cell Culture

The identified primary ICCs were cultured in a 1640 medium supplemented with 10% fetal bovine serum, 100 units/ml of penicillin, and 100 units/ml of streptomycin. All the cells were cultured in a humidified incubator at 37°C in a 5% CO_2 atmosphere.

Cell Viability Assay

The extracts of XZT, SCF, and imatinib were initially dissolved in sterile PBS as a stock solution. To confirm a suitable concentration for the drugs on ICCs *in vitro*, ICCs were cultured in 96-well plates with the three drugs at the concentrations of 0, 0.1, 1, 10, 50, and 100 ng/ml. After a 48 h treatment, cell viability assays were performed using the Cell Counting Kit 8 (CCK8) (Dojindo Laboratories, Kumamoto, Japan), which identified the most suitable concentrations of the drugs on ICCs to be 100 ng/ml for SCF, 100 ng/ml for imatinib, and 50 ng/ml for XZT.

To evaluate the effects of different drugs and drug combinations on the cell viability of primary ICCs, the cells were divided into six groups and incubated with the most suitable concentrations of the drugs and with drug combinations (**Table 1**) for 48 h, and CCK8 was employed to evaluate the viability of ICCs.

Electrophysiology of ICCs

To study the effects of XZT on the electrophysiology of ICCs, a whole-cell patch clamp was used to detect K^+ and Na^+ channel currents in the ICC membrane. The resistance of the glass pipette was 2–4 MΩ, and whole-cell recording mode was established using a suction after a gigaohm (KMΩ) seal was obtained. For the detection of Na^+ channel currents, the following reagents were used: 140 mM NaCl, 0.1 Mm $CdCl_2$, 20 mM TEA-Cl, 5 mM CsCl, 2 mM $CaCl_2$, 1 mM $MgCl_2.6H_2O$, 10 mM HEPES, and 10 mM glucose in the extracellular solution and 10 mM NaCl, 10 mM HEPES, 130 mM CsF, and 10 mM EGTA in the internal solution. In the extracellular solution, a sodium hydroxide solution was used to adjust the pH to 7.4 and the osmolality to 300–310 mOsm, and a cesium hydroxide solution was used in the pipette solution to adjust the pH to 7.2 and osmolality to 295–300 mOsm. The holding potential was set at −60 mV, and the current of Na^+ channel was brought out by a 0 mV voltage for 20 ms every 2 s. To

avoid influencing the detection of Na^+ channel currents, the components TEA, Cs^+, and Cd^{2+} in the extracellular solution were applied to block other ion channels. For the detection of the K^+ channel current, the extracellular solution contained 135 mM NaCl, 5.4 mM KCl, 0.2 mM $CdCl_2$, 1 mM $CaCl_2$, 1 mM $MgCl_2$, 0.33 mM NaH_2PO_4, 5 mM HEPES, and 5 mM glucose, whereas the internal solution consisted of 140 mM KCl, 1 mM $MgCl_2$, 5 mM HEPES, 10 mM EGTA, and 2 mM Na_2ATP. Similarly, a sodium hydroxide solution was added to the extracellular solution to adjust the pH to 7.4 and osmolality to 300–310 mOsm, and potassium hydroxide was used in a pipette solution to adjust the pH to 7.2 and osmolality to 295–300 mOsm. ICCs were claimed at the holding potential of −40 mV, and the experimental potential stepped to +50 mV from −120 mV by + 20 mV increments for 300 ms at a frequency of 0.2 kHz.

Western Blotting

ICCs were lysed in RIPA lysis buffer containing 150 mmol/L NaCl, 1% NP-40, 0.1% SDS, 50 mmol/L Tris–HCl pH 7.4, 1 mmol/L EDTA, 1 mmol/L PMSF, and 1 × complete mini. Lysates were centrifuged at 10,000 × g at 4 °C for 15 min to collect lysate. The protein concentration was quantified using a bicinchoninic acid protein assay. Under denaturing and nonreducing conditions, 50 μg of total protein was separated by 10% SDS gel electrophoresis and then transferred to immunobilon-p transfer membranes. Membranes were blocked with 5% nonfat milk in TBST (20 mmol/L Tris–HCl, pH 7.5, 150 mmol/L NaCl, 0.1% Tween 20) at room temperature for 1 h and incubated with c-kit (Art. No. SC-365504), Akt (Art. No. ab4691), STAT3 (Art. No. ab12640), ERK1/2 (Art. No. ab4695), p-Akt (Art. No. ab4060), p-STAT3 (Art. No. ab98543), and p-ERK1/2 (Art. No. ab9101) primary antibodies overnight at a temperature of 4°C. After washing with TBST, blots were incubated with a horseradish-coupled secondary antibody in wash buffer. Signals were developed and immunoreactive bands were visualized using an ECL kit (Upstate Biotechnology, Lake Placid, NY, USA) according to the manufacturer's instructions and were quantified using a Chemi-Doc image analyzer (Bio-Rad, Hercules, CA, USA).

Function of Isolated Gastrointestinal Muscle

The present study involved pre-experiments and formal experiments. A cirrhotic ascites model was established in rats as described. Laparotomy was carried out as soon as the four model rats and two normal rats were decapitated. Their stomachs and jejunums were separated and placed in a Tyrode's solution bath. The solution was set at a temperature of 37°C, and a mixed gas of 95% O_2 + 5% CO_2 was passed into the bath through an L-shaped hook. Contents in the gastrointestinal tract were cleared and the intestinal villus, mesentery, blood vessels, and adipose tissues affiliated with gastrointestinal tissues were carefully removed. The gastrointestinal segments were cut into 2 × 5 mm^2 muscle strips and separately placed in Tyrode's solution baths. The upper ends of the muscle strips were connected to a tension

TABLE 1 | Grouping and treatment of ICCs.

	Blank	Imatinib	Imatinib and XZT	Imatinib and SCF	XZT	SCF
SCF	−	−	−	+	−	+
Imatinib	−	+	+	+	−	−
XZT	−	−	+	−	+	−

ICCs, interstitial cells of Cajal; XZT, Xiaozhang Tie; SCF, stem cell factor.

transducer, and the lower ends were fixed to the L-shaped hook. The tension transducer was connected to a BL-420 biology function laboratory system (Chengdu Instruments Factory Co., Ltd., Sichuan, China), and the contractile activities of the muscle strips were recorded.

In the pre-experiment, an XZT extract solution was added to the bath separately at different concentrations (0.001, 0.1, 1, 10, 50, and 100 µg/ml), and the muscle-contraction curves were recorded. Because the XZT extract solution at the concentrations of 0.001, 0.1, and 1 µg/ml showed no obvious effect on tension or contractile frequency of the gastrointestinal muscle *in vitro*, solution concentrations of 10, 50, and 100 µg/ml were selected for the formal experiment, in which the steps were repeated with escalating concentrations of 10, 50, and 100 µg/ml of the XZT extract solution. The tension and contraction frequency of gastrointestinal muscle obtained from healthy rats and those with cirrhotic ascites were both measured and recorded before and after XZT treatment.

Statistical Analysis

All data were analyzed with PASW Statistics 18 software. Differences between groups were assessed using nonparametric one-way analysis of variance, and $p < 0.05$ was considered statistically significant. Values in the text are presented as the mean ± SD.

RESULTS

XZT Improved Urine Volume and Fecal Water Content in Cirrhotic Ascites in Rats

Fluid dark areas in the abdomen were detected through B ultrasound in the 29 model rats. High ascites/weight ratio accompanied by reduced 24 h urine volume and fecal water content were observed in the cirrhotic rats, and all pathological phenomena were effectively reversed by XZT but not by mosapride (**Figures 1A–E**). In the model rats, serum transaminases levels increased markedly significantly, and a large amount of collagen was deposited as a result of the formation of pseudo lobules in the interstitial space of liver tissue sections. Neither XZT nor mosapride had an effect on serum liver function parameters or histological changes in the cirrhotic model rats (data not shown).

XZT Improved Intestinal Motility of Rats With Cirrhosis And Ascites *In Vivo* and *In Vitro*

In vivo, both XZT and mosapride considerably increased the small intestinal propulsion rate, which was restricted by model establishment (**Figure 2A**), and neither affected the gastric residue ratio (**Figure 2B**). *In vitro*, gastric and jejunal muscle strips isolated from two normal and four cirrhotic ascites rats were incubated with XZT extract at different concentrations to screen for the optimal concentration. It was found that 10–
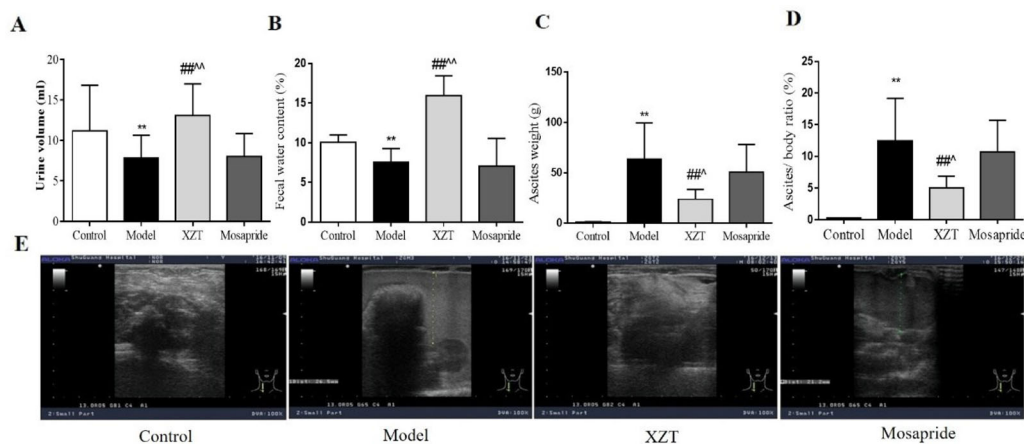
FIGURE 1 | Xiaozhang Tie (XZT) increased the urine volume and fecal water content in rats with cirrhotic ascites. Cirrhosis with ascites was established as follows. A total of 70 rats were injected intraperitoneally with a 20% CCl₄–olive oil solution for the first week, 30% CCl₄ for the second week, then 40% CCl₄ at a dose of 2 ml·kg⁻¹ twice a week until B ultrasound confirmed the ascites model of cirrhosis. Eventually, cirrhotic ascites was successfully induced in 29 rats, and the model rats were randomly divided into the following three groups: model group (n = 9), XZT group (n = 8), and mosapride group (n = 8). The remaining model rats were subjected to further electrophysiological testing of the gastrointestinal tract (n = 4). In the normal control group, 10 rats were injected with the same volume of pure olive oil. All rats were transferred to metabolic cages. Rats in the XZT group were administered XZT in the umbilical region at a daily dose of 2.25 cm² once a day for 7 days, and those in the positive control group were orally administered mosapride citrate tablets at a dose of 2 mg·kg⁻¹ once a day for 7 days. After a 7-day intervention and observation period in metabolic cages, urine and feces were collected over a period of 24 h before the experiment concluded. Body weight and ascites weight were recorded during the execution of the rats. **(A)** 24 h urine volume. **(B)** Wet feces were dried in an oven at 60°C for 24 h. Fecal water content was calculated using the following calculation formula: [wet weight (g) – dry weight (g)]/wet weight (g) × 100%. **(C)** The weight of ascites and **(D)** ratio of ascites weight to body weight was calculated. **(E)** The amount of ascites was roughly assessed through B ultrasound. Each bar represents the mean ± SD. **$p < 0.01$ compared with the normal group; ##$p < 0.01$ compared with the model group; ^$p < 0.05$ and ^^$p < 0.01$ compared with the mosapride group.
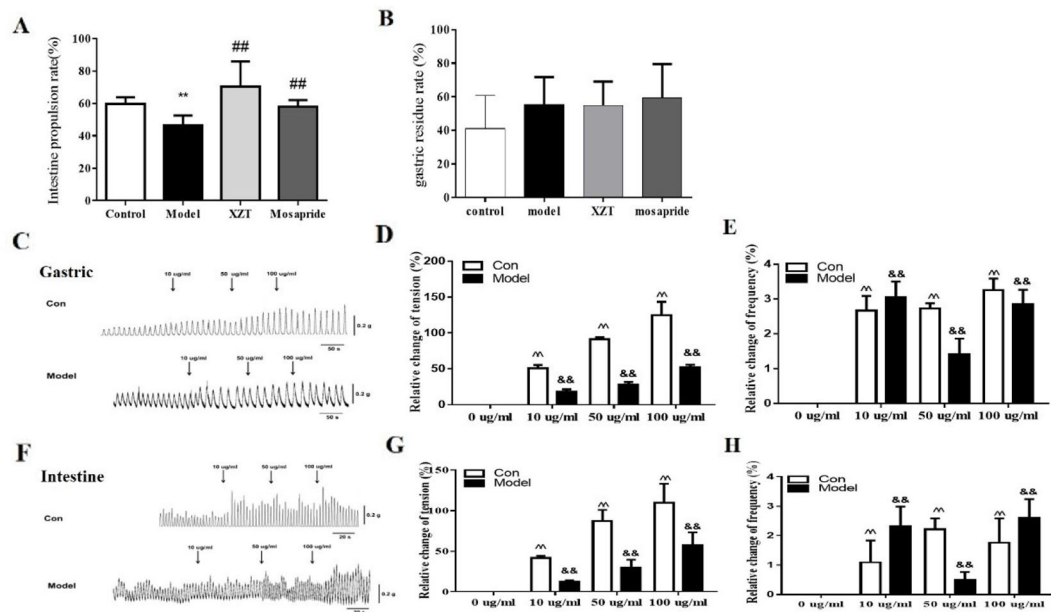
FIGURE 2 | XZT improved intestinal motility of rats with cirrhosis and ascites *in vivo* and *in vitro*. The small intestine propulsion ratio **(A)** and gastric residual ratio **(B)** were determined with ink *in vivo*. After a 7-day intervention, all rats were intragastrically administrated nutritious semisolid paste (5.0 g of sodium carboxymethyl cellulose, 8.0 g of milk powder, 4.0 g of sucrose, 4 g of starch, 2.0 ml of carbon ink, and 125 ml of distilled water) containing ink to determine the gastric residual ratio and intestinal propulsion ratio. The rats were given 1 ml/kg semisolid nutritional paste and then deprived of food for 12 h before sacrifice; 30 min later, the rats were anesthetized with 3% pentobarbital sodium. The stomachs of the rats were cut off at the distant part of the cardia and duodenum at the lower end of the esophagus, and the small part above the intestine was removed and straightened. The formula for calculating gastric residual ratio was as follows: (total weight of stomach – net weight of stomach)/semisolid nutrition paste weight × 100%. The movement distance in the small intestine of the paste was measured using a soft ruler. The formula used for calculation the small intestine propulsion ratio is as follows: migration distance of ink/whole length of small intestine × 100%. **(C–H)** *In vivo*, two normal control rats and four rats with cirrhotic ascites were sacrificed, and the jejunums and stomachs with appropriate sizes were used to measure gastrointestinal muscle strip tension and contraction frequency. First, XZT extract was screened and its optimal concentrations were confirmed to be from 10 to 100 μg/ml (data not shown). The frequency and tension of the gastric and jejunal muscle strips were recorded using a biosignal collection system **(C, G)**. **p < 0.01 compared with the control (normal) group; ##p < 0.01 compared with the model group; ^^p < 0.01 compared with the normal group muscle strips; &&p < 0.01 compared with the model control group muscle strips.

100 μg/ml of XZT obviously increased the frequency and tension of isolated gastric and jejunal muscle contraction (data not shown). Thus, muscle strips were treated with XZT extract at concentrations of 10, 50, and 100 μg/ml (**Figures 2C–H**). The results suggested that XZT extract at these three concentrations increased the frequency and tension of isolated gastric and jejunal muscle contraction in both the control and model groups. A biosignal collection system was used to record the experiment and process the results (**Figures 2C, F**), which underwent semiquantitative analysis (**Figures 2D**, **E**, **G**, and **H**).

XZT Regulated the Dysfunction of Gastrointestinal Hormones in Cirrhotic Rats

Gastrointestinal hormone levels in rat serum were tested through radioimmunoassay. As can be seen in **Figure 3**, model establishment significantly reduced MTL level (**Figure 3A**) but notably elevated SP (**Figure 3B**), SS (**Figure 3C**), and VIP (**Figure 3D**) levels. The gastrointestinal hormone levels of MTL, SP, and SS were considerably reversed after the

administration of XZT; mosapride upregulated the level of MTL and downregulated SS and VIP levels.

XZT Regulated SCF/c-kit Pathway in ICCs

Immunohistochemical staining revealed that XZT upregulated the expression of c-kit in jejunal tissues in cirrhotic ascites rats (**Figures 4A, B**). The SCF level and phosphorylation of c-kit, Akt, Stat3, and Erk1/2 in rat serum were measured using ELISA *in vivo* (**Figure 4C**), and XZT upregulated the expressions of p-c-kit, p-Akt, p-STAT3, and p-ERK1/2. The effect of XZT was similar to that of mosapride.

In the concentration range of 0–100 ng/ml, SCF promoted ICCs activity and imatinib inhibited ICCs activity, both in a dose-dependent manner. XZT had no influence on ICCs activity at concentrations in the range of 0–50 ng/ml but inhibited ICCs activity at 100 ng/ml according to CCK8 (data not shown). Therefore, the final concentration in subsequent experiments was 100 ng/ml for SCF and imatinib and 50 ng/ml for XZT. The influence of XZT on the SCF/c-kit signaling pathway was comprehensively evaluated and found to exert critical effects on ICCs activity (**Figure 5A**). The expressions of c-kit, p-Akt, p-
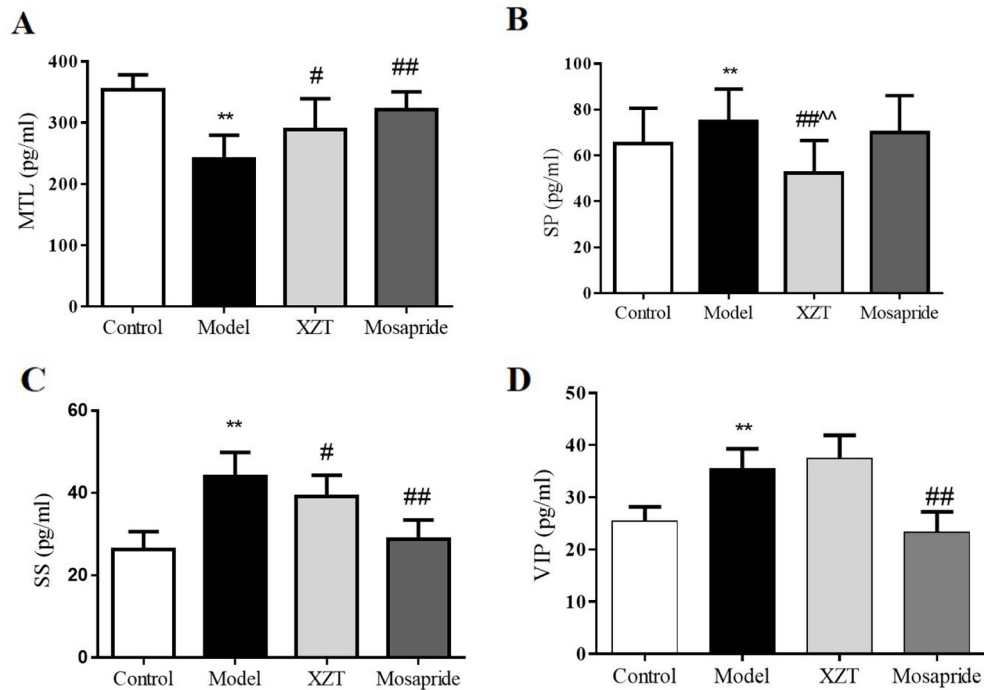
FIGURE 3 | XZT regulated the dysfunction of gastrointestinal hormones of rats with cirrhosis and ascites. *In vivo*, gastrointestinal hormones of **(A)** MTL, **(B)** SP, **(C)** SS, and **(D)** VIP in serum were measured using a radioimmunoassay technique. ******$p < 0.01$ compared with the control (normal) group; #$p < 0.05$ and ##$p < 0.01$ compared with the model group; ^^ $p < 0.01$ compared with the Mosapride group.

STAT3, and p-ERK1/2 in ICCs were tested using western blotting *in vitro* (**Figure 5F**). As revealed in **Figure 4C**, XZT had a reverse effect on SCF level and the phosphorylation of c-kit, Akt, STAT3, and ERK1/2 in rats with cirrhotic ascites. Moreover,

XZT not only enhanced the expression of c-kit, p-Akt, p-STAT3, and p-ERK1/2 in ICCs but also antagonized the inhibition of imatinib, whereas the effect of XZT was similar to that of SCF (**Figure 5F**). The whole-cell patch clamp technique was used to

Group	n	SCF(pg/ml)	p-Akt(μmol/ml)	p-c-kit(pg/ml)	p-Stat3(pg/ml)	p-Erk(μmol/ml)
Control	8	660.07±160.61	17.93±5.24	1135.00±81.33	554.73±122.44	121.14±25.09
Model	9	479.03±67.02*	5.89±2.69**	729.00±134.61**	93.30±44.81**	42.40±17.00**
XZT	8	729.60±175.35##^	22.38±2.50##^	840.00±67.02	723.79±181.10##^	141.13±23.63##^
Mosapride	8	581.36±75.62#	12.62±7.54#	789.00±131.43	337.05±175.65##	88.41±37.27#
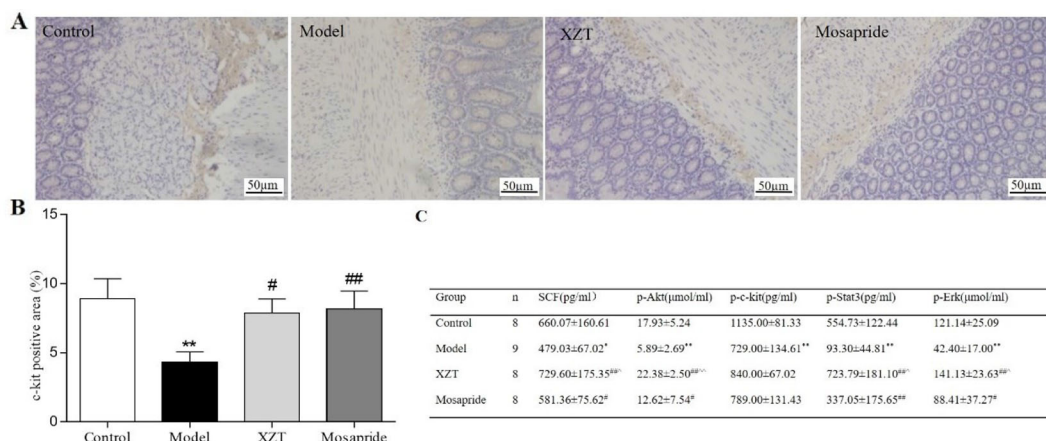
FIGURE 4 | XZT regulated the stem cell factor (SCF)/c-kit pathway in interstitial cells of Cajal (ICCs) *in vivo*. **(A)** A 1 cm segment of jejunum at a distance of 1 cm from the duodenum was taken for kit immunostaining, then a full slide of immunostained tissue was digitally scanned. Semiquantitative analysis was conducted with Image-Pro Plus 6.0 software. **(A)** Expression of ICCs in jejunal tissues according to immunohistochemical staining (×200). **(B)** Semiquantitative analysis of the positive staining rate (%) of c-kit in jejunal tissues. **(C)** Serum SCF level and phosphorylation of the downstream factors in the SCF/c-kit signaling pathway of small intestine tissues in rats were calculated using Enzyme-Linked Immunosorbent Assay (ELISA). *$p < 0.05$, **$p < 0.01$ compared with the blank group; #$p < 0.05$, ##$p < 0.01$ compared with the mosapride group.
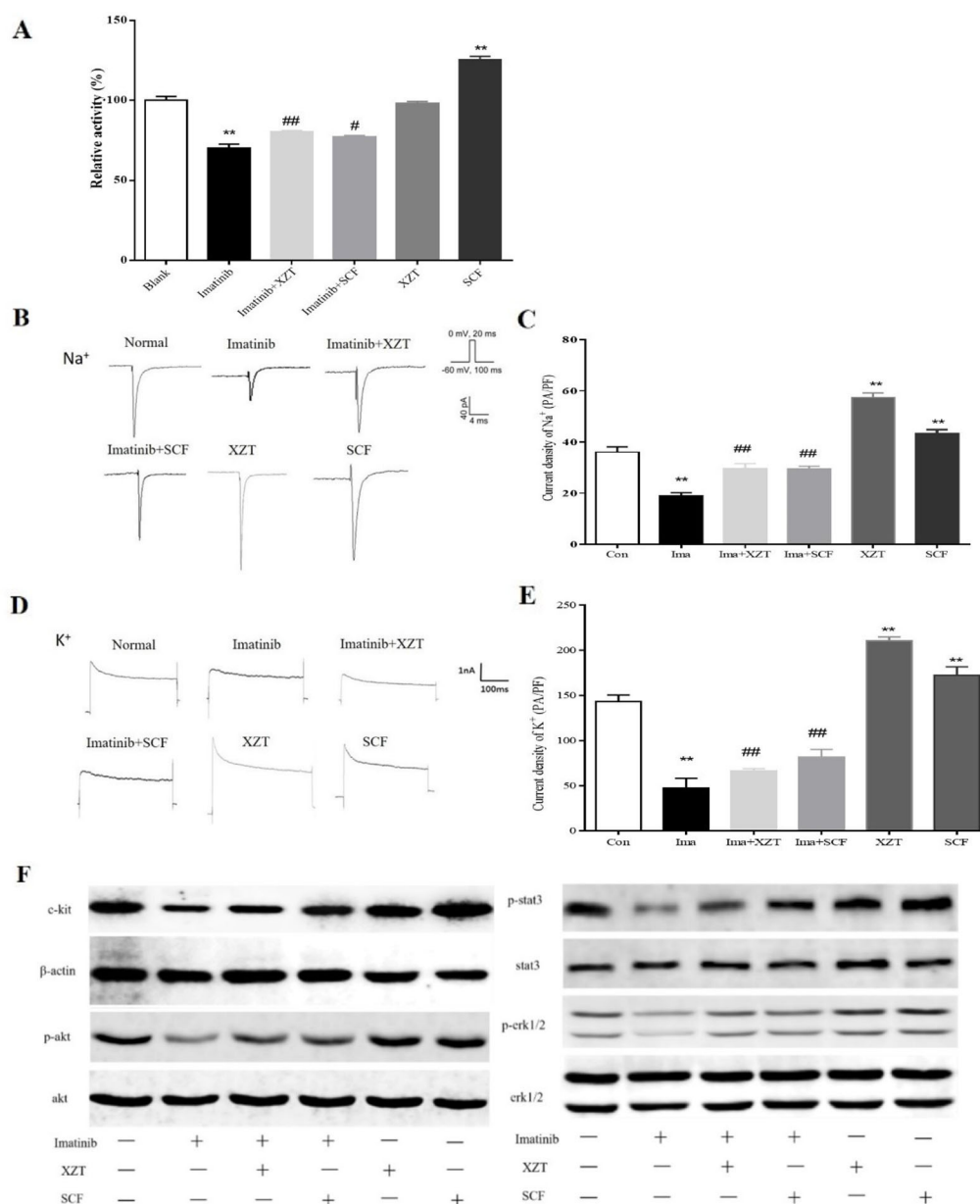
FIGURE 5 | XZT regulated the SCF/c-kit pathway in ICCs *in vitro*. ICCs in the jejunum were separated from 10 g germ-free 3-day-old C57/BL6 neonatal mice. After isolation, the cells were cultured for 96 h and then incubated with (1) 100 ng/ml imatinib, (2) 100 ng/ml imatinib plus 50 ng/ml XZT, (3) 100 ng/ml imatinib plus 100 ng/ml SCF, and (4) 50 ng/ml XZT. (5) The cells were incubated with 100 ng/ml SCF for 48 h and then harvested as described. All experiments were performed at least three times using independent cell cultures. **(A)** Cell viability was detected by CCK8; **(B, D)** the whole-cell patch recording technique was used for the study of the effect of XZT on the current of Na^+ and K^+ channels in the ICC membrane. **(C, E)** Results of quantitative analysis of the current of the Na^+ and K^+ channels. **(F)** Effect of XZT on the expression of phosphorylation of c-kit, Akt, STAT3, and ERK1/2 in ICCs, as determined by western blotting. $**p < 0.01$ compared with the normal control group; $^\#p < 0.05$ and $^{\#\#}p < 0.01$ compared with the imatinib group.

study the influence of XZT on K^+ and Na^+ channel currents in ICCs membranes (**Figures 5B, D**), and the final results were quantitatively analyzed (**Figures 5C, E**). As disclosed in **Figures 5C, E**, XZT plays a valuable role in enhancing the current of K^+ and Na^+ channels in ICCs membranes as well as in reversing the inhibition effect of imatinib (**Figures 5C, E**).

DISCUSSION

Cirrhosis is the final stage of various chronic liver diseases and leads not only to impaired liver function but also portal hypertension. Ascites is a common complication in which cirrhosis becomes decompensated, and it results in poor life

quality and high mortality. Several studies have suggested that cirrhotic ascites and gastrointestinal dysfunction might interact, but the underlying mechanism has not been revealed (Kalaitzakis et al., 2009).

CCl_4 is a classical reagent used in model establishment of cirrhotic ascites. Relevant studies have reported that the animal model of cirrhotic ascites induced by CCl_4 can closely duplicate the pathological features of human cirrhotic ascites, including water-sodium retention and a hyperdynamic circulation state (Lopez-Talavera et al., 1997; Domenicali et al., 2005; Ros et al., 2005). In our experiment, intraperitoneal injection with CCl_4 was employed to induce cirrhotic ascites. To avoid high mortality caused by exposure to a heavy CCl_4 concentration, the rats were administrated gradient concentrations of CCl_4 in the model establishment process. A sizable fluid dark area could be seen in the abdomens of 29 rats through B ultrasound and false liver acinus caused by collagen deposition was apparent in the tissue pathology evaluated using a microscope, indicating that the cirrhotic ascites model was established successfully.

In our study, XZT obviously attenuated cirrhotic ascites in rats, as evidenced by ascites weight and measurement results through B ultrasound. Urination and fecal excretion are two principal means of exhausting water from the body. However, although conventional therapy with diuresis is commonly used, the promotion of ascites regression through diarrhea is not. In refractory ascites, bacteria translocation, disorders of proinflammatory molecules, vasoactive factors, and other disorders lead to further vasodilation of peripheral and splanchnic arteriolar vessels, resulting in hyperdynamic circulation (Hsu and Huang, 2013). In hyperdynamic circulation, the effective arterial blood volume and renal perfusion decrease and cause body resistance to dieresis. Therefore, diarrhea or the promotion of fecal water content is an alternative method for eliminating ascites. In the present study, XZT increased both 24 h urine and fecal water output, which contributed to its effect on ascites. Increases in diarrhea and fecal water content are also associated with gastrointestinal motility, and in a previous study, we observed that XZT could increase excretion and defecation, alleviating abdominal distention (Xing et al., 2012), and the results suggested that this finding was related to gastrointestinal motility. In the present study, the model rats had ascites and a delayed intestinal transit rate, but XZT ameliorated intestinal motility disorder *in vivo* and *in vitro* and increased fecal water content in the models, indicating that XZT action on ascites may be associated with the regulation of gastrointestinal motility.

Gastrointestinal motility is regulated by gastrointestinal hormones, including MTL, SP, SS, and VIP. These hormones are secreted by endocrine cells and islet cells. They stimulate smooth muscle cells and play a central role in gastrointestinal motility. In cirrhotic states, endocrinology disorder and nerve dysfunction may result in abnormal secretion and the deactivation of gastrointestinal hormones, leading to further gastrointestinal dysfunction. Thus, altering the hormone level would promote gastrointestinal motility. In the model group in

our study, the MTL level was decreased and SP and SS levels were increased. XZT had a reversal effect on them, suggesting that the improvement of gastrointestinal hormone secretion could be a key action mechanism of XZT in intestinal motility.

ICCs are the pacemaker of gastrointestinal electrical activity, initiator of gastrointestinal rhythm movement, and transmitter of gastrointestinal rhythmic potential. They are widely distributed in the alimentary canal, connecting smooth muscle cells, and play a pivotal role in gastrointestinal motility (Daniel, 2004). ICC function is related to the currents of voltage-dependent ion channels and is mainly mediated by the SCF/c-Kit signaling pathway. As a type III tyrosine kinase receptor, c-kit is a specific receptor of ICCs and is mainly secreted by smooth muscle cells and liganded by SCF. Once SCF binds to a c-kit receptor in ICCs, cytoplasmic mediators are activated, including PI3K/AKT, RAS/ERK, and JAK/STAT, resulting in downstream signaling and biological effects, including with respect to gastrointestinal motility. In cases of cirrhosis, ICCs in the gastrointestinal tract reportedly decrease in number and undergo microstructural changes, which results in impaired intestinal transmission and abnormal gastrointestinal motility (Isobe et al., 1994).

To comprehensively understand the effect of XZT on the SCF/c-kit signaling pathway, which plays a critical role in ICC functions, we tested the number and viability of ICCs and their electronic activities, in particular the signaling of mediator expression and phosphorylation, *in vivo* and *in vitro* with the inhibitor imatinib as the control. Our results indicated decreased c-kit expression and cell viability and downregulated current of sodium and potassium ions in ICCs in the model rats. XZT appeared to increase c-kit expression, enhance the ICC cell number and viability, and promote voltage-dependent sodium and potassium current. In addition, XZT countered the influence of imatinib, an inhibitor of tyrosine kinase, on ICC activities, such as the movement of sodium and potassium ions. Finally, XZT improved the expression and phosphorylation of mediators such as ERK1/2 and STAT3 in SCF/c-kit signaling. The results indicate that XZT at least partially restores ICCs functions, mainly through the regulation of the SCF/c-kit signaling pathway, which is closely associated with its regulation of gastrointestinal motility in rats with cirrhotic ascites. Our findings not only reveal the main molecular mechanism of XZT on gastrointestinal motility in cirrhosis but also provide a novel method for the treatment of cirrhotic ascites.

CONCLUSION

XZT alleviated ascites and improves gastrointestinal motility disorders in cirrhotic rats. XZT action on gastrointestinal motility may be associated with its effect on ascites, and the mechanism of XZT on gastrointestinal motility was mainly regarded as regulating SCF/c-kit pathway in ICCs and gastrointestinal hormone secretion.

DATA AVAILABILITY STATEMENT

The raw data supporting the conclusions of this manuscript will be made available by the authors, without undue reservation, to any qualified researcher.

AUTHOR CONTRIBUTIONS

QZ and FX performed the experiments. QZ, FX, and YT analyzed the data and wrote the manuscript. KH and HL assisted with the animal experiment. YP assisted with the cell culture. CL and NF designed the study, NF made the XZT extract, and CL made critical revisions to the manuscript. CL and NF serve as the corresponding authors for the project.

REFERENCES

Chander Roland, B., Garcia-Tsao, G., Ciarleglio, M. M., Deng, Y., and Sheth, A. (2013). Decompensated cirrhotics have slower intestinal transit times as compared with compensated cirrhotics and healthy controls. *J. Clin. Gastroenterol.* 47, 888–893. doi: 10.1097/MCG.0b013e31829006bb

Daniel, E. E. (2004). Communication between interstitial cells of Cajal and gastrointestinal muscle. *Neurogastroenterol. Motil.* 16 Suppl 1, 118–122. doi: 10.1111/j.1743-3150.2004.00486.x

Domenicali, M., Caraceni, P., Principe, A., Pertosa, A. M., Ros, J., Chieco, P., et al. (2005). A novel sodium overload test predicting ascites decompensation in rats with CCl4-induced cirrhosis. *J. Hepatol.* 43, 92–97. doi: 10.1016/j.jhep.2005.01.034

Hsu, S. J., and Huang, H. C. (2013). Management of ascites in patients with liver cirrhosis: recent evidence and controversies. *J. Chin. Med. Assoc.* 76, 123–130. doi: 10.1016/j.jcma.2012.11.005

Isobe, H., Sakai, H., Satoh, M., Sakamoto, S., and Nawata, H. (1994). Delayed gastric emptying in patients with liver cirrhosis. *Dig. Dis. Sci.* 39, 983–987. doi: 10.1007/BF02087548

Kalaitzakis, E., Sadik, R., Holst, J. J., Ohman, L., and Bjornsson, E. (2009). Gut transit is associated with gastrointestinal symptoms and gut hormone profile in patients with cirrhosis. *Clin. Gastroenterol. Hepatol.* 7, 346–352. doi: 10.1016/j.cgh.2008.11.022

Lopez-Talavera, J. C., Levitzki, A., Martinez, M., Gazit, A., Esteban, R., and Guardia, J. (1997). Tyrosine kinase inhibition ameliorates the hyperdynamic state and decreases nitric oxide production in cirrhotic rats with portal hypertension and ascites. *J. Clin. Invest.* 100, 664–670. doi: 10.1172/JCI119578

Planas, R., Montoliu, S., Balleste, B., Rivera, M., Miquel, M., Masnou, H., et al. (2006). Natural history of patients hospitalized for management of cirrhotic ascites. *Clin. Gastroenterol. Hepatol.* 4, 1385–1394. doi: 10.1016/j.cgh.2006.08.007

FUNDING

SUPPLEMENTARY MATERIAL

The Supplementary Material for this article can be found online at: https://www.frontiersin.org/articles/10.3389/fphar.2020.00001/full#supplementary-material

Ros, J., Fernandez-Varo, G., Munoz-Luque, J., Arroyo, V., Rodes, J., Gunnet, J. W., et al. (2005). Sustained aquaretic effect of the V2-AVP receptor antagonist, RWJ-351647, in cirrhotic rats with ascites and water retention. *Br. J. Pharmacol.* 146, 654–661. doi: 10.1038/sj.bjp.0706375

Runyon, B. A., and Committee, A. P. G. (2009). Management of adult patients with ascites due to cirrhosis: an update. *Hepatology* 49, 2087–2107. doi: 10.1002/hep.22853

Xing, F., Tan, Y., Yan, G. J., Zhang, J. J., Shi, Z. H., Tan, S. Z., et al. (2012). Effects of Chinese herbal cataplasm Xiaozhang Tie on cirrhotic ascites. *J. Ethnopharmacol.* 139, 343–349. doi: 10.1016/j.jep.2011.10.040

Zhang, D., Zhang, K., Su, W., Zhao, Y., Ma, X., Qian, G., et al. (2017). Aquaporin-3 is down-regulated in jejunum villi epithelial cells during enterotoxigenic Escherichia coli-induced diarrhea in mice. *Microb. Pathog.* 107, 430–435. doi: 10.1016/j.micpath.2017.04.031

Zhang, K., Zhang, Y., Li, N., Xing, F., Zhao, J., Yang, T., et al. (2019). An herbal-compound-based combination therapy that relieves cirrhotic ascites by affecting the L-arginine/nitric oxide pathway: a metabolomics-based systematic study. *J. Ethnopharmacol.* 241, 112034. doi: 10.1016/j.jep.2019.112034

Uncovering the Anticancer Mechanisms of Chinese Herbal Medicine Formulas: Therapeutic Alternatives for Liver Cancer

Feiyu Chen, Zhangfeng Zhong, Hor Yue Tan, Wei Guo, Cheng Zhang, Chi-wing Tan, Sha Li, Ning Wang and Yibin Feng*

School of Chinese Medicine, Li Ka Shing Faculty of Medicine, The University of Hong Kong, Hong Kong, Hong Kong

The potential values of Chinese herbal formulas in treating various diseases are well known. In addition to more than 2,000 years of history, herbal medicine is appreciated for its remarkable efficacy in a lot of cases, which warrants a role in public health care worldwide, especially in East Asian countries. Liver cancer is the second most fatal cancer across the world. Recent studies have extensively investigated the chemical profiles and pharmacological effects of Chinese herbal medicine formulas on liver cancer. Either through observational follow-up or experimental studies, multiple herbal formulas have benefits implicated in the management of liver cancer. However, complex composition of each formula imposes restrictions on promoting clinical practice and global recognition. Therefore, understanding the mode of action of Chinese herbal medicine formulas in depth may offer sufficient evidence for their clinical use. This review highlighted the chemical characteristics and molecular mechanisms of actions of prominent Chinese herbal medicine formulas and summarized the correlated findings on the potential use in liver cancer treatment. At last, the present progresses of Chinese herbal medicine formulas in the perspective of clinical trials are discussed.

Keywords: cancer, liver cancer, hepatocellular carcinoma, Chinese herbal medicine formula, alternative therapy

INTRODUCTION

Liver cancer is highly fatal, with an estimation of 841,000 new cases and 782,000 new deaths for liver cancer that occurred around the world in 2018 (Bray et al., 2018). In contrast to any other cancers, liver cancer incidence and mortality are both increasing at a faster pace by almost 3% per year (Siegel et al., 2017). As of now, liver transplantation, image-guided ablation, and chemoembolization are state-of-the-art therapeutic modalities in practice. Even so, Asian countries are still undergoing the rapidly increasing cancer burden due largely to immense scale of population as well as less abundant medical resources. Compared to the United States, China has relatively poorer survival rate, with 40% higher cancer-related death among patients diagnosed with cancer (Feng et al., 2019).

Various forms of complementary and alternative medicine have been studied and practiced to deal with cancers or ailments (Barnes et al., 2008). A wide spectrum of medicinal herbs as well as their natural constituents or extracts has been demonstrated to possess anticancer properties with

involvement of possible mechanisms including cell cycle arrest, cell apoptosis induction, inflammation suppression, immune modification, and angiogenesis inhibition. For example, *Coptidis chinensis* Franch (Huanglian) extract and its main active compound, berberine, were revealed antineoplastic activity via inducing cell cycle arrest and cell apoptosis, as well as inhibiting metastasis and angiogenesis (Wang et al., 2015b), partly involving tumor suppressor p53 and miR-23a pathway (Wang et al., 2014). Moreover, targeting the hypoxia-inducible factor 1 signaling pathway is a key antiangiogenic mechanism behind cancer treatment with the formula Pien Tze Huang, as well as famous compounds such as curcumin, ginsenosides, and baicalein (Hong et al., 2019). Based on the fact that Danshensu is the major bioactive constituent of *Salvia miltiorrhiza* Bunge (Danshen), novel compounds were designed as multidrug resistance reversal agents, and Danshensu-tetramethylpyrazine conjugate was observed to overcome multidrug resistance via simultaneously inhibiting P-gp activity and regulating metabolic process (Zhou et al., 2019).

Nevertheless, with 2,000-year empirical evidence, Chinese medicine has always been characterized with holistic perspective and syndrome differentiation. Based on these principles of diagnosis and treatment, cancer is rather believed as the "cumulative toxicity" of internal organs that combines several patterns of syndrome (Liu et al., 2015). The application of herbal formulas is being well recognized for those multicomponents in confronting complexity of cancer. More so, formulas are favorable in cancer complications management, leading to less function impairment, pain alleviation, sleep improvement, and depression remission (Tao et al., 2015b). In the Chinese Pharmacopoeia (2015 edition), a total of 25 formulas are documented with antineoplastic efficacy, featuring with Qi invigorating, heat clearing and detoxifying, blood activating, and stasis removing, as well as phlegm removing (Huang et al., 2019). Among them, Qi tonifying and detoxification are two main strategies for liver cancer therapy. Combining herbal medicines with diverse functions could synergistically benefit cancer patients (**Figure 1**).

To better understand molecular mechanisms whereby Chinese herbal medicine formulas exert their antineoplastic efficacies in liver cancer as well as current status of formulas in clinical practice, database retrieval was conducted in PubMed and Web of Science, as well as China National Knowledge Infrastructure, with terms including *liver cancer*, *hepatocellular carcinoma*, *Chinese medicine*, *herbal formula*, and *Chinese medicine herbal formula*, alone or in randomized combination (**Figure 2**). Publications in English and Chinese were both included (**Table 1**).

CHINESE HERBAL MEDICINE FORMULAS INTERVENE LIVER CANCER PROGRESSION

According to the principles of Chinese medicine, liver cancer is being considered the cumulative toxicity of internal organs that combines several patterns of syndrome such as Qi-blood deficiency, phlegm stagnation, blood stasis, spleen deficiency, or damp-toxin condensation. However, there is a consensus in terms of the selection of therapeutic strategy, which is to invigorate Qi and eliminate toxic pathogens (Huang et al., 2019). As more than 5,000 medicinal herbs have been documented and practiced in Asia to date, as well as the same herbs usually present disparate functions in different formulas due to interactions with each other in different combinations, a valid and successful formula normally goes through several modifications in dosage or choice of herbs. As such, clarifying the molecular mechanisms underground the anticancer action of Chinese herbal medicine formulas might shed new light on liver cancer treatment.
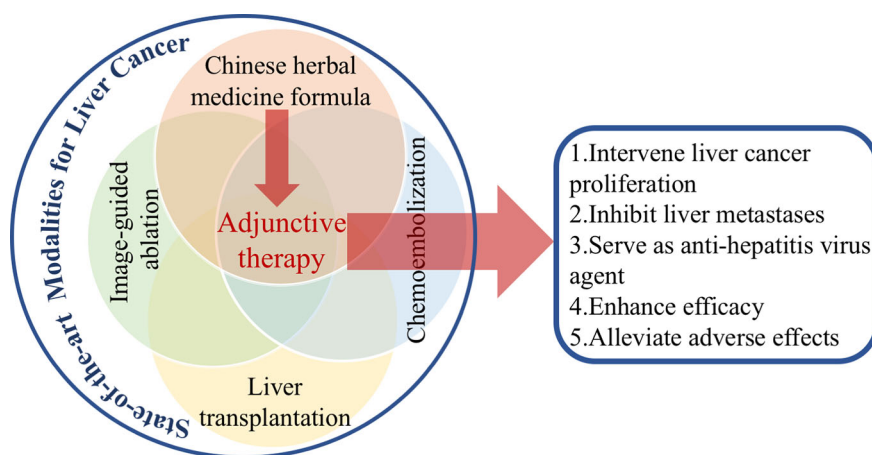
FIGURE 1 | The roles of Chinese herbal medicine formulas in liver cancer treatment.
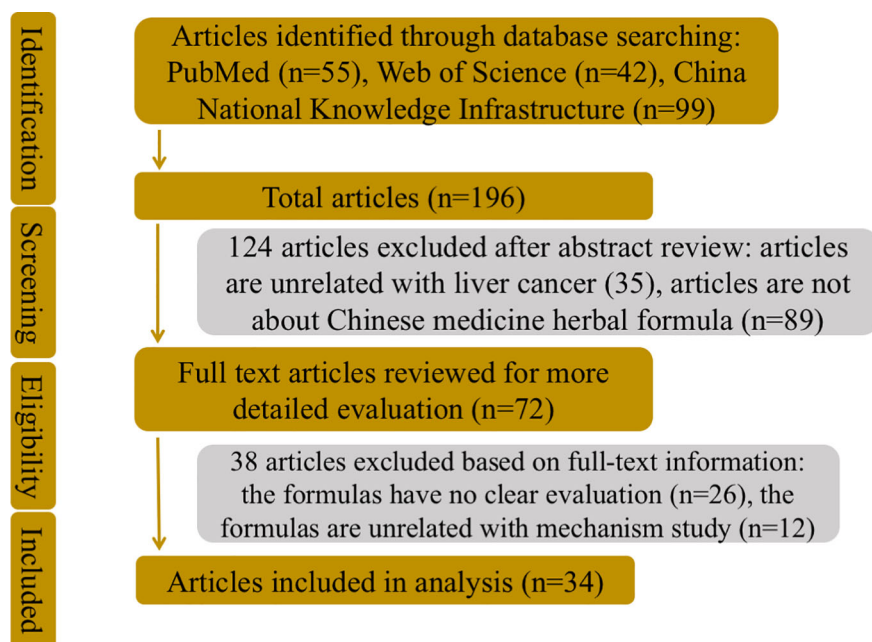
FIGURE 2 | The flowchart of the literatures search strategy, inclusion and exclusion criteria.

Ancient Herbal Formulas in Liver Cancer Treatment

Yi Guan Jian (YGJ) was established by Wei Zhixiu in Qing Dynasty. Its application in treating liver disease with liver-YIN deficiency has been well documented in Chinese medical monograph (Liu et al., 2005). With consideration that hepatoma generation may be attributed to liver-YIN insufficiency (Wu et al., 2007), YGJ has long been an optimal formula for liver cancer. Yet its tumor suppression activity is not as stable and sustained as anticipated; researchers optimized the original prescription by changing dosages of some herbs. After exposure of hepatoma Bel-7402 cells to modified YGJ, considerable decline in cell proliferation was observed, and the inhibitory action was further reported to be correlated with the induction of anoikis and p38 phosphorylation (Hu et al., 2011). The formula named San Huang Xie Xin Tang (SHXXT) is made up of three herbs, which are *Coptis chinensis* Franch (Huanglian), *Scutellaria baicalensis* Georgi (Huangqin), and *Rheum palmatum* L. (Dahuang). Their individual effects to restrain hepatocellular carcinoma have been demonstrated to modulate cell cycle or apoptotic profiles (Chang et al., 2002; Lin et al., 2004; Chan et al., 2006; Lu et al., 2007). Researchers analyzed gene profiles of HepG2 cells after exposure to SHXXT, indicating that SHXXT displayed antiproliferation pattern via p53 signaling and DNA damage (Cheng et al., 2008). Huanglian Jiedu decoction (HJD) is a canonical herbal formula that has been used for heat-damp– related diseases since its inception 1,300 years ago. Recently, its curative effect in several types of cancer is appreciated in the Asian community. Chinese medical practitioners have postulated HJD as a regimen for cancer treatment. Previous

reports identified the tumor suppression of hepatocellular carcinoma after HJD administration, and further investigation indicated that eukaryotic elongation factor 2 might be a new target of the formula in attenuating cancer progression (Wang et al., 2015a). Zuo Jin Wan (ZJW) is a well-known drug pair composed of *C. chinensis* Franch and *Fructus rutaecarpa* Benth (*Wuzhuyu*), which was prescribed to remove heat and dampness from liver. Recent works have identified antineoplastic activity of ZJW in several types of tumors including gastric cancer (Tang et al., 2012), colorectal cancer (Sui et al., 2013), breast cancer (Du et al., 2013), and liver cancer (Chao et al., 2011; Chou et al., 2017). The mode of action underlying the antiproliferation effect of ZJW on these malignancies involved the induction of mitochondria-dependent apoptosis (Xu et al., 2014). Gansui Banxia Tang (GBT) is proposed and practiced dating back centuries by Zhang Zhongjing, who has been a Chinese medical sage of considerable standing. The formula has been used for treatment of effusion of pleural, peritoneal, pericardial, and cranial cavities and intestinal tuberculosis, as well as gastrointestinal inflammation. In modern times, it was shown that it may be effective in some malignancies and cancerous ascites, such as hepatocellular carcinoma and esophageal cancer (Xia, 1989; Song, 1993), yet the pharmacological mechanism behind the anticancer effect has not been fully elucidated. *Euphobiae kansui* S. L. Liou ex S.B.Ho (Gansui) and *Glycyrhiza glabra* L. (Daji), two herbs in GBT, which are traditionally regarded as prohibited combination in "18 antagonisms," are, however, intriguingly included in the same formula. In order to illuminate the synergy as well as the action mechanism of the ingredients on hepatocellular carcinoma, Zhang and colleagues

TABLE 1 | Chinese herbal medicine formulas for liver cancer treatment.

Name of formula	Composition	Dosage or interval	Key findings	Mechanism of action	Reference
Compound *Astragalus* and *Salvia miltiorrhiza* extract	*Astragalus membranaceus Bunge, Salvia miltiorrhiza Bunge*	60, 120, or 240 mg/kg per day for 12–16 weeks	Repressed proliferation of hepatic stellate cells and HepG2 cells, inhibited tumor growth in HCC rats	MAPK (mitogen-activated protein kinases)–regulated TGF (transforming growth factor)-β/Smad signaling pathway	(Boye et al., 2015)
Ciji Hua'ai Baosheng granule	*Codonopsis pilosula (Franch.) Nannf., Astragalus membranaceus Bunge, Arisaema erubescens (Wall.) Schott, Ostreae Concha, Ganoderma, Sparganium stoloniferum (Buch.-Ham. ex Graebn.) Buch.-Ham. ex Juz., Gleditsia sinensis Lam., Cullen corylifolium (L.) Medik., Citrus aurantium L.*	5.85, 2.93, or 1.46 g/mL per day for 10 days	Prolonged survival time of H22 mice model	Increasing serum IL-2 (interleukin 2), IFN-γ (Interferon-γ) and TNF-α, but decreased IL-6 levels in serum and tumor tissue	(Xi et al., 2014; Xi et al., 2018)
Dachaihu decoction	*Bupleurum chinense DC., Scutellariae baicalensis Georgi, Paeonia lactiflora Pall., Pinellia ternata (Thunb.) Makino, Citrus aurantium L., Zingiber officinale Roscoe, Ziziphus jujube Mill.*	50 mL/time twice a day (BID), for 5 days	Attenuated adverse reactions (fever, abdominal pain, , nausea and vomiting, insomnia) in HCC patients	NA	(Wang et al., 2019)
Dahuang Zhechong formula	*Rheium palmatum L., Prunus persica (L.) Batsch, Scutellariae baicalensis Georgi, Prunus armeniacae L., Inula helenium L., Eupolyphaga seu Steleophaga, Tabanus, Hirudo, , Holotrichia diomphalia Bates, Paeoniae lactiflora Pall., Glycyrrhiza uralensis Fisch, Rehmannia glutinosa (Gaertn.) DC.*	In types of pill and capsule for 12 weeks to 12 months	Reduced fibrosis markers in liver fibrosis patients with Hepatitis B virus, potential benefits for liver cancer patients	NA	(Zhang et al., 2013)
Danzhi Xiaoyao San	*Paeonia suffruticosa Andrews, Gardenia jasminoides J. Ellis, Bupleurum chinense DC., Angelica sinensis (Oliv.) Diels, Paeonia lactiflora Pall., Atractylodis Macrocephalae Koidz, Campsis grandiflora (Thunb.) K. Schum., Glycyrrhiza uralensis Fisch.*	250 mL/time BID, for 15 days	Tumor inhibition and reduced incidence of adverse reactions in HCC patients	NA	(Zhao et al., 2011)
Fuzheng Jiedu Tongluo Fang	*Curcuma longa L., Lobelia chinensis Lour., Scutellaria barbata D. Don, Reynoutria japonica Houtt., Atractylodis Macrocephalae Koidz, Astragalus membranaceus Bunge, Angelica sinensis (Oliv.) Diels, Spatholobus suberectus Dunn, Cinnamomum cassia (L.) J. Presl*	2.65 mg/mL	Inhibited invasion of HepG2 cells.	MMP-2 (matrix metalloproteinase 2) and MMP-9 downregulation	(Zhang et al., 2017)
Fuzheng Kang'ai Formula	*Astragalus membranaceus Bunge, Ligustrum lucidum W. T. Aiton, Curcuma longa L., Actinidia arguta (Sieb. & Zucc) Planch. ex Miq., Salvia miltiorrhiza Bunge*	13.6 µmol/L	Blocked invasion and migration capacities in HepG2 cells	Reversing epithelial-to-mesenchymal transition	(Fang et al., 2019)
Fuzheng Yiliu decoction	*Sparganium emersum Rehmann, Curcuma longa L., Solanum nigrum L., Solanum lyratum Thunb., Scutellariae baicalensis Georgi, Hedyotis Diffusa Willd, Astragalus membranaceus Bunge, Angelica sinensis (Oliv.) Diels, Atractylodis Macrocephalae Koidz*	400 mg/mL	Inhibited tumor progression, invasion, and migration ability in MHC97-H cells	NA	(Peng et al., 2018)
Gansui Banxia Tang	*Euphobiae Kansui T. N. Liou ex S. B. Ho, Pinelliae ternata (Thunb.) Makino, Glycyrrhiza glabra L., Paeonia lactiflora Pall.*	7.2–14.4 g/kg per day	Inhibited tumor growth in xenografted nude mice	Targeting Hsp90a (heat shock protein 90a), ATP1A1 (ATPase Na+/K+ transporting subunit α1) and STAT3 (Signal transducer and activator of transcription 3) proteins	(Zhang et al., 2014)
Hedyotis diffusa Willd. detoxification spleen prescription	*Hedyotis diffusa Willd., Atractylodis Macrocephalae Koidz, Codonopsis pilosula (Franch.) Nannf., Dioscorea japonica Thunb., Citrus aurantium L., Setaria italica (L.) P. Beauv., Glycyrrhiza uralensis Fisch*	NA	Alleviated the pain of patients and side effects, inhibited the proliferation of tumor cells in patients	NA	(Cai and Liao, 2017)

(Continued)

TABLE 1 | Continued

Name of formula	Composition	Dosage or interval	Key findings	Mechanism of action	Reference
Huanglian Jiedu decoction	*Coptis chinensis Franch., Phellodendron chinense C. K. Schneid., Scutellaria baicalensis Georgi., Gardeniae jasminoides J. Ellis.*	25, 50, and 100 mg/kg, BID, for 3 weeks	Attenuated cell progression in HepG2, MHCC97L cells; suppressed xenografted growth of nude mice	Targeting eukaryotic elongation factor 2	(Wang et al., 2015a)
JDF granule	*Actinidia chinensis Planch., Salvia miltiorrhiza Bunge, Cremastra appendiculata (D. Don) Makino, Galli gigerii endothelium Corneum*	8 g/time BID	Prolonged survival of patients with unresectable HCC	NA	(Yu et al., 2009)
Jiedu Xiaozheng Yin	*Hedyotis diffusa* Willd., *Sophora flavescens Aiton, Pseudobulbus cremastrae (D. Don) Makino, Prunella vulgaris L.*	200 mg/mL	Inhibited cell growth of HepG2 cells	Cell arrest at G0/G1 phase via regulated expressions of cyclin D and cyclin E	(Cao et al., 2013)
Ka-mi-kae-kyuk-tang	*Benincasa hispida* (Thunb.) Cogn., *Bletilla striata* (Thunb.) Rchb.f., *Amana edulis* (Miq.) Honda, *Panax ginseng C. A. Mey., Vigna angularis* (Willd.) Ohwi & H. Ohashi, *Zanthoxylum piperitum* (L.) DC., *Patrinia villosa* (Thunb.) Dufr., *Astragalus membranaceus Bunge, Angelica sinensis* (Oliv.) Diels, *Achyranthes* BIDentata *Blume*	3 times/week for 36 days	Anti–liver metastasis and invasiveness in C57BL/6 mice model	NA	(Lee et al., 2006)
KCT-01	*Artemisia capillaris Thunb., Sanguisorba officinalis L., Curcuma longa L.*	5,000 mg/kg per day	Cell proliferation reduced in HepG2 and HepG2.2.15 cells; anti-HBV in C57BL/6 mice	Reduction in TNF-α, IL-6, and MCP (methyl-accepting chemotaxis proteins) mRNA synthesis	(Kim et al., 2018)
Liujunzi Decoction	*Corydalis yanhusuo* (Y. H. Chou & Chun C. Hsu) W. T. Wang ex Z.Y.Su & C.Y.Wu, *Glycyrrhiza uralensis Fisch, Aucklandia costus Falc., Amomum villosum Lour., Pseudostellaria heterophylla* (Miq.) Pax, *Artemisia scoparia* Waldst. & Kit., *Atractylodis Macrocephalae Koidz, Pinellia ternata* (Thunb.) Makino, *Paeonia lactiflora Pall., Scutellariae baicalensis Georgi, Bupleurum chinense DC.*	BID for 9 days	Better scores in life quality and liver function (alanine aminotransferase, aspartate aminotransferase) in HCC patients	NA	(Zhang, 2019)
Pien Tze Huang	*Moschus, Bos taurus domesticus Gmelin, Agkistrodon halys* (Pallas)., *Panax notoginseng* (Burkill) F. H. Chen	234 mg/kg per day	Anti–liver metastasis	Inhibition of epithelial-to-mesenchymal transition; regulation of Hif-1 (hypoxia-inducible factor 1) pathway	(Lin et al., 2015; Hong et al., 2019)
PHY906	*Scutellariae baicalensis Georgi, Glycyrrhiza uralensis Fisch, Paeonia lactiflora Pall., Ziziphus jujube Mill*	800 mg BID	Median overall survival was 9.2 months in advanced HCC patients	Synergistically acting with chemotherapy	(Yen et al., 2009)
QHF (Q, Qingrejiedu; H, Huoxuehuayu; and F, Fuzhengguben)	*Panax ginseng C. A. Mey., Panax notoginseng* (Burkill) F. H. Chen.	20, 40, 80, 160, and 320 µg/mL	Inhibited migration and invasion in HepG2 cells	Inhibitory action in migration and invasion activities	(Tao et al., 2010; Chen et al., 2016)
Qingyihuaji formula	*Scutellaria barbata D. Don, Hedyotis fruticosa L., Amorphophallus kiusianus, Coix lacryma-jobi L., Gynostemma pentaphyllum* (Thunb.) Makino, *Geranium lucidum L., Amomum villosum Lour.*	NA	Anti–liver metastasis in nude mice	Reversing epithelial-to-mesenchymal transition	(Zhang et al., 2013)
San-Huang-Xie Xin-Tang	*Rheum palmatum L., Coptis chinensis Franch., Scutellaria baicalensis Georgi.*	3.66 mg/mL	Cell proliferation decreased in HepG2 cells	p53 signaling and DNA damage	(Cheng et al., 2008)
Shen-Ling-Bai-Zhu Powder	*Panax ginseng C. A. Mey., Poria cocos* (Schw.) Wolf, *Atractylodis Macrocephalae Koidz., Dioscoreae oppositifolia L., Lablab purpureus Subsp., Nelumbo nucifera Gaertn., Coix lacryma-jobi L., Amomum villosum Lour., Platycodon grandiflorus* (Jacq.) A.DC., *Glycyrrhiza uralensis Fisch*	0.075, 0.15, or 0.3 g/mL per day	Inhibited tumor growth and accelerated apoptosis in H22 mice model	Descending levels of tumor growth promoters signaling and apoptotic suppressor proteins	(Kim et al., 2018)

(Continued)

TABLE 1 | Continued

Name of formula	Composition	Dosage or interval	Key findings	Mechanism of action	Reference
Shuangbai powder	*Phellodendron chinense C. K. Schneid.*, *Platycladus orientalis* (*L.*) *Franco*, *Rheum palmatum L.*, *Mentha canadensis L.*, *Lycopus lucidus Turcz. ex Benth.*	BID for 7 days	Enhanced analgesic effect, reduced side effects, and improved patients' quality of life	NA	(Liu et al., 2016)
Shuihonghuazi formula	*Polygonum orientale L.*, *Ophicalcitum Serpentine*, *Coix lacryma-jobi L.*, *Imperata cylindrica* (*L.*) *Raeusch.*	757 mg/ kg per day	Enhanced the organism immunity of cancer rats	Mediation of phosphatidylethanolamine *N*-methyltransferase (PEMT), lysophospholipase D, methylenetetrahydrofolate reductase (MTHFR) and lysophospholipase	(Bao et al., 2017)
Sijunzi decoction	*Panax ginseng C. A. Mey.*, *Atractylodis Macrocephalae Koidz*, *Glycyrrhiza uralensis Fisch*	300 mL/ day, for 2 years	Reduced tumor recurrence and increased survival rate in HCC patients	Regulation of T lymphocytes and natural killer cells	(Chen et al., 2017; Song and Wu, 2017)
Simo decoction	*Panax ginseng C. A. Mey.*, *Areca catechu L.*, *Aquilaria sinensis* (*Lour.*) *Spreng.*, *Lindera aggregata* (*Sims*) *Kosterm.*	300 mL/ day	Recovery of gastrointestinal function and reduced complications in HCC patients	NA	(Li, 2019)
Songyou Yin	*Salvia miltiorrhiza Bunge*, *Astragalus membranaceus Bunge*, *Lycium barbarum L.*, *Crataegus pinnatifida Bunge*, *Trionyx sinensis Wiegmann*	4 g/kg per day	Tumor suppression and metastasis inhibition in C57BL/6 mice	Enhancing immunity (CD4, CD8), reduced serum TGF-β1 and CD4 + CD25 + Foxp3 + Treg (regulatory T cells) proportion in PBMC (peripheral blood mononuclear cell), spleen lymphocytes, and TIL (tumor-infiltrating lymphocytes)	(Zhang et al., 2016)
Weichang'an	*Pseudostellaria heterophylla* (*Miq.*) *Pax*, *Atractylodes macrocephala Koidz.*, *Poria cocos* (*Schw.*) *Wolf*, *Glycyrrhiza uralensis Fisch.*, *Sargentodoxa cuneata* (*Oliv.*) *Rehd. et Wilson*, *Prunella vulgaris L.*	0.5 mL/ day	Cytotoxicity in HCT-116 cells; reduced metastasis in nude mice	Decreasing expressions of β-catenin and MMP-7	(Tao et al., 2015a)
Xiaotongsan	*Boswellia sacra Flueck.*, *Myrrha Mitch*, *Corydalis DC*, *Melia azedarach L.*, *Curcuma aromatica Salisb.*, *Cinnamomum camphora* (*L.*) *J. Presl*, *Daemonorops draco Bl*	Every day for 4 weeks	Relieved the pain of patients, decreased dosage of morphine	NA	(Shen et al., 2014)
Yanggan Huayu KangaiSan	*Astragalus membranaceus Bunge*, *Ziziphus jujube Mill*, *Atractylodis Macrocephalae Koidz*, *Dioscorea japonica Thunb.*, *Paeonia lactiflora Pall.*, *Glycyrrhiza uralensis Fisch*, *Praeparata Cum Melle*, *Pseudostellaria heterophylla* (*Miq.*) *Pax*, *Angelica sinensis* (*Oliv.*) *Diels*, *Lycium barbarum L.*, *Corydalis yanhusuo* (*Y. H. Chou & Chun C. Hsu*) *W. T. Wang ex Z. Y. Su & C. Y. Wu*, *Ligustrum lucidum W. T. Aiton*, *Scutellaria barbata D. Don*, *Curcuma longa L.*, *Citrus aurantium L.*, *Cinnamomum cassia* (*L.*) *J. Presl*, *Sargentodoxa cuneata* (*Oliv.*) *Rehder & E. H. Wilson*, *Magnoliae Officinalis Cortex*, *Curcuma longa L.*, *Bupleurum chinense DC.*, *Salvia miltiorrhiza Bunge*, *Arisaema Cum Bile*, *Solanum Nigrum L.*, *Pinellia ternata* (*Thunb.*) *Makino*, *Rheum palmatum L.*, *Euphorbia kansui S. L. Liou ex S.B.Ho.*	12 g/ time, thrice a day	Inhibited anchorage-independent growth and induced caspase-mediated anoikis in Bel-7402 cells	Reducing glutamate aminotransferase, aspartate aminotransferase, serum total bilirubin, serum α-fetoprotein	(Zhao et al., 2011)
Yanggan Jiedu Sangjie formula	*Ligustrum lucidum W. T. Aiton*, *Duchesnea indica* (*Andr.*) *Focke*, *Solanum nigrum L.*, *Euphorbia helioscopia L.*, *Ranunculus ternatus Thunb.*, *Curcuma longa L.*	400 mg/ mL	Inhibited anchorage-independent	ROS (reactive oxygen species) generation and PTK2 (PTK2 protein	(Hu et al., 2018)

(Continued)

TABLE 1 | Continued

Name of formula	Composition	Dosage or interval	Key findings	Mechanism of action	Reference
			growth and induced caspase-mediated anoikis in Bel-7402 cells	tyrosine kinase 2) downregulation	
Yi Guan Jian	*Glehnia littoralis* (*A Gray*) *F. Schmidt ex Miq.*, *Ophiopogon japonicus* (*Thunb.*) *Ker Gawl.*, *Angelica archangelica L.*, *Rehmannia glutinosa* (*Gaertn.*) *DC.*, *Lycium barbarum L.*, *Melia azedarach L.*, *Reynoutria japonica Houtt.*	400 mg/mL	Cell proliferation decreased in Bel-7402 cells	Anoikis induction and phosphorylation of p38 MAPK	(Hu et al., 2011)
Zuo Jin Wan	*Coptis chinensis Franch.*, *Tetradium ruticarpum* (*A. Juss.*) *T. G. Hartley*	19, 38, 76, 152, and 304 µg/mL	Inhibitory effects in SMMC-7721, BEL-7402, BEL-7404, HepG2 cells	Induction of mitochondria-dependent apoptosis	(Xu et al., 2014)
ZYD	*Phyllanthus urinaria L.*, *Salvia miltiorrhiza Bunge.*, *Arnebia guttata Bunge*	500, 1,000 µg/mL	Attenuated migratory and adhesion abilities in SMMC-7721	Anti–hepatitis B virus, deregulations of Snail, MMP-2 and MMP-9	(Guo et al., 2018)

developed a comprehensive system of integrating disease-specific and drug-specific network, which revealed the associations of GBT ingredients with their putative targets, concurrently with hepatoma-related pathways. Moreover, further experiments showed that Hsp90a, ATP1A1, and STAT3 proteins might be targeting molecules in tumor repression (Zhang et al., 2014). Shuihonghuazi formula (SHHZF) is made up of four medical herbs including *Polygonum orientale* L. (Shuihonghuazi), *Ophicalcitum* Serpentine (Huaruishi), *Coix lacryma-jobi* L. (Yiyiren), and *Imperata cylindrica* L. Raeusch (Baimao). Over the past 30 years, growing clinical experiences have demonstrated considerable antineoplastic ability of SHHZF in liver cancer patients (Lee et al., 2008; Zhou et al., 2012). Since the mode of action remains obscure, researchers have adopted the metabolomics method to facilitate the understanding of metabolomic characteristics related to its function. The study indicated metabolic profiles involving mediation of phosphatidylethanolamine *N*-methyltransferase, lysophospholipase D, methylenetetrahydrofolate reductase, and lysophospholipase are responsible for the antitumor effect (Bao et al., 2017).

As we know, clinical employment of some formulas remains unsatisfactory due in part to extraction approach barrier. Successful discovery of artemisinin by Nobel Laureate Tu Youyou exemplifies the fact that inappropriate extraction method may undermine effectiveness. Screening for optimal extraction methods of herbal formulas may help to achieve better therapeutic outcome. Rather than the conventional method utilizing water to extract active constituents from herbal formulas, present works place much focus on extraction using different polarity solvents (Cao et al., 2013). Thus, Chinese herbal medicine formulas may deserve more attention in the field.

Nascent Herbal Formulas in Liver Cancer Treatment

Beyond ancient formulas generally used in clinical practice, a wealth of nascent formulas has been used over the past few decades, and the relevant pharmacological actions have been investigated. Fuzheng Yiliu decoction (FYD) is a polyherbal formula consisting of Qi-blood–tonifying and heat toxin–clearing herbs. Human hepatocellular carcinoma HepG2 and MHC97H cells were exposed to FYD, and the findings showed inhibitory actions of FYD in tumor progression, invasion, and migration (Peng et al., 2018). Another formula composed of eight herbs is an empirical prescription initiated by a Chinese medical physician from Shaanxi province. The formula was demonstrated to reverse epithelial–mesenchymal transition in HepG2 cells, by which invasion and migration capacities were remarkably blocked (Fang et al., 2019). Matrix metallopeptidases (MMPs) are a family of proteases known to degrade extracellular matrix proteins, which in turn renders the reduction in cell adhesion, following the disruption of cellular processes. Upregulation of MMPs has been well documented in multiple types of tumor (Shay et al., 2015). Fuzheng Jiedu Tongluo formula is made up of 10 herbs and was reported to restrain invasion and migration abilities by decreasing the expression levels of MMP-2 and MMP-9 (Zhang et al., 2017). Based on clinical medications and related studies, Yanggan Jiedu Sangjie formula (YJSF) was established for hepatoma treatment. In present study, they evaluated the anticancer potential of YJSF on suspension human hepatocellular carcinoma Bel-7402 cells. YJSF inhibited anchorage-independent growth and induced caspase-mediated anoikis in Bel-7402 cells, which may be related to ROS generation and PTK2 downregulation (Hu et al., 2018). Several lines of evidence have identified the hepatoprotective role of *Astragalus membranaceus* Bunge (*Huangqi*) and *S. miltiorrhiza* Bunge (Roxas and Jurenka, 2007). The two herbs have seen positive efficacy in both *in vitro* and *in vivo* models of liver fibrosis and hepatoma (Chan et al., 2009; Chen et al., 2011). Researchers designed a synergized formula with active ingredients extracted from the two herbs using orthogonal studies and named it CASE (Yang et al., 2008). Mechanistically, CASE modulated TGF-β/Smad signaling

pathway and inhibited TGF-β–specific target gene expression in liver fibrosis and hepatocellular carcinoma, whereas the amelioration of hepatoma phenotypic hallmarks was verified (Boye et al., 2015). Herbal formula QHF is composed of three types of herbs with characteristics of clear heating (Qingrejiedu, Q), blood circulation promoting (Huoxuehuayu, H), and energy consolidating (Fuzhengguben, F). Researchers optimized the composition ratios of the formula (Tao et al., 2010), followed by the underlying mechanism of the prescription in liver cancer being investigated, which showed dramatic improvement of QHF in inhibiting migration and invasion activities in hepatic carcinoma HepG2 cells (Chen et al., 2016).

CHINESE HERBAL MEDICINE FORMULAS INHIBIT LIVER METASTASES

Cancer metastasis is one of the major barriers to successful management of carcinomas. As a critical hub in the body, the liver is involved in numerous physiological processes (Trefts et al., 2017). With two large blood vessels connected to the liver, it is a main site of metastatic disease from gastrointestinal tract, particularly colonic, gastric, and pancreatic malignancies. Reciprocal interactions between tumor cells and adjacent normal cells are implicated in hepatic metastases. Drugs that reverse or attenuate such intercellular communication will be in favor of suppressing tumor metastasis. Because diverse cross-communications occur in cancer metastasis, Chinese medicine holds the holistic perspective that might be beneficial in metastasis suppression. In fact, some formulas have been investigated in dealing with liver metastasis. A well-known formula named Pien Tze Huang (PZH) has been demonstrated effective in the management of several types of tumors (Wan et al., 2017; Chen et al., 2018). Recent work reported that PZH could not only repress colorectal tumor growth, but also exert anti–liver metastasis through the inhibition of epithelial-to-mesenchymal transition (Lin et al., 2015). Moreover, upregulated miR-16 expression was observed in its anti–hepatocellular carcinoma activity (Qi et al., 2017). Herbal medicine is popular not only in China, but also in Korea with its development based on Chinese medicine. Ka-mi-kae-kyuk-tang (KMKKT) is a formula that comprises 10 oriental herbs. Korean researchers reported with bench experiments and preclinical trials that KMKKT inhibited invasiveness of mouse colon cancer 26-L5 cells, and liver metastasis was less likely to occur in mice model (Lee et al., 2006). Weichang'an (WCA) is a herbal formula prescribed by practitioners, and the principal functions are spleen invigorating and heat clearing. Previous efforts have identified that patients with gastric (Zhao et al., 2010; Xu et al., 2013) or colon cancer (Gu et al., 2006) could benefit from WCA, whereas recent work showed positive efficacy of WCA in colorectal tumor with hepatic metastasis, in which decreased expressions of β-catenin and MMP-7 may be involved in the inhibitory action (Tao et al., 2015a). Pancreatic cancer is a common digestive system disease. A seven-herb formula named QYHJ has been used to treat pancreatic cancer,

and patients receiving it reported prolonged survival time. Several scholars established the model of pancreatic cancer with liver metastasis using nude mice and found that QYHJ suppressed liver metastasis from pancreatic tumor, at least by reversing epithelial-to-mesenchymal transition (Zhang et al., 2013).

CHINESE HERBAL MEDICINE FORMULAS SERVE AS ANTIVIRAL AGENTS TO PREVENT LIVER CANCER

The infection of hepatitis viruses accounts for the majority of liver cancer occurrence. The most predominant contributor to this high burden is the dissemination of chronic infections with hepatitis B virus (HBV) and hepatitis C virus. Infection of hepatitis viruses can progress toward liver cirrhosis, which is tightly associated with hepatocellular carcinoma (Feng et al., 2019).

Hepatocellular carcinoma is characterized as the most prevalent cancer in China in recent decades. Recent decline in incidence has been partly attributed to effective prevention and suppression of hepatitis viruses (Sherman, 2008). Chinese medicine has long been used to diminish viruses and bacteria, which are risk factors for many ailments and diseases. On account of effective and multitargeting actions against viral infections, herbal formulas are lately receiving increasing attention. Dahuang Zhechong formula (DZF) has been used for the treatment of chronic hepatitis B, but its efficacy in liver fibrosis is conflicting. For this purpose, researchers made a meta-analysis for the effect of DZF on liver fibrosis, suggesting that DZF as adjuvant treatment could reverse liver fibrosis in patients with HBV infection, and robust conclusion was reached that antifibrotic effect might be a potential benefit of DZT. Nevertheless, for long-term clinical use in liver cancer patients with HBV infection, more investigations should be carried out in laboratory and clinical trials (Wei et al., 2015). The herbal formula has capacity of being anti-HBV, namely, ZYD. Its effect on the biological behavior of liver cancer was evaluated using hepatocellular carcinoma SMMC-7721 cells, displaying that ZYD could considerably attenuate migratory and adhesion abilities of hepatoma cells by a dose-dependent manner. Further investigation demonstrated the deregulations of Snail, MMP-2, and MMP-9 expression at nucleic acid level (Guo et al.). Recent work from a Korean group newly developed an oriental formula, KCT-01, which is extracted from *Artemisia capillaris* Thunb (Yinchen), *Sanguisorba officinalis* L. (Diyu), and *Curcuma longa* L. (Jianghuang). They reported that KCT-01 is able to suppress HBV replication and inflammatory cytokine production with low risk of toxicity either in cell or in animal models, indicating the antiviral potential of using KCT-01 alone or in combination with entecavir (Kim et al., 2018).

Collectively, there is currently no eradication cure for hepatitis viruses because of the characteristic obstacle that viral minichromosome covalently closed circular DNA persistently exists in infected subjects (Charre et al., 2019). To some extent,

Chinese herbal medicine formulas represent an alternative choice for antiviral therapy. In this situation, a range of liver cancer incidence could possibly be averted.

COMPLEMENTARY THERAPY FOR LIVER CANCER MANAGEMENT

To our knowledge, curative outcome of current advanced therapeutic modalities including liver transplantation, image-guided ablation, and chemoembolization remains suboptimal in liver cancer patients due partly to multiple side effects. In this case, Chinese medicine herbal formulas have gained increasing attention because of fewer adverse effects and less toxicity to adjacent cells or tissues (Li et al., 2019; Zeng et al., 2019). Herein, several relevant examples are illustrated to show adjunctive and complementary roles of formulas in the treatment of malignancies. Shen-Ling-Bai-Zhu powder (SLBZP) is a classic herbal remedy that has been used in the management of gastrointestinal carcinoma for a long period of time. A comprehensive analysis was conducted to determine the precise role of SLBZP in hepatocellular carcinoma, which identified the antitumor property of the formula in hepatoma. More than that, compared to patients simply receiving chemotherapy, hepatoma subjects synchronously undertaking the formula reported better curative outcome, indicating the therapeutic merit of SLBZP coupled with chemotherapy for hepatoma. The mechanism behind involved descending levels of tumor growth promoters and apoptotic suppressor proteins (Xi et al., 2016). JDF granule comprised detoxifying endotoxic herbs and has been commonly used in Chinese clinics, and some compositions of the formula have demonstrated cytotoxic activity against several hepatoma cells such as BEL-7402 and SMMC-7721 (Xu et al., 2010). As hepatocellular carcinoma is an intricate disease with multivariate etiology, a synergistic strategy that Chinese herbal medicine is combined with modern therapeutic modalities has acquired extensive attention. Lately, a retrospective case study was performed to analyze the combinate employment of transcatheter arterial chemoembolization (TACE) with JDF for hepatocellular carcinoma therapy. The conclusion could be made that JDF granule considerably improved the prognosis of hepatocellular carcinoma patients undertaking TACE (Yu et al., 2009). PHY906 is a formula that has long been used for 1,800 years to treat distressing conditions of the gastrointestinal disorder. In the recent past, preclinical and early-phase clinical trials of PHY906 coupled with chemotherapy in patients with advanced hepatocellular carcinoma (Yen et al., 2009), pancreatic cancer and other gastrointestinal malignancies (Saif et al., 2010) have yielded promising results. Ciji Hua'ai Baosheng granule (CHBG) is an empirical formula originated by a Chinese medical practitioner from Fujian. The herbal compositions possess multiple capacities of reinforcing Qi, removing blood stasis, and dissipating phlegm, which have been confirmed to effectively alleviate symptoms of cancer patients. The group investigated the effect of CHBG on general health and survival

time in H22 mice model with chemotherapy treatment, showing that CHBG obviously contributed to survival time of mice bearing subcutaneous transplanted tumor or ascitic tumor (Xi et al., 2014). One step further, CHBG was identified as complementary therapy for patients undertaking chemotherapy by improving immune function and attenuating side effects (Xi et al., 2018). It is well known that exercise is favorable in overcoming and preventing ailments and diseases; the combined application of exercise and herbal formulas has not yet been largely studied. Intriguingly, researchers investigated the possibility of Songyou Yin (SYY) in parallel with swimming in liver cancer treatment. SYY is a five-herb formula that was demonstrated to exert enhanced effect on tumor suppression and metastasis inhibition. Combined use of SYY and swimming exercise showed protective effects against liver cancer in animal models (Zhang et al., 2016).

CLINICAL TRIALS OF CHINESE HERBAL MEDICINE FORMULA OFFER OPTIONS FOR LIVER CANCER TREATMENT

Extensive laboratory experiments have been conducted to explore the mechanisms of action by herbal formulas in liver cancer management. Nevertheless, herbal formulas have not yet been incorporated into conventional health care due to a series of obstacles, such as safety concerns, quality control of herbs, and evidence from clinical trials. Systematic and rigorous clinical evaluation are essential to transform oriental herbal practices into evidence-based prescriptions, which could provide an insight into the application of herbal formulas in the management of hepatic cancer (Yu et al., 2009; Du et al., 2010).

As stated above, in contrast to classical herbal formulas, growing nascent formulas have been introduced and prescribed by Chinese medicine practitioners. To observe clinical effectiveness of Yanggan Huayu KangaiSan (YHKS) on advanced primary liver cancer, 25 patients were recruited and orally received the formula for two courses. After treatment, glutamate aminotransferase, aspartate aminotransferase, serum total bilirubin, serum α-fetoprotein descended obviously; other clinical complications including pain relief was improved, implying that YHKS could improve life quality of patients (Zhao et al., 2011). To investigate the clinical efficacy of Danzhi Xiaoyao San (DXS) plus ablation on liver tumor, a study comparing microwave ablation treatment with combinate use of ablation and DXS found significant differences. Within 80 cases, patients who took oral DXS reported reduced α-fetoprotein, as well as less incidence of adverse reactions (Zhu et al., 2017). Transcatheter hepatic arterial chemoembolization is one of the efficient therapeutic avenues for hepatic tumor, yet postoperative syndrome is a tough problem in most cases. Researchers recruited 60 patients with hepatic cancer, who had been diagnosed as postoperative syndrome prior to recruiting. After receiving Dachaihu decoction, a premier choice by medical sage Zhang Zhongjing for soothing liver and eliminating pathogens, adverse reactions

including fever, abdominal pain, nausea and vomiting, and insomnia were found alleviated, which warrant further investigations and clinical practices (Wang et al., 2019). Around the same time, another study reported the curative outcome of combinatory employment of Dachaihu decoction and another canonical formula Liujunzi decoction, in the management of postoperative syndrome. The finding showed that patients who received combinatory formulas had better scores in life quality and liver function (Zhang, 2019). In addition, a recent work reported Sijunzi decoction, a tonic prescription documented in "Prescriptions People's Welfare Pharmacy," could improve immune function of patients who received TACE as well as relieve their adverse reactions (Song and Wu, 2017).

Despite surgery is an effective modality for hepatic cancer patients with no extrahepatic metastasis, the postoperative surgery still negatively influences patients' life quality. Scholars recruited 128 postoperative patients, and half of the cases received Sijunzi decoction, while the remaining received placebo. They found that the recurrence rate in the treated group was reduced compared to placebo group, and the mechanism possibly involved regulation of T lymphocytes and natural killer cells (Chen et al., 2017). Interestingly, beyond combinatory use of a couple of formulas, Tui-na (Chinese massage) was also employed with classic formulas. Simo decoction in combination with acupoint massage exerted significant therapeutic efficacy in recovery of gastrointestinal function of primary liver cancer patients (Li, 2019).

Based on clinical knowledge, cancer patients are prevalently living with cancer pain, leading to limitations in daily activity. Recognizing cancer-induced pain and initiating specialist management are important for patients' welfare. *Hedyotis diffusa* Willd. is the principal component of the formula with abilities of clearing heat and detoxicating, promoting circulation, and removing stasis. In a recent observational study of 80 patients with cancer, patients who received *H. diffusa* Willd. Detoxification Spleen Prescription (HDSP) were found to have lower incidence of pain (Cai and Liao, 2017). Shuangbai powder has been an option in promoting blood circulation, removing blood stasis, reducing swelling, and relieving pain; current advice is therefore to use Shuangbai powder in cancer pain treatment. However, extensive evidence from clinics indicated modified Shuangbai powder was preferred when the original formula failed to relieve pain. An observational study of 90 patients showed that those applied modified Shuangbai powder reported consistent pain relief in comparison with patients applying placebo (Liu et al., 2016). There are many analgesics of first-line management, and pain relief could be observed immediately, but the effectiveness could not last for a longer time; also, adverse effects have been reported such as gastrointestinal damage (Ruchita et al., 2017). Xiaotongsan, an empirical formula for external use, was practiced for years by practitioners to treat cancer-induced pain. It could enhance efficacy of conventional drug morphine through multiple targets including improvement of immune function and repression of metastasis. That said, herbal formulas could be employed coupled with first-line management of refractory pain triggered by malignant cancer (Shen et al., 2014). Taken together, on the basis of laboratory and clinical evidence-based investigations, Chinese herbal medicine formulas might have potential as latent therapeutic alternatives for liver cancer treatment.

CONCLUSION

Extensive evidence has highlighted the clinical application of Chinese herbal medicine formulas in cancer therapy. For liver cancer treatment, Chinese herbal medicine formulas improve the curative outcome whereby multicomponent and thereby multitarget against complex symptoms in liver cancer. Moreover, because current chemotherapy or radiotherapy leads to dose-limiting toxicities and substantial side effects, various functions as well as modifiable herbal compositions of the formula ensure synergistic effects and even fewer side effects. However, complexed and modifiable herbal constituents are exactly the major hurdle to clarify the underlying molecular mechanisms. On the other hand, there are cases that Chinese herbs may be harmful to the human body and cause serious toxicity when taken excessively or under inappropriate circumstances. It is also the complexed and unprecise constituents that have to take the large blame for incidences. Therefore, further optimization and large-scale validation are always imperative in order to improve the precision and safety of Chinese herbal medicine formulas used in liver cancer management. Attempts to develop herbal formulas into stable and potent modalities may offer options of considerable merit for global health care.

AUTHOR CONTRIBUTIONS

FC and ZZ retrieved the data and draft the manuscript. HT, WG, and CZ retrieved the data. C-WT, SL, and NW revised the manuscript. YF initiated the idea and drafted the manuscript.

FUNDING

REFERENCES

Bao, Y., Wang, S., Yang, X., Li, T., Xia, Y., and Meng, X. (2017). Metabolomic study of the intervention effects of Shuihonghuazi Formula, a Traditional Chinese Medicinal formulae, on hepatocellular carcinoma (HCC) rats using performance HPLC/ESI-TOF-MS. *J. Ethnopharmacol* 198, 468–478. doi: 10.1016/j.jep.2017.01.029

Barnes, P. M., Bloom, B., and Nahin, R. L. (2008). Complementary and alternative medicine use among adults and children: United States 2007. *Natl. Health Stat. Rep.*, 1–23.

Boye, A., Wu, C., Jiang, Y., Wang, J., Wu, J., Yang, X., et al. (2015). Compound Astragalus and Salvia miltiorrhiza extracts modulate MAPK-regulated TGF-beta/Smad signaling in hepatocellular carcinoma by multi-target mechanism. *J. Ethnopharmacol* 169, 219–228. doi: 10.1016/j.jep.2015.04.013

Bray, F., Ferlay, J., Soerjomataram, I., Siegel, R. L., Torre, L. A., and Jemal, A. (2018). Global cancer statistics 2018: GLOBOCAN estimates of incidence and mortality worldwide for 36 cancers in 185 countries. *CA Cancer J. Clin.* 68, 394–424. doi: 10.3322/caac.21492

Cai, L., and Liao, B. N. (2017). Effects of Hedyotis diffusa Willd detoxification Spleen Prescription on tumour related index and pain in patients with advanced primary liver cancer. *J. Southeast Univ* 36, 44. doi: 10.3969/j.issn.1671-6264.2017.01.011

Cao, Z., Lin, W., Huang, Z., Chen, X., Zhao, J., Zheng, L., et al. (2013). Ethyl acetate extraction from a Chinese herbal formula, Jiedu Xiaozheng Yin, inhibits the proliferation of hepatocellular carcinoma cells via induction of G0/G1 phase arrest in vivo and in vitro. *Int. J. Oncol.* 42, 202–210. doi: 10.3892/ijo.2012.1703

Chan, J. Y., Tang, P. M., Hon, P. M., Au, S. W., Tsui, S. K., Waye, M. M., et al. (2006). Pheophorbide a, a major antitumor component purified from Scutellaria barbata, induces apoptosis in human hepatocellular carcinoma cells. *Planta Med.* 72, 28–33. doi: 10.1055/s-2005-873149

Chan, W. S., Durairajan, S. S., Lu, J. H., Wang, Y., Xie, L. X., Kum, W. F., et al. (2009). Neuroprotective effects of Astragaloside IV in 6-hydroxydopamine-treated primary nigral cell culture. *Neurochem. Int.* 55, 414–422. doi: 10.1016/j.neuint.2009.04.012

Chang, W. H., Chen, C. H., and Lu, F. J. (2002). Different effects of baicalein, baicalin and wogonin on mitochondrial function, glutathione content and cell cycle progression in human hepatoma cell lines. *Planta Med.* 68, 128–132. doi: 10.1055/s-2002-20246

Chao, D. C., Lin, L. J., Kao, S. T., Huang, H. C., Chang, C. S., Liang, J. A., et al. (2011). Inhibitory effects of Zuo-Jin-Wan and its alkaloidal ingredients on activator protein 1, nuclear factor-kappaB, and cellular transformation in HepG2 cells. *Fitoterapia* 82, 696–703. doi: 10.1016/j.fitote.2011.02.009

Charre, C., Levrero, M., Zoulim, F., and Scholtes, C. (2019). Non-invasive biomarkers for chronic hepatitis B virus infection management. *Antiviral Res.* 169, 104553. doi: 10.1016/j.antiviral.2019.104553

Chen, R., Shao, H., Lin, S., Zhang, J. J., and Xu, K. Q. (2011). Treatment with Astragalus membranaceus produces antioxidative effects and attenuates intestinal mucosa injury induced by intestinal ischemia-reperfusion in rats. *Am. J. Chin Med.* 39, 879–887. doi: 10.1142/S0192415X11009275

Chen, T., Wang, Q., Li, Y., Huang, H., and Hu, W. (2016). Chinese herbal formula QHF inhibits liver cancer cell invasion and migration. *Exp. Ther. Med.* 11, 2413–2419. doi: 10.3892/etm.2016.3247

Chen, Y., Hu, H., Zhang, S. J., Sun, B. G., and Yang, H. Z. (2017). Effect of the Sijunzi decoction on the T lymphocyte and NK cell of the Hepatocellular Carcinoma patients with radical operation. *Zhong XI Yi Jie He Gan Bing Za Zhi* 27, 8. doi: 10.3969/j.issn.1005-0264.2017.01.003

Chen, X., Qi, F., Shen, A. L., Chu, J. F., Sferra, T. J., Chen, Y. Q., et al. (2018). Pien Tze Huang (片仔癀) Overcomes Doxorubicin Resistance and Inhibits Epithelial-Mesenchymal Transition in MCF-7/ADR Cells. *Chin J. Integr. Med* 25, 598–603. doi: 10.1007/s11655-018-2992-4

Cheng, W. Y., Wu, S. L., Hsiang, C. Y., Li, C. C., Lai, T. Y., Lo, H. Y., et al. (2008). Relationship Between San-Huang-Xie-Xin-Tang and its herbal components on the gene expression profiles in HepG2 cells. *Am. J. Chin Med.* 36, 783–797. doi: 10.1142/S0192415X08006235

Chou, S. T., Hsiang, C. Y., Lo, H. Y., Huang, H. F., Lai, M. T., Hsieh, C. L., et al. (2017). Exploration of anti-cancer effects and mechanisms of Zuo-Jin-Wan and its alkaloid components in vitro and in orthotopic HepG2 xenograft immunocompetent mice. *BMC Complement Altern. Med.* 17, 121. doi: 10.1186/s12906-017-1586-6

Du, Q., Hu, B., Shen, K. P., and An, H. M. (2010). Progress in TCM pathogenesis and treatment of liver cancer. *World J. Integr. Tradit. West. Med.* 5, 814.

Du, J., Sun, Y., Wang, X. F., Lu, Y. Y., Zhou, Q. M., and Su, S. B. (2013). Establishment of an Experimental Breast Cancer ZHENG Model and Curative Effect Evaluation of Zuo-Jin Wan. *Evid Based Complement Alternat Med.* 2013, 324732. doi: 10.1155/2013/324732

Fang, Y., Xiao, H. J., Li, R. T., Yang, Y., and Chen, G. W. (2019). Effect of Fuzheng Kang'ai Formula on Anti-hepatoma by Reversing EMT Transformation of HepG2 Cells. *China Med. Herald* 25, 60.

Feng, R. M., Zong, Y. N., Cao, S. M., and Xu, R. H. (2019). Current cancer situation in China: good or bad news from the 2018 Global Cancer Statistics? *Cancer Commun. (Lond)* 39, 22. doi: 10.1186/s40880-019-0368-6

Gu, Y., Zheng, Y. Y., and Yang, J. K. (2006). Analysis of therapeutic effect of Wei Chang An in Colorectal Cancer. *Liaoning Zhongyiyao Daxue Xuebao* 8, 5. doi: 10.3969/j.issn.1673-842X.2006.05.001

Guo, P., Huang, H., Kang, C., Zhong, Y., Li, N., and Zhang, B. (2018). Studies on the biological behavior and mechanism of human hepatocellular carcinoma cells SMMC-7721 by the traditional Chinese medicine ZYD of anti-hepatitis B virus. *World Clin. Drugs* 39, 306. doi: 10.13683/j.wph.2018.05.005

Hong, M., Shi, H., Wang, N., Tan, H. Y., Wang, Q., and Feng, Y. (2019). Dual Effects of Chinese Herbal Medicines on Angiogenesis in Cancer and Ischemic Stroke Treatments: Role of HIF-1 Network. *Front. Pharmacol.* 10, 696. doi: 10.3389/fphar.2019.00696

Hu, B., An, H. M., Shen, K. P., Xu, L., Du, Q., Deng, S., et al. (2011). Modified Yi Guan Jian, a Chinese herbal formula, induces anoikis in Bel-7402 human hepatocarcinoma cells in vitro. *Oncol. Rep.* 26, 1465–1470. doi: 10.3892/or.2011.1414

Hu, B., Zhang, T., An, H. M., Zheng, J. L., Yan, X., and Huang, X. W. (2018). Herbal formula YGJDSJ inhibits anchorage-independent growth and induces anoikis in hepatocellular carcinoma Bel-7402 cells. *BMC Complement Altern. Med.* 18, 17. doi: 10.1186/s12906-018-2083-2

Huang, Y., Zhu, J., Lin, X., Hong, Y., Feng, Y., and Shen, L. (2019). Potential of Fatty Oils from Traditional Chinese Medicine in Cancer Therapy: A Review for Phytochemical, Pharmacological and Clinical Studies. *Am. J. Chin Med.* 47, 727–750. doi: 10.1142/S0192415X19500381

Kim, H., Jang, E., Kim, S. Y., Choi, J. Y., Lee, N. R., Kim, D. S., et al. (2018). Preclinical Evaluation of In Vitro and In Vivo Antiviral Activities of KCT-01, a New Herbal Formula against Hepatitis B Virus. *Evid. Based Complement Alternat. Med.* 2018, 1073509. doi: 10.1155/2018/1073509

Lee, H. J., Lee, E. O., Rhee, Y. H., Ahn, K. S., Li, G. X., Jiang, C., et al. (2006). An oriental herbal cocktail, ka-mi-kae-kyuk-tang, exerts anti-cancer activities by targeting angiogenesis, apoptosis and metastasis. *Carcinogenesis* 27, 2455–2463. doi: 10.1093/carcin/bgl104

Lee, M. Y., Lin, H. Y., Cheng, F., Chiang, W., and Kuo, Y. H. (2008). Isolation and characterization of new lactam compounds that inhibit lung and colon cancer cells from adlay (Coix lachryma-jobi L. var. ma-yuen Stapf) bran. *Food Chem. Toxicol.* 46, 1933–1939. doi: 10.1016/j.fct.2008.01.033

Li, L., Yin Tang, L., Liang, B., Wang, R., Sun, Q., Bik San Lau, C., et al. (2019). Evaluation of in vitro embryotoxicity tests for Chinese herbal medicines. *Reprod. Toxicol.* 89, 45–53. doi: 10.1016/j.reprotox.2019.06.001

Li, S. S. (2019). Experience of Simo Decoction Combined with Acupoint Massage in the Treatment of Gastrointestinal Dysfunction of Primary Liver Cancer. *Chin. Med. Modern Distance Educ. China* 17, 50. doi: 10.3969/j.issn.1672-2779.2019.08.021

Lin, C. C., Ng, L. T., Hsu, F. F., Shieh, D. E., and Chiang, L. C. (2004). Cytotoxic effects of Coptis chinensis and Epimedium sagittatum extracts and their major constituents (berberine, coptisine and icariin) on hepatoma and leukaemia cell growth. *Clin. Exp. Pharmacol. Physiol.* 31, 65–69. doi: 10.1111/j.1440-1681.2004.03951.x

Lin, W., Zhuang, Q., Zheng, L., Cao, Z., Shen, A., Li, Q., et al. (2015). Pien Tze Huang inhibits liver metastasis by targeting TGF-beta signaling in an orthotopic model of colorectal cancer. *Oncol. Rep.* 33, 1922–1928. doi: 10.3892/or.2015.3784

Liu, Q., Zhang, Y. B., Ma, C. H., Yue, X. Q., and Ling, C. Q. (2005). [Analysis of literature on therapeutic methods and medicines of traditional Chinese medicine for primary liver cancer]. *Zhong Xi Yi Jie He Xue Bao* 3, 260–262. doi: 10.3736/jcim20050403

Liu, J., Wang, S., Zhang, Y., Fan, H. T., and Lin, H. S. (2015). Traditional Chinese medicine and cancer: History, present situation, and development. *Thorac. Cancer* 6, 561–569. doi: 10.1111/1759-7714.12270

Liu, Z., Tian, X., and Cheng, L. (2016). Effect of Modified Shuangbai Powder Combined with Three-Step Method Analgesic on Patients with Primary Hepatic Cancer Pain. *Zhong Yi Yao Dao Bao* 22, 45. doi: CNKI:SUN: HNZB.0.2016-23-015

Lu, G. D., Shen, H. M., Chung, M. C., and Ong, C. N. (2007). Critical role of oxidative stress and sustained JNK activation in aloe-emodin-mediated apoptotic cell death in human hepatoma cells. *Carcinogenesis* 28, 1937–1945. doi: 10.1093/carcin/bgm143

Peng, J. X., He, J. M., Cai, B. Q., Chen, G. H., and Liu, M. (2018). Study on the effect of Fuzheng Yiliu Decoction on invasion and metastasis of hepatocellular carcinoma cells. *China Med. Herald* 15, 25. doi: CNKI:SUN:YYCY.0.2018-10-007

Qi, F., Zhou, S., Li, L., Wei, L., Shen, A., Liu, L., et al. (2017). Pien Tze Huang inhibits the growth of hepatocellular carcinoma cells by upregulating miR-16 expression. *Oncol. Lett.* 14, 8132–8137. doi: 10.3892/ol.2017.7240

Roxas, M., and Jurenka, J. (2007). Colds and influenza: a review of diagnosis and conventional, botanical, and nutritional considerations. *Altern. Med. Rev.* 12, 25–48. doi: 10.1016/j.jep.2006.09.034

Ruchita, S., Nanda, S., and Pathak, D. (2017). Analgesic Prodrugs for Combating their Side-Effects: Rational Approach. *Curr. Drug Deliv.* 14, 16–26. doi: 10.2174/1567201813666160504100705

Saif, M. W., Lansigan, F., Ruta, S., Lamb, L., Mezes, M., Elligers, K., et al. (2010). Phase I study of the botanical formulation PHY906 with capecitabine in advanced pancreatic and other gastrointestinal malignancies. *Phytomedicine* 17, 161–169. doi: 10.1016/j.phymed.2009.12.016

Shay, G., Lynch, C. C., and Fingleton, B. (2015). Moving targets: Emerging roles for MMPs in cancer progression and metastasis. *Matrix Biol.*, 44–46, 200–206. doi: 10.1016/j.matbio.2015.01.019

Shen, L. X., Wang, M. B., and Zhang, H. Y. (2014). Clinical observation on therapeutic effect of Xiaotongsan combined with morphine sustained release tablets in treating late-stage liver cancer pain patients. *Zhong Xi Yi Jie He Gan Bing Za Zhi* 24, 267. doi: 10.3969/j.issn.1005-0264.2014.05.004

Sherman, M. (2008). Recurrence of hepatocellular carcinoma. *N Engl. J. Med.* 359, 2045–2047. doi: 10.1056/NEJMe0807581

Siegel, R. L., Miller, K. D., and Jemal, A. (2017). Cancer Statistics 2017. *CA Cancer J. Clin.* 67, 7–30. doi: 10.3322/caac.21387

Song, P., and Wu, J. (2017). Effect of Huangqi Sijunzi Decoction Combined with Blood Component Transfusion on Postoperative Immune Function in Patients with Liver Cancer. *China Med. Herald* 23, 50. doi: 10.ssss/j.issn.1672-951X.2017.21.015

Song, W. Q. (1993). Utilization pattern of GSBXT in clinics. *J. Tradit. Chin. Med.* 34, 492.

Sui, H., Liu, X., Jin, B. H., Pan, S. F., Zhou, L. H., Yu, N. A., et al. (2013). Zuo Jin Wan, a Traditional Chinese Herbal Formula, Reverses P-gp-Mediated MDR In Vitro and In Vivo. *Evid. Based Complement Alternat. Med.* 2013, 957078. doi: 10.1155/2013/957078

Tang, Q. F., Liu, X., and Ge, Y. (2012). Experimental study on inhibiting proliferation and inducing apoptosis of zuo jin wan alcohol extracts on human gastric cancer cells infected by Helicobacter pylori. *Chongqing Med.* 41, 1462.

Tao, C., Dan, L., Ling, F., and Peng, G. (2010). In vivo and in vitro effects of QHF combined with chemotherapy on hepatocellular carcinoma. *J. BioMed. Res.* 24, 161–168. doi: 10.1016/S1674-8301(10)60025-5

Tao, L., Yang, J. K., Gu, Y., Zhou, X., Zhao, A. G., Zheng, J., et al. (2015a). Weichang'an and 5-fluorouracil suppresses colorectal cancer in a mouse model. *World J. Gastroenterol.* 21, 1125–1139. doi: 10.3748/wjg.v21.i4.1125

Tao, W., Luo, X., Cui, B., Liang, D., Wang, C., Duan, Y., et al. (2015b). Practice of traditional Chinese medicine for psycho-behavioral intervention improves quality of life in cancer patients: A systematic review and meta-analysis. *Oncotarget* 6, 39725–39739. doi: 10.18632/oncotarget.5388

Trefts, E., Gannon, M., and Wasserman, D. H. (2017). The liver. *Curr. Biol.* 27, R1147–R1151. doi: 10.1016/j.cub.2017.09.019

Wan, Y., Shen, A., Qi, F., Chu, J., Cai, Q., Sferra, T. J., et al. (2017). Pien Tze Huang inhibits the proliferation of colorectal cancer cells by increasing the expression of miR-34c-5p. *Exp. Ther. Med.* 14, 3901–3907. doi: 10.3892/etm.2017.4972

Wang, N., Zhu, M., Wang, X., Tan, H. Y., Tsao, S. W., and Feng, Y. (2014). Berberine-induced tumor suppressor p53 up-regulation gets involved in the regulatory network of MIR-23a in hepatocellular carcinoma. *Biochim. Biophys. Acta* 1839, 849–857. doi: 10.1016/j.bbagrm.2014.05.027

Wang, N., Feng, Y., Tan, H. Y., Cheung, F., Hong, M., Lao, L., et al. (2015a). Inhibition of eukaryotic elongation factor-2 confers to tumor suppression by a herbal formulation Huanglian-Jiedu decoction in human hepatocellular carcinoma. *J. Ethnopharmacol* 164, 309–318. doi: 10.1016/j.jep.2015.02.025

Wang, N., Tan, H. Y., Li, L., Yuen, M. F., and Feng, Y. (2015b). Berberine and Coptidis Rhizoma as potential anticancer agents: Recent updates and future perspectives. *J. Ethnopharmacol* 176, 35–48. doi: 10.1016/j.jep.2015.10.028

Wang, X., Yang, Y., and Yang, X. W. (2019). Therapeutic Effect of Dachaihu Decoction on Postoperative Syndrome of Hepatocellular Carcinoma after TACE. *J. Shananxi Univ. Chin. Med.* 42, 130. doi: 10.13424/j.cnki.jsctcm. 2019.01.039

Wei, F., Lang, Y., Gong, D., and Fan, Y. (2015). Effect of Dahuang zhechong formula on liver fibrosis in patients with chronic hepatitis B: a meta-analysis. *Complement Ther. Med.* 23, 129–138. doi: 10.1016/j.ctim.2014.12.011

Wu, Y. F., Wang, S. P., Sun, J. M., and Wei, J. N. (2007). Clinical distribution and standards of TCM Syndrome of primary hepatic carcinoma. *Shanxi Coll. Tradit Chin. Med.* 8, 21.

Xi, S., Hong, R., Huang, J., Lu, D., Qian, L., Li, P., et al. (2014). Effects of Ciji Hua'ai Baosheng granule formula (CHBGF) on life time, pathology, peripheral blood cells of tumor chemotherapy model mouse with H22 hepatoma carcinoma cells. *Afr J. Tradit Complement Altern. Med.* 11, 94–100. doi: 10.4314/ajtcam.v11i4.16

Xi, S., Peng, Y., Minuk, G. Y., Shi, M., Fu, B., Yang, J., et al. (2016). The combination effects of Shen-Ling-Bai-Zhu on promoting apoptosis of transplanted H22 hepatocellular carcinoma in mice receiving chemotherapy. *J. Ethnopharmacol* 190, 1–12. doi: 10.1016/j.jep.2016.05.055

Xi, S., Fu, B., Loy, G., Minuk, G. Y., Peng, Y., Qiu, Y., et al. (2018). The effects of Ciji-Hua'ai-Baosheng on immune function of mice with H22 hepatocellular carcinoma receiving chemotherapy. *BioMed. Pharmacother.* 101, 898–909. doi: 10.1016/j.biopha.2018.03.027

Xia, B. (1989). Application of GSBXT in treatment of liver cancer. *Shanxi J. Tradit. Chin. Med.* 5, 24.

Xu, Y. X., Xiang, Z. B., Jin, Y. S., Shen, Y., and Chen, H. S. (2010). Two new triterpenoids from the roots of Actinidia chinensis. *Fitoterapia* 81, 920–924. doi: 10.1016/j.fitote.2010.06.007

Xu, Y., Zhao, A. G., Li, Z. Y., Zhao, G., Cai, Y., Zhu, X. H., et al. (2013). Survival benefit of traditional Chinese herbal medicine (a herbal formula for invigorating spleen) for patients with advanced gastric cancer. *Integr. Cancer Ther.* 12, 414–422. doi: 10.1177/1534735412450512

Xu, L., Qi, Y., Lv, L., Xu, Y., Zheng, L., Yin, L., et al. (2014). In vitro anti-proliferative effects of Zuojinwan on eight kinds of human cancer cell lines. *Cytotechnology* 66, 37–50. doi: 10.1007/s10616-013-9534-x

Yang, Y., Yang, S., Chen, M., Zhang, X., Zou, Y., and Zhang, X. (2008). Compound Astragalus and Salvia miltiorrhiza Extract exerts anti-fibrosis by mediating TGF-beta/Smad signaling in myofibroblasts. *J. Ethnopharmacol* 118, 264–270. doi: 10.1016/j.jep.2008.04.012

Yen, Y., So, S., Rose, M., Saif, M. W., Chu, E., Liu, S. H., et al. (2009). Phase I/II study of PHY906/capecitabine in advanced hepatocellular carcinoma. *Anticancer Res.* 29, 4083–4092.

Yu, Y., Lang, Q., Chen, Z., Li, B., Yu, C., Zhu, D., et al. (2009). The efficacy for unresectable hepatocellular carcinoma may be improved by transcatheter arterial chemoembolization in combination with a traditional Chinese herbal medicine formula: a retrospective study. *Cancer* 115, 5132–5138. doi: 10.1002/cncr.24567

Zeng, L., Tang, G., Wang, J., Zhong, J., Xia, Z., Li, J., et al. (2019). Safety and efficacy of herbal medicine for acute intracerebral hemorrhage (CRRICH): a multicentre randomised controlled trial. *BMJ Open* 9, e024932. doi: 10.1136/bmjopen-2018-024932

Zhang, J., Wang, P., Ouyang, H., Yin, J., Liu, A., Ma, C., et al. (2013). Targeting cancer-related inflammation: Chinese herbal medicine inhibits epithelial-to-mesenchymal transition in pancreatic cancer. *PLoS One* 8, e70334. doi: 10.1371/journal.pone.0070334

Zhang, Y., Guo, X., Wang, D., Li, R., Li, X., Xu, Y., et al. (2014). A systems biology-based investigation into the therapeutic effects of Gansui Banxia Tang on

reversing the imbalanced network of hepatocellular carcinoma. *Sci. Rep.* 4, 4154. doi: 10.1038/srep04154

Zhang, Q. B., Meng, X. T., Jia, Q. A., Bu, Y., Ren, Z. G., Zhang, B. H., et al. (2016). Herbal Compound Songyou Yin and Moderate Swimming Suppress Growth and Metastasis of Liver Cancer by Enhancing Immune Function. *Integr. Cancer Ther.* 15, 368–375. doi: 10.1177/1534735415622011

Zhang, J. Z., Feng, X. W., and Meng, F. P. (2017). Effect of Fuzheng Jiedu Tongluofang on MMP-2 and MMP-9 and invasion of human hepatoma HepG2 cells. *Zhong Guo Mian Yi Xue Za Zhi* 33, 542. doi: 10.3969/j.issn.1000-484X.2017.04.013

Zhang, X. T. (2019). Clinical effect of addition and subtraction of Dachaihu Decoction and Liujunzi Decoction in the treatment of post-embolization syndrome of liver cancer. *China Modern Med.* 26, 89. doi: 10.3969/j.issn.1674-4721.2019.05.028

Zhao, A. G., Cao, W., Xu, Y., Zhao, G., Liu, B. Y., Cai, Y., et al. (2010). [Survival benefit of an herbal formula for invigorating spleen for elderly patients with gastric cancer]. *Zhong Xi Yi Jie He Xue Bao* 8, 224–230. doi: 10.3736/jcim20100305

Zhao, W. J., Zhao, D. M., and Zhang, Z. (2011). Treatment Efficacy of 25 Cases of Primary Liver Cancer Treatrd by YangGan HuaYu KangAiSan. *Western J. Traditional Chin. Med.* 24, 8. doi: 10.3969/j.issn.1674-7860.2017.08.026

Zhou, X. Y., Su, B. H., Zhang, Y. Y., and Zhai, Y. J. (2012). [Effects of different processing on active components in fructus polygoni orientalis by HPLC analysis]. *Zhong Yao Cai* 35, 540–542.

Zhou, X., Wang, A., Wang, L., Yin, J., Wang, L., Di, L., et al. (2019). A Danshensu-Tetramethylpyrazine Conjugate DT-010 Overcomes Multidrug Resistance in Human Breast Cancer. *Front. Pharmacol.* 10, 722. doi: 10.3389/fphar.2019.00722

Zhu, Z., Yang, C. W., Chen, Y. Q., and Peng, S. Z. (2017). Observation on treating liver tumor with Danzhi Xiaoyao San plus ablation. *Clin. J. Chin. Med.* 9, 54. doi: 10.3969/j.issn.1674-7860.2017.08.026

The Impacts of Herbal Medicines and Natural Products on Regulating the Hepatic Lipid Metabolism

Sha Li, Yu Xu, Wei Guo, Feiyu Chen, Cheng Zhang, Hor Yue Tan, Ning Wang and Yibin Feng*

School of Chinese Medicine, Li Ka Shing Faculty of Medicine, The University of Hong Kong, Hong Kong, Hong Kong

The dysregulation of hepatic lipid metabolism is one of the hallmarks in many liver diseases including alcoholic liver diseases (ALD) and non-alcoholic fatty liver diseases (NAFLD). Hepatic inflammation, lipoperoxidative stress as well as the imbalance between lipid availability and lipid disposal, are direct causes of liver steatosis. The application of herbal medicines with anti-oxidative stress and lipid-balancing properties has been extensively attempted as pharmaceutical intervention for liver disorders in experimental and clinical studies. Although the molecular mechanisms underlying their hepatoprotective effects warrant further exploration, increasing evidence demonstrated that many herbal medicines are involved in regulating lipid accumulation processes including hepatic lipolytic and lipogenic pathways, such as mitochondrial and peroxisomal β-oxidation, the secretion of very low density lipoprotein (VLDL), the non-esterified fatty acid (NEFA) uptake, and some vital hepatic lipogenic enzymes. Therefore, in this review, the pathways or crucial mediators participated in the dysregulation of hepatic lipid metabolism are systematically summarized, followed by the current evidences and advances in the positive impacts of herbal medicines and natural products on the lipid metabolism pathways are detailed. Furthermore, several herbal formulas, herbs or herbal derivatives, such as Erchen Dection, Danshen, resveratrol, and berberine, which have been extensively studied for their promising potential in mediating lipid metabolism, are particularly highlighted in this review.

Keywords: herbal medicines, natural products, lipid metabolism, fatty liver, lipolysis, lipogenesis

INTRODUCTION

Generally, liver regulates lipid metabolism by three major processes: (1) uptake free fatty acids from circulation, and *de novo* fatty acid synthesis (FAS); (2) lipid storage, including converting fatty acids into triglyceride (TG) and other lipid droplets, which are subsequently exported to adipose tissue or stored in liver; and (3) lipid consumption, including lipolysis, β-oxidation, and the generation of lipoproteins (Reddy and Rao, 2006; Musso et al., 2009; Ponziani et al., 2015; Mato et al., 2019). These processes are presented in **Figure 1**. Correct control of lipid level is critical for cellular and organismal homeostasis, while interferences with the lipogenic pathways are accompanied with a variety of metabolic syndromes. The disorders of lipid metabolism, such as decreased β-oxidation,
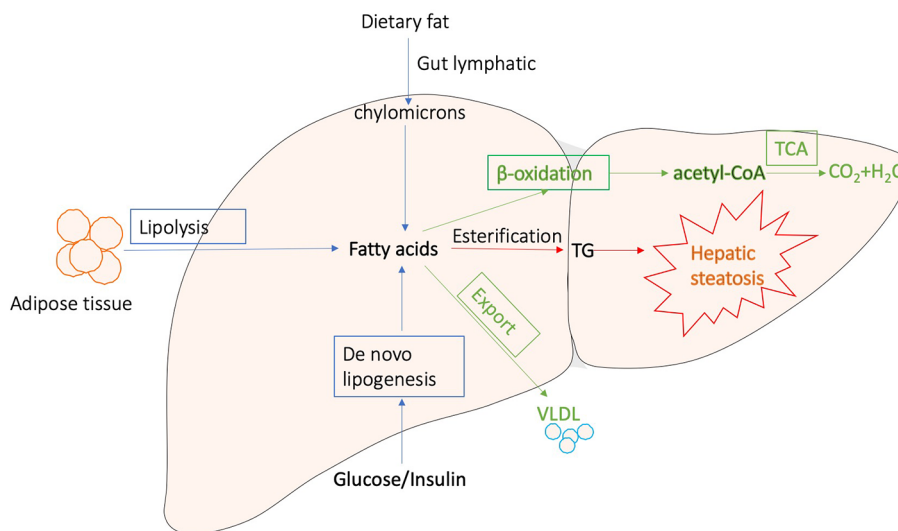
FIGURE 1 | Major processes involved in hepatic lipid metabolism.

enhanced lipolysis, and secretion of very low-density lipoprotein (VLDL), as well as altered pathways involved in the FAS, drive the accumulation of lipid droplets into the hepatocytes, eventually leading to the development of hepatic steatosis, which is a common pathological feature in various liver diseases (Reddy and Rao, 2006; Nguyen et al., 2008; Tessari et al., 2009; Perla et al., 2017).

The most prevalent liver diseases resulting from lipid metabolism disorder are alcoholic and non-alcoholic fatty liver diseases. Except difference in alcohol consumption, alcoholic and non-alcoholic fatty liver diseases show similar pathological process, which is characterized by long-term excessive fat accumulation in the liver (Younossi, 2019). They represent a wide range of liver injury, from simple fatty liver through steatosis with necrosis and inflammation to fibrosis and cirrhosis (Lomonaco et al., 2013; Heeboll et al., 2018). In particular, non-alcoholic fatty liver diseases (NAFLD), as the metabolic diseases induced by obesity and type 2 diabetes mellitus, are the second leading causes of death globally, becoming a heavy economic burden in many countries due to the high prevalence (Albhaisi and Sanyal, 2018; Al-Dayyat et al., 2018). Since inordinate lipid metabolism is intensively involved in fatty liver diseases progression, reducing lipid accumulation is a major target of development of pharmaceutical agents for various liver diseases (Ipsen et al., 2018). Simvastatin has been used as lipid-lowing drug in patients with hyperlipidemia (Aronow, 2006). However, it shows side effects, such as constipation headaches, nausea, myopathy, elevated blood sugar, and even liver damage. As a matter of fact, there is currently no satisfying therapeutic drug for fatty liver diseases (Issa et al., 2018; Moctezuma-Velazquez, 2018).

Over the past decades, due to the positive efficacy and minimal side effects, herbal medicines, and natural products have obtained increasing attention as alternative therapeutic agents for liver disorders and dyslipidemia (Xiao et al., 2013; Yao et al., 2016; Liu Q. et al., 2017). Growing evidence from preclinical studies suggests that many herbs and isolated compounds could inhibit the progression of hepatic steatosis (Dong et al., 2012; Liu Z. L. et al., 2013). A variety of mechanisms have been demonstrated to be implicated in preventing hepatic steatosis, including reducing lipogenesis, enhancing β-oxidation, increasing insulin sensitivity, suppressing oxidative stress, and inhibiting activation of inflammatory pathways (Dong et al., 2012; Yao et al., 2016). In recent studies, sterol regulatory elementbinding protein 1c (SREBP-1c), peroxisome proliferator activated receptor α (PPARα), AMP-activated protein kinase (AMPK) and sirtuin 1 (SIRT1) signaling pathways have been highlighted as crucial molecular targets of action mechanisms by which herbal medicines regulate hepatic lipid metabolism (Liu Z. L. et al., 2013). In this review, herbal medicines involved in regulating hepatic lipolytic and lipogenic pathways, such as mitochondrial and peroxisomal β-oxidation, the secretion of very low-density lipoprotein (VLDL), the non-esterified fatty acid (NEFA) uptake, and some vital hepatic lipogenic enzymes are summarized. Current clinical evidences and meta-analysis in the positive impacts of herbal medicines on the hepatic lipid metabolism pathways have also been reviewed. Furthermore, several herbal formulae, herbs or herbal derivatives, such as Erchen Dection, Danshen, resveratrol, and berberine which have been extensively studied for their promising potential in mediating lipid metabolism, are particularly highlighted in this review. This review aims to update and summarize current evidence from laboratory and clinic studies to provide alternative and complementary medical therapies with the regulatory property of hepatic lipid metabolism to current pharmaceuticals for the treatment of liver diseases.

HERBAL MEDICINES AND NATURAL PRODUCTS REGULATE ON THE HEPATIC LIPID METABOLISM PATHWAYS

Increasing evidence indicated that many herbs, natural products, and their derived compounds could inhibit the progression of hepatic steatosis. A variety of mechanisms have been demonstrated to be implicated in preventing hepatic steatosis and modulating lipid metabolism by herbs, including anti-oxidative stress, anti-inflammation, reducing hepatocyte fatty acid uptake and trafficking, reducing hepatic *de novo* lipogenesis, increasing lipolysis, induction of lipophagy, enhancing fatty acid β-oxidation. In particular, SREBP-1c, PPARα, AMPK, and SIRT1 signaling pathways have been highlighted as crucial molecular targets of action mechanisms by which herbal medicines regulate hepatic lipid metabolism. In **Table 1**, we reviewed the effects and mechanisms of herbs and some natural products on fatty liver diseases from recent studies. In the following section, we will discuss herbs that attenuate hepatic steatosis *via* reducing hepatocyte fatty acid uptake and trafficking, reducing hepatic *de novo* lipogenesis, increasing lipolysis, induction of lipophagy, and enhancing fatty acid β-oxidation in detail.

Reducing Hepatocyte Fatty Acid Uptake and Trafficking

Nonesterified fatty acids (NEFAs) and glycerol are generated and released from adipose tissue *via* lipolysis (Kawano and Cohen, 2013). Then NEFAs enter into hepatocytes principally through CD36, and fatty acid transports (FATPs)(Kawano and Cohen, 2013). Several mediators have been demonstrated to play a role in regulating CD36 and FATPs, such as pregnane X receptor (PXR), which impact the hepatocyte fatty acid uptake. Increasing evidence has shown that a variety of herbs and natural compounds attenuate hepatic steatosis *via* modulating genes for fatty acid uptake.

Scutellarin, one of the Traditional Chinese Medicines (TCM) used for liver diseases and diabetes, was found to reduce insulin-dependent lipid accumulation and the mRNA expression of CD36 in HepG2 cells-treated with palmitic acid (Luan et al., 2019). Several other TCM and isolated compounds, babaodan, licorice extract, polyphenol-enriched fraction from Herba Erigerontis, and magnesium lithospermate B, reduced hepatic CD36 expression in mice fed with High Fat Diet (HFD) (Wu and Wang, 2012; Wang et al., 2016; Sheng et al., 2019). Dansameum reduced the expression level of CD36 in liver of apolipoprotein E-Knockout mice with NAFLD (Ahn et al., 2019). In another mice model of NAFLD induced by high-fat and high-cholesterol diet, gypenosides which are a type of TCM extracted from plants downregulated CD36 level in the liver, alleviating the progression of hepatic steatosis (Huang et al., 2019). Berberine attenuated fat accumulation in the liver partially *via* suppressing the expression of FATP gene in HFD-fed mice (Zhou et al., 2019).

Reducing Hepatic De Novo Lipogenesis

De novo lipogenesis in the liver is tightly controlled by metabolic hormones such as insulin, and glucose level (Wang Y. et al., 2015). In the normal physiological status, high level of glucose promotes the

secretion of insulin, activates carbohydrate-responsive element-binding protein (ChREBP), and meanwhile, provides substrate to facilitate lipogenesis in the liver (Wang Y. et al., 2015). In terms of insulin, it activates sterol regulatory element-binding protein 1c (SREBP-1c) to up-regulate lipogenic enzymes, and then promotes *de novo* lipogenesis (Eissing et al., 2013; Chao et al., 2019). **Figure 2** shows the overview of lipogenesis in hepatocytes. Herbs and isolated natural compounds have been demonstrated by animal studies and *in vitro* studies to alleviate hepatic steatosis by ChREBP pathway and insulin-SREBP-1c pathway, as well as other factors, such as AMPK, PPARγ, SIRT1, inflammatory cytokines, immuno-modulation, and microRNAs. We summarized medicinal herbs and isolated natural compounds from recent literatures with the effects of reducing hepatic lipogenesis in **Table 2** and discussed some representative studies in detail as following.

Magnolia officinalis Rehder & E.H.Wilson, *Houttuynia cordata* Thunb., 3-Caffeoyl, 4-dihydrocaffeoylquinic acid from *Salicornia europaea* L., puerarin and four kinds metabolites of berberine attenuated lipid accumulation in HepG2 cells *in vitro* via down-regulation of lipogenesis gene expressions through activation of the AMPK signaling pathway (Cao et al., 2013) (Pil Hwang et al., 2013; Kang and Koppula, 2014). Gyeongshingangjeehwan 18 (an herbal drug composed of *Laminaria japonica*, *Rheum palmatum*, and *Ephedra sinica*), Herbal Formula HT048 (*Citrus unshiu* and *Crataegus pinnatifida*), Fructus Xanthii (*Xanthium sibiricum* Patr.), *Lycium barbarum* polysaccharide, Jatrorrhizine hydrochloride, oxyresveratrol, and alisol A isolated from *Rhizoma alismatis* (Oriental Waterplantain Tuber.) attenuated liver steatosis in HFD-fed animals *via* regulating lipogenic genes, predominantly relating with downregulation of SREBP-1c expression *via* AMPK activation (Li et al., 2013; Li W. et al., 2014; Lee Y. H. et al., 2016; Yang et al., 2016; Lee et al., 2018; Lim et al., 2018; Ho et al., 2019). Gangjihwan, a polyherbal composition of *Ephedra intermedia* Schrenk & C.A.Mey., *Lithospermum erythrorhizon* Siebold & Zucc., and *Rheum palmatum* L., showed anti-obesity and anti-nonalcoholic steatohepatosis effects in HFD-fed mice. Lipogenic transcription factors, SREBP-1c, PPAR-γ, and ChREBP alpha were involved in the action mechanism (Jang et al., 2018); (Roh et al., 2017). Molecular targets of FAS, ACC1, ChREBP alpha, and SREBP-1c were also found to be involved in the underlying mechanism of anti-hepatic steatosis and anti-obesity-related hepatic inflammation effect of Gambigyeongsinhwan in Otsuka Long-Evans Tokushima fatty rats and HepG2 cells (Yoon et al., 2017).

Glycycoumarin, a representative of coumarin compounds isolated from licorice, and Alisol B 23-acetate exert ability of reducing hepatic lipogenesis in methionine-choline-deficient (MCD) diet-fed mice (Meng et al., 2017; Zhang E. et al., 2019). MCD diet is a classical dietary model of non-alcoholic steato-hepatitis. With the lack of methionine and choline and high sucrose (40%) and fat (10%), impaired hepatic mitochondrial β-oxidation and very low-density lipoprotein (VLDL) synthesis are observed in mice (Ibrahim et al., 2016). Glycycoumarin activated AMPK signaling pathway to reduce lipogenesis. Alisol B 23-acetate, a natural triterpenoid derived from TCM *Rhizoma alismatis* (Oriental Waterplantain Tuber.), decreased hepatic

TABLE 1 | The effects and mechanisms of herbs and some natural products on fatty liver diseases.

Herbs or Natural products	Model	Effects	Mechanisms	References
Rosmarinus officinalis Linn.	Orotic acid induced NAFLD model in rats	Reduced the levels of hepatic TG, TC, FFA and improved cell hypertrophy, vacuolation, and cell necrosis in the liver	↑Phosphorylation of AMPK and ↓SREBP-1c cracking into the nucleus, following ↓FAS	(Wang et al., 2019)
Chinese Herbal Formula (CHF03, composition confidentiality)	HFD induced NAFLD model in mice; AML12 cells treated with palmitic acid *in vitro*	Reduced hepatic steatosis	↓lipogenesis *via* down-regulating the expression of SREBF1, Fasn, and Acaca, ↓ lipid accumulation	(Cui et al., 2019)
Dachaihu Decoction (Bupleuri Radix, Scutellaria baicalensis Georgi, Pinellia ternate, Paeonia lactiflora, Citrus trifoliata, Rheum rhabarbarum, Zingiber officinale, Ziziphus jujuba Mill)	High-fat high-fructose diet induced NAFLD model in rats	Reduced the levels of elevated liver coefficient, serum TG, TC, LDL, AST, and ALT, blood glucose, plasma endotoxin, reduced TG, TNF-α, TGF-β, NF-κB, and TLR4 in liver tissues	↓oxidative stress and inflammation	(Yang J.M. et al., 2019)
Leaves of *Aloysia citrodora* Paláu (syn. Lippia triphylla)	KK-Ay mice	Improved hepatic lipid metabolism	via activating AMPK	(Zhang Y. et al., 2019)
Polygonatum kingianum	HFD induced NAFLD model in rats	↓ALT, AST, TC, LDL in serum, and hepatic TC and TG	↑mRNA expression of carnitine palmitoyl transferase-1 and ↓uncoupling protein-2 respectively, ↓caspase 9, caspase 3 and Bax expression in hepatocytes, ↑expression of Bcl-2 in hepatocytes and cytchrome c in mitochondria	(Yang X. X. et al., 2019)
Bangpungtongseong-san (Bofutsushosan)	HFD induced NAFLD model in C57BL/6J mice	Ameliorated dyslipidemia and hepatic steatosis, reduced body weight gain	Altered transcriptional changes in the liver, ↓mitochondrial oxidative phosphorylation-related genes in the liver, ↓hepatic fibrosis-related transcriptome.	(Choi et al., 2019)
Thymbra spicata L. extracts	endothelial cells *in vitro*	Ameliorated lipid accumulation, oxidative stress and inflammation, reduced hepatic steatosis	Preventing endothelium dysfunction	(Khalil et al., 2019)
Swertiamarin	fructose-fed mice	Lowed levels of serum glucose, TG, uric acid, ALT, AST, alleviation of hepatic ballooning degeneration and steatosis	↓SREBP-1, FAS and acetyl-CoA carboxylase 1 (ACC1) in liver	(Yang Y. et al., 2019)
Si He Decoction (Zingiber officinale., Cyperus rotundus L., Lilium, Lindera aggregate, Salvia miltiorrhiza, Santalum album, Amomum villosum, *Typha angustifolia* L., Trogopterus xanthipes Milne)	HFD induced NAFLD model in rats	Improved liver pathological conditions	↓expression level of TNF-alpha and IL-6, ↑visfatin, adiponectin, leptin and resistin, targeting adipokines	(Sun et al., 2019)
Modified Longdan Xiegan Tang (composed of *Scutellaria baicalnsis* Geprgi, *Gardenia jasminoides, Adenophora capillaris, Akebia quinate, Plantago asiatica, Angelica sinensis, Rehmannia glutinosa, Alisma plantago-aquatica, Bupleurum gibraltaicum,* and *Glycyrrhiza uralensis*)	Olanzapine-induced fatty liver in rats	↓TG, cell vacuolar degeneration and Oil Red O-stained area	Regulating hepatic *de novo* lipogenesis and fatty acid β-oxidation-associated Gene expression mediated by SREBP-1c, PPAR-α and AMPK-α	(Ren et al., 2019)
LongShengZhi Capsule	apoE-Deficient Mice	Reduced atherosclerosis	↓lipogenic and cholesterol synthetic genes while activating expression of triglyceride catabolism genes	(Ma et al., 2019)
Thymoquinone	Hypothyroidism with NAFLD rats	Reduced steatosis and lobular inflammation	↑antioxidant CAT gene	(Ayuob et al., 2019)
Monomer Hairy Calycosin	NAFLD rats	Control the lipid peroxidation, and reduce the levels of serum TNF-alpha, IL-6, MDA and FFA, improve the steatosis and inflammation of liver tissue	↓CYP2E1, ↓apoptosis of hepatocytes.	(Liu X. et al., 2019)

(Continued)

TABLE 1 | Continued

Herbs or Natural products	Model	Effects	Mechanisms	References
Hongqi Jiangzhi Formula (Astragali Radix, Red yeast rice, Nelumbinis Folium, Curcumae Longae Rhizoma, Lych Fructus, Magnoliae Officinals Cortex, Artemisiae Scopariae Herba)	HFD induced NAFLD model in rats	Reduced lipid accumulation	↓the expression of NF-kappa B through TLR4 downstream signalling pathways	(Liang et al., 2019)
Jiang Zhi Granule (Herba Gynostemmatis, Folium Nelumbinis, Radix Salviae, Rhizoma Polygoni Cuspidati, and Herba Artemisiae Scopariae)	NAFLD in animal and PA-treated hepatocytes *in vitro*	Showed anti-steatotic effects	droplet degradation *via* autophagy though the mTOR signalling	(Zheng et al., 2018)
Curcumin	Steatotic hepatocyte model *in vitro* and NAFLD rat models	Improved lipid accumulation	Reversed the DNA methylation at the PPAR-alpha gene	(Li Y. Y. et al., 2018)
Samjunghwan Herbal Formula (Mori Fructus, *Lycium chinensis* Miller, Atractylodis Rhizoma)	HepG2 Cells and OLETF Rats	↓Body weights, and visceral adipose tissue (VAT) weights, AST and ALT levels,	↑HMGCOR, SREBP, and ACC, and ↓AMPK and LDLR gene expressions levels.	(Ansari et al., 2018)
Oxyresveratrol	NAFLD in mice	Ameliorated NAFLD	↓LXR alpha agonists-mediated SREBP-1c induction and expression of the lipogenic genes, ↑mRNA of fatty acid beta-oxidation-related genes in hepatocytes; induced AMPK activation, helped inhibit SREBP-1c using compound C.	(Lee et al., 2018)
Sedum sarmentosum Bunge extract	Tilapia fatty liver model	Restored the changes to feed coefficient, immune capacity, and pathological characters	Altered expression of genes in the lipid metabolic process, metabolic process, and oxidation-reduction process. Our results suggest that disorders of the PPAR and p53 signaling pathways	(Huang et al., 2018)
Berberine and curcumin	HFD induced NAFLD model in rats	↓LDL-c, ALT, AST, ALP, MDA, LSP	↓SREBP-1c, pERK, TNF-alpha, and pJNK	(Feng et al., 2018)
Gegen Qinlian decoction (Pueraria lacei Craib, Scutellaria baicalensis Georgi, Coptis chinensis Franch., and Glycyrrhiza uralensis Fisch.) and resveratrol	Rat model of HFD-induced NAFLD	Restored lipid metabolism and inflammatory and histological abnormalities	Triggering the Sirt1 pathway	(Guo et al., 2017)
Gegenqinlian Decoction	Rat model of HFD-induced NAFLD and HepG2	Suppress inflammation and regulate lipid	Improving PPAR-γ	(Wang Y. L. et al., 2015)
Lingguizhugan Decoction (Poria, Ramulus Cinnamomi, Rhizoma Atractylodis Macrocephalae, and Radix Glycyrrhizae)	Rat model of HFD-induced NAFLD	Attenuated phenotypic characteristics of NAFLD	By affecting insulin resistance and lipid metabolism related pathways (e.g., PI3K-Akt, AMPK); activating cholesterol secretio; increasing serum thyroid hormone levels, improving beta-oxidation (via modulation of TR beta 1 and CPT1A expression), metabolism and transport (through modulation of SREBP-1c, ACSL and ApoB100 expression) of fatty acid.	(Liu X. et al., 2017; Yang et al., 2017; Zhu et al., 2017)
Chinese herb extract, QSHX (*Bupleurum falcatum, Salvia miltiorrhiza,* rhubarb, lotus leaf, capillary Artemisia, rhizome polygoni cuspide and gyn*ostemma pentaphyllum*)	High-fat and high-sugar diet-induced NAFLD in rat	↓Body weight, liver index, and serum levels of AST, ALT and TG; and increased the serum level of adiponectin	Promoting the expression of HMW APN and DsbA-L, which may have been induced by inhibiting the activation and expression of FOXO1 in adipocytes	(Liu X. et al., 2017)
Qushi Huayu Decoction (*Herba Artemisiae* capillaris, *Polygonum cuspidatum, Hypericum japonicum* Thunb, Gardenia, and *Rhizoma Curcumae* Longae)	NAFLD rats	Attenuated phenotypic characteristics of NAFLD	↑Hepatic anti-oxidative mechanism, ↓hepatic lipid synthesis, and promoted the regulatory T cell inducing microbiota in the gut.	(Feng et al., 2017)

(Continued)

TABLE 1 | Continued

Herbs or Natural products	Model	Effects	Mechanisms	References
Rhododendron oldhamii Maxim. leaf extract	HepG2 cells and HFD-fed mice	Improves fatty liver syndrome	Increasing lipid oxidation and decreasing the lipogenesis pathway	(Liu Y. L. et al., 2017)
Herbal Formula HT048 (*Crataegus pinnatifida* leaf and *Citrus unshiu* peel extracts.)	HFD-fed rats	Attenuates Diet-Induced Obesity	↓Genes involved in lipogenesis, gluconeogenesis, and adipogenesis, ↑β–oxidation genes	(Lee Y. H. et al., 2016)
Angelica dahurica (Hoffm.) Benth. & Hook.f. ex Franch. & Sav.	HFD-induced hyperlipidemic mice	↓TC and TG in the livers	↓CAT and sterol carrier protein2 (SCP2), ↑ the expression of lipid metabolism related genes-lipase member C (LIPC) and PPAR-γ	(Lu et al., 2016)
Daisaikoto (Bupleuri Radix, Scutellaria baicalensis Georgi, Pinellia ternate, Paeonia lactiflora, Citrus trifoliata, Rheum rhabarbarum, Zingiber officinale, Ziziphus jujuba Mill)	Diabetic fatty liver rats induced by a high-fat diet and streptozotocin (STZ)	Reversing dyslipidemia and insulin resistance	Regulating expressions of SIRT1 and NF-κB	(Qian et al., 2016)
Herb Formula KIOM2012H (*Arctium lappa* Linne, *Glycyrrhiza uralensis* Fischer, *Magnolia officinalis* Rehder & Wilson, Zingiber officinale Roscoe)	HFD-fed mice	Inhibited lipid accumulation	Gene expressions involved in lipogenesis and related regulators	(Park et al., 2015)
Hawthorn (Crataegus) leaf flavonoids	HFD-fed rats	Alleviated NAFLD	Enhancing the adiponectin/AMPK pathway	(Li et al., 2015)
Herbal SGR Formula (Semen Hoveniae extract, *Ginkgo biloba* extract, and *Rosa roxburghii* Tratt extract)	Acute ethanol-induced liver steatosis in mice	Inhibited acute ethanol-induced liver steatosis, ↓serum and hepatic TG level, and improved classic histopathological changes	↓Protein expression of hepatic SREBP-1c and TNF-α and increased adiponectin, PPAR-α, and AMPK phosphorylation in the liver	(Qiu et al., 2015)
Nitraria retusa (Forssk.) Asch. ethanolic extract	db/db mice model	↓Increases in body and fat mass weight, ↓TG and LDL-c levels	↑Gene expression related to lipid homeostasis in liver, modulating the lipolysis-lipogenesis balance	(Zar Kalai et al., 2014)
14-Deoxyandrographolide	Ethanol-induced hepatosteatosis in rats	Alleviate hepatosteatosis	↑AMPK, ↓SREBP-1c, ACC, and FAS, ↑sirtuin I and depletion of malonyl-CoA, ↑fatty acid oxidation	(Mandal et al., 2014)
Total Alkaloids in Rubus aleaefolius Poir	Modified HFD-fed rats	↓TG, TC, and LDL-C levels and ↑HDL-C level	↓Expression of FAS, ACC, ↑carnitine palmitoyltransferase (CPT)	(Li Y. et al., 2014)
Lycium barbarum L. polysaccharide	HFD-fed mice	Improved body compositions and lipid metabolic profiles, ↓hepatic intracellular TG	↓SREBP-1c, ↑AMPK activation	(Li W. et al., 2014)
Salacia oblonga Wall. ex Wight & Arn. root	fructose-induced fatty liver in rats	Diminished fructose-induced fatty liver	↓SREBP-1/1c mRNA and nuclear protein	(Liu L. et al., 2013)
Chunggan extract (*Artemisia capillaries* Thunberg, *Trionyx sinensis* Wiegmann, *Raphanus sativus* Linne, *tractylodes macrocephala* Koidz, *Poria cocos* Wolf, *Alisma orientalis (Sam.)* Juzepczuk, *Atractylodes chinensis* Koidzumi, *Salvia miltiorrhiza* Bunge, *Polyporus umbellatus* Fries, *Poncirus trifoliate* Rafin, *Amomum villosum* Lour, *Glycyrrhiza uralensis* Fisch., *Aucklandia lappa* Decne.)	methionine- and choline-deficient (MCD) diet	↓TG, AST, ALT, ALP, and total bilirubin	Anti-oxidative stress	(Park et al., 2013)
Celastrus orbiculatus Thunb.	HFD-induced NAFLD in guinea pigs	↓TC, free cholesterol (FC), cholesterol ester (CE) and TG in liver	↑mRNA abundance of cholesterol 7 alpha-hydroxylase A1 (CYP7A1) and 3-hydroxy-3-methyl-glutaryl-CoA reductase (HMGCR).	(Zhang et al., 2013)
Oxymatrine	NAFLD rats fed with high fructose diet	↓Body weight gain, liver weight, liver index, dyslipidemia, and TG, ↓liver lipid accumulation.	↓ SREBF1 and ↑PPAR-α	(Shi et al., 2013)

(Continued)

TABLE 1 | Continued

Herbs or Natural products	Model	Effects	Mechanisms	References
Rhein	HFD-induced obese mice	↓Body weight, particularly body fat content, improved insulin resistance, and ↓circulating cholesterol levels, ↓TG, reversed hepatic steatosis, and normalized ALT	Mediated negative energy balance, metabolic regulatory pathways, and immunomodulatory activities involved in hepatic steatosis	(Sheng et al., 2011)
Osthol	Alcohol-induced fatty liver in mice	Inhibit alcohol-induced fatty liver	Anti-oxidation and suppression of TNF-α production	(Sun et al., 2009)

↑ means increase and up-regulate and ↓ means decrease and down-regulate.

lipogenesis *via* FXR-dependent pathway. It decreased hepatic levels of SREBP-1c, FAS, ACC1 and SCD1, and promoted lipid metabolism *via* inducing PPAR α, CPT1 α, ACADS, and LPL (Meng et al., 2017). In an apolipoprotein E-knockout mice model, Dansameum (*Salvia miltiorrhiza* root), a kind of Korean polyherbal medicine, reduced hepatic lipogenesis, and inflammation *via* regulating PPAR-γ, SREBP-1c, FAS, ACC1, and CD36 (Ahn et al., 2019).

Dangguiliuhuang Decoction, a TCM formula composed of *radix rehmanniae* (root of Rehmannia Glutinosa), *angelica* (*Angelica acutiloba* Siebold et Zucc.), *Coptis chinensis* Franch., *Radix Rehmanniae Praeparata* (Rehmannia root), *Astragalus propinquus* (the root of *astragalus membranaceus*), Chinese skullcap (*Scutellaria baicalensis*) and *Phellodendron amurense* (*Phellodendron chinense* Schneid.), is used for the treatment of autoimmune diseases and diabetes (Cao et al., 2017; Cao et al., 2018). In a study of ob/ob mice model, it normalized glucose and insulin level, diminished fat accumulation and lipogenesis, increased the expression of adiponectin, and promoted glucose uptake (Cao et al., 2017). It showed modulation abilities on inflammation and immune response. Dangguiliuhuang Decoction (composition as listed above) promoted the shift of pro-inflammatory to anti-inflammatory cytokines. Furthermore, it decreased T cells proliferation while increased regulatory T cells (Tregs) differentiation, reduced dendritic cells (DCs) maturation and secretion of IL-12p70 cytokine, decreased DCs-stimulated T cells proliferation, and promoted, the interaction of DCs with Tregs. In adipocytes and hepatocytes as well as DCs and T cells, Dangguiliuhuang Decoction treatment altered PI3K/Akt signaling pathway and increased PPAR-γ expression, indicating the ameliorated glucose and lipid metabolism (Cao et al., 2017).

MicroRNA (miR), a small non-coding RNA molecule, has been recently demonstrated to play a role in mediating the anti-hepatic steatosis effects of natural compounds derived from herbs. Berberine reduced steatosis in MIHA and HepG2 cells by mechanism associating with up-regulation of miR-373, which decreased its mRNA level target gene AKT serine/threonine kinase 1 (AKT1), resulting in the suppression of AKT-mTOR-S6K signaling pathway in hepatocytes (Cao et al., 2018). Genipin reduced HFD-induced hyperlipidemia and hepatic lipid accumulation in mice *via* increasing the expression levels of miR-142a-5p, which bound to 3'-untranslated region of SREBP-1c, thus leading to the inhibition of lipogenesis (Zhong et al., 2018).

Increasing Lipolysis

Lipolysis is the catabolic process of hydrolytic cleavage of ester bonds in TG, leading to the production of fatty acids and glycerol, which could be further utilized for β-oxidation and subsequent ATP generation (Lass et al., 2011). It predominantly occurs in adipose tissues, but also in the liver, with different physiological functions. Dietary fat is digested into the gut lymphatic system as chylomicrons, which arrives at the liver through the circulation and release NEFAs through lipolysis which mediated mainly by lipoprotein lipase (LPL) (Rui, 2014). Other lipolytic enzymes contributing to hepatic TG metabolism include adiponutrin/
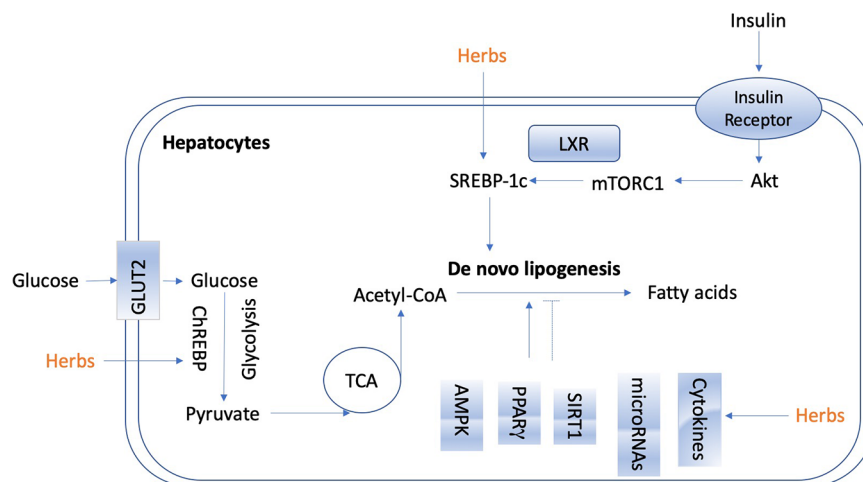
FIGURE 2 | The overview of lipogenesis in hepatocytes.

patatin-like phospholipase domain containing 3 (PNPLA3) (Kumashiro et al., 2013), lysosomal acid lipase (LAL) (Quiroga and Lehner, 2018), arylacetamide deacetylase (Lo et al., 2010), hepatic lipase (HL)(Chatterjee and Sparks, 2011) and some members of the carboxylesterase family. In adipose tissue, inhibition of lipolysis improves glucose metabolism and insulin sensitivity, whereas in liver tissue, increasing lipolysis facilitates the attenuation of hepatic steatosis.

As far from now, limited herbs were found to show regulatory effect on hepatic lipolysis. *Lavatera critica* (Cornish mallow), a green leafy vegetable, attenuated hepatic lipid accumulation induced by HFD *via* reversing lipolysis genes acetyl-CoA carboxylase (Veeramani et al., 2017). *Nitraria retusa* (Forssk.) Asch. ethanolic extract modulated the lipolysis-lipogenesis balance in the liver of db/db mice (Veeramani et al., 2017). Caffeic acid upregulated the phosphorylation of AMPK and its primary downstream targeting enzyme, acetyl-CoA carboxylase, to promote the lipolysis in HepG2 cells with oleic acid administration (Liao et al., 2014). *Polygonatum stenophyllum* (PS) Maxim. rhizome showed efficacy on menopausal obesity by activating lipolysis-related genes including hormone-sensitive lipase (HSL) and adipose triglyceride lipase (ATGL) (Lee J. E. et al., 2016). Mulberry (Fructus Mori) water extracts promoted hepatic lipolysis and protected liver from steatosis in obesity (Peng et al., 2011). More herbs or natural compounds exerted effects on lipolysis in adipose tissues and attenuated hepatic steatosis *via* liver-adipose tissue crosstalk, which are not going to be discussed in detail here.

Induction of Lipophagy

In addition to lipolysis, lipid breakdown can also be accessed *via* lipophagy, a special kind of autophagy to degrade lipid droplets (Singh and Cuervo, 2012; Kounakis et al., 2019). It is a process that the double membrane wraps lipid droplets and sends them to lysosomes to form autolysosomes for degradation of excessive lipid droplets deposited in cells (Liu and Czaja, 2013; Ward et al., 2016). It plays a vital role in maintaining the cellular steady state.

During the early stage of NAFLD, lipophagy is activated in response to acute increase in lipid availability, thus reduce lipid deposition (Czaja, 2016; Ipsen et al., 2018). However, in the condition of such as long-lasting high fat dieting, hepatic lipophagy is impaired when lipids are sustained overwhelmed (Kwanten et al., 2014; Czaja, 2016; Ipsen et al., 2018). Growing evidence raised from recent studies indicate that lipophagy is partially suppressed in patients and animal models of NAFLD and restoring lipophagy may slow the progression of hepatic steatosis. Lipophagy could be activated by various approaches, such as mTOR and AMPK-targeting agents. Glycycoumarin, a representative of coumarin compounds isolated from licorice, mitigated hepatic steatosis partially through AMPK-mediated lipophagy in a murine model of NAFLD induced by MCD diet (Zhang et al., 2016). Dioscin is a saponin extracted and isolated from *Polygonatum zanlanscianense* Pamp. It has been proposed as a healthcare product against hepatic fibrosis with remarkable ability to inhibit the expression of p-mTOR/mTOR level and sequentially promote autophagy (Xu et al., 2017). In another study, Bergamot polyphenol fraction prevents NAFLD *via* stimulation of lipophagy in cafeteria dietinduced rat model of metabolic syndrome. The increased levels of LC3 and Beclin 1, and concomitant reduction of SQSTM1/p62 proved the promoted lipophagy with the treatment of Bergamot polyphenol fraction (Parafati et al., 2015). Increasing number of herbs or natural products have been demonstrated to exert significant effects on regulating lipophagy in the liver. Current understanding of mechanisms associated with autophagy/lipophagy of herbal medicines and natural products in preventing and treating NAFLD has been well reviewed in Zhang et al. (2018), which could be referred for further reading.

In alcoholic liver diseases (ALD), upon acute consumption of alcohol, lipophagy is activated in hepatocytes, serving as a defensive mechanism against injury to steatosis (Yan et al., 2019). However, it is impaired by chronic alcohol exposure, which is likely due to the activation of mTOR signaling and decreased lysosomal biogenesis in hepatocytes (Kounakis et al., 2019; Yang L. et al., 2019). There are

TABLE 2 | Medicinal herbs and isolated natural compounds with the effect of hepatic lipogenesis reduction.

Herbs or compounds	Model	Effect	Mechanism	References
Dansameum (*Salvia miltiorrhiza* root)	Apolipoprotein E-Knockout mice	Reduced hepatic lipogenesis and inflammation	Regulating LXR-α, PPAR-γ, SREBP-1, FAS, ACC1, and CD36	(Ahn et al., 2019)
Alisol A	HFD-induced obese mice	Reduced hepatic steatosis and improved liver function	AMPK/ACC/SREBP-1c pathway	(Ho et al., 2019)
Ling-gui-zhu-gan decoction (*Poria cocos, Ramulus cinnamomi, Atractylodis macrocephalae Rhizoma* and *Radix glycyrrhizae*)	HFD-fed rats	Reduced hepatic glycogen	Inhibited the activity of ACC, SREBP-1c and HMGCR, *via* inhibiting PPP1R3C targeting pathways	(Dang et al., 2019)
Salvianolic acids	Ovariectomized rats	Reduced body weight gain and attenuated	Blocking STAT-3/SREBP1 signaling	(Dang et al., 2019)
Gyeongshingangjeehwan 18 (*Laminaria japonica, Rheum palmatum*, and *Ephedra sinica*)	HFD-induced obese mice	Attenuated visceral obesity and NAFLD	Down-regulated lipogenesis-related genes	(Lim et al., 2018)
Cordycepin	Oleic acid-induced mouse FL83B hepatocytes	Attenuated lipid accumulation	Activating AMPK and regulating mitochondrial function	(Uen et al., 2018)
Oxyresveratrol	HFD-fed mice	Ameliorated NAFLD	AMPK/SREBP-1c pathway	(Lee et al., 2018)
Berberine	MIHA and HepG2 cells	Reduced hepatosteatosis	Up-regulation of miR-373 decreased mRNA level target gene AKT1, leading to inhibition of AKT-mTOR-S6K signaling pathway in hepatocytes	(Li C. H. et al., 2018)
Genipin	HFD-fed mice	Reduced HFD-induced hyperlipidemia and hepatic lipid accumulation	Increased the expression levels of miR-142a-5p, which bound to 3 untranslated region of SREBP-1c	(Zhong et al., 2018)
Gangjihwan (*Ephedra intermedia* Schrenk & C.A.Mey., *Lithospermum erythrorhizon* Siebold & Zucc., and *Rheum palmatum* L.)	HFD-induced obese mice	Inhibited fat accumulation	Modulation of lipogenic transcription factors SREBP-1c, PPAR-γ and ChREBP-α	(Jang et al., 2018)
Gangjihwan (*Ephedra intermedia* Schrenk & C.A.Mey., *Lithospermum erythrorhizon* Siebold & Zucc., and *Rheum palmatum* L.)	HFD-fed C57BL/6 J mice and HepG2 cells	Anti-obesity and anti-nonalcoholic steatohepatosis	Increased mRNA levels of fatty acid oxidation genes and decreased mRNA levels of genes for lipogenesis	(Roh et al., 2017)
Dangguiliuhuang Decoction (root of Rehmannia Glutinosa, *Angelica acutiloba* Siebold et Zucc., *Coptis chinensis* Franch., *Radix Rehmanniae Praeparata, Astragalus propinquus, Scutellaria baicalensis,* and *Phellodendron chinense* Schneid.)	ob/ob mice	Normalized glucose and insulin level, increased the expression of adiponectin, diminished fat accumulation and lipogenesis, and promoted glucose uptake	↓T cells, ↑ Tregs differentiation, ↓DCs maturation, ↓ DCs-stimulated T cells proliferation and secretion of IL-12p70 cytokine, promoted the interaction of DCs with Tregs, changed PI3K/Akt signaling pathway and↑ PPAR-γ.	(Cao et al., 2017)
Glycycoumarin	MCD diet mice	Prevented hepatic steatosis	Activation of AMPK signaling pathway	(Zhang et al., 2016)
Gambigyeongsinhwan (Curcuma longa, Alnus japonica, and Massa Medicata Fermentata)	Otsuka Long-Evans Tokushima fatty rats and HepG2 cells	Suppressed hepatic steatosis and obesity-related hepatic inflammation	↓mRNA levels of FAS, ACC1, ChREBP alpha, and SREBP-1c	(Yoon et al., 2017)
Alisol B 23-acetate	MCD diet-fed mice	↓ALT, AST, TG	FXR-dependent, ↓hepatic lipogenesis through decreasing hepatic levels of SREBP-1c, FAS, ACC1 and SCD1 and ↑lipid metabolism *via* inducing PPAR α, CPT1 α, ACADS and LPL	(Meng et al., 2017)
Herbal Formula HT048 (*Crataegus pinnatifida* leaf and *Citrus unshiu* peel extracts)	HFD-fed obese rats	Decreased obesity and insulin resistance	↓Genes involved in lipogenesis	(Lee Y. H. et al., 2016)
Jatrorrhizine hydrochloride	HFD-induced obesity mouse model	Attenuated hyperlipidemia	↓ SREBP-1c and FAS, and induced PPAR- and CPT1A	(Yang et al., 2016)
Puerarin	Oleic acid (OA)-treated HepG2 cells	Ameliorated hepatic steatosis	↑PPAR-α and AMPK signaling pathways, ↓SREBP-1 and FAS expression	(Kang et al., 2015)
Protopanaxatriol	HFD-induced obesity (DIO) mice	Alleviated steatosis	Inhibition of PPAR-γ activity	(Zhang et al., 2014)
Magnolia officinalis Rehder & E.H.Wilson	HepG2 cells and mouse	Attenuated TG biosynthesis	Inhibition of SREBP-1c *via* AMPK phosphorylation	(Seo et al., 2014)

(Continued)

TABLE 2 | Continued

Herbs or compounds	Model	Effect	Mechanism	References
	normal FL83B hepatocytes			
Lycium barbarum polysaccharide	HFD-fed mice	Attenuate liver steatosis	↓SREBP-1c expression *via* AMPK activation	(Li W. et al., 2014)
Houttuynia cordata Thunb.	HepG2	Attenuates Lipid Accumulation	AMPK signaling	(Kang and Koppula, 2014)
Berberine metabolites	HepG2	TG-lowering effects	↓Lipogenesis gene expressions through activation of the AMPK signaling pathway	(Cao et al., 2013)
3-Caffeoyl, 4-dihydrocaffeoylquinic acid from *Salicornia herbacea Salicornia europaea* L.	HepG2	Attenuated high glucose-induced hepatic lipogenesis	Prevented lipid accumulation by blocking the expression of SREBP-1c and FAS through LKB1/SIRT1 and AMPK activation	(Pil Hwang et al., 2013)
Fructus Xanthii (*Xanthium strumarium*)	HFD-fed rats	Attenuated hepatic steatosis	↓The expression of lipogenic genes	(Li et al., 2013)

↑ means increase and up-regulate and ↓ means decrease and down-regulate.

growing number of herbs and natural products have been found to protect liver from injury induced by alcohol by mechanism of lipophagy stimulation. Corosolic acid, a compound derived from the leaves of *Langertroemia speciosa* L Pers., protected the liver from alcoholic-induced liver injury partially *via* restoring hepatic lipophagy due to mTORC1 suppression after AMPK activation (Guo et al., 2016). Another natural compound, quercitin, which is extensively found in many fruits and herbal plants, remarkably reversed the alcohol-induced blockade of TFEB nuclear localization, *via* restoring lysosome function and autophagic flux in livers of ethanol-fed C57BL6 mice (Li et al., 2019). Salvianolic acid A, a phenolic carboxylic acid extracted from *Salvia miltiorrhiza Bunge*, reduced hepatic steatosis induced by alcohol administration in rats. The action mechanism is attributed to enhanced autophagosome-lysosome fusion after restoring lysosomal cathepsin activities (Shi et al., 2018).

As a matter of fact, the field of lipophagy in liver diseases has yet to be fully developed. Its pathological role in different stages and circumstances of various liver disorders still needs to be revealed. Nevertheless, current studies concerning lipophagy have already provided new insights on lipid metabolism and energy homeostasis in the liver. It represents a promising path forward to the therapeutic of hepatic steatosis. Pharmaceutic agents including herbs, natural products or compounds targeting lipophagy in the liver deserve to be further investigated in future basic and clinic researches.

Enhancing Fatty Acid β-Oxidation

Fatty acid could be oxidized by β-oxidation, α-oxidation, omega-oxidation, and peroxisomal oxidation, among which β-oxidation is the major type occurring in the mitochondria matrix (Wanders et al., 2015). In β-oxidation, two carbon subunits from fatty acids are removed repeatedly until the fatty acid carbon chain is fully degraded to form acetyl-CoA, which is further oxidized to carbon dioxide and H_2O in the tricarboxylic acid cycle (TCA) (Canbay et al., 2007). β-oxidation plays a vital role in hepatic lipid consumption. A variety of proteins and enzymes are involved in the process of mitochondrial fatty acid β-oxidation, such as plasma membrane fatty acid binding protein (FABPpm) (Furuhashi and Hotamisligil, 2008), fatty acid transport protein (FATP) (Ouali et al., 2000), carnitine acylcarnitine translocase (CACT) (Pierre et al., 2007), carnitine palmitoyltransferases

1 and 2 (CPT1/2), etc. (Bonnefont et al., 2004; Houten and Wanders, 2010). More importantly, mitochondrial fatty acid β-oxidation is regulated by both transcriptional and posttranscriptional mechanisms. Peroxisome proliferator-activated receptors (PPARs) are activated by fatty acids, having specific roles in physiology of different tissues (Yu et al., 2003; Lamichane et al., 2018). In liver, PPARα controls many genes involved in mitochondrial fatty acid β-oxidation (Lamichane et al., 2018). In terms of posttranscriptional mechanism, the inhibition of CPT1 by malonyl-CoA is a vital regulatory step. The levels of malonyl-CoA in hepatocytes are regulated *via* degradation induced by malonyl-CoA decarboxylase and *via* production by acetyl-CoA carboxylase (ACC)(Park et al., 2002). PPARs-mediated activation persuades transcription of malonyl-CoA decarboxylase, and phosphorylated AMPK inactivated ACC (Saha and Ruderman, 2003). They stimulate mitochondrial fatty acid β-oxidation by reducing malonyl-CoA levels. Additionally, peroxisome proliferator activated receptor gamma coactivator 1-alpha (PGC-1α) has also been regarded as a factor of posttranscriptional regulation of β-oxidation (Fernandez-Marcos and Auwerx, 2011). The activation of PGC-1α is mediated by AMPK *via* SIRT1-mediated deacetylation (Canto and Auwerx, 2009).

Many herbs and active compounds protect liver from steatosis *via* regulation of fatty acid β-oxidation. Herbacetin is a dietary flavonoid with plenty of pharmacological activities. Its anti-hyperglycemic and anti-hyperlipidemic properties was associated with up-regulation of CPT to enhanced β-oxidation and hepatic lipid metabolism (Veeramani et al., 2018). Acteoside, a major compound isolated from leaves of *Aloysia citriodora* Palau (syn. *Lippia triphylla*), promoted lipolysis and fatty acid oxidation by enhancing mRNA expression level of adipose triglyceride lipase (ATGL) and CPT-1, and thus improved hepatic lipid metabolism (Zhang Y. et al., 2019). Cordycepin enhanced β-oxidation and suppressed lipid accumulation *via* regulating AMPK pathway and mitochondrial fusion in hepatocytes (Uen et al., 2018).

In China, the modified Longdan Xiegan Tang (mLXT, composed of Scutellaria baicalnsis Geprgi, Gardenia jasminoides, Adenophora capillaris, Akebia quinate, Plantago asiatica, Angelica sinensis, Rehmannia glutinosa, Alisma plantago-aquatica, Bupleurum gibraltaicum, and Glycyrrhiza uralensis) has been used clinically for various liver diseases such as NAFLD. It was

found to activate hepatic expression of PPAR α and its target genes associated with fatty acid β-oxidation (Ren et al., 2019). Babaodan, a TCM, up-regulated the expression of CPT-1 and PPAR α in liver of HFD-fed mice with NAFLD, leading to the enhanced β-oxidation (Sheng et al., 2019). Rosa rugosa Thunb., another TCM, is used for treatment of cardiovascular diseases and diabetes, hypertension, hyperlipidemia, and inflammation. R. rugosa flavonoids, the major components in R. rugosa Thunb., were observed to up-regulate the mRNA expression of PPAR α and its downstream gene of acyl-coenzyme A oxidas X (ACOX) in a mouse model of hypertriglyceridemia (Baiyisaiti et al., 2019). Thereby, R. rugosa flavonoids could reduce TG in hepatocytes via rising β-oxidation. Gynura procumbens Merr., one of precious medicinal herbs of Asterceaes, up-regulated the mRNA expression of genes involved in β-oxidation, including PPAR α, CPT1 α, ACOX, fatty acid-binding proteins 5 (FABP5), stearoyl-coenzyme A desaturase-1 (SCD-1), glycerol-3-phosphate acyltransferase (mGPAT), microsomal triglyceride transfer protein (MTTP), to increase β-oxidation and efflux of fatty acids in liver of mice fed with MCD diet, and consequently decreased hepatic lipid accumulation (Liu Y. Y. et al., 2019). An herbal formula Gyeongshingangjeehwan 18 (GGEx18), composed of Laminaria japonica Aresch (Laminariaceae), Rheum palmatum L. (Polygonaceae) and Ephedra sinica Stapf (Ephedraceae), has traditionally been described to against obesity and related metabolic disease such as dyslipidemia. In HFD-fed mice receiving GGEx18, genes related to hepatic fatty acid β-oxidation was higher compared to mice fed with only HFD (Lim et al., 2018).

Evidence from recent studies has also indicated that some natural compounds promoted fatty acid oxidation by regulating the AMPK/PGC-1α signaling pathway. Yellow pigments, monascin, and ankaflavin, as secondary metabolites derived from monascus-fermented products, could reduce fatty acid accumulation partly mediated by the AMPK signaling activation and enhancement of β-oxidation by PGC-1α (Hsu et al., 2014). Myricetin, a natural flavonol with many biological activities, decreased PGC-1α acetylation through SIRT1 activation, and thus enhanced mitochondrial activity, suggesting its potential role in regulating hepatic lipid metabolism (Jung et al., 2017).

CLINICAL TRIALS

Given to the encouraging effects of herbal medicines on liver diseases, plenty of clinical trials have been extensively performed. The potential therapeutic benefits of herbal medicines in patients with NAFLD have been reviewed in several papers in recent years (Xiao et al., 2013; Bedi et al., 2016; Perumpail et al., 2018). In present review, we focused on the efficacy of herbal medicines to mediate lipid metabolism and attenuate hepatic steatosis.

Dava Al-Balgham, as one of the traditional medicine products composed of Nigella sativa L., Pistacia lentiscus L., Zataria multiflora Boiss. (ZM), and Trachyspermum ammi, was tested for its effect on NAFLD by a randomized, double-blinded, placebo-controlled trial with 76 NAFLD patients. Placebo or Dava Al-Balgham were consumed with each meal for three months. The

results showed that Dava Al-Balgham could cause weight loss and have anti-hypolipidemic effect (Hormati et al., 2019).

The effect of Z. multiflora supplementation on NAFLD was studied by a randomized double-blind placebo-controlled clinical trial. Total 85 patients with NAFLD were treated with ZM powder (700 mg) or placebo twice daily for 3 months. However, no significant difference between two ZM-treated groups and placebo groups regarding ALT, TNF-α, grade of fatty liver in ultrasonography, lipid profiles, and high sensitive C-reactive protein (hs-CRP), while it could improve insulin resistance in patients with NAFLD. Further studies with larger sample size and longer duration are recommended (Zamani et al., 2018).

A 12-weeks randomized, controlled, double-blind trial included with was 44 NAFLD patients, was performed to evaluate the efficacy of Capparis spinosa L. on disease regression of NAFLD. Patients are randomly divided into control (n=22) or caper (n=22) group. The caper group was treated with 40-50 g caper fruit pickles with meals every day. Results obtained after treatment of 12 weeks indicated that the grade of fatty liver and serum lipoproteins were improved by C. spinosa administration (Khavasi et al., 2017).

We further checked the registered clinical trials about testing effects of the herbs and natural products on fatty liver via the website of www.clinialtrial.gov. The intensively studied herbs and derived compounds are resveratrol, ginseng, and ginger, which were discussed in detail in following. Other herbs and some natural products that are undergoing or were performed clinical trials on fatty liver diseases are listed in **Table 3**.

Resveratrol is a stilbenoid and a phytoalexin generated by several plants, such as red grapes in response to stimuli (Hasan and Bae, 2017). It is an activator of AMPK and SIRT1, and thus has a critical role in promoting fat breakdown and removal from the liver, preventing liver damage and inhibiting the progression of NAFLD (Shang et al., 2008; Charytoniuk et al., 2017; Theodotou et al., 2019). Resveratrol has been involved in three trials (NCT01446276; NCT01464801; NCT02030977) included patients of fatty liver, NAFLD, and obesity.

Another herb, ginseng, has been traditionally used for more than 2,000 years with various biological effects. A great deal of preclinical studies have demonstrated the protective effects of ginseng on liver diseases, including ALD and NAFLD. Korean Red Ginseng (Panax ginseng) (Park et al., 2017) enhanced the decreased phosphorylation of AMPK induced by ethanol consumption. Notably, it reduced the accumulation of fat in hepatocytes caused by ethanol via regulation of SREBP-1, SIRT-1 and PPAR-α (Huu Tung et al., 2012; Park et al., 2017). Clinical trial (NCT0394512) has been performed to study the effect of red ginseng on liver dysfunction. Fermented ginseng powder has also been tested to study its efficacy on NAFLD (NCT03260543).

Ginger is the root of Zingiber officinale Roscoe and is one of the most used spices in many countries (Huu Tung et al., 2012). It contains active compounds, such as shogaol, gingerol, zingerone, and β-bisabolene. It has been shown that ginger can reduce insulin resistance and serum TG level in patients with Type II diabetes and hyperlipidemia (Arablou et al., 2014). In a randomized, double-blind, placebo-controlled clinical trial with 44 patients of NAFLD, ginger supplementation significantly

TABLE 3 | Registered clinical trials of herbs and natural products on fatty liver diseases (Referred to http://www.ClinicalTrials.gov website).

NCT number	Status	Conditions	Interventions	Outcome Measures	Population	Dates
NCT02030977	Completed	NAFLD	Resveratrol	ALT	Enrollment: 50 Age: 18 Years to 80 Years (Adult, Older Adult) Sex: All	Study Start: June 2012 Study Completion: March 2013
NCT01464801	Completed	Fatty liver	Resveratrol	• Change in hepatic steatosis and inflammation • Assessment of tolerability and side-effects	Enrollment: 28 Age: 18 Years to 70 Years (Adult, Older Adult) Sex: All	Study Start: September 2011 Study Completion: June 2015
NCT01446276	Completed	Obesity • NAFLD	Resveratrol	• Hepatic VLDL-TG secretion and peripheral VLDL-TG clearance • Basal and insulin stimulated free fatty acid (FFA) and glucose turnover • VLDL-TG oxidation • Body composition (fat mass, fat-free mass, percent fat, visceral fat mass) • lipoprotein lipase activity and fat cell size in abdominal and femoral adipose tissue biopsy • Baseline data	Enrollment: 26 Age: 25 Years to 65 Years (Adult, Older Adult) Sex: Male	Study Start: November 2011 Study Completion: April 2014
NCT04130321	Not yet recruiting	• Overweight • Microtia • Endotoxemia • Metabolic Syndrome • Insulin Resistance • NAFLD	Camu camu (Myrciaria dubia)	• Change in Gut Microbiota Composition and Diversity • Change in fat accumulation in the liver • Change in Endotoxemia • Change in Intestinal permeability • Change in Inflammation state of the tissue • Change in Short chain and branched chain fatty acids in the feces • Change in gut health • Change in stool consistency • Change in Glucose homeostasis • Change in Lipid profile and 8 more	Enrollment: 32 Age: 18 Years to 75 Years (Adult, Older Adult) Sex: All	Study Start: January 6, 2020 Study Completion: June 30, 2022
NCT0394512	Completed	Liver Dysfunction	Red ginseng	Liver enzyme	Enrollment: 94 Age: 37 Years to 63 Years (Adult) Sex: All	Study Start: January 1, 2018 Study Completion: December 31, 2018
NCT03260543	Completed	NAFLD	Fermented ginseng powder	Changes of ALT • Changes of Liver function index • Changes of fatty liver grade • Changes of lipid metabolism index • Changes of total antioxidant capacity • Changes of imflammation index • Changes of Multidimensional Fatigue Scale	Enrollment: 90 Age: 19 Years to 70 Years (Adult, Older Adult) Sex: All	Study Start: July 2016 Study Completion: August 2017
NCT04049396	Completed	NAFLD	Berberine	ALT; AST; ALP; fasting blood sugar; total cholesterol; LDL-Cholesterol; HDL -Cholesterol; TG	Enrollment: 50 Age: 18 Years to 65 Years (Adult, Older Adult) Sex: All	Study Start: October 1, 2018 Study Completion: June 15, 2019
NCT02535195	Completed	• NAFLD	Ginger	• Serum levels of the ALT liver enzyme • Serum levels of the AST liver enzyme • controlled attenuation parameter(CAP) score	Enrollment: 60 Age: 18 Years to 70 Years (Adult, Older Adult) Sex: All	Study Start: March 2013 Study Completion: August 2015

(Continued)

TABLE 3 | Continued

NCT number	Status	Conditions	Interventions	Outcome Measures	Population	Dates
NCT02289235	Enrolling by invitation	• Fatty Liver • Diabetes Mellitus, Type 2	Ginger	• Change in ALT level • Change in AST level • Change in score of fatty liver in fibroscan • Change in Gama GT (#- glutamyl transpeptidase) levels • Number of patients with adverse events	Enrollment: 90 Age: 20 Years to 65 Years (Adult, Older Adult) Sex: All	Study Start: November 1, 2018 Study Completion: December 1, 2019
NCT03864783	Recruiting	• NAFLD • Insulin Resistance • Glucose Tolerance Impaired • Obesity, Abdominal	Curcumin (Meriva®)	• Curcumin's effect on steatosis • Total amino acids in plasma • Total amino acids in plasma • Curcumin's effect on plasma concentration of urea • Curcumin's effect on urin concentration of urea • Curcumin's effect on serum concentration of inflammatory marker interleukin (IL)-1b • Curcumin's effect on serum concentration of inflammatory marker IL-2 • Curcumin's effect on serum concentration of inflammatory marker IL-6 • Curcumin's effect on serum concentration of inflammatory marker IL-10 • Curcumin's effect on serumconcentration of inflammatory marker tumor necrosis factor (TNF)- alpha • Curcumin's effect on plasma concentration of adipokines • and 34 more	Enrollment: 40 Age: 20 Years and older (Adult, Older Adult) Sex: Male	Study Start: March 5, 2019 Study Completion: October 2020
NCT03073343	Recruiting	Non-Alcoholic Fatty Liver Disease • Non Insulin Dependent Diabetes • ALT	Betaine	• ALT	Enrollment: 48 Age: 18 Years to 75 Years (Adult, Older Adult) Sex: All	Study Start: November 12, 2013 Study Completion: June 30, 2020
NCT02973295	Recruiting	NAFLD	Silymarin	• Change (Reduction) • of parameters of liver steatosis defined by CAP (Controlled Attenuation Parameter) and liver fibrosis defined by • LSM (liver stiffness measurements) during the 6 months period • Change in liver enzymes in period of 6 months • Change in insulin resistance in period of 6 months • Change in lipidogram in period of 6 months	Enrollment: 400 Age: 18 Years to 70 Years (Adult, Older Adult) Sex: All	Study Start: September 20, 2019 Study Completion: June 30, 2021
NCT02929901	Completed	Type 2 Diabetes Nonalcoholic Fatty Liver	Caffeine and chlorogenic acid	• Hepatic steatosis • Glucose • Glycated hemoglobin (HBA1C) • ALT • AST • hs- CRP) • gut microbiota	Enrollment: 200 Age: 30 Years to 65 Years (Adult, Older Adult) Sex: All	Study Start: December 2016 Study Completion: March 2019
NCT02908152	Unknown status	• Type 2 Diabetes • Nonalcoholic Fatty Liver	Curcumin	• Hepatic steatosis • Glucose • HBA1C • ALT • AST	Enrollment: 50 Age: 30 Years to 65 Years (Adult, Older Adult) Sex: All	Study Start: February 2017 Study Completion: October 2017
NCT02006498	Completed	NAFLD	Sillymarin	• To assess the efficacy • of Silymarin as defined by an improvement in non-alcoholic steatosis (NAS) activity score by at least 30% from baseline compared to placebo • To assess the safety and adverse event profile of Silymarin compared to placebo	Enrollment: 99 Age: 18 Years and older (Adult, Older Adult) Sex: All	Study Start: June 2012 Study Completion: December 2015

(Continued)

TABLE 3 | Continued

NCT number	Status	Conditions	Interventions	Outcome Measures	Population	Dates
NCT01940263	Completed	NAFLD	Anthocyanin	• Biomarkers related to oxidative stress • Biomarkers related to inflammation	Enrollment: 63 Age: 18 Years to 65 Years (Adult, Older Adult) Sex: All	Study Start: June 2013 Study Completion: June 2014
NCT02307344	Unknown status	• Nonalcoholic Steatohepatitis • Liver Steatosis	Nigella sativa L.	• Effect of Nigella Sativa on Liver Triglyceride Concentration • Effect of Nigella Sativa on Improvement in NASH Activity Index • Effect of Nigella Sativa on Fibrosis Staging	Enrollment: 100 Age: 18 Years and older (Adult, Older Adult) Sex: All	Study Start: January 2015 Study Completion: January 2017
NCT02303314	Completed	NAFLD	Trigonella Foenum-graecum Seed Extract	Liver stiffness change	Enrollment: 35 Age: 18 Years to 70 Years (Adult, Older Adult) Sex: All	Study Start: November 2014 Study Completion: September 2017
NCT01707914	Completed	NAFLD	Chinese bayberry juice (Myrica rubra)	Plasma lipids profile	Enrollment: 44 Age: 18 Years to 25 Years (Adult) Sex: All	Study Start: June 2012
NCT01677325	Completed	NAFLD	Drug: Chinese herb (YiQiSanJu) (Angelica sinensis, Rehmannia, Cinnamomum cassia, Glycyrrhiza uralensis, Eucommia ulmoides, Achyranthes bidentate, Lycium chinense)	• The CT ratio of liver/spleen • BMI(Body Mass Index) • liver function • lipid profile • NEFA • HOMA index • adiponectin • IL-6 • hs-CRP (C-reactive protein) • TNF-a • leptin	Enrollment: 40 Age: 18 Years to 65 Years (Adult, Older Adult) Sex: Male	Study Start: January 2007 Study Completion: January 2008
NCT01210989	Completed	NAFLD	Phyllanthus urinaria L.	• Histologic NAFLD activity score • ALT normalization • Metabolic endpoints • Changes in magnetic resonance spectroscopy • Liver stiffness measurement • Biomarkers of NASH and liver fibrosis	Enrollment: 60 Age: 18 Years to 70 Years (Adult, Older Adult) Sex: All	Study Start: May 2010 Study Completion: May 2012
NCT00816465	Completed	NAFLD	Hoodia gordonii (Masson) Sweet ex Decne.	• Decreased insulin resistance • Safety • Reduced hepatic injury • Reduced weight/BMI/abdominal circumference	Enrollment: 20 Age: 18 Years to 65 Years (Adult, Older Adult) Sex: All	Study Start: May 2009 Study Completion: August 2010

reduced the levels of ALT, inflammatory cytokines, γ-glutamyl transferase, as well as hepatic steatosis grade and the insulin resistance index in comparison to the control group. Another clinical trial of ginger supplement on fatty liver or Type 2 Diabetes Mellitus is still undergoing (NCT02289235).

META-ANALYSIS STUDIES

HuoXueHuaYu (HXHY), a TCM formula, has been widely used in clinic for patients with NAFLD. Cai et al. performed a meta-analysis of randomized controlled trial of HXHY in NAFLD. There are 13 studies involving 1429 patients which 654 patients receiving conventional treatment group and 775 patients belonged to HXHY group. HXHY showed better ability on lowing TC and TG levels than that of conversational treatment. HXHY might be an effective and safe therapy for NAFLD, and trials with rigorous design, multicenter, large-scale, and high-quality worldwide are still expected (Cai et al., 2019).

Erchen Decoction (ECD), a TCM formula, is often used in the therapy of various diseases. A meta-analysis of the efficacy of ECD for the treatment of NAFLD by PRISMA systematic review standard has been performed. Seven randomized controlled trial with a total of 1951 participants were included in this study. The analysis results showed that patients with ECD treatment showed an improved status compared to the conventional treatment. Longer follow-up periods and larger-scale randomized controlled trial are still required to evaluate the efficacy of ECD in NAFLD (Li et al., 2017).

The efficiency and safety of a famous TCM Danshen in the treatment of NAFLD has also been analyzed by a meta-analysis study. Eight randomized controlled trials with 800 patients of NAFLD were identified. The results indicated that Danshen had improved total effectiveness rate, lower level of TC, TG, LDL, ALT, and AST, suggesting that Danshen may have potential effects on NAFLD, while multicenter large-sample clinical trials are still expected to confirm the efficacy and safety of Danshen (Peng et al., 2016).

Another study performed by Narjes et al. on 2017 has evaluated the efficiency of all kinds of TCM on the treatment of NAFLD. Literature were searched on China National Knowledge and PubMed from 1995 to 2010. Total 5904 patients from 62 randomized controlled trials were included for meta-analysis. Results showed that TCM had a better effect on the normalization of ALT level and disappearance of radiological steatosis for the patients of NAFLD. Finally, authors concluded that TCM is of modest benefit to the therapy of NAFLD (Shi et al., 2012).

CONCLUSIONS AND PERSPECTIVES

Due to the positive efficacy and minimal side effects, herbal medicines have obtained increasing attention as alternative therapeutic agents for liver disorders and dyslipidemia. Increasing evidence from laboratory studies suggests that many herbs, natural products, and derived compounds could inhibit the progression of hepatic steatosis. A variety of mechanisms have been demonstrated to be implicated in preventing hepatic steatosis and modulating lipid metabolism by herbs, including reducing hepatocyte fatty acid uptake and trafficking, reducing hepatic *de novo* lipogenesis, increasing lipolysis, inducing lipophagy, enhancing fatty acid β-oxidation. In particular, SREBP-1c, PPARα, AMPK, and SIRT1 signaling pathways have been highlighted as crucial molecular targets of action mechanisms by which herbal medicines regulate hepatic lipid metabolism. Current clinical evidences and meta-analysis showing the positive impacts of herbal medicines on the hepatic lipid metabolism pathways are still not strong enough. Further multicenter large-sample randomized clinical trials are still required to confirm the efficacy and safety of herbal medicines on hepatic lipid metabolism. Herbs mix and single medical plants as well as their components have been widely applied in the treatment of NAFLD. We consider the main actor should be the active components. For both herbs mix and single medical plants, they are containing many compounds, which may act synergistically in ways to enhance the therapeutic effects. Identifying the active components in herbs is a crucial and significant subject for the development of TCM. Currently, network pharmacology-based strategy has been extensively used for the prediction of the active components from herbs. Network pharmacology is an approach based on systems biology, poly-pharmacology, and molecular networks, to analyze relationships between drugs and diseases in recent decade, which has attracted considerable attention among Chinese medicine researchers for its ability in predicting and illustrating interactive relationships between numerous components and targets of herbal medicines. Network-based pharmacological analysis is a desirable approach as well as a good tool of in silico prediction for investigating the mechanisms of action for herbs and formulae and their potential bioactive components at molecular and systematic levels, which renders more effective subsequent exploration with experimental approaches. With the promising and effective prediction, subsequently validation experiments in laboratory and bench would be performed to confirm their pivotal role. In conclusion, herbal medicines have the potency to be alternative and complementary medical therapies to current pharmaceuticals for the treatment of liver diseases with lipid metabolism disorder.

AUTHOR CONTRIBUTIONS

YF designed and conceived the study. SL and YF retrieved and analyzed the data, and drafted the manuscript. SL, YX, WG, FC, CZ, HT, and NW discussed and revised the manuscript. All authors confirmed final version of the manuscript.

FUNDING

REFERENCES

Ahn, S. H., Lee, K. P., Kim, K., Choi, J. Y., Park, S. Y., and Cheon, J. H. (2019). Dansameum regulates hepatic lipogenesis and inflammation *in vitro* and *in vivo*. *Food Sci. Biotechnol.* 28 (5), 1543–1551. doi: 10.1007/s10068-019-00579-8

Albhaisi, S., and Sanyal, A. (2018). Recent advances in understanding and managing non-alcoholic fatty liver disease. *F1000Res* 7. doi: 10.12688/f1000research.14421.1

Al-Dayyat, H. M., Rayyan, Y. M., and Tayyem, R. F. (2018). Non-alcoholic fatty liver disease and associated dietary and lifestyle risk factors. *Diabetes Metab. Syndr.* 12 (4), 569–575. doi: 10.1016/j.dsx.2018.03.016

Ansari, A., Bose, S., Patra, J. K., Shin, N. R., Lim, D. W., Kim, K. W., et al. (2018). A Controlled Fermented Samjunghwan Herbal Formula Ameliorates Non-alcoholic Hepatosteatosis in HepG2 Cells and OLETF Rats. *Front. Pharmacol.* 9, 596. doi: 10.3389/fphar.2018.00596

Arablou, T., Aryaeian, N., Valizadeh, M., Sharifi, F., Hosseini, A., and Djalali, M. (2014). The effect of ginger consumption on glycemic status, lipid profile and some inflammatory markers in patients with type 2 diabetes mellitus. *Int. J. Food Sci. Nutr.* 65 (4), 515–520. doi: 10.3109/09637486.2014.880671

Aronow, W. S. (2006). Management of hyperlipidemia with statins in the older patient. *Clin. Interv. Aging* 1 (4), 433–438. doi: 10.2147/ciia.2006.1.4.433

Ayuob, N. N., Abdel-Hamid, A., Helal, G. M. M., and Mubarak, W. A. (2019). Thymoquinone reverses nonalcoholic fatty liver disease (NAFLD) associated with experimental hypothyroidism. *Rom. J. Morphol. Embryol.* 60 (2), 479–486.

Baiyisaiti, A., Wang, Y., Zhang, X., Chen, W., and Qi, R. (2019). Rosa rugosa flavonoids exhibited PPARalpha agonist-like effects on genetic severe hypertriglyceridemia of mice. *J. Ethnopharmacol.* 240, 111952. doi: 10.1016/j.jep.2019.111952

Bedi, O., Bijjem, K. R. V., Kumar, P., and Gauttam, V. (2016). Herbal Induced Hepatoprotection and Hepatotoxicity: A Critical Review. *Indian J. Physiol. Pharmacol.* 60 (1), 6–21.

Bonnefont, J. P., Djouadi, F., Prip-Buus, C., Gobin, S., Munnich, A., and Bastin, J. (2004). Carnitine palmitoyltransferases 1 and 2: biochemical, molecular and medical aspects. *Mol. Aspects Med.* 25 (5-6), 495–520. doi: 10.1016/j.mam.2004.06.004

Cai, Y., Liang, Q., Chen, W., Chen, M., Chen, R., Zhang, Y., et al. (2019). Evaluation of HuoXueHuaYu therapy for nonalcoholic fatty liver disease: a systematic review and meta-analysis of randomized controlled trial. *BMC Complement Altern. Med.* 19 (1), 178. doi: 10.1186/s12906-019-2596-3

Canbay, A., Bechmann, L., and Gerken, G. (2007). Lipid metabolism in the liver. *Z. Gastroenterol.* 45 (1), 35–41. doi: 10.1055/s-2006-927368

Canto, C., and Auwerx, J. (2009). PGC-1alpha, SIRT1 and AMPK, an energy sensing network that controls energy expenditure. *Curr. Opin. Lipidol.* 20 (2), 98–105. doi: 10.1097/MOL.0b013e328328d0a4

Cao, S., Zhou, Y., Xu, P., Wang, Y., Yan, J., Bin, W., et al. (2013). Berberine metabolites exhibit triglyceride-lowering effects via activation of AMP-activated protein kinase in Hep G2 cells. *J. Ethnopharmacol.* 149 (2), 576–582. doi: 10.1016/j.jep.2013.07.025

Cao, H., Tuo, L., Tuo, Y., Xia, Z., Fu, R., Liu, Y., et al. (2017). Immune and Metabolic Regulation Mechanism of Dangguiliuhuang Decoction against Insulin Resistance and Hepatic Steatosis. *Front. Pharmacol.* 8, 445. doi: 10.3389/fphar.2017.00445

Cao, H., Li, S., Xie, R., Xu, N., Qian, Y., Chen, H., et al. (2018). Exploring the Mechanism of Dangguiliuhuang Decoction Against Hepatic Fibrosis by Network Pharmacology and Experimental Validation. *Front. Pharmacol.* 9, 187. doi: 10.3389/fphar.2018.00187

Chao, H. W., Chao, S. W., Lin, H., Ku, H. C., and Cheng, C. F. (2019). Homeostasis of Glucose and Lipid in Non-Alcoholic Fatty Liver Disease. *Int. J. Mol. Sci.* 20 (2). doi: 10.3390/ijms20020298

Charytoniuk, T., Drygalski, K., Konstantynowicz-Nowicka, K., Berk, K., and Chabowski, A. (2017). Alternative treatment methods attenuate the development of NAFLD: A review of resveratrol molecular mechanisms and clinical trials. *Nutrition* 34, 108–117. doi: 10.1016/j.nut.2016.09.001

Chatterjee, C., and Sparks, D. L. (2011). Hepatic lipase, high density lipoproteins, and hypertriglyceridemia. *Am. J. Pathol.* 178 (4), 1429–1433. doi: 10.1016/j.ajpath.2010.12.050

Choi, J. Y., Kwon, E. Y., and Choi, M. S. (2019). Elucidation of the Metabolic and Transcriptional Responses of an Oriental Herbal Medicine, Bangpungtongseongsan, to Nonalcoholic Fatty Liver Disease in Diet-Induced Obese Mice. *J. Med. Food* 22 (9), 928–936. doi: 10.1089/jmf.2018.4383

Cui, Y., Chang, R., Zhang, T., Zhou, X., Wang, Q., Gao, H., et al. (2019). Chinese Herbal Formula (CHF03) Attenuates Non-Alcoholic Fatty Liver Disease (NAFLD) Through Inhibiting Lipogenesis and Anti-Oxidation Mechanisms. *Front. Pharmacol.* 10, 1190. doi: 10.3389/fphar.2019.01190

Czaja, M. J. (2016). Function of Autophagy in Nonalcoholic Fatty Liver Disease. *Dig. Dis. Sci.* 61 (5), 1304–1313. doi: 10.1007/s10620-015-4025-x

Dang, Y., Hao, S., Zhou, W., Zhang, L., and Ji, G. (2019). The traditional Chinese formulae Ling-gui-zhu-gan decoction alleviated non-alcoholic fatty liver disease via inhibiting PPP1R3C mediated molecules. *BMC Complement Altern. Med.* 19 (1), 8. doi: 10.1186/s12906-018-2424-1

Dong, H., Lu, F. E., and Zhao, L. (2012). Chinese herbal medicine in the treatment of nonalcoholic fatty liver disease. *Chin. J. Integr. Med.* 18 (2), 152–160. doi: 10.1007/s11655-012-0993-2

Eissing, L., Scherer, T., Todter, K., Knippschild, U., Greve, J. W., Buurman, W. A., et al. (2013). De novo lipogenesis in human fat and liver is linked to ChREBP-beta and metabolic health. *Nat. Commun.* 4, 1528. doi: 10.1038/ncomms2537

Feng, Q., Liu, W., Baker, S. S., Li, H., Chen, C., Liu, Q., et al. (2017). Multi-targeting therapeutic mechanisms of the Chinese herbal medicine QHD in the treatment of non-alcoholic fatty liver disease. *Oncotarget* 8 (17), 27820–27838. doi: 10.18632/oncotarget.15482

Feng, W. W., Kuang, S. Y., Tu, C., Ma, Z. J., Pang, J. Y., Wang, Y. H., et al. (2018). Natural products berberine and curcumin exhibited better ameliorative effects on rats with non-alcohol fatty liver disease than lovastatin. *BioMed. Pharmacother.* 99, 325–333. doi: 10.1016/j.biopha.2018.01.071

Fernandez-Marcos, P. J., and Auwerx, J. (2011). Regulation of PGC-1alpha, a nodal regulator of mitochondrial biogenesis. *Am. J. Clin. Nutr.* 93 (4), 884S–8890.

Furuhashi, M., and Hotamisligil, G. S. (2008). Fatty acid-binding proteins: role in metabolic diseases and potential as drug targets. *Nat. Rev. Drug Discovery* 7 (6), 489–503. doi: 10.1038/nrd2589

Guo, X., Cui, R., Zhao, J., Mo, R., Peng, L., and Yan, M. (2016). Corosolic acid protects hepatocytes against ethanol-induced damage by modulating mitogen-activated protein kinases and activating autophagy. *Eur. J. Pharmacol.* 791, 578–588. doi: 10.1016/j.ejphar.2016.09.031

Guo, Y., Li, J. X., Mao, T. Y., Zhao, W. H., Liu, L. J., and Wang, Y. L. (2017). Targeting Sirt1 in a rat model of high-fat diet-induced non-alcoholic fatty liver disease: Comparison of Gegen Qinlian decoction and resveratrol. *Exp. Ther. Med.* 14 (5), 4279–4287. doi: 10.3892/etm.2017.5076

Hasan, M., and Bae, H. (2017). "An Overview of Stress-Induced Resveratrol Synthesis in Grapes: Perspectives for Resveratrol-Enriched Grape Products. *Molecules* 22 (2). doi: 10.3390/molecules22020294

Heeboll, S., Vilstrup, H., and Gronbaek, H. (2018). "[Treatment of non-alcoholic fatty liver disease]. *Ugeskr Laeger* 180 (31).

Ho, C., Gao, Y., Zheng, D., Liu, Y., Shan, S., Fang, B., et al. (2019). Alisol A attenuates high-fat-diet-induced obesity and metabolic disorders via the AMPK/ACC/SREBP-1c pathway. *J. Cell Mol. Med.* 23 (8), 5108–5118. doi: 10.1111/jcmm.14380

Hormati, A., Tooiserkany, F., Mohammadbeigi, A., Aliasl, F., and Dehnavi, H. M. (2019). Effect of an Herbal Product on the Serum Level of Liver Enzymes in Patients with Non-Alcoholic Fatty Liver Disease: A Randomized, Double-Blinded, Placebo-Controlled Trial. *Iranian Red Crescent Med. J.* 21 (7), 7. doi: 10.5812/ircmj.91024

Houten, S. M., and Wanders, R. J. (2010). A general introduction to the biochemistry of mitochondrial fatty acid beta-oxidation. *J. Inherit. Metab. Dis.* 33 (5), 469–477. doi: 10.1007/s10545-010-9061-2

Hsu, W. H., Chen, T. H., Lee, B. H., Hsu, Y. W., and Pan, T. M. (2014). Monascin and ankaflavin act as natural AMPK activators with PPARalpha agonist activity to down-regulate nonalcoholic steatohepatitis in high-fat diet-fed C57BL/6 mice. *Food Chem. Toxicol.* 64, 94–103. doi: 10.1016/j.fct.2013.11.015

Huang, L., Cheng, Y., Huang, K., Zhou, Y., Ma, Y., and Zhang, M. (2018). Ameliorative effect of Sedum sarmentosum Bunge extract on Tilapia fatty liver via the PPAR and P53 signaling pathway. *Sci. Rep.* 8 (1), 8456.

Huang, X., Chen, W., Yan, C., Yang, R., Chen, Q., Xu, H., et al. (2019). Gypenosides improve the intestinal microbiota of non-alcoholic fatty liver in mice and alleviate its progression. *BioMed. Pharmacother.* 118, 109258. doi: 10.1016/j.biopha.2019.109258

Huu Tung, N., Uto, T., Morinaga, O., Kim, Y. H., and Shoyama, Y. (2012). Pharmacological effects of ginseng on liver functions and diseases: a minireview. *Evid. Based Complement Alternat. Med.* 2012, 173297.

Ibrahim, S. H., Hirsova, P., Malhi, H., and Gores, G. J. (2016). Animal Models of Nonalcoholic Steatohepatitis: Eat, Delete, and Inflame. *Dig. Dis. Sci.* 61 (5), 1325–1336. doi: 10.1007/s10620-015-3977-1

Ipsen, D. H., Lykkesfeldt, J., and Tveden-Nyborg, P. (2018). Molecular mechanisms of hepatic lipid accumulation in non-alcoholic fatty liver disease. *Cell Mol. Life Sci.* 75 (18), 3313–3327. doi: 10.1007/s00018-018-2860-6

Issa, D., Patel, V., and Sanyal, A. J. (2018). Future therapy for non-alcoholic fatty liver disease. *Liver Int.* 38 Suppl 1, 56–63. doi: 10.1111/liv.13676

Jang, J., Jung, Y., Chae, S., Cho, S. H., Yoon, M., Yang, H., et al. (2018). Gangjihwan, a polyherbal composition, inhibits fat accumulation through the modulation of lipogenic transcription factors SREBP1C, PPARgamma and C/EBPalpha. *J. Ethnopharmacol.* 210, 10–22. doi: 10.1016/j.jep.2017.08.024

Jung, H. Y., Lee, D., Ryu, H. G., Choi, B. H., Go, Y., Lee, N., et al. (2017). Myricetin improves endurance capacity and mitochondrial density by activating SIRT1 and PGC-1alpha. *Sci. Rep.* 7 (1), 6237.

Kang, H., and Koppula, S. (2014). Houttuynia cordata attenuates lipid accumulation via activation of AMP-activated protein kinase signaling pathway in HepG2 cells. *Am. J. Chin. Med.* 42 (3), 651–664. doi: 10.1142/S0192415X14500426

Kang, O. H., Kim, S. B., Mun, S. H., Seo, Y. S., Hwang, H. C., Lee, Y. M., et al. (2015). Puerarin ameliorates hepatic steatosis by activating the PPARalpha and AMPK signaling pathways in hepatocytes. *Int. J. Mol. Med.* 35 (3), 803–809. doi: 10.3892/ijmm.2015.2074

Kawano, Y., and Cohen, D. E. (2013). Mechanisms of hepatic triglyceride accumulation in non-alcoholic fatty liver disease. *J. Gastroenterol.* 48 (4), 434–441. doi: 10.1007/s00535-013-0758-5

Khalil, M., Khalifeh, H., Baldini, F., Salis, A., Damonte, G., Daher, A., et al. (2019). Antisteatotic and antioxidant activities of Thymbra spicata L. extracts in hepatic and endothelial cells as in vitro models of non-alcoholic fatty liver disease. *J. Ethnopharmacol.* 239, 111919.

Khavasi, N., Somi, M. H., Khadem, E., Faramarzi, E., Ayati, M. H., Fazljou, S. M. B., et al. (2017). Effect of Daily Caper Fruit Pickle Consumption on Disease Regression in Patients with Non-Alcoholic Fatty Liver Disease: a Double-Blinded Randomized Clinical Trial. *Adv. Pharm. Bull.* 7 (4), 645–650. doi: 10.15171/apb.2017.077

Kounakis, K., Chaniotakis, M., Markaki, M., and Tavernarakis, N. (2019). Emerging Roles of Lipophagy in Health and Disease. *Front. Cell Dev. Biol.* 7, 185. doi: 10.3389/fcell.2019.00185

Kumashiro, N., Yoshimura, T., Cantley, J. L., Majumdar, S. K., Guebre-Egziabher, F., Kursawe, R., et al. (2013). Role of patatin-like phospholipase domain-containing 3 on lipid-induced hepatic steatosis and insulin resistance in rats. *Hepatology* 57 (5), 1763–1772. doi: 10.1002/hep.26170

Kwanten, W. J., Martinet, W., Michielsen, P. P., and Francque, S. M. (2014). Role of autophagy in the pathophysiology of nonalcoholic fatty liver disease: a controversial issue. *World J. Gastroenterol.* 20 (23), 7325–7338. doi: 10.3748/wjg.v20.i23.7325

Lamichane, S., Dahal Lamichane, B., and Kwon, S. M. (2018). Pivotal Roles of Peroxisome Proliferator-Activated Receptors (PPARs) and Their Signal Cascade for Cellular and Whole-Body Energy Homeostasis. *Int. J. Mol. Sci.* 19 (4). doi: 10.3390/ijms19040949

Lass, A., Zimmermann, R., Oberer, M., and Zechner, R. (2011). Lipolysis - a highly regulated multi-enzyme complex mediates the catabolism of cellular fat stores. *Prog. Lipid Res.* 50 (1), 14–27. doi: 10.1016/j.plipres.2010.10.004

Lee, J. E., Kim, E. J., Kim, M. H., Hong, J., and Yang, W. M. (2016). Polygonatum stenophyllum improves menopausal obesity via regulation of lipolysis-related enzymes. *J. Nat. Med.* 70 (4), 789–796. doi: 10.1007/s11418-016-1018-9

Lee, Y. H., Jin, B., Lee, S. H., Song, M., Bae, H., Min, B. J., et al. (2016). Herbal Formula HT048 Attenuates Diet-Induced Obesity by Improving Hepatic Lipid

Metabolism and Insulin Resistance in Obese Rats". *Molecules* 21 (11). doi: 10.3390/molecules21111424

Lee, J. H., Baek, S. Y., Jang, E. J., Ku, S. K., Kim, K. M., Ki, S. H., et al. (2018). Oxyresveratrol ameliorates nonalcoholic fatty liver disease by regulating hepatic lipogenesis and fatty acid oxidation through liver kinase B1 and AMP-activated protein kinase. *Chem. Biol. Interact.* 289, 68–74. doi: 10.1016/j.cbi.2018.04.023

Li, X., Li, Z., Xue, M., Ou, Z., Liu, M., Yang, M., et al. (2013). Fructus Xanthii attenuates hepatic steatosis in rats fed on high-fat diet. *PloS One* 8 (4), e61499. doi: 10.1371/journal.pone.0061499

Li, W., Li, Y., Wang, Q., and Yang, Y. (2014). Crude extracts from Lycium barbarum suppress SREBP-1c expression and prevent diet-induced fatty liver through AMPK activation. *BioMed. Res. Int.* 2014, 196198.

Li, Y., Zhao, J., Zheng, H., Zhong, X., Zhou, J., and Hong, Z. (2014). Treatment of Nonalcoholic Fatty Liver Disease with Total Alkaloids in Rubus aleaefolius Poir through Regulation of Fat Metabolism. *Evid. Based Complement Alternat. Med.* 2014, 768540. doi: 10.1155/2014/768540

Li, Z., Xu, J., Zheng, P., Xing, L., Shen, H., Yang, L., et al. (2015). Hawthorn leaf flavonoids alleviate nonalcoholic fatty liver disease by enhancing the adiponectin/AMPK pathway. *Int. J. Clin. Exp. Med.* 8 (10), 17295–17307.

Li, W. S., Wu, Y., Ge, W. Z., Fan, L., and Sun, W. (2017). A herbal formula Erchen decoction for non-alcoholic fatty liver disease: a systematic review and meta-analysis of randomized controlled trials. *Int. J. Clin. Exp. Med.* 10 (6), 9110–9116.

Li, C. H., Tang, S. C., Wong, C. H., Wang, Y., Jiang, J. D., and Chen, Y. (2018). Berberine induces miR-373 expression in hepatocytes to inactivate hepatic steatosis associated AKT-S6 kinase pathway. *Eur. J. Pharmacol.* 825, 107–118. doi: 10.1016/j.ejphar.2018.02.035

Li, Y. Y., Tang, D., Du, Y. L., Cao, C. Y., Nie, Y. Q., Cao, J., et al. (2018). Fatty liver mediated by peroxisome proliferator-activated receptor-alpha DNA methylation can be reversed by a methylation inhibitor and curcumin. *J. Dig. Dis.* 19 (7), 421–430. doi: 10.1111/1751-2980.12610

Li, Y. Y., Chen, M., Wang, J., Guo, X. P., Xiao, L., Liu, P. Y., et al. (2019). Quercetin ameliorates autophagy in alcohol liver disease associated with lysosome through mTOR-TFEB pathway. *J. Funct. Foods* 52, 177–185. doi: 10.1016/j.jff.2018.10.033

Liang, Z. E., Zhang, Y. P., Tang, K. R., Deng, Y. J., Liang, Y. Q., Liang, S., et al. (2019). Anti-inflammation effect via TLR4-mediated MyD88-dependent and -independent signalling pathways in non-alcoholic fatty liver disease rats: Chinese herb formula. *Int. J. Clin. Exp. Med.* 12 (3), 2265–2277.

Liao, C. C., Ou, T. T., Huang, H. P., and Wang, C. J. (2014). The inhibition of oleic acid induced hepatic lipogenesis and the promotion of lipolysis by caffeic acid via up-regulation of AMP-activated kinase. *J. Sci. Food Agric.* 94 (6), 1154–1162. doi: 10.1002/jsfa.6386

Lim, J., Lee, H., Ahn, J., Kim, J., Jang, J., Park, Y., et al. (2018). The polyherbal drug GGEx18 from Laminaria japonica, Rheum palmatum, and Ephedra sinica inhibits hepatic steatosis and fibroinflammtion in high-fat diet-induced obese mice. *J. Ethnopharmacol.* 225, 31–41. doi: 10.1016/j.jep.2018.06.034

Liu, K., and Czaja, M. J. (2013). Regulation of lipid stores and metabolism by lipophagy. *Cell Death Differ.* 20 (1), 3–11. doi: 10.1038/cdd.2012.63

Liu, L., Yang, M., Lin, X., Li, Y., Liu, C., Yang, Y., et al. (2013). Modulation of hepatic sterol regulatory element-binding protein-1c-mediated gene expression contributes to Salacia oblonga root-elicited improvement of fructose-induced fatty liver in rats. *J. Ethnopharmacol.* 150 (3), 1045–1052. doi: 10.1016/j.jep.2013.10.020

Liu, Z. L., Xie, L. Z., Zhu, J., Li, G. Q., Grant, S. J., and Liu, J. P. (2013). Herbal medicines for fatty liver diseases. *Cochrane Database Syst. Rev.* (8), CD009059. doi: 10.1002/14651858.CD009059.pub2

Liu, Q., Zhu, L., Cheng, C., Hu, Y. Y., and Feng, Q. (2017). Natural Active Compounds from Plant Food and Chinese Herbal Medicine for Nonalcoholic Fatty Liver Disease. *Curr. Pharm. Des.* 23 (34), 5136–5162.

Liu, X., Tong, W., Zhao, X., Zhang, H., Tang, Y., and Deng, X. (2017). Chinese herb extract improves liver steatosis by promoting the expression of high molecular weight adiponectin in NAFLD rats. *Mol. Med. Rep.* 16 (4), 5580–5586. doi: 10.3892/mmr.2017.7284

Liu, Y. L., Lin, L. C., Tung, Y. T., Ho, S. T., Chen, Y. L., Lin, C. C., et al. (2017). Rhododendron oldhamii leaf extract improves fatty liver syndrome by increasing lipid oxidation and decreasing the lipogenesis pathway in mice. *Int. J. Med. Sci.* 14 (9), 862–870. doi: 10.7150/ijms.19553

Liu, X., Xie, Z. H., Liu, C. Y., and Zhang, Y. (2019). Effect of Chinese Herbal Monomer Hairy Calycosin on Nonalcoholic Fatty Liver Rats and its Mechanism. *Comb. Chem. High Throughput Screen* 22 (3), 194–200. doi: 10.2174/1386207322666190411112814

Liu, Y. Y., You, J. J., Xu, W., Zhai, T., Du, C. Y., Chen, Y., et al. (2019). Gynura procumbens aqueous extract alleviates nonalcoholic steatohepatitis through CFLAR-JNK pathway in vivo and in vitro. *Chin. Herb. Medicines* 11 (4), 369–378. doi: 10.1016/j.chmed.2019.09.005

Lo, V., Erickson, B., Thomason-Hughes, M., Ko, K. W., Dolinsky, V. W., Nelson, R., et al. (2010). Arylacetamide deacetylase attenuates fatty-acid-induced triacylglycerol accumulation in rat hepatoma cells. *J. Lipid Res.* 51 (2), 368–377. doi: 10.1194/jlr.M000596

Lomonaco, R., Sunny, N. E., Bril, F., and Cusi, K. (2013). Nonalcoholic fatty liver disease: current issues and novel treatment approaches. *Drugs* 73 (1), 1–14. doi: 10.1007/s40265-012-0004-0

Lu, X., Yuan, Z. Y., Yan, X. J., Lei, F., Jiang, J. F., Yu, X., et al. (2016). Effects of Angelica dahurica on obesity and fatty liver in mice. *Chin. J. Nat. Med.* 14 (9), 641–652. doi: 10.1016/S1875-5364(16)30076-0

Luan, H., Huo, Z., Zhao, Z., Zhang, S., Huang, Y., Shen, Y., et al. (2019). Scutellarin, a modulator of mTOR, attenuates hepatic insulin resistance by regulating hepatocyte lipid metabolism via SREBP-1c suppression. *Phytother. Res.* doi: 10.1002/ptr.6582

Ma, J., Zhao, D., Wang, X., Ma, C., Feng, K., Zhang, S., et al. (2019). LongShengZhi Capsule Reduces Established Atherosclerotic Lesions in apoE-Deficient Mice by Ameliorating Hepatic Lipid Metabolism and Inhibiting Inflammation. *J. Cardiovasc. Pharmacol.* 73 (2), 105–117. doi: 10.1097/FJC.0000000000000642

Mandal, S., Mukhopadhyay, S., Bandhopadhyay, S., Sen, G., and Biswas, T. (2014). 14-Deoxyandrographolide alleviates ethanol-induced hepatosteatosis through stimulation of AMP-activated protein kinase activity in rats. *Alcohol* 48 (2), 123–132. doi: 10.1016/j.alcohol.2013.11.005

Mato, J. M., Alonso, C., Noureddin, M., and Lu, S. C. (2019). Biomarkers and subtypes of deranged lipid metabolism in non-alcoholic fatty liver disease. *World J. Gastroenterol.* 25 (24), 3009–3020. doi: 10.3748/wjg.v25.i24.3009

Meng, Q., Duan, X. P., Wang, C. Y., Liu, Z. H., Sun, P. Y., Huo, X. K., et al. (2017). Alisol B 23-acetate protects against non-alcoholic steatohepatitis in mice via farnesoid X receptor activation. *Acta Pharmacol. Sin.* 38 (1), 69–79. doi: 10.1038/aps.2016.119

Moctezuma-Velazquez, C. (2018). Current treatment for non-alcoholic fatty liver disease. *Rev. Gastroenterol. Mex.* 83 (2), 125–133. doi: 10.1016/j.rgmxen.2018.05.014

Musso, G., Gambino, R., and Cassader, M. (2009). Recent insights into hepatic lipid metabolism in non-alcoholic fatty liver disease (NAFLD). *Prog. Lipid Res.* 48 (1), 1–26. doi: 10.1016/j.plipres.2008.08.001

Nguyen, P., Leray, V., Diez, M., Serisier, S., Le Bloc'h, J., Siliart, B., et al. (2008). Liver lipid metabolism. *J. Anim. Physiol. Anim. Nutr. (Berl.)* 92 (3), 272–283. doi: 10.1111/j.1439-0396.2007.00752.x

Ouali, F., Djouadi, F., Merlet-Benichou, C., Riveau, B., and Bastin, J. (2000). Regulation of fatty acid transport protein and mitochondrial and peroxisomal beta-oxidation gene expression by fatty acids in developing rats. *Pediatr. Res.* 48 (5), 691–696. doi: 10.1203/00006450-200011000-00023

Parafati, M., Lascala, A., Morittu, V. M., Trimboli, F., Rizzuto, A., Brunelli, E., et al. (2015). Bergamot polyphenol fraction prevents nonalcoholic fatty liver disease via stimulation of lipophagy in cafeteria diet-induced rat model of metabolic syndrome. *J. Nutr. Biochem.* 26 (9), 938–948. doi: 10.1016/j.jnutbio.2015.03.008

Park, H., Kaushik, V. K., Constant, S., Prentki, M., Przybytkowski, E., Ruderman, N. B., et al. (2002). Coordinate regulation of malonyl-CoA decarboxylase, sn-glycerol-3-phosphate acyltransferase, and acetyl-CoA carboxylase by AMP-activated protein kinase in rat tissues in response to exercise. *J. Biol. Chem.* 277 (36), 32571–32577. doi: 10.1074/jbc.M201692200

Park, H. J., Han, J. M., Kim, H. G., Choi, M. K., Lee, J. S., Lee, H. W., et al. (2013). Chunggan extract (CGX), methionine-and choline-deficient (MCD) diet-induced hepatosteatosis and oxidative stress in C57BL/6 mice. *Hum. Exp. Toxicol.* 32 (12), 1258–1269. doi: 10.1177/0960327113485253

Park, H., Hwang, Y. H., Kim, D. G., Jeon, J., and Ma, J. Y. (2015). Hepatoprotective effect of herb formula KIOM2012H against nonalcoholic fatty liver disease. *Nutrients* 7 (4), 2440–2455. doi: 10.3390/nu7042440

Park, T. Y., Hong, M., Sung, H., Kim, S., and Suk, K. T. (2017). Effect of Korean Red Ginseng in chronic liver disease. *J. Ginseng Res.* 41 (4), 450–455. doi: 10.1016/j.jgr.2016.11.004

Peng, C. H., Liu, L. K., Chuang, C. M., Chyau, C. C., Huang, C. N., and Wang, C. J. (2011). Mulberry water extracts possess an anti-obesity effect and ability to inhibit hepatic lipogenesis and promote lipolysis. *J. Agric. Food Chem.* 59 (6), 2663–2671. doi: 10.1021/jf1043508

Peng, H., He, Y., Zheng, G., Zhang, W., Yao, Z., and Xie, W. (2016). Meta-analysis of traditional herbal medicine in the treatment of nonalcoholic fatty liver disease. *Cell Mol. Biol. (Noisy-le-grand)* 62 (4), 88–95.

Perla, F. M., Prelati, M., Lavorato, M., Visicchio, D., and Anania, C. (2017). The Role of Lipid and Lipoprotein Metabolism in Non-Alcoholic Fatty Liver Disease. *Children (Basel)* 4 (6). doi: 10.3390/children4060046

Perumpail, B. J., Li, A. A., Iqbal, U., Sallam, S., Shah, N. D., Kwong, W., et al. (2018). Potential Therapeutic Benefits of Herbs and Supplements in Patients with NAFLD. *Diseases* 6 (3). doi: 10.3390/diseases6030080

Pierre, G., Macdonald, A., Gray, G., Hendriksz, C., Preece, M. A., and Chakrapani, A. (2007). Prospective treatment in carnitine-acylcarnitine translocase deficiency. *J. Inherit. Metab. Dis.* 30 (5), 815. doi: 10.1007/s10545-007-0518-x

Pil Hwang, Y., Gyun Kim, H., Choi, J. H., Truong Do, M., Tran, T. P., Chun, H. K., et al. (2013). 3-Caffeoyl, 4-dihydrocaffeoylquinic acid from Salicornia herbacea attenuates high glucose-induced hepatic lipogenesis in human HepG2 cells through activation of the liver kinase B1 and silent information regulator T1/AMPK-dependent pathway. *Mol. Nutr. Food Res.* 57 (3), 471–482. doi: 10.1002/mnfr.201200529

Ponziani, F. R., Pecere, S., Gasbarrini, A., and Ojetti, V. (2015). Physiology and pathophysiology of liver lipid metabolism. *Expert Rev. Gastroenterol. Hepatol.* 9 (8), 1055–1067. doi: 10.1586/17474124.2015.1056156

Qian, W., Cai, X., Zhang, X., Wang, Y., Qian, Q., and Hasegawa, J. (2016). Effect of Daisaikoto on Expressions of SIRT1 and NF-kappaB of Diabetic Fatty Liver Rats Induced by High-Fat Diet and Streptozotocin. *Yonago Acta Med.* 59 (2), 149–158.

Qiu, P., Li, X., Kong, D. S., Li, H. Z., Niu, C. C., and Pan, S. H. (2015). Herbal SGR Formula Prevents Acute Ethanol-Induced Liver Steatosis via Inhibition of Lipogenesis and Enhancement Fatty Acid Oxidation in Mice. *Evid. Based Complement Alternat. Med.* 2015, 613584. doi: 10.1155/2015/613584

Quiroga, A. D., and Lehner, R. (2018). Pharmacological intervention of liver triacylglycerol lipolysis: The good, the bad and the ugly. *Biochem. Pharmacol.* 155, 233–241. doi: 10.1016/j.bcp.2018.07.005

Reddy, J. K., and Rao, M. S. (2006). Lipid metabolism and liver inflammation. II. Fatty liver disease and fatty acid oxidation. *Am. J. Physiol. Gastrointest Liver Physiol.* 290 (5), G852–G858.

Ren, L., Sun, D., Zhou, X., Yang, Y., Huang, X., Li, Y., et al. (2019). Chronic treatment with the modified Longdan Xiegan Tang attenuates olanzapine-induced fatty liver in rats by regulating hepatic de novo lipogenesis and fatty acid beta-oxidation-associated gene expression mediated by SREBP-1c, PPAR-alpha and AMPK-alpha. *J. Ethnopharmacol.* 232, 176–187. doi: 10.1016/j.jep.2018.12.034

Roh, J. S., Lee, H., Lim, J., Kim, J., Yang, H., Yoon, Y., et al. (2017). Effect of Gangjihwan on hepatic steatosis and inflammation in high fat diet-fed mice. *J. Ethnopharmacol.* 206, 315–326. doi: 10.1016/j.jep.2017.06.008

Rui, L. (2014). Energy metabolism in the liver. *Compr. Physiol.* 4 (1), 177–197. doi: 10.1002/cphy.c130024

Saha, A. K., and Ruderman, N. B. (2003). Malonyl-CoA and AMP-activated protein kinase: an expanding partnership. *Mol. Cell Biochem.* 253 (1-2), 65–70. doi: 10.1023/A:1026053302036

Seo, M. S., Hong, S. W., Yeon, S. H., Kim, Y. M., Um, K. A., Kim, J. H., et al. (2014). Magnolia officinalis attenuates free fatty acid-induced lipogenesis via AMPK phosphorylation in hepatocytes. *J. Ethnopharmacol.* 157, 140–148. doi: 10.1016/j.jep.2014.09.031

Shang, J., Chen, L. L., Xiao, F. X., Sun, H., Ding, H. C., and Xiao, H. (2008). Resveratrol improves non-alcoholic fatty liver disease by activating AMP-activated protein kinase. *Acta Pharmacol. Sin.* 29 (6), 698–706. doi: 10.1111/j.1745-7254.2008.00807.x

Sheng, X., Wang, M., Lu, M., Xi, B., Sheng, H., and Zang, Y. Q. (2011). Rhein ameliorates fatty liver disease through negative energy balance, hepatic

lipogenic regulation, and immunomodulation in diet-induced obese mice. *Am. J. Physiol. Endocrinol. Metab.* 300 (5), E886–E893. doi: 10.1152/ajpendo.00332.2010

Sheng, D., Zhao, S., Gao, L., Zheng, H., Liu, W., Hou, J., et al. (2019). BabaoDan attenuates high-fat diet-induced non-alcoholic fatty liver disease via activation of AMPK signaling. *Cell Biosci.* 9, 77. doi: 10.1186/s13578-019-0339-2

Shi, K. Q., Fan, Y. C., Liu, W. Y., Li, L. F., Chen, Y. P., and Zheng, M. H. (2012). Traditional Chinese medicines benefit to nonalcoholic fatty liver disease: a systematic review and meta-analysis. *Mol. Biol. Rep.* 39 (10), 9715–9722. doi: 10.1007/s11033-012-1836-0

Shi, L. J., Shi, L., Song, G. Y., Zhang, H. F., Hu, Z. J., Wang, C., et al. (2013). Oxymatrine attenuates hepatic steatosis in non-alcoholic fatty liver disease rats fed with high fructose diet through inhibition of sterol regulatory element binding transcription factor 1 (Srebf1) and activation of peroxisome proliferator activated receptor alpha (Pparalpha). *Eur. J. Pharmacol.* 714 (1-3), 89–95. doi: 10.1016/j.ejphar.2013.06.013

Shi, X., Sun, R. M., Zhao, Y., Fu, R., Wang, R. W., Zhao, H. Y., et al. (2018). Promotion of autophagosome-lysosome fusion via salvianolic acid A-mediated SIRT1 up-regulation ameliorates alcoholic liver disease. *Rsc Adv.* 8 (36), 20411–20422. doi: 10.1039/C8RA00798E

Singh, R., and Cuervo, A. M. (2012). Lipophagy: connecting autophagy and lipid metabolism. *Int. J. Cell Biol.* 2012, 282041. doi: 10.1155/2012/282041

Sun, F., Xie, M. L., Zhu, L. J., Xue, J., and Gu, Z. L. (2009). Inhibitory effect of osthole on alcohol-induced fatty liver in mice. *Dig. Liver Dis.* 41 (2), 127–133. doi: 10.1016/j.dld.2008.01.011

Sun, X. H., Zhang, L. D., and Wei, W. (2019). A study on the mechanism of adipokine in non-alcoholic fatty liver in rats treated by four herbs decoction. *Eur. J. Inflammation* 17, 8. doi: 10.1177/2058739219853970

Tessari, P., Coracina, A., Cosma, A., and Tiengo, A. (2009). Hepatic lipid metabolism and non-alcoholic fatty liver disease. *Nutr. Metab. Cardiovasc. Dis.* 19 (4), 291–302. doi: 10.1016/j.numecd.2008.12.015

Theodotou, M., Fokianos, K., Moniatis, D., Kadlenic, R., Chrysikou, A., Aristotelous, A., et al. (2019). Effect of resveratrol on non-alcoholic fatty liver disease. *Exp. Ther. Med.* 18 (1), 559–565. doi: 10.3892/etm.2019.7607

Uen, W. C., Shi, Y. C., Choong, C. Y., and Tai, C. J. (2018). Cordycepin suppressed lipid accumulation via regulating AMPK activity and mitochondrial fusion in hepatocytes. *J. Food Biochem.* 42 (5), 7. doi: 10.1111/jfbc.12569

Veeramani, C., Alsaif, M. A., and Al-Numair, K. S. (2017). Lavatera critica, a green leafy vegetable, controls high fat diet induced hepatic lipid accumulation and oxidative stress through the regulation of lipogenesis and lipolysis genes. *BioMed. Pharmacother.* 96, 1349–1357. doi: 10.1016/j.biopha.2017.11.072

Veeramani, C., Alsaif, M. A., and Al-Numair, K. S. (2018). Herbacetin, a flaxseed flavonoid, ameliorates high percent dietary fat induced insulin resistance and lipid accumulation through the regulation of hepatic lipid metabolizing and lipid-regulating enzymes. *Chem. Biol. Interact.* 288, 49–56. doi: 10.1016/j.cbi.2018.04.009

Wanders, R. J., Waterham, H. R., and Ferdinandusse, S. (2015). Metabolic Interplay between Peroxisomes and Other Subcellular Organelles Including Mitochondria and the Endoplasmic Reticulum. *Front. Cell Dev. Biol.* 3, 83.

Wang, Y. L., Liu, L. J., Zhao, W. H., and Li, J. X. (2015). Intervening TNF-alpha via PPARgamma with Gegenqinlian Decoction in Experimental Nonalcoholic Fatty Liver Disease. *Evid. Based Complement Alternat. Med.* 2015, 715638.

Wang, Y., Viscarra, J., Kim, S. J., and Sul, H. S. (2015). Transcriptional regulation of hepatic lipogenesis. *Nat. Rev. Mol. Cell Biol.* 16 (11), 678–689. doi: 10.1038/nrm4074

Wang, Y. P., Wat, E., Koon, C. M., Wong, C. W., Cheung, D. W., Leung, P. C., et al. (2016). The beneficial potential of polyphenol-enriched fraction from Erigerontis Herba on metabolic syndrome. *J. Ethnopharmacol.* 187, 94–103. doi: 10.1016/j.jep.2016.04.040

Wang, S. J., Chen, Q., Liu, M. Y., Yu, H. Y., Xu, J. Q., Wu, J. Q., et al. (2019). Regulation effects of rosemary (Rosmarinus officinalis Linn.) on hepatic lipid metabolism in OA induced NAFLD rats. *Food Funct.* 10 (11), 7356–7365.

Ward, C., Martinez-Lopez, N., Otten, E. G., Carroll, B., Maetzel, D., Singh, R., et al. (2016). Autophagy, lipophagy and lysosomal lipid storage disorders. *Biochim. Biophys. Acta* 1861 (4), 269–284. doi: 10.1016/j.bbalip.2016.01.006

Wu, W. Y., and Wang, Y. P. (2012). Pharmacological actions and therapeutic applications of Salvia miltiorrhiza depside salt and its active components. *Acta Pharmacol. Sin.* 33 (9), 1119–1130. doi: 10.1038/aps.2012.126

Xiao, J., Fai So, K., Liong, E. C., and Tipoe, G. L. (2013). Recent advances in the herbal treatment of non-alcoholic Fatty liver disease. *J. Tradit. Complement Med.* 3 (2), 88–94. doi: 10.4103/2225-4110.110411

Xu, L., Yin, L., Tao, X., Qi, Y., Han, X., Xu, Y., et al. (2017). Dioscin, a potent ITGA5 inhibitor, reduces the synthesis of collagen against liver fibrosis: Insights from SILAC-based proteomics analysis. *Food Chem. Toxicol.* 107 (Pt A), 318–328. doi: 10.1016/j.fct.2017.07.014

Yan, S., Khambu, B., Hong, H., Liu, G., Huda, N., and Yin, X. M. (2019). Autophagy, Metabolism, and Alcohol-Related Liver Disease: Novel Modulators and Functions. *Int. J. Mol. Sci.* 20 (20). doi: 10.3390/ijms20205029

Yang, W., She, L., Yu, K., Yan, S., Zhang, X., Tian, X., et al. (2016). Jatrorrhizine hydrochloride attenuates hyperlipidemia in a high-fat diet-induced obesity mouse model. *Mol. Med. Rep.* 14 (4), 3277–3284. doi: 10.3892/mmr.2016.5634

Yang, L., Lin, W., Nugent, C. A., Hao, S., Song, H., Liu, T., et al. (2017). Lingguizhugan Decoction Protects against High-Fat-Diet-Induced Nonalcoholic Fatty Liver Disease by Alleviating Oxidative Stress and Activating Cholesterol Secretion. *Int. J. Genomics* 2017, 2790864. doi: 10.1155/2017/2790864

Yang, J. M., Sun, Y., Wang, M., Zhang, X. L., Zhang, S. J., Gao, Y. S., et al. (2019). Regulatory effect of a Chinese herbal medicine formula on non-alcoholic fatty liver disease. *World J. Gastroenterol.* 25 (34), 5105–5119. doi: 10.3748/wjg.v25.i34.5105

Yang, L., Yang, C., Thomes, P. G., Kharbanda, K. K., Casey, C. A., McNiven, M. A., et al. (2019). Lipophagy and Alcohol-Induced Fatty Liver. *Front. Pharmacol.* 10, 495. doi: 10.3389/fphar.2019.00495

Yang, X. X., Wang, X., Shi, T. T., Dong, J. C., Li, F. J., Zeng, L. X., et al. (2019). Mitochondrial dysfunction in high-fat diet-induced nonalcoholic fatty liver disease: The alleviating effect and its mechanism of Polygonatum kingianum. *BioMed. Pharmacother.* 117, 109083. doi: 10.1016/j.biopha.2019.109083

Yang, Y., Li, J., Wei, C., He, Y., Cao, Y., Zhang, Y., et al. (2019). Amelioration of nonalcoholic fatty liver disease by swertiamarin in fructose-fed mice. *Phytomedicine* 59, 152782. doi: 10.1016/j.phymed.2018.12.005

Yao, H., Qiao, Y. J., Zhao, Y. L., Tao, X. F., Xu, L. N., Yin, L. H., et al. (2016). Herbal medicines and nonalcoholic fatty liver disease. *World J. Gastroenterol.* 22 (30), 6890–6905. doi: 10.3748/wjg.v22.i30.6890

Yoon, S., Kim, J., Lee, H., Lee, H., Lim, J., Yang, H., et al. (2017). The effects of herbal composition Gambigyeongsinhwan (4) on hepatic steatosis and inflammation in Otsuka Long-Evans Tokushima fatty rats and HepG2 cells. *J. Ethnopharmacol.* 195, 204–213. doi: 10.1016/j.jep.2016.11.020

Younossi, Z. M. (2019). Non-alcoholic fatty liver disease - A global public health perspective. *J. Hepatol.* 70 (3), 531–544. doi: 10.1016/j.jhep.2018.10.033

Yu, S., Rao, S., and Reddy, J. K. (2003). Peroxisome proliferator-activated receptors, fatty acid oxidation, steatohepatitis and hepatocarcinogenesis. *Curr. Mol. Med.* 3 (6), 561–572. doi: 10.2174/1566524033479537

Zamani, N., Shams, M., Nimrouzi, M., Zarshenas, M. M., Abolhasani Foroughi, A., Fallahzadeh Abarghooei, E., et al. (2018). The effects of Zataria multiflora Boiss. (Shirazi thyme) on nonalcoholic fatty liver disease and insulin resistance: A randomized double-blind placebo-controlled clinical trial. *Complement Ther. Med.* 41, 118–123. doi: 10.1016/j.ctim.2018.09.010

Zar Kalai, F., Han, J., Ksouri, R., Abdelly, C., and Isoda, H. (2014). Oral administration of Nitraria retusa ethanolic extract enhances hepatic lipid metabolism in db/db mice model 'BKS.Cg-Dock7(m)+/+ Lepr(db/)J' through the modulation of lipogenesis-lipolysis balance. *Food Chem. Toxicol.* 72, 247–256. doi: 10.1016/j.fct.2014.07.029

Zhang, Y., Si, Y., Zhai, L., Yang, N., Yao, S., Sang, H., et al. (2013). Celastrus orbiculatus Thunb. ameliorates high-fat diet-induced non-alcoholic fatty liver disease in guinea pigs. *Pharmazie* 68 (10), 850–854.

Zhang, Y., Yu, L., Cai, W., Fan, S., Feng, L., Ji, G., et al. (2014). Protopanaxatriol, a novel PPARgamma antagonist from Panax ginseng, alleviates steatosis in mice. *Sci. Rep.* 4, 7375. doi: 10.1038/srep07375

Zhang, E., Yin, S., Song, X., Fan, L., and Hu, H. (2016). Glycycoumarin inhibits hepatocyte lipoapoptosis through activation of autophagy and inhibition of ER stress/GSK-3-mediated mitochondrial pathway. *Sci. Rep.* 6, 38138. doi: 10.1038/srep38138

Zhang, L., Yao, Z., and Ji, G. (2018). Herbal Extracts and Natural Products in Alleviating Non-alcoholic Fatty Liver Disease via Activating Autophagy. *Front. Pharmacol.* 9, 1459. doi: 10.3389/fphar.2018.01459

Zhang, E., Yin, S., Zhao, S., Zhao, C., Yan, M., Fan, L., et al. (2019). Protective effects of glycycoumarin on liver diseases. *Phytother. Res*. doi: 10.1002/ptr.6598

Zhang, Y., Liu, M., Chen, Q., Wang, T., Yu, H., Xu, J., et al. (2019). Leaves of Lippia triphylla improve hepatic lipid metabolism via activating AMPK to regulate lipid synthesis and degradation. *J. Nat. Med.* 73 (4), 707–716. doi: 10.1007/s11418-019-01316-5

Zheng, Y., Wang, M., Zheng, P., Tang, X., and Ji, G. (2018). Systems pharmacology-based exploration reveals mechanisms of anti-steatotic effects of Jiang Zhi Granule on non-alcoholic fatty liver disease. *Sci. Rep.* 8 (1), 13681.

Zhong, H., Chen, K., Feng, M., Shao, W., Wu, J., Chen, K., et al. (2018). Genipin alleviates high-fat diet-induced hyperlipidemia and hepatic lipid accumulation in mice via miR-142a-5p/SREBP-1c axis. *FEBS J.* 285 (3), 501–517. doi: 10.1111/febs.14349

Zhou, W., Rahimnejad, S., Lu, K., Wang, L., and Liu, W. (2019). Effects of berberine on growth, liver histology, and expression of lipid-related genes in blunt snout bream (Megalobrama amblycephala) fed high-fat diets. *Fish Physiol. Biochem.* 45 (1), 83–91. doi: 10.1007/s10695-018-0536-7

Zhu, M., Hao, S., Liu, T., Yang, L., Zheng, P., Zhang, L., et al. (2017). Lingguizhugan decoction improves non-alcoholic fatty liver disease by altering insulin resistance and lipid metabolism related genes: a whole trancriptome study by RNA-Seq. *Oncotarget* 8 (47), 82621–82631. doi: 10.18632/oncotarget.19734

Polyherbal Medicine Divya Sarva-Kalp-Kwath Ameliorates Persistent Carbon Tetrachloride Induced Biochemical and Pathological Liver Impairments in Wistar Rats and in HepG2 Cells

*Acharya Balkrishna[1,2], Sachin Shridhar Sakat[1], Ravikant Ranjan[1], Kheemraj Joshi[1], Sunil Shukla[1], Kamal Joshi[1], Sudeep Verma[1], Abhishek Gupta[1], Kunal Bhattacharya[1] and Anurag Varshney[1,2]**

[1] *Drug Discovery and Development Division, Patanjali Research Institute, Haridwar, India,* [2] *Department of Allied and Applied Sciences, University of Patanjali, Patanjali Yog Peeth, Haridwar, India*

Divya Sarva-Kalp-Kwath (SKK) is a poly-herbal ayurvedic medicine formulated using plant extracts of *Boerhavia diffusa* L. (Nyctaginaceae), *Phyllanthus niruri* L. (Euphorbiaceae), and *Solanum nigrum* L. (Solanaceae), described to improve liver function and general health. In the present study, we have explored the hepatoprotective effects of SKK in ameliorating carbon tetrachloride (CCl_4) induced liver toxicity using *in-vitro* and *in-vivo* test systems. Chemical analysis of SKK using Liquid Chromatography-Mass Spectroscopy (LC-MS-QToF) and High-Performance Liquid Chromatography (HPLC) revealed the presence of different bioactive plant metabolites, known to impart hepatoprotective effects. In human hepatocarcinoma (HepG2) cells, co-treatment of SKK with CCl_4 effectively reduced the hepatotoxicity induced by the latter. These effects were confirmed by studying parameters such as loss of cell viability; release of hepatic injury enzymatic biomarkers- aspartate aminotransferase (AST), and alkaline phosphatase (ALP); and changes in reactive oxygen species and in mitochondrial membrane potentials. *In-vivo* safety analysis in Wistar rats showed no loss in animal body weight, or change in feeding habits after repeated oral dosing of SKK up to 1,000 mg/kg/day for 28 days. Also, no injury-related histopathological changes were observed in the animal's blood, liver, kidney, heart, brain, and lung. Pharmacologically, SKK played a significant role in modulating CCl_4 induced hepatic injuries in the Wistar rats at a higher dose. In the 9 weeks' study, SKK (200 mg/kg) reduced the CCl_4 stimulated increase in the release of enzymes (ALT, AST, and ALP), bilirubin, total cholesterol, and uric acid levels in the Wistar rats. It also reduced the CCl_4 stimulated inflammatory lesions such as liver fibrosis, lymphocytic infiltration, and hyper-plasticity. In conclusion, SKK showed pharmacological effects in improving the CCl_4 stimulated liver injuries in HepG2 cells and in Wistar rats. Furthermore, no adverse effects were observed up to $10\times$ higher human equivalent dose of SKK during 28-days repeated dose exposure in Wistar rats. Based on

the literature search on the identified plant metabolites, SKK was found to act in multiple ways to ameliorate CCl_4 induced hepatotoxicity. Therefore, polyherbal SKK medicine has shown remarkable potentials as a possible alternative therapeutics for reducing liver toxicity induced by drugs, and other toxins.

INTRODUCTION

Liver is the principal organ involved in the enzymatic metabolism of drugs, xenobiotics, and toxins. Following hepatic expsure, xenobiotics and harsh chemicals such as carbon tetrachloride (CCl_4; haloalkene) are metabolized by liver microsomal enzyme CYP2E1 into reactive intermediates such as tetrachloromethane radical ($CCl_3^{\bullet}$) and trichloromethyl peroxy radical ($CCl_3OO^{\bullet}$) (Abraham and Wilfred, 2002; Nada et al., 2010). These reactive intermediates interact and induce oxidation of the membrane lipids and proteins of hepatic stellate, kupffer, and endothelial cells. These damages lead to the elevation of injury associated biomarkers- aspartate aminotransferase (AST), acid phosphatase (ASP), alkaline phosphatase (ALP), alanine transaminase (ALT), gamma-glutamyl-transferase, lactate dehydrogenase (LDH), glucose, globulin, bilirubin, and cholesterol levels (Yadav and Kumar, 2014). Chronic and long-term injuries can lead to the development of liver cirrhosis (Debnath et al., 2013).

Recent publications have drawn focus on the importance of herbal formulation in modulating complex life-changing diseases such as rheumatoid arthritis and psoriasis (Balkrishna et al., 2019b,c,d). The traditional medicinal system is based on the application of polyherbal formulations. Pharmacological effects obtained from multiple plant extract metabolites are much higher as compared to single herb extracts (Yadav et al., 2008; Balkrishna et al., 2019a). In modern medicine, the treatment for chronic diseases has shifted from the "one drug, one target, one disease" paradigm toward combination therapies (Williamson, 2001; Zhou et al., 2016). Synergistic treatments also significantly reduce possible incidences of health-related side-effects.

Divya Sarva-kalp-kwath (SKK) decoction having a poly-herbal origin has been given for healing acute hepatic diseases and have been found effective in ameliorating CCl_4 stimulated sub-acute hepatotoxicity in Wistar rats following a 7 days' treatment (Yadav and Kumar, 2014). It is prepared using aqueous extracts from *Boerhavia diffusa* L. (Nyctaginaceae), *Phyllanthus niruri* L. (Euphorbiaceae), and *Solanum nigrum* L. (Solanaceae) plants mixed in the ratio of 2:1:1. These plants have been cited in the traditional medicinal texts to provide protection against hepatic diseases and other injuries (Kirtikar and Basu, 1956). Herbal component of SKK, *B. diffusa* L. plant also known as "Punarnava" possesses a variety of isoflavinoids such as rotenoids, flavonoids, flavonoid glycosides, xanthones, lignans, ecdysteroids, and steroids. Several of these plant metabolites such as rotenoids (Boeravinone A- G), kaempferol, and quercetin have been proven for their role in hepatoprotective activity (Lami et al., 1990; Borrelli et al., 2005; Ferreres et al., 2005; Pereira

et al., 2009; Bairwa et al., 2013). *B. diffusa* L. plant extract has been found to modulate CCl_4 induced liver injury in stimulated animals through the reduction of cytochrome (CYP) enzyme activities (Ramachandra et al., 2011; Venkatesh et al., 2012; Bairwa et al., 2013; Patel and Verma, 2014; Ekow Thomford et al., 2018; Juneja et al., 2020). *P. niruri* L. also known as 'bhumi amalaki' is composed of alkaloids, anthrocyanins, chlorogenic acids, flavonoids, lignans, phenolic acids, tannins, terpenoids, saponins, and substitutes that attribute to its bioactivity (Kaur et al., 2017; Jantan et al., 2019). Metabolites present in the plant extract act as antioxidants reducing CCl_4 stimulated liver injuries in hepatocyte (Syamasundar et al., 1985; Harish and Shivanandappa, 2006; Bhattacharjee and Sil, 2007). *S. nigrum* L. also known as "Makoy" contains several steroidal glycosides, steroidal alkaloids and steroidal oligoglycosides that also act as antioxidants reducing CCl_4 induced hepatic injuries through amelioration of oxidative stress (Lin et al., 2008; Mir et al., 2010; Elhag et al., 2011; Sivgami et al., 2012).

Therefore, in the present study, we explore the safety and long-term pharmacological effects of SKK decoction with a possible synergistic effect from the presence of three potent plant species having hepatoprotective effects in ameliorating chronic liver injuries induced in Wistar rats following 9 weeks' stimulation with CCl_4. For the study, we screened, identified and quantified essential metabolites present in the SKK decoction using Liquid Chromatography-Mass Spectroscopy QToF (LC-MS QToF) and High-Performance Liquid Chromatography (HPLC) analytical techniques. Using human hepatocarcinoma (HepG2) cells, we verified the biological effect and mode of action of SKK in ameliorating the chronic CCl_4 induced cytotoxicity and injuries. We also studied the safety profile of SKK decoction in Wistar rats through the measurement of cellular and biochemical parameters after 28 days of repeated dosing. The pharmacological effect of SKK decoction in reducing CCl_4 induced chronic toxicity in Wistar rats was explored over 9 weeks' time-period through analysis of the physiological, biochemical, and histopathological changes. As a positive control drug, Silymarin (SLM) treatment was also given to the CCl_4 stimulated Wistar rats to ameliorate the CCl_4 induced liver injuries.

MATERIALS AND METHODS

Chemicals and Reagents

SKK was obtained from Divya Pharmacy, Haridwar, India, under its brand name "Divya Sarva-Kalp-Kwath" (Batch no- #A-SKK056). Plant identification of the SKK herbal components was performed at the Council of Scientific and Industrial Research—National Institute of Science Communication and

Information Resources (CSIR—NISCAIR), Delhi, India and provided the following plant identification voucher numbers– *Phyllanthus amarus* Schum. & Thonn. Syn. *Phyllanthus fraternus* Webster (NISCAIR/RHMD/Consult/2019/3453-54-30), *P. niruri sensu* Hook. f. (NISCAIR/RHMD/Consult/2019/3453-54-149) and *B. diffusa* L. and *S. nigrum* L. (NISCAIR/RHMD/Consult/2019/3453-54-119). CCl_4 was purchased from MP Biomedicals India Private Limited Mumbai, India. SLM was purchased from Sigma Aldrich, St. Louis, USA. All the solvents and reagents used for LC-MS QToF and HPLC assays were of high spectroscopy grade and purchased from Merck India Pvt. Ltd., Mumbai, India. Haematoxylin, Potassium Aluminum Sulfate Dodecahydrate, Mercury (II) Oxide red were purchased from Merck India Pvt. Ltd., Mumbai, India. Eosin Yellow and Ferric chloride were purchased from Hi-Media Laboratories, Mumbai, India. Biochemistry reagents were procured from Randox Laboratories Ltd., United Kingdom. Food grade olive oil was purchased from the local market. All other chemicals and reagents used for the tissue processing work were of the highest analytical grade.

Extract Preparation and Dose Calculation

Animal equivalent doses of SKK for rat studies were estimated based on the body surface area of the animals. The human therapeutic recommended dose of the SKK is 5–10 g of powder boiled in 400 mL of water until approximately 100 mL decoction remains.

Accordingly, 7.5 g (average quantity) of SKK was weighed, and boiled in 400 mL of water until a volume of 100 mL remained. The resultant decoction was dried using lyophilizer, and ~853 mg of powder was obtained. Based on the decoction preparation protocol, the human dose was calculated as 14.21 mg/kg. Human equivalent doses (mg/kg) for rat were calculated by multiplying human dose (mg/kg) by factor 6.2 (Nair and Jacob, 2016) and was estimated at 88.14 mg/kg. Taking a round-off, we considered 100 mg/kg as the human equivalent dose and 200 mg/kg as effective and higher doses, respectively.

Metabolite Analysis of SKK Decoction

Identification of the metabolites present in the SKK decoction was performed using a Xevo G2-XS QToF with Acquity UPLC-I Class and Unifi software (Waters, MA, USA). Separation of the metabolites was performed using an Acquity UPLC HSS - T3 column (100 x 2.1 mm i.d., 1.7 μm). The elution was carried out at a flow rate of 0.4 mL/min using gradient elution of mobile phase 0.1% formic acid in water (mobile phase A) and 0.1 % formic acid in acetonitrile (mobile phase B). Two microliters of the final test solution were injected during the analysis and record the chromatograph for 15 min. The gradient program was set between 0 and 18 min retention time with a flow of 0.4 mL/min.

The LC-MS equipment was equipped with an ESI ion source operating in positive and negative ion mode. A mass range of 50–1,000 Da was set with a 0.2 s scan time, the acquisition time of 15 min, the capillary voltage of 1 kV (for positive mode) and 2 kV (for negative mode). Mass was corrected during acquisition using an external reference (Lock-Spray) consisting of a 0.2 ng/mL solution of leucine-enkephalin.

Quantitative analysis of SKK decoction was performed using Waters HPLC equipped with a Binary pump (1525), photodiode detector array (2998), and auto-sampler (2707). Elution was performed at a flow rate of 1 mL/min using a gradient elution of mobile phase A (0.1% Orthophosphoric acid, pH-2.5 with Diethylamine) and mobile phase B (Acetonitrile). For gallic acid, catechin, caffeic acid, rutin, and quercetin, the solvent gradient program selected was 5% of mobile phase B from 0 to 5 min, 5 to 100% of mobile phase B from 5 to 35 min, 100% of mobile phase B from 35 to 45 min, 100 to 50% of mobile phase B from 45 to 47 min, 50 to 5% of mobile phase B from 47 to 48 min, 5% of mobile phase B from 48 to 55 min. For corilagin, the solvent gradient program selected was 5% of mobile phase B from 0 to 5 min, 5 to 20% of mobile phase B from 5 to 20 min, 20 to 30% of mobile phase B from 20 to 25 min, 30 to 75% of mobile phase B from 25 to 30 min, 75 to 90% of mobile phase B from 30 to 35 min, 90% of mobile phase B from 35 to 40 min, 90 to 5% of mobile phase B from 40 to 41 min, 5% of mobile phase B from 41 to 45 min. The X-Bridge Phenyl Column (5 μm, 4.6 × 250 mm) was used for gallic acid, catechin, caffeic acid, rutin and quercetin, and Shodex C18-4E column (5 μm, 4.6 × 250 mm) was used for corilagin. Detector wavelength was kept at 270 nm for gallic acid- catechin- corilagin and at 325 nm for caffeic acid- rutin-quercetin. The column temperature was maintained 35°C and 10 μL of test solution was injected during the analysis.

In-vitro Biological Effect of SKK in Ameliorating CCl_4 Induced Injury

HepG2 cells were sourced from the ATCC authorized cell repository, National Center for Cell Sciences, Pune, India and grown in Dulbecco's Modified Eagle Hi-glucose medium supplemented with 10% fetal bovine serum and 1% penicillin-streptomycin antibiotics at 37°C and 5% CO_2 under humid conditions. For the experiments, the cells were seeded in 96 and 24 well plates at a density of 1×10^5 cells/mL. The cells were pre-incubated overnight. The next day, they were pre-treated for 1 h with SKK at final concentrations of 0.25, 0.5, and 1 mg/mL and then with 10 mM CCl_4. The exposed cells were incubated further for 18 h. At the end of the treatment time period, the exposure medium was replaced with 100 μL of fresh media containing 0.5 mg/mL of 3-(4,5-dimethylthiazol-2-yl)-2,5-diphenyltetrazolium bromide (MTT) in each well. The plates were incubated for an additional 3 h at 37°C and at the end of the time period, 50 of 75 μL of MTT containing media was removed from each well and 50 μL of pure DMSO was added. The plates were placed on a shaker for 10 min at 200 rpm. The absorbance of each well was recorded using the PerkinElmer Envision microplate reader, at 595 nm wavelength and cell viability percentage was calculated. For the analysis of AST, and ALT released from the HepG2 cells, the supernatant was collected from 24 well plates exposed to SKK and CCl_4 following the method mentioned for MTT and analyzed using Randox chemical analyzer (RX Monaco) and associated standard test kits (Randox Laboratories Ltd., United Kingdom).

For the detection of reactive oxygen species (ROS) and mitochondrial membrane potential (MMP), the HepG2 cells were seeded on the transparent bottom 96 well black plate at
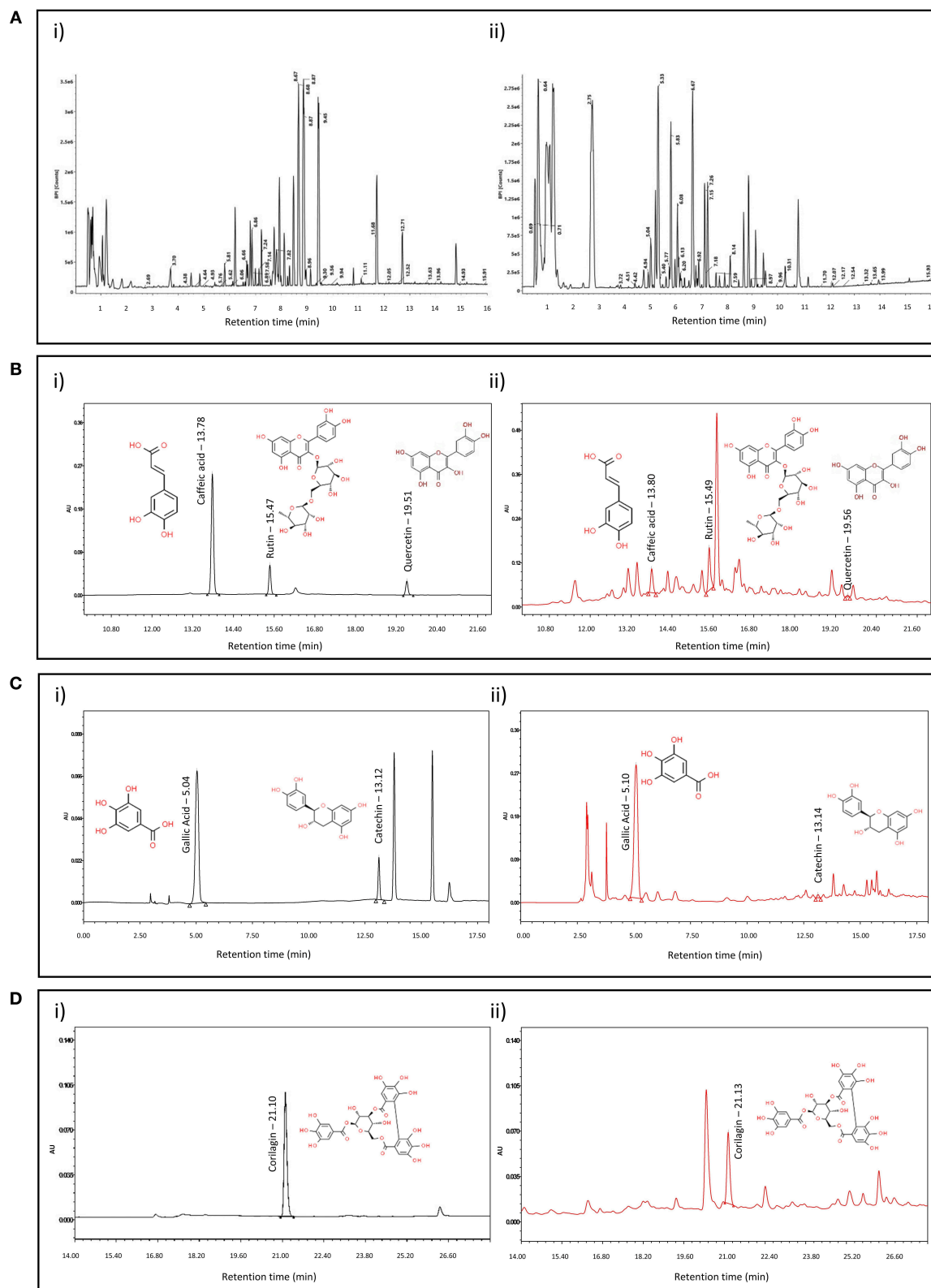
FIGURE 1 | Plant metabolite analysis of Divya Sarva-Kalp-Kwath (SKK): Aqueous extract of the SKK was screened for plant metabolites using liquid chromatography (LC)-based mass spectroscopy (MS). Spectral analysis revealed the presence of (**A**, i) 46 metabolites were detected in the positive mode and (**A**, ii) 48 metabolites

(Continued)

FIGURE 1 | were detected in the negative mode at different retention time (RT; min) (see **Table 1**). Using High Performance Liquid Chromatography (HPLC) analysis, SKK was analyzed and quantified for the metabolites, (**B**, i) Standards of caffeic acid, rutin, and quercetin, (**B**, ii) SKK contents of caffeic acid, rutin, and quercetin detected at 325 nm, (**C**, i) standards of gallic acid and catechin, (**C**, ii) SKK contents of gallic acid and catechin detected at 270 nm, and (**D**, i) standards of corilagin, (**D**, ii) SKK contents of corilagin detected at 270 nm. Gallic acid (RT: 5.10 min), catechin (RT: 13.14 min), caffeic acid (RT: 13.80 min), rutin (RT: 15.50 min), quercetin (RT: 19.56 min), and corilagin (RT: 21.13 min) were detected at their respective retention time (RT) in the developed and validated analytical HPLC method.

a density of 5×10^5 cells/mL and pre-incubated as mentioned above. The next day, cells were pre-treated with SKK at a final concentration of 1 mg/mL. After 1 h, cells were induced with CCl_4 (10 mM) for 12 h treatment. For measuring ROS and MMP, CellROX, and Mitotracker Red reagents (Thermo Fisher) were added, respectively, following the manufacturer's protocols. High-content analysis (HCA) of the cells was performed using a Nikon epifluorescence microscope, and images were analyzed using the HCS Studio software suite.

Experimental Animal Model

Male albino rats of Wistar strain (body weight 180–200 g) were used for the safety and pharmacological studies. Animals were procured from Liveon Life Sciences Pvt. Ltd., India and were housed in polypropylene cages in controlled room temperature $22 \pm 2°C$ and relative humidity of 60–70% with 12:12 h light and dark cycle in a registered animal house (1964/PO/Rc/S/17/CPCSEA). All animals were fed standard nutritionally balanced pellet diet (Purina Lab Diet, St. Louis, MO, USA) and sterile filtered water *ad libitum*. Animal experimentation ethical clearance was obtained from the Institutional Animal Ethical Committee of the Patanjali Research Institute, Haridwar, India. For the study, standard operating procedures and protocols were followed according to the approval numbers: PRIAS/LAF/IAEC-048 and PRIAS/LAF/IAEC-007.

Grouping of Experimental Animals

For the safety assessment, animals were randomized and divided into four treatment groups ($n = 5$ animals per group).

Group 1: Normal control (NC) animals were administered with distilled water only.
Group 2: SKK doses of 100 mg/kg.
Group 3: SKK dose of 500 mg/kg.
Group 4: SKK dose of 1,000 mg/kg.

For the pharmacological study, animals were divided randomly into five groups ($n = 7$ animals per group):

Group 1: NC animals administered with olive oil (intraperitoneal injection; 0.25 ml/kg; every 3rd day for 9 weeks) and 0.25% Na-CMC orally.
Group 2: Disease control (DC) animals administered with CCl_4 in olive oil v/v (intraperitoneal injection; 0.5 ml/kg; every 3rd day for 9 weeks).
Group 3: Animals were administered with CCl_4 in olive oil v/v (intraperitoneal injection; 0.5 ml/kg; every 3rd day for 9 weeks), and concurrent oral treatment of SLM (100 mg/kg; once daily for 9 weeks).

Group 4: Animals were administered with CCl_4 in olive oil v/v (intraperitoneal injection; 0.5 ml/kg; every 3rd day for 9 weeks), and concurrent oral treatment of SKK (100 mg/kg; once daily for 9 weeks).
Group 5: Animals were administered with CCl_4 in olive oil v/v (intraperitoneal injection; 0.5 ml/kg; every 3rd day for 9 weeks), and concurrent oral treatment of SKK (200 mg/kg; once daily for 9 weeks).

For the safety study, all SKK doses were dissolved in distilled water and given once a day through gavage administration for 28 days. In the case of pharmacological study, fresh suspension of SLM (using 0.25% Na-CMC) and solution of SKK were prepared daily and administered to the corresponding group of animals at the dose volume of 10 ml/kg. The animals were observed for body weight changes daily throughout the study period and averaged on a per-day basis for the safety study, whereas for the pharmacological study, they were averaged per week. Similarly, animal feed and water consumption were recorded daily until the end of the experiment. Histopathological, pathological, and biochemical changes in the animals were analyzed at the end of the study period following the euthanization of the animals.

Hematological and Serum Biochemical Analysis

Whole blood samples were collected from all the rats using the tail-snip method. In the safety study, parameters such as hemoglobin (Hb), total red blood corpuscles (RBC), hemoglobin per RBC (MCH), mean corpuscular hemoglobin concentration per unit volume (MCHC), mean corpuscular size (MCV), the total and differential counts of leukocytes were analyzed in the whole blood samples using the hematology analyzer BC-2800 (Mindray, Haryana, India).

In both the safety and pharmacological effect studies, analysis of biochemical parameters in the blood serum such as aspartate aminotransferase (AST), and alanine aminotransferase (ALT), urea, albumin, total bilirubin, total cholesterol, and creatinine levels were performed following manufacturer's protocol using Randox chemical analyser (RX Monaco) and associated standard test kits (Randox Laboratories Ltd, United Kingdom).

Histopathological Evaluation

The euthanized animals were dissected, and their target organs were excised. A portion of each tissue was fixed at 10% buffered formalin and embedded in paraffin. Solid sections of 5 μm thickness were made using a microtome and stained with hematoxylin-eosin (H&E). Blinded histopathological analysis of the H&E stained tissue sections was done by a veterinarian pathologist using an Olympus Magnus microscope camera. For the safety study, liver and kidney tissue samples were analyzed for determining the presence and distribution of focal, multifocal,

TABLE 1 | Liquid chromatography based metabolite analysis of the aqueous extract of Divya Sarva-Kalp-Kwath (SKK) showed the presence of 68 metabolites.

S.No.	Component name	Formula	RT (min)	Ionization mode	Observed m/z	Plant species
1	Citric acid monohydrate	$C_6H_{10}O_8$	0.64	–ve	209.0304	*Solanum nigrum* L. (Atanu et al., 2011; Albouchi et al., 2018)
2	Tartaric acid	$C_4H_6O_6$	0.69	–ve	149.0095	*Solanum nigrum* L. (Atanu et al., 2011)
3	D-(-)-Quinic acid	$C_7H_{12}O_6$	0.71	–ve	191.0567	
4	Gallic acid	$C_7H_6O_5$	2.69/2.75	+ve/–ve	171.0295/169.0141	*Solanum nigrum* L., *Phyllanthus* species (Huang et al., 2010; Mao et al., 2016; Jantan et al., 2019)
5	Gentiatibetine	$C_9H_{11}NO_2$	3.7/3.72	+ve/–ve	166.0873/164.0717	
6	Pseudolaroside C	$C_{14}H_{18}O_8$	4.38	+ve	315.1059	
7	Gentisic acid	$C_7H_6O_4$	4.42	–ve	153.0195	*Phyllanthus* species (Huang et al., 2010)
8	Gentianine	$C_{10}H_9NO_2$	4.43	+ve	176.0715	
9	Koaburaside	$C_{14}H_{20}O_9$	4.51	–ve	331.1027	*Phyllanthus* species (Mao et al., 2016)
10	Pyrogallic acid	$C_6H_6O_3$	4.64	+ve	127.0399	*Phyllanthus* species (Mao et al., 2016)
11	3-O-trans-Coumaroylquinic acid	$C_{16}H_{18}O_8$	4.66	+ve	339.1057	*Solanum* species (Daji et al., 2018)
12	Cornoside	$C_{14}H_{20}O_8$	4.67	–ve	315.1076	
13	1-O-Caffeoyquinic acid	$C_{16}H_{18}O_9$	4.93/4.94	+ve/–ve	355.1034	*Phyllanthus* species (Mao et al., 2016)
14	Picrasidine V	$C_{12}H_8N_2O_4$	5.03/5.04	+ve/–ve	245.0562/243.0439	
15	Demethylcoclaurine	$C_{16}H_{17}NO_3$	5.13	+ve	272.1285	
16	Camphoronic Acid	$C_9H_{14}O_6$	5.32/5.33	+ve/–ve	219.087/217.0712	
17	Protocatechuic aldehyde	$C_7H_6O_3$	5.4	–ve	137.0245	*Solanum* species (Kaunda and Zhang, 2019)
18	5-Caffeoylquinic acid	$C_{16}H_{18}O_9$	5.62/5.64	+ve/–ve	355.103/353.0871	*Solanum* species (Daji et al., 2018)
19	Umbelliferone	$C_9H_6O_3$	5.62	+ve	163.04	
20	Catechin	$C_{15}H_{14}O_6$	5.67	–ve	289.0712	*Phyllanthus* species (Huang et al., 2010; Mao et al., 2016)
21	Chlorogenic acid	$C_{16}H_{18}O_9$	5.76/5.77	+ve/–ve	355.104/353.087	*Solanum nigrum* L., *Phyllanthus* species (Huang et al., 2010; Mao et al., 2016)
22	Brevifolincarboxylic acid	$C_{13}H_8O_8$	5.81/5.83	+ve/–ve	293.0298/291.0142	*Phyllanthus* species (Mao et al., 2016)
23	Caffeic acid	$C_9H_8O_4$	6.02	–ve	179.0347	*Solanum nigrum* L. (Huang et al., 2010)
24	Phyllanthusiin E	$C_{13}H_8O_8$	6.06/6.08	+ve/–ve	293.0296/291.014	
25	Corilagin	$C_{27}H_{22}O_{18}$	6.13	–ve	633.074	*Phyllanthus* species (Mao et al., 2016)
26	Gallocatechin	$C_{15}H_{14}O_7$	6.2	–ve	305.0695	*Phyllanthus* species (Mao et al., 2016)
27	Coumurrin	$C_{16}H_{18}O_6$	6.27	–ve	305.1049	
28	Brevifolin	$C_{12}H_8O_6$	6.66/6.67	+ve/–ve	249.0401/247.0243	*Phyllanthus* species (Mao et al., 2016)
29	Quercetin 3,7-diglucoside	$C_{27}H_{30}O_{17}$	6.73/6.74	+ve/–ve	627.1566/625.1418	
30	Evodionol	$C_{14}H_{16}O_4$	6.86	+ve	249.1125	
31	Kaempferol-3-O-rutinoside	$C_{27}H_{30}O_{15}$	6.89	+ve	595.164	*Solanum* species, *Boerhavia diffusa* L. (Daji et al., 2018; Kumar et al., 2018)
32	m-coumaric acid	$C_9H_8O_3$	6.92	–ve	163.0401	*Solanum nigrum* L. (Huang et al., 2010)
33	Rutin	$C_{27}H_{30}O_{16}$	7.14/7.15	+ve/–ve	611.1609/609.1468	*Solanum nigrum* L., *Phyllanthus* species, *Solanum* species (Huang et al., 2010; Mao et al., 2016; Daji et al., 2018)
34	Citrusin B	$C_{27}H_{36}O_{13}$	7.18	–ve	567.2089	*Solanum* species (De Souza et al., 2019)
35	Ellagic Acid	$C_{14}H_6O_8$	7.24/7.26	+ve/–ve	303.0142/300.9985	*Phyllanthus* species (Mao et al., 2016)
36	Myricitrin	$C_{21}H_{20}O_{12}$	7.34/7.35	+ve/–ve	465.1024/463.0879	*Solanum nigrum* L. (Huang et al., 2010)
37	(3R)-Abruquinone B	$C_{20}H_{22}O_8$	7.37	–ve	389.1235	
38	Ecdysterone	$C_{27}H_{44}O_7$	7.42	+ve	481.3165	
39	Kaempferol-3-o-beta-glucopyranosyl7-o-alpha-rhamnopyranoside	$C_{27}H_{30}O_{15}$	7.58/7.59	+ve/–ve	595.1668/593.1516	
40	Astragalin	$C_{21}H_{20}O_{11}$	7.81	–ve	447.0911	*Phyllanthus* species (Mao et al., 2016)
41	Solamargine	$C_{45}H_{73}NO_{15}$	7.82	+ve	868.5101	*Solanum* species (Daji et al., 2018)

(Continued)

TABLE 1 | Continued

S.No.	Component name	Formula	RT (min)	Ionization mode	Observed m/z	Plant species
42	Dipropylmalonic acid	$C_9H_{16}O_4$	8.14	−ve	187.0973	
43	Naringenin	$C_{15}H_{12}O_5$	8.19/8.21	+ve/−ve	273.0765/271.0601	*Solanum nigrum* L. (Huang et al., 2010)
44	Rhoifolin	$C_{27}H_{30}O_{14}$	8.36	+ve	579.1694	*Solanum* species (Refaat et al., 2015)
45	Apigenin	$C_{15}H_{10}O_5$	8.92	−ve	269.0454	*Solanum nigrum* L. (Huang et al., 2010)
46	Chuanbeinone	$C_{27}H_{43}NO_2$	8.67	+ve	414.3369	
47	Solasonin	$C_{45}H_{73}NO_{16}$	8.68	+ve	884.5064	*Solanum* species (Daji et al., 2018)
48	Eupalitin 3-galactoside	$C_{23}H_{24}O_{12}$	8.79/8.8	+ve/−ve	493.1346/491.12	*Boerhavia diffusa* L. (Pereira et al., 2009)
49	Solasodine glucoside	$C_{33}H_{53}NO_7$	8.87	+ve	576.3908	
50	Solanine	$C_{45}H_{73}NO_{15}$	8.87	+ve	868.5114	*Solanum nigrum* L. (Albouchi et al., 2018)
51	Eupalitin-3-O-b-D-glucoside	$C_{23}H_{24}O_{12}$	8.93	−ve	491.1198	*Boerhavia diffusa* L. (Pereira et al., 2009)
52	Moupinamide	$C_{18}H_{19}NO_4$	8.96/8.97	+ve/−ve	314.139/312.1236	
53	Quercetin	$C_{15}H_{10}O_7$	9.3/9.32	+ve/−ve	303.0501/301.0348	*Solanum nigrum* L. (Huang et al., 2010; Mishra et al., 2014)
54	Solasodine 3-b-D-glucopyranoside	$C_{33}H_{53}NO_7$	9.45	+ve	576.3906	*Solanum* species (Li et al., 2015)
55	Apigenin-7-O-α-L-rhamnose(1→4)-6"-O-acetyl-β-D-glucoside	$C_{29}H_{32}O_{15}$	9.56	+ve	621.1809	
56	Butein	$C_{15}H_{12}O_5$	9.94/9.96	+ve/−ve	273.0765/271.0608	*Solanum* species (Bovy et al., 2007)
57	Kaempferol	$C_{15}H_{10}O_6$	10.31	−ve	285.0402	*Solanum nigrum* L., *Boerhavia diffusa* L. (Huang et al., 2010; Mishra et al., 2014)
58	Solasodine	$C_{27}H_{43}NO_2$	11.11	+ve	414.3364	*Solanum nigrum* L. (Albouchi et al., 2018)
59	Eupalitin	$C_{17}H_{14}O_7$	11.68/11.7	+ve/−ve	331.0814/329.0662	*Boerhavia diffusa* L. (Pandey et al., 2005)
60	Coccineone B	$C_{16}H_{10}O_6$	12.05/12.07	+ve/−ve	299.056/297.0399	*Boerhavia diffusa* L. (Mishra et al., 2014)
61	Boeravinone E	$C_{17}H_{12}O_7$	12.17	−ve	327.0508	*Boerhavia diffusa* L. (Lami et al., 1990; Bairwa et al., 2013; Mishra et al., 2014)
62	Boeravinone K	$C_{17}H_{12}O_6$	12.52/12.54	+ve/−ve	313.0714/311.0559	*Boerhavia diffusa* L. (Bairwa et al., 2013)
63	Veratramine	$C_{27}H_{39}NO_2$	12.71	+ve	410.3059	
64	Boeravinone I	$C_{18}H_{14}O_7$	13.32	−ve	341.0664	*Boerhavia diffusa* L. (Mishra et al., 2014)
65	Boeravinone B	$C_{17}H_{12}O_6$	13.63/13.65	+ve/−ve	313.0713/311.0552	*Boerhavia diffusa* L. (Bairwa et al., 2013; Mishra et al., 2014)
66	Boeravinone G	$C_{18}H_{14}O_7$	13.96/13.99	+ve/−ve	343.0856/341.066	*Boerhavia diffusa* L. (Mishra et al., 2014)
67	Tigogenin	$C_{27}H_{44}O_3$	14.93	+ve	417.3361	*Solanum nigrum* L. (Albouchi et al., 2018)
68	Boeravinone A	$C_{18}H_{14}O_6$	15.91/15.93	+ve/−ve	327.0872/325.071	*Boerhavia diffusa* L. (Mishra et al., 2014)

*Out of these 46 metabolites were detected in the positive mode. Forty-eight metabolites were detected in the negative mode (see **Figure 1**). Based on a literature search, sources of these metabolites were identified as- (a) Boerhavia diffusa L., (b) Phyllanthus niruri L., and (c) Solanum nigrum L. and listed on the basis of their retention time (RT; min), respective charge and observed mass to charge (m/z) ratio.*

and diffuse lesions. For the pharmacological effect study, only the liver tissue samples were analyzed for severity of the lesions that were scored as 0 = Not Present, 1 = Minimal (<1%), 2 = Mild (1–25%), 3 = Moderate (26–50%), 4 = Moderately Severe (51–75%), 5 = Severe (76–100%). Average of the individual scores obtained from all the animals present in a group were calculated to generate each lesion score. Finally, the mean of respective tissue lesions score were considered for the final calculations.

Statistical Analysis

Data are expressed as mean ± standard error of means (SEM) for each group. A one-way analysis of variance (ANOVA) followed by Dunnett's multiple comparison t-test was used to calculate the statistical difference. Values of $p < 0.05$ were considered statistically significant. Statistical analysis was done using GraphPad Prism version 7.0 software (GraphPad Software, CA).

RESULTS

LC-MS-QToF and HPLC Based Metabolite Analysis of SKK

Aqueous extract of the SKK was first analyzed using LC-MS QToF technique. Results showed the presence of 68 identifiable metabolites present in SKK decoction. Among these, 46 metabolites were detected in the positive mode and 48 metabolites in the negative mode (**Figure 1A**i,ii). Metabolites identified were citric acid monohydrate, gallic acid, gentisic acid, catechin, brevifolincarboxylic acid, caffeic acid, corilagin, rutin, ellagic acid, naringenin, apigenin, quercetin, kaempferol,
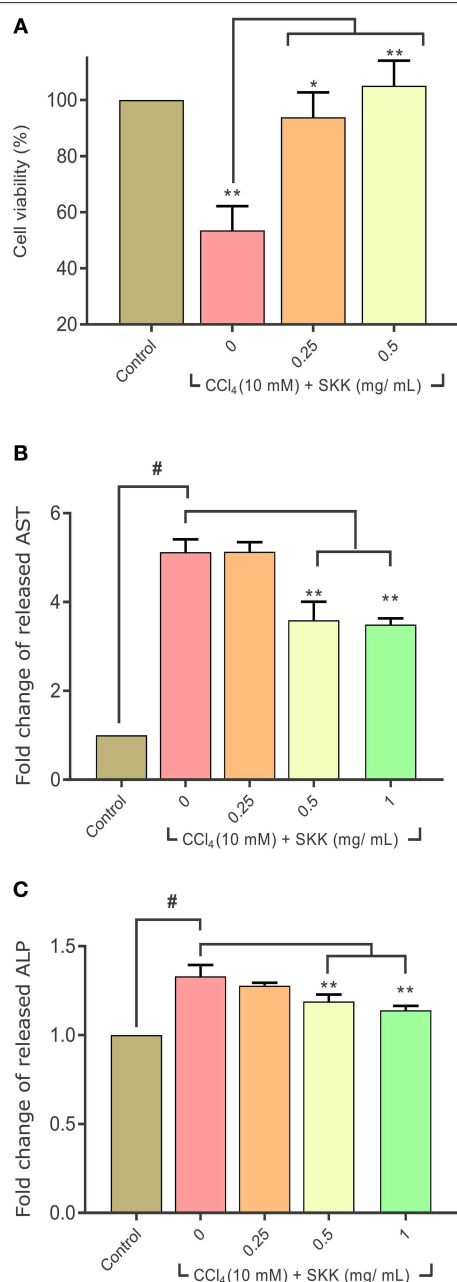
FIGURE 2 | *In-vitro* analysis of cellular and biochemical effects of Divya Sarva-Kalp-Kwath (SKK): **(A)** significant loss of cell viability was observed following the stimulation of HepG2 cells with 10 mM of CCl_4. Co-treatment of the CCl_4 stimulated HepG2 cells with SKK led to a significant recovery of cell viability. Also, CCl_4 stimulation of the HepG2 cells led to an augmented release of liver injury serum-based biomarkers, **(B)** aspartate aminotransferase (AST), and **(C)** alkaline phosphatase (ALP). Release of these serum hepatotoxicity biomarkers was ameliorated following co-treatment of the CCl_4 stimulated HepG2 cells with SKK (0.5 and 1 mg/mL). Results are expressed as mean ± standard deviation. One-way analysis of variance (ANOVA) followed by Dunnett's multiple comparison *t*-test was used to calculate the statistical difference. *p*-value *<0.05; **<0.01; #<0.01.

solasodine, and coccineone B as a major metabolites. Based on a literature search, sources of these metabolites were identified as, *B. diffusa* L., *P. niruri* L., and *S. nigrum* L. (**Table 1**).

Furthermore, the spectral signature of several other metabolites was also identified in the SKK decoction which is currently under investigation.

Quantitative analysis of selected metabolite present in the SKK decoction was performed using HPLC method and confirmed the presence of gallic acid (RT: 5.10 min), catechin (RT: 13.14 min), caffeic acid (RT: 13.80 min), rutin (RT: 15.49 min), quercetin (RT: 19.56 min), corilagin (RT: 21.13 min; **Figures 1B–D**). Using internal standards, the metabolites were quantified as, gallic acid: 1.929 μg/mg, catechin: 0.197 μg/mg, rutin: 0.223 μg/mg, caffeic acid: 0.028 μg/mg, quercetin 0.011 μg/mg, and corilagin 2.954 μg/mg (**Figures 1B**i,ii,**C**i,ii,**D**i,ii).

In-vitro Biological Effect Study of SKK Decoction in Reducing CCl_4 Stimulated Hepatotoxicity

Under *in-vitro* conditions, stimulation of the HepG2 cells with 10 mM carbon tetrachloride (CCl_4), induced a significant ($p < 0.01$) loss of cell viability (53 ± 9%) (**Figure 2A**). Treatment of these CCl_4 stimulated HepG2 cells with SKK at the concentrations of 0.25 and 0.5 mg/mL significantly reversed the loss in cell viability to 94 ± 9% ($p < 0.05$) and 105 ± 9% ($p < 0.01$), respectively. Analysis of the released AST and ALP enzymatic biomarkers in the CCl_4 stimulated HepG2 cell culture supernatant showed a ∼1.5–2-folds' increase, compared to the untreated normal control (NC) cells (**Figures 2B,C**). Treatment of the CCl_4 stimulated HepG2 cells with SKK (0.5 and 1 mg/mL) significantly ($p < 0.01$) attenuated the release of the liver injury AST and ALP biomarkers (**Figures 2B,C**). SLM treatment of the CCl_4 stimulated HepG2 cells also showed a reversal of the CCl_4 induced cytotoxicity and release of hepatotoxicity biomarkers (data not shown).

High content analysis (HCA) of the CCl_4 stimulated HepG2 cells was done to study the modulation of ROS and MMP following treatment with SKK (1 mg/mL) (**Figure 3A**). The representative figures showed an expression of ROS in green colored fluorescence and MMP in red-colored fluorescence; the merged fluorescence images produced yellow-colored spots due to co-localization within the HepG2 cells (**Figure 3A**). Quantitative analysis of the microscopic images showed a high induction of ROS levels in the HepG2 cells following stimulation with CCl_4 (10 mM) (**Figure 3B**). Treatment of these stimulated cells with SKK (1 mg/mL) led to a significant ($p < 0.01$) reduction in the intracellular release of ROS. Similarly, enhanced MMP levels in the CCl_4 stimulated HepG2 cells as compared to control cells, were also found to be significantly reduced ($p < 0.05$) following treatment with SKK decoction (**Figure 3C**).

In-vivo Safety of SKK Decoction

In a 28 days repeat dose safety study, no change was observed in the daily body weight of the Wistar rats treated with SKK decoction at the concentrations of 100, 500, and 1,000 mg/kg/day (**Figures 4A,B**). Similarly, no variation was observed in the daily average feed consumption of the different animal groups throughout the study period (**Figure 4C**). Histopathological analysis of the lung, brain, heart, liver and kidney tissues in the SKK treated rats showed the absence of any focal, multifocal, or diffuse inflammatory lesions (**Figure 4D**). Whole blood analysis
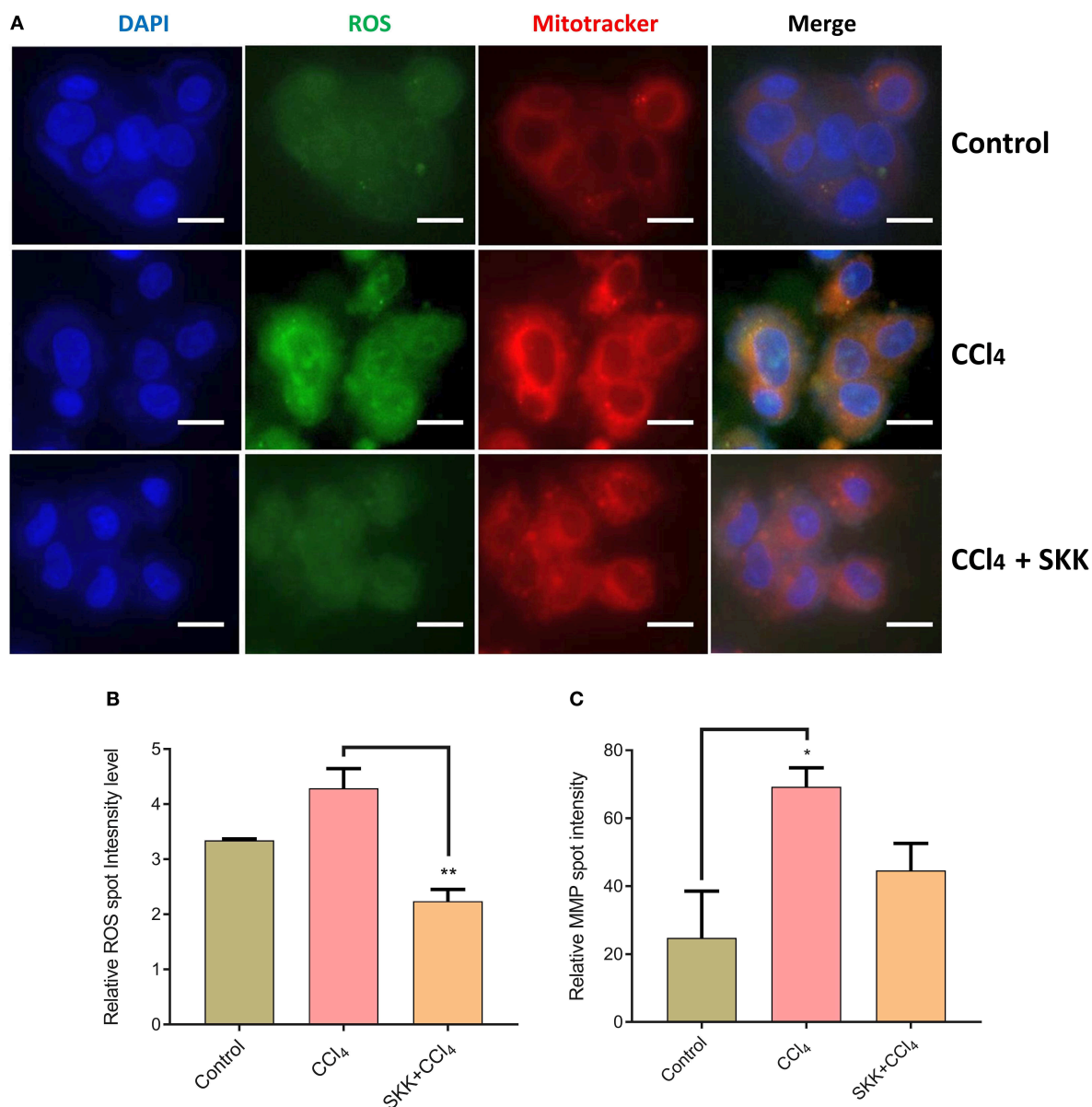
FIGURE 3 | Reactive oxygen species and mitochondrial membrane potential measurement in Divya Sarva-Kalp-Kwath (SKK) and carbon tetrachloride (CCl$_4$) treated HepG2 cells: **(A)** Oxidative stress was induced in the HepG2 cells following stimulation with the CCl$_4$. Intracellular presence of reactive oxygen species (ROS; green color) and an increase in mitochondrial membrane potential (MMP; red color) were determined through epifluorescence microscope based imaging and HCS Studio software based analysis. Co-treatment of the HepG2 cells with SKK and CCl$_4$ significantly reduced the production of ROS and MMP. **(B)** Quantitatively, ROS levels in the CCl$_4$ stimulated HepG2 cells showed an upregulation. **(C)** Similarly, MMP in the CCl$_4$ stimulated HepG2 cells showed an upregulation. Both these parameters showed a reduction following the co-treatment of the HepG2 cells with CCl$_4$ and SKK. Results are expressed as Mean ± Standard Error of Means. One-way analysis of variance (ANOVA) followed by Dunnett's multiple comparison t-test was used to calculate the statistical difference. p-value *<0.05; **<0.01. Bars represent 200 μm.

also showed no change in the levels of hemoglobin, red blood cells (RBC) indices, total and differential leucocyte counts in the SKK-treated animals (**Table 2**). Similarly, albumin, glucose, AST, ALT ($p < 0.05$ at 1,000 mg kg day), ALP, total bilirubin urea, creatinine, and total cholesterol levels remained unchanged in the serum of the SKK treated groups, compared with the NC animals (**Tables 2**, **3**). Thus, 28 days treatment of the Wistar rats with SKK did not produce any adverse effects up to the dose of 1,000 mg/kg/day.

In-vivo Pharmacological Effects of SKK Decoction in Modulating CCl$_4$ Induced Hepatotoxicity

Liver injury was induced in the male Wistar rats using an intraperitoneal injection of CCl$_4$ at the dose of 0.5 mg/kg. A variety of physiological, biochemical, and histopathological markers were tested during the study (**Figure 5A**). Compared to the NC animals, the disease control (DC) animals showed

FIGURE 4 | *In-vivo* Safety Analysis of Divya Sarva-Kalp-Kwath (SKK): **(A)** Male Wistar rats were randomized and divided into four treatment groups (*n* = 5): Group 1: Normal control (NC) animals were administered with distilled water only; Group 2: SKK doses of 100 mg/kg; Group 3: SKK dose of 500 mg/kg; and Group 4: SKK

(Continued)
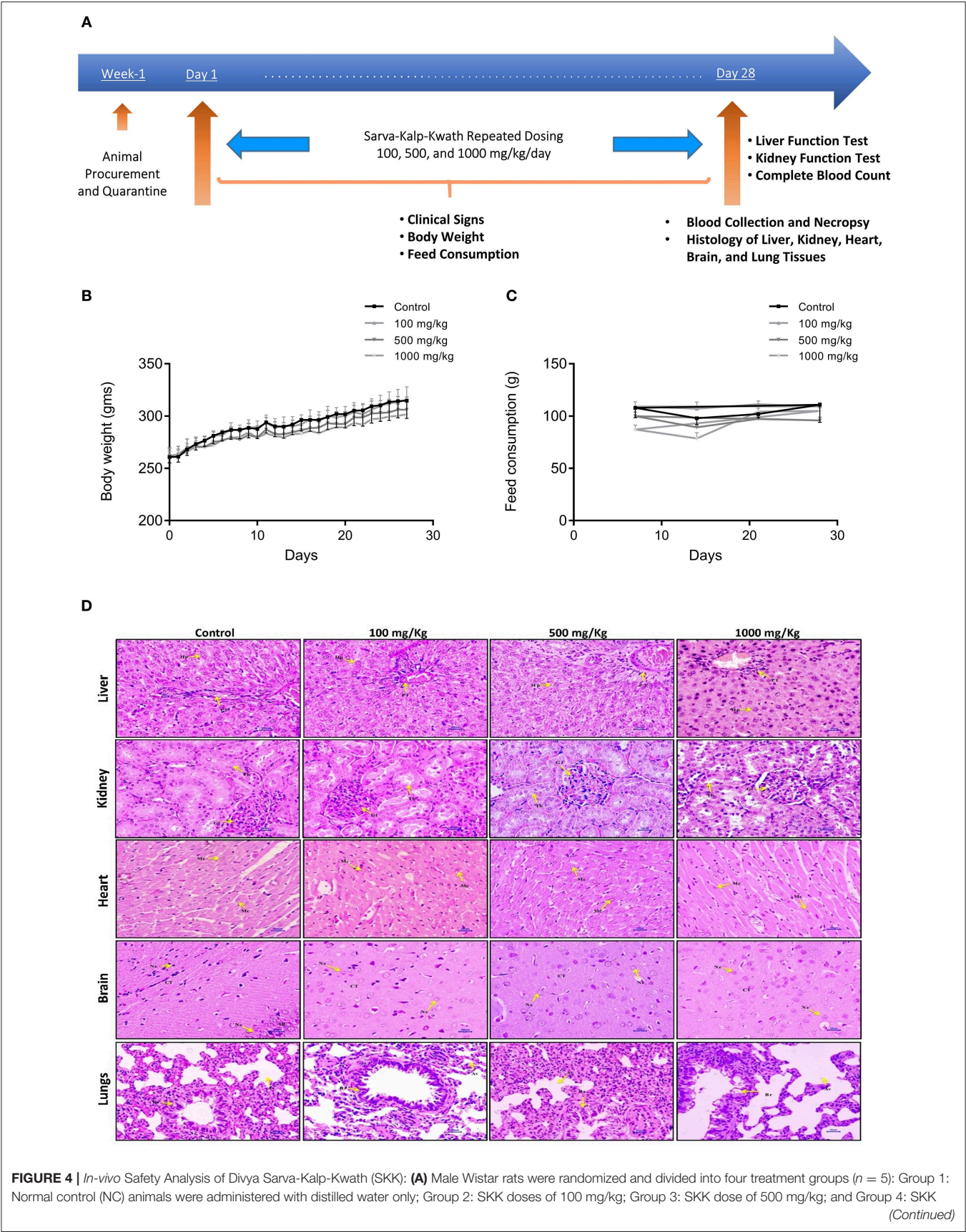
FIGURE 4 | dose of 1,000 mg/kg. Water extract of SKK was dissolved in distilled water and administered daily by gavage for 28 days. The animals were observed for physiological, histopathological, and biochemical changes. **(B)** Body weight change in the SKK exposed animals was measured daily and no changes were detected throughout the study period. **(C)** Feed consumption of the SKK treated animals was determined daily and averaged per week. The animals did not show any change in their feed consumption. Histopathological analysis of the **(D)** Liver, kidney, heart, brain, and lung tissue samples obtained from the Wistar rats, did not show any pathological lesions following exposure- Control, SKK 100 mg/kg, SKK 500 mg/ml, and SKK 1,000 mg/kg treatment. Results are expressed as a Mean ± Standard Error of Means. One-way analysis of variance (ANOVA) followed by Dunnett's multiple comparison t-test was used to calculate the statistical difference. No statistical significance was detected.

TABLE 2 | Hematological safety analysis of 28 days repeated dosing of SKK in male Wistar rats: Parameters such as hemoglobin (Hb), total red blood corpuscles (RBC), hemoglobin per RBC (MCH), mean corpuscular hemoglobin concentration per unit volume (MCHC), mean corpuscular size (MCV), the total and differential counts of leukocytes were tested in the whole blood collected from the Wistar rats exposed to Divya Sarva-Kalp-Kwath (SKK) decoction up to the concentration of 1,000 mg/kg.

Gr. no.	Dose (mg/kg)	Hb (g/dL)	Total RBC ($\times 10^6$/mm^3)	RBC indices			Total WBC ($\times 10^3$/mm^3)	Differential leucocyte count (%)				
				MCH (pg/cell)	MCV (fL/cell)	MCHC (g/dL)		Neutrophil	Lymphocyte	Eosinophil	Macrophage	Basophil
1	0	16 ± 1	7.8	21 ± 1	53 ± 3	39	16 ± 5	21 ± 8	73 ± 9	1	4 ± 2	1
2	100	16	7.7	21 ± 1	53 ± 2	39 ± 1	14 ± 6	22 ± 6	70 ± 6	2	4 ± 1	1
3	500	16 ± 1	7.5	10 ± 2	54 ± 1	39 ± 1	15 ± 5	24 ± 5	70 ± 5	1	3 ± 1	2
4	1,000	15 ± 4	7 ± 1	21 ± 1	53 ± 1	39 ± 1	15 ± 4	20 ± 5	72 ± 5	2 ± 2	5 ± 2	1

No changes were observed in the SKK treated animals in comparison to the normal control animals (0 mg/kg). The results indicated that SKK was safe up to five times the human equivalent oral dose given to the CCl$_4$ treated Wistar rats in the pharmacological effect study.

TABLE 3 | Effect of 28-days oral exposure of SKK on blood biochemistry in wistar rats: Biochemical parameters such as urea, creatine, albumin, alanine transaminase (ALT), aspartate aminotransferase (AST), alkaline phosphatase (ALP), total bilirubin, glucose, and cholesterol levels were determined in the serum of Wistar rats exposed to varying concentrations of the Divya Sarva-Kalp-Kwath (SKK).

Gr. no.	Dose (mg/kg)	Urea (mg/dL)	Creatinine (mg/dL)	Albumin (g/dL)	ALT (U/L)	AST (U/L)	ALP (U/L)	Total Bilirubin (mg/dL)	Glucose (mg/dL)	Total Cholesterol (mg/dL)
1	0	53 ± 3	1	4	112 ± 15	288 ± 36	446 ± 100	0.04 ± 0.05	103 ± 5	63 ± 4
2	100	48 ± 4	0.6	3	109 ± 22	264 ± 24	464 ± 100	0.04 ± 0.09	101 ± 7	54 ± 6
3	500	51 ± 4	0.5	3	114 ± 18	224 ± 36	387 ± 79	0.04 ± 0.05	102 ± 8	56 ± 11
4	1,000	48 ± 7	0.5	3	115 ± 1	199 ± 47	439 ± 137	0.06 ± 0.09	100 ± 6	57 ± 10

Based on the analysis, no change in these serum-based biochemical parameters was observed in the animals exposed up to the dose of 1,000 mg/kg of SKK in comparison to the normal control animals (0 mg/kg). No changes were observed in the SKK treated animals in comparison to the normal control animals (0 mg/kg). The results indicated that SKK was safe up to five times the human equivalent oral dose given to the CCl$_4$ treated Wistar rats in the pharmacological effect study.

a significant decline ($p < 0.01$) in their body weights (**Figure 5B**). Treatment of the CCl$_4$ stimulated animals with human equivalent dose (100 mg/kg), and a higher dose (200 mg/kg) of SKK displayed significant ($p < 0.01$) recovery of their body weight (**Figure 5B**). This SKK induced recovery was comparable to those induced by SLM (100 mg/kg). Following, a 6 weeks' treatment of the CCl$_4$ stimulated rats, significant recovery was observed in the feeding habit of the animals following treatment with the 200 mg/kg dose of SKK decoction. This recovery was found to be stable until the end of the 9 weeks' study period. Further, animals treated with SKK at the concentration of 100 mg/kg and reference drug, SLM showed no change in their feed consumption (**Figure 5C**). Similar to the observations made under *in-vitro* conditions, Wistar rats showed a significant ($p < 0.01$) elevation in their serum levels of ALT, AST, ALP, bilirubin, total cholesterol, and uric acid following stimulation with CCl$_4$ (**Figure 6**). Enhanced levels of these serum biomarkers indicated CCl$_4$ induced injury to the liver and kidney of the

stimulated animals. Treatment of the CCl$_4$ pre-treated rats with equivalent concentration (100 mg/kg) of SKK or, SLM showed no alteration in the release of ALT enzyme (**Figure 6A**). Treatment of the CCl$_4$ stimulated rats with a higher concentration of SKK (200 mg/kg) showed a considerable but statistically non-significant reduction in ALT levels in comparison to the DC animals. The CCl$_4$ stimulated increase in the AST levels of rats, was significantly reduced following treatment of the animals with SKK (200 mg/kg; $p < 0.01$) and the reference drug SLM (100 mg/kg; $p < 0.05$) (**Figure 6B**). Serum ALP levels also showed a significant ($p < 0.05$) reduction in the CCl$_4$ stimulated rats following treatment with SKK (200 mg/kg) (**Figure 6C**). Total bilirubin, cholesterol, and uric acids were also prominently reduced in the CCl$_4$ stimulated rats following treatments with the different concentrations of SKK or SLM (**Figures 6D–F**).

Histopathological analysis of the liver tissue obtained from the euthanized CCl$_4$ stimulated Wistar rats showed the development of inflammatory fibrosis, lymphocytic infiltration,
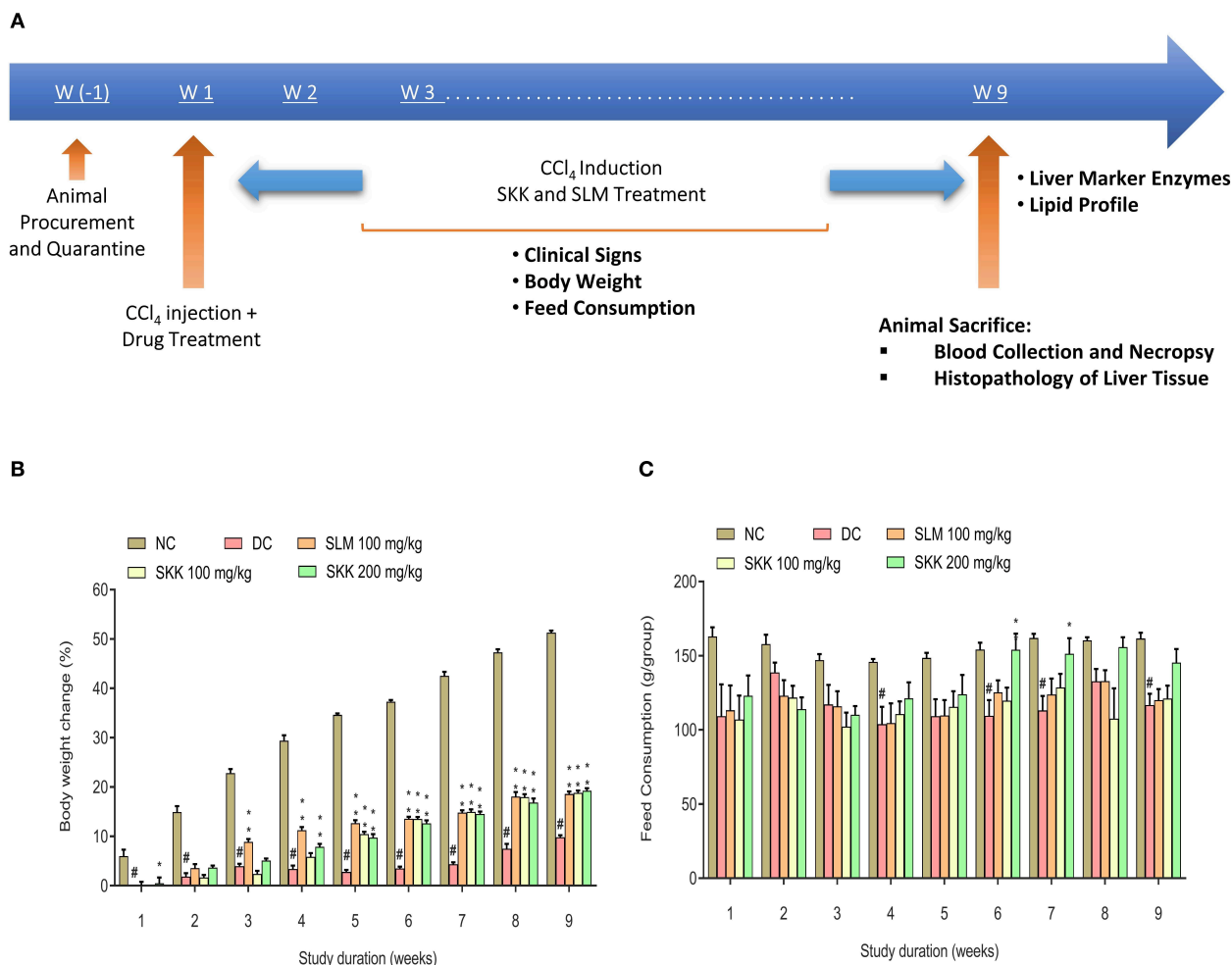
FIGURE 5 | *In-vivo* pharmacological effect study of Divya Sarva-Kalp-Kwath (SKK) in carbon tetrachloride (CCl$_4$) treated wistar Rats: **(A)** Wistar rats were divided randomly into four groups ($n = 5$): Group 1 (NC): Animals were administered with olive oil (intraperitoneal injection; 0.25 ml/kg; every 3rd day for 9 weeks) and 0.25% Na-CMC, Group 2 (DC): Animals were administered with CCl$_4$ in olive oil v/v (intraperitoneal injection; 0.5 ml/kg; every 3rd day for 9 weeks), Group 3 (PC): Animals were administered with CCl$_4$ in olive oil v/v (intraperitoneal injection; 0.5 ml/kg; every 3rd day for 9 weeks) with the concurrent oral treatment of SLM (100 mg/kg; once daily for 9 weeks), Group 4 (SKK-treated): Animals were administered with CCl$_4$ in olive oil v/v (intraperitoneal injection; 0.5 ml/kg; every 3rd day for 9 weeks) with the concurrent oral treatment of SKK (100 and 200 mg/kg; once daily for 9 weeks). The animals were observed for physiological, histopathological, and biochemical changes during and after completion of the study period. **(B)** Substantial loss of body weight was detected in the CCl$_4$ stimulated Wistar rats. Treatment of the CCl$_4$ stimulated animals with human equivalent and higher dose of SKK (100 and 200 mg/kg) resulted in the minor recovery in body weight loss. **(C)** Wistar rats treated with CCl$_4$ showed loss of food habits over a period of 28 days. Recovery was detected in the CCl$_4$ stimulated animals following treatment with the high dose of SKK (200 mg/kg). SLM (100 mg/kg) was used as a positive control in the study and did not induce any changes in the feed habits. Results are expressed as Mean ± Standard Error of Means. One-way analysis of variance (ANOVA) followed by Dunnett's multiple comparison *t*-test was used to calculate the statistical difference. *p*-value # <0.01; * <0.05; ** <0.01.

and hyperplastic bile duct (**Figure 7A**i,ii). Treatment of the CCl$_4$ stimulated rats with SKK (100 and 200 mg/kg) or SLM (100 mg/kg) displayed a remarkable reduction in the severity and distribution of these inflammatory lesions in the liver tissue viz. moderate fibrosis, lymphocytic infiltration, hyperplastic bile duct, and vacuolation (**Figure 7A**iii–v). Based on the lesion score criteria, CCl$_4$ stimulated rats showed an approximately 10-fold increase in their "total lesion score" (**Figure 7E**). Further, treatment with SKK at 100 and 200 mg/kg significantly ($p < 0.01$) reduced the "total lesion score" in a dose-dependent manner

(**Figure 7E**). Reference drug, SLM (100 mg/kg) treatment showed a significant ($p < 0.01$) reduction in "total lesion score" as compared to DC animals.

Individual lesion score analysis, further confirmed the histopathological observations, showing significant induction ($p < 0.01$) of bile duct hyperplasia, hepatocellular vacuolation, interlobular fibrosis, and lymphocytic infiltrations, in the DC animals. Treatment of the stimulated animals with SKK (200 mg/kg) showed signs of significant ($p < 0.01$) improvements in CCl$_4$ induced injuries through reduction of the inflammatory
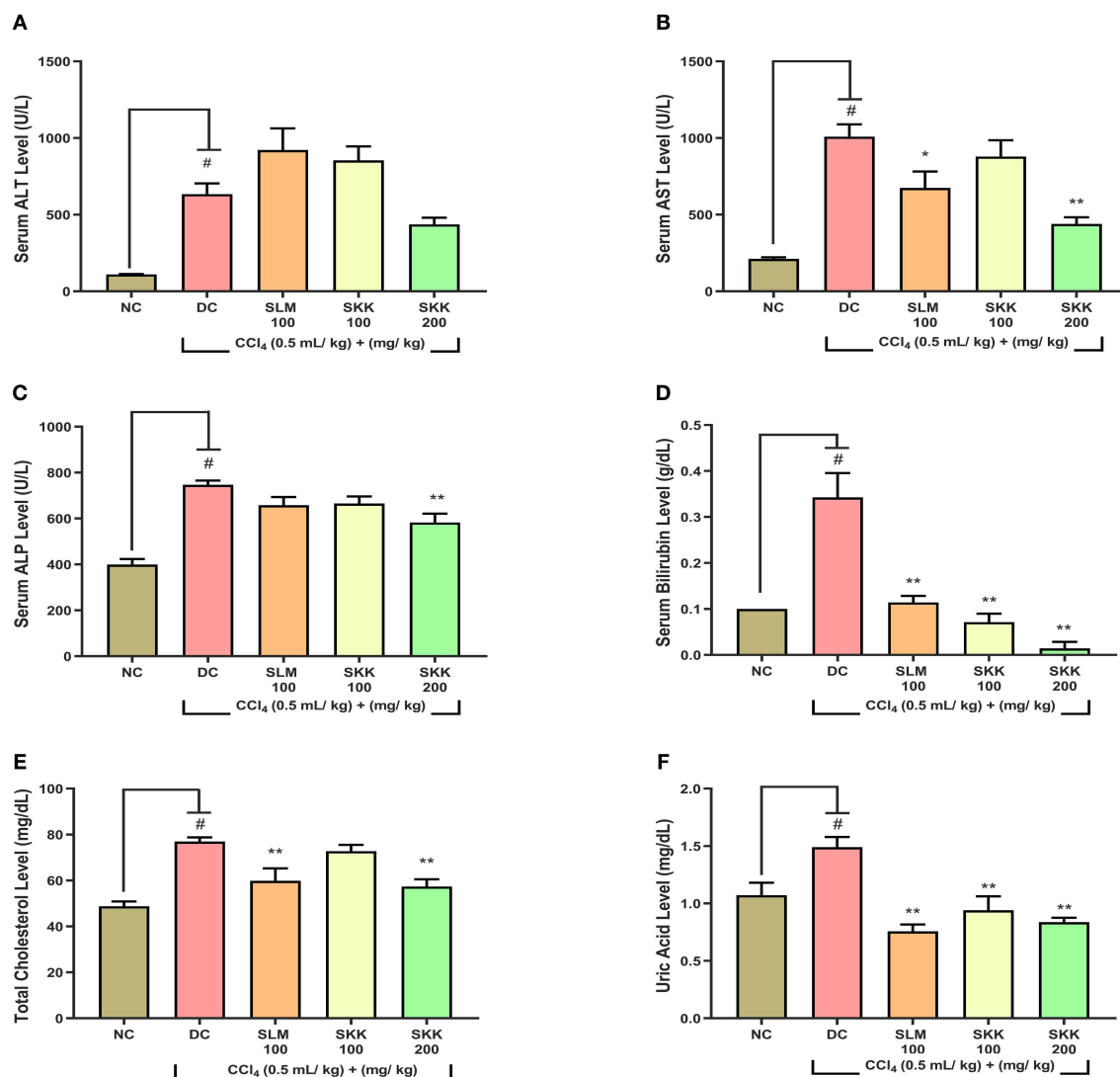
FIGURE 6 | *In-vivo* biochemical analysis of CCl_4 stimulated wistar rats treated with Divya Sarva-Kalp-Kwath (SKK): Wistar rats stimulated with CCl_4 showed a significant upsurge in their serum enzyme levels–**(A)** alanine transaminase (ALT), **(B)** aspartate aminotransferase (AST), **(C)** alkaline phosphatase (ALP), **(D)** total bilirubin, **(E)** total cholesterol, and **(F)** uric acid. Co-treatment of the CCl_4 stimulated rats with SKK (100 and 200 mg/kg) showed a significant reduction in their serum liver injury biomarkers. SLM (100 mg/kg) was used as a positive control in the study. Results are expressed as Mean $\pm$ Standard Error Mean. One-way analysis of variance (ANOVA) followed by Dunnett's multiple comparison *t*-test was used to calculate the statistical difference. *p*-value #<0.01; *<0.05; **<0.01.

lesions. Low dose treatment of the stimulated animals with SKK (100 mg/kg) could only lessen the induced bile duct hyperplasia ($p < 0.01$). Similarly, reference drug SLM (100 mg/kg) displayed prominent ($p < 0.01$) reduction in the induced bile duct hyperplasia, hepatocellular vacuolation, interlobular fibrosis (IF), and lymphocytic infiltration (**Figures 7B–E**).

It is interesting to note that in the overall study, we could observe that the treatment of CCl_4 stimulated rats with both the concentrations of SKK (100 and 200 mg/kg) and reference drug- SLM (100 mg/kg) significantly reduced the liver injuries. The human equivalent dose of SKK (100 mg/kg) in several parameters showed an equivalent pharmacological effect to SLM (100 mg/kg). However, a higher dose of SKK (200 mg/kg) showed

a better hepatoprotective effect than the SLM, against the CCl_4 induced hepatic damages.

DISCUSSION

CCl_4 is well-documented for inducing hepatotoxicity in both animals and humans and extensively used as a study model for evaluating the pharmacological effects of newly synthesized drugs and herbal formulations (Manibusan et al., 2007; Ingawale et al., 2014; Dong et al., 2016). The three herbal components of SKK decoction (*B. diffusa* L., *P. niruri* L., and *S. nigrum* L.) are well-known to have anti-oxidant, anti-inflammatory, and
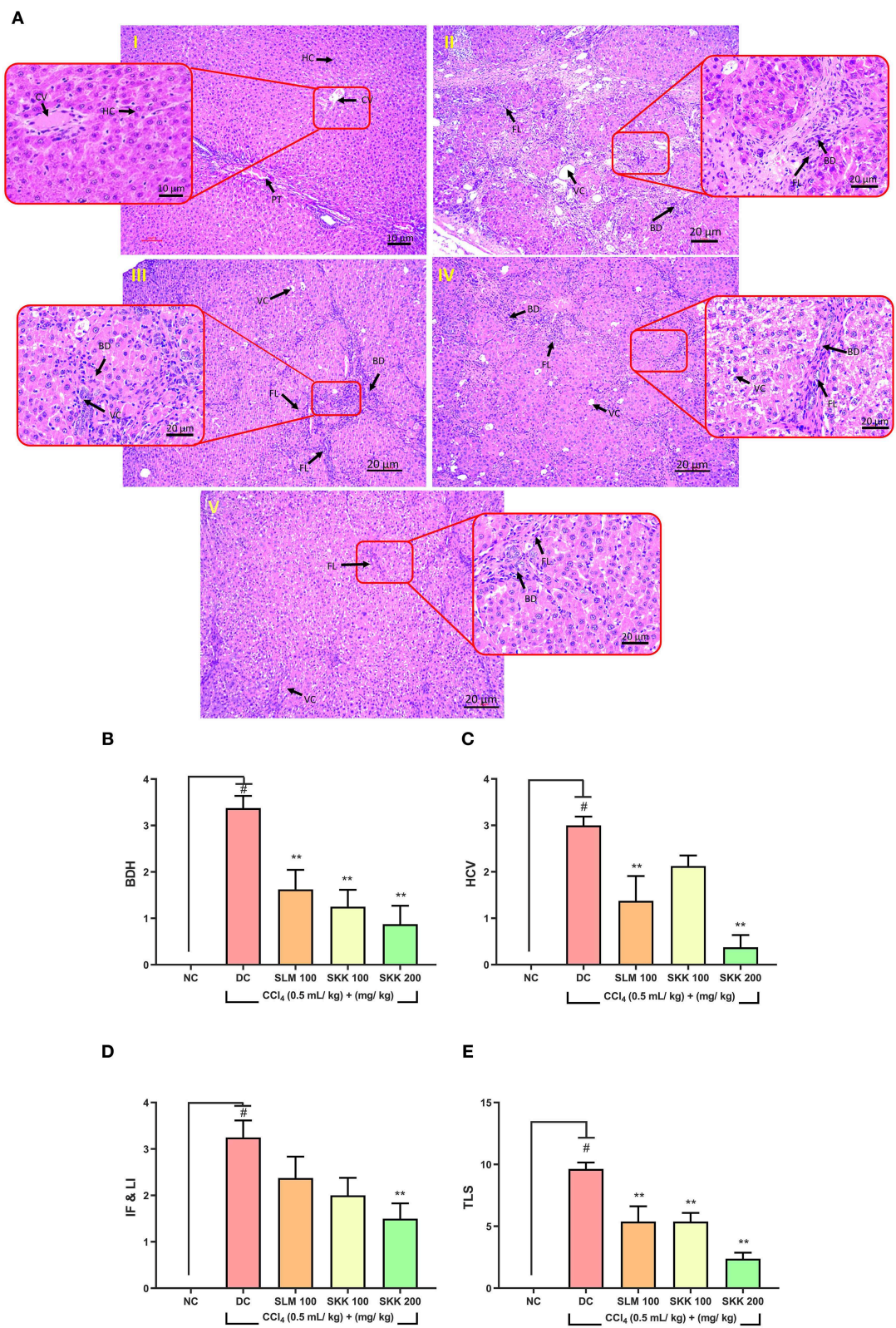
FIGURE 7 | Histopathological Analysis of Wistar Rats Treated with CCl$_4$ and Co-Treated with Divya Sarva-Kalp-Kwath (SKK): **(A)** Histopathological investigation was performed in the liver tissue samples obtained from the Wistar rats treated for 9 weeks with CCl$_4$, reference drug: SLM (100 mg/kg) and SKK (100 and 200 mg/kg).

(Continued)

FIGURE 7 | Results indicated- (i) Untreated animal liver tissue represents normal histology of liver tissue; portal triad (PT), central vein (CV), hepatocyte, (ii) CCl$_4$ treated animals showed the presence of severe fibrosis and lymphocytic infiltration (FL), hyperplastic bile duct in the hepatic regions, (iii) Wistar rats treated with SLM (100 mg/kg) showed the development of moderate fibrosis and lymphocytic infiltration (FL), hyperplastic bile duct (BD), vacuolation (VC) in the hepatic tissues; (iv) CCl$_4$ and SKK (100 mg/kg) co-treated animals showed moderate levels of fibrosis and lymphocytic infiltration (FL), hyperplastic bile duct (BD), vacuolation (VC) in their hepatic region; (v) Wistar rats treated with CCl$_4$ and higher dose of SKK (200 mg/kg) showed the presence of mild fibrosis and lymphocytic infiltration (FL), hyperplastic bile duct (BD) in their hepatic regions. Finally, based on individual lesion scoring, the CCl$_4$ treated animals showed marked increase in- **(B)** hyperplastic bile duct (BDH), **(C)** Hepatocellular vacuolation (HCV), **(D)** interlobular fibrosis and lymphocytic infiltration (IF & LI), and **(E)** Total Lesion Score (TLS). The positive control drug, SLM (100 mg/kg) significantly ameliorated the hepatic injuries induced by CCl$_4$ treatment. CCl$_4$ stimulated animals co-treated with SKK at 100 and 200 mg/kg also showed significant amelioration in their hepatic lesion score. Results are expressed as Mean $\pm$ Standard Error of Means. One-way analysis of variance (ANOVA) followed by Dunnett's multiple comparison t-test was used to calculate the statistical difference. p-value $^{\#}$ <0.01; ** <0.01.

hepatoprotective properties (Lin et al., 2008; Manjrekar et al., 2008; Ramachandra et al., 2011).

Plant metabolites play a major role in the active prevention of diseases. Hence, our chemical analysis of the SKK decoction revealed the presence of several plant metabolites such as rotenoids (boeravinones: A, B, E, G, I, K), eupalitin 3-galactoside, eupalitin, coccineone B, koaburaside, pyrogallic acid, 1-O-caffeoyquinic acid, phyllanthusiin E, corilagin, gallocatechin, astragalin, tartaric acid, gentisic acid, 3-O-trans-coumaroylquinic acid, protocatechuic aldehyde, 5-caffeoylquinic acid, caffeic acid, m-coumaric acid, citrusin B, myricitrin, solamargine, naringenin, rhoifolin, apigenin, solasonin, solanine, solasodine 3-b-D-glucopyranoside, butein, solasodine, and tigogenin. Based on literature search, the origin of these plant metabolites was identified from *B. diffusa* L., *P. niruri* L., and *S. nigrum* L. (Pandey et al., 2005; Bairwa et al., 2013; Mishra et al., 2014; Sarin et al., 2014; Jantan et al., 2019). Other plant metabolites identified through the chemical analysis were common to the three plant species.

In our 28 days' chronic safety study, SKK did not induce any form of toxicity in the Wistar rats following repeated dosing up to the highest tested concentration of 1,000 mg/kg (10× human equivalent dose for rats). Earlier sub-acute safety study of SKK had reported similar findings where the authors calculated the lethal-dose 50% of SKK at concentration >2,000 mg/kg (Yadav and Kumar, 2014). Toxicity studies performed on the individual plant extract of *B. diffusa* L. and *P. niruri* L. have reported them to be non-toxic in rats (Asare et al., 2011). Raw plant materials obtained from *S. nigrum* L. have been reported to have high toxicity in humans and cattle. However, pre-treatment of these plant parts on boiling (decocting) can render them non-toxic (Kuete, 2013; Mishra et al., 2014).

In-vitro and *in-vivo* treatment of the CCl$_4$ stimulated human hepatocyte (HepG2 cells) and Wistar rats, with SKK decoction, showed noteworthy hepatoprotective effects through the amelioration of cytotoxicity, generation of ROS, down-regulation of MMP and reduction in the release of AST, ALP, bilirubin, and total cholesterol. Compared to the positive control drug SLM (100 mg/kg), low (100 mg/kg), and high (200 mg/kg) dose treatments of SKK showed sizable pharmacological effects in ameliorating CCl$_4$ stimulated hepatic injuries in the Wistar rats. Uric acid level recovery in the CCl$_4$ stimulated rats also indicated a vital role for SKK in providing kidney protection against

chemical-induced injury. Our study showed a good correlation with the earlier short-term (7 days), sub-acute, single-dose (120 mg/kg) exposure study performed by Yadav and Kumar (2014). They also observed that the SKK decoction treatment of Wistar rats inhibited CCl$_4$ induced hepatotoxicity and inhibited the release of serum ALT, ALP, bilirubin, and albumin levels (Yadav and Kumar, 2014). However, it is interesting to observe that the low dose of SKK (100 mg/kg) applied in our chronic, long-term study did not perform well compared to the sub-acute study performed by Yadav and Kumar (2014). Hence, from our study, it can be inferred that under chronic exposure to CCl$_4$ inducing severe hepatic injuries, SKK is required at a higher dose of ∼200 mg/kg in Wistar rats.

Finally, the hepatoprotective effect of SKK can be attributed to the presence of plant metabolites detected using the LC-MS QToF analytical method. Several of the detected plant metabolites have been reported to have excellent antioxidant, anti-inflammatory and hepatoprotective properties (Pandey et al., 2005; Bairwa et al., 2013; Mishra et al., 2014; Sarin et al., 2014; Jantan et al., 2019). Rotenoids (boeravinones) also possess anti-oxidant properties as they have been observed to have inhibitory effects on the production of cyclooxygenase (COX)-1, COX-2, and generation of cellular reactive oxygen species (Aviello et al., 2011; Bairwa et al., 2013; Son and Phan, 2014). Six plant metabolites further quantified using HPLC (caffeic acid, rutin, gallic acid, catechin, quercetin, and corilagin) have been studied extensively for their hepatoprotective activities against CCl$_4$ and drug exposures (Janbaz et al., 2004; Wang et al., 2014, 2019; Elsawy et al., 2019; Ezzat et al., 2020). Owing to the different mode of action for the three plants *per se* and the presence of large variety of plant metabolites, it can be speculated that SKK probably functions at multiple levels in inhibiting CCl$_4$ induced hepatic injuries, i.e., through inhibition of oxidative stress, pro-inflammatory responses, and metabolizing enzymes CYPs (Khan et al., 2012; Wang et al., 2014; Ekstrand et al., 2015; Li et al., 2018). Finally, the presence of three herbal components also produced a possible synergistic effect in ameliorating CCl$_4$ induced hepatic injury that needs to be explored further. The dose of individual plant extract applied at the highest tested dose of SKK (200 mg/kg) was relatively low as compared to several other published studies using individual plant extracts of *B. diffusa* L. , *P. niruri* L., and *S. nigrum* L. for hepatoprotection in CCl$_4$ stimulated murine models (Chandan et al., 1991; Manjrekar et al., 2008; Patel et al., 2014; Beedimani and Jeevangi, 2017; Krithika and Verma, 2019).

CONCLUSION

Finally, the present work revealed that SKK has prominent pharmacological effects against long-term, chronic CCl_4 induced liver damages in Wistar rats and in human hepatocytes. Therefore, it is important to perform further experiments to understand its mode of action. This would reconfirm the overall biological effect of "Divya Sarva-Kalp-Kwath" medicine as the potent hepatoprotective therapeutics.

DATA AVAILABILITY STATEMENT

All datasets generated for this study are included in the article/supplementary material.

ETHICS STATEMENT

The animal study was reviewed and approved by Institutional Animal Ethical Committee of the Patanjali Research Institute, Haridwar, India.

AUTHOR CONTRIBUTIONS

AB provided broad direction for the study, identified the test formulation, generated resources, and gave final approval for the manuscript. SSS did the *in-vivo* study execution, and data analysis. RR performed the *in-vitro* experiments and manuscript reviewing. KhJ assisted in performing *in-vivo* studies. SS executed the safety studies. KaJ prepared the histopathological slides. SV performed the LC-MS analysis. AG analyzed the data. KB performed *in-vitro* experiments, wrote, and revised the overall manuscript. SSS, SS, RR, SV, AG, KB, and AV contributed in final manuscript revision. AV supervised overall research project planning, generated resources, reviewed, and finally approved the manuscript.

ACKNOWLEDGMENTS

REFERENCES

Abraham, P., and Wilfred, G. (2002). A massive increase in serum beta-glucuronidase after a single dose of carbon tetrachloride to the rat. *Clin. Chim. Acta* 322, 183–184. doi: 10.1016/s0009-8981(02)00170-5

Albouchi, F., Attia, M., Hanana, M., and Hamrouni, L. (2018). Ethnobotanical notes and phytopharmacologiques on *Solanum nigrum* Linn. (Family: Solanaceae). *Am. J. Phytomed. Clin. Ther.* 6:5. doi: 10.21767/2321-2748.100341

Asare, G. A., Addo, P., Bugyei, K., Gyan, B., Adjei, S., Otu-Nyarko, L. S., et al. (2011). Acute toxicity studies of aqueous leaf extract of *Phyllanthus niruri*. *Interdiscip. Toxicol.* 4, 206–210. doi: 10.2478/v10102-011-0031-9

Atanu, F., Ebiloma, G., and Ajayi, E. (2011). A review of the pharmacological aspects of *Solanum nigrum* Linn. *Biotechnol. Mol. Biol. Rev.* 6, 1–7.

Aviello, G., Canadanovic-Brunet, J. M., Milic, N., Capasso, R., Fattorusso, E., Taglialatela-Scafati, O., et al. (2011). Potent antioxidant and genoprotective effects of boeravinone G, a rotenoid isolated from Boerhaavia diffusa. *PLoS ONE* 6:e19628. doi: 10.1371/journal.pone.0019628

Bairwa, K., Singh, I. N., Roy, S. K., Grover, J., Srivastava, A., and Jachak, S. M. (2013). Rotenoids from Boerhaavia diffusa as potential anti-inflammatory agents. *J. Nat. Prod.* 76, 1393–1398. doi: 10.1021/np300899w

Balkrishna, A., Pokhrel, S., Tomer, M., Verma, S., Kumar, A., Nain, P., et al. (2019a). Anti-Acetylcholinesterase activities of mono-herbal extracts and exhibited synergistic effects of the phytoconstituents: a biochemical and computational study. *Molecules* 24:4175. doi: 10.3390/molecules24224175

Balkrishna, A., Sakat, S. S., Joshi, K., Joshi, K., Sharma, V., Ranjan, R., et al. (2019b). Cytokines driven anti-inflammatory and anti-psoriasis like efficacies of nutraceutical sea buckthorn (*Hippophae rhamnoides*) Oil. *Front. Pharmacol.* 10:1186. doi: 10.3389/fphar.2019.01186

Balkrishna, A., Sakat, S. S., Joshi, K., Paudel, S., Joshi, D., Joshi, K., et al. (2019c). Anti-inflammatory and anti-arthritic efficacies of an indian traditional herbo-mineral medicine "divya amvatari ras" in collagen antibody-induced arthritis (CAIA) mouse model through modulation of IL-6/IL-1beta/TNF-alpha/NFkappaB signaling. *Front. Pharmacol.* 10:659. doi: 10.3389/fphar.2019.00659

Balkrishna, A., Sakat, S. S., Joshi, K., Paudel, S., Joshi, D., Joshi, K., et al. (2019d). Herbo-mineral formulation 'Ashwashila' attenuates rheumatoid arthritis symptoms in collagen-antibody-induced arthritis (CAIA) mice model. *Sci. Rep.* 9:8025. doi: 10.1038/s41598-019-44485-9

Beedimani, R. S., and Jeevangi, S. K. (2017). Evaluation of hepatoprotective activity of Boerhaavia diffusa against carbon tetrachloride induced liver toxicity in albino rats. *Int. J. Basic Clin. Pharmacol.* 4:153. doi: 10.5455/2319-2003.ijbcp20150230

Bhattacharjee, R., and Sil, P. C. (2007). Protein isolate from the herb *Phyllanthus niruri* modulates carbon tetrachloride-induced cytotoxicity in hepatocytes. *Toxicol. Mech. Methods* 17, 41–47. doi: 10.1080/15376510600970034

Borrelli, F., Milic, N., Ascione, V., Capasso, R., Izzo, A. A., Capasso, F., et al. (2005). Isolation of new rotenoids from Boerhaavia diffusa and evaluation of their effect on intestinal motility. *Planta Med.* 71, 928–932. doi: 10.1055/s-2005-871282

Bovy, A., Schijlen, E., and Hall, R. D. (2007). Metabolic engineering of flavonoids in tomato (*Solanum lycopersicum*): the potential for metabolomics. *Metabolomics* 3, 399–412. doi: 10.1007/s11306-007-0074-2

Chandan, B. K., Sharma, A. K., and Anand, K. K. (1991). Boerhaavia diffusa: a study of its hepatoprotective activity. *J. Ethnopharmacol.* 31, 299–307. doi: 10.1016/0378-8741(91)90015-6

Daji, G., Steenkamp, P., Madala, N., and Dlamini, B. (2018). Phytochemical composition of *Solanum retroflexum* analysed with the aid of ultra-performance liquid chromatography hyphenated to quadrupole-time-of-flight mass spectrometry (UPLC-qTOF-MS). *J. Food Qual.* 2018:8. doi: 10.1155/2018/3678795

De Souza, G. R., De-Oliveira, A. C. A. X., Soares, V., Chagas, L. F., Barbi, N. S., et al. (2019). Chemical profile, liver protective effects and analgesic properties of a *Solanum paniculatum* leaf extract. *Biomed. Pharmacother.* 110, 129–138. doi: 10.1016/j.biopha.2018.11.036

Debnath, S., Ghosh, S., and Hazra, B. (2013). Inhibitory effect of *Nymphaea pubescens* Willd. flower extract on carrageenan-induced inflammation and

CCl(4)-induced hepatotoxicity in rats. *Food Chem. Toxicol.* 59, 485–491. doi: 10.1016/j.fct.2013.06.036

Dong, S., Chen, Q. L., Song, Y. N., Sun, Y., Wei, B., Li, X. Y., et al. (2016). Mechanisms of CCl4-induced liver fibrosis with combined transcriptomic and proteomic analysis. *J. Toxicol. Sci.* 41, 561–572. doi: 10.2131/jts.41.561

Ekow Thomford, N., Dzobo, K., Adu, F., Chirikure, S., Wonkam, A., and Dandara, C. (2018). Bush mint (*Hyptis suaveolens*) and spreading hogweed (*Boerhavia diffusa*) medicinal plant extracts differentially affect activities of CYP1A2, CYP2D6 and CYP3A4 enzymes. *J. Ethnopharmacol.* 211, 58–69. doi: 10.1016/j.jep.2017.09.023

Ekstrand, B., Rasmussen, M. K., Woll, F., Zlabek, V., and Zamaratskaia, G. (2015). *In vitro* gender-dependent inhibition of porcine cytochrome p450 activity by selected flavonoids and phenolic acids. *Biomed. Res. Int.* 2015:387918. doi: 10.1155/2015/387918

Elhag, R. A. M., Sma, E. B., Bakhiet, A. O., and Galal, M. (2011). Hepatoprotective activity of Solanum nigrum extracts on chemically induced liver damage in rats. *J. Vet. Med. Ani. Health* 3, 45–50.

Elsawy, H., Badr, G. M., Sedky, A., Abdallah, B. M., Alzahrani, A. M., and Abdel-Moneim, A.M. (2019). Rutin ameliorates carbon tetrachloride (CCl4)-induced hepatorenal toxicity and hypogonadism in male rats. *Peer J.* 7:e7011. doi: 10.7717/peerj.7011

Ezzat, M. I., Okba, M. M., Ahmed, S. H., El-Banna, H. A., Prince, A., Mohamed, S. O., et al. (2020). In-depth hepatoprotective mechanistic study of *Phyllanthus niruri*: in vitro and in vivo studies and its chemical characterization. *PLoS ONE* 15:e0226185. doi: 10.1371/journal.pone.0226185

Ferreres, F., Sousa, C., Justin, M., Valentão, P., Andrade, P. B., Llorach, R., et al. (2005). Characterisation of the phenolic profile of Boerhaavia diffusa L. by HPLC-PAD-MS/MS as a tool for quality control. *Phytochem. Anal.* 16, 451–458. doi: 10.1002/pca.869

Harish, R., and Shivanandappa, T. (2006). Antioxidant activity and hepatoprotective potential of *Phyllanthus niruri*. *Food Chem.* 95, 180–185. doi: 10.1016/j.foodchem.2004.11.049

Huang, H. C., Syu, K. Y., and Lin, J. K. (2010). Chemical composition of *Solanum nigrum* linn extract and induction of autophagy by leaf water extract and its major flavonoids in AU565 breast cancer cells. *J. Agric Food Chem.* 58, 8699–8708. doi: 10.1021/jf101003v

Ingawale, D. K., Mandlik, S. K., and Naik, S. R. (2014). Models of hepatotoxicity and the underlying cellular, biochemical and immunological mechanism(s): a critical discussion. *Environ. Toxicol. Pharmacol.* 37, 118–133. doi: 10.1016/j.etap.2013.08.015

Janbaz, K. H., Saeed, S. A., and Gilani, A. H. (2004). Studies on the protective effects of caffeic acid and quercetin on chemical-induced hepatotoxicity in rodents. *Phytomedicine* 11, 424–430. doi: 10.1016/j.phymed.2003.05.002

Jantan, I., Haque, M. A., Ilangkovan, M., and Arshad, L. (2019). An insight into the modulatory effects and mechanisms of action of phyllanthus species and their bioactive metabolites on the immune system. *Front. Pharmacol.* 10:878. doi: 10.3389/fphar.2019.00878

Juneja, K., Mishra, R., Chauhan, S., Gupta, S., Roy, P., Sircar, D., et al. (2020). Metabolite profiling and wound-healing activity of Boerhavia diffusa leaf extracts using *in vitro* and *in vivo* models. *J. Trad. Comp. Med.* 10, 52–59. doi: 10.1016/j.jtcme.2019.02.002

Kaunda, J. S., and Zhang, Y.-J. (2019). The genus solanum: an ethnopharmacological, phytochemical and biological properties review. *Nat. Prod. Bioprosp.* 9:6. doi: 10.1007/s13659-019-0201-6

Kaur, N., Kaur, B., and Sirhindi, G. (2017). Phytochemistry and pharmacology of *Phyllanthus niruri* L.: a review. *Phytother. Res.* 31, 980–1004. doi: 10.1002/ptr.5825

Khan, R. A., Khan, M. R., and Sahreenm, S. (2012). CCl4-induced hepatotoxicity: protective effect of rutin on p53, CYP2E1 and the antioxidative status in rat. *BMC Complement Altern. Med.* 12:178. doi: 10.1186/1472-6882-12-178

Kirtikar, K. R., and Basu, B. D. (1956). *Indian Medicinal Plants*. Allahabad: Lalit Mohan Basu.

Krithika, R., and Verma, R. J. (2019). *Solanum nigrum* confers protection against CCl4-induced experimental hepatotoxicity by increasing hepatic protein synthesis and regulation of energy metabolism. *Clin. Phytosci.* 5:1. doi: 10.1186/s40816-018-0096-5

Kuete, V. (2013). *Physical, Hematological, and Histopathological Signs of Toxicity Induced by African Medicinal Plants*. Oxford: Elsevier. doi: 10.1016/B978-0-12-800018-2.00022-4

Kumar, S., Singh, A., Singh, B., Maurya, R., and Kumar, B. (2018). Structural characterization and quantitative determination of bioactive compounds in ethanolic extracts of *Boerhaavia diffusa* L. by liquid chromatography with tandem mass spectrometry. *Sep. Sci. Plus* 1, 588–596. doi: 10.1002/sscp.201800056

Lami, N., Kadota, S., Tezuka, Y., and Kikuchi, T. (1990). Constituents of the roots of Boerhaavia diffusa Linn. IV. Isolation and structure determination of boeravinones D, E and F. *Chem. Pharm. Bull.* 38, 1558–1562. doi: 10.1248/cpb.38.1558

Li, X., Deng, Y., Zheng, Z., Huang, W., Chen, L., Tong, Q., et al. (2018). Corilagin, a promising medicinal herbal agent. *Biomed Pharmacother.* 99, 43–50. doi: 10.1016/j.biopha.2018.01.030

Li, Y., Chang, W., Zhang, M., Ying, Z., and Lou, H. (2015). Natural product solasodine-3-O-beta-D-glucopyranoside inhibits the virulence factors of Candida albicans. *FEMS Yeast Res.* 15:fov060. doi: 10.1093/femsyr/fov060

Lin, H. M., Tseng, H. C., Wang, C. J., Lin, J. J., Lo, C. W., and Chou, F. P. (2008). Hepatoprotective effects of *Solanum nigrum* Linn extract against CCl(4)-induced oxidative damage in rats. *Chem. Biol. Interact.* 171, 283–293. doi: 10.1016/j.cbi.2007.08.008

Manibusan, M. K., Odin, M., and Eastmond, D. A. (2007). Postulated carbon tetrachloride mode of action: a review. *J. Environ. Sci. Health C Environ. Carcinog. Ecotoxicol. Rev.* 25, 185–209. doi: 10.1080/10590500701569398

Manjrekar, A. P., Jisha, V., Bag, P. P., Adhikary, B., Pai, M. M., Hegde, A., et al. (2008). Effect of *Phyllanthus niruri* Linn. treatment on liver, kidney and testes in CCl4 induced hepatotoxic rats. *Indian J. Exp. Biol.* 46, 514–520.

Mao, X., Wu, L. F., Guo, H. L., Chen, W. J., Cui, Y. P., Qi, Q., et al. (2016). The genus phyllanthus: an ethnopharmacological, phytochemical, and pharmacological review. *Evid. Based Compl. Alternat. Med.* 2016:7584952. doi: 10.1155/2016/7584952

Mir, A., Anjum, F., Riaz, N., Iqbal, H., Wahedi, H. M., Khattak, J. Z. K., et al. (2010). Carbon tetrachloride (CCl4) - induced hepatotoxicity in rats: curative role of *Solanum nigrum*. *J. Med. Plants Res.* 4, 2525–2532. doi: 10.5897/JMPR10.482

Mishra, S., Aeri, V., Gaur, P. K., and Jachak, S. M. (2014). Phytochemical, therapeutic, and ethnopharmacological overview for a traditionally important herb: *Boerhavia diffusa* Linn. *Biomed. Res. Int.* 2014:808302. doi: 10.1155/2014/808302

Nada, S. A., Omara, E. A., Abdel-Salam, O. M., and Zahran, H. G. (2010). Mushroom insoluble polysaccharides prevent carbon tetrachloride-induced hepatotoxicity in rat. *Food Chem. Toxicol.* 48, 3184–3188. doi: 10.1016/j.fct.2010.08.019

Nair, A. B., and Jacob, S. (2016). A simple practice guide for dose conversion between animals and human. *J. Basic Clin. Pharm.* 7:27. doi: 10.4103/0976-0105.177703

Pandey, R., Maurya, R., Singh, G., Sathiamoorthy, B., and Naik, S. (2005). Immunosuppressive properties of flavonoids isolated from *Boerhaavia diffusa* Linn. *Int. Immunopharmacol.* 5, 541–553. doi: 10.1016/j.intimp.2004.11.001

Patel, A., Biswas, S., Shoja, M. H., Ramalingayya, G. V., and Nandakumar, K. (2014). Protective effects of aqueous extract of *Solanum nigrum* Linn. leaves in rat models of oral mucositis. *Sci. World J.* 2014:10. doi: 10.1155/2014/345939

Patel, M., and Verma, R. (2014). Hepatoprotective activity of *Boerhavia diffusa* extract. *Int. J. Pharm. Clin. Res.* 6, 233–240.

Pereira, D. M., Faria, J., Gaspar, L., Valentão, P., De Pinho, P. G., and Andrade, P. B. (2009). *Boerhaavia diffusa*: metabolite profiling of a medicinal plant from Nyctaginaceae. *Food Chem. Toxicol.* 47, 2142–2149. doi: 10.1016/j.fct.2009.05.033

Ramachandra, Y. L., Shilali, K., Ahmed, M., Sudeep, H. V., Kavitha, B. T., Gurumurthy, H., et al. (2011). Hepatoprotective properties of *Boerhavia diffusa* and aerva lanata against carbon tetra chloride induced hepatic damage rats. *Pharmacology Online* 3, 435–441.

Refaat, J., Yehia, S., Ramadan, M., and Kamel, M. (2015). Rhoifolin: a review of sources and biological activities. *Int. J. Pharmacog.* 2, 102–109.

Sarin, B., Verma, N., Martín, J. P., and Mohanty, A. (2014). An overview of important ethnomedicinal herbs of Phyllanthus species: present status and future prospects. *Sci. World J.* 2014:839172. doi: 10.1155/2014/839172

Sivgami, S., Gayathri, P., and Ramapriya, R. (2012). The antioxidant potential of two selected varieties of *Solanum nigrum*. *J. Pharm. Res.* 5, 2221–2223.

Son, H., and Phan, Y. (2014). Preliminary phytochemical screening, acute oral toxicity and anticonvulsant activity of the berries of *Solanum nigrum* Linn. *Trop. J. Pharm. Res.* 13:907. doi: 10.4314/tjpr.v13i6.12

Syamasundar, K. V., Singh, B., Thakur, R. S., Husain, A., Kiso, Y., and Hikino, H. (1985). Antihepatotoxic principles of *Phyllanthus niruri* herbs. *J. Ethnopharmacol.* 14, 41–44. doi: 10.1016/0378-8741(85)90 026-1

Venkatesh, P., Dinakar, A., and Senthilkumar, N. (2012). Hepatoprotective activity of alcoholic extracts of *Boerhaavia diffusa* and Anisochlilus Carnosus against carbon tetrachloride induced hepatotoxicity in rats. *Asian J. Pharm. Clin. Res.* 5, 232–234.

Wang, J., Tang, L., White, J., and Fang, J. (2014). Inhibitory effect of gallic acid on CCl4-mediated liver fibrosis in mice. *Cell Biochem. Biophys.* 69, 21–26. doi: 10.1007/s12013-013-9761-y

Wang, L., Yang, G., Yuan, L., Yang, Y., Zhao, H., Ho, C. T., et al. (2019). Green tea catechins effectively altered hepatic fibrogenesis in rats by inhibiting ERK and Smad1/2 phosphorylation. *J. Agric Food Chem.* 67, 5437–5445. doi: 10.1021/acs.jafc.8b05179

Williamson, E. M. (2001). Synergy and other interactions in phytomedicines. *Phytomedicine* 8, 401–409. doi: 10.1078/0944-7113-00060

Yadav, A., and Kumar, S. (2014). Hepatoprotective effect of sarvakalp kwath against carbon tetrachloride induced hepatic injury in albino rats. *Biomed. Pharmacol. J.* 7, 659–663. doi: 10.13005/bpj/538

Yadav, N. P., Pal, A., Shanker, K., Bawankule, D. U., Gupta, A. K., Darokar, M. P., et al. (2008). Synergistic effect of silymarin and standardized extract of Phyllanthus amarus against CCl4-induced hepatotoxicity in *Rattus norvegicus*. *Phytomedicine* 15, 1053–1061. doi: 10.1016/j.phymed.2008.08.002

Zhou, X., Seto, S. W., Chang, D., Kiat, H., Razmovski-Naumovski, V., Chan, K., et al. (2016). Synergistic effects of chinese herbal medicine: a comprehensive review of methodology and current research. *Front. Pharmacol.* 7:201. doi: 10.3389/fphar.2016.00201

Interpreting the Pharmacological Mechanisms of Huachansu Capsules on Hepatocellular Carcinoma Through Combining Network Pharmacology and Experimental Evaluation

Jihan Huang[1,2,3†], Feiyu Chen[2†], Zhangfeng Zhong[2], Hor Yue Tan[2], Ning Wang[2], Yuting Liu[3], Xinyuan Fang[4], Tao Yang[1,3*] and Yibin Feng[2*]

[1] Center for Drug Clinical Research, Shuguang Hospital, Shanghai University of Traditional Chinese Medicine, Shanghai, China, [2] School of Chinese Medicine, Li Ka Shing Faculty of Medicine, The University of Hong Kong, Hong Kong, Hong Kong, [3] Department of Cardiology, Cardiovascular Research Institute, Shuguang Hospital affiliated to Shanghai University of Traditional Chinese Medicine, Shanghai, China, [4] Marine College, Shandong University (Weihai), Weihai, China

Hepatocellular carcinoma (HCC) is one of the most fatal cancers across the world. Chinese medicine has been used as adjunctive or complementary therapy for the management of HCC. Huachansu belongs to a class of toxic steroids isolated from toad venom that has important anti-cancer property. This study was aimed to identify the bioactive constituents and molecular targets of Huachansu capsules (HCSCs) for treating HCC using network pharmacology analysis and experimental assays. The major bioactive components of HCSCs were determined using ultra-performance liquid chromatography-tandem mass spectrometry (UPLC-MS/MS). A series of network pharmacology methods including target prediction, pathway identification, and network establishment were applied to identify the modes of action of HCSCs against HCC. Furthermore, a series of experiments, including MTT, clonogenic assay, 3-D transwell, wound healing assay, as well as flow cytometry, were conducted to verify the inhibitory ability of HCSCs on HCC *in vitro*. The results showed that 11 chemical components were identified from HCSCs. The network pharmacological analysis showed that there were 82 related anti-HCC targets and 14 potential pathways for these 11 components. Moreover, experimental assays confirmed the inhibitory effects of HCSCs against HCC *in vitro*. Taken together, our study revealed the synergistic effects of HCSCs on a systematic level, and suggested that HCSCs exhibited anti-HCC effects in a multi-component, multi-target, and multi-pathway manner.

Keywords: Huachansu capsules, network pharmacology, hepatocellular carcinoma, molecular targets, KEGG pathway

INTRODUCTION

Hepatocellular carcinoma (HCC) is an aggressive malignancy and the third leading cause of cancer-related death (Colagrande et al., 2016). Up to now, surgical resection is the principal therapy for HCC patients who were diagnosed at the early stage (Daher et al., 2018), but it is not satisfying for those were diagnosed in the middle or later stages. There is first-line systemic treatment such as sorafenib in the clinical practice, which is the first molecular-targeted agent for HCC treatment, and has been approved in Japan for the treatment of unresectable HCC (Daoudaki and Fouzas, 2014; Omata et al., 2017). Although sorafenib has been shown to provide survival benefits for patients, there are many side effects such as fatigue, diarrhea, hypertension, baldness, and hand-foot skin reaction (Li et al., 2015). With the empirical applications and refinements of Chinese medicine for over two thousand years, it becomes a prominent part of the medical system in China. Using alone or in combination with conventional chemo- or radio- therapy, Chinese medicine has been demonstrated to improve immunity, enhance quality of life and progression-free survival in patients with HCC (Huang et al., 2013). Besides, Chinese herbal formulas are widely used in clinical practice due to its multi-component and multi-target for the treatment of cancers.

Huachansu, a class of toxic steroids isolated from toad venom, has a range of properties including detoxification, detumescence, and pain relief (Zhan et al., 2020). It has been widely used in various diseases and ailments such as chronic hepatitis B and cancer (Cui et al., 2010). Although Huachansu has remarkable inhibitory effects against many types of cancer, it is mainly used for the treatment of advanced tumors (Meng et al., 2009). It has been demonstrated that Huachansu has good therapeutic effects against various advanced malignant tumors including HCC, lung, and pancreatic cancer (Meng et al., 2009). Huachansu capsules (HCSCs) have been approved by the China Food and Drug Administration (No. Z20050846) in 2005 and are produced by Shanxi Eastantai Pharmaceutical Corporation Limited. A study reported that when used in combination with conventional chemotherapy, HCSCs could synergistically enhance the efficacy of chemotherapy and reduce its toxicity (Qin et al., 2008).

A range of pharmacological studies of HCSCs revealed that toad venom lactones are the main active ingredients of HCSCs, which contain cinobufagin (Qi et al., 2010), resibufogenin (Xie et al., 2012), and bufalin (Meng et al., 2016). These studies also demonstrated that these three compounds are the major cardiac glycosides that exert the anti-tumor activities of HCSCs. However, the underlying mechanisms of these anti-tumor effects remain unclear because of the complex compositions. Indeed, the complex compositions of Chinese herbal formulas make it difficult to characterize their active substances, the activities of the active substances, and the compatibilities with multiple ingredients, which have the characteristics of multi-target and multi-pathway. The approaches of systematic pharmacology and network pharmacology provide a new perspective for studying Chinese herbal formulas (Zineh, 2019). Our previous studies have successfully predicted the bioactive substances and molecular targets of several Chinese herbal formulas, which included Yinchenhao decoction (Huang et al., 2017), Danlu capsule (Huang et al., 2017a), Xuangui dropping pill (Huang et al., 2017b), and Fructus Schisandrae (Hong et al., 2017).

In the current study, we identified the major bioactive components of HCSCs. Moreover, a series of network pharmacological analyses, including target prediction and enrichment, pathway analysis, and network construction, were also conducted to identify the HCC-related targets and potential mechanisms of HCSCs. On the other hand, a series of experimental assays were performed in HCC cell lines, PLC/PRF/5 and MHCC97L, to confirm the inhibitory effects of HCSCs including cell proliferation, colony formation, cell invasion and migration, cell cycle, and cell apoptosis in HCC. The workflow of our network pharmacological and experimental studies of HCSCs in HCC is shown in **Figure 1**. Our results did not only demonstrate the synergistic anti-cancer activities of HCSCs components and their potential targets, but also offer an in-depth knowledge of the molecular mechanisms of HCSCs.

METHODS

Network Pharmacology-Based Analysis
Ultra-Performance Liquid Chromatography-Tandem Mass Spectrometry (UPLC-MS/MS)
The pulverized HCSCs (ca. 0.25 g) was accurately weighed and added to methanol-water (30: 70, v/v; 10 ml). The mixture was processed with ultrasonication for 25 min and centrifugation at 3000 g for 10 min, and then was filtered using a filter (0.25 μm; Millipore, USA). An aliquot (3 μl) of the filtered supernatant was injected for UPLC-Q/ExactiveHybrid Quadrupole-Orbitrap system analysis with the Compound Discoverer 2.1 software package (Thermo Finnigan, San Jose, CA, USA). The detail conditions of the assay are as follows: mobile phase A was 0.1% aqueous solution of formic acid and mobile phase B was acetonitrile. Chromatographic separation was performed on an Acquity UPLC® HSS T3 column (2.1 mm × 100 mm, 1.8 μm); the column temperature was 45°C, flow rate was 0.3 ml/min, and the sample volume was 3 μl. Then the data was analyzed under the model of cation and anion by the means of UHPLC-Q/Exactive, electrospray ionization (ESI) source; scanning model: full MS (resolution 70,000) and ddMS2 (resolution 17,500, NCE35, stepped NCE50%; voltage of the ESI source, +3.2 kV/−2.8 kV). The temperature and voltage of the capillary tube were 320°C and 75.0 V, respectively. The flow rate of the sheath and auxiliary gas were 32.0 and 10.0 arbitrary unit, respectively (scanned area m/z: 80–1,050).

Identification of Associated Molecular Targets of HCSCs
The potential molecular targets of HCSCs were predicted using SwissTargetPrediction (Gfeller et al., 2014), similarity ensemble approach (SEA) (Keiser et al., 2007), the Traditional Chinese Medicines for Systems Pharmacology Database and Analysis
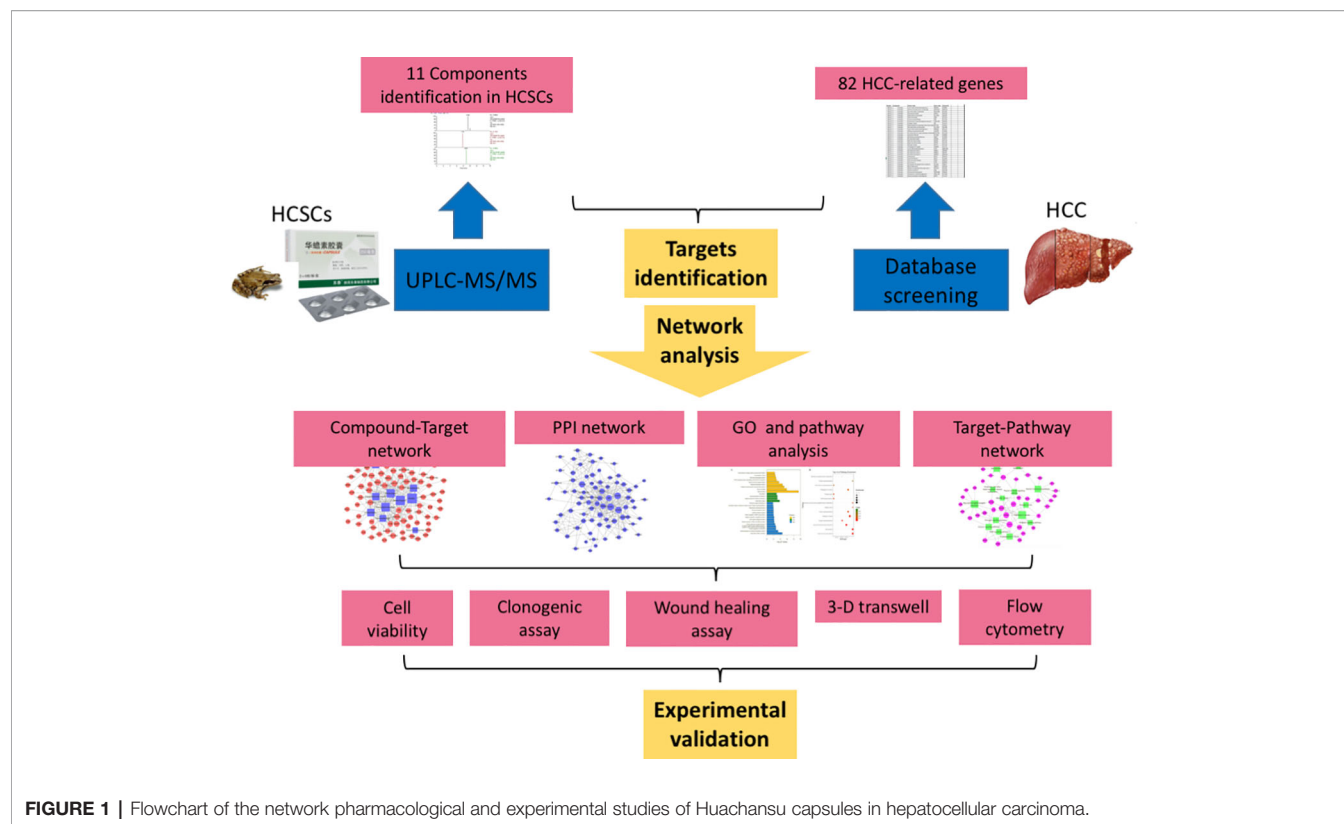
FIGURE 1 | Flowchart of the network pharmacological and experimental studies of Huachansu capsules in hepatocellular carcinoma.

Platform (TCMSP) (Ru et al., 2014), and the Search Tool for Interacting Chemicals (STITCH) (Szklarczyk et al., 2016).

The HCC-associated human genes were comprehensively retrieved from five databases, which were OncoDB.HCC (Su et al., 2007), Liverome (Lee et al., 2011), Therapeutic Target Database (*TTD*), Kyoto Encyclopedia of Genes and Genomes (KEGG), the Comparative Toxicogenomics Database (CTD), and GeneCards.

Protein-Protein Interaction (PPI) Network

The STRING online database was applied to obtain the PPI data of the molecular targets of HCSCs (Szklarczyk et al., 2019), where the parameter organism was set to Homo sapiens, other basic settings were the default value. Cytoscape software was employed to establish the PPI relationship network and perform topological analysis.

Gene Ontology (GO) and KEGG Pathway Enrichment Analyses

The GO analysis and KEGG pathway enrichment were employed by using the Database for Annotation, Visualization and Integrated Discovery (DAVID). The biological process (BP), cellular component (CC), and molecular function (MF) in GO were selected to annotate the gene function. Terms with expression analysis systematic explorer scores of ≤0.05 were collected for functional annotation clustering. The pathway enrichment analysis was performed using the KEGG database to verify the functional categories of statistically significant genes

($p < 0.05$). Terms with thresholds of count of ≥2 and Expression Analysis Systemic Explorer (EASE) scores of ≤0.05 were screened for functional annotation clustering.

Network Construction and Analysis

The compound-target network was generated by linking bioactive constituents and putative targets. The target-pathway network was established with the predicted targets and signaling pathways that were postulated to be involved in HCC. The compound-pathway network was constructed with all the compounds and the signaling pathways. In our network, the nodes represent the candidate compounds, potential targets, or signaling pathways, while the edges represent the compound-target or target-pathway interactions. The Cytoscape software was employed to construct the networks.

Experimental Analyses
Chemicals and Reagents

HCSCs (Batch No. 7D05) was provided by Shanxi Eastantai Pharmaceutical Co., Ltd. Dulbecco's Modified Eagle Medium (DMEM), fetal bovine serum (FBS), penicillin-streptomycin, and phosphate buffered saline (PBS) were purchased from Gibco. Thiazolyl Blue Tetrazolium Blue (MTT), paraformaldehyde (PFA), crystal violet solution, and propidium iodide (PI) were purchased from Sigma. Transwell chamber system, matrigel matrix, and FITC Annexin V/PI Apoptosis Detection kit were purchased from BD Bioscience.

Cell Lines and Cell Culture

The human HCC cell line, PLC/PRF/5, was purchased from ATCC (USA), while another human HCC cell line, MHCC97L, was a kind gift from Dr. Man Kwan, Department of Surgery, The University of Hong Kong. The cells were maintained in DMEM (Gibco, USA) with 10% FBS (Gibco, USA) and 1% penicillin-streptomycin (Gibco, USA). The cells were cultured and maintained at 37°C, and equilibrated with 95% air and 5% CO_2. In addition, HCSCs (Batch No. 7D05) was provided by Shanxi Eastantai Pharmaceutical Co., Ltd, and stored at ambient temperature. The ingredient of HCSCs is toad skin. It was dissolved in PBS (Gibco, USA) in the experiments.

MTT Assay

The cell viability was measured with MTT assay. In brief, the cells were seeded onto 96-well plates, and treated with PBS or different dosages of HCSCs (0, 0.05, 0.1, 0.2, 0.4, 0.8, and 1.2 mg/ml) on the next day. After incubation for 48 h, 10 μl of MTT (Thiazolyl Blue Tetrazolium Blue; 5 mg/ml; Sigma, USA) was added to each well, followed by 4 h incubation at 37°C. The MTT was then discarded, and 100 μl of DMSO was added to each well. The absorbance of formazan formed was measured at 595 nm using a Multiskan MS microplate reader (Labsystems, Finland).

Clonogenic Assay

The cells were seeded onto six-well plates (10^4 cells/well), and treated with indicated concentration of HCSCs for 12 d. At the end of the treatment, the medium was removed, and the cells were fixed using 4% paraformaldehyde (PFA; Sigma, USA) for 2 h, and stained with 0.1% crystal violet solution (Sigma-Aldrich, USA) for 30 min. Images were captured using an optical microscope, and clonogenic spheres were measured by manual counting in three random fields.

3-D Transwell

The transwell invasion assay was conducted using a transwell chamber system (BD Biosciences, USA) with 8 μm pore. We firstly performed the proliferation assay with HCSCs treatment for 48 h, and then the survived population was collected and used for this assay. Briefly, the upper chamber was coated with matrigel matrix (BD, USA), and filled with 100 μl serum-free medium containing 5×10^4 cells, while 500 μl DMEM containing 10% FBS and the indicated concentrations of HCSCs was added into the lower chamber. After incubation for 48 h, the non-invading cells on the upper surface of the chamber were removed using cotton swabs, and the cells, that have invaded across the matrigel matrix to the lower chamber, were fixed with 4% PFA and stained with 0.1% crystal violet solution. An inverted microscope at 200× magnification was used to image the stained cells in three random fields, and the cell number in each field was manually counted. The relative cell invasion rate was calculated by the number of invaded cells normalized to the total number of cells in the upper chamber.

Wound Healing Assay

The cells were cultured in 24-well plates until 100% confluence. A narrow section of the cells was removed using a sterile micropipette tip to create a wound of around 0.5 mm in width. The medium was then discarded, and the monolayer was gently rinsed twice using warm PBS. Next, the medium containing vehicle or indicated dosages of HCSCs was added to each well. The cell migration data were obtained with an inverted microscope (Olympus, Japan) at 0, 24, and 48 h incubation. The wound width of the cell-free area was also assessed by Image-J software (NIH, Bethesda, MD, USA).

Flow Cytometry

The cells were seeded onto six-well tissue culture plates and exposed to specified dosages of HCSCs for 48 h. For cell cycle analysis, the cells were harvested and fixed in 70% ethanol at 4°C overnight, followed by staining with propidium iodide (PI; Sigma-Aldrich, USA) in the dark for 15 min, and acquired with Canto II flow cytometer (BD Biosciences, USA). For the measurement of apoptosis, the cells were stained using the FITC Annexin V/PI Apoptosis Detection kit (BD Biosciences, USA) as per the manufacturer's instructions. The percentage of apoptotic cells was calculated as the sum of percentages at Q2 and Q3. All the data were analyzed using the FlowJo software (BD, USA).

RESULTS

Identification of Bioactive Components From HCSCs

The major components of HCSCs were separated and determined using UPLC-Q/ExactiveHybrid Quadrupole-Orbitrap system with the Compound Discoverer 2.1 software package (Thermo Finnigan, San Jose, CA, USA). As shown in **Figure 2**, phytochemical profile of HCSCs was detected, and 11 bioactive compounds were identified from HCSCs with chromatographic peaks. Then, mzCloud (ddMS2) and ChemSpider (exact mass or formula) were used to identify these compounds and search for their analogues. On the basis of their spectral data and chemical properties, 10 of the compounds were identified as nonsteroidal, including cinobufagin, bufotoxin, bufalin, bufotalin, resibufogenin, bufadienolide, telocinobufagin, cinobufotalin, desacetylcinobufotalin, and desacetylcinobufagin; the other compound was alkaloid, namely dehydrobufotenine. The details were shown in **Table 1** and **Figure 2**.

HCC-Related Target Identification of HCSCs

Based on the 11 identified compounds, a total of 402 targets were collected from the SwissTargetPrediction, SEA, TCMSP, and STITCH databases, and there are 268 repetitive genes in 402 targets. The remaining 134 targets shared the common compounds. The detailed information was presented in **Supplementary Table 1**. Moreover, we collected HCC-associated human genes from five databases including OncoDB.HCC, Liverome, TTD, KEGG, CTD, and GeneCards, which presented specifically in **Supplementary Table 2**. According to the results presented in **Supplementary Tables 1**
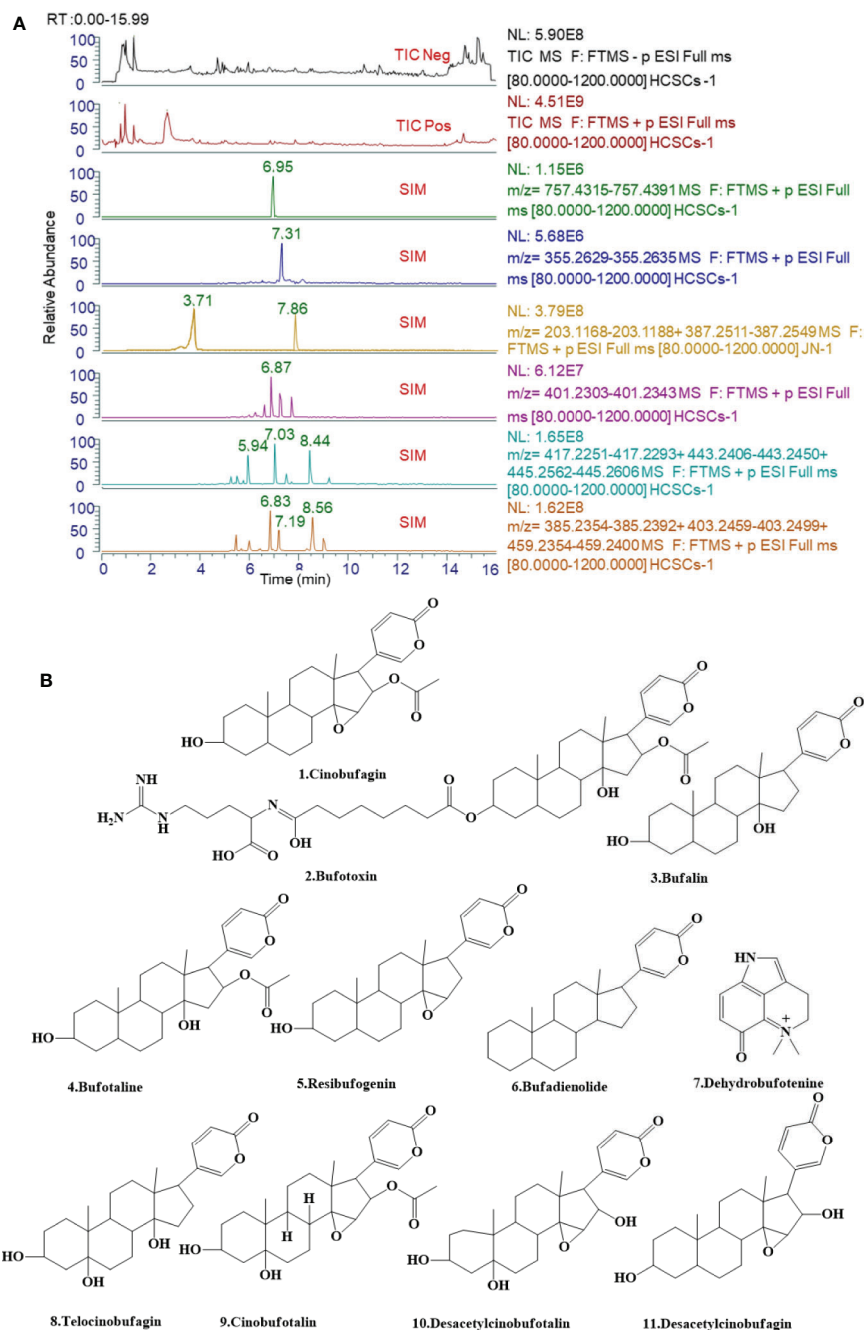
FIGURE 2 | Ultra-performance liquid chromatography-tandem mass spectrometry (UPLC-MS/MS) analyses of Huachansu capsules (HCSCs) and their active compounds. **(A)** Total-ion chromatograms (TIC) and select-ion chromatograms (SIC) of HCSCs samples [Stationary phase: ACQUITY UPLC HSS T3 (2.1 mm×100 mm, 1.8 μm); mobile phase: 0.1% aqueous solution of formic acid **(A)** and acetonitrile **(B)** in gradient. The following gradient elution program was used: 0–12 min, 5%–98% B; 12–12.01 min, 98%–5% B; 12.01–15 min, 5% B; flow rate: 0.3 μl/min. (Peak No: Rt, 8.44 min, Cinobufagin; 6.95 min, Bufotoxin; 7.86 min, Bufalin; 7.03 min, Bufotalin; 8.56 min, Resibufogenin; 7.31 min, Bufadienolide; 3.71 min, Dehydrobufotenine; 6.83 min, Telocinobufagin; 7.19 min, Cinobufotalin; 5.94 min, Desacetylcinobufotalin; 6.87 min, and Desacetylcinobufagin. **(B)** The molecular formulas of the 11 bioactive components identified from Huachansu capsules (HCSCs).

TABLE 1 | Chemical formulae of the 11 bioactive components identified from Huachansu capsules (HCSCs).

No	Compound	Chemical formula	$[M+H]^+$ Measured mass	$[M+H]^+$ True mass	Accuracy (ppm)	RT (min)
1	Cinobufagin	$C_{26}H_{34}O_6$	443.2428	443.2413	3.38	8.44
2	Bufotoxin	$C_{40}H_{60}N_4O_{10}$	757.4382	757.4353	3.83	6.95
3	Bufalin	$C_{24}H_{34}O_4$	387.2517	387.2530	−3.36	7.86
4	Bufotalin	$C_{26}H_{36}O_6$	445.2585	445.2570	3.37	7.03
5	Resibufogenin	$C_{24}H_{32}O_4$	385.236	385.2373	−3.37	8.56
6	Bufadienolide	$C_{24}H_{34}O_2$	355.2637	355.2631	1.69	7.31
7	Dehydrobufotenine	$C_{12}H_{14}N_2O$	203.1175	203.1178	−1.48	3.71
8	Telocinobufagin	$C_{24}H_{34}O_5$	403.2464	403.2479	−3.72	6.83
9	Cinobufotalin	$_{C26}H_{34}O_7$	459.2362	459.2377	−3.27	7.19
10	Desacetylcinobufotalin	$C_{24}H_{32}O_6$	417.2254	417.2272	−4.31	5.94
11	desacetylcinobufagin	$C_{24}H_{32}O_5$	401.231	401.2323	−3.24	6.87

RT, retention time.

and **2**, the overlapping genes for compound targets and HCC-associated human genes was obtained by using Venny 2.1.0 (Liang et al., 2019). As a result, 82 HCC-related genes were identified for the 11 components of HCSCs (**Table 2**).

Compound-Target Network Analysis

Chinese herbal formulas present a range of pharmacological activities through a range of targets, so we investigated the potential mechanisms of HCSCs against HCC. Based on the compounds and predicted targets, we constructed a network of components and targets using Cytoscape. The centralization and heterogeneity of the network were 0.393 and 1.400, respectively. As presented in **Figure 3**, the network contained a total of 93 nodes, 11 compound nodes and 82 target nodes, which formed 261 compound-target associations. The network indicated the potential relationships between the compounds and the targets, thereby revealing the potential pharmacological mechanisms of HCSCs for the treatment of HCC. The nodes with the highest degree of connections to other compounds or targets represented hubs within the entire network, and hence were potential drugs or targets. For example, the compound with the highest degree of connections was bufalin (degree=41). Resibufogenin, desacetylcinobufagin, and cinobufagin also have higher degree of connections of 37, 32, and 29, respectively. These findings indicated that a single compound affected multiple targets, and these targets were potentially related to action of HCSCs. In terms of target analysis, SRD5A1, AR, and MAPT individually linked to 56 compounds; ATP1A1, MBNL2, and MBNL3 were individually connected to nine compounds; NR3C1, VDR, HSD11B2, SLC10A2, UGT2B7, CYP27B1, OPRM1, and OPRK1 individually linked to seven compounds; OPRD1, SERPINA6, G6PD, GABBR1, GPBAR1, NR1I3, and SHBG connected to six compounds, respectively. These findings indicated that multiple compounds could target a single gene in an interactional manner, supporting that HCSCs exhibited inhibitory function through multi-components and multi-target treatment.

PPI Network of HCSC-Related HCC Targets

The PPI network was constructed based on the PPIs for the candidate protein targets of HCSCs. **Figure 4** showed that the PPI network consisted of 77 nodes and 324 edges. The

centralization and heterogeneity of the network were 0.292 and 0.751, respectively. In the PPI network, the nodes with higher degree might play important roles in the pharmacological processes. It demonstrated that 10 key nodes, including ESR1, CASP3, EGFR, AR, CYP3A4, ERBB2, NR3C1, PGR, ADAM17, and MMP2 were likely to be the key targets of HCSCs to inhibit HCC (**Supplementary Table 3**).

GO and KEGG Pathway Enrichment Analyses

To verify the biological characteristics of involved target genes of HCSCs against HCC, the GO enrichment analysis of putative targets was performed using DAVID Bioinformatics Resources, a type of functional annotation tool. Among the 77 genes, 68 GO terms met the requirements with the count of ≥2 and EASE scores of ≤0.05, in which 31 items were BP-related, 10 items were CC-related, and 27 were MF-related. The GO information was presented in detail in **Supplementary Table 4**. **Figure 5A** showed the top 27 enriched terms in BP, CC, and MF categories, suggesting that HCSCs may regulate cancer cell proliferation through protein, enzyme, and transcription factor binding in the extracellular space, plasma membrane, or cytosol, to exhibit inhibitory effects in HCC.

To further identify the potential pathways involved in the inhibitory effects of HCSCs against HCC, the KEGG pathway enrichment analysis of the 77 genes was performed. As shown in **Figure 5B**, a total of 14 enriched pathways of HCSCs against HCC were identified (p < 0.05). The KEGG pathway information was presented in detail in **Supplementary Table 5**. The enriched genes were linked to a variety of pathways, including pathways in cancer, bladder cancer, prostate cancer, proteoglycans in cancer, as well as metabolic, immune, and apoptotic pathways. To further clarify the modes of action, a target-pathway network was constructed based on all these target proteins and the corresponding signaling pathways. The centralization and heterogeneity of the network were 0.149 and 0.804, respectively. As shown in **Figure 6**, this network was composed of 87 edges and 56 nodes, including 14 for pathways and 42 for proteins. Among these protein targets, ERBB2, EGFR, ESR1, GSK3B, MMP2, CASP3, ATP1A1, BDKRB2, and AR were identified as relatively high-involved molecules, which suggested that these proteins may play essential roles in HCC progression.

TABLE 2 | Hepatocellular carcinoma-related targets of Huachansu capsules (HCSCs).

Number	Protein name	Gene name
01	Steroid 5 Alpha-Reductase 1	SRD5A1
02	Aldo-Keto Reductase Family 1 Member B10	AKR1B10
03	Nuclear Receptor Subfamily 3 Group C Member 1	NR3C1
04	Solute Carrier Family 10 Member 1	SLC10A1
05	Vitamin D Receptor	VDR
06	Tyrosine Aminotransferase	TAT
07	Hydroxysteroid 11-Beta Dehydrogenase 2	HSD11B2
08	Androgen Receptor	AR
09	ATPase Na$^+$/K$^+$ Transporting Subunit Alpha 1	ATP1A1
10	Solute Carrier Family 10 Member 2	SLC10A2
11	UDP Glucuronosyltransferase Family 2 Member B7	UGT2B7
12	Cytochrome P450 Family 27 Subfamily B Member 1	CYP27B1
13	Cytochrome P450 Family 3 Subfamily A Member 4	CYP3A4
14	Microtubule-associated protein tau	MAPT
15	Opioid Receptor Mu 1	OPRM1
16	Opioid Receptor Delta 1	OPRD1
17	Opioid Receptor Kappa 1	OPRK1
18	Muscleblind Like Splicing Regulator 2	MBNL2
19	Muscleblind Like Splicing Regulator 3	MBNL3
20	Butyrylcholinesterase	BCHE
21	Acetylcholinesterase (Cartwright Blood Group)	ACHE
22	ATP Binding Cassette Subfamily B Member 11	ABCB11
23	Serpin Family A Member 6	SERPINA6
24	Glucose-6-Phosphate Dehydrogenase	G6PD
25	Gamma-Aminobutyric Acid Type B Receptor Subunit 1	GABBR1
26	G Protein-Coupled Bile Acid Receptor 1	GPBAR1
27	Nuclear Receptor Subfamily 1 Group H Member 4	NR1H4
28	Nuclear Receptor Subfamily 1 Group I Member 3	NR1I3
29	Sex Hormone Binding Globulin	SHBG
30	Bradykinin Receptor B2	BDKRB2
31	ATP Binding Cassette Subfamily C Member 4	ABCC4
32	ST6 Beta-Galactoside Alpha-2,6-Sialyltransferase 1	ST6GAL1
33	Matrix Metallopeptidase 3	MMP3
34	Matrix Metallopeptidase 1	MMP1
35	Matrix Metallopeptidase 10	MMP10
36	Matrix Metallopeptidase 8	MMP8
37	Matrix Metallopeptidase 12	MMP12
38	Matrix Metallopeptidase 13	MMP13
39	Growth Factor, Augmenter Of Liver Regeneration	GFER
40	Angiotensin I Converting Enzyme	ACE
41	Angiotensin I Converting Enzyme 2	ACE2
42	ADAM Metallopeptidase Domain 17	ADAM17
43	Carboxyl Ester Lipase	CEL
44	Cytochrome P450 Family 17 Subfamily A Member 1	CYP17A1
45	Matrix Metallopeptidase 2	MMP2
46	Eukaryotic Translation Initiation Factor 2 Alpha Kinase 3	EIF2AK3
47	Caspase 3	CASP3
48	MYB Proto-Oncogene, Transcription Factor	MYB
49	Poly(ADP-Ribose) Polymerase 1	PARP1
50	Interferon Regulatory Factor 3	IRF3
51	Cytochrome P450 Family 3 Subfamily A Member 5	CYP3A5
52	TNF Receptor Superfamily Member 10a	TNFRSF10A
53	Glycogen Synthase Kinase 3 Beta	GSK3B
54	Cannabinoid Receptor 1	CNR1
55	Estrogen Receptor 1	ESR1
56	Estrogen Receptor 2	ESR2
57	Cannabinoid Receptor 2	CNR2
58	Carbonic Anhydrase 1	CA1
59	Carbonic Anhydrase 2	CA2
60	Nuclear Receptor Subfamily 3 Group C Member 2	NR3C2
61	Sonic Hedgehog	SHH
62	Histone Deacetylase 1	HDAC1

(Continued)

TABLE 2 | Continued

Number	Protein name	Gene name
63	Histone Deacetylase 3	HDAC3
64	Histone Deacetylase 2	HDAC2
65	Fatty Acid Binding Protein 1	FABP1
66	Progesterone Receptor	PGR
67	Solute Carrier Family 22 Member 2	SLC22A2
68	Steroid 5 Alpha-Reductase 2	SRD5A2
69	Hydroxysteroid 17-Beta Dehydrogenase 12	HSD17B12
70	5-Hydroxytryptamine Receptor 2B	HTR2B
71	Epidermal Growth Factor Receptor	EGFR
72	Erb-B2 Receptor Tyrosine Kinase 2	ERBB2
73	Erb-B2 Receptor Tyrosine Kinase 4	ERBB4
74	Erb-B2 Receptor Tyrosine Kinase 3	ERBB3
75	Kruppel Like Factor 5	KLF5
76	Carbonic Anhydrase 3	CA3
77	Secreted Frizzled Related Protein 1	SFRP1
78	Coagulation Factor II Thrombin Receptor	F2R
79	Monoglyceride Lipase	MGLL
80	Galactosidase Beta 1	GLB1
81	Histone Deacetylase 6	HDAC6
82	Solute Carrier Family 5 Member 1	SLC5A1

To further clarify the pathways that regulated by the compounds, a compound-pathway network was constructed based on all the compounds and signaling pathways. The centralization and heterogeneity of the network were 0.230 and 0.364, respectively. As shown in **Figure 7**, the network was composed of 25 nodes (14 pathways and 11 compounds) and 99 edges. Taken together, we suggested that HCSCs exerted anti-tumor effects against HCC through multiple mechanisms.

HCSCs Inhibited HCC Proliferation

To validate the effects of HCSCs against HCC as predicted from network pharmacology analyses, a series of cell biological function assays were performed. MTT assay was conducted to identify the effects of HCSCs on cell viability in HCC, PLC/PRF/5, and MHCC97L cells. After exposure to 0–1.2 mg/ml of HCSCs for 48 h, the HCC cells were observed a dose-dependent decrease in cell viability (**Figure 8A**). The IC$_{50}$ (the half maximal inhbitory concentration) values of HCSCs were 0.1132 and 0.1807 mg/ml for PLC/PRF/5 and MHCC97L cells, respectively.

Next, we examined the anti-cancer effects of HCSCs in PLC/PRF/5 and MHCC97L cells. The cells were exposed to HCSCs (0.05 and 0.1 mg/ml) for 48 h. The colony formation assay was performed to examine the colony formation abilities of the HCC cells in the presence of HCSCs. The colony counts of PLC/PRF/5 and MHCC97L cells were significantly reduced by HCSCs (**Figure 8B**). Moreover, the transwell invasion assay was also carried out to measure the invasive ability of the HCC cells in the presence of HCSCs. After incubation with HCSCs, the invasive abilities of the HCC cells were significantly reduced (**Figure 8C**). Likewise, we observed that HCSCs significantly increased the wound width in HCC cells (**Figure 8D**), indicating its wound healing abilities. Interestingly, the cell cycle arrest at the G2/M stage was observed in HCC cells (**Figure 8E**). Furthermore, the apoptotic profile showed that HCSCs significantly induced apoptosis in HCC cells (**Figure 8F**). To further validate the
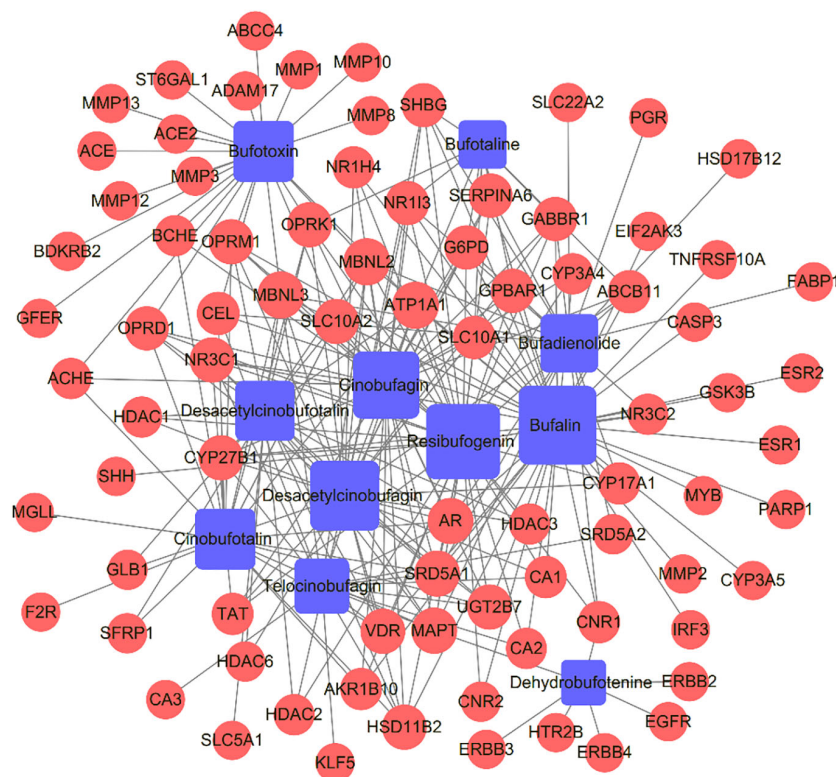
FIGURE 3 | Compound-target network of Huachansu capsules (HCSCs) and hepatocellular carcinoma. The blue nodes represent candidate active compounds, and the red nodes represent potential protein targets. The edges represent the interactions between them, and the node sizes are proportional to the node degrees.

feasibility of pharmacology network analysis, we selected the top proteins with high degree from PPI network results and found that the proteins expression of EGFR, ERBB2 were significantly decreased after HCSCs treatment, but ESR1, a tumor suppression gene, had no obvious changes after HCSCs treatment (**Figure 8G**). We reasoned that HCSCs inhibited HCC growth in part through inhibiting ERBB, EGFR signaling pathways. Taken together, this indicated that HCSCs have strong anti-cancer effects in HCC.

DISCUSSION

HCC is one of the main types of liver cancer, which has high incidence and mortality around the world. According to GLOBOCAN 2018 China, Southeastern Asia, Eastern Africa, and sub-Saharan western have the highest incidence of HCC. Up to now, there is still lack of effective medicine to inhibit the progression of HCC, so new effective agents are needed to be developed. According to the principles of Chinese medicine, liver cancer is being considered as the cumulative toxicity of internal organs that combines several patterns of syndrome. Chinese herbal formulas are composed of multi-components for treating complex symptoms in liver cancer. Being made up of various

components, Chinese herbal formulas play a variety of functions through synergistic or contradictory actions between multiple compositions (Wang et al., 2014). The multiple compositions may be responsible for multi-targets and -pathways underlying the effects of Chinese herbal formulas in liver cancer. Considering that the underlying mechanisms of Chinese herbal formulas in diseases are difficult to be clarified (Liu and Du, 2010), network pharmacology analysis may shed the light to the study of the mechanisms of Chinese herbal formulas. This analysis can predict the target profiles and pharmacological mechanisms of the active constituents in Chinese herbal formulas, thereby suggesting some interactions between drugs and organisms at a systematic level (Li and Zhang, 2013). In this study, we identified the chemical compounds with biological activity from HCSCs and the possible targets and pathways in relation to HCC, and also investigated the anti-cancer effects of HCSCs in HCC, PLC/PRF/5, and MHCC97L cells.

Huachansu, one type of Chinese medicine derived from dried toad venom, has been shown to display efficacy for the treatment of several cancers such as gastric and bladder cancer (Xie et al., 2013; Yang et al., 2015; Ni et al., 2019). A study demonstrated that with the combination of cinobufacin, one of the bioactive compounds from Huachansu, the transcatheter arterial chemoembolization could significantly improve the life quality

FIGURE 4 | Protein-Protein Interaction (PPI) network of Huachansu capsules (HCSCs)-related targets in hepatocellular carcinoma. The size of the nodes is proportional to the degree of the nodes.

and increase the 2-year survival rate in advanced HCC patients (Wu et al., 2014). Chinese herbal formulas are widely used in China to treat diseases. HCSCs, a formula of Huachansu, has been produced and consumed in China for many years. In this study, 11 chemical components of HCSCs were identified using UPLC-MS/MS. Among these 11 bioactive components, several compounds have been reported to possess pharmacological actions against cancers including HCC. Previous work reported that bufotalin and telocinobufagin were promising anti-HCC agents (Zhang et al., 2012), while cinobufotalin was a potential anti-hepatoma component (Cheng et al., 2015). In addition, bufalin (Qiu et al., 2013), cinobufagin (Qi et al., 2011), resibufogenin (Xie et al., 2012), and bufadienolide (Wei et al., 2017) are the main anti-cancer components of Huachansu injection.

The network pharmacology analysis may predict the potential targets and pathways underlying the anti-cancer effects of HCSCs against HCC. We applied a series of databases to retrieve HCC-related targets for these 11 bioactive compounds of HCSCs. The PPI network analysis was used to identify key proteins related to the anti-HCC effects of HCSCs, which were implied by the crucial nodes in the PPI network. The top 10 key targets, namely ESR1, CASP3, EGFR, AR, CYP3A4, ERBB2, NR3C1, PGR, ADAM17, and MMP2, were demonstrated as hub-bottleneck proteins according to

the topological parameters. The interactive structure indicated that HCSCs could interact directly or indirectly with these molecular targets to exert anti-cancer effects. We also observed that ESR1 connected 30 nodes in the PPI network. ESR1 encodes the estrogen receptor, which is important for hormone binding, DNA binding, and transcription activation. The silence of ESR1 significantly increased the size of tumor in HCC tissues, implying that ESR1 is a tumor suppressor in human HCC (Hishida et al., 2013). Moreover, EGFR, a transmembrane receptor tyrosine kinase, connected 28 nodes in the PPI network. The activation of EGFR could lead to the activation of diverse signaling pathways that regulate cell proliferation, differentiation, and survival (Komposch and Sibilia, 2015). CASP3, a type of cysteinyl aspartate-specific proteases, functions as an important effector in apoptotic process (Hong et al., 2017), while CYP3A4 encodes a member of the cytochrome P450 superfamily of enzymes and is used as a biomarker for HCC prognosis (Ashida et al., 2017). Therefore, we concluded that these proteins are important for tumor-suppressing activity of HCSCs in HCC.

Sixty-eight GO terms and 14 KEGG pathways were identified using enrichment analysis. Our results indicated that HCSCs may exert anti-tumor effects through the dysregulation of HCC cell proliferation, which characterize the potential mode of action of
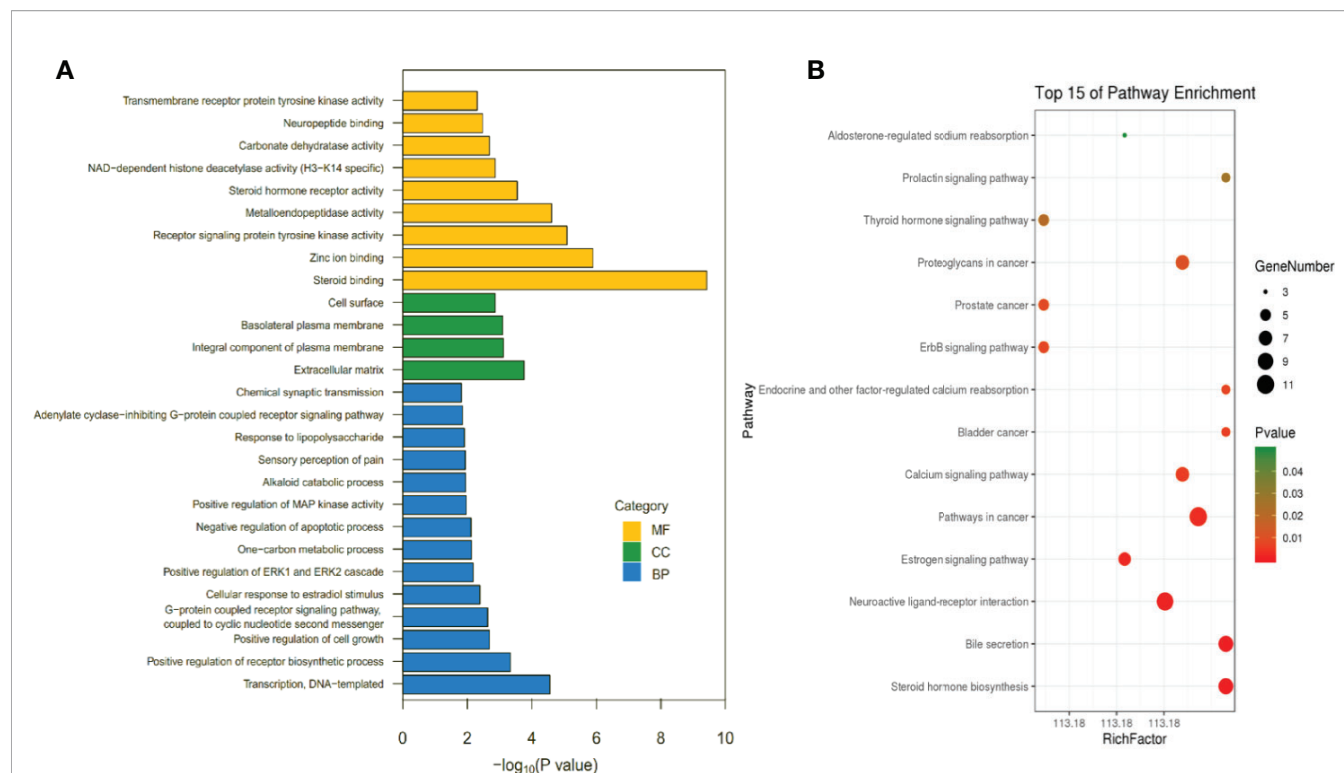
FIGURE 5 | List of Gene Ontology (GO) and Kyoto Encyclopedia of Genes and Genomes (KEGG) pathway enrichment results in relation to the potential targets of Huachansu capsules (HCSCs). **(A)** The first 27 GO terms were identified based on $p < 0.01$. **(B)** The top 15 pathways were identified based on $p < 0.05$.

HCC progression. Based on a series of network pharmacology analyses, HCSCs may exhibit inhibitory actions in HCC *via* directly modulating cancer, metabolism and immune-related pathways. For example, the ERBB signaling pathway is involved in multiple human cancers, and signaling through the ERBB/HER receptors already serves as a target for several cancer drugs (Citri and Yarden, 2006). This is in consistence with our compound-pathway network analysis showing that the ERBB signaling pathway was a potential underlying mechanism for bufalin and dehydrobufotenine. Moreover, among these 14 pathways, bufalin was involved in 13 pathways of them, resibufogenin, desacetylcinobufagin, and cinobufotalin was involved in 10 pathways, and other compounds involved in at least six pathways. It also showed that the cancer pathways were linked with 10 compounds, and the remaining pathways interacted with at least two compounds. Taken together, we suggested that HCSCs regulate multiple targets and pathways in HCC cells.

To further verify the anti-HCC ability of HCSCs, a series of biological function assays were performed in HCC cell lines, PLC/PRF/5 and MHCC97L. We showed that HCSCs induced cell death and cell cycle arrest at G2/M phase in HCC cells. Moreover, we found that HCSCs inhibited colony formation, cell invasion and migration, and apoptosis in HCC cells. This is in consistent with a previous study of gastric cancer, which reported that HCSCs has significant anti-proliferative and apoptotic effects in gastric cancer cells (Ni et al., 2019).

Taken together, we identified 11 bioactive components in HCSCs and the potential targets and pathways underlying the effects of HCSCs in HCC using the network pharmacology method. The results identified some pathways and biological processes that could be related to anti-cancer effects of HCSCs again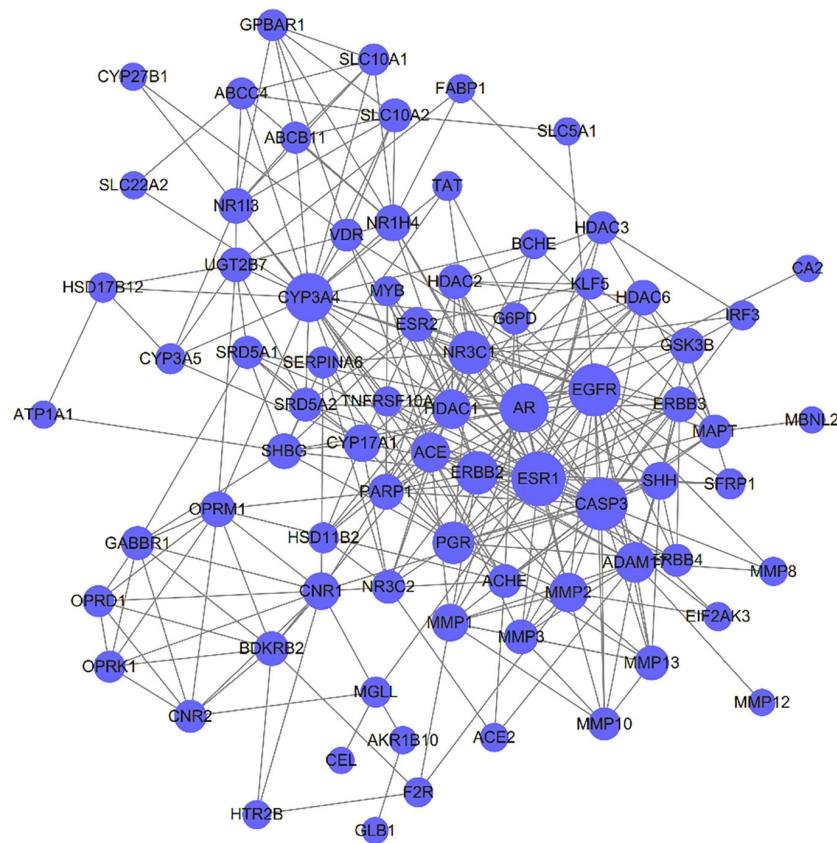st HCC. To further validate the feasibility of pharmacology network analysis, we selected the top proteins with high degree from PPI network results and found that the proteins expression of EGFR, ERBB2 were significantly decreased after HCSCs treatment, but ESR1, a tumor suppression gene, had no obvious changes after HCSCs treatment. We reasoned that HCSCs inhibited HCC growth in part through inhibiting ERBB, EGFR signaling pathways. Therefore, this study provides an alternative method for the comprehensive understanding of the anti-HCC mechanisms of HCSCs.

CONCLUSION

In conclusion, the current study identified, for the first time, the bioactive components in HCSCs, as well as the multiple targets and pathways of HCSCs against HCC. The network pharmacological method developed and the experimental evaluations in this study pointed to a new window for laboratory research and clinical application of HCSCs for the treatment of HCC.
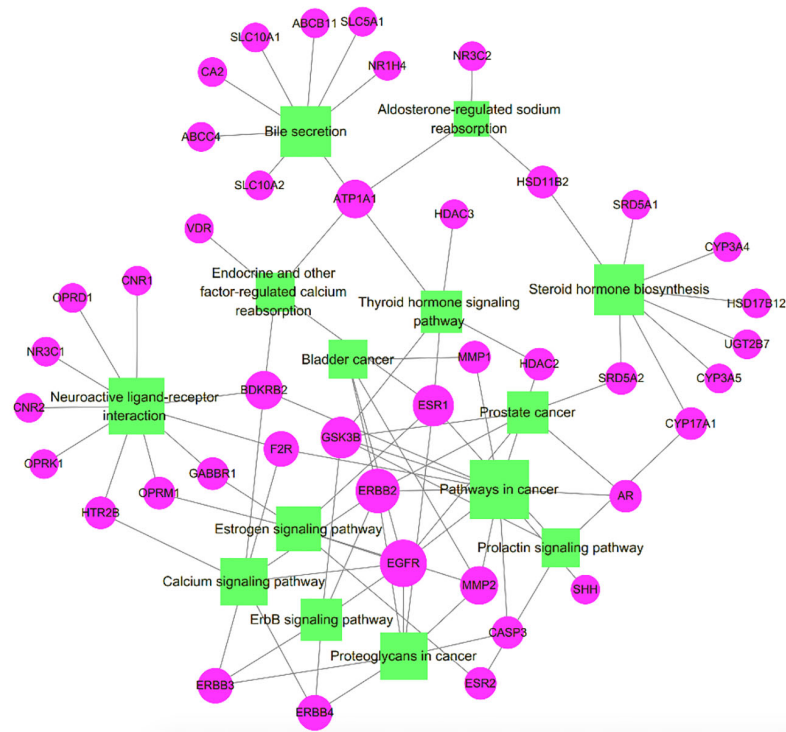
FIGURE 6 | Target-pathway network of Huachansu capsules (HCSCs). The green nodes represent the pathways, the pink nodes represent the targets, and the edges represent the interactions between them. The size of the node is proportional to the degree of the node.
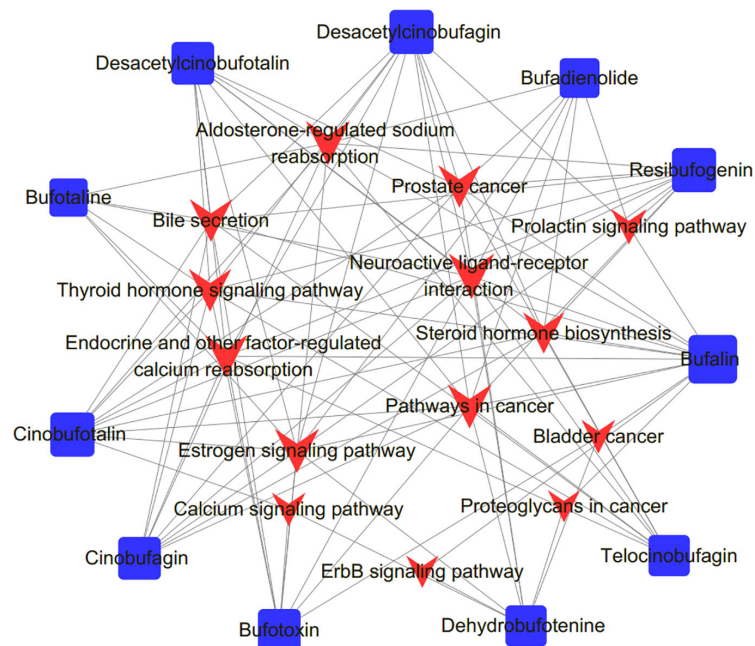
FIGURE 7 | Compound-pathway network of Huachansu capsules (HCSCs). The red nodes represent significant pathways, the blue nodes represent candidate active compounds, and the edges represent the interactions between them. The size of the node is proportional to the degree of the node.

FIGURE 8 | Huachansu capsules (HCSCs) exhibited anti-cancer effects in PLC/PRF/5 and MHCC97L cells. **(A)** The cell viability was assessed by MTT assay after HCSCs administration for 48 h. The cells were incubated with 0–1.2 mg/ml HCSCs. n=3. **(B)** Colony formation in the presence of HCSCs. n=3. **(C)** Transwell invasion abilities of HCC cells in the presence of HCSCs. n=3. **(D)** Wound healing abilities of HCC cells in the presence of HCSCs. n=3. **(E)** Cell cycle analysis in HCSCs-treated HCC cells. n=3. **(F)** Apoptosis analysis of HCSCs-treated HCC. n=3. **(G)** Western blot analysis of ESR1, EGFR, and ERBB2 in HCC cells after 48 h treatment with HCSCs of 0.05 mg/ml. **(B–G)** The cells were treated with 0.05 and 0.1 mg/ml HCSCs for 48 h. $*p < 0.05$, $**p < 0.01$, $***p < 0.001$ vs. 0 mg/ml.

DATA AVAILABILITY STATEMENT

Publicly available datasets were analyzed in this study. This data can be found here: OncoDB.HCC (http://oncodb.hcc.ibms. sinica.edu.tw/index.htm), Liverome (http://liverome.kobic.re.kr/ index.php), Therapeutic Target Database (TTD, http://bidd.nus. edu.sg/group/cjttd/TTD_HOME.asp), Comparative Toxicogenomics Database (CTD, http://ctdbase.org/), PharmGKB (https://www.pharmgkb.org/), DAVID Bioinformatics Resources 6.7 (http://david.abcc.ncifcrf.gov/), and Chinese medicine systems pharmacology (TCMSP) database (http://lsp.nwsuaf.edu.cn/tcmsp.php).

AUTHOR CONTRIBUTIONS

YF and JH designed and conceived the study. JH and FC conceived the study and drafted the manuscript. ZZ, HT, NW, YL, and XF retrieved and analyzed the data. ZZ and TY revised the manuscript. All authors have read and approved the final manuscript.

SUPPLEMENTARY MATERIAL

The Supplementary Material for this article can be found online at: https://www.frontiersin.org/articles/10.3389/fphar.2020. 00414/full#supplementary-material

REFERENCES

Ashida, R., Okamura, Y., Ohshima, K., Kakuda, Y., Uesaka, K., Sugiura, T., et al. (2017). CYP3A4 Gene Is a Novel Biomarker for Predicting a Poor Prognosis in Hepatocellular Carcinoma. *Cancer Genomics Proteomics* 14 (6), 445–453. doi: 10.21873/cgp.20054

Cheng, L., Chen, Y. Z., Peng, Y., Yi, N., Gu, X. S., Jin, Y., et al. (2015). Ceramide production mediates cinobufotalin-induced growth inhibition and apoptosis in cultured hepatocellular carcinoma cells. *Tumour Biol.* 36 (8), 5763–5771. doi: 10.1007/s13277-015-3245-1

Citri, A., and Yarden, Y. (2006). EGF-ERBB signalling: towards the systems level. *Nat. Rev. Mol. Cell Biol.* 7 (7), 505–516. doi: 10.1038/nrm1962

Colagrande, S., Inghilesi, A. L., Aburas, S., Taliani, G. G., Nardi, C., and Marra, F. (2016). Challenges of advanced hepatocellular carcinoma. *World J. Gastroenterol.* 22 (34), 7645–7659. doi: 10.3748/wjg.v22.i34.7645

Cui, X., Inagaki, Y., Xu, H., Wang, D., Qi, F., Kokudo, N., et al. (2010). Anti-hepatitis B virus activities of cinobufacini and its active components bufalin and cinobufagin in HepG2.2.15 cells. *Biol. Pharm. Bull.* 33 (10), 1728–1732. doi: 10.1248/bpb.33.1728

Daher, S., Massarwa, M., Benson, A. A., and Khoury, T. (2018). Current and Future Treatment of Hepatocellular Carcinoma: An Updated Comprehensive Review. *J. Clin. Transl. Hepatol* 6 (1), 69–78. doi: 10.14218/JCTH.2017.00031

Daoudaki, M., and Fouzas, I. (2014). Hepatocellular carcinoma. *Wien Med. Wochenschr* 164 (21-22), 450–455. doi: 10.1007/s10354-014-0296-7

Gfeller, D., Grosdidier, A., Wirth, M., Daina, A., Michielin, O., and Zoete, V. (2014). SwissTargetPrediction: a web server for target prediction of bioactive small molecules. *Nucleic Acids Res.* 42 (Web Server issue), W32–W38. doi: 10.1093/nar/gku293

Hishida, M., Nomoto, S., Inokawa, Y., Hayashi, M., Kanda, M., Okamura, Y., et al. (2013). Estrogen receptor 1 gene as a tumor suppressor gene in hepatocellular carcinoma detected by triple-combination array analysis. *Int. J. Oncol.* 43 (1), 88–94. doi: 10.3892/ijo.2013.1951

Hong, M., Zhang, Y., Li, S., Tan, H. Y., Wang, N., Mu, S., et al. (2017). A Network Pharmacology-Based Study on the Hepatoprotective Effect of Fructus Schisandrae. *Molecules* 22 (10), 1617. doi: 10.3390/molecules22101617

Hong, H., An, J. C. , de La Cruz, J. F., and Hwang, S. G. (2017). Cnidium officinale Makino extract induces apoptosis through activation of caspase-3 and p53 in human liver cancer HepG2 cells. *Exp. Ther. Med.* 14 (4), 3191–3197. doi: 10.3892/etm.2017.4916

Huang, Z., Wang, Y., Chen, J., Wang, R., and Chen, Q. (2013). Effect of Xiaoaiping injection on advanced hepatocellular carcinoma in patients. *J. Tradit Chin Med.* 33 (1), 34–38. doi: 10.1016/S0254-6272(13)60097-7

Huang, J., Cheung, F., Tan, H. Y., Hong, M., Wang, N., Yang, J., et al. (2017). Identification of the active compounds and significant pathways of yinchenhao decoction based on network pharmacology. *Mol. Med. Rep.* 16 (4), 4583–4592. doi: 10.3892/mmr.2017.7149

Huang, J., Tang, H., Cao, S., He, Y., Feng, Y., Wang, K., et al. (2017a). Molecular Targets and Associated Potential Pathways of Danlu Capsules in Hyperplasia of Mammary Glands Based on Systems Pharmacology 2017. *Evid. Based Complement Alternat. Med.* 1930598. doi: 10.1155/2017/1930598

Huang, J., Li, L., Cheung, F., Wang, N., Li, Y., Fan, Z., et al. (2017b). Network Pharmacology-Based Approach to Investigate the Analgesic Efficacy and Molecular Targets of Xuangui Dropping Pill for Treating Primary Dysmenorrhea. 2017. *Evid. Based Complement Alternat. Med.*, 7525179. doi: 10.1155/2017/7525179

Keiser, M. J., Roth, B. L., Armbruster, B. N., Ernsberger, P., Irwin, J. J., and Shoichet, B. K. (2007). Relating protein pharmacology by ligand chemistry. *Nat. Biotechnol.* 25 (2), 197–206. doi: 10.1038/nbt1284

Komposch, K., and Sibilia, M. (2015). EGFR Signaling in Liver Diseases. *Int. J. Mol. Sci.* 17 (1), 30. doi: 10.3390/ijms17010030

Lee, L., Wang, K., Li, G., Xie, Z., Wang, Y., Xu, J., et al. (2011). Liverome: a curated database of liver cancer-related gene signatures with self-contained context information. *BMC Genomics* 12 (Suppl 3), S3. doi: 10.1186/1471-2164-12-S3-S3

Li, S., and Zhang, B. (2013). Traditional Chinese medicine network pharmacology: theory, methodology and application. *Chin J. Nat. Med.* 11 (2), 110–120. doi: 10.1016/S1875-5364(13)60037-0

Li, Y., Gao, Z. H., and Qu, X. J. (2015). The adverse effects of sorafenib in patients with advanced cancers. *Basic Clin. Pharmacol. Toxicol.* 116 (3), 216–221. doi: 10.1111/bcpt.12365

Liang, Y., Zhang, X., Zou, J., Shi, Y., Wang, Y., Tai, J., et al. (2019). Pharmacology mechanism of Flos magnoliae and Centipeda minima for treating allergic rhinitis based on pharmacology network. *Drug Dev. Ind. Pharm.* 45 (9), 1547–1555. doi: 10.1080/03639045.2019.1635150

Liu, A. L., and Du, G. H. (2010). Network pharmacology: new guidelines for drug discovery. *Yao Xue Xue Bao* 45 (12), 1472–1477.

Meng, Z., Yang, P., Shen, Y., Bei, W., Zhang, Y., Ge, Y., et al. (2009). Pilot study of huachansu in patients with hepatocellular carcinoma, nonsmall-cell lung cancer, or pancreatic cancer. *Cancer* 115 (22), 5309–5318. doi: 10.1002/cncr.24602

Meng, Q., Zhao, Y., An, L., Li, X., and Liu, P. (2016). Inhibitory effect of bufalin on retinoblastoma cells (HXO-RB44) via the independent mitochondrial and death receptor pathway. *Am. J. Transl. Res.* 8 (11), 4968–4974.

Ni, T., Wang, H., Li, D., Tao, L., Lv, M., Jin, F., et al. (2019). Huachansu Capsule inhibits the proliferation of human gastric cancer cells via Akt/mTOR pathway. *BioMed. Pharmacother.* 118, 109241. doi: 10.1016/j.biopha.2019.109241

Omata, M., Cheng, A. L., Kokudo, N., Kudo, M., Lee, J. M., Jia, J., et al. (2017). Asia-Pacific clinical practice guidelines on the management of hepatocellular carcinoma: a 2017 update. *Hepatol Int.* 11 (4), 317–370. doi: 10.1007/s12072-017-9799-9

Qi, F. H., Li, A. Y., Zhao, L., Zhang, L., Du, G. H., and Tang, W. (2010). [Apoptosis-inducing effect of cinobufacini on human hepatoma cell line HepG2 and its mechanism of action]. *Yao Xue Xue Bao* 45 (3), 318–323.

Qi, F., Inagaki, Y., Gao, B., Cui, X., Xu, H., Kokudo, N., et al. (2011). Bufalin and cinobufagin induce apoptosis of human hepatocellular carcinoma cells via Fas- and mitochondria-mediated pathways. *Cancer Sci.* 102 (5), 951–958. doi: 10.1111/j.1349-7006.2011.01900.x

Qin, T. J., Zhao, X. H., Yun, J., Zhang, L. X., Ruan, Z. P., and Pan, B. R. (2008). Efficacy and safety of gemcitabine-oxaliplatin combined with huachansu in patients with advanced gallbladder carcinoma. *World J. Gastroenterol.* 14 (33), 5210–5216. doi: 10.3748/wjg.14.5210

Qiu, D. Z., Zhang, Z. J., Wu, W. Z., and Yang, Y. K. (2013). Bufalin, a component in Chansu, inhibits proliferation and invasion of hepatocellular carcinoma cells. *BMC Complement Altern. Med.* 13, 185. doi: 10.1186/1472-6882-13-185

Ru, J., Li, P., Wang, J., Zhou, W., Li, B., Huang, C., et al. (2014). TCMSP: a database of systems pharmacology for drug discovery from herbal medicines. *J. Cheminform* 6, 13. doi: 10.1186/1758-2946-6-13

Su, W. H., Chao, C. C., Yeh, S. H., Chen, D. S., Chen, P. J., and Jou, Y. S. (2007). OncoDB.HCC: an integrated oncogenomic database of hepatocellular carcinoma revealed aberrant cancer target genes and loci. *Nucleic Acids Res.* 35 (Database issue), D727–D731. doi: 10.1093/nar/gkl845

Szklarczyk, D., Santos, A., von Mering, C., Jensen, L. J., Bork, P., and Kuhn, M. (2016). STITCH 5: augmenting protein-chemical interaction networks with tissue and affinity data. *Nucleic Acids Res.* 44 (D1), D380–D384. doi: 10.1093/nar/gkv1277

Szklarczyk, D., Gable, A. L., Lyon, D., Junge, A., Wyder, S., Huerta-Cepas, J., et al. (2019). STRING v11: protein-protein association networks with increased coverage, supporting functional discovery in genome-wide experimental datasets. *Nucleic Acids Res.* 47 (D1), D607–D613. doi: 10.1093/nar/gky1131

Wang, C. Y., Bai, X. Y., and Wang, C. H. (2014). Traditional Chinese medicine: a treasured natural resource of anticancer drug research and development. *Am. J. Chin Med.* 42 (3), 543–559. doi: 10.1142/S0192415X14500359

Wei, X., Si, N., Zhang, Y., Zhao, H., Yang, J., Wang, H., et al. (2017). Evaluation of Bufadienolides as the Main Antitumor Components in Cinobufacin Injection for Liver and Gastric Cancer Therapy. *PloS One* 12 (1), e0169141. doi: 10.1371/journal.pone.0169141

Wu, T., Sun, R., Wang, Z., Yang, W., Shen, S., and Zhao, Z. (2014). A meta-analysis of Cinobufacini combined with transcatheterarterial chemoembolization in the treatment of advanced hepatocellular carcinoma. *J. Cancer Res. Ther.* 10 (Suppl 1), 60–64. doi: 10.4103/0973-1482.139763

Xie, R. F., Li, Z. C., Gao, B., Shi, Z. N., and Zhou, X. (2012). Bufothionine, a possible effective component in cinobufocini injection for hepatocellular carcinoma. *J. Ethnopharmacol* 141 (2), 692–700. doi: 10.1016/j.jep.2011.12.018

Xie, X., Huang, X., Li, J., Lv, X., Huang, J., Tang, S., et al. (2013). Efficacy and safety of Huachansu combined with chemotherapy in advanced gastric cancer: a meta-analysis. *Med. Hypotheses* 81 (2), 243–250. doi: 10.1016/j.mehy.2013.04.038

Yang, T., Shi, R., Chang, L., Tang, K., Chen, K., Yu, G., et al. (2015). Huachansu suppresses human bladder cancer cell growth through the Fas/Fasl and TNF-alpha/TNFR1 pathway in vitro and in vivo. *J. Exp. Clin. Cancer Res.* 34, 21. doi: 10.1186/s13046-015-0134-9

Zhan, X., Wu, H., Wu, H., Wang, R., Luo, C., Gao, B., et al. (2020). Metabolites from Bufo gargarizans (Cantor, 1842): A review of traditional uses, pharmacological activity, toxicity and quality control. *J. Ethnopharmacol* 246, 112178. doi: 10.1016/j.jep.2019.112178

Zhang, D. M., Liu, J. S., Tang, M. K., Yiu, A., Cao, H. H., Jiang, L., et al. (2012). Bufotalin from Venenum Bufonis inhibits growth of multidrug resistant HepG2 cells through G2/M cell cycle arrest and apoptosis. *Eur. J. Pharmacol.* 692 (1-3), 19–28. doi: 10.1016/j.ejphar.2012.06.045

Zineh, I. (2019). Quantitative Systems Pharmacology: A Regulatory Perspective on Translation. *CPT Pharmacometrics Syst. Pharmacol.* 8 (6), 336–339. doi: 10.1002/psp4.12403

Xiaochaihutang Improves the Cortical Astrocyte Edema in Thioacetamide-Induced Rat Acute Hepatic Encephalopathy by Activating NRF2 Pathway

Weiyi Jia[1,2†], Jiajia Liu[3†], Rui Hu[4], Anling Hu[3], Weiwei Tang[5], Lijuan Li[5] and Jin Li[1,2*]

[1] Key Laboratory of Infectious Disease and Biosafety, and Provincial Department of Education, Zunyi Medical University, Zunyi, China, [2] Research Center for Medicine and Biology, Zunyi Medical University, Zunyi, China, [3] Key Laboratory of Basic Pharmacology of Ministry of Education and Joint International Research Laboratory of Ethnocentric of Ministry of Education, Zunyi Medical University, Zunyi, China, [4] Key Laboratory of Brain Science, Zunyi Medical University, Zunyi, China, [5] Department of Pathophysiology, Basic Medical College, Zunyi Medical University, Zunyi, China

Oxidative stress induced by high ammonia, which leads to astrocyte edema, is the key to acute hepatic encephalopathy (AHE). Nuclear factor erythroid 2-related factor 2 (NRF2) has been implicated in oxidative stress, but the mechanism of NRF2 against ammonia-induced astrocytes edema has not been fully studied. We confirmed that the NRF2 pathway is related to brain edema caused by AHE and found that Xiaochaihutang (XCHT) could effectively activate the NRF2 pathway to treat AHE. The model of AHE was established with thioacetamide (TAA) in rats. Rat behaviors were observed, brain water content, blood ammonia levels, glutamine synthetase (GS), malondialdehyde (MDA), and total superoxide dismutase (T-SOD) were determined after XCHT treatment. Furthermore, the expression of NRF2 pathway proteins and mRNA, glial fibrillary acidic protein (GFAP) and aquaporins 4 (AQP4) were examined. In order to determine whether XCHT has a direct effect on cerebral edema caused by high ammonia, we examined the effect of XCHT compound serum on cortical astrocytes in the presence of ammonia, through microscopic observation and immunofluorescence (IF). Results showed that AHE induced by TAA changed the behavior of the rats, and increased brain water content, blood ammonia levels, GS and MDA content meanwhile decreasing T-SOD, but these symptoms were improved by treatment with XCHT. XCHT protected brain edema by activating the NRF2 pathway and increasing the expression of downstream proteins and genes. Astrocytes treated with 5 mM ammonia also showed an increase in the AQP4 protein expression but a decrease in XCHT compound serum and ammonia-induced cell edema groups. This study demonstrates that the NRF2 pathway is involved in the brain edema in AHE, and XCHT may represent a useful prescription for the treatment of AHE.

Keywords: Xiaochaihutang, acute hepatic encephalopathy, NRF2 pathway, brain edema, astrocyte edema

INTRODUCTION

Hepatic Encephalopathy (HE) is a series of neuropsychological abnormalities secondary to liver dysfunction after excluding other known brain diseases, such as behavioral, intellectual and cognitive changes (Ferenci et al., 2002). Acute liver failure (ALF) is also called fulminant hepatic failure (FHF), which refers to various causes leading to severe acute liver injury, thus causing some potential and reversible diseases such as electrolyte metabolic disorder, jaundice, HE, etc (Trey and Davidson, 1970). Although the diseases are potentially reversible, they are all based on the loss of the detoxification function of the liver. The increase of toxins affects various systems in the body, and the mortality rate is high (Capocaccia and Angelico, 1991). One of the main components of ALF is the development of brain edema, which leads to increased intracranial pressure and brain herniation, eventually leading to death (Blei, 2010). The disease is also called AHE.

Evidence shows that brain edema in AHE is due to edema of astrocytes (Traber et al., 1987; Traber et al., 1989; Butterworth, 2003; Reinehr et al., 2010). An elevated ammonia level always exists in HE patients (Hazell and Butterworth, 1999). The occurrence of astrocyte edema seems to be affected by ammonia toxicity (Gregorios et al., 1985a; Gregorios et al., 1985b; Swain et al., 1992). Astrocytes mainly convert glutamic acid into glutamine through ammonia detoxification reaction, mediated by glutamine synthetase (Martinez et al., 1977). The dysfunction of astrocytes caused by ammonia-induced oxidative stress is also the core of AHE (Norenberg, 2003). GFAP is a landmark structural protein of astrocytes and participates in cell volume regulation. AQP4 specifically expresses on the capillary side of the protuberant foot plate of brain astrocytes and regulates the transmembrane flow of water. The changes in their expression are involved in astrocyte edema (Papadopoulos et al., 2002).

NRF2 is a major regulator in the redox balance (Cao et al., 2016). In normal conditions, NRF2 combines with Kelch-like ECH-associated protein1 (KEAP1) in an activity inhibition state (Tong et al., 2006). Under the action of the oxidative stress, NRF2 releases from KEAP1 and combines with the antioxidant response element (ARE) in the nucleus, then activates antioxidant enzyme genes expression such as heme oxygenase 1 (HO-1), NADPH quinine oxidoreductase 1 (NQO1), and GSH synthesis (GCLM, GCLC) (Kaspar et al., 2009; Liu et al., 2013). HO-1 is one of the most extensive antioxidant defense enzymes and a member of the heat shock protein family. It has anti-inflammatory, antioxidant, anti-apoptosis, and anti-proliferative effects. NQO1 is a flavin enzyme, which plays a key role in collective detoxification metabolism. GCLM and GCLC form glutamic acid cysteine ligase, which are two important genes in cell antioxidant defense mechanisms and play an important role in regulating glutathione synthesis. When cells are damaged by oxidative stress, gene expressions are up-regulated, glutathione synthesis is increased, and oxidative defense mechanism is enhanced (Liu et al., 2008; Reisman et al., 2009). It was found that NRF2 regulated the activity of the antioxidant enzymes and the expression of down-stream genes to protect against brain edema (Zhang et al., 2017; Chen et al., 2018; Duan et al., 2019). However, whether NRF2 plays a regulatory role in the occurrence and development of AHE needed further research and confirmation.

Xiaochaihutang (XCHT, Sho-Saiko-to, SST in Japan) is a classic formula of traditional Chinese medicine, which is first recorded in 'Shang Han Lun' and has the effects of anti-inflammation, hepatic protection, antipyretic and analgesic treatment. Our previous research found that XCHT can reduce liver cell necrosis and enhance liver function by activating the NRF2 pathway, thus playing a role in protecting the liver (Li et al., 2017; Hu et al., 2019; Jia et al., 2019). Moreover, studies have shown that XCHT can play a role in neurological diseases, such as the treatment of depression (Su et al., 2014), etc. However, whether XCHT treats brain edema through the NRF2 pathway in AHE rats remains to be clarified.

Therefore, this study aimed to investigate the pharmacological effects of XCHT on AHE rats, and subsequently delineated the underlying mechanisms which might be involved in it.

MATERIALS AND METHODS

Animals, Drugs, and Treatments

Male Sprague-Dawley rats weighing 180-220 g (Experimental Animal Centre of the Third Military Medical University) were used for the experiments. Animals were fed in a room with a 12-h light/dark cycle at constant humidity and temperature (22-25°C) and had chow and water ad libitum placed in the cages. Animal maintenance and experimental protocols were carried out in accordance with guidelines approved by the Care Committee of Zunyi Medical University and the NIH guide of Humane Use.

Xiaochaihutang is a traditional Chinese Medicine. Xiaochaihu granule (containing Bupleurum falcatum L. (1.5 g), Scutellaria baicalensis Georgi (0.56 g), Codonopsis pilosula Franch (0.56 g), Pinellia temata Breitenbach (0.56 g), Glycyrrhiza glabra L.(0.56 g), Zingiber officinale Roscoe (0.56 g), and Zizyphus vulgaris Lam. (0.56 g)), referring to the ancient method of decocting, was purchased from Baiyunshan Guanghua Pharmaceutical Co., Ltd. (approval number K70079, Guangzhou, China). According to the 2015 edition of the Pharmacopeia Committee of China (Pharmacopeia Committee of China, 2015), baicalin is used as the index of Xiaochaihu granule, and the content of baicalin in Xiaochaihu granule, measured by high performance liquid chromatography (HPLC) in our previous studies, is 24.307 mg/10g. This conforms to the requirement of not less than 20 mg/10g.

After acclimatization for one week, rats were randomly divided into five groups (50, n = 10): vehicle group, model group, XCHT treatment groups (the instruction of Xiaochaihu granule suggests that patients should take 6-12 g/day, and considering the dose conversion from human to rats, the dose of XCHT is clinically relevant: 1.0 g/kg, 2.0 g/kg, 4.0 g/kg). To induce acute hepatic encephalopathy, rats in model and XCHT groups were given TAA (300 mg/kg/day, i.p.) for three consecutive days (Jayakumar et al., 2014). Starting from the 4th

day, the animals in treatment groups were given the appropriate doses of XCHT granules for 2 weeks (1 mL/100 g/day, i.g.). In the end after 2 weeks of treatment, the mortality rate of rats was about 10%. Then behavior was tested and all rats were sacrificed to obtain blood and cerebral cortex samples.

Observation and Measurement of Rat Behaviors

Rats were observed after administrations and recorded in an open field. Behaviors included mortality, body weight and auto-activity. All studies were performed under strictly standardized conditions in a dark room for 10 min. The total distances were recorded to reflect the auto-activities of rats with AHE. The activities were defined as zero in dead rats (Wang et al., 2017).

Brain Water Measurement

Brain water content was evaluated as previously described (Duris et al., 2011). The cerebral cortex was removed and separated into 2 parts. The left hemisphere was weighed for wet weight. Tissue dried for 72 h in an oven at 110°C, and dry weights were determined. The percentage of water content was calculated as [(wet weight − dry weight)/wet weight] × 100%.

Biochemical Analysis

The plasma was separated and the blood ammonia level was detected according to the instructions of the kit (Nanjing Jiancheng Bioengineering Institute, Nanjing, China). The cortex was isolated from the brain of rat. After homogenizing the cortex, the levels of GS, MDA and T-SOD were determined according to the instructions of the kit (Nanjing Jiancheng Bioengineering Institute, Nanjing, China). Protein concentrations were determined using the Bradford method.

IHC of GFAP in AHE

IHC for GFAP was carried out on cerebral cortex tissue slices after deparaffinization, rehydration, antigen unmasking by heat treatment, and 5% normal goat serum blocking. Slices were incubated with a specific primary antibody overnight at 4 °C, then processed using a GTVision kit (Gene Tech, Shanghai, China) according to the technical manual. Five areas of each slice were randomly examined under an optical microscope (OLYMPUS, BX5, Japan).

Astrocyte Cultures

Primary cultures of cortical astrocytes were prepared as described previously (Guo et al., 2014). Primary cultures of cortical astrocytes were prepared from 1/2-day-old rats. Briefly, the cerebral cortex was stripped from the meninges, minced and dissociated by trituration, passed through sterile nylon sieves and then placed in Dulbecco's modified Eagle medium (DMEM) containing 10% FBS. The medium was changed after 24 h. Astrocytes were incubated at 37 °C in a humidified chamber provided with 5% CO_2 and 95% air. Cultures consisted of at least 95% astrocytes and were determined by GFAP IF.

There were three groups: 10% (v/v) control-serum group (vehicle group), 10% (v/v) control-serum and NH_4Cl (5 nM) group (model group), and 10% (v/v) XCHT compound serum and NH_4Cl (5 nM) group (XCHT group). Serums were provided by preliminary work of our group (Hu et al., 2019). In brief, 30 rats were randomly divided into two equal groups, which includes the control (vehicle) group (n=15) and XCHT treatment group (n=15). The XCHT group received an oral administration of 2 g/kg decoction for 6 days (considering the dose conversion from human to rat, the dose of XCHT was clinically relevant; according to the results of previous in vivo experiments, we chose 2.0 g/kg for administration). A distilled water vehicle control was given to the control group. Then the blood samples were obtained from the abdominal aorta 2 h after oral administration and centrifuged at 3500 rpm for 15 min. The serum samples were mixed and inactivated.

IF Microscopy

Astrocytes were cultured on glass coverslips for 24 h and treated for a further 24 h. Coverslips were washed with PBS, fixed in 4% (v/v) paraformaldehyde for 20 min at room temperature, washed prior to detergent extraction with 0.5% (v/v) Triton X-100 for 20 min., then saturated with PBS containing 5% (v/v) normal goat serum for 30 min. Next, cells were incubated with the specific primary antibody for AQP4 over-night, washed, then incubated with secondary antibody for 1 h at 37 °C. Finally, cells were stained for 5 min with 4,6-diamidino-2-phenylindole (DAPI). OLYMPUS IX73 microscope was used to observe the slides.

Real Time PCR Analysis

Total RNA was extracted from cerebral cortex tissues and treated cortical astrocytes using RNAiso plus (TAKARA, Dalian, China). The primers were designed and synthesized by TAKARA Systems. The sequences of the primers were listed in **Table 1**. The total RNA was reverse-transcribed with 5 × PrimeScripe TM Buffer, Prime Script TMRT Enzyme Mix, and Oligo dT Primer. The SYBR green PCR Master Mix was chosen for real time PCR analysis. A relative quantitative method was used for analysis of results.

Western Blot Analysis

Cytoplasmic and nuclear protein of cerebral cortex tissues and treated cortical astrocytes were extracted by NE-PER Nuclear and Cytoplasmic Extraction Reagents (Thermo-Scientific, Rockford, United States). Equal amounts of protein (15 μg) were separated on 10% SDS-polyacrylamide gel. The blots were incubated overnight with individual protein anti-bodies (1:1000, Abcam, Cambridge, UK), washed, incubated with anti-rabbit IgG, anti-mouse IgG (1:5000, ZSGB-BIO, Beijing, China) for 2 h, and developed by ECL western blotting substrate. Western blot signals were quantified by Imager (Bio-Rad, America).

Statistical Analysis

All data were expressed as mean ± standard deviation (S.D). Statistical analysis was performed with Student's t test and ANOVA with the Tukey post hoc test was used if more than two experimental groups were compared, and $p < 0.05$ was considered statistically significant. Data were analyzed with GraphPad Prism 5.0 (La Jolla, CA, USA).

TABLE 1 | The primer sequence for RT-PCR.

Gene	Sequence (5′~3′)	
	Forward primer	**Reverse primer**
β-actin	GGAGATTACTGCCCTGGCTCCTA	GACTCATCGTACTCCTGCTTGCTG
NRF2	TTGGCAGAGACATTCCCATTTGTA	GAGCTATCGAGTGACTGAGCCTGA
KEAP1	CATCGGCATCGCCAACTTC	GCTGGCAGTGTGACAGGTTGA
HO-1	AGGTGCACATCCGTGCAGAG	CTTCCAGGGCCGTATAGATATGGTA
NQO1	TGGAAGCTGCAGACCTGGTG	CCCTTGTCATACATGGTGiGCATAC
GCLC	CTGCACATCTACCACGCAGTCA	ATCGCCGCCATTCAGTAACAA
GCLM	AGACCGGGAACCTGCTCAAC	GATTTGGGAGCTCCATTCATTCA
GFAP	TCGTGTGGATCTGGAGAGGAAGG	AGAGCCGCTGTGAGGTCTGG
AQP4	GAAGGCGGTCACAGCAGAGTTC	TGATGTGGCCGAAGCACTGAAC

RESULTS

XCHT Treatment Suppressed the Development of TAA-Induced AHE

To analyze the effect of XCHT on TAA-induced AHE in rats, the degree of liver injury in the rats was at first measured (**Supplementary Figure 1**). Subsequently the behaviors [scoring (**Figure 1A**), total distance traveled (**Figure 1B**)], the brain cortical water content (**Figure 1C**), the ammonia plasma (**Figure 2A**), and the GS (**Figure 2B**) levels in all groups of rats were measured. Compared with the vehicle group, significant changes in behavior, decreased auto-action, increased brain water content, blood ammonia and GS in the cerebral cortex were observed in the TAA group relative to the vehicle group. Whereas in rats treated with XCHT behavior scoring improved during the first week, and increased automatic action, decreased brain water content, blood ammonia, and GS were observed. Together, the data presented here demonstrated that XCHT enabled the healing of TAA-induced AHE.

XCHT Reduced the Degree of TAA-induced Oxidative Damage in AHE Rats

In order to detect the oxidative damage degree of AHE rat, we measured the levels of MDA (**Figure 3A**) and T-SOD (**Figure 3B**) in the cerebral cortex by colorimetry. Compared with the vehicle group, MDA level was found to be dramatically increased in the TAA group, and in contrast the level of T-SOD was obviously decreased. However, the groups of XCHT treatment noticeably prevented oxidative stress production in a dose-dependent manner. The data presented here demonstrated that XCHT enabled the healing of TAA-induced AHE by reducing oxidative stress damage.

XCHT Activated NRF2 Pathway in AHE Rats

To examine whether different doses of XCHT inhibit the destruction of cortical astrocytes in an experimental model of AHE (TAA treated rats), cortical sections from each group (n=3)
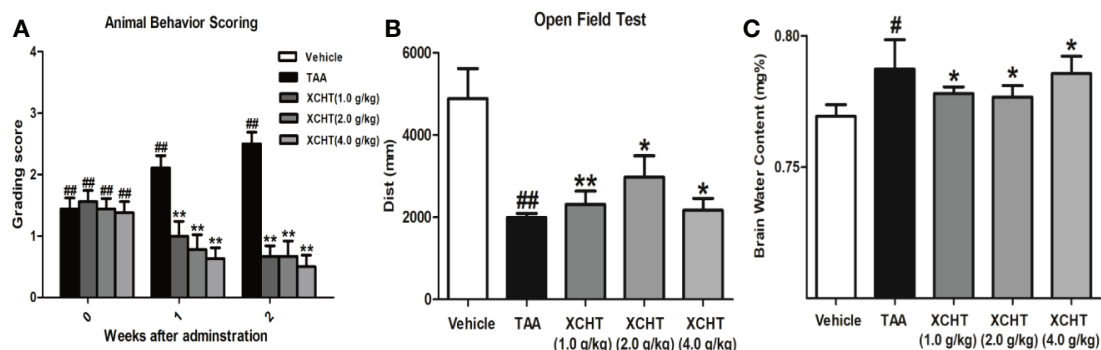
FIGURE 1 | Acute hepatic encephalopathy (AHE) was induces by repeated injection of 300 mg/kg/day thioacetamide (TAA) for 3 days (1 mL/kg in saline, i.p.). From the 4th day, the animals in treatment groups were given the XCHT granules (1.0 g/kg, 2.0 g/kg and 4.0 g/kg, 1mL/100 g/day, i.g.) for 2 weeks. **(A, B)** Measurement of the rat behaviors [**(A)** Animal behavior scoring. **(B)** Open field test. Rats in each group were evaluated for total distance traveled]. **(C)** Brain water content ([(wet weight – dry weight)/wet weight] × 100%). Data were expressed as mean ± SD (n = 5-7). $^{\#}p < 0.05$, $^{\#\#}p < 0.01$ vs. the vehicle group. $^{*}p < 0.05$, $^{**}p < 0.01$ vs. the TAA group.
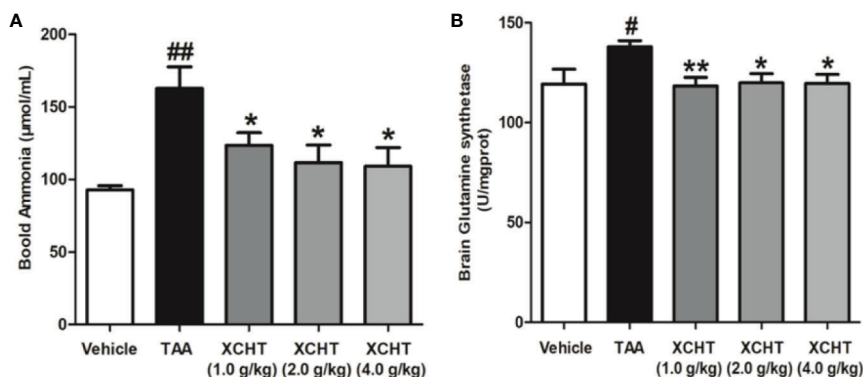
FIGURE 2 | Effect of XCHT on ammonia level in TAA induced AHE rats. **(A)** Ammonia plasma levels in all groups of rats. **(B)** GS levels in cerebral cortex of rats. Data were expressed as mean ± SD (n = 5-7). #p < 0.05, ##p < 0.01 vs. the vehicle group. *p < 0.05, **p < 0.01 vs. the TAA group.
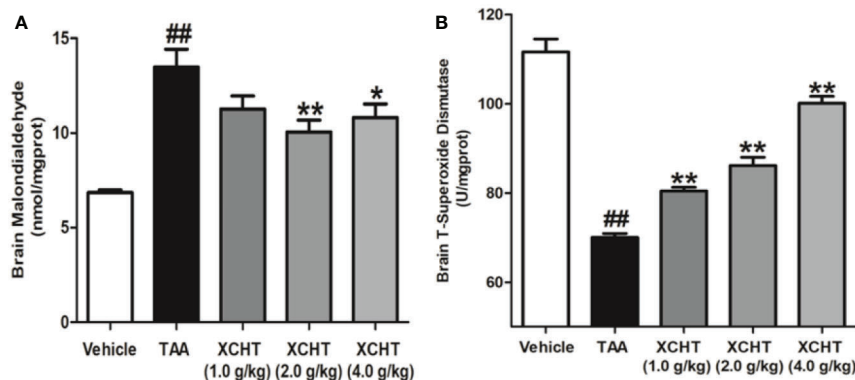
FIGURE 3 | Effects of different doses of XCHT on oxidative stress level [MDA **(A)** and T-SOD **(B)**] in cerebral cortex of TAA induced AHE rats. Data were expressed as mean ± SD (n = 5-7). ##p < 0.01 vs. the vehicle group. *p < 0.05, **p < 0.01 vs. the TAA group.

were immunostained with GFAP, and images were captured with a microscope. Faint GFAP staining of astrocytes were observed in the TAA group. However, intense GFAP IHC was found in XCHT treatment groups (**Figure 4**). In order to determine whether XCHT could protect the cerebral cortex by activating the NRF2 pathway, the expression of NRF2 pathway proteins and genes (Nucl-NRF2 (**Figure 5B**), Cyto-NRF2, KEAP1, HO-1, NQO1, GCLC, GCLM) (**Figures 5A, C**) were further quantified in each group by western blots and real time PCR. Compared with the vehicle group, the TAA group showed a decrease in Nucl-NRF2 and proteins on the NRF2 pathway. In contrast, XCHT treatment groups showed an increase in Nucl-NRF2 and proteins on the NRF2 pathway. At the same time, the level of GFAP and AQP4 in the cerebral cortex was detected and compared with the model group. The expression of GFAP in the XCHT treatment group was increased while there was a decrease in AQP4 protein (**Figures 5A, C**). These results indicated that XCHT might activate the NRF2 pathway to improve brain edema induced by AHE in rats.

Effect of XCHT Compound Serum on the Ammonia-Induced Cell Edema in Astrocytes

The obtained astrocyte culture purity and maturity was put under immunocytochemical examination using an antibody against to the GFAP protein. The astrocyte purity was greater than 95% for the following experiments (**Figure 6A**).

Since XCHT has a protective effect on the liver and reduces the ammonia level in the body, whether or not XCHT has a direct therapeutic effect on cerebral edema caused by AHE needs to be further determined. Cultures were divided between the vehicle group (10% control-serum), the model group (5 mM NH_4Cl and 10% control-serum) and the XCHT group (5 mM NH_4Cl and 10% XCHT compound serum). After 24 h treatment, the cell morphology was observed by a microscope. An increased tense had been seen in cell volume and the cell refractive index was observed after exposure to ammonia for 24 h. Such edema was attenuated by treatment of cells with XCHT compound serum (**Figure 6B**). Compared with the vehicle group, intense
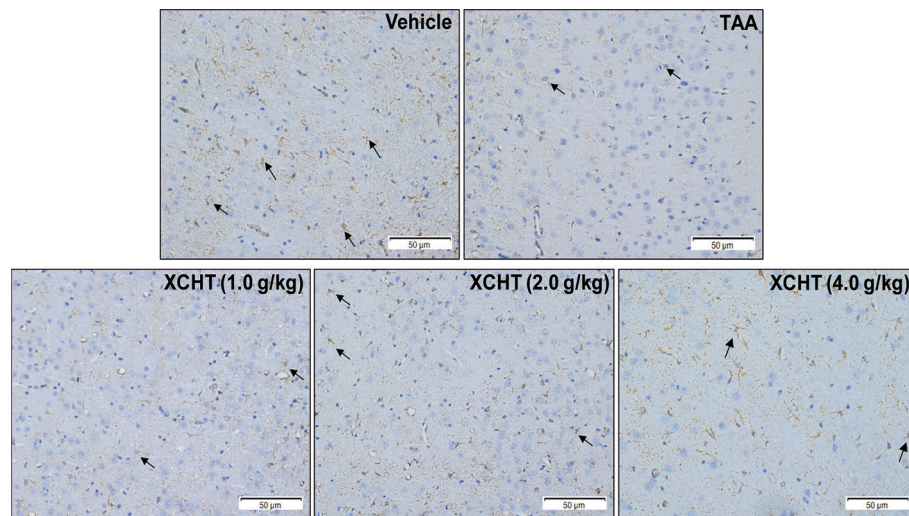
FIGURE 4 | Effect of XCHT on structure of the astrocytes in cerebral cortex of AHE rats. GFAP expression in cerebral cortex of rat brain (IHC, 200×). The decrease of GFAP immunostaining in cortex of TAA group rats compared to the vehicle group, which indicated that the structure of astrocytes was destroyed and brain edema occurred. In contrast, the expression of GFAP in astrocytes increased in the treatment groups with different doses.

AQP4 IF cortical astrocytes were found in the model group. But faint AQP4 staining of astrocytes were observed in the XCHT group (**Figure 6C**).

DISCUSSION

In our present study, we investigated whether XCHT has a potentially protective effect on brain edema associated with AHE, which works by activating the NRF2 pathway. To clarify the effect of XCHT on brain edema caused by AHE, we performed in vivo and vitro experiments respectively and detected the expression of GFAP, AQP4 involved in astrocyte edema as well as the NRF2 pathway (Nucl-NRF2, Cyto-NRF2, HO-1, NQO-1, GCLC and GCLM). This study demonstrates for the first time that the occurrence of AHE-related brain edema may be associated with the NRF2 pathway, and that XCHT, by offering a protective role against ammonia-induced brain/astrocyte edema through activating the NRF2 pathway, may be a promising candidate for AHE treatment.

As mentioned earlier, studies demonstrated that the occurrence of brain edema caused by AHE was related to oxidative stress (Bodega et al., 2015; Mladenović et al., 2015). Since it is the central regulator of cell antioxidant response, the NRF2 pathway plays an important role in the mechanism of cell resistance to internal and external oxidative stress. Studies elaborated that the NRF2 pathway was involved in brain edema caused by various factors (Yang et al., 2016; Gao et al., 2018; Jin et al., 2018). Although some studies analyzed that AHE-induced astrocyte edema was related to the downstream gene HO-1 of the NRF2 pathway (Oenarto et al., 2016), there is no evidence that it is directly related to NRF2 pathway. Therefore, we assumed that the occurrence of brain edema caused by AHE

may be related to the NRF2 pathway. In vivo and vitro, the results showed that ammonia inhibited and reduced the activation of the NRF2 pathway in astrocytes, thus leading to the occurrence of brain edema (**Figures 4, 6**), which is consistent with our hypothesis.

XCHT plays a protective role in disease models damaged by oxidative stress. Our previous studies proved that XCHT could reduce the related symptoms of liver fibrosis and ALF in rats by activating the NRF2 pathway (Jia et al., 2019). Wang et al. proved that XCHT could protect human skin fibroblasts from oxidative stress injury induced by hydrogen peroxide through blocking NF-κB (Wang et al., 2018). At present, studies showed that XCHT could be able to treat neurological related diseases, such as depression (Ma et al., 2017). Therefore, we assumed that XCHT could also activate the NRF2 pathway in the brain after AHE, and reduce the occurrence of brain edema by inhibiting oxidative stress. For this reason, XCHT was given to treat AHE rats in this study. The results showed that XCHT activated the NRF2 pathway and promoted NRF2 translocation from cytoplasm to the nucleus. This translocation alleviates the symptoms of brain edema caused by oxidative stress injury and also alleviates the occurrence of AHE. However, the effect of XCHT treatment with 1.0 or 4.0 mg/kg on rats was not as good as that with 2.0 mg/kg (**Figure 5**). Although the cause of this effect is not clear, low or high concentrations of XCHT may produce non-specific effects.

Previously, it was proved that administration of XCHT to ALF rats could improve liver oxidative damage through the NRF2 pathway, which indicated that XCHT had beneficial effects on ALF (Jia et al., 2019). As XCHT is reported to have a hepato-protective effect, the beneficial effect of XCHT on AHE-induced brain edema observed in this study might be because of the secondary one liver function improvement. And we further verified this conjecture.
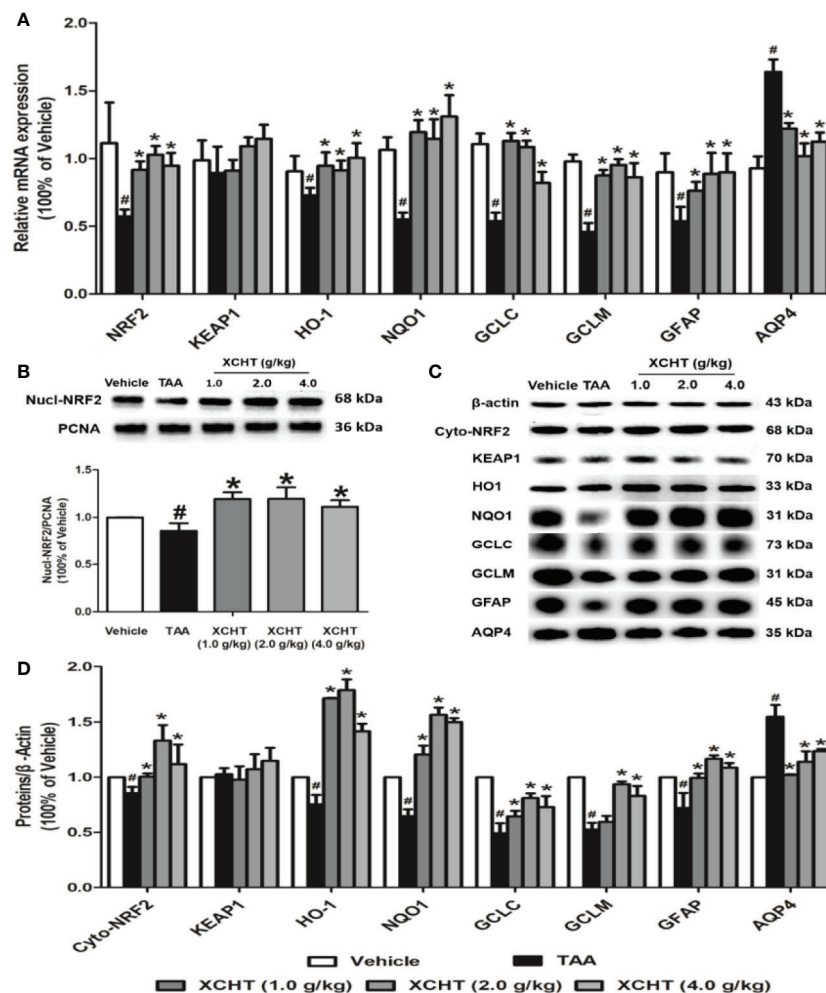
FIGURE 5 | Effect of XCHT on TAA-induced AHE in rats by activating cortical astrocytes NRF2 pathway. **(A)** The mRNA expression of NRF2, KEAP-1, HO-1, NQO-1, GCLC, GCLM, GFAP and AQP4. **(B)** The protein expression of Nucl-NRF2. **(C, D)** The protein expression of Cyto-NRF2, KEAP-1, HO-1, NQO-1, GCLC, GCLM, GFAP and AQP4. Data were expressed as mean ± SD (n = 5-7). #$p < 0.05$, *$p < 0.01$ vs. the TAA group.

In order to simulate the environment in vivo, we selected 10% XCHT compound serum to treat astrocytes in ammonia environment according to previous studies. Studies found that XCHT compound serum contained a variety of active ingredients (such as liquiritin, rutin, zingerone, baicalin, quercetin, etc.) (Sun et al., 2015; Chen et al., 2017). We also detected baicalin in the serum used in this study (**Supplementary Figure 2**), and previous studies found that liquiritin, rutin, baicalin and other components could enter the brain through the blood-brain barrier (BBB) (Huang et al., 2015; Chen et al., 2017; Enogieru et al., 2018). These results showed that XCHT compound serum could protect the structure of astrocytes and reduce AQP4 expression in cells. These results were consistent with our previous work in vitro. All the results proved that the recovery from the brain edema in TAA-induced AHE rats after treatment with XCHT might be due to a direct effect of XCHT on brain edema and a direct effect of improvement in liver function.

However, the study had several limitations. Firstly, since XCHT is a compound Chinese Medicine, which has multitarget features and a variety of protective effects such as antioxidative and anti-inflammatory properties (Hu et al., 2019), we should consider if its protection in AHE is related to its anti-inflammation or other properties in our study. Secondly, in order to simulate the internal environment, we should choose drug-containing cerebrospinal fluid for the cell part. However, considering the small amount of cerebrospinal fluid in rats and the large amount needed in the experimental process, we chose drug-containing serum for this study. Although it was proven that baicalin produced after XCHT entering the body for metabolism could enter the brain, the effect of serum on astrocytes may cause slight deviation in the experimental results. Thirdly, our experiment treated XCHT only at the beginning of AHE. The therapeutic effect of XCHT on AHE in different clinical stages needed further study.
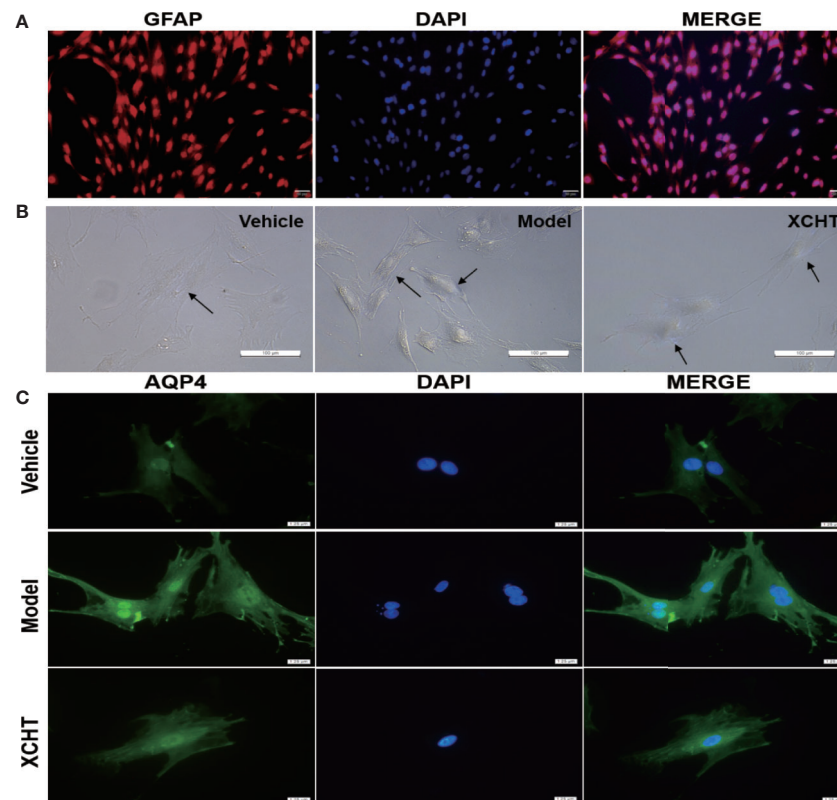
FIGURE 6 | Effect of XCHT compound serum on ammonia-induced astrocyte swelling. **(A)** Purity of primary astrocyte culture. Immunolabeling of primary rat astrocyte cultures with the markers GFAP (Red) revealed pure primary astrocyte culture. Nucleus were stained with 4′,6′-diamidino-2-phenylindole (DAPI) (Blue). (Staining, 100×) **(B)** Morphological overview of astrocyte culture after treatment. **(C)** Immunolabeling of primary rat astrocyte cultures with the markers AQP4 (Green), Nucleus were stained with 4′,6′-diamidino-2-phenylindole (DAPI) (Blue).

In summary, NRF2 pathway protein and mRNA levels were decreased in the cerebral cortex in the TAA model of AHE rats, but treatment with XCHT reduced the brain edema as well as improved their clinical status. Decreased NRF2 was associated with brain edema and activating this pathway with XCHT significantly reduced the edema. Astrocytes treated with ammonia showed the same change in AQP4 as the TAA model of AHE. Our findings suggest that the NRF2 pathway is related to brain/astrocyte edema in AHE, and XCHT might be an effective method for the treatment of brain edema associated with AHE.

DATA AVAILABILITY STATEMENT

The raw data supporting the conclusions of this manuscript will be made available by the authors, without undue reservation, to any qualified researcher.

ETHICS STATEMENT

Animal maintenance and experimental protocols were carried out in accordance with guidelines approved by the Care Committee of Zunyi Medical University and the NIH guide of Humane Use.

AUTHOR CONTRIBUTIONS

All authors contributed to the study conception and design. JL and WJ participated in research design. Material preparation, data collection and analysis and the manuscript were performed by WJ, JJL, and RH. AH, WT, and LL performed the data analysis. All authors commented on previous versions of the manuscript. All authors read and approved the final manuscript.

FUNDING

SUPPLEMENTARY MATERIAL

The Supplementary Material for this article can be found online at: https://www.frontiersin.org/articles/10.3389/fphar.2020.00382/full#supplementary-material

REFERENCES

Blei, A. T. (2010). Cerebral edema and intracranial hypertension in acute liver failure: distinct aspects of the same problem. *Hepatology* 13, 376–379. doi: 10.1002/hep.1840130227

Bodega, G., Segura, B., Ciordia, S., Mena, M. C., López-Fernández, L. A., García, M. I., et al. (2015). Ammonia affects astroglial proliferation in culture. *PloS One* 10, e0139619. doi: 10.1371/journal.pone.0139619

Butterworth, R. F. (2003). Pathogenesis of hepatic encephalopathy: new insights from neuroimaging and molecular studies. *J. Hepatol.* 39, 278–285. doi: 10.1016/S0168-8278(03)00267-8

Cao, L.-J., Li, H.-D., Yan, M., Li, Z.-H., Gong, H., Jiang, P., et al. (2016). The protective effects of isoliquiritigenin and glycyrrhetinic acid against triptolide-induced oxidative stress in HepG2 cells involve Nrf2 activation. *Evid. Based. Complement. Alternat. Med.* 2016, 8912184. doi: 10.1155/2016/8912184

Capocaccia, L., and Angelico, M. (1991). Fulminant hepatic failure. Clinical features, etiology, epidemiology, and current management. *Digest. Dis. Sci.* 36, 775–779. doi: 10.1007/BF01311236

Chen, T.-F., Liu, J.-X., Zhang, Y., Lin, L., Song, W.-T., and Yao, M.-J. (2017). Analysis on microdialysis probe recovery of baicalin in vitro and in vivo based on LC-MS /MS. *Chin. J. Chin. Mater. Med.* 42, 2168–2174. doi: 10.19540/j.cnki.cjcmm.20170307.001

Chen, H.-Y., Cao, J., Zhu, Z.-Y., Zhang, G.-X., Shan, L.-C., Yu, P., et al. (2018). A novel tetramethylpyrazine derivative protects against glutamate-induced cytotoxicity through PGC1α/Nrf2 and PI3K/Akt signaling pathways. *Front. Neurosci.* 12, 567. doi: 10.3389/fnins.2018.00567

Duan, J.-L., Cui, J., Yang, Z.-F., Guo, C., Cao, J.-Y., Xi, M.-M., et al. (2019). Neuroprotective effect of Apelin 13 on ischemic stroke by activating AMPK/GSK-3β/Nrf2 signaling. *J. Neuroinflamm.* 16, 24. doi: 10.1186/s12974-019-1406-7

Duris, K., Manaenko, A., Suzuki, H., Rolland, W., Tang, J., and Zhang, J. H. (2011). Sampling of CSF via the cisterna magna and blood collection via the heart affects brain water content in a rat SAH model. *Transl. Stroke Res.* 2, 232–237. doi: 10.1007/s12975-010-0063-z

Enogieru, A. B., Haylett, W., Hiss, D. C., Bardien, S., and Ekpo, O. E. (2018). Rutin as a Potent Antioxidant: Implications for Neurodegenerative Disorders. *Oxid. Med. Cell. Longev.* 27, 6241017. doi: 10.1155/2018/6241017

Ferenci, P., Lockwood, A., Mullen, K., Tarter, R., Weissenborn, K., and Blei, A. T. (2002). Hepatic encephalopathy-Definition, nomenclature, diagnosis, and quantification: Final report of the Working Party at the 11th World Congresses of Gastroenterology, Vienn. *Hepatology* 35, 716–721. doi: 10.1053/jhep.2002.31250

Gao, Y., Fu, R.-R., Wang, J., Yang, X., Wen, L., and Feng, J. (2018). Resveratrol mitigates the oxidative stress mediated by hypoxic-ischemic brain injury in neonatal rats via Nrf2/HO-1 pathway. *Pharm. Biol.* 56, 440–449. doi: 10.1080/13880209.2018.1502326

Gregorios, J. B., Mozes, L. W., Norenberg, L. O., and Norenberg, M. D. (1985a). Morphologic effects of ammonia on primary astrocyte cultures. I. Light microscopic studies. *J. Neuropathol. Exp. Neurol.* 44, 397–403. doi: 10.1097/00005072-198507000-00003

Gregorios, J. B., Mozes, L. W., and Norenberg, M. D. (1985b). Morphologic effects of ammonia on primary astrocyte cultures. II. Electron microscopic studies. *J. Neuropathol. Exp. Neurol.* 44, 404–414. doi: 10.1097/00005072-198507000-00004

Guo, H., Mao, M., Yu, D., Zhou, H., and Tong, Y. (2014). A modified culture method for astrocytes from rat cortical tissue in vitro. *Zhongguo. Dang. Dai. Er. Ke. Za. Zhi.* 16, 1271–1274. doi: 10.7499/j.issn.1008-8830.2014.12.017

Hazell, A. S., and Butterworth, R. F. (1999). Hepatic encephalopathy: an update of pathophysiologic mechanisms. *Exp. Biol. Med.* 222, 99–112. doi: 10.1046/j.1525-1373.1999.d01-120.x

Hu, R., Jia, W.-Y., Xu, S.-F., Zhu, Z.-W., Xiao, Z., Yu, S.-Y., et al. (2019). Xiaochaihutang inhibits the activation of hepatic stellate cell line T6 through the Nrf2 pathway. *Front. Pharmacol.* 9, 1516. doi: 10.3389/fphar.2018.01516

Huang, X., Wang, Y., and Ren, K. (2015). Protective Effects of Liquiritin on the Brain of Rats with Alzheimer's Disease. *West. Indian Med. J.* 64, 468–472. doi: 10.7727/wimj.2016.058

Jayakumar, A. R., Valdes, V., Tong, X. Y., Shamaladevi, N., Gonzalez, W., and Norenberg, M. D. (2014). Sulfonylurea receptor 1 contributes to the astrocyte swelling and brain edema in acute liver failure. *Transl. Stroke Res.* 5, 28–37. doi: 10.1007/s12975-014-0328-z

Jia, W.-Y., Liu, J.-J., Hu, R., Hu, A.-L., Xu, S.-F., Wang, H., et al. (2019). Therapeutic mechanism of xiaochaihu granule on acute liver injury induced by thioacetamide in rats through Nrf2 pathway. *Chin. J. Exp. Tradit. Med. Form.* 25, 54–59. doi: 10.13422/j.cnki.syfjx.20190840

Jin, X.-X., Liao, Y.-J., Tan, X.-Q., Wang, G., Zhao, F., and Jin, Y. (2018). Involvement of CYP2E1 in the course of brain edema induced by subacute poisoning with 1,2-Dichloroethane in mice. *Front. Pharmacol.* 9, 1317. doi: 10.3389/fphar.2018.01317

Kaspar, J. W., Niture, S. K., and Jaiswal, A. K. (2009). Nrf2: INrf2 (Keap1) signaling in oxidative stress. *Free. Radic. Biol. Med.* 47, 1304–1309. doi: 10.1016/j.freeradbiomed.2009.07.035

Li, J., Hu, R., Xu, S.-F., Li, Y., Qin, Y., Wu, Q., et al. (2017). Xiaochaihutang attenuates liver fibrosis by activation of Nrf2 pathway in rats. *Biomed. Pharmacother.* 96, 847–853. doi: 10.1016/j.biopha.2017.10.065

Liu, J., Wu, Q., Lu, Y.-F., and Pi, J. (2008). New insights into generalized hepatoprotective effects of oleanolic acid: key roles of metallothionein and Nrf2 induction. *Biochem. Pharmacol.* 76, 922–928. doi: 10.1016/j.bcp.2008.07.021

Liu, J., Wu, K.-C., Lu, Y.-F., Ekuase, E., and Klaassen, C. D. (2013). NRF2 protection against liver injury produced by various hepatotoxicants. *Oxid. Med. Cell. Longev.* 2013, 305861. doi: 10.1155/2013/305861

Ma, J., Wang, F., Yang, J., Dong, Y., Su, G., Zhang, K., et al. (2017). Xiaochaihutang attenuates depressive/anxiety-like behaviors of social isolation-reared mice by regulating monoaminergic system, neurogenesis and BDNF expression. *J. Ethnopharmacol.* 208, 94–104. doi: 10.1016/j.jep.2017.07.005

Martinez, H. A., Bell, K. P., and Norenberg, M. D. (1977). Glutamine synthetase: glial localization in brain. *Science* 195, 1356–1358. doi: 10.1126/science.14400

Mladenović, D., Petronijević, N., Stojković, T., Velimirović, M., Jevtić, G., Hrnčić, D., et al. (2015). Finasteride has regionally different effects on brain oxidative stress and acetylcholinesterase activity in acute thioacetamide-induced hepatic encephalopathy in rats. *Plos. One* 10, e0134434. doi: 10.1371/journal.pone.0134434

Norenberg, M. D. (2003). Oxidative and nitrosative stress in ammonia neurotoxicity. *Hepatology* 37, 245–248. doi: 10.1053/jhep.2003.50087

Oenarto, J., Karababa, A., Castoldi, M., Bidmon, H. J., Görg, B., and Häussinger, D. (2016). Ammonia-induced miRNA expression changes in cultured rat astrocytes. *Sci. Rep.* 6, 18493. doi: 10.1038/srep18493

Papadopoulos, M. C., Krishna, S., and Verkman, A. S. (2002). Aquaporin water channels and brain edema. *Mt. Sinai. J. Med.* 69, 242–248. doi: 10.1097/01.md.0000032520.993581e

Pharmacopeia Committee of China (2015) (Beijing: Chinese Medical Press), 576–577.

Reinehr, R., Görg, B., Becker, S., Qvartskhava, N., Bidmon, H. J., Selbach, O., et al. (2010). Hypoosmotic swelling and ammonia increase oxidative stress by NADPH oxidase in cultured astrocytes and vital brain slices. *Glia* 55, 758–771. doi: 10.1002/glia.20504

Reisman, S. A., Aleksunes, L. M., and Klaassen, C. D. (2009). Oleanolic acid activates Nrf2 and protects from acetaminophen hepatotoxicity via Nrf2-dependent and Nrf2-independent processes. *Biochem. Pharmacol.* 77, 1273–1282. doi: 10.1016/j.bcp.2008.12.028

Su, G.-Y., Yang, J.-Y., Wang, F., Xiong, Z.-L., Hou, Y., Zhang, K., et al. (2014). Xiaochaihutang prevents depressive-like behaviour in rodents by enhancing the serotonergic system. *J. Pharm. Pharmacol.* 66, 823–834. doi: 10.1111/jphp.12201

Sun, R., Zeng, M., Du, T., Li, L., Yang, G., Hu, M., et al. (2015). Simultaneous determinations of 17 marker compounds in Xiao-Chai-Hu-Tang by LC-MS/MS: Application to its pharmacokinetic studies in mice. *J. Chromatogr. B. Analyt. Technol. Biomed. Life Sci.* 15, 12–21. doi: 10.1016/j.jchromb.2015.09.004

Swain, M., Butterworth, R. F., and Blei, A. T. (1992). Ammonia and related amino acids in the pathogenesis of brain edema in acute ischemic liver failure in rats. *Hepatology* 15, 449–453. doi: 10.1002/hep.1840150316

Tong, K. I., Kobayashi, A., Katsuoka, F., and Yamamoto, M. (2006). Two-site substrate recognition model for the Keap1-Nrf2 system: a hinge and latch mechanism. *Biol. Chem.* 387, 1311–1320. doi: 10.1515/BC.2006.164

Traber, P. G., Canto, M. D., Ganger, D. R., and Blei, A. T. (1987). Electron microscopic evaluation of brain edema in rabbits with galactosamine-induced fulminant hepatic failure: Ultrastructure and integrity of the blood-brain barrier. *Hepatology* 7, 1272–1277. doi: 10.1002/hep.1840070616

Traber, P., Dalcanto, M., Ganger, D., and Blei, A. T. (1989). Effect of body temperature on brain edema and encephalopathy in the rat after hepatic devascularization. *Gastroenterology* 96, 885–891. doi: 10.1016/S0016-5085(89)80092-7

Trey, C., and Davidson, C. S. (1970). The management of fulminant hepatic failure. *Prog. Liver Dis.* 3, 282–298. doi: 10.1007/BF01738610

Wang, W.-W., Zhang, Y., Huang, X.-B., You, N., Zheng, L., and Li, J. (2017). Fecal microbiota transplantation prevents hepatic encephalopathy in rats with carbon tetrachloride-induced acute hepatic dysfunction. *World J. Gastroenterol.* 23, 6983–6994. doi: 10.3748/wjg.v23.i38.6983

Wang, C.-Y., Jiang, M., Hou, G.-Y., and Hou, J. G. (2018). Saikokeishito Protecting HumanDermal Fibroblast Cell from Oxidative Damage Induced by H_2O_2. *Chin. J. Lab. Diagn.* 22, 1074–1077. doi: 10.3969/j.issn.1007-4287.2018.06.044

Yang, Y.-Q., Wang, H.-D., Li, L.-W., Li, X., Wang, Q., Ding, H., et al. (2016). Sinomenine provides neuroprotection in model of traumatic brain injury via the Nrf2-ARE pathway. *Front. Neurosci.* 10, 580. doi: 10.3389/fnins.2016.00580

Zhang, L., Wang, H., Fan, Y., Gao, Y., Li, X., Hu, Z., et al. (2017). Fucoxanthin provides neuroprotection in models of traumatic brain injury via the Nrf2-ARE and Nrf2-autophagy pathways. *Sci. Rep.* 7, 46763. doi: 10.1038/srep46763

Protective Actions of Acidic Hydrolysates of Polysaccharide Extracted From *Mactra veneriformis* Against Chemical-Induced Acute Liver Damage

Lingchong Wang[1,2†], Ying Yang[1†], Hor-Yue Tan[2], Sha Li[2] and Yibin Feng[2*]

[1] School of Pharmacy, Nanjing University of Chinese Medicine, Nanjing City, China, [2] School of Chinese Medicine, LKS Faculty of Medicine, The University of Hong Kong, Hong Kong, Hong Kong

The present study aimed to explore the hepatoprotective effects of acidic hydrolysates of polysaccharide extracted from the marine clam *M. veneriformis* (Ah-MVPS) against ethanol- and CCl_4-induced liver damage. Moreover, we also seek to probe the mechanism associated with the liver protection effect of Ah-MVPS. A series of animal and cell experiments were executed to detect suitable serological and histological indicators in hepatic tissues. Ah-MVPS can significantly reduce liver damage by means of an increase in hepatocyte superoxidase dismutase and inhibition of leakages of alanine aminotransferase and aspartate transaminase, as well as through alleviation of malondialdehyde excalation. Ah-MVPS inhibited steatosis and water-like hepatic deterioration in histological examination. They can suppress membrane destruction in boundaries and the collapse of reticular scaffolds of injured mouse hepatocytes and can substantially reduce the inflammatory extent of liver tissue aroused by excessive intake of ethanol or CCl_4. In cell assays, Ah-MVPS markedly elevated the viability of L-02 cells exposed to an intoxication of ethanol or H_2O_2. The beneficial effect of Ah-MVPS might arise, at least in part, because of the amelioration of peroxidation or oxidative stress. Taken together, our findings reveal that Ah-MVPS have potential for development as protective agents to attenuate acute liver injuries.

Keywords: *Mactra veneriformis*, hydrolysates, polysaccharide, acute liver damage, liver-protection agent

INTRODUCTION

As the largest digestive gland, the liver has the capacity to defend against chemical jeopardy *via* decomposition or metabolism of exogenous or endogenous toxins that damage the health of the human body (Yang et al., 2013; Uyanoglu et al., 2014). However, the liver itself may suffer from such harmful attacks from, e.g., ethanol, virus, drugs, out-of-control immune response, and hypoxia (Xiao et al., 2018). Damage to the liver involves many pathological changes, such as hepatocyte inflammation, steatosis, fibrosis, and necrosis, which can be broadly divided into infection and chemical injuries. Chemical liver injury is usually defined as chemical-driven hepatocyte damage

accompanying acute inflammation, since the hepatocyte is susceptible to many absorbable chemical toxins, and the severity of the pathology is strongly related to type, dose, and period of chemical intakes (Gu and Manautou, 2012). Chemical liver injuries easily progress to severe terminal liver disease, such as cirrhosis and hepatocarcinogenesis, by combination with other causes or through repeated episodes. It is essential to find or screen out some compounds that are protective to liver, given the recognized urgency of prevention and treatment of liver diseases. Animals with liver injury induced by CCl_4 or ethanol are typical experimental models that have been comprehensively applied in efficacy evaluation and pharmacological investigation of liver-protective drugs, as well as for screening of active compounds (Sun et al., 2013).

Reactive oxygen species (ROS) play an important role in the initiation and progression of chemical liver damage (Poli, 1993; Muriel, 2009). Excessive ROS generation, inducing imbalance of the intracellular oxidative-antioxidant system, is perhaps the chief pathological mechanism of chemical liver injury. Specifically, long-term or high doses of chemical intake and subsequent metabolism will produce multitudinous ROS beyond the elimination ability of the hepatic antioxidant enzymes, such as superoxidase dismutase (SOD), and will finally disturb the cellular homeostasis and lead to accumulation of liver damage (Pushpavalli et al., 2010). Excess free radicals bind to important biomolecules on the surfaces of mitochondria or endoplasmic reticulum, leading to lipid peroxidation and producing malondialdehyde (MDA). This will cause endoplasmic reticulum stress (ERS) and mitochondrial outer membrane permeabilization (MOMP), which are characterized by a decrease in fluidity and an increase in permeability of the membrane, release of cytochrome C, activation of capsase, and eventual cell apoptosis or necrosis (Liu et al., 2018).

It has been widely confirmed by the contemporary academic community that natural polysaccharides and/or their oligomer derivatives are free radical scavengers that are successfully applied in Chinese medicine or alternative medicine as protective agents to prevent liver damage (Tong et al., 2015; Xiao et al., 2018). Numerous natural polysaccharides/ oligosaccharides can reduce consumption of the antioxidant factors that are induced by an increase in oxidative stress, thus inhibiting the oxidative degeneration of lipids, enzymes, and nucleic acids and ultimately protecting the cell membrane structure and safeguarding the organelles (Wang et al., 2014; Wang et al., 2019).

Mactra veneriformis, sometimes termed *M. quadrangularis,* is an edible seashore clam (shellfish) that has been widely cultured and largely consumed as a seafood resource in many Asian countries (http://www.sealifebase.org/summary/Mactra-quadrangularis.html). Its fleshy part is also historically used as traditional Chinese Medicine (TCM) to remedy liver function injured by alcohol abuse (http://zhongyaocai360.com/g/geli.html). The hepatoprotective effect of *M. veneriformis* and the related active ingredients has been primarily investigated by our research group (Luan et al., 2011; Wang et al., 2011a). The first

result obtained was that the extracted polysaccharide (MVPS) could provide hepatoprotective benefits for CCl_4-induced liver-damaged mice. One derivative, hydrolysates of MVPS from HCl reaction, were then verified to have more superior antioxidant activity in comparison with the maternal polysaccharide (Wang et al., 2016). It was finally acknowledged that HCl hydrolysis might modify the physicochemical characters of the polysaccharide and improve its biological activity. In brief, the hydrolyzing products of MVPS varied in compositions and oligosaccharide contents and performed significant antioxidant actions by scavenging DPPH radicals, inhibiting the hydroxyl radicals, and generating reducing power. This indicated that some oligosaccharides might be functional ingredients since the hydrolysate exhibited stronger antioxidant effect than the initial polysaccharide of MVPS.

The above beneficial effect of MVPS and its hydrolysis products on mouse liver-injury or radical scavenging shifted our attention in subsequent studies toward the *in vivo* antioxidant mechanism and liver-protective actions. In the current study, we investigated the potential protective effects of the acidic hydrolysates of *M. veneriformis* polysaccharides (Ah-MVPS) in mitigating ethanol- or CCl_4-elicited liver injuries. Moreover, at the cellular level, the liver protective effect was further verified. Our findings demonstrate that Ah-MVPS have promising potentials for development as protective agents for patients who are susceptible to liver diseases.

MATERIALS AND METHOD

Materials

Three-year-old clams were collected by hand picking from the sea beach of Lvsi harbor at Nantong, Jiangsu province, China (32°06 N; 122°30 E) and were identified as *M. veneriformis* by Jiangsu Marine Fisheries Research Institute. The captured clams were starved in an aquarium for 24 h to evacuate their gut contents, and then their flesh was excavated from their shells and stored at −10 °C for further use.

Dulbecco's modified Eagle medium (DMEM) and Dulbecco's phosphate-buffered saline (DPBS) was obtained from Invitrogen. Fetal bovine serum (FBS) was acquired from Gibco. Phenazine methosulfate (PMS) and ethylenediaminetetraacetic acid (EDTA) were purchased from Amresco. A methanethiosulfonate (MTS) kit was purchased from Promega. Pancreatin was obtained from Beijing Dingguo Biological Reagent Co., Ltd. Carbon tetrachloride (CCl_4) was purchased from Sinopharm Chemical Reagent Co., Ltd. Bifendatatum (Biphenyl diester dropping pills) was provided by Beijing Union Pharmaceutical Factory. Standard commercial bioassay kits for alanine aminotransferase (ALT), aspartate transaminase (AST), superoxidase dismutase (SOD) malondialdehyde (MDA), and protein BCA determinations were purchased from Nanjing Jiancheng Bioengineering Institute. All other reagents and chemicals employed in the present work were analytical grade and supplied by local chemical suppliers in Nanjing city.

Preparation of Ah-MVPS

Water-soluble polysaccharide from the clam, utilized as the initial material in this study, was prepared by hot-water extraction and alcoholic precipitation, as described in our previous publication (Wang et al., 2011b). Briefly, pre-washed flesh materials of *M. veneriformis* were cut into pieces by a mincer and then decocted for 2 h in six-fold volumes of boiling water. The decoctions were centrifuged at 6000 rpm for 20 min, and the supernatant was concentrated to double volume and then precipitated by the addition of quadruple volumes of alcohol at room temperature. After overnight reaction, the precipitates were collected by filtration with 400-mesh fabrics. The products were dehydrated by 95% ethanol and then freeze-dried to obtain crude polysaccharide product. The crude product was dissolved in distilled water and trichloroacetic acid (TCA) (10% w/v) was added to remove its protein impurities by centrifugation (6000 rpm for 10 min) and 2 or 3 repeats of the reaction. The supernatant was collected was and dialyzed against distilled water for 24 h and then freeze-dried to obtain the pure polysaccharide of *M. veneriformis* (MVPS). The MVPS is an opalescent powder and was measured to have an over 97.3% total sugar content by reference to D-glucose *via* the anthrone-sulfuric acid method (Laurentin and Edwards, 2003; Piccolo et al., 2008).

The product Ah-MVPS were correspondingly prepared by incomplete degradation of HCl, as reported in our previous study (Wang et al., 2016). In brief, about 2.0g MVPS was dissolved in 100 mL distilled water to prepare 20 mg/mL of solution. Ten milliliter MVPS solutions were carefully transferred into a tapered flask (50 mL) and 1.0 mol/L of HCl was added under ice-bath conditions. Afterward, the flasks were transferred to a water bath (80 °C) to initiate the acidic hydrolyzing reaction, without agitation. The reaction lasted for 2 h and was then stopped by neutralization with NaOH (10 mol/L) containing a small amount of sodium borohydride (0.05 mol/L). The hydrolysates were supplemented with a two-fold volume of ethanol and centrifuged at 12000 rpm for 10 min to remove the generated salts or impurities. One final products, termed Ah-MVPS, were retrieved by freeze-drying and were preserved in a glass desiccator for further use.

Analysis of Ah-MVPS

About 100 mg of Ah-MVPS were precisely weighted and dissolved in 100 mL distilled water to prepare 1.0 mg/mL of stock solution. Ah-MVPS stock solution was diluted to anticipative concentrations to determine the content of total sugar and reducing sugar. The total sugar content was measured by the anthrone-sulfuric acid method (Laurentin and Edwards, 2003; Piccolo et al., 2008), while the reducing sugar content was quantified by the 3,5-dinitrosalicylic acid (DNS) method in calibration with D-glucose (Zhao et al., 2008). The oligosaccharides of Ah-MVPS were initially analyzed by high-performance liquid chromatography (HPLC), adopting the methods of Chen (Chen et al., 2004) and using a Waters ™ Alliance 2695 HPLC Separation Module in combination with a Shodex Asahipak NH2P-4E column (4.6mm×250mm) and a Dionex PA-1 guard column (4.0mm×50mm). Further

identification of the oligosaccharides of Ah-MVPS was executed on an HPLC-ESI-TOF-MS system. The system consisted of two successive coupled apparatuses: a Waters 2695 HPLC Separation Module equipped with a Shodex Asahipak NH2P-4E column (4.6mm×250mm) and a Time-of-Flight Mass Spectrometer (QTOF-MS, Waters QTOF Premier) equipped with an electrospray source.

Animal experiments

Animals and Grouping

The Kunming strain mice (male, 8-week-old, 20 ± 2 g), purchased from the Experimental Animal Research Center of Nanjing Medical University (Certificate no. SCXKC (Su) 2008-2014), were housed in cages and kept under conditions of a 12 h light/dark cycle, 22 ± 2°C, 50-55% humidity, and free access to water and standard food. All experiments were performed following the Regulations of Experimental Animal Administration issued by the State Committee of Science and Technology of the People's Republic of China.

After a week of acclimatization, all mice were randomly divided into six groups (eight mice per group), including one normal control (NC) group, one model control (MC) group, one positive control (PC) group, and three treatment groups. The mouse grouping reflected the different gavage procedures. During the animal experiment, mice in the three treatment groups received Ah-MVPS once daily at doses of 62.5, 125, and 250 mg/kg-b.w., mice in the PC group were administrated with a well-known liver-protective reagent, bifendatatum (150 mg/kg-b.w.), that is commonly used to treat the transaminase elevation caused by viral hepatitis, while mice in the NC and MC groups only received an equivalent volume of saline.

Acute Hepatic Damage Induced by CCl_4

For this experiment, the groups of Kunming mice were processed by intragastric gavage (i.g.) once daily and continued for 7 successive days. Eight hours after the last gavage, all animals except for the NC group were intraperitoneally administered (10 mL/kg-b.w.) a CCl4/peanut oil mixture (0.1% v/v) to induce acute hepatic injury, while the NC group mice only received the same volume of physiological saline at that time (**Figure 2A**). All mice were then fasted but allowed to drink water as usual.

Acute Hepatic Damage Induced by Ethanol

In another experiment, all mice received test samples once daily for 25 successive days *via* intragastric gavage according to a protocol. From day 26 for the next consecutive 7 days, all mice except the NC group were orally intoxicated (15 mL/kg-b.w.) with intense liquor (Hongxing Erguotou®, 56%v/v of alcohol) after 8 h of the normal treatment once daily, while the NC group received an equal volume of physiological saline instead of liquor (**Figure 3A**). During this experiment, all animals were fasted but permitted to drink water as usual.

Detections of Biological Indicators of Hepatic Damages

After 4 h of the CCl_4 intoxication or 8 h of the last liquor intoxication of animals in the above two experiments, about 0.5

mL of blood was collected from each mouse by excising the eyeballs to acquire the serum (seen in **Figures 2A** and **3A**). ALT and AST levels in the serum were measured using standard enzymatic assays according to the kit protocols (Nanjing Jiancheng Bioengineering Institute, China). All mice were subjected to cervical detachments at another eight hours after the blood collection. At that time point, the peritoneal cavity was opened along the abdominal middle line, and the liver was carefully isolated and removed to calculate the liver index (wet liver weight/body weight×100%). Partial hepatic tissues were then cut off from the whole liver specimen and homogenized (1:9, w/v) in saline after being washed with cold saline. The SOD activities and contents of MDA, calibrating to the protein measurement of the hepatic tissue, were analyzed using a commercial kit according to the instructions.

Histological Examination
Mouse liver specimens were immersed in PBS buffer containing 10% formalin (pH 7.4) for 24 h and embedded in paraffin. Thin sections were prepared by using a microtome and stained with hematoxylin-eosin (H&E). Each section was photographed under a microscope to show the histopathological changes in the liver. Images of each tissue slice were taken at a magnification of 400×. At the same time, pathological scoring was performed for the liver tissues to access their degree of injury with the help of two experts. The liver specimens were classed into five degrees of injury according to their tissue lesions under optical observation, including slight (< 5%), mild (5~15%), moderate (15~30%), significant (30~50%), and severe (≥50%) lesions. Six out of eight mice in each group were evaluated with the pathological scoring.

Cell Experiments
Cell Culturing
L-02 human normal liver cells were obtained from the cell bank of the pharmacology and toxicology room of Nanjing University of Traditional Chinese Medicine. The normal human hepatocyte cell line L-02 was cultured in DMEM medium supplemented with 10% FBS, 100 IU/mL of penicillin, and 100 µg/mL of streptomycin. Cells were incubated in a humidified atmosphere of 5% CO_2 at 37°C and passaged according to the recommended procedures of the ATCC (American Type Culture Collection). They were used for experiments from the logarithmic phase of growth, seeded into 96-well plates ($5×10^3$ cells per well, 180 µL).

Cell Viability Assay
L-02 cells were seeded into a 96-well plate at a density of 5000 cells per well and incubated for 24 h. Varying concentrations of Ah-MVPS pre-dissolved in culture media were then added to the L-02 cells. Cell proliferation after another 4 h of co-incubation was assayed using the MTS/PMS method. Briefly, 100 µL of MTS/PMS working solution was added to each well and then incubated at 37°C for 1 h. The absorbance of each well was measured at 490 nm using a full-length microplate reader (Beckman AD-340, USA).

Determinations of Protection Against Cytotoxicity
We here examine the protective effects of Ah-MVPS on H_2O_2- or ethanol-induced L-02 cell damage. In these examinations, L-02 cells were seeded on 96-well plates ($2.0×10^4$ per well) and randomly divided into eight sets (ten wells per set) including normal control (NC), model control (MC), and positive control (PC) wells, as well as five sets with various concentrations of Ah-MVPS. The cultured cells were then supplemented with 200 µL of different reagents for pre-incubation. The PC wells had 50 µg/mL bifendatatum in culture media added to them, and the wells for As-MVPS sets had 20, 40, 80, 160, or 320 µg/mL of the tested sample added to them, while the NC and MC wells received only blank culture media of equivalent volume. After 2 h of incubation (37°C, 5% CO_2), 200 µL of H_2O_2 (10% v/v) or ethanol (50% v/v) as the cytotoxic agent was add into each well of all sets except NC, for which the toxicants were replaced with an equivalent volume of culture medium (Junming et al., 2015). The L-02 cells were grown for another 8 h, and finally, each well was investigated for corresponding biochemical markers that can reflect cell damages. Supernatants (0.2 mL) above the cultured cells were withdrawn, and the activities of ALT and AST in them were determined using the commercial enzymatic assay kits according to standard protocols. The cells were also collected after removing the supernatants, and Triton-100 (0.2 mM) was then used to lyse the cells and release cytoplasm. After that, MDA content and SOD activity were determined by the standard commercial kit by using standard protocols and calibrated with the protein measurement of L-02 cells, respectively.

Statistical Analysis
All the data are expressed as the mean ± S.D. The data were assessed using professional statistics software (SPSS version 19.0, Chicago, IL, USA). A non-parametrial Kolmogorov-Smirnov test was employed for verifying a normal distribution of the data. Differences between groups were assessed by one-way analysis of variance (ANOVA) with either LSD (assuming equal variances) or Dunnett's T3 (not assuming equal variances) for posthoc analyses. Statistical significance was recognized at $p < 0.05$.

RESULTS
Chemical Characterization of Ah-MVPS
The Ah-MVPS product mainly consisted of numerous oligosaccharide molecules with various degrees of polymerization (DP) because it was derived from MVPS polysaccharide. Almost all ingredients in the Ah-MVPS product are short-chain sugars. Its total sugar content is near to 98.7%, and the reducing sugar content was determined to be 32.8%. Its oligosaccharide compositions were examined with sugar-affinity column (NH2P-4E) coupled HPLC, and nine oligomer ingredients were detected in the sample (**Figure 1A**). Its oligosaccharides were subsequently identified with the LC-QTOF-MS analysis (**Figure 1B**), and seven oligomers were
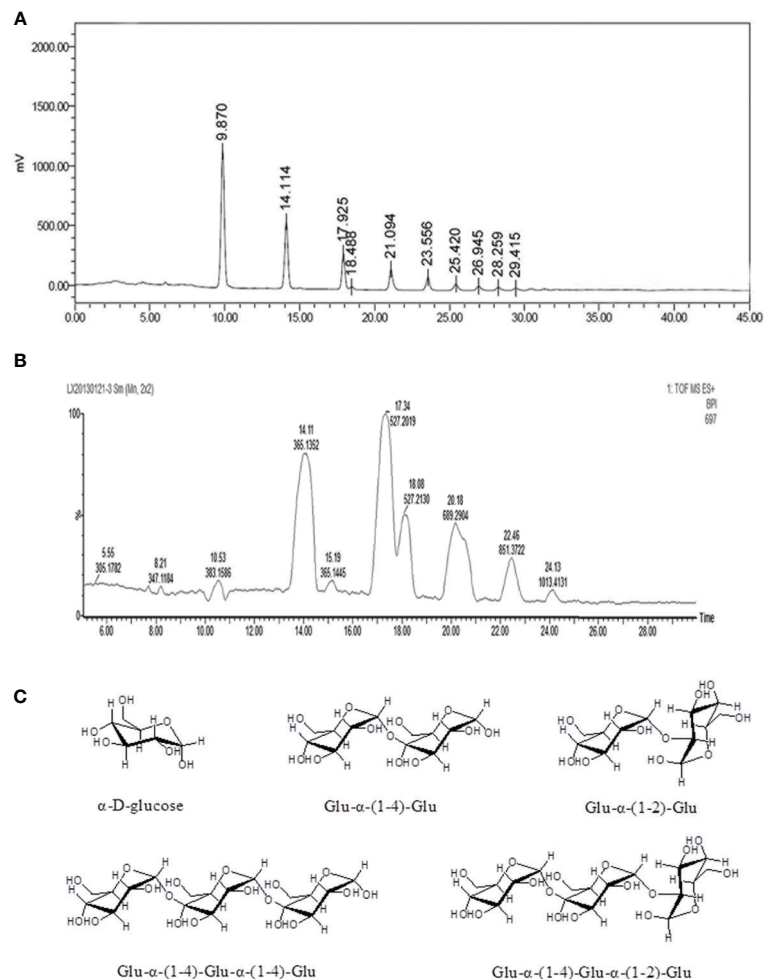
FIGURE 1 | Chemical composition analysis of the Ah-MVPS exhibited by HPLC profile **(A)** and the total ion flow chromatography of LC-QTOF-MS **(B)**, and structural drawing of representative oligosaccharides detected in the Ah-MVPS product **(C)**.

recognized from their structural attributions in chemistry due to retrieval of their MS signal responses. This mass identification showed the Ah-MVPS to be mainly composed of α-D-glucose and Glu-α-(1-4)-Glu and/or Glu-α-(1-2)-Glu dimers, as well as Glu-α-(1-4)-Glu-α-(1-4)-Glu or Glu-α-(1 -4)-Glu-α-(1-2)-Glu as trimers. Their chemical structures were completely drafted and are shown in **Figure 1C**. There are 42.6% of Glu, 27.5% of dimers, and about 18.7% of trimers in the molar composition of Ah-MVPS, as calculated from the peak areas of the HPLC curve. Other oligosaccharides with higher DP might be minor components of Ah-MVPS and are no reported on here because they made up only 11.1% of the composition.

Effects of Ah-MVPS on Acute CCl$_4$ Induced Liver Injury

Oral administration of Ah-MVPS could effectively attenuate the increase of serum alanine aminotransferase (ALT) and aspartate transaminase (AST) vitality that resulted from liver injury due to the injection of CCl$_4$. As depicted in **Figures 2B, C**, the enzymatic activities of serum AST and ALT of model control (MC) mice dramatically increased to 136 and 110 U/L ($p < 0.01$) from 54 and 14 U/L in the normal control (NC) mice, correspondingly. When the dose of Ah-MVPS was increased to 125 mg/kg-b.w., AST and ALT vitality dropped to 58 and 30 U/L ($p < 0.01$, *vs.* MC mice), and at a further elevating dose with 250 mg/kg-b.w. of Ah-MVPS, serum AST and ALT activities of mice were depressed to 55 and 23 U/L, individually ($p < 0.01$). In this experiment, bifendatatum as positive control also sharply reduced the enzyme activities of serum AST and ALT by 59.5% and 83.9% relative to CCl$_4$-intoxicated mice ($p < 0.01$). As shown in **Figure 2D**, Ah-MVPS reduced the liver index in a dose-dependent manner.

The measurements for hepatic superoxidase dismutase (SOD) activity in all mice are displayed in **Figure 2E**. A single application of CCl$_4$ led to a significant reduction of SOD, with the SOD levels in liver of MC mice decreased to 155 U/mg-protein ($p < 0.01$) from 219 U/mg-protein in liver of NC mice (without injection of CCl$_4$). The reduction of hepatic SOD
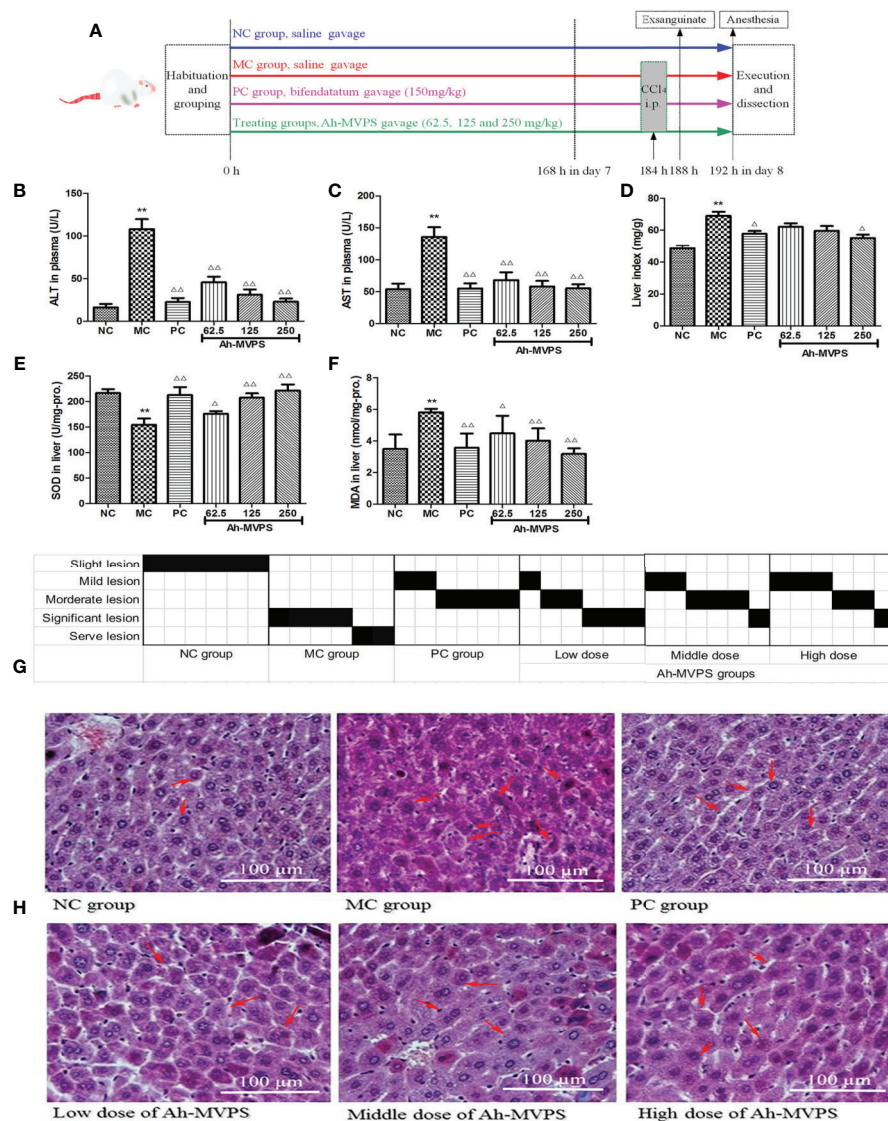
FIGURE 2 | Protective effects of Ah-MVPS on the injury of mouse liver induced by CCl_4. The time protocols of animal disease model setting and administration **(A)**. Comparative analysis of ALT (serum alanine aminotransferase, **B**), AST (aspartate transaminase, **C**), LI (liver index, **D**), SOD (superoxide dismutase, **E**), and MDA (malondialdehyde, **F**) of mice in each group, ******$P < 0.01$ vs. normal control (NC) group, $^{\Delta}P < 0.05$, $^{\Delta\Delta}P < 0.01$ vs. model control (MC) group. Recording table of pathological scoring **(G)**, and typical H&E section images **(H)** of mouse liver tissues (400-fold magnification); red arrows indicate normal and/or injured hepatocytes.

activity in CCl_4-intoxicated groups was weakened by pretreatment with Ah-MVPS at 125 and 250 mg/kg-b.w. (p < 0.01), and the SOD-promoting effect of Ah-MVPS exhibited dose-dependent behavior. Furthermore, the levels of SOD activity-promotion caused by middle or high dosage of Ah-MVPS gavages are basically the same to that of bifendatatum as positive SOD accelerant at doses of 150 mg/kg, the effect of which is obvious in inhibiting the reduction of SOD activity in liver tissue with CCl_4-induced hepatic injuries (p < 0.01 vs. MC mice). The generation of malondialdehyde (MDA) can be used to signify the lipid peroxidation levels in liver (Maheshwari et al., 2011); thus, detection of the MDA content of liver tissue was focused upon in our research. The measured results for mouse

hepatic MDA are shown in **Figure 2F**. The hepatic MDA levels of the NC mice were 3.5nmol/mg-protein. However, the liver MDA levels of CCl_4-induced mice (MC) were remarkably elevated to 5.8nmol/mg-protein (p < 0.01 vs. NC). Pretreatment with Ah-MVPS at doses of 62.5, 125, and 250 mg/kg-b.w. to mice could effectively decrease the CCl_4-induced production of MDA (p <0.01 vs. MC); this accords with prior expectations. Moreover, an obvious dose-dependent MDA inhibition was observed in the Ah-MVPS groups, and a higher dose had a more significant effect, near that of bifendatatum at a dose of 250 mg/kg. The bifendatatum was used as a positive hepatoprotective drug and could also prominently inhibit the elevation of MDA to 3.6nmol/mg-protein. These results suggest
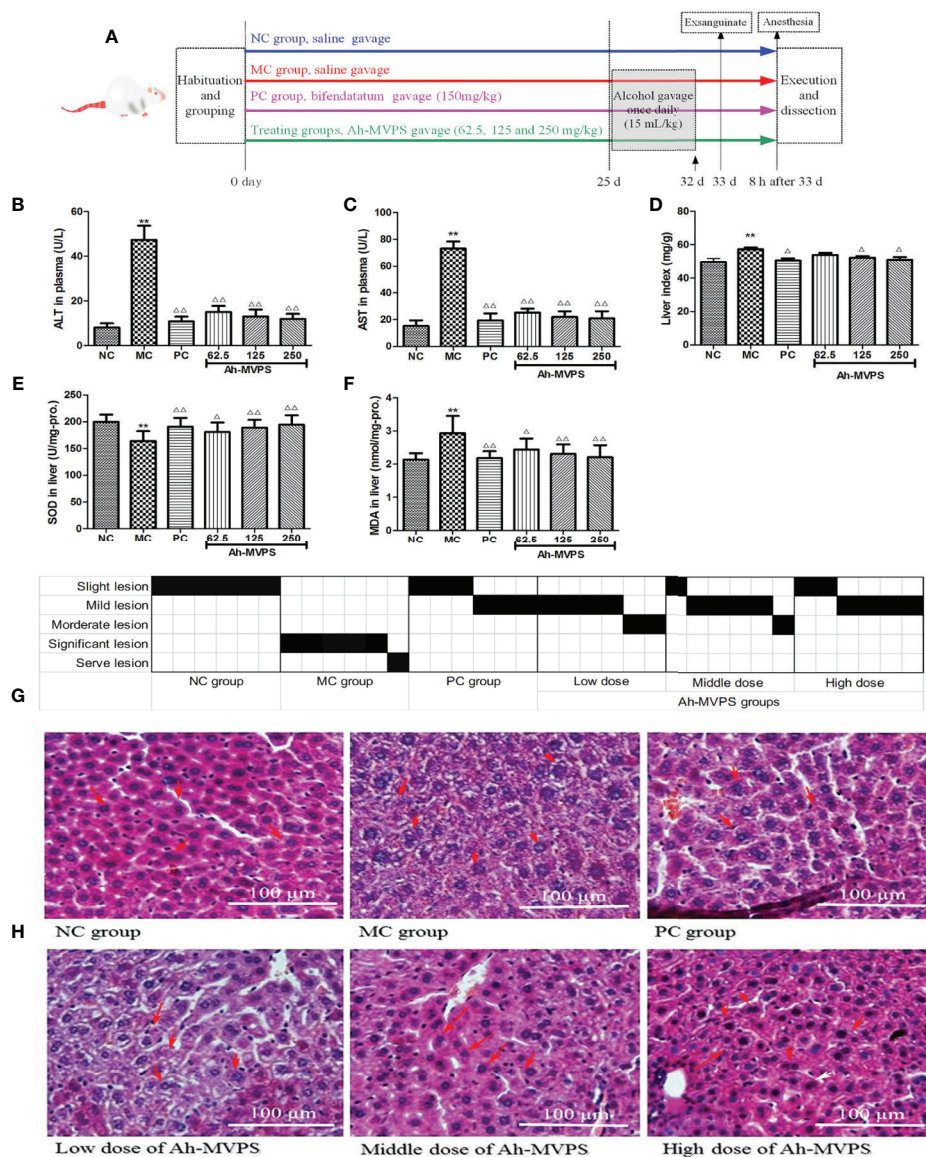
FIGURE 3 | Protective effects of Ah-MVPS on the injury of mouse liver induced by alcohol. The time protocols of animal disease model setting and administration **(A)**. Comparative analysis of ALT (serum alanine aminotransferase, **B**), AST (aspartate transaminase, **C**), LI (liver index, **D**), SOD (superoxide dismutase, **E**), and MDA (malondialdehyde, **F**) of mice in each group, **$P < 0.01$ vs. normal control (NC) group, $^{\triangle}P < 0.05$, $^{\triangle\triangle}P < 0.01$ vs. model control (MC) group. Recording table of pathological scoring **(G)**, and typical H&E section images **(H)** of the mouse liver tissues (400-fold magnification); red arrows indicate normal and/or injured hepatocytes.

that Ah-MVPS may prevent liver against chemical damage by suppressing lipid peroxidation *in vivo*.

Liver protection by Ah-MVPS could also be confirmed through histopathological examinations of the morphological changes of liver tissue derived from CCl₄-injured mice. As showed in **Figure 2H**, H&E tissue slices of liver of mice in the NC group exhibited a normal cellular architecture with clear hepatic cells, a central vein, and sine spaces. In contrast, quite serious damage can be seen in a slice from the MC group, whose H&E image shows severe hepatocyte necrosis, massive fatty changes, hepatocellular swelling, water-like deterioration of

hepatocytes, loss of cellular boundaries, and collapse of reticular scaffolds, as well as the formation of eosinophils and broad infiltration of lymphocytes. However, liver tissue belonging to Ah-MVPS-treated mice showed a repaired liver lobular H&E morphology by exhibiting a slight hepatic fatty change, less necrosis, and lobular inflammation as compared with the liver H&E slices of the NC group. These results demonstrate that Ah-MVPS can protect liver tissue from acute CCl₄-intoxication hepatic damage (**Figure 2H**). A more intuitive result is displayed in **Figure 2G**, which gives semi-quantitative values (pathological score) to describe the degrees of damage to

mice livers of the six groups. Six mice per group were examined, and the value of each was marked in black on the scoring sheet. It is exhibited that the degree of liver damage in the mice was in the order of MC > low dose of Ah-MVPS > middle dose of Ah-MVPS > high dose of Ah-MVPS > PC > NC. The dose-dependent liver protective effect of Ah-MVPS is clearly obvious in this ranking.

Effects of Ah-MVPS on Acute Alcoholic Liver Injury

After the relatively long term gavage, mice exhibited unusual resistance to alcoholic damages, preserving their liver morphology and function. This animal experiment provided further information besides showing the definite effectiveness of Ah-MVPS. Firstly, an alcoholic-liver-injured animal model was established successfully. It was seen that the serum ALT and AST levels (**Figures 3B, C**), liver index (**Figure 3D**), and hepatic MDA content (**Figure 3E**) and SOD activity (**Figure 3E**) of MC mice were obviously increased as compared to NC mice (P < 0.01), which was also reflected by the relatively serious lesions found in mouse liver under histological examination (**Figure 3G**). The pathological consequences were that the hepatic cords in the liver tissues of MC mice exhibited irregular lobules in combination with membrane destruction of hepatocyte boundaries, collapse of reticular scaffolds, and cytoplasmic leakages (**Figure 3H**). Secondly, the liver protection effect of Ah-MVPS pre-gavage continued for 25 days was confirmed through a comparison of biochemical and histological indexes between the subjects and MC mice. Serum ALT and AST of every Ah-MVPS group were significantly decreased by 2~4 folds compared to MC mice (P < 0.01), and they reached the level of the PC group. The significant drop in serum transaminase reflects the ability of Ah-MVPS to moderate the hepatic damages caused by excessive alcohol intake and protect liver functions in a dose-dependent manner. Administration of Ah-MVPS to mice not only reduced the liver index (**Figure 3D**) and MDA content (**Figure 3F**) but also increased the SOD activity (**Figure 3E**) of mouse livers. The liver index and hepatic MDA levels declined markedly in Ah-MVPS-treated and PC mice as compared to the MC. Moreover, liver SOD activity was enhanced in Ah-MVPS-treated groups and PC groups. The reduction in MDA content and liver index, as well as the increase in SOD activity, are extremely significant in the middle and high Ah-MVPS dose groups (P < 0.01), and the high-dose treatment even resulted in a stronger effect than in the positive control (PC) group. In histological observation, the liver cells of mice administered a high dose of Ah-MVPS were arranged regularly, and the ballooning degeneration of liver cell cytoplasm was alleviated (**Figure 3H**). Finally, Ah-MVPS are more suitable for protecting liver from alcoholic damage than against CCl$_4$ intoxication based on comparison of the direct data (**Figures 2** and **3**), which might correlate with the low level of injuries in intoxicated liver and long-term of administration with Ah-MVPS. It was noted from the pathological scoring that two

mice were restored to no tissue lesions, while the other four examined mice had only mild liver lesions after receiving 250 mg/kg of Ah-MVPS (**Figure 3G**). This beneficial result was hard to obtain for the CCl$_4$-induced serve liver injury in mice, indicating that Ah-MPVS might be a suitable antagonist of ethanol.

Effects of Ah-MVPS on the Injury of L-02 Cells Induced by H$_2$O$_2$ or Ethanol

There was no obvious influence of the addition of Ah-MVPS on the viability of L-02 cells (**Figure 4A**). Under co-incubation with Ah-MVPS, L-02 cells fluctuated within 90~130% of viability under lab setting conditions, indicating that the Ah-MVPS are not toxic to hepatocytes over a wide range of concentrations in cell assays. This conclusion can be corroborated by the optical observations (**Figure 4B**), in which the density and morphology of L-02 cells were hardly altered by supplementation of Ah-MVPS in the concentrations range 0~5000 μg/mL.

However, supplementation of Ah-MVPS in concentrations of 80~320 μg/mL can effectively prevent damage to L-02 cells aroused by H$_2$O$_2$ (**Figures 4C–F**) or ethanol (**Figures 4G–J**). These results indicate that Ah-MVPS could decrease the cell damage by the suppression of ALT and AST leakage, promotion of SOD activity, and inhibition of MDA production. The protective effects were increased at increased concentrations of Ah-MVPS. At a concentration of 320μg/mL, the effect of Ah-MVPS is equivalent to that of bifendatatum, the positive control.

DISCUSSION

In our previous research (Wang et al., 2016), we degraded MVPS by mild H$_2$SO$_4$ or HCl hydrolysis and found that hydrolysates were extremely influenced by adding an amount of acid and by the reaction time. To avoid thorough hydrolysis and obtain more oligosaccharide content in the product, degradation with 0.5 h of HCl was adopted to process MVPS due to its controllability. HCl hydrolysates contained many oligosaccharides that could be considered active ingredients. The superior ability of Ah-MVPS in scavenging hydroxyl radicals was confirmed by activity screening among polysaccharides and various hydrolysates. We also elucidated the composition and content of oligosaccharides in the Ah-MVPS, which include many oligomers of glucan that are varied in DP and linkages, as shown in **Figure 1**. The results were especially noteworthy in that linkages of α-(1-2) residues were identified in oligomers of Ah-MVPS, which would be exploitable for drug candidates functioning in a new way. However, there is still a long way to go to clarify its functions and mechanism due to a lack of data accumulation.

In this study, we exhibit the liver-protective activities of the HCl-hydrolysis products of marine clam polysaccharide (Ah-MVPS). A suitable animal model is a good basis for investigation of the pathogenesis and pathology of liver injury and is also an
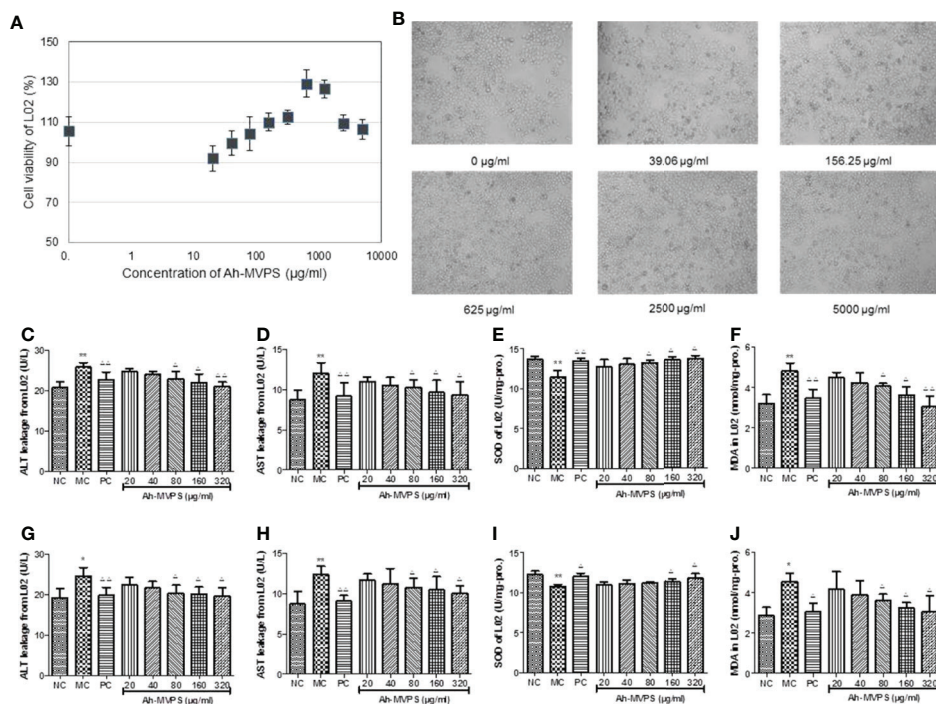
FIGURE 4 | Protection of Ah-MVPS against chemical damage to L-02 cell. The influence of MVPS concentrations on L-02 cell viability and after 24h of co-incubation **(A)**, and optical images of L-02 incubated with MVPS **(B)**. Quantitation of leakage of ALT (serum alanine aminotransferase, **C, G**) and AST (aspartate transaminase, **D, H**), SOD (superoxidase dismutase, **E, I**) activity, and MDA (malondialdehyde, **F, J**) content for L-02 cells injured by H_2O_2 and ethanol, respectively; $*P < 0.05$, $**P < 0.01$ vs. normal control (NC) set, $^\Delta P < 0.05$, $^{\Delta\Delta}P < 0.01$ vs. model control (MC) set.

effective way of screening active ingredients. The toxic reagents CCl_4 and ethanol are commonly used at present to establish acute chemical liver injury in mice, though the potential model designs are diverse in terms of animal strain, administration route, dose, and time of exposure (Liu et al., 2015; Zhou et al., 2017). For our experiment, the administration route, time of exposure, and dosage of the model established were decided by literature review, pre-experiments, and screens. One acute alcoholic liver injury model was established by the oral gavage route to cause mouse liver function loss so significant that it accords with human drinking habits, which avoided the shortcomings usually arising with intraperitoneal injections, such as organ adhesion, infection, and ascite formation (Wang et al., 2012; Zhao et al., 2017). However, the other acute liver injury model was induced by intraperitoneal CCl_4 injection of mice since the toxicant was absorbed quickly, and just one injection would bring an overall toxic response to animals. Otherwise, many repeats of oral administration CCl_4 are required by a combination of peanut oil as a solvent, which usually results in diarrhea. Diarrhea not only pollutes the environment but can also easily cause secondary absorption through the mouth and the skin, generating a large dose error (Zeng et al., 2017; Sun et al., 2018a). Oxidative stress is

commonly recognized as indispensable factor for exploring injury mechanisms in most chemical liver injury models (Recknagel and Glende, 1989; Sun et al., 2018a; Sun et al., 2018b). Therefore, we chose a very representative oxidative stress injury model induced by H_2O_2 and/or ethanol to further evaluate the protective activities of Ah-MVPS in cellular experiments in association with comparing with the results of bifendatatum as the positive drug. It has an obvious antioxidant effect, inhibiting hepatic lipid peroxidation by stabilizing the hepatocyte membrane, alleviating the structural damage of hepatic tissue, and reducing the ALT and AST leakages arising due to various pathogenic damages, such as CCl_4 and ethanol intoxication of hepatocytes (Liu et al., 2016; Jing et al., 2017; Song et al., 2018).

It was finally confirmed in this study that Ah-MVPS have excellent liver-protective activities that perhaps correlate with their antioxidant nature as oligosaccharides that are complex in chemistry. To some extent, the liver protection effect of Ah-MVPS is even stronger than that of other similar products that are already well known. For example, enzymatic hydrolysates of the polysaccharide extract (EPS) from *Pleurotus eryngii* exhibited significant hepatoprotective activities to CCl_4-injured mice (Zhang et al., 2017) only when its dose was near to 400 mg/kg-b.w. and it

was administered by continuous oral gavage for 28 days. In another study, enzymatic and acidic hydrolysates of polysaccharides isolated from *Pleurotus geesteranus* mycelium were also effective in protecting mouse liver against injury by ethanol, but the efficiency was not obvious unless the dose was increased to 200 mg/kg-b.w. and treatment course was extended to 25 days (Song et al., 2018). In our study, just seven days of Ah-MVPS treatment to mice by oral gavage at a dose of 62.5 mg/kg-b.w. can significantly protect the liver against CCl_4-induced injuries. Hepatoprotection of Ah-MVPS at the high dose (250 mg/kg) is essentially equal to that of bifendatatum (250 mg/kg) in the mouse model. The liver protective effect of Ah-MVPS was subsequently authenticated again in ethanol-induced liver-damaged mice and chemically injured hepatic parenchymal cells. Further investigations may focus on the specific oligosaccharide ingredients in the Ah-MVPS product, such as Glu-α-(1-2)-Glu or Glu-α-(1-4)-Glu-α-(1-2)-Glu, whose liver-protective effects could be confirmed by rapid comparison and screening in animals or cellular experiments. The biochemical mechanism also needs to be considered as a part of the comprehensive research so as to interpret the roles of the specific oligosaccharides in liver protection.

CONCLUSION

In conclusion, our results confirm the preventative effects of Ah-MVPS against hepatic injury both *in vivo* and *in vitro*. The defensive mechanism of Ah-MVPS is, at least in part, related to the improvement of oxidative stress and lipid peroxidation. Taken together, our results show that Ah-MVPS have the potential to be developed as pharmaceutical or functional ingredients to benefit patients suffering from liver injury.

DATA AVAILABILITY STATEMENT

The datasets generated for this study are available on request to the corresponding author.

ETHICS STATEMENT

The animal study was reviewed and approved by Laboratory Animal Welfare Ethics Committee in Nanjing University of Chinese Medicine.

AUTHOR CONTRIBUTIONS

LW and YF conceived and designed the project. LW and YY performed experiments and wrote the manuscripts. H-YT and SL analyzed the data and gave some helpful advice.

FUNDING

REFERENCES

Chen, H. M., Zheng, L., Lin, W., and Yan, X. J. (2004). Product monitoring and quantitation of oligosaccharides composition in agar hydrolysates by precolumn labeling HPLC. *Talanta* 64, 773–777. doi: 10.1016/j.talanta.2004.04.002

Gu, X., and Manautou, J. E. (2012). Molecular mechanisms underlying chemical liver injury. *Exp. Revi. Mol. Med.* 14, e4. doi: 10.1017/s1462399411002110

Jing, L. Y., Zone, S., Li, J. L., Ye, M., Surahio, M., and Yang, L. (2017). Potential mechanism of protection effect of exopolysaccharide from Lachnum YM406 and its derivatives on carbon tetrachloride-induced acute liver injury in mice. *J. Funct. Foods* 36, 203–214. doi: 10.1016/j.jff.2017.06.057

Junming, W., Yueyue, Z., Ruixin, L., Xiaobing, L., Ying, C., and Lingbo, Q. (2015). Geniposide protects against acute alcohol-induced liver injury in mice via up-regulating the expression of the main antioxidant enzymes. *Can. J. Physiol. Pharmacol.* 93, 261–267. doi: 10.1139/cjpp-2014-0536

Laurentin, A., and Edwards, C. A. (2003). A microtiter modification of the anthrone-sulfuric acid colorimetric assay for glucose-based carbohydrates. *Anal. Biochem.* 315, 143–145. doi: 10.1016/S0003-2697(02)00704-2

Liu, Y. J., Du, J. L., Cao, L. P., Jia, R., Shen, Y. J., Zhao, C. Y., et al. (2015). Anti-inflammatory and hepatoprotective effects of Ganoderma lucidum polysaccharides on carbon tetrachloride-induced hepatocyte damage in common carp (Cyprinus carpio L.). *Int. Immunopharmacol.* 25, 112–120. doi: 10.1016/j.intimp.2015.01.023

Liu, M., Meng, G. Y., Zhang, J. J., Zhao, H. J., and Jia, L. (2016). Antioxidant and Hepatoprotective Activities of Mycelia Selenium Polysaccharide by Hypsizigus marmoreus SK-02. *Biol. Trace Element Res.* 172, 437–448. doi: 10.1007/s12011-015-0613-z

Liu, S., Wang, Q. K., Song, Y. F., He, Y. H., Ren, D. D., Cong, H. H., et al. (2018). Studies on the hepatoprotective effect of fucoidans from brown algae Kjellmaniella crassifolia. *Carbohydr. Polym.* 193, 298–306. doi: 10.1016/j.carbpol.2018.03.077

Luan, H. M., Wang, L. C., Wu, H., Jin, Y., and Ji, J. (2011). Antioxidant activities and antioxidative components in the surf clam, Mactra veneriformis. *Nat. Product Lett.* 25, 1838–1848. doi: 10.1080/14786419.2010.530268

Maheshwari, D. T., Yogendra Kumar, ,. M. S., Verma, S. K., Singh, V. K., and Som Nath, S. (2011). Antioxidant and hepatoprotective activities of phenolic rich fraction of Seabuckthorn (Hippophae rhamnoides L.) leaves. *Food Chem. Toxicol.* 49, 2422–2428. doi: 10.1016/j.fct.2011.06.061

Muriel, P. (2009). Role of free radicals in liver diseases. *Hepat. Int.* 3, 526–536. doi: 10.1007/s12072-009-9158-6

Piccolo, A., Zena, A., and Conte, P. (2008). A comparison of acid hydrolyses for the determination of carbohydrate content in soils. *Commun.Soil Sci. Plant Anal.* 27, 2909–2915. doi: 10.1080/00103629609369749

Poli, G. (1993). Liver damage due to free radicals. *Br. Med. Bull.* 49, 604–620. doi: 10.1093/oxfordjournals.bmb.a072634

Pushpavalli, G., Kalaiarasi, P., Veeramani, C., and Pugalendi, K. V. (2010). Effect of chrysin on hepatoprotective and antioxidant status in -galactosamine-induced hepatitis in rats. *Eur. J. Pharmacol.* 631, 36–41. doi: 10.1016/j.ejphar.2009.12.031

Recknagel, R. O., and Glende, ,. E. G.Jr. (1989). Mechanisms of carbon tetrachloride toxicity. *Pharmacol. Ther.* 43, 139–154. doi: 10.1016/0163-7258(89)90050-8

Song, X. L., Liu, Z. H., Zhang, J. J., Zhang, C., Dong, Y. H., Ren, Z. Z., et al. (2018). Antioxidative and hepatoprotective effects of enzymatic and acidic-hydrolysis of Pleurotus geesteranus mycelium polysaccharides on alcoholic liver diseases. *Carbohydr. Polym.* 201, 75–86. doi: 10.1016/j.carbpol.2018.08.058

Sun, Y. F., Yang, X. B., Lu, X. S., Wang, D. Y., and Zhao, Y. (2013). Protective effects of Keemun black tea polysaccharides on acute carbon tetrachloride-caused oxidative hepatotoxicity in mice. *Food Chem. Toxicol.* 58, 184–192. doi: 10.1016/j.fct.2013.04.034

Sun, J., Wen, X. Y., Liu, J., Kan, J., Qian, C. L., Wu, C. S., et al. (2018a). Protective effect of an arabinogalactan from black soybean against carbon tetrachloride-induced acute liver injury in mice. *Int. J. Biol. Macromol.* 117, 659–664. doi: 10.1016/j.ijbiomac.2018.05.203

Sun, J., Zhou, B., Tang, C., Gou, Y. R., Chen, H., Wang, Y., et al. (2018b). Characterization, antioxidant activity and hepatoprotective effect of purple sweetpotato polysaccharides. *Int. J. Biol. Macromol.* 115, 69–76. doi: 10.1016/j.ijbiomac.2018.04.033

Tong, C. Q., Zheng, Y. X., Guo, G. L., and Li, W. (2015). Hepatoprotective effect of a polysaccharide from Auricularia auricula root on acute model of liver injury. *Glycobiology* 25, 1287–1287.

Uyanoglu, M., Canbek, M., Van Griensven, L. J. L. D., Yamac, M., Senturk, H., Kartkaya, K., et al. (2014). Effects of polysaccharide from fruiting bodies of Agaricus bisporus, Agaricus brasiliensis, and Phellinus linteus on alcoholic liver injury. *Int. J. Food Scie. Nutr.* 65, 482–488. doi: 10.3109/09637486.2013.869796

Wang, L., Wu, H., Chang, N., and Zhang, K. (2011a). Anti-hyperglycemic effect of the polysaccharide fraction isolated from mactra veneriformis. *Front. Chem. Sci. Eng.* 5, 238–244. doi: 10.1007/s11705-010-0002-2

Wang, L. C., Zhang, K., Di, L. Q., Liu, R., and Wu, H. (2011b). Isolation and structural elucidation of novel homogenous polysaccharide from Mactra veneriformis. *Carbohydr. Polyme.* 86, 982–987. doi: 10.1016/j.carbpol.2011.05.052

Wang, M. C., Zhu, P. L., Jiang, C. X., Ma, L. P., Zhang, Z. J., and Zeng, X. X. (2012). Preliminary characterization, antioxidant activity in vitro and hepatoprotective effect on acute alcohol-induced liver injury in mice of polysaccharides from the peduncles of Hovenia dulcis. *Food Chem. Toxicol.* 50, 2964–2970. doi: 10.1016/j.fct.2012.06.034

Wang, L., Wang, X., Wu, H., and Liu, R. (2014). Overview on Biological Activities and Molecular Characteristics of Sulfated Polysaccharides from Marine Green Algae in Recent Years. *Marine Drugs* 12, 4984–5020. doi: 10.3390/md12094984

Wang, L. C., Wu, H., Ji, J., Xue, F., and Liu, R. (2016). Preparation, analysis and antioxidant evaluation of the controlled product of polysaccharide from Mactra veneriformis by mild acid hydrolysis. *Carbohydr. Polym.* 137, 709–718. doi: 10.1016/j.carbpol.2015.11.030

Wang, L. C., Di, L. Q., Li, J. S., Hu, L. H., Cheng, J. M., and Wu, H. (2019). Elaboration in type, primary structure, and bioactivity of polysaccharides derived from mollusks. *Crit. Rev. Food Sci. Nutr.* 59, 1091–1114. doi: 10.1080/10408398.2017.1392289

Xiao, M., Li, Y., Sha, L., Gan, R. Y., and Li, H. B. (2018). Natural Products for Prevention and Treatment of Chemical-Induced Liver Injuries. *Compr. Revi/ Food Sci. Food Saf.* 17, 472–495. doi: 10.1111/1541-4337.12335

Yang, X., Yang, S., Guo, Y., Jiao, Y., and Zhao, Y. (2013). Compositional characterisation of soluble apple polysaccharides, and their antioxidant and hepatoprotective effects on acute CCl4-caused liver damage in mice. *Food Chem.* 138, 1256–1264. doi: 10.1016/j.foodchem.2012.10.030

Zeng, B. Y., Su, M. H., Chen, Q. X., Chang, Q., Wang, W., and Li, H. H. (2017). Protective effect of a polysaccharide from Anoectochilus roxburghii against carbon tetrachloride-induced acute liver injury in mice. *J. Ethnopharmacol* 200, 124–135. doi: 10.1016/j.jep.2017.02.018

Zhang, C., Li, J., Wang, J., Song, X. L., Zhang, J. J., Wu, S., et al. (2017). Antihyperlipidaemic and hepatoprotective activities of acidic and enzymatic hydrolysis exopolysaccharides from Pleurotus eryngii SI-04. *BMC Complement. Alternat. Med.* 17, 403. doi: 10.1186/s12906-017-1892-z

Zhao, K., Xue, P. J., and Guang-Ye, G. U. (2008). Study on Determination of Reducing Sugar Content Using 3,5-Dinitrosalicylic Acid Method. *Food Sci.* 29, 534–536. doi: 10.3321/j.issn:1002-6630.2008.08.127

Zhao, H. J., Lan, Y. F., Liu, H., Zhu, Y. F., Liu, W. R., Zhang, J. J., et al. (2017). Antioxidant and Hepatoprotective Activities of Polysaccharides from Spent Mushroom Substrates (Laetiporus sulphureus) in Acute Alcohol-Induced Mice. *Oxi. Med. Cell. Long.* 2017, 1–12. doi: 10.1155/2017/5863523

Zhou, X., Deng, Q. F., Chen, H. G., Hu, E. M., Zhao, C., and Gong, X. J. (2017). Characterizations and hepatoprotective effect of polysaccharides from Mori Fructus in rats with alcoholic-induced liver injury. *Int. J. Biol. Macromol.* 102, 60–67. doi: 10.1016/j.ijbiomac.2017.03.083

Paeoniflorin, a Natural Product With Multiple Targets in Liver Diseases—A Mini Review

Xiao Ma[1], Wenwen Zhang[1], Yinxiao Jiang[1], Jianxia Wen[1,2], Shizhang Wei[1,2] and Yanling Zhao[2]*

[1] School of Pharmacy, Chengdu University of Traditional Chinese Medicine, Chengdu, China, [2] Department of Pharmacy, Fifth Medical Center of PLA General Hospital, Beijing, China

Paeoniflorin is derived from *Paeonia suffruticosa* Andr., *Paeonia lactiflora* Pall., or *Paeonia veitchii* Lynch and has been used in traditional medical applications for more than 2,000 years. Paeoniflorin is a monoterpenoid glycoside with various effects on liver diseases. Recent studies have revealed that paeoniflorin demonstrates a wide range of activities, including hepatic protection, cholestasis alleviation, liver fibrosis attenuation, nonalcoholic fatty liver disease prevention, and hepatocellular carcinoma inhibition involved in multiple pathways. Moreover, anti-inflammation, antioxidation, and immune regulation with the regulation of TLR4-NF-κB, ROCK/NF-κB, HO-1, mitochondria-dependent as well as HMGB1-TLR4 signaling pathways are correlated with hepatic protection in liver injury and nonalcoholic fatty liver disease. Antioxidative mechanisms, anti-inflammation, and hepatic transporter regulation involved in NOX4, PI3K/Akt/Nrf2, NF-κB, NTCP, BSEP, as well as MRP2 signals are mainly relevant to the anticholestatic effect of paeoniflorin. The inhibition of hepatic stellate cell activation and alleviation of extracellular matrix deposition *via* vast signals such as mTOR/HIF-1α, TGF-β1/Smads, and JAK2/STAT6 are primarily involved in the antifibrotic effect of paeoniflorin. The regulation of macrophages also contributes to the alleviation effect on liver fibrosis. In addition, the reduction of invasion, metastasis, and adhesion and the induction of apoptosis-related targets, including Bax, Bcl-2, and caspase-3, are related to its effect on hepatocellular carcinoma. The literature indicates that paeoniflorin might have potent efficacy in complex liver diseases and demonstrates the profound medicinal value of paeoniflorin.

Keywords: paeoniflorin, hepatic protection, cholestasis, liver fibrosis, nonalcoholic fatty liver disease, hepatocellular carcinoma, mini-review

Abbreviations: ALP, Alkaline phosphatase. ANIT, Alpha-naphthylisothiocyanate. BCG, Bacillus Calmette-Guérin. BSEP, Bile salt export pump. CCl₄, Carbon tetrachloride. Con-A, Concanavalin A. DMN, Dimethylnitrosamine. ECM, Extracellular matrix. GalN, D-galactosamine. LPS, lipopolysaccharide. GSH, Glutathione. GCLc, Glutamate-cysteine ligase catalytic subunit. GCLm, Glutamate-cysteine ligase modifier subunit. HCC, Hepatocellular carcinoma. HHSECs, Primary human hepatic sinusoidal endothelial cells. HSCs, Hepatic stellate cells. I/R, Ischemia/reperfusion. MRP2, Multidrug resistance-associated protein 2. NAFL, Nonalcoholic fatty liver. NAFLD, Nonalcoholic fatty liver disease. NASH, Nonalcoholic steatohepatitis. NTCP, Na⁺/taurocholate-cotransporting polypeptide. TBA, Total bile acid. γ-GT, γ-Glutamyltranspeptidase. i.g., Intragastric. i.v., Intravenous injection.

INTRODUCTION

Since the "one gene, one drug, one disease" concept was challenged, more and more agents have been confirmed to be multiple targets and signals rather than a single approach (Hasin et al., 2017). Several natural products applied for thousands of years in traditional medicine demonstrate a wide range of pharmacological activities *via* multiple pathways (Park and Pezzuto, 2017; Kunnumakkara et al., 2017; Ren et al., 2019). These natural products might have potent efficacy in complex human diseases and display profound medicinal value. Among these natural compounds, paeoniflorin has gained attention as a promising compound for drug development.

Paeoniflorin is the major bioactive ingredient derived from *Paeonia suffruticosa* Andr., *Paeonia lactiflora* Pall., or *Paeonia veitchii* Lynch, which have been used for cerebrovascular disease, cardiovascular disease, nervous system disease, and liver disease in traditional Chinese medicine for more than 2,000 years (Zhao et al., 2016). Paeoniflorin was first isolated from *Paeonia lactiflora* Pall. as a monoterpenoid glycoside in 1963 (Zhang J. et al., 2018). Since then, an increasing number of studies have reported the numerous pharmacologic effects of paeoniflorin, such as cerebrovascular protection, cardiovascular protection, neuroprotection, antihyperglycemia, tumor inhibition, immunoregulation, abirritation, and hepatoprotection (Zhang et al., 2017; Chen et al., 2018; Zhai et al., 2018; Tu et al., 2019). Paeoniflorin has gained a large amount of attention for its effect on liver diseases as the growth rate of liver diseases has increased in recent years (Ma et al., 2020). Hence, this mini-review provides a comprehensive summary of the pharmacologic activities of paeoniflorin in liver diseases.

HEPATIC PROTECTION

The liver is a vital organ for metabolic functions and for the purification of toxic chemicals. However, the liver can be overloaded (Singh et al., 2016). Once the function of the liver is dysregulated, liver damage will occur. Under certain circumstances, liver injuries can be induced by various factors, including chemical pollutants, drugs, alcohols, and liver ischemia (Peralta et al., 2013; Wang et al., 2016; Kullak-Ublick et al., 2017). Liver injury is recognized as a highly complex process accompanied by extensive apoptosis in hepatic cells. Oxidative stress and inflammatory reactions are thought to play key roles in this process (Brenner et al., 2013; Li et al., 2015). Moreover, immune reactions resulting from immune cells such as Kupffer cells have also drawn much attention due to the unique characteristics of hepatic sinusoids (Heymann et al., 2015).

Hepatic Ischemia/Reperfusion Alleviation

Hepatic ischemia/reperfusion (I/R) injury is the major manifestation after liver transplantation or hemorrhagic shock with relatively high morbidity and mortality (Go et al., 2015). Currently, paeoniflorin is considered to be highly effective in hepatic I/R injury treatment. A study from Xie reported that compared with hepatic I/R injury rats, rats pretreated with paeoniflorin (100 mg/kg) showed significantly decreased serum alanine aminotransferase (ALT) and aspartate aminotransferase (AST) activities by 40.3% and 53.8%, respectively. This liver protection effect is strongly relevant to directly alleviating hepatic cell apoptosis and decreasing caspase-3 levels. Furthermore, an inflammatory response was also observed in this study. This study demonstrated that paeoniflorin pretreatment could inhibit CD45+/Ly6G+ neutrophils and the production of proinflammatory cytokines [tumor necrosis factor alpha (TNF-α) and interleukin-1 beta (IL-1β)]. Therefore, a reduction in the innate immune response might contribute to this process. This research finally found that inhibiting the HMGB1-TLR4 signaling pathway is the crucial mechanism of paeoniflorin in hepatic I/R injury (Xie et al., 2018). Another study also supported this conclusion. Tao's study demonstrated that treatment with paeoniflorin at a dose of 5 to 20 mg/kg could markedly reduce the expression levels of inflammatory mediators, including nuclear factor kappa-B (NF-κB), TNF-α, IL-1β, and IL-6. At the same time, the apoptosis marker caspase-3 was decreased after paeoniflorin treatment (Tao et al., 2016). Therefore, antioxidative, anti-inflammatory, and antiapoptotic activities are clearly involved in the mechanism of paeoniflorin treatment.

Protection From Toxic Chemical-Induced Liver Injury

There are a variety of toxic chemicals, including carbon tetrachloride (CCl₄), concanavalin A (Con-A), D-galactosamine (GalN), bacillus Calmette-Guérin (BCG), and lipopolysaccharide (LPS), that can induce liver injury (Zhang H.Y. et al., 2018). Toxic chemical-induced liver injury is mainly characterized by an immune response and inflammation. Moreover, hepatic tissue apoptosis is a key outcome. A large amount of evidence indicates that paeoniflorin has a profound effect on toxic chemical-induced liver injury. Paeoniflorin at a dose of 100 mg/kg was able to decrease liver injury, significantly decrease ALT and AST, and alleviate the histopathological changes induced by CCl₄. Moreover, the significant pharmacological effect was related to the reduction of HO-1 mRNA expression and proinflammatory cytokine (TNF-α and IL-6) excretion (Guo et al., 2018). Other studies have indicated the protective effect of paeoniflorin on Con A-induced hepatitis with immune regulation. Chen's results suggested that intravenous paeoniflorin pretreatment could attenuate plasma levels of ALT and AST and diminish apoptosis or necrosis of liver tissue. These results demonstrated a protective effect of paeoniflorin against Con A-induced liver injury in mice. The mechanism may at least in part be the suppression of CD4+, CD8+, and NKT cell infiltration in the liver. Moreover, the downregulation of TLR4 expression and the inhibition of NF-κB activation are key signaling pathways in this process (Chen M. et al., 2015). *In vitro* research from primary human hepatic sinusoidal endothelial cells (HHSECs) also confirmed this result. Paeoniflorin at doses from 50 to 800 μM most likely contributed to the alleviation of Con-A-induced inflammation in HHSECs. Preincubation with paeoniflorin caused a concentration-

dependent downregulation of IL-8. Furthermore, paeoniflorin was able to inhibit IL-8 release by 52.8% at a dose of 800 μM. The mechanism might be closely related to blocking IL-8 secretion *via* the downregulation of ERK1/2 and Akt phosphorylation (Gong et al., 2015). In addition, GalN/TNF-α-induced apoptosis of human L-02 hepatocytes was decreased by paeoniflorin in a dose-dependent manner. The antiapoptotic effect was further evidenced by the inhibition of caspase-3/9 activities and by the suppression of ER stress activation in L-02 cells. These results revealed that paeoniflorin might target ER stress and calcium, leading to mitochondria-dependent pathway regulation (Jiang et al., 2014). A study of immunological liver injury based on BCG combined with LPS was also performed in 2006. Paeoniflorin administration was able to protect against immunological liver injury by ameliorating TNF-α and IL-6 secretion and downregulating LPS receptor expression (Liu et al., 2006).

CHOLESTASIS ALLEVIATION

Cholestasis is characterized by decreased bile flow and bile acid accumulation. It is one of the most common but devastating liver diseases. Hepatocyte injury and cholangitis will ultimately occur with cholestasis progression. Furthermore, portal myofibroblast and hepatic stellate cell activation rapidly result in biliary fibrosis or even cirrhosis without prompt treatment (Ghonem et al., 2015). It is currently believed that the pathogenesis of cholestasis involves multiple signaling pathways with the simultaneous activation of inflammation, dysregulation of hepatocyte transporters, and oxidative stress injury in liver tissue (Copple et al., 2010; Allen et al., 2011; Trauner et al., 2017).

A series of studies from Zhao's group indicated that paeoniflorin exerts a dose-dependent (50–200 mg/kg) protective effect on alpha-naphthylisothiocyanate (ANIT)-induced cholestasis in rats by decreasing serum ALT, AST, TBIL, DBIL, total bile acid (TBA), γ-glutamyltranspeptidase (γ-GT), and alkaline phosphatase (ALP). Moreover, the extremely suppressed bile flow induced by ANIT was also increased by paeoniflorin treatment. The mechanism of this activity is partially related to attenuating oxidative stress with reactive oxygen species (ROS) inhibition by suppressing nicotinamide adenine dinucleotide phosphate (NADPH) oxidase 4 expression and the mitochondria-dependent pathway (Zhao et al., 2013; Zhou et al., 2017). In addition, an alternative antioxidative mechanism was also investigated. The results indicated that paeoniflorin could regulate glutathione (GSH) and its related synthase glutamate-cysteine ligase catalytic subunit (GCLc) and glutamate-cysteine ligase modifier subunit (GCLm). The enhancement of GSH synthesis was further proven to increase Nrf2 through the PI3K/Akt-dependent pathway (Chen Z. et al., 2015). Regarding inflammation, histological examination revealed that paeoniflorin-treated rats demonstrated less neutrophil infiltration. The research suggested that paeoniflorin could remarkably reduce the overexpression of NF-κB and IL-1β induced by ANIT in liver tissue (Zhao et al., 2017). Moreover, a study focusing on *Paeonia lactiflora* Pall., one of the sources of paeoniflorin, was in accordance with the previous result showing the

suppression of the inflammatory response (Ma et al., 2018). Another study further revealed that paeoniflorin could mainly regulate primary bile acid biosynthesis by serum metabolomic profiling analysis (Chen et al., 2016)]. Therefore, transporters might be the central regulatory process. In 2017, Zhao reported that ANIT-induced dysregulated hepatocyte transporters, such as Na$^+$/taurocholate-cotransporting polypeptide (NTCP), bile salt export pump (BSEP), and multidrug resistance-associated protein 2 (MRP2), were restored by paeoniflorin treatment (Zhao et al., 2017).

LIVER FIBROSIS ATTENUATION

Liver fibrosis is the process of chronic liver injury caused by hepatitis B and C, alcohol consumption, fatty liver disease, cholestasis, and autoimmune hepatitis (Seki and Brenner, 2015). Hepatic stellate cell (HSC) activation plays a key role in myofibroblasts that produce extracellular matrix (ECM) in the liver (Tsuchida and Friedman, 2017). Currently, a variety of inflammatory and fibrogenic pathways are thought to participate in liver fibrosis (Seki and Schwabe, 2015; Higashi et al., 2017; Wree et al., 2018).

In the CCl$_4$-induced liver fibrosis model, paeoniflorin was proven to effectively attenuate serum ALT, AST, HA, IV-C, and liver tissue Hyp at the doses of 20, 40, 80, and 200 mg/kg (Min et al., 2011). This result indicated that paeoniflorin could significantly decrease liver fibrosis development. Moreover, the inhibition of HIF-1α expression partly through the mTOR pathway might be the crucial mechanism (Zhao et al., 2014). This pharmacologic effect was also confirmed in two other liver fibrosis models. Hu reported that paeoniflorin treatment from 20 to 80 mg/kg for 26 consecutive weeks was able to inhibit radiation-induced hepatic fibrosis. The expression levels of TGF-β1, Smad3/4, and Smad7 were significantly lower in the paeoniflorin-treated groups than in the model group. This result indicated that paeoniflorin alleviated fibrosis *via* the TGF-β1/Smad signaling pathway (Hu et al., 2018). In addition to the radiation model, dimethylnitrosamine (DMN) was also used to induce liver fibrosis. Paeoniflorin treatment demonstrated an antifibrosis effect in rats with less collagen fiber deposition and gentle centrilobular necrosis observed in paeoniflorin-treated rats compared with DMN-induced model rats. These results were at least in part due to restored macrophage disruption and reduced inflammatory cytokines (Chen et al., 2012).

In addition, schistosomiasis is a kind of special chronic disease leading to liver fibrosis. A recent study demonstrated that paeoniflorin at 50 mg/kg/d improved parasitological parameters, such as decreased worm burden, immature eggs, and mature eggs, in a schistosomiasis *mansoni*-induced hepatic fibrosis model. Meanwhile, paeoniflorin treatment also significantly decreased the hepatic mean granuloma diameter and fibrosis area. The mechanism was partially recognized as targeting the apoptosis pathway by regulating caspase-3 and P53 expression (Abd El-Aal et al., 2017). Moreover, the key role of IL-13 was also explored in this model. Three other studies confirmed that paeoniflorin had a significant suppressive effect

on the establishment of the ECM. Paeoniflorin could not only directly inhibit the alternative activation of macrophages by inhibiting the JAK2/STAT6 signaling pathway but also indirectly suppressed macrophages by decreasing IL-13 secretion (Li et al., 2009; Li et al., 2010; Chu et al., 2011).

NONALCOHOLIC FATTY LIVER DISEASE PREVENTION

Nonalcoholic fatty liver disease (NAFLD) has been the most common chronic liver disease worldwide in recent years. More than 40% of the population is affected in some countries. NAFLD has attracted concern worldwide since becoming a public health burden (Neuschwander-Tetri et al., 2010; Estes et al., 2018). NAFLD includes a wide range of liver disorders extending from nonalcoholic fatty liver (NAFL) to nonalcoholic steatohepatitis (NASH). Fibrosis, cirrhosis, and hepatocellular carcinoma will ultimately occur without treatment (Lebeaupin et al., 2018).

Paeoniflorin is a potential NAFLD prevention compound according to many studies. Zhang revealed that paeoniflorin attenuated NAFLD by restoring serum ALT, AST, TC, TG, HDL, and LDL. At the same time, paeoniflorin alleviated high-fat diet-induced hepatic adipose infiltration by decreasing steatosis, inflammation, ballooning degeneration, and necrosis. The potential mechanism might be cardiovascular protection by decreasing body weight and hyperlipidemia, blocking inflammation, and inhibiting lipid deposition (Zhang et al., 2015). Further research indicated that paeoniflorin ameliorated hepatic steatosis and inhibited CD68 and TGF-β1 expression. Downregulation of the ROCK/NF-κB signaling pathway might be relevant to the effect of paeoniflorin on NAFLD (Ma et al., 2016). Ma's investigation indicated that 20 mg/kg paeoniflorin remarkably inhibited lipid ectopic deposition *via* the lipid metabolism pathway. On the other hand, paeoniflorin treatment also exerted insulin sensitizing effects *via* IRS/Akt/GSK3β and antioxidation (Ma et al., 2017). In addition, a recent study also confirmed that paeoniflorin significantly reduced serum insulin and glucagon levels, enhanced insulin sensitivity, restored serum lipid profiles, and attenuated hepatic steatosis. All these effects should be relevant to the activation of the LKB1/AMPK and Akt signaling pathways in NAFLD (Li et al., 2018).

HEPATOCELLULAR CARCINOMA INHIBITION

Hepatocellular carcinoma (HCC) is believed to be the most common and malignant type of tumor. HCC is the third most common cancer-related cause of death due to poor prognosis. Over 700,000 HCC cases are diagnosed every year (Robinson et al., 2019). The situation is particularly concerning in China. China accounts for 55% of HCC cases worldwide (Su et al., 2016). HCC is recognized to involve multiple signaling cascades in cell adhesion, cell migration, and extracellular matrix proteolysis (Brown and Murray, 2015). Therefore, potential agents for HCC treatment should efficiently address multiple aspects of this process.

In an *in vitro* study, paeoniflorin at the doses of 6.25–200 μM was found to significantly inhibit the growth of HepG2 and Bel-7402 cell lines. Proteolysis could reduce the invasion, metastasis, and adhesion of HCC cell lines. In addition, paeoniflorin was able to decrease MMP-9 and ERK levels and increase E-cad expression in HepG2 and Bel-7402 cells (Lu et al., 2014). Moreover, another study also indicated paeoniflorin as a promising agent in the treatment of liver cancer. Its mechanism might be partially related to apoptosis induction in hepatocellular carcinoma cells by downregulating prostaglandin E receptor EP_2 levels, increasing the Bax/Bcl-2 ratio and thus upregulating the activation of caspase-3 (Hu et al., 2013).

OUTLOOK AND CONCLUSION

As evidenced by the numerous studies that have focused on the mechanism in-depth, many attempts have been made to investigate the efficacy of natural compounds such as paeoniflorin in liver disease treatment. This mini-review summarizes the pharmacologic activities and liver protection provided by paeoniflorin and demonstrates that paeoniflorin from the dosage of 5–200 mg/kg *in vivo* is an important compound for hepatic protection, cholestasis alleviation, liver fibrosis attenuation, NAFLD prevention, and HCC inhibition (**Table 1**). It is also crucial to reveal the mechanism to determine how paeoniflorin exerts its pharmacological effect. Paeoniflorin displays remarkable anti-inflammation effects *via* the TLR4-NF-κB and ROCK/NF-κB signaling pathways during liver injury and NAFLD. Antioxidation signals such as HO-1, mitochondria-dependent pathways, and immune regulation containing HMGB1-TLR4 are closely correlated. Moreover, paeoniflorin also alleviates cholestasis through an antioxidative mechanism by downregulating ROS and NOX4 and upregulating the PI3K/Akt/Nrf2 pathway. The anti-inflammatory effects of NF-κB and IL-1β and the regulation of NTCP, BSEP, and MRP2 are mainly relevant to the anti-cholestatic effects of paeoniflorin. Several important signaling pathways, such as mTOR/HIF-1α, TGF-β1/Smads, and JAK2/STAT6, are involved in the effect of paeoniflorin on activated HSC and ECM inhibition during liver fibrosis. Macrophage regulation is also considered the crucial mechanism for the antifibrotic effect. The reduction in invasion, metastasis, and adhesion and the induction of apoptosis signals, including Bax, Bcl-2, and caspase-3, are related to the effect on hepatocellular carcinoma (**Figure 1**).

The common mechanisms could be summarized from the current literature. The anti-inflammation, anti-oxidative and anti-apoptosis in hepatocytes are the core functions for its effect on liver diseases. Moreover, the immune and macrophage regulation are also important for its special effect on liver damage and liver fibrosis. The effect of paeoniflorin on liver diseases has been vastly developed, accompanied by deep insight into mechanistic

TABLE 1 | The pharmacological activities of paeoniflorin in liver diseases.

Disease Treatment	Experimental model	Doses (Route)	Targets/Pathways	Reference
Liver injury	Hepatic I/R-induced injury	100 mg/kg (i.g.)	HMGB1-TLR4 pathway	Xie et al., 2018
	Hepatic I/R-induced injury	5–20 mg/kg (i.v.)	NF-κB signaling pathway and caspase-3	Tao et al., 2016
	CCl$_4$-induced liver injury	10–100 mg/kg (i.g.)	HO-1, TNF-α, IL-6, and caspase-3	Guo et al., 2018
	Con A-induced liver injury	50 mg/kg (i.v.)	TLR4-NF-κB pathway	Chen M. et al., 2015
	Con A-treated HHSECs	50–800 μM (*in vitro*)	ERK1/2 and Akt phosphorylation	Gong et al., 2015
	GalN/TNF-α-treated L02	1–100 μM (*in vitro*)	ER stress and mitochondria-dependent pathway	Jiang et al., 2014
	BCG/LPS-induced immunological liver injury	25–100 mg/kg (i.g.)	TNF-α, IL-6, and LPS receptor	Liu et al., 2006
Cholestasis	ANIT-induced cholestasis	100–200 mg/kg (i.g.)	ROS-related NADPH and NOX4	Zhao et al., 2013
	ANIT-induced cholestasis	50–200 mg/kg (i.g.)	Apoptosis-related Bax, Caspase-9, and caspase-3	Zhou et al., 2017
	ANIT-induced cholestasis	50–200 mg/kg (i.g.)	PI3K/Akt/Nrf2 pathway	Chen Z. et al., 2015
	ANIT-induced cholestasis	50–200 mg/kg (i.g.)	NF-κB, IL-1β and the hepatic transporters NTCP, BSEP, and MRP2	Zhao et al., 2017
	ANIT-induced cholestasis	50–200 mg/kg (i.g.)	Primary bile acid biosynthesis	Chen et al., 2016
Liver fibrosis	CCl$_4$-induced liver fibrosis	20–80 mg/kg (i.g.)	IV-C, LN, and Hyp reduction	Min et al., 2011
	CCl$_4$-induced liver fibrosis	80–200 mg/kg (i.g.)	mTOR/HIF-1α signaling pathway	Zhao et al., 2014
	Radiation-induced liver fibrosis	20–80 mg/kg (i.g.)	TGF-β1/Smads signaling pathway	Hu et al., 2018
	DMN-induced liver fibrosis	20 mg/kg (i.g.)	Macrophage disruption	Chen et al., 2012
	Schistosomiasis *mansoni*-induced liver fibrosis	50 mg/kg (i.g.)	Apoptosis pathway related to caspase-3 and P53	Abd El-Aal et al., 2017
	Schistosomiasis *japonica*-induced liver fibrosis	60 mg/kg (i.g.)	JAK2/STAT6 signaling pathway and IL-13	Chu et al., 2011
	Schistosomiasis *japonica*-induced liver fibrosis/ Hepatic stellate cells	30 mg/kg (i.g.) /30–120 mg/L (*in vitro*)	SOCS-1, STAT6, and IL-13	Li et al., 2010
	Schistosomiasis *japonica*-induced liver fibrosis	30 mg/kg (i.g.)	IL-13 and IL-13Ra2	Li et al., 2009
NAFLD	AIN76A diet-induced NAFLD	0.05% (in diet)	Lipid synthesis, inflammation, and hyperglycemia pathway	Zhang et al., 2015
	HCF diet-induced NAFLD	20–100 mg/kg (i.g.)	ROCK/NF-κB signaling pathway	Ma et al., 2016
	2% cholesterol and 15% lard diet-induced NAFLD	20 mg/kg (i.g.)	IRS/Akt/GSK3β, antioxidation, and insulin sensitizing	Ma et al., 2017
	Fructose-induced insulin resistance and hepatic steatosis	10–40 mg/kg (i.g.)	LKB1/AMPK and Akt signaling pathway	Li et al., 2018
HCC	Human HCC Bel-7402 and HepG2 cell lines	6.25–200 μM (*in vitro*)	MMP-9, ERK, and E-cad	Lu et al., 2014
	Human HCC HepG2 and SMMC-7721 cell lines	10^{-8}–10^{-5} mol/L (*in vitro*)	Prostaglandin E receptor EP2, Bax, Bcl-2, and caspase-3	Hu et al., 2013

ANIT, alpha-naphthylisothiocyanate; BCG, bacillus Calmette-Guérin; CCl$_4$, carbon tetrachloride; Con-A, concanavalin A; DMN, dimethylnitrosamine; HCC, hepatocellular carcinoma; HCF, High-fat; HHSECs, human hepatic sinusoidal endothelial cells; i.g., intragastric; I/R, ischemia/reperfusion; i.v., intravenous injection; LPS, lipopolysaccharide; NAFLD, Nonalcoholic fatty liver disease.
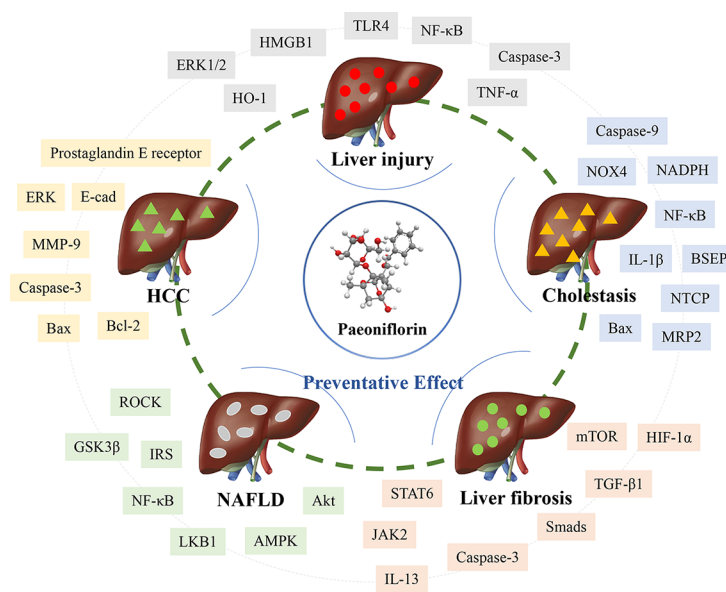
FIGURE 1 | The pharmacological effect of paeoniflorin on liver diseases through multiple targets.

investigation. Even so, two essential aspects ought to be noted based on this mini-review. First, most of the signals mentioned above are the downstream targets in various liver diseases. The upstream of signals which paeoniflorin targets directly will be drawn with special attention. Second, particular focus should also be paid to the 'from bench to bedside' concept for further clinical discovery. The clinical conversion with rigorous randomized controlled trial is the golden index to check the efficacy and medicinal value of paeoniflorin. Therefore, the deeper mechanistic investigation and the further clinical confirmation seem as the two key processes in the future development.

In summary, paeoniflorin demonstrates multiple effects on liver diseases correlating with complex and complicated signaling pathways. Therefore, paeoniflorin might be a potential agent to treat liver disease and alleviate liver damage.

AUTHOR CONTRIBUTIONS

XM, WZ, and YJ prepared the manuscript. JW and SW reviewed the drafts and provided important information for the completion. YZ conceived the idea and provided important information for the completion.

FUNDING

REFERENCES

Abd El-Aal, N. F., Hamza, R. S., and Harb, O. (2017). Paeoniflorin targets apoptosis and ameliorates fibrosis in murine schistosomiasis mansoni: A novel insight. *Exp. Parasitol.* 183, 23–32. doi: 10.1016/j.exppara.2017.10.005

Allen, K., Jaeschke, H., and Copple, B. L. (2011). Bile acids induce inflammatory genes in hepatocytes: a novel mechanism of inflammation during obstructive cholestasis. *Am. J. Pathol.* 178 (1), 175–186. doi: 10.1016/j.ajpath.2010.11.026

Brenner, C., Galluzzi, L., Kepp, O., and Kroemer, G. (2013). Decoding cell death signals in liver inflammation. *J. Hepatol.* 59 (3), 583–594. doi: 10.1016/j.jhep.2013.03.033

Brown, G. T., and Murray, G. I. (2015). Current mechanistic insights into the roles of matrix metalloproteinases in tumour invasion and metastasis. *J. Pathol.* 237 (3), 273–281. doi: 10.1002/path.4586

Chen, X., Liu, C., Lu, Y., Yang, Z., Lv, Z., Xu, Q., et al. (2012). Paeoniflorin regulates macrophage activation in dimethylnitrosamine-induced liver fibrosis in rats. *BMC Complement. Altern. Med.* 12, 254. doi: 10.1186/1472-6882-12-254

Chen, M., Cao, L., Luo, Y., Feng, X., Sun, L., Wen, M., et al. (2015). Paeoniflorin protects against concanavalin A-induced hepatitis in mice. *Int. Immunopharmacol.* 24 (1), 42–49. doi: 10.1016/j.intimp.2014.11.006

Chen, Z., Ma, X., Zhu, Y., Zhao, Y., Wang, J., Li, R., et al. (2015). Paeoniflorin ameliorates ANIT-induced cholestasis by activating Nrf2 through an PI3K/Akt-dependent pathway in rats. *Phytother. Res.* 29 (11), 1768–1775. doi: 10.1002/ptr.5431

Chen, Z., Zhu, Y., Zhao, Y., Ma, X., Niu, M., Wang, J., et al. (2016). Serum Metabolomic Profiling in a Rat Model Reveals Protective Function of Paeoniflorin Against ANIT Induced Cholestasis. *Phytother. Res.* 30 (4), 654–662. doi: 10.1002/ptr.5575

Chen, H., Dong, Y., He, X., Li, J., and Wang, J. (2018). Paeoniflorin improves cardiac function and decreases adverse postinfarction left ventricular remodeling in a rat model of acute myocardial infarction. *Drug Des. Devel. Ther.* 12, 823–836. doi: 10.2147/DDDT.S163405

Chu, D., Du, M., Hu, X., Wu, Q., and Shen, J. (2011). Paeoniflorin attenuates schistosomiasis japonica-associated liver fibrosis through inhibiting alternative activation of macrophages. *Parasitology.* 138 (10), 1259–1271. doi: 10.1017/S0031182011001065

Copple, B. L., Jaeschke, H., and Klaassen, C. D. (2010). Oxidative stress and the pathogenesis of cholestasis. *Semin. Liver. Dis.* 30 (2), 195–204. doi: 10.1055/s-0030-1253228

Estes, C., Razavi, H., Loomba, R., Younossi, Z., and Sanyal, A. J. (2018). Modeling the epidemic of nonalcoholic fatty liver disease demonstrates an exponential increase in burden of disease. *Hepatology.* 67 (1), 123–133. doi: 10.1002/hep.29466

Ghonem, N. S., Assis, D. N., and Boyer, J. L. (2015). Fibrates and cholestasis. *Hepatol.* 62 (2), 635–643. doi: 10.1002/hep.27744

Go, K. L., Lee, S., Zendejas, I., Behrns, K. E., and Kim, J. S. (2015). Mitochondrial Dysfunction and Autophagy in Hepatic Ischemia/Reperfusion Injury. *Biomed. Res. Int.* 2015, 183469. doi: 10.1155/2015/183469

Gong, W. G., Lin, J. L., Niu, Q. X., Wang, H. M., Zhou, Y. C., Chen, S. Y., et al. (2015). Paeoniflorin diminishes ConA-induced IL-8 production in primary human hepatic sinusoidal endothelial cells in the involvement of ERK1/2 and Akt phosphorylation. *Int. J. Biochem. Cell Biol.* 62, 93–100. doi: 10.1016/j.biocel.2015.02.017

Guo, X. Y., Yin, X. R., Yuan, H. M., and Wan, J. Y. (2018). Paeoniflorin Attenuates CCl4-Induced Acute Liver Injury. *Genom. Applied. Biol.* 37 (8), 3693–3698. doi: 10.13417/j.gab.037.003693

Hasin, Y., Seldin, M., and Lusis, A. (2017). Multi-omics approaches to disease. *Genome Biol.* 18 (1), 83. doi: 10.1186/s13059-017-1215-1

Heymann, F., Peusquens, J., Ludwig-Portugall, I., Kohlhepp, M., Ergen, C., Niemietz, P., et al. (2015). Liver inflammation abrogates immunological tolerance induced by Kupffer cells. *Hepatology* 62 (1), 279–291. doi: 10.1002/hep.27793

Higashi, T., Friedman, S. L., and Hoshida, Y. (2017). Hepatic stellate cells as key target in liver fibrosis. *Adv. Drug Deliv. Rev.* 121, 27–42. doi: 10.1016/j.addr.2017.05.007

Hu, S., Sun, W., Wei, W., Wang, D., Jin, J., Wu, J., et al. (2013). Involvement of the prostaglandin E receptor EP2 in paeoniflorin-induced human hepatoma cell apoptosis. *Anticancer. Drugs* 24 (2), 140–149. doi: 10.1097/CAD.0b013e32835a4dac

Hu, Z., Qin, F., Gao, S., Zhen, Y., Huang, D., and Dong, L. (2018). Paeoniflorin exerts protective effect on radiation-induced hepatic fibrosis in rats via TGF-β1/Smads signaling pathway. *Am. J. Transl. Res.* 10 (3), 1012–1021.

Jiang, Z., Chen, W., Yan, X., Bi, L., Guo, S., and Zhan, Z. (2014). Paeoniflorin protects cells from GalN/TNF-α-induced apoptosis via ER stress and mitochondria-dependent pathways in human L02 hepatocytes. *Acta Biochim. Biophys. Sin.* 46 (5), 357–367. doi: 10.1093/abbs/gmu010

Kullak-Ublick, G. A., Andrade, R. J., Merz, M., End, P., Benesic, A., Gerbes, A. L., et al. (2017). Drug-induced liver injury: recent advances in diagnosis and risk assessment. *Gut* 66 (6), 1154–1164. doi: 10.1136/gutjnl-2016-313369

Kunnumakkara, A. B., Bordoloi, D., Padmavathi, G., Monisha, J., Roy, N. K., Prasad, S., et al. (2017). Curcumin, the golden nutraceutical: multitargeting for multiple chronic diseases. *Br. J. Pharmacol.* 174 (11), 1325–1348. doi: 10.1111/bph.13621

Lebeaupin, C., Vallée, D., Hazari, Y., Hetz, C., Chevet, E., and Bailly-Maitre, B. (2018). Endoplasmic reticulum stress signalling and the pathogenesis of non-alcoholic fatty liver disease. *J. Hepatol.* 69 (4), 927–947. doi: 10.1016/j.jhep.2018.06.008

Li, X., Shen, J., Zhong, Z., Wen, H., Luo, Q., and Wei, W. (2009). Paeoniflorin: a monomer from traditional Chinese medical herb ameliorates Schistosoma japonicum egg-induced hepatic fibrosis in mice. *J. Parasitol.* 95 (6), 1520–1524. doi: 10.1645/GE-1994.1

Li, X., Shen, J., Zhong, Z., Peng, J., Wen, H., Li, J., et al. (2010). Paeoniflorin ameliorates schistosomiasis liver fibrosis through regulating IL-13 and its signalling molecules in mice. *Parasitology* 137 (8), 1213–1225. doi: 10.1017/S003118201000003X

Li, S., Tan, H. Y., Wang, N., Zhang, Z. J., Lao, L., Wong, C. W., et al. (2015). The Role of Oxidative Stress and Antioxidants in Liver Diseases. *Int. J. Mol. Sci.* 16 (11), 26087–26124. doi: 10.3390/ijms161125942

Li, Y. C., Qiao, J. Y., Wang, B. Y., Bai, M., Shen, J. D., and Cheng, Y. X. (2018). Paeoniflorin Ameliorates Fructose-Induced Insulin Resistance and Hepatic Steatosis by Activating LKB1/AMPK and AKT Pathways. *Nutrients* 10 (8), E1024. doi: 10.3390/nu10081024

Liu, D. F., Wei, W., and Song, L. H. (2006). Protective effect of paeoniflorin on immunological liver injury induced by bacillus Calmette-Guerin plus lipopolysaccharide: modulation of tumour necrosis factor-alpha and interleukin-6 MRNA. *Clin. Exp. Pharmacol. Physiol.* 33 (4), 332–339. doi: 10.1111/j.1440-1681.2006.04371.x

Lu, J. T., He, W., Song, S. S., and Wei, W. (2014). Paeoniflorin inhibited the tumor invasion and metastasis in human hepatocellular carcinoma cells. *Bratisl. Lek. Listy.* 115 (7), 427–433. doi: 10.4149/BLL_2014_084

Ma, Z., Chu, L., Liu, H., Li, J., Zhang, Y., Liu, W., et al. (2016). Paeoniflorin alleviates non-alcoholic steatohepatitis in rats: Involvement with the ROCK/NF-κB pathway. *Int. Immunopharmacol.* 38, 377–384. doi: 10.1016/j.intimp.2016.06.023

Ma, Z., Chu, L., Liu, H., Wang, W., Li, J., Yao, W., et al. (2017). Beneficial effects of paeoniflorin on non-alcoholic fatty liver disease induced by high-fat diet in rats. *Sci. Rep.* 7, 44819. doi: 10.1038/srep44819

Ma, X., Wen, J. X., Gao, S. J., He, X., Li, P. Y., Yang, Y. X., et al. (2018). *Paeonia lactiflora* Pall. regulates the NF-κB-NLRP3 inflammasome pathway to alleviate cholestasis in rats. *J. Pharm. Pharmacol.* 70 (12), 1675–1687. doi: 10.1111/jphp.13008

Ma, X., Jiang, Y., Zhang, W., Wang, J., Wang, R., Wang, L., et al. (2020). Natural products for the prevention and treatment of cholestasis: A review. *Phytother. Res.* doi: 10.1002/ptr.6621

Min, J., Han, Z., and Jing, C. (2011). Protective effect of paeoniflorin on rat with chronic liver injury and fibrosis. *Modern. J. Integrated. Tradit. Chin. Western Med.* 20 (36), 4618–4624.

Neuschwander-Tetri, B. A., Clark, J. M., Bass, N. M., Van Natta, M. L., Unalp-Arida, A., Tonascia, J., et al. (2010). Clinical, laboratory and histological associations in adults with nonalcoholic fatty liver disease. *Hepatology* 52 (3), 913–924. doi: 10.1002/hep.23784

Park, E. J., and Pezzuto, J. M. (2015). The pharmacology of resveratrol in animals and humans. *Biochim. Biophys. Acta* 1852 (6), 1071–1113. doi: 10.1016/j.bbadis.2015.01.014

Peralta, C., Jiménez-Castro, M. B., and Gracia-Sancho, J. (2013). Hepatic ischemia and reperfusion injury: effects on the liver sinusoidal milieu. *J. Hepatol.* 59 (5), 1094–1106. doi: 10.1016/j.jhep.2013.06.017

Ren, J., Fu, L., Nile, S. H., Zhang, J., and Kai, G. (2019). *Salvia miltiorrhiza* in Treating Cardiovascular Diseases: A Review on Its Pharmacological and Clinical Applications. *Front. Pharmacol.* 10, 753. doi: 10.3389/fphar.2019.00753

Robinson, A., Tavakoli, H., Cheung, R., Liu, B., Bhuket, T., and Wong, R. J. (2019). Low Rates of Retention Into Hepatocellular Carcinoma (HCC) Surveillance Program After Initial HCC Screening. *J. Clin. Gastroenterol.* 53 (1), 65–70. doi: 10.1097/MCG.0000000000001024

Seki, E., and Brenner, D. A. (2015). Recent advancement of molecular mechanisms of liver fibrosis. *J. Hepatobiliary. Pancreat. Sci.* 22 (7), 512–518. doi: 10.1002/jhbp.245

Seki, E., and Schwabe, R. F. (2015). Hepatic inflammation and fibrosis: functional links and key pathways. *Hepatology* 61 (3), 1066–1079. doi: 10.1002/hep.27332

Singh, D., Cho, W. C., and Upadhyay, G. (2016). Drug-Induced Liver Toxicity and Prevention by Herbal Antioxidants: An Overview. *Front. Physiol.* 6, 363. doi: 10.3389/fphys.2015.00363

Su, L., Zhou, T., Zhang, Z., Zhang, X., Zhi, X., Li, C., et al. (2016). Optimal staging system for predicting the prognosis of patients with hepatocellular carcinoma in China: a retrospective study. *BMC Cancer.* 16, 424. doi: 10.1186/s12885-016-2420-0

Tao, Y. E., Wen, Z., Song, Y., and Wang, H. (2016). Paeoniflorin attenuates hepatic ischemia/reperfusion injury via anti-oxidative, anti-inflammatory and anti-apoptotic pathways. *Exp. Ther. Med.* 11 (1), 263–268. doi: 10.3892/etm.2015.2902

Trauner, M., Fuchs, C. D., Halilbasic, E., and Paumgartner, G. (2017). New therapeutic concepts in bile acid transport and signaling for management of cholestasis. *Hepatology* 65 (4), 1393–1404. doi: 10.1002/hep.28991

Tsuchida, T., and Friedman, S. L. (2017). Mechanisms of hepatic stellate cell activation. *Nat. Rev. Gastroenterol. Hepatol.* 14 (7), 397–411. doi: 10.1038/nrgastro.2017.38

Tu, J., Guo, Y., Hong, W., Fang, Y., Han, D., Zhang, P., et al. (2019). The regulatory effects of Paeoniflorin and its derivative Paeoniflorin-6'-O-benzene sulfonate CP-25 on inflammation and immune diseases. *Front. Pharmacol.* 10, 57. 2019. doi: 10.3389/fphar.2019.00057

Wang, S., Pacher, P., De,, Lisle, R. C., Huang, H., and Ding, W. X. (2016). A Mechanistic Review of Cell Death in Alcohol-Induced Liver Injury. *Alcohol. Clin. Exp. Res.* 40 (6), 1215–1223. doi: 10.1111/acer.13078

Wree, A., McGeough, M. D., Inzaugarat, M. E., Eguchi, A., Schuster, S., Johnson, C. D., et al. (2018). NLRP3 inflammasome driven liver injury and fibrosis: Roles of IL-17 and TNF in mice. *Hepatology* 67 (2), 736–749. doi: 10.1002/hep.29523

Xie, T., Li, K., Gong, X., Jiang, R., Huang, W., Chen, X., et al. (2018). Paeoniflorin protects against liver ischemia/reperfusion injury in mice via inhibiting HMGB1-TLR4 signaling pathway. *Phytother. Res.* 32 (11), 2247–2255. doi: 10.1002/ptr.6161

Zhai, W., Ma, Z., Wang, W., Song, L., and Yi, J. (2018). Paeoniflorin inhibits Rho kinase activation in joint synovial tissues of rats with collagen-induced rheumatoid arthritis. *Biomed. Pharmacother.* 106, 255–259. doi: 10.1016/j.biopha.2018.06.130

Zhang, L., Yang, B., and Yu, B. (2015). Paeoniflorin Protects against Nonalcoholic Fatty Liver Disease Induced by a High-Fat Diet in Mice. *Biol. Pharm. Bull.* 38 (7), 1005–1011. doi: 10.1248/bpb.b14-00892

Zhang, Y., Qiao, L., Xu, W., Wang, X., Li, H., Xu, W., et al. (2017). Paeoniflorin Attenuates Cerebral Ischemia-Induced Injury by Regulating Ca^{2+}/CaMKII/CREB Signaling Pathway. *Molecules* 22 (3), E359. doi: 10.3390/molecules22030359

Zhang, H. Y., Wang, H. L., Zhong, G. Y., and Zhu, J. X. (2018). Molecular mechanism and research progress on pharmacology of traditional Chinese medicine in liver injury. *Pharm. Biol.* 56 (1), 594–611. doi: 10.1080/13880209.2018.1517185

Zhang, J., Yu, K., Han, X., Zhen, L., Liu, M., Zhang, X., et al. (2018). Paeoniflorin influences breast cancer cell proliferation and invasion via inhibition of the Notch−1 signaling pathway. *Mol. Med. Rep.* 17 (1), 1321–1325. doi: 10.3892/mmr.2017.8002

Zhao, Y., Zhou, G., Wang, J., Jia, L., Zhang, P., Li, R., et al. (2013). Paeoniflorin protects against ANIT-induced cholestasis by ameliorating oxidative stress in rats. *Food Chem. Toxicology* 58, 242–248. doi: 10.1016/j.fct.2013.04.030

Zhao, Y., Ma, X., Wang, J., Zhu, Y., Li, R., Wang, J., et al. (2014). Paeoniflorin alleviates liver fibrosis by inhibiting HIF-1α through mTOR-dependent pathway. *Fitoterapia* 99, 318–327. doi: 10.1016/j.fitote.2014.10.009

Zhao, D. D., Jiang, L. L., Li, H. Y., Yan, P. F., and Zhang, Y. L. (2016). Chemical Components and Pharmacological Activities of Terpene Natural Products from the Genus Paeonia. *Molecules* 21 (10), E1362. doi: 10.3390/molecules21101362

Zhao, Y., He, X., Ma, X., Wen, J., Li, P., Wang, J., et al. (2017). Paeoniflorin ameliorates cholestasis via regulating hepatic transporters and suppressing inflammation in ANIT-fed rats. *Biomed. Pharmacother.* 89, 61–68. doi: 10.1016/j.biopha.2017.02.025

Zhou, H. Q., Liu, W., Wang, J., Huang, Y. Q., Li, P. Y., Zhu, Y., et al. (2017). Paeoniflorin attenuates ANIT-induced cholestasis by inhibiting apoptosis *in vivo* via mitochondria-dependent pathway. *Biomed. Pharmacother.* 89, 696–704. doi: 10.1016/j.biopha.2017.02.084

Targeting Hepatic Stellate Cells for the Treatment of Liver Fibrosis by Natural Products: Is It the Dawning of a New Era?

Yau-Tuen Chan, Ning Wang, Hor Yue Tan, Sha Li and Yibin Feng*

School of Chinese Medicine, The University of Hong Kong, Hong Kong, Hong Kong

Liver fibrosis is a progressive liver damage condition that is worth studying widely. It is important to target and alleviate the disease at an early stage before turning into later cirrhosis or liver cancer. There are currently no direct medicines targeting the attenuation or reversal of liver fibrosis, and so there is an urgent need to look into this area. Traditional Chinese Medicine has a long history in using herbal medicines to treat liver diseases including fibrosis. It is time to integrate the ancient wisdom with modern science and technology to look for the best solution to the disease. In this review, the principal concept of the pathology of liver fibrosis will be described, and then some of the single compounds isolated from herbal medicines, including salvianolic acids, oxymatrine, curcumin, tetrandrine, *etc.* will be discussed from their effects to the molecular mechanism behind. Molecular targets of the compounds are analyzed by network pharmacology approach, and TGFβ/SMAD was identified as the most common pathway. This review serves to summarize the current findings of herbal medicines combining with modern medicines in the area of fibrosis. It hopefully provides insights in further pharmaceutical research directions.

Keywords: hepatic stellate cells, liver fibrosis, cirrhosis, natural product, herbal medicine, network pharmacology

INTRODUCTION

Liver fibrosis is a great concern in public health, as it could result in cirrhosis, portal hypertension, liver failure, and possibly hepatocellular carcinoma (HCC) that cause deaths. A common result of progressive liver fibrosis is cirrhosis, which affects 1–2% of the world population (Higashi et al., 2017); it causes over one million deaths annually ranking the 11th most common cause of mortality worldwide (Asrani et al., 2019) and has an incidence of over five million in 2017 (James et al., 2018). Liver fibrosis is a chronic state of hepatic injuries, which could be the result of viral infection (HBV, HCV), alcohol consumption, drug abuse, fatty liver, steatohepatitis, as well as autoimmune disease (Seki and Schwabe, 2015). Fibrogenesis initiates with activation of effector cells by the primary injury response that leads to an elaboration and deposition of extracellular matrix. With insufficient restoration, fibrogenesis progresses and develops into organ failure.

Diverse types of cells are involved in fibrogenesis, including epithelial cells, endothelial cells, inflammatory cells, and most importantly fibrogenic effector cells. Specifically, the hepatic epithelial

cells are injured by external causes and are followed by an inflammatory response. Wound healing response is stimulated and results in recruitment of inflammatory cells and activation of fibrogenic effector cells. The inflammatory cells, including Kupffer cells, mast cells, and T cells, secrete inflammation mediators and factors like chemokines and cytokines, inducing immune response with inflammation (Rockey, 2013). Those released factors could promote the activation of the fibrogenic effector cells, which is the central key in fibrogenesis, through the paracrine pathways. Fibroblasts, myofibroblasts, and certain types of cells derived from bone marrow and epithelial-to-mesenchymal transition are the crucial effectors in liver fibrosis, which are mainly responsible for producing extracellular matrix proteins (EMP) (Hinz et al., 2007). Stimulators of the cells like transforming growth factor beta (TGFβ) are also secreted by themselves, which contribute to the autocrine activation (Meng et al., 2014). Scar tissues accumulate with EMP which are synthesized and released from the effector cells, mainly fibroblasts and myofibroblasts. The EMP include prominently collagens type I and type III, fibronectin, laminin, and some other trace amount elements (Friedman, 2008a).

Activation of hepatic stellate cells (HSCs) from its quiescent state is an indispensable and critical step of liver fibrogenesis. HSCs are mesenchymal cells that contribute to about 15% of normal resident cells in the liver (Friedman, 2008b). They serve as the storage of vitamin A (retinoid) in normal liver, but this characteristic is deprived once the HSCs start to transdifferentiate under the stimulation of cellular mediators, cytokines, and chemokines from injured or inflammatory cells.

At the initiating stage of fibrogenesis, HSCs are activated to become proliferative and contractile myofibroblasts. The transdifferentiated HSCs accelerate the secretion and attenuate the degradation of the extracellular matrix elements, which eventually lead to fibrogenesis (**Figure 1**). Studies showed that selective inhibition of HSCs exhibited prominent potential in preventing and reversing fibrogenic process in rodents (Marti-Rodrigo et al., 2019; Yan et al., 2019).

Current therapeutic strategy on liver fibrosis is to remove and eliminate the etiology. Until now, there are no "golden standard" therapies for liver fibrosis. However, accumulating preclinical evidence has suggested that the scarring process of the liver is not unidirectional and permanent, but instead plastic and reversible (Campana and Iredale, 2017; Higashi et al., 2017; Zoubek et al., 2017; Schuppan et al., 2018). Owing to the primary role in mediating fibrogenesis in the liver, HSCs have become arousing interesting drug targets to the prevention and treatment of hepatic fibrosis (Lotersztajn et al., 2005). Inhibition of HSCs could be achieved by reversing transdifferentiation of HSCs into myofibroblast, reducing the fibrogenic activity of the HSCs, and inducing death or apoptosis of HSCs. Natural products derived from medicinal plants and animals, such as silymarin, catechins, schisantherin, and ursodeoxycholic acid, have shown proofs of beneficial effects and were approved as healthy supplements for patients with chronic liver diseases (Paumgartner and Beuers, 2002; Levy et al., 2004; Hong et al., 2017; Bagheriya et al., 2018; Daniyal et al., 2019). Moreover, a great number of herbal medicine and bioactive compounds are under investigation for their antifibrotic activity. In this review, we summarized the
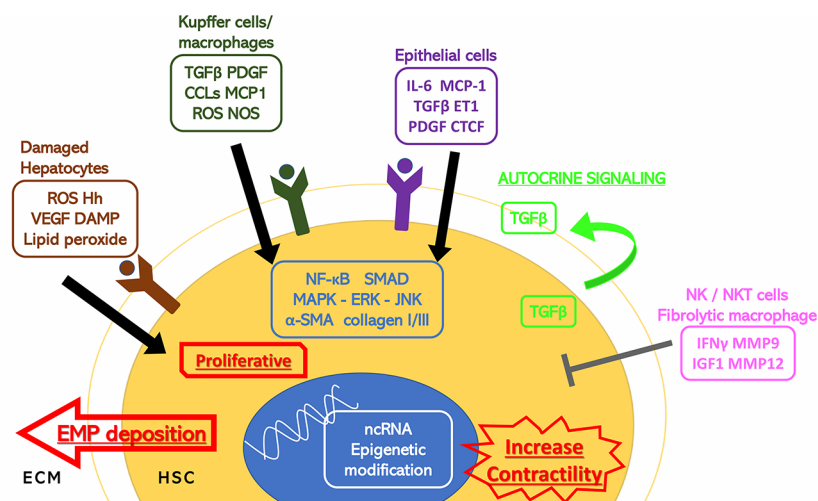
FIGURE 1 | Stimuli to HSC activation. Hepatic cells surrounding the hepatic stellate cells (HSCs) including damaged hepatocytes, Kupffer cells, macrophages, epithelial cells, and natural killer/natural kill T cells have extracellular secretion to either stimulate or inhibit the activation of the HSCs through cytokines and hormones. The HSC activation response is also shown. α-SMA, alpha smooth muscle actin; CCL2, C-C motif chemokine 2; CTCF, connective tissue growth factor; DAMP, damage associated molecular patterns; ECM, extracellular matrix; EMP, extracellular matrix proteins; ERK, extracellular signal-regulated kinase; ET1, endothelin 1; Hh, hedgehog; HSC, hepatic stellate cell; IFNγ, interferon gamma; IGF1, insulin-like growth factor 1; IL-6, interleukin 6; JNK, c-Jun N-terminal kinase; MAPK, mitogen-activated protein kinase; MCP1, monocyte chemoattractant protein 1; MMP, matrix metalloproteinase; ncRNA, noncoding ribonucleic acid; NF-κB, nuclear factor kappa-light-chain-enhancer of activated B cells; NOS, nitric oxide synthase; PDGF, platelet-derived growth factor; ROS, reactive oxygen species; TGFβ, transforming growth factor beta; VEGF, vascular endothelial growth factor.

current research progress on compounds isolated from herbal medicine in treating liver fibrosis by targeting HSCs. We searched through the PubMed database with the keywords "liver fibrosis", "hepatic stellate cells", and "herbal medicine". We aim to highlight the role of herbal drugs in modern medicine and provide insights and perspectives on the research and development of first-line fibrosis therapies targeting hepatic stellate cells.

HEPATIC STELLATE CELLS AS THERAPEUTIC TARGETS OF LIVER FIBROSIS

Activation of Hepatic Stellate Cells From Their Quiescent State

The first step of HSCs involvement in fibrosis is the initiation stage, where there are primary modulations in genetic expressions and phenotypic changes sensitized by paracrine cytokine and chemokine stimulation. HSCs locate in the perisinusoidal space where neighboring cells including Kupffer cells, hepatocytes, and endothelial cells could cause reshaping in the microenvironment (Wake, 1971). Cytokines, mainly platelet-derived growth factor (PDGF), TGFβ, interleukin 1 beta (IL-1β), tumor necrosis factor (TNF), monocyte chemoattractant protein 1 (MCP1), C-C motif chemokine (CCL)-3, CCL5, are secreted by Kupffer cell (Marra et al., 1993; Pinzani, 2002; Pradere et al., 2013). Damage-associated molecular patterns (DAMP), reactive oxygen species (ROS), and such inflammatory mediators are released from injured hepatocytes which trigger innate immune response. Hepatic nuclear factor κB (NF-κB)-inducing kinase is activated, while lipid peroxides and TNF-related apoptosis-inducing ligand (TRAIL), hedgehog ligands, and so forth are released from leukocytes (Canbay et al., 2002; Shen et al., 2014; Lan et al., 2015). These can cause activation of the HSCs, resulting in matrix synthesis, proliferation, and loss of retinoids. Instead of causing damage to normal hepatocytes, those activators induce the transdifferentiation of the quiescent HSCs into activated form. Carbon tetrachloride (CCl$_4$)-induced liver injury model in rodent showed the HSC activation and liver fibrosis mechanism (Miao et al., 2019). The free radical product CCl$_3$ produced by the cytochrome CYP2E1 in liver cells leads to elevated activation of HSCs (Bedossa et al., 1994). Depletion of macrophages by transgenic means and administrated liposomal clodronate caused suppressed HSC activation and fibrogenesis in CCl$_4$ chronic hepatic injury mice model (Duffield et al., 2005; Sunami et al., 2012).

Subsequently, the HSCs would enter into the second stage, which was first named "perpetuation" by Friedman twenty years ago (Friedman, 2000). In this stage, the phenotypes of the activated HSCs are amplified and results in elevated proliferation, scar formation, contractility, reduced matrix degradation, and fibrogenesis (Iwaisako et al., 2014). The apparent net change of these behaviors is the accumulation of extracellular matrix.

Major Factors Involved in Hepatic Stellate Cell Activation

While many factors are able to activate the HSCs from their quiescent state in *in vitro* studies, there are two major cytokines proven to be the dominant inducers that lead to HSC activation *in vivo*. The sustained interaction between HSCs and paracrine and autocrine TGFβ and PDGF in the hepatic microenvironment results in consecutive activation of the cells throughout the initiation and progression of liver fibrosis.

Transforming Growth Factor Beta

TGFβ has long been identified as one of the most potent cytokines to induce fibrogenesis (Hellerbrand et al., 1999). HSCs are activated by signals from the TGFβ, but at the same time they secrete TGFβ, which completes an autocrine positive feedback mechanism. The direct downstream effector of the signaling pathway is the SMAD proteins, predominantly SMAD2 and SMAD3 (Shi et al., 2011). The binding of TGFβ to its type 1 receptor (TGFβR1) brings phosphorylation to the receptor and thus the SMAD2/3 proteins. The p-SMAD proteins then bind to SMAD4, which forms a complex translocating to the nucleus. It could affect the epigenetic modifications, noncoding RNA (ncRNA) expressions, as well as the induction of myofibroblast and matrix deposition (Meng et al., 2016). TGFβ may also act on the mitogen-activated protein kinase (MAPK) pathway, with extracellular signal-regulated kinase (ERK), p38, c-jun N-terminal kinase (JNK) as downstream cascades (Engel et al., 1999; Hanafusa et al., 1999). Alpha-smooth muscle actin (α-SMA), EMP like fibronectin, proteoglycans (George et al., 2000), and especially collagen types I and III are upregulated through induced transcription (Breitkopf et al., 2006). α-SMA induction is one of the critical markers demonstrating HSC activation (Tomasek et al., 2002) due to its absence in the surrounding resident hepatocytes except the smooth muscle cells inside blood vessels (Friedman, 2008a). Extracellular collagen type I and III levels are elevated in fibrotic liver, whereas type I is the most characteristic one leading to cirrhosis (Rojkind et al., 1979). It was elucidated that the augmentation of collagen I by TGFβ stimulation is dependent of the mediator hydrogen peroxide and the CCAAT/enhancer binding protein-β (C/EBPβ) (Garcia-Trevijano et al., 1999).

Platelet-Derived Growth Factor

Animal studies have shown the critical role of the mitogen PDGF as well as its receptor PDGF receptor-β (PDGFRβ) in HSC proliferation and migration (Wong et al., 1994; Kostallari et al., 2018). The extent of inflammation so as fibrosis is correlated with the expression of PDGF in patients with chronic liver diseases (Zuo et al., 2019). Interestingly, the mRNA expression of PDGFRβ was confirmed in both quiescent and activated HSCs, but protein production was mainly limited to the activated cells (Henderson et al., 2013). The PDGF-induced proliferation could be attenuated by an adipocytokine adiponectin (Kamada et al., 2003), whereas leptin had the opposite effect (Saxena and Anania, 2015).

Vascular Endothelial Growth Factor

The vascular endothelial growth factor (VEGF) induces cell proliferation especially HSCs, which includes angiogenesis in the damaged liver tissue. It has a complicated role which takes part in both fibrogenesis and hepatic tissue repair and reversal of fibrosis (Kantari-Mimoun et al., 2015). VEGF may be a pathological factor in the induction of HSC activation, in hypoxic environment (Ankoma-Sey et al., 2000), but it also regulates liver sinusoidal permeability, monocyte migration, and scar-associated macrophage function, which are fibrotic resolution and tissue repair processes (Yang et al., 2014).

Connective Tissue Growth Factor

The connective tissue growth factor (CTGF) is highly expressed in fibrotic liver when compared to normal liver. It is a potent fibrogenic cytokine similar to PDGF. Its contribution to ECM accumulation brings about a series of hepatic fibrogenic actions (Huang and Brigstock, 2012). CTGF activates and at the same time is produced mainly by HSCs. It is particularly important because it is one of the primary drivers to fibrillar collagen productions. CTGF expression is reported to be associated with the microRNA miR-214 in an inverse proportion (Chen et al., 2014a; Chen et al., 2015).

Hedgehog Pathway

The hedgehog (Hh) pathway is an essential system in the regulation of progenitor cells' fate in the fibrosis of liver. Smoothened homolog (SMO), which is released and activated with the upregulation of Hh ligands, drives the epithelial regeneration by promoting mesenchymal-to-epithelial transitions of the myofibroblasts derived from HSCs (Omenetti et al., 2011). Mice experiments have demonstrated that the deletion of SMO could attenuate fibrogenesis in liver injury models. Other studies also proved that the blockade of Hh signaling could inhibit the liver fibrosis and reduce liver progenitor cells (Greenbaum and Wells, 2011). The Hh pathway could possess the possible targets of fibrotic treatment (Shen et al., 2017).

Toll-Like Receptor

Dietary or free cholesterol in the liver could worsen fibrosis by activating HSCs. The elevated intracellular cholesterol level in HSCs leads to Toll-like Receptor (TLR) 4 signaling (Teratani et al., 2012). The accompanying result is the sensitization of HSC to TGFβ-activation by the reduction of TGFβ pseudoreceptor bone morphogenetic protein and activin membrane-bound inhibitor (Bambi). The deficiency of a cholesterol acyltransferase accelerates the fibrosis develop through the insufficient removal of free cholesterol in HSCs (Tomita et al., 2014). Therefore, cholesterol-lowering drugs could help alleviate the fibrosis by slowing down the accumulation of free cholesterol (Van Rooyen et al., 2013).

Molecular Strategies of Hepatic Stellate Cell Suppression

Despite the advancement of effective antiviral agents that could target the underlying causes of the fibrotic result by hepatitis B

and C (Schuppan et al., 2018), there are some other etiologies of these liver diseases including alcoholic and nonalcoholic steatohepatitis, autoimmune diseases, etc. that remain poorly solved. A viable therapeutic approach is arising with HSCs as the target. Since HSCs is the major mediator in the process of fibrogenesis, reducing the activity of HSCs could slow down or possibly revert the fibrosis condition. On the purpose of HSCs regression and clearance, currently there are three therapeutic approaches, namely apoptosis, senescence, and reversion.

Apoptosis

The transdifferentiated HSCs express antiapoptotic activity under proinflammatory stimuli TNF and IL-1β through the NF-κB signaling pathway (Pradere et al., 2013), and the production of antiapoptotic proteins like Bcl-2 is the result (Lee et al., 2015). Tissue inhibitors of metalloproteinase 1 (TIMP-1) and TGFβ also promote antiapoptotic signals and survival of HSCs (Murphy et al., 2002). As such, the treatment on the HSCs should induce susceptibility to cell death in order to reduce the number of transdifferentiated HSCs. The activated HSCs have receptors such as apoptosis antigen 1 (FAS, CD95), TNF receptor 1 (TNFR1), TRAIL receptors, and p75 neurotrophin receptor (p75NTR), which stimulate apoptosis when engaged (Pellicoro et al., 2014). NF-κB inhibitor BAY 11-7082 and proteasome inhibitors bortezomib and MG132 can inhibit the NF-κB gene and so its pathway on the HSCs, which can in turn reduce liver fibrosis (Anan et al., 2006). Natural killer cells (NK) also play an essential role in the induction of HSC apoptosis (Heymann and Tacke, 2016). Interferon gamma (IFNγ) is extensively produced by NK, which can block the HSCs activation. This cytokine can also enhance the cytotoxicity of NK on HSCs by increasing NKG2D and TRAIL related apoptosis induction (Radaeva et al., 2006). Target-constructed-IFNγ could also bind to the PDGFRβ on the HSCs to cease activation and induce fibrolysis (Bansal et al., 2011). Sorafenib is a first-line tyrosine kinase inhibitor that is used to treat renal cell and hepatocellular carcinoma (HCC) (Lyons et al., 2001). It also shows inhibitory effect and induces autophagic cell death on HSCs through the Akt/mTOR/p70S6K and JNK signaling pathways (Hao et al., 2016).

Senescence

When cell proliferation exceeds a finite number of times, cellular senescence occurs, and the cell-cycle would arrest to prevent genetic damages. Senescence is mainly mediated by the p53-dependent pathway, and the attenuation of this program in HSCs enhances liver fibrosis and exacerbates the chances of developing into HCCs (Lujambio et al., 2013). IL-6 and IFNγ is normally secreted in senescent p53 pathway from the HSCs, while IL-3, IL-4, and IL-5 from proliferating HSCs stimulate M2-polarization of macrophages that can promote malignant cell growth. The CCN family matricellular proteins, cysteine-rich protein 6_1 (CCN$_1$/CYR6$_1$) contribute to HSC senescence and apoptosis by attenuating the TGFβ signaling (Borkham-Kamphorst et al., 2014). OSU-03012, which is a celecoxib derivative, can suppress the proliferation of HSCs and result in senescence (Zhang et al., 2015). During activation of HSCs, the retinol

storage is depleted and the level of peroxisome proliferator-activated receptor gamma (PPARγ) is decreased (Lee and Jeong, 2012). So, retinoid receptor and PPARγ agonists are suggested to have a role in antifibrotic treatment (Panebianco et al., 2017).

Reversal of the Activation
Evidences have shown that activated HSCs could be reverted to a quiescent-like but distinct form. When the stimuli for transdifferentiation were removed from the rodent models, half of the myofibroblasts escaped from apoptosis, with fibrogenic genes downregulated and reverted phenotypes. The HSCs remained in an inactivated state until resensitized by fibrogenic stimuli again. The reverted HSCs were not completely identical to the preactivated quiescent ones, with fibrogenic genes as well as quiescence-associated genes expressed in a lesser extent. (Kisseleva et al., 2012; Troeger et al., 2012). A recent study has revealed the possibility of reprogramming the profibrogenic myofibroblasts into hepatocyte-like cells, named induced hepatocytes (iHeps). Using chronic liver disease mouse models, liver myofibroblasts were treated with a set of transcription factors including FOXA3, GATA4, HNF1A, and HNF4A and resulted in ameliorated liver fibrosis. Most iHeps were found near the portal vein and central vein regions, and they assisted in restoring the deprived liver function (Song et al., 2016).

HSC-TARGETING NATURAL COMPOUNDS FROM HERBAL MEDICINE FOR LIVER FIBROSIS TREATMENT

Although there are currently countable numbers of approaches on the treatment targeting HSCs undergoing clinical trials, the use of herbal drugs or the isolated active single compounds are also worth investigating due to its cheap cost and low risk of side effects. There has been a long history in using herbal medicines and natural compounds in treating liver diseases. In the following, plenty of small molecular compounds derived from herbal medicines are discussed in detail and summarized in **Table 1**.

Salvianolic Acids
Salvianolic acids (SAs) are water-soluble extracted compounds isolated from the dried root of *Salvia miltiorrhiza* Bunge *(Radix Salviae miltiorrhizae)*, a herbal TCM medicine, *Danshen* that have been used thousands of years for the treatment of cardiovascular diseases (Li et al., 2018). With modern understanding in chemistry and pharmacology, SAs are also demonstrated to have observable antioxidative and anticancer effects. Moreover, SAs can modulate fibrogenesis through signal transduction.

Traditionally, *S. miltiorrhiza* was used to enhance blood circulation, attenuate congestion, and modulate menstrual cycle. It is also commonly used in modern Chinese Medicine to treat ischemic stroke, atherosclerosis, viral myocarditis, chronic hepatitis, cancers, as well as liver fibrosis (Zhou et al., 2005; Liu et al., 2010; Zhu et al., 2018). Among the water-soluble

compounds in *S. miltiorrhiza*, SAs have the highest solubility (Liu et al., 2007). Until now there are more than 10 different types of SAs identified, which are coded as salvianolic acid A, B, C, D, *etc.* (Ma et al., 2019). Salvianolic acid A (SAA) and salvianolic acid B (SAB) are the most abundant ones in the extract. All the salvianolic acids are possessing a common subunit Danshensu [(R)-3-(3, 4-Dihydroxyphenyl)-2-hydroxypropanoic acid] (Chen et al., 2014b) (**Figure 2**). SAA is composed of one Danshensu unit, while SAB is composed of three. SA showed higher anti-inflammatory and antioxidative activity than other compounds in *S. miltiorrhiza* (Du et al., 2016).

There are recent studies showing the antifibrosis effect of SA, particularly on liver fibrosis. These effects are inevitably related to the inhibition of HSC activation or the induction of apoptosis of HSCs. SAAs are believed to suppress lipid peroxidation, reduce alanine aminotransferase (ALT) and aspartate aminotransferase (AST) activity, as well as deprive the deposition of collagens I and III (Liu et al., 2000). HSCs induced apoptosis and inhibited activation by SAA, through the depression level of Bcl-2, cyclin D1, and E proteins, phosphorylation of AKT and PDGF, with elevated expression of p21 and p27 (Lin et al., 2006). Liver function was repaired; hydroxyproline (Hyp) and malondialdehyde (MDA) contents were attenuated by SAA in a rat model (Liu et al., 2001). In streptozotocin-induced diabetic rat model, SAA has shown to slow down the progression of liver fibrosis by reducing the expression of α-SMA and TGFβ (Qiang et al., 2014). SAA was also suggested to have a protective effect against bile duct ligation induced liver fibrosis through sirtuin 1 (SIRT1)/heat shock factor 1 (HSF1) signaling pathway (Zhu et al., 2018). Endoplasmic reticulum stress was abrogated by increased HSF1 expression.

SAB has all the aforementioned effects on countering fibrosis like the SAA (Luk et al., 2007; Li et al., 2012). Moreover, it was reported that SAB could also inhibit the cyclooxygenase activity in rat liver (Liu et al., 1994). SAB was proved to have a reversal effect on fibrosis in a double-blinded randomized control clinical study (Liu et al., 2002a). It was reported that SAB has as much, if not more, therapeutic effects and anti-inflammatory effects compared to IFNγ. Up to 10 µM of SAB could result in inhibition of cell proliferation and cell cycle arrest at G1 to S phase (Cui et al., 2002; Yang et al., 2003). SAB is, at the same time, limiting the PDGF stimulation through MAPK activity (Liu et al., 2002b). This mediation is suggested to be of the reduction of TGFβ-induced HSCs undergoing SMAD signaling pathway. SAB suppressed SMAD2/3 protein phosphorylation at the linker region of SMAD2/3 and the C-terminal in SMAD2, while it increased at the C-terminal in SMAD3 (Wu et al., 2019a).

Oxymatrine
Oxymatrine (OM) is one of the many effective quinolizidine alkaloids extracted from the herbal medicine root of *Sophora flavescens* Aiton *(Kushen)*. It is an oxygenated form of another alkaloid matrine. *Kushen* has been traditionally used with other herbal medicines together to treat fever, hematochezia, dysentery, jaundice, oliguria, *etc.* (He et al., 2015). Its extracted active compound, OM, has the effect of antiarrhythmia, myocardial

TABLE 1 | Molecular mechanism of compounds isolated from herbal medicine on hepatic stellate cells against liver fibrosis.

Compounds	Effects	References
Salvianolic acid A	⬇ lipid peroxidation, ALT, AST, deposition of collagens I and III	(Liu et al., 2000)
	Induce apoptosis and inhibit activation of HSC, through depression of Bcl-2, cyclin D1, E, phosphorylation of AKT and PDGF, and elevated p21 and p27	(Lin et al., 2006)
	⬆ liver function	(Liu et al., 2001)
	⬇ Hyp and MDA content	
	α-SMA and TGFβ	(Qiang et al., 2014)
	⬆ HSF1, regulate SIRT1 pathway	(Zhu et al., 2018)
Salvianolic acid B	⬇ cyclooxygenase activity	(Liu et al., 1994)
	⬇ ALT/AST and total bilirubin, reverse fibrotic score in clinical trial	(Liu et al., 2002a)
	⬇ HSC proliferation, cell cycle arrest at G1-S phase	(Cui et al., 2002; Yang et al., 2003)
	⬇ PDGF stimulation through MAPK signaling	(Liu et al., 2002b)
	⬇ SMAD2/3 protein activity	(Wu et al., 2019a)
	⬇ H$_2$O$_2$ induced mitochondrial dysfunction	(Liu et al., 2017)
	Regulate NF-κB/I-κB-α pathway	(Wang et al., 2012)
Oxymatrine	Antihepatitis B and C virus	(Wu and Wang, 2004; Wang et al., 2011)
	⬇ IL-6, TNFα, SMAD3, CREBBP, TLR4 via TGFβ pathway	(Zhao et al., 2016)
	⬆ IL-10, Bambi, SMAD7	
	⬇ SMAD3	(Wu et al., 2005; Wu et al., 2008)
	⬆ SMAD7	
	⬇ HSC-T6 cell	(Song et al., 2019)
	⬇ miR-195	
	⬆ SMAD7	
	⬇ procollagen I	(Du et al., 2015)
	YB-1 nuclear translocate	
	Regulate ERK1/2 pathway	
	⬇ TIMP-1	(Shi and Li, 2005)
	⬆ effect with RGD-liposome	(Chai et al., 2012)
Curcumin	⬇ ALT, TGFβ	(Reyes-Gordillo et al., 2008)
	⬇ PDGFRβ, ERK, serum PDGF, CTGF	(Zhang et al., 2012)
	⬆ MMP-9, ECM degradation	
	⬇ α-SMA, TGFβ, SMAD2, SMAD3, CTGF	(Yao et al., 2012)
	⬆ SMAD7	
	⬇ TNFα, IL-6, MCP-1, HMGB-1, TLR4, TLR2, activated HSC	(Tu et al., 2012)

(Continued)

TABLE 1 | Continued

Compounds	Effects	References
	⬇ ALT, AST, TGFα	(Morsy et al., 2012)
	⬆ MMP-13, reduced GSH	
	⬇ Collagen deposition, NF-κB, TNFα, IL-1β, IL-6	(Wu et al., 2010)
	⬆ IL-10	
	⬇ TNFα, NF-κB, IL-6	(Bassiouny et al., 2011)
	⬇ the leptin activation on HSC	(Tang et al., 2009)
	⬆ PPARγ	
	⬆ AMPK activity	(Tang and Chen, 2010)
	⬇ HSC activation	
	⬇ GLUT-2	(Lin and Chen, 2011)
	Disrupt p38 MAPK pathway	
	⬆ PPARγ	
Tetrandrine	Block calcium ion channel	(Bataller et al., 1998)
	⬇ collagen deposition, α-SMA, DNA synthesis	(Park et al., 2000)
	⬇ Hyp, α_1-collagen and TIMP-1	(Lee et al., 2001)
	⬆ HSC apoptosis	(Yin et al., 2007)
	⬇ TGFβ	(Chen et al., 2005)
	⬆ SMAD7	
	⬇ TNF-α, NF-κB, α-SMA, collagen deposition	(Hsu et al., 2007)
	⬇ Phosphorylation of IκBα, ICAM-1 expression	
	⬇ α-SMA, TRADD, TAK1, p-JNK	(Li et al., 2016)
	⬆ IκBα, JNK, NF-κB, p-ERK, caspase-3, PARP	
	⬇ autophagic, fibrogenic signals	(Miyamae et al., 2016)
	⬆ lipid accumulation	
Quercetin	⬇ TGFβ, ECM, collagen I, α-SMA, p-SMAD2/3	(Wu et al., 2017)
	⬆ PI3K, p-Akt	
Artesunate	⬇ Hyp, MMP-2, MMP-9, α-SMA, collagen I	(Xu et al., 2014)
	⬆ MMP-13	
	⬇ p-FAK, Akt, GSK-3β	(Lv et al., 2018)
	Induce ferroptosis in HSC	(Kong et al., 2019)
Glycyrrhetinic acid	⬇ Collagen I, nuclear SMAD3, COL1A2	(Moro et al., 2008)
	⬇ cleaved caspase-3, Bax, CTGF, α-SMA, collagen I and III, MMP-2, MMP-9	(Liang et al., 2015)
	⬇ Inflammation, Hyp, α-SMA, collagen I, TGFβ1, SMAD2/3, SMAD3 mRNA, p-SMAD2/3	(Zhou et al., 2016)
Resveratrol	⬆ SOD, MDA, ATPase	(Ahmad and Ahmad, 2014)
		Zhang et al., 2016

(Continued)

TABLE 1 | Continued

Compounds	Effects	References
Deoxyschizandrin	↓ protein carbonyls, α-SMA, collagen deposition	
	↓ cell viability, α-SMA, collagen I, TLR4, MyD88, PI3K, Akt, translocation of NF-κb	(Zhang et al., 2016)
	↑ CYP3A4, CYP3A5	(Yang et al., 2015)
	↑ LC3-II	(Lu et al., 2014)
	↓ p62, beclin 1	
Ligustrazine	↑ PPARγ	(Zhang et al., 2018)
	↓ HIF-1α, VEGF, bFGF, ICAM-1, VCAM-1, p-MLC2, migration and adhesion of HSC	
	↓ SMO, Gli 1, bcl-2, cyclin-D1, HSP90, HIF-1α, VEGF, angiopoietin 1	(Zhang et al., 2017)
Astragaloside	↑ MMP-2, GSH, SOD, p-SMAD2, p-SMAD3	(Yuan et al., 2018)
	↓ TGFβ1, SMAD7, collagen I, collagen III, TIMP-2, α-SMA, MDA	
	↓ α-SMA, collagen I	(Guo et al., 2018)
Paeonol	↓ AST, ALT, TNF-α, IL-6, IL-1, p-PI3K/PI3K, p-Akt/Akt, p-mTOR/mTOR	(Wei et al., 2019)
	↓ HSC migration, α-SMA, collagen, p-p38, p-ERK, p-JNK, p-PDGFRβ	(Kuo et al., 2012)
	↑ GSH-PX, SOD, CAT	(Wu et al., 2019b)
	↓ TGFβ, SMAD3, ALT, AST, Hyp, IL-6, TNF-α, MDA, collagen 1a, α-SMA, vimentin, desmin	
	↑ Bax, cleaved caspase-9 & caspase-3, cleaved PARP	(Kong et al., 2013)
	↓ p-NF-κB, IκBα, ALT, AST, Hyp, α-SMA, collagen 1a, CTGF, bcl-2,	

ischemia prevention, prophylactic, anti-inflammation and reducing oversensitivity (Deng et al., 2019). In recent years, its ability to attenuate fibrogenesis and carcinogenesis is being widely studied (Halim et al., 2019; Lan et al., 2019).

OM was proved to be antihepatitis B and C virus, which is effective to reduce viral-caused hepatitis and fibrosis (Wu and Wang, 2004; Wang et al., 2011). It is also effective against fibrosis from other causes. OM attenuated liver fibrosis by limiting the CCl₄-induced proinflammatory cytokines IL-6 and TNFα while promoting IL-10 and Bambi such anti-inflammatory factors (Zhao et al., 2016). It was suggested that OM modulates the HSC activation by suppressing TLR4 *via* the TGFβ signaling pathway. Collagen deposition in the liver is significantly reduced by OM-treated rats, which is accompanied by an elevation of SMAD7 and inhibition of SMAD3 as well as cAMP-response element-binding protein binding protein (CREBBP). This is consistent with the modulation of the fibrogenesis *via* TGFβ pathway with SMAD as the downstream effecter (Wu et al., 2008). OM was observed to have a similar effect on the pig serum-induced liver rat fibrosis (Wu et al., 2005).

The molecular mechanisms of OM on HSCs were studied *in vitro*. It was found that OM has an inhibitory effect on HSC-T6

cell line *in vitro* with concentration higher than 200 µg/ml after 24 h and 10 µg/ml after 72 h. miR-195, which is essential in HSC activation, was significantly down-regulated. SMAD7 level was augmented in the meantime (Song et al., 2019). Another study working on the LX-2 human HSC line has shown the possible mechanism of reducing procollagen I expression (Du et al., 2015). A transcription factor Y-box binding protein 1 (YB-1) was observed to have nuclear translocation under OM treatment at a concentration of 960 mg/L. The phosphorylation level of ERK1/2 was found to be positively associated with YB-1 expression. Thus, it is suggested that OM also regulates HSC activity *via* the ERK1/2 signaling pathway. The expression level of TIMP-1 was significantly lowered by OM in a CCl₄-induced fibrosis rat model, with no differences in α-SMA expression between the control or treatment group (Shi and Li, 2005). The therapeutic effect of OM on HSCs was reported to be enhanced using the Arg-Gly-Asp (RGD)-mediated targeting delivery liposome (Chai et al., 2012). This combined formulation could increase the inhibitory effect of OM on hepatic fibrosis by reducing HSC viability, inducing apoptosis, and limiting fibrogenesis gene expressions.

Curcumin

Curcumin is the principal phenol found in the rhizome of the herb *Curcuma longa* L., or turmeric as the common name, which has been a Chinese medicinal herb *Jianghuang*. It is a kind of curcuminoid, which is responsible for most of the biological activity of *C. longa*. In traditional Chinese medicine, it has been used in the treatment of chest and gut pain, dysmenorrhea, abdominal mass, wound healing, as well as rheumatic numb and pain. In modern pharmacology, curcumin was reported to have anti-inflammatory, antioxidant, antimicrobial, chemopreventive, chemotherapeutic, and anticancer activity (Anand et al., 2007; Hatcher et al., 2008).

The major effect of curcumin on liver fibrosis has been extensively studied, and it has been documented that the mechanism is a major target on HSC activation. There are many studies proving the effect of curcumin on HSCs, and this has been a potential therapeutic approach to be researched. There are reported evidences that TGFβ (Reyes-Gordillo et al., 2008), PDGFRβ, serum PDGF, CTGF (Zhang et al., 2012), SMAD2-3 (Yao et al., 2012), TNFα (Tu et al., 2012), matrix metalloproteinases (MMPs) (Morsy et al., 2012), TLRs (Tu et al., 2012), and some inflammatory cytokines (Wu et al., 2010; Bassiouny et al., 2011) are targeted and attenuated.

As mentioned previously leptin is a mediator in the development of liver fibrosis, especially in patients with obesity and type II diabetes mellitus (Stefanovic et al., 2008; Watanabe et al., 2008). During HSC activation, the cellular lipid storage is depleted, and lipid accumulation related gene expressions are downregulated. Leptin as a hormone in regulating lipid metabolism and energy balance (Friedman, 2004) was shown to stimulate HSC activation during fibrogenesis (Aleffi et al., 2005; Cayon et al., 2006). However, it is suggested that curcumin could revert this stimulation action by leptin on HSCs. Curcumin was demonstrated to have an inhibitory effect on leptin activation by reducing the phosphorylation level of the leptin
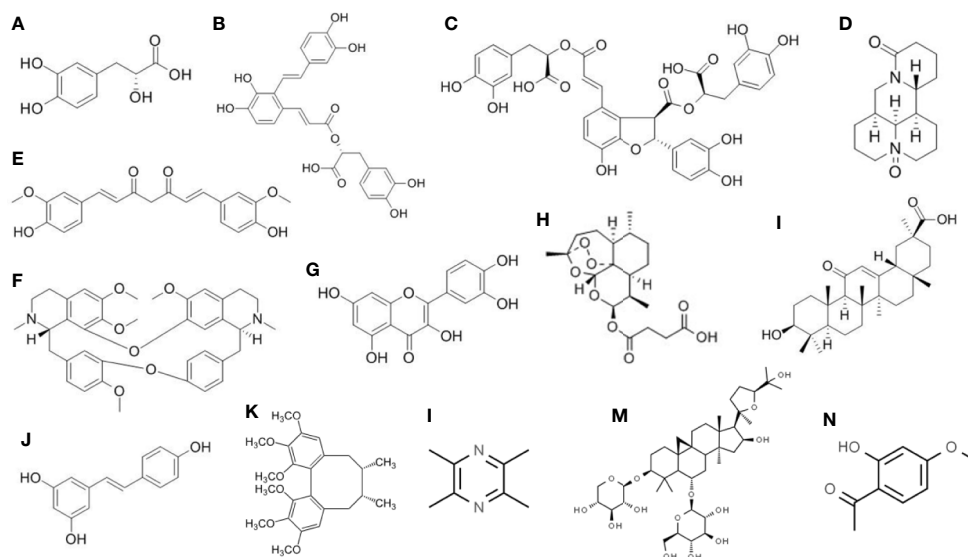
FIGURE 2 | Chemical structure of the isolated active compounds from herbal medicine with therapeutic effects on liver fibrosis. **(A)** Denshensu. **(B)** Salvianolic acid A. **(C)** Salvianolic acid B. **(D)** Oxymatrine. **(E)** Curcumin. **(F)** Tetrandrine. **(G)** Quercetin. **(H)** Artesunate. **(I)** Glycyrrhetinic acid. **(J)** Resveratrol. **(K)** Deoxyschizandrin. **(L)** Ligustrazine. **(M)** Astragaloside. **(N)** Paeonol.

receptor while stimulating PPARγ activity and leading to the interruption of leptin signaling (Tang et al., 2009). In another study performed by the same group later in 2010, curcumin was found also to attenuate the effect of leptin by promoting the activity of AMP-activated protein kinase (AMPK). The increased AMPK level results in induction of expression of lipid accumulation genes, which in turn slows down the HSC activation (Tang and Chen, 2010).

On the other hand, there are arising evidences showing that high blood glucose or the state of hyperglycemia could lead to the activation of HSCs (Aggarwal, 2010). Curcumin could restore this situation (Lin and Chen, 2011). The phytochemical could suppress the translocation of glucose transporter (GLUT)-2 to the cell membrane by disrupting the p38 MAPK pathway. The GLUT2 gene expression was downregulated by stimulating PPARγ activity. Less glucose could be imported by HSCs, and the diabetes-associated hepatic fibrogenesis was under control.

Tetrandrine

Tetrandrine (Tet) is an alkaloid extracted from the herbal medicine, *Stephania tetrandra* S. Moore, or called *Fangji* in Chinese Medicine, which acts on the calcium ion channel (Li et al., 2001). *Fangji* has been prescribed to treat rheumatic diseases, hypertension, numbness, edema, urination problems, and sores traditionally. In modern Chinese Medicine, Tet is also used for the purpose of analgesic, anti-inflammation, treating tuberculosis, lowering blood pressure, antimyocardial ischemia, antiarrhythmia, antifibrosis, and anticancer *etc.* (Yin et al., 2007; Bhagya and Chandrashekar, 2018).

The antifibrosis effect of Tet is due to its function of abrogating HSC activation as well as inducing HSC apoptosis.

It has a blocking action of the calcium ion channels on the HSCs, which could suppress their contractility and thus the activation (Liu et al., 1995; Bataller et al., 1998). Tet was shown to reduce collagen deposition in ECM in liver fibrosis induced by bile duct ligation and scission in rat (Park et al., 2000). Reduced α-SMA was observed in the HSCs, while DNA synthesis was also attenuated. Another study suggested that Tet reduced liver Hyp content through reducing the α1-collagen and TIMP-1 mRNA level (Lee et al., 2001). HSC apoptosis could also be the result of Tet treatment as described by (Yin et al., 2007). The effect has almost no differences when compared with the group treated with IFNγ. Tet has a similar suppressive effect on TGFβ and an inductive effect on SMAD7, which results in reduced activation of HSCs (Chen et al., 2005).

A more detailed mechanism was illustrated in 2007, where Tet inhibition on TNF-α-induced NF-κB transcription was found to be concentration dependent (Hsu et al., 2007). In addition, Tet attenuates TGFβ induced α-SMA production and collagen deposition in cultured HSC-T6 cells. Phosphorylation of IκBα and ICAM-1 expression is reduced, resulting in a total decrease of activated α-SMA positive HSCs. Tet was also reported to have the counter effect to TNF-α on HSCs activation. With dose-dependent effect, Tet could attenuate the α-SMA and TNF-receptor-1-associated death domain (TRADD) expression. It also has the inhibitory effect on the TGFβ-activated kinase-1 (TAK1) and JNK phosphorylation. Furthermore, the phosphorylation of NF-κB and degradation of IκBα was suppressed by Tet treatment (Li et al., 2016). Apoptosis of HSCs was confirmed by the increased level of caspase-3 and poly (ADP-ribose) polymerase (PARP) at higher concentration (>12.5 μM) of Tet. A more recent study suggested another role of Tet in the

deactivation of HSCs (Miyamae et al., 2016). As discussed above, there exists lipid degradation during HSC activation. Tet was found to inhibit the degradation of the lipid droplets as autophagic cargo and induce lipid accumulation which makes the HSC-T6 cell line remain quiescent. This result suggested that Tet could also target the late autophagy regulators.

Other Compounds From Herbs or Plants

Quercetin is a common flavonoid found in many fruits and vegetables such as onions, kales, green tea, apples, berries, *etc.*, which has been used as a supplement for its antioxidant and anti-inflammatory effects. There are researches suggesting its potential in preventing hepatic fibrosis. It was reported that quercetin could inhibit HSC activation and possibly reduce autophagy by acting on the TGFβ1/SMAD signaling pathway, as well as activating the phosphoinositide 3-kinase (PI3K)/Akt pathway. ECM, collagen I, and α-SMA production is inhibited, MMPs are increased by quercetin on the CCl$_4$ fibrosis model, and TIMP-1 was upregulated (Wu et al., 2017). Quercetin derivatives have also similar antifibrotic effects as well. By adding methyl group to a different position on the quercetin, there are different singular effects against various features of fibrosis respectively. This provides potentials in studying the enhancement of quercetin's therapeutic effect (Ganbold et al., 2019).

Artesunate is a semisynthetic derivative of the artemisinin group of drugs that is most commonly used to treat malaria. Artemisinin was isolated from the Chinese medicine *Artemisia annua* L. by the 2015 Nobel Prize laureate Tu Youyou. Artesunate was found to have the attenuation effect on liver fibrosis. Hyp content was significantly decreased; MMP-2, MMP-9, α-SMA, and collagen I were inhibited in a bovine serum albumin induced fibrosis rat model. MMP-13 level was promoted by artesunate, and it can be concluded that it is inhibiting the activation of HSC (Xu et al., 2014). Artemisinin was also proved to reduce the phosphorylation level of focal adhesion kinase (FAK), Akt, as well as glycogen synthase kinase 3 beta (GSK-3β). HSC proliferation and activation are inhibited by artesunate, and apoptosis is promoted through the FAK/Akt/β-catenin pathway (Lv et al., 2018). One study suggested that artesunate could also bring antifibrosis effect by inducing ferroptosis in activated HSCs (Kong et al., 2019).

Glycyrrhetinic acid is a main active compound from the herbal medicine *Glycyrrhiza uralensis* Fisch. ex DC., or *Gancao* in Chinese. It was shown to significantly inhibit liver fibrosis induced by CCl$_4$. It has a similar effect in cultured HSCs, that collagen I, nuclear accumulation of SMAD3, and alpha2(I) collagen gene (COL1A2) are abolished (Moro et al., 2008). It was confirmed again that hepatocyte apoptosis, *i.e.* cleaved caspase-3, Bax, CTGF, and HSC activation, *i.e.* α-SMA, collagens I and III, MMP-2, MMP-9, were all decreased by treatment of glycyrrhetinic acid (Liang et al., 2015). In addition, it was suggesting that a combination of glycyrrhetinic acid and astragalus saponins, components isolated from *Astragalus mongholicus* Bunge (Huangqi), could effectively reduce liver inflammation, ECM deposition, and HSC

activation in liver fibrosis rats. The combined therapy significantly reduced SMAD3 mRNA, TGFβ1, SMAD3, and p-SMAD2/3 protein levels, when compared with the phytochemicals used alone (Zhou et al., 2016).

Resveratrol is a polyphenol that is mostly found on the skin of red grapes, and sometimes in peanuts and berries. It has antioxidative, anti-inflammatory, anticancer, and cardioprotective properties and has been used as a nutrient supplement. Recently, there are studies of using resveratrol in treating liver fibrosis. Resveratrol could significantly restore levels of liver function biomarkers of oxidative damage, suggesting that the antifibrotic effect may come from the reduced oxidation and HSC inactivation by down-regulating α-SMA (Ahmad and Ahmad, 2014). It was also suggested that the antifibrotic effect of resveratrol is because of the inhibition of NF-κB activation, PI3K/Akt phosphorylation, and TLR4 level, which results in attenuation of HSC activation (Zhang et al., 2016).

Deoxyschizandrin is a lignan isolated from the *Schisandra chinensis* (Turcz.) Baill. or magnolia-vine as common name. The fruit of this plant could be prepared into a Chinese medicine five-flavor-fruit, or *Wuweizi*. *Schisandra chinensis* is one of the crucial components in the Chinese prescription, *Fuzheng Huayu Recipe*, to treat liver diseases mainly hepatitis B induced fibrosis (Liu et al., 2019a). Deoxyschizandrin was identified as a compound possessing the function to change the cytochrome P450 enzyme activity during hepatic fibrogenesis (Liu et al., 2019b). It was reported that the metabolism of deoxyschizandrin involved the P450 isoforms CYP3A4 and CYP3A5 (Yang et al., 2015). Deoxyschizandrin was also reported to have liver protective activity by activation of autophagy flux and reduction of apoptosis (Lu et al., 2014).

Ligustrazine, or tetramethylpyrazine, is the bioactive compound isolated from the Chinese herb *Conioselinum anthriscoides* 'Chuanxiong' (Chuanxiong). The antifibrotic action of ligustrazine was reported to be suppression of HSCs *via* SMRT-mediated transrepression of HIF-1α. It was shown to attenuate the HSC activities by inhibition of proangiogenic cytokines, suppression of migration and adhesion, restriction of contraction, and lowering the pericyte functions of HSCs (Zhang et al., 2018). The suppression of angiogenic properties of HSCs was also found to be related to the inhibition of canonical hedgehog signaling. SMO, HSP90, and HIF-1α were down-regulated while the VEGF and angiopoietin 1 level were depressed by ligustrazine in rat and mice models (Zhang et al., 2017).

Astragalosides are a type of compounds found from the herb *Astragalus mongholicus* Bunge, which are the sources of the Chinese medicine *Huangqi*. Astragalosides are reported to have therapeutic effects on hepatic fibrosis. Its antioxidant properties inhibit the activation of HSCs and regulate MMP-2, TIMP-2, and collagens. The pharmacological pathway was suggested to be TGFβ/SMAD signaling (Yuan et al., 2018). Astragaloside I, a compound of the astragaloside family, was shown to proliferate inhibition on the HSC cell line LX-2 (Guo et al., 2018). Astragaloside IV, on the other hand, was reported to have an effect on the PI3K/Akt/mTOR signaling pathway in a rat model. It could suppress the inflammatory response so as to limit the fibrogenesis through the action on HSCs (Wei et al., 2019). There

were some other reports suggesting the effects of astragalosides on different pathways, including PAR2 and Notch signaling (Mu et al., 2015; Wang et al., 2017).

Paeonol is a phenolic compound isolated from the flowering plant *Paeonia lactiflora* Pall. which roots could be prepared into the Chinese medicine *Baishao*. It was also reported to possess antifibrotic effect as a compound. In a PDGF-induced fibrosis rat model, *Baishao* extract, including paeonol, was shown to inhibit HSC migration and collagen production. The effect was believed to be associated with ERK, p38, and JNK deactivation (Kuo et al., 2012). Paeonol showed similar inhibition effect on HSCs in another CCl_4-induced fibrosis mice model. Liver injury and fibrosis were decreased through the effect on the TGFβ/SMAD signaling (Wu et al., 2019b). Paeonol also exhibited its antifibrogenesis effect through the NF-κB inhibition pathway (Kong et al., 2013).

NETWORK PHARMACOLOGY-ASSOCIATED STUDY

In order to identify the most important molecular target or pathway of these herbal compounds, we carried out network pharmacology study to understand the global regulation of natural compounds in the treatment of liver fibrosis targeting

HSCs. The reported candidate targets of those compounds isolated from the herbal medicine are collected from the Pubmed database. The molecular interactions between the compounds and the targets are analyzed and summarized by the Cytoscape software. The network analysis was performed using "NetworkAnalyzer", a plug-in function of Cytoscape. The correlation degree of the compounds as well as the gene target was calculated and visualized using the network diagram.

As shown as a result in **Figure 3**, the compounds labeled in red color, while the molecular targets are put in the outside region. The genes as common targets to more than one compound are labeled in blue, while the unique targets are labeled in yellow at the outermost area. As a result, the five targets with the highest degree are identified as TGFβ, α-SMA, collagen I, TNFα, and SMAD3 and are located at the center of the network from which, TGFβ is the most common one and is reported to have interactions with almost all the drugs mentioned in this review.

It is obvious to see that the TGFβ/SMAD signaling pathway play an essential role in the therapy of liver fibrosis through HSCs. The compounds have the aim to lower the TGFβ level of the HSCs, which could slow down the signaling of the particular pathway, and so the expression of α-SMA, as the translational product of the pathway and the characteristic of activated HSCs. Moreover, as discussed before, collagen I is an essential indicator of the HSC activation. It is obvious that the therapeutic

FIGURE 3 | Network pharmacology-based target identification of herbal medicine isolated compounds for the treatment of hepatic fibrosis. TGFβ, α-SMA, Collagen I, TNFα and SMAD3 are the five targets with the highest degree (green). Pure compounds from herbal drugs are labeled in (red). Common targets of the compounds are labeled in (blue), while unique targets of compounds are labeled in (yellow).

compounds would have effects on the expression of collagen. The relationship with TNFα signifies the anti-inflammatory nature of the herbal compounds, which is also an important property of antifibrotic drugs. This network pharmacology result shows that, even though there are different herbal medicines reported to have antifibrosis functions, with different active compounds and receptors, the ultimate therapeutic targets may actually be similar, as the most potent curative effect.

DISCUSSION

Liver fibrosis is becoming a huge public health burden in recent years, due to the unhealthy lifestyles in more developed countries. Progressive fibrosis leading to cirrhosis or eventually cancer will become irreversible, so diagnosis and treatment must be centered in the early stage. Although there are clinical trials for the development of antifibrosis drug, there still lacks a direct therapy method to cure liver fibrosis. Current therapeutic directions include anti-inflammation, antioxidative, and inhibition of effector cells, or HSCs. There are now RAS inhibitors, collagen synthesis inhibitors, antioxidants, PPARγ agonists, and direct inhibition inducers such as IFNγ going through different phases of clinical trials. As an ancient wisdom developed for thousands of years, Chinese medicine, or other alternative medicines have their own methodologies in treating liver diseases including fibrosis. Therefore, it is useful to provide insight of the herbal drugs used to treat fibrosis, and there are possibilities to isolate one or more feasible therapeutic compounds.

With the extensive research mentioned previously, it is optimistic that there is indeed more than one compound isolated from herbal medicine that is useful or beneficial to the treatment of liver fibrosis. Many of them are having drug targets on the HSC activators that could help remove the etiology. Since there are limited therapeutic approaches currently, we must extend the research directions to different possibilities, including Chinese herbal medicine. From the result of the network pharmacology, we could clearly see that the herbal compounds are having shared drug targets with each other, and they are consistent with the modern pharmaceutical research also. This greatly raises our confidence on the studies and usage of herbal medicine on the treatment of hepatic fibrosis.

There are some arising clinical trials using Chinese medicine formula as intervention or treatment to target liver fibrosis. For example, the effect of curcumin on diabetes-caused fatty liver diseases was investigated in a randomized placebo-controlled clinical trial (NCT02908152). The TCM Fuzheng Huayu formula was tested in several clinical trials for its antifibrotic activity in viral-induced hepatic fibrosis (NCT00854087, NCT00540397, NCT00543426). The TCM was prescribed to a group of patients while placebo was given as control. The corresponding liver function parameters were measured within different timepoints. However, none of them were shown with promising results. Another trial is using the Fuzheng Huayu tablet with the current approved antiviral drug Entecavir and is currently in the phase 4 clinical trial (NCT02241590). A pilot study using *Yo Jyo Hen Shi Ko*, an herbal-based compound to treat nonalcohol steatohepatitis was performed in a randomized, double-blinded placebo-controlled manner (Chande et al., 2006). All eight patients in the treatment group had a significant decrease in ALT level during the fourth and eighth weeks of intervention, and the level was returned to normal after removing the treatment. Only pilot clinical studies are in progress, and there is still a long way to get an herbal compound approved by the FDA for therapies of liver fibrosis.

There are also some challenges encountered that must be overcome before the extensive clinical use of herbal medicine on the treatment of hepatic fibrosis. One is the possible toxicity issue of the herbs in patients with liver diseases. There are still very limited researches or randomized clinical trial data on the testing of Chinese medicine, especially pure compounds isolated from herbs, and make the progression of the application difficult. Due to the complex nature of the action of herbal medicine on the human body, it is not easy to assess the risk-to-benefit ratio before novel drug development. The pharmaceutical industries are reluctant to carry out related research before extensive scientific evidence is reported. The patients' benefits are also of a great concern. However, we are positive that these problems and obstacles could be overcome in the coming future and better therapeutic approaches will be developed.

In conclusion, as discussed in the context of the present review, there are some examples of novel bioactive compounds isolated or identified from natural plants or herbal medicines, such as salvianolic acids, oxymatrine, curcumin, tetrandrine, and more, possessing different levels of antifibrosis activity as shown mainly in animal experiments. The TGFβ/SMAD signaling pathway was identified as the most common drug targets for the compounds *via* network pharmacological strategy. There is sensational possibility of passing through one of them into human clinical trials for the development of derivative drugs. Before that, the exact underlying molecular mechanism must be systematically identified, and the best and useful chemical properties would be kept while improving it with modern derivatives and adjuvants if necessary. This will be foreseeable as a perfect example of the integration of traditional Chinese and modern Western medicine.

AUTHOR CONTRIBUTIONS

YF and NW designed the study and prepared the manuscript. Y-TC retrieved data and drafted the manuscript. HT and SL revised and comments the manuscript. All authors confirmed the final manuscript.

FUNDING

REFERENCES

Aggarwal, B. B. (2010). "Targeting Inflammation-Induced Obesity and Metabolic Diseases by Curcumin and Other Nutraceuticals," in *Annual Review of Nutrition*, vol. 30 Ed. R. J. Cousins (Palo Alto: Annual Reviews), 173–199.

Ahmad, A., and Ahmad, R. (2014). Resveratrol mitigate structural changes and hepatic stellate cell activation in N′-nitrosodimethylamine-induced liver fibrosis via restraining oxidative damage. *Chem. Biol. Interact.* 221, 1–12. doi: 10.1016/j.cbi.2014.07.007

Aleffi, S., Petrai, I., Bertolani, C., Parola, M., Colombatto, S., Novo, E., et al. (2005). Upregulation of proinflammatory and proangiogenic cytokines by leptin in human hepatic stellate cells. *Hepatology* 42 (6), 1339–1348. doi: 10.1002/hep.20965

Anan, A., Baskin-Bey, E. S., Bronk, S. F., Werneburg, N. W., Shah, V. H., and Gores, G. J. (2006). Proteasome inhibition induces hepatic stellate cell apoptosis. *Hepatology* 43 (2), 335–344. doi: 10.1002/hep.21036

Anand, P., Kunnumakkara, A. B., Newman, R. A., and Aggarwal, B. B. (2007). Bioavailability of curcumin: Problems and promises. *Mol. Pharmaceut.* 4 (6), 807–818. doi: 10.1021/mp700113r

Ankoma-Sey, V., Wang, Y., and Dai, Z. H. (2000). Hypoxic stimulation of vascular endothelial growth factor expression in activated rat hepatic stellate cells. *Hepatology* 31 (1), 141–148. doi: 10.1002/hep.510310122

Asrani, S. K., Devarbhavi, H., Eaton, J., and Kamath, P. S. (2019). Burden of liver diseases in the world. *J. Hepatol.* 70 (1), 151–171. doi: 10.1016/j.jhep.2018.09.014

Bagheriya, M., Nobili, V., Blesso, C. N., and Sahebkar, A. (2018). Medicinal plants and bioactive natural compounds in the treatment of non-alcoholic fatty liver disease: A clinical review. *Pharmacol. Res.* 130, 213–240. doi: 10.1016/j.phrs.2017.12.020

Bansal, R., Prakash, J., Post, E., Beljaars, L., Schuppan, D., and Poelstra, K. (2011). Novel Engineered Targeted Interferon-gamma Blocks Hepatic Fibrogenesis in Mice. *Hepatology* 54 (2), 586–596. doi: 10.1002/hep.24395

Bassiouny, A. R., Zaky, A., Fawky, F., and Kandeel, K. M. (2011). Alteration of AP-endonuclease1 expression in curcumin-treated fibrotic rats. *Ann. Hepatol.* 10 (4), 516–530. doi: 10.1016/s1665-2681(19)31521-2

Bataller, R., Nicolas, J. M., Gines, P., Gorbig, M. N., Garcia-Ramallo, E., Lario, S., et al. (1998). Contraction of human hepatic stellate cells activated in culture: a role for voltage-operated calcium channels. *J. Hepatol.* 29 (3), 398–408. doi: 10.1016/s0168-8278(98)80057-3

Bedossa, P., Houglum, K., Trautwein, C., Holstege, A., and Chojkier, M. (1994). Stimulation of collagen α1(I) gene expression is associated with lipid peroxidation in hepatocellular injury: A link to tissue fibrosis? *Hepatology* 19 (5), 1262–1271. doi: 10.1002/hep.1840190527

Bhagya, N., and Chandrashekar, K. R. (2018). Tetrandrine and cancer - An overview on the molecular approach. *Biomed. Pharmacother.* 97, 624–632. doi: 10.1016/j.biopha.2017.10.116

Borkham-Kamphorst, E., Schaffrath, C., Van de Leur, E., Haas, U., Tihaa, L., Meurer, S. K., et al. (2014). The anti-fibrotic effects of CCN1/CYR61 in primary portal myofibroblasts are mediated through induction of reactive oxygen species resulting in cellular senescence, apoptosis and attenuated TGF-beta signaling. *Biochim. Et Biophys. Acta-Mol. Cell Res.* 1843 (5), 902–914. doi: 10.1016/j.bbamcr.2014.01.023

Breitkopf, K., Godoy, P., Ciuclan, L., Singer, M. V., and Dooley, S. (2006). TGF-beta/Smad signaling in the injured liver. *Z. Fur Gastroenterol.* 44 (1), 57–66. doi: 10.1055/s-2005-858989

Campana, L., and Iredale, J. P. (2017). Regression of Liver Fibrosis. *Semin. Liver Dis.* 37 (1), 1–10. doi: 10.1055/s-0036-1597816

Canbay, A., Higuchi, H., Bronk, S. F., Taniai, M., Sebo, T. J., and Gores, G. J. (2002). Fas enhances fibrogenesis in the bile duct ligated mouse: A link between apoptosis and fibrosis. *Gastroenterology* 123 (4), 1323–1330. doi: 10.1053/gast.2002.35953

Cayon, A., Crespo, J., Mayorga, M., Guerra, A., and Pons-Romero, F. (2006). Increased expression of Ob-Rb and its relationship with the overexpression of TGF-beta 1 and the stage of fibrosis in patients with nonalcoholic steatohepatitis. *Liver Int.* 26 (9), 1065–1071. doi: 10.1111/j.1478-3231.2006.01337.x

Chai, N. L., Fu, Q., Shi, H., Cai, C. H., Wan, J., Xu, S. P., et al. (2012). Oxymatrine liposome attenuates hepatic fibrosis via targeting hepatic stellate cells. *World J. Gastroenterol.* 18 (31), 4199–4206. doi: 10.3748/wjg.v18.i31.4199

Chande, N., Laidlaw, M., Adams, P., and Marotta, P. (2006). Yo Jyo Hen Shi Ko (YHK) improves transaminases in nonalcoholic steatohepatitis (NASH): A randomized pilot study. *Digestive Dis. Sci.* 51 (7), 1183–1189. doi: 10.1007/s10620-006-8030-y

Chen, Y. W., Li, D. G., Wu, J. X., Chen, Y. W., and Lu, H. M. (2005). Tetrandrine inhibits activation of rat hepatic stellate cells stimulated by transforming growth factor-beta in vitro via up-regulation of Smad 7. *J. Ethnopharmacol.* 100 (3), 299–305. doi: 10.1016/j.jep.2005.03.027

Chen, L., Charrier, A., Zhou, Y., Chen, R. J., Yu, B., Agarwal, K., et al. (2014a). Epigenetic Regulation of Connective Tissue Growth Factor by MicroRNA-214 Delivery in Exosomes From Mouse or Human Hepatic Stellate Cells. *Hepatology* 59 (3), 1118–1129. doi: 10.1002/hep.26768

Chen, X. P., Guo, J. J., Bao, J. L., Lu, J. J., and Wang, Y. T. (2014b). The Anticancer Properties of Salvia Miltiorrhiza Bunge (Danshen): A Systematic Review. *Med. Res. Rev.* 34 (4), 768–794. doi: 10.1002/med.21304

Chen, L., Chen, R. J., Kemper, S., Charrier, A., and Brigstock, D. R. (2015). Suppression of fibrogenic signaling in hepatic stellate cells by Twist1-dependent microRNA-214 expression: Role of exosomes in horizontal transfer of Twist1. *Am. J. Physiol. Gastrointestinal Liver Physiol.* 309 (6), G491–G499. doi: 10.1152/ajpgi.00140.2015

Cui, Y., Wang, X., Liu, Q., and Liu, P. (2002). Influences of anti-oxidation of salvianolic acid B on proliferation of rat cultured hepatic stellate cells. *World Chin. J. Digestol.* 10 (3), 317–319.

Daniyal, M., Akram, M., Zainab, R., Munir, N., Sharif, A., Shah, S. M. A., et al. (2019). Prevalence and current therapy in chronic liver disorders. *Inflammopharmacology* 27 (2), 213–231. doi: 10.1007/s10787-019-00562-z

Deng, X., Wang, R., Wu, X., Gao, Q., Han, L., Gao, X., et al. (2019). Sophora alopecuroides L.: An ethnopharmacological, phytochemical, and pharmacological review. *J. Ethnopharmacol.* 248, 112172. doi: 10.1016/j.jep.2019.112172

Du, M. L., Zhang, J., Xu, D. N., Li, W. S., Liu, J., and Liu, F. (2015). Inhibition of pro-collagen I expression by oxymatrine in hepatic stellate cells is mediated via nuclear translocation of Y-box binding protein 1. *Mol. Med. Rep.* 12 (6), 8101–8106. doi: 10.3892/mmr.2015.4428

Du, G. H., Sun, L., Zhao, R., Du, L. D., Song, J. K., Zhang, L., et al. (2016). Polyphenols: Potential source of drugs for the treatment of ischaemic heart disease. *Pharmacol. Ther.* 162, 23–34. doi: 10.1016/j.pharmthera.2016.04.008

Duffield, J. S., Forbes, S. J., Constandinou, C. M., Clay, S., Partolina, M., Vuthoori, S., et al. (2005). Selective depletion of macrophages reveals distinct, opposing roles during liver injury and repair. *J. Clin. Invest.* 115 (1), 56–65. doi: 10.1172/jci200522675

Engel, M. E., McDonnell, M. A., Law, B. K., and Moses, H. L. (1999). Interdependent SMAD and JNK signaling in transforming growth factor-beta-mediated transcription. *J. Biol. Chem.* 274 (52), 37413–37420. doi: 10.1074/jbc.274.52.37413

Friedman, S. L. (2000). Molecular regulation of hepatic fibrosis, an integrated cellular response to tissue injury. *J. Biol. Chem.* 275 (4), 2247–2250. doi: 10.1074/jbc.275.4.2247

Friedman, J. M. (2004). Modern science versus the stigma of obesity. *Nat. Med.* 10 (6), 563–569. doi: 10.1038/nm0604-563

Friedman, S. L. (2008a). Hepatic stellate cells: Protean, multifunctional, and enigmatic cells of the liver. *Physiol. Rev.* 88 (1), 125–172. doi: 10.1152/physrev.00013.2007

Friedman, S. L. (2008b). Mechanisms of hepatic fibrogenesis. *Gastroenterology* 134 (6), 1655–1669. doi: 10.1053/j.gastro.2008.03.003

Ganbold, M., Shimamoto, Y., Ferdousi, F., Tominaga, K., and Isoda, H. (2019). Antifibrotic effect of methylated quercetin derivatives on TGFβ-induced hepatic stellate cells. *Biochem. Biophysics Rep.* 20, 100678.

Garcia-Trevijano, E. R., Iraburu, M. J., Fontana, L., Dominguez-Rosales, J. A., Auster, A., Covarrubias-Pinedo, A., et al. (1999). Transforming growth factor beta(1) induces the expression of alpha 1(I) procollagen mRNA by a hydrogen peroxide-C/EBP beta-dependent mechanism in rat hepatic stellate cells. *Hepatology* 29 (3), 960–970. doi: 10.1002/hep.510290346

George, J., Wang, S. S., Sevcsik, A. M., Sanicola, M., Cate, R. L., Koteliansky, V. E., et al. (2000). Transforming growth factor-beta initiates wound repair in rat liver through induction of the EIIIA-fibronectin splice isoform. *Am. J. Pathol.* 156 (1), 115–124. doi: 10.1016/s0002-9440(10)64711-6

Greenbaum, L. E., and Wells, R. G. (2011). The role of stem cells in liver repair and fibrosis. *Int. J. Biochem. Cell Biol.* 43 (2), 222–229. doi: 10.1016/j.biocel.2009.11.006

Guo, T., Liu, Z. L., Zhao, Q., Zhao, Z. M., and Liu, C. H. (2018). A combination of astragaloside I, levistilide A and calycosin exerts anti-liver fibrosis effects in vitro and in vivo. *Acta Pharmacol. Sin.* 39 (9), 1483–1492. doi: 10.1038/aps.2017.175

Halim, C. E., Xinjing, S. L., Fan, L., Vitarbo, J. B., Arfuso, F., Tan, C. H., et al. (2019). Anti-cancer effects of oxymatrine are mediated through multiple molecular mechanism(s) in tumor models. *Pharmacol. Res.* 147, 12. doi: 10.1016/j.phrs.2019.104327

Hanafusa, H., Ninomiya-Tsuji, J., Masuyama, N., Nishita, M., Fujisawa, J., Shibuya, H., et al. (1999). Involvement of the p38 mitogen-activated protein kinase pathway in transforming growth factor-beta-induced gene expression. *J. Biol. Chem.* 274 (38), 27161–27167. doi: 10.1074/jbc.274.38.27161

Hao, H. Y., Zhang, D., Shi, J. L., Wang, Y., Chen, L., Guo, Y. Z., et al. (2016). Sorafenib induces autophagic cell death and apoptosis in hepatic stellate cell through the JNK and Akt signaling pathways. *Anti-Cancer Drugs* 27 (3), 192–203. doi: 10.1097/cad.0000000000000316

Hatcher, H., Planalp, R., Cho, J., Tortia, F. M., and Torti, S. V. (2008). Curcumin: From ancient medicine to current clinical trials. *Cell. Mol. Life Sci.* 65 (11), 1631–1652. doi: 10.1007/s00018-008-7452-4

He, X. R., Fang, J. C., Huang, L. H., Wang, J. H., and Huang, X. Q. (2015). Sophora flavescens Ait.: Traditional usage, phytochemistry and pharmacology of an important traditional Chinese medicine. *J. Ethnopharmacol.* 172, 10–29. doi: 10.1016/j.jep.2015.06.010

Hellerbrand, C., Stefanovic, B., Giordano, F., Burchardt, E. R., and Brenner, D. A. (1999). The role of TGF beta 1 in initiating hepatic stellate cell activation in vivo. *J. Hepatol.* 30 (1), 77–87. doi: 10.1016/s0168-8278(99)80010-5

Henderson, N. C., Arnold, T. D., Katamura, Y., Giacomini, M. M., Rodriguez, J. D., McCarty, J. H., et al. (2013). Targeting of alpha(v) integrin identifies a core molecular pathway that regulates fibrosis in several organs. *Nat. Med.* 19 (12), 1617–1624. doi: 10.1038/nm.3282

Heymann, F., and Tacke, F. (2016). Immunology in the liver - from homeostasis to disease. *Nat. Rev. Gastroenterol. Hepatol.* 13 (2), 88–110. doi: 10.1038/nrgastro.2015.200

Higashi, T., Friedman, S. L., and Hoshida, Y. (2017). Hepatic stellate cells as key target in liver fibrosis. *Adv. Drug Delivery Rev.* 121, 27–42. doi: 10.1016/j.addr.2017.05.007

Hinz, B., Phan, S. H., Thannickal, V. J., Galli, A., Bochaton-Piallat, M. L., and Gabbiani, G. (2007). The myofibroblast - One function, multiple origins. *Am. J. Pathol.* 170 (6), 1807–1816. doi: 10.2353/ajpath.2007.070112

Hong, M., Zhang, Y., Li, S., Tan, H. Y., Wang, N., Mu, S., et al. (2017). A Network Pharmacology-Based Study on the Hepatoprotective Effect of Fructus Schisandrae. *Mol. (Basel Switzerland)* 22 (10), 1617. doi: 10.3390/molecules22101617

Hsu, Y. C., Chiu, Y. T., Cheng, C. C., Wu, C. F., Lin, Y. L., and Huang, Y. T. (2007). Antifibrotic effects of tetrandrine on hepatic stellate cells and rats with liver fibrosis. *J. Gastroenterol. Hepatol.* 22 (1), 99–111. doi: 10.1111/j.1440-1746.2006.04361.x

Huang, G. C., and Brigstock, D. R. (2012). Regulation of hepatic stellate cells by connective tissue growth factor. *Front. Biosci. Landmark* 17, 2495–2507. doi: 10.2741/4067

Iwaisako, K., Jiang, C. Y., Zhang, M. J., Cong, M., Moore-Morris, T. J., Park, T. J., et al. (2014). Origin of myofibroblasts in the fibrotic liver in mice. *Proc. Natl. Acad. Sci. U. S. A.* 111 (32), E3297–E3305. doi: 10.1073/pnas.1400062111

James, S. L., Abate, D., Abate, K. H., Abay, S. M., Abbafati, C., Abbasi, N., et al. (2018). Global, regional, and national incidence, prevalence, and years lived with disability for 354 diseases and injuries for 195 countries and territories 1990-2017: a systematic analysis for the Global Burden of Disease Study 2017. *Lancet* 392 (10159), 1789–1858. doi: 10.1016/s0140-6736(18)32279-7

Kamada, Y., Tamura, S., Kiso, S., Matsumoto, H., Saji, Y., Yoshida, Y., et al. (2003). Enhanced carbon tetrachloride-induced liver fibrosis in mice lacking adiponectin. *Gastroenterology* 125 (6), 1796–1807. doi: 10.1053/s0016-5085(03)01509-9

Kantari-Mimoun, C., Castells, M., Klose, R., Meinecke, A. K., Lemberger, U. J., Rautou, P. E., et al. (2015). Resolution of liver fibrosis requires myeloid cell-driven sinusoidal angiogenesis. *Hepatology* 61 (6), 2042–2055. doi: 10.1002/hep.27635

Kisseleva, T., Cong, M., Paik, Y., Scholten, D., Jiang, C. Y., Benner, C., et al. (2012). Myofibroblasts revert to an inactive phenotype during regression of liver fibrosis. *Proc. Natl. Acad. Sci. U. S. A.* 109 (24), 9448–9453. doi: 10.1073/pnas.1201840109

Kong, D. S., Zhang, F., Wei, D. H., Zhu, X. J., Zhang, X. P., Chen, L., et al. (2013). Paeonol inhibits hepatic fibrogenesis via disrupting nuclear factor-B pathway in activated stellate cells: In vivo and in vitro studies. *J. Gastroenterol. Hepatol.* 28 (7), 1223–1233. doi: 10.1111/jgh.12147

Kong, Z. Y., Liu, R., and Cheng, Y. R. (2019). Artesunate alleviates liver fibrosis by regulating ferroptosis signaling pathway. *Biomed. Pharmacother.* 109, 2043–2053. doi: 10.1016/j.biopha.2018.11.030

Kostallari, E., Hirsova, P., Prasnicka, A., Verma, V. K., Yaqoob, U., Wongjarupong, N., et al. (2018). Hepatic stellate cell-derived platelet-derived growth factor receptor-alpha-enriched extracellular vesicles promote liver fibrosis in mice through SHP2. *Hepatology* 68 (1), 333–348. doi: 10.1002/hep.29803

Kuo, J. J., Wang, C. Y., Lee, T. F., Huang, Y. T., and Lin, Y. L. (2012). Paeoniae Radix Reduces PDGF-Stimulated Hepatic Stellate Cell Migration. *Planta Med.* 78 (4), 341–348. doi: 10.1055/s-0031-1280472

Lan, T., Kisseleva, T., and Brenner, D. A. (2015). Deficiency of NOX1 or NOX4 Prevents Liver Inflammation and Fibrosis in Mice through Inhibition of Hepatic Stellate Cell Activation. *PloS One* 10 (7), 19. doi: 10.1371/journal.pone.0129743

Lan, X., Zhao, J., Zhang, Y., Chen, Y., Liu, Y., and Xu, F. (2019). Oxymatrine Exerts Organ-and Tissue-Protective Effects by Regulating Inflammation, Oxidative Stress, Apoptosis, and Fibrosis: From Bench to Bedside. *Pharmacol. Res.* 151, 104541. doi: 10.1016/j.phrs.2019.104541

Lee, Y. S., and Jeong, W. I. (2012). Retinoic acids and hepatic stellate cells in liver disease. *J. Gastroenterol. Hepatol.* 27, 75–79. doi: 10.1111/j.1440-1746.2011.07007.x

Lee, S. H., Nan, J. X., and Sohn, D. H. (2001). Tetrandrine prevents tissue inhibitor of metalloproteinase-1 messenger RNA expression in rat liver fibrosis. *Pharmacol. Toxicol.* 89 (4), 214–216. doi: 10.1111/j.0901-9928.2001.890412.x

Lee, Y. A., Wallace, M. C., and Friedman, S. L. (2015). Pathobiology of Liver Fibrosis - A Translational Success Story (vol 64, pg 830, 2015). *Gut* 64 (8), 1337–1337. doi: 10.1136/gutjnl-2014-306842corr1

Levy, C., Seeff, L. D., and Lindor, K. D. (2004). Use of herbal supplements for chronic liver disease. *Clin. Gastroenterol. Hepatol.* 2 (11), 947–956. doi: 10.1016/s1542-3565(04)00455-0

Li, D. G., Wang, Z. R., and Lu, H. M. (2001). Pharmacology of tetrandrine and its therapeutic use in digestive diseases. *World J. Gastroenterol.* 7 (5), 627–629.

Li, S., Wang, L. N., Yan, X. C., Wang, Q. L., Tao, Y. Y., Li, J. X., et al. (2012). Salvianolic Acid B Attenuates Rat Hepatic Fibrosis via Downregulating Angiotensin II Signaling. *Evidence-Based Complementary Altern. Med.* 10. 1–10 doi: 10.1155/2012/160726

Li, X., Jin, Q., Wu, Y. L., Sun, P., Jiang, S., Zhang, Y., et al. (2016). Tetrandrine regulates hepatic stellate cell activation via TAK1 and NF-kappa B signaling. *Int. Immunopharmacol.* 36, 263–270. doi: 10.1016/j.intimp.2016.04.039

Li, Z. M., Xu, S. W., and Liu, P. Q. (2018). Salvia miltiorrhiza Burge (Danshen): a golden herbal medicine in cardiovascular therapeutics. *Acta Pharmacol. Sin.* 39 (5), 802–824. doi: 10.1038/aps.2017.193

Liang, B., Guo, X. L., Jin, J., Ma, Y. C., and Feng, Z. Q. (2015). Glycyrrhizic acid inhibits apoptosis and fibrosis in carbon-tetrachloride-induced rat liver injury. *World J. Gastroenterol.* 21 (17), 5271–5280. doi: 10.3748/wjg.v21.i17.5271

Lin, J. G., and Chen, A. P. (2011). Curcumin diminishes the impacts of hyperglycemia on the activation of hepatic stellate cells by suppressing membrane translocation and gene expression of glucose transporter-2. *Mol. Cell. Endocrinol.* 333 (2), 160–171. doi: 10.1016/j.mce.2010.12.028

Lin, Y. L., Lee, T. F., Huang, Y. J., and Huang, Y. T. (2006). Antiproliferative effect of salvianolic acid A on rat hepatic stellate cells. *J. Pharm. Pharmacol.* 58 (7), 933–939. doi: 10.1211/jpp.58.7.0008

Liu, P., Noirfumi, K., Mizoguchi, Y., and Morisawa, S. (1994). Effects of magnesium lithospermate B on cyclooxygenase activity in rat liver, adherent cells and enzyme's product. *Zhongguo Zhongyao Zazhi* 19 (2), 110–128.

Liu, Q.-Y., Li, B., Gang, J.-M., Karpinski, E., and Pang, P. (1995). Tetrandrine, a Ca++ antagonist: effects and mechanisms of action in vascular smooth muscle cells. *J. Pharmacol. Exp. Ther.* 273 (1), 32–39.

Liu, C. H., Liu, P., Hu, Y. Y., Xu, L. M., Tan, Y. Z., Wang, Z. N., et al. (2000). Effects of salvianolic acid-A on rat hepatic stellate cell proliferation and collagen production in culture. *Acta Pharmacolog. Sin.* 21 (8), 721–726.

Liu, P., Hu, Y. Y., Liu, C. H., Liu, C., and Zhu, D. Y. (2001). Effects of salviainolic acid A (SA-A) on liver injury: SA-A action on hepatic peroxidation. *Liver* 21 (6), 384–390. doi: 10.1034/j.1600-0676.2001.210604.x

Liu, P., Hu, Y. Y., Liu, C., Zhu, D. Y., Xue, H. M., Xu, Z. Q., et al. (2002a). Clinical observation of salvianolic acid B in treatment of liver fibrosis in chronic hepatitis B. *World J. Gastroenterol.* 8 (4), 679–685. doi: 10.3748/wjg.v8.i4.679

Liu, P., Liu, C. H., Wang, H. N., Hu, Y. Y., and Liu, C. (2002b). Effect of salvianolic acid B on collagen production and mitogen-activated protein kinase activity in rat hepatic stellate cells. *Acta Pharmacol. Sin.* 23 (8), 733–738.

Liu, M., Li, Y. G., Zhang, F., Yang, L., Chou, G. X., Wang, Z. T., et al. (2007). Chromatographic fingerprinting analysis of Danshen root (Salvia miltiorrhiza Radix et Rhizoma) and its preparations using high performance liquid chromatography with diode array detection and electrospray mass spectrometry (HPLC-DAD-ESI/MS). *J. Separation Sci.* 30 (14), 2256–2267. doi: 10.1002/jssc.200700149

Liu, X., Yang, Y., Zhang, X. X., Xu, S. X., He, S. F., Huang, W. J., et al. (2010). Compound Astragalus and Salvia miltiorrhiza extract inhibits cell invasion by modulating transforming growth factor-beta/Smad in HepG2 cell. *J. Gastroenterol. Hepatol.* 25 (2), 420–426. doi: 10.1111/j.1440-1746.2009.05981.x

Liu, Y. X., Hu, Y. Y., E, Q. K., Zuo, J., Yang, L., and Liu, W. (2017). Salvianolic acid B inhibits mitochondrial dysfunction by up-regulating mortalin. *Sci. Rep.* 7, 13. doi: 10.1038/srep43097

Liu, H. L., Lv, J., Zhao, Z. M., Xiong, A. M., Tan, Y., Glenn, J. S., et al. (2019a). Fuzhenghuayu Decoction ameliorates hepatic fibrosis by attenuating experimental sinusoidal capillarization and liver angiogenesis. *Sci. Rep.* 9, 11. doi: 10.1038/s41598-019-54663-4

Liu, W., Li, Z. X., Sun, Z. L., Xu, Y. B., Wang, S. C., Hu, Y. Y., et al. (2019b). The components data of fuzheng huayu extracts, cordyceps sinensis mycelia polysaccharide, gypenosides and amygdalin. *Data Brief* 25, 7. doi: 10.1016/j.dib.2019.104087

Loterszatjn, S., Julien, B., Teixeira-Clerc, F., Grenard, P., and Mallat, A. (2005). Hepatic fibrosis: Molecular mechanisms and drug targets. *Annu. Rev. Pharmacol. Toxicol.* 45, 605–628. doi: 10.1146/annurev.pharmtox.45.120403.095906

Lu, Y., Wang, W. J., Song, Y. Z., and Liang, Z. Q. (2014). The protective mechanism of schisandrin A in D-galactosamine-induced acute liver injury through activation of autophagy. *Pharmaceut. Biol.* 52 (10), 1302–1307. doi: 10.3109/13880209.2014.890232

Lujambio, A., Akkari, L., Simon, J., Grace, D., Tschaharganeh, D. F., Bolden, J. E., et al. (2013). Non-Cell-Autonomous Tumor Suppression by p53. *Cell* 153 (2), 449–460. doi: 10.1016/j.cell.2013.03.020

Luk, J. M., Wang, X. L., Liu, P., Wong, K. F., Chan, K. L., Tong, Y., et al. (2007). Traditional Chinese herbal medicines for treatment of liver fibrosis and cancer: from laboratory discovery to clinical evaluation. *Liver Int.* 27 (7), 879–890. doi: 10.1111/j.1478-3231.2007.01527.x

Lv, J., Bai, R. D., Wang, L., Gao, J. F., and Zhang, H. (2018). Artesunate may inhibit liver fibrosis via the FAK/Akt/beta-catenin pathway in LX-2 cells. *BMC Pharmacol. Toxicol.* 19, 7. doi: 10.1186/s40360-018-0255-9

Lyons, J. F., Wilhelm, S., Hibner, B., and Bollag, G. (2001). Discovery of a novel Raf kinase inhibitor. *Endocrine-Related Cancer* 8 (3), 219–225. doi: 10.1677/erc.0.0080219

Ma, L. K., Tang, L. L., and Yi, Q. (2019). Salvianolic Acids: Potential Source of Natural Drugs for the Treatment of Fibrosis Disease and Cancer. *Front. Pharmacol.* 10, 13. doi: 10.3389/fphar.2019.00097

Marra, F., Valente, A. J., Pinzani, M., and Abboud, H. E. (1993). Cultured Human Liver Fat-Storing Cells Produce Monocyte Chemotactic Protein-1 - Regulation By Proinflammatory Cytokines. *J. Clin. Invest.* 92 (4), 1674–1680. doi: 10.1172/jci116753

Marti-Rodrigo, A., Alegre, F., Moragrega, A. B., Garcia-Garcia, F., Marti-Rodrigo, P., Fernandez-Iglesias, A., et al. (2019). Rilpivirine attenuates liver fibrosis through selective STAT1-mediated apoptosis in hepatic stellate cells. *Gut.* 69 (5), 920–932. doi: 10.1136/gutjnl-2019-318372

Meng, X. M., Nikolic-Paterson, D. J., and Lan, H. Y. (2014). Inflammatory processes in renal fibrosis. *Nat. Rev. Nephrol.* 10 (9), 493–503. doi: 10.1038/nrneph.2014.114

Meng, X. M., Nikolic-Paterson, D. J., and Lan, H. Y. (2016). TGF-beta: the master regulator of fibrosis. *Nat. Rev. Nephrol.* 12 (6), 325–338. doi: 10.1038/nrneph.2016.48

Miao, H., Zhang, Y., Huang, Z. L., Lu, B., and Ji, L. L. (2019). Lonicera japonica Attenuates Carbon Tetrachloride-Induced Liver Fibrosis in Mice: Molecular Mechanisms of Action. *Am. J. Chin. Med.* 47 (2), 351–367. doi: 10.1142/s0192415x19500174

Miyamae, Y., Nishito, Y., Nakai, N., Nagumo, Y., Usui, T., Masuda, S., et al. (2016). Tetrandrine induces lipid accumulation through blockade of autophagy in a hepatic stellate cell line. *Biochem. Biophys. Res. Commun.* 477 (1), 40–46. doi: 10.1016/j.bbrc.2016.06.018

Moro, T., Shimoyama, Y., Kushida, M., Hong, Y. Y., Nakao, S., Higashiyama, R., et al. (2008). Glycyrrhizin and its metabolite inhibit Smad3-mediated type I collagen gene transcription and suppress experimental murine liver fibrosis. *Life Sci.* 83 (15-16), 531–539. doi: 10.1016/j.lfs.2008.07.023

Morsy, M. A., Abdalla, A. M., Mahmoud, A. M., Abdelwahab, S. A., and Mahmoud, M. E. (2012). Protective effects of curcumin, alpha-lipoic acid, and N-acetylcysteine against carbon tetrachloride-induced liver fibrosis in rats. *J. Physiol. Biochem.* 68 (1), 29–35. doi: 10.1007/s13105-011-0116-0

Mu, Y. P., Zhang, X., Li, X. W., Fan, W. W., Chen, J. M., Zhang, H., et al. (2015). Astragaloside prevents BDL-induced liver fibrosis through inhibition of notch signaling activation. *J. Ethnopharmacol.* 169, 200–209. doi: 10.1016/j.jep.2015.04.015

Murphy, F. R., Issa, R., Zhou, X. Y., Ratnarajah, S., Nagase, H., Arthur, M. J. P., et al. (2002). Inhibition of apoptosis of activated hepatic stellate cells by tissue inhibitor of metalloproteinase-1 is mediated via effects on matrix metalloproteinase inhibition - Implications for reversibility of liver fibrosis. *J. Biol. Chem.* 277 (13), 11069–11076. doi: 10.1074/jbc.M111490200

Omenetti, A., Choi, S., Michelotti, G., and Diehl, A. M. (2011). Hedgehog signaling in the liver. *J. Hepatol.* 54 (2), 366–373. doi: 10.1016/j.jhep.2010.10.003

Panebianco, C., Oben, J. A., Vinciguerra, M., and Pazienza, V. (2017). Senescence in hepatic stellate cells as a mechanism of liver fibrosis reversal: a putative synergy between retinoic acid and PPAR-gamma signalings. *Clin. Exp. Med.* 17 (3), 269–280. doi: 10.1007/s10238-016-0438-x

Park, P. H., Nan, J. X., Park, E. J., Kang, H. C., Kim, J. Y., Ko, G., et al. (2000). Effect of tetrandrine on experimental hepatic fibrosis induced by bile duct ligation and scission in rats. *Pharmacol. Toxicol.* 87 (6), 261–268. doi: 10.1034/j.1600-0773.2000.pto870604.x

Paumgartner, G., and Beuers, U. (2002). Ursodeoxycholic acid in cholestatic liver disease: mechanisms of action and therapeutic use revisited. *Hepatol. (Baltimore Md.)* 36 (3), 525–531. doi: 10.1053/jhep.2002.36088

Pellicoro, A., Ramachandran, P., Iredale, J. P., and Fallowfield, J. A. (2014). Liver fibrosis and repair: immune regulation of wound healing in a solid organ. *Nat. Rev. Immunol.* 14 (3), 181–194. doi: 10.1038/nri3623

Pinzani, M. (2002). PDGF and signal transduction in hepatic stellate cells. *Front. Biosci.* 7, D1720–D1726. doi: 10.2741/pinzani

Pradere, J. P., Kluwe, J., De Minicis, S., Jiao, J. J., Gwak, G. Y., Dapito, D. H., et al. (2013). Hepatic Macrophages But Not Dendritic Cells Contribute to Liver Fibrosis by Promoting the Survival of Activated Hepatic Stellate Cells in Mice. *Hepatology* 58 (4), 1461–1473. doi: 10.1002/hep.26429

Qiang, G. F., Yang, X. Y., Xuan, Q., Shi, L. L., Zhang, H. G., Chen, B. N., et al. (2014). Salvianolic Acid A Prevents the Pathological Progression of Hepatic Fibrosis in High-Fat Diet-Fed and Streptozotocin-Induced Diabetic Rats. *Am. J. Chin. Med.* 42 (5), 1183–1198. doi: 10.1142/s0192415x14500748

Radaeva, S., Sun, R., Jaruga, B., Nguyen, V. T., Tian, Z. G., and Gao, B. (2006). Natural killer cells ameliorate liver fibrosis by killing activated stellate cells in NKG2D-dependent and tumor necrosis factor-related apoptosis-inducing ligand-dependent manners. *Gastroenterology* 130 (2), 435–452. doi: 10.1053/j.gastro.2005.10.055

Reyes-Gordillo, K., Segovia, J., Shibayama, M., Tsutsumi, V., Vergara, P., Moreno, M. G., et al. (2008). Curcumin prevents and reverses cirrhosis induced by bile duct obstruction or CCl(4) in rats: role of TGF-beta modulation and oxidative stress. *Fundam. Clin. Pharmacol.* 22 (4), 417–427. doi: 10.1111/j.1472-8206.2008.00611.x

Rockey, D. C. (2013). Translating an Understanding of the Pathogenesis of Hepatic Fibrosis to Novel Therapies. *Clin. Gastroenterol. Hepatol.* 11 (3), 224–22+. doi: 10.1016/j.cgh.2013.01.005

Rojkind, M., Giambrone, M. A., and Biempica, L. (1979). Collagen Types In Normal And Cirrhotic Liver. *Gastroenterology* 76 (4), 710–719.

Saxena, N. K., and Anania, F. A. (2015). Adipocytokines and hepatic fibrosis. *Trends Endocrinol. Metab.* 26 (3), 153–161. doi: 10.1016/j.tem.2015.01.002

Schuppan, D., Ashfaq-Khan, M., Yang, A. T., and Kim, Y. O. (2018). Liver fibrosis: Direct antifibrotic agents and targeted therapies. *Matrix Biol.* 68-69, 435–451. doi: 10.1016/j.matbio.2018.04.006

Seki, E., and Schwabe, R. F. (2015). Hepatic Inflammation and Fibrosis: Functional Links and Key Pathways. *Hepatology* 61 (3), 1066–1079. doi: 10.1002/hep.27332

Shen, H., Sheng, L., Chen, Z., Jiang, L., Su, H. R., Yin, L., et al. (2014). Mouse Hepatocyte Overexpression of NF-kappa B-Inducing Kinase (NIK) Triggers Fatal Macrophage-Dependent Liver Injury and Fibrosis. *Hepatology* 60 (6), 2065–2076. doi: 10.1002/hep.27348

Shen, X., Peng, Y., and Li, H. M. (2017). The Injury-Related Activation of Hedgehog Signaling Pathway Modulates the Repair-Associated Inflammation in Liver Fibrosis. *Front. Immunol.* 8, 11. doi: 10.3389/fimmu.2017.01450

Shi, G. F., and Li, Q. (2005). Effects of oxymatrine on experimental hepatic fibrosis and its mechanism in vivo. *World J. Gastroenterol.* 11 (2), 268–271. doi: 10.3748/wjg.v11.i2.268

Shi, M. L., Zhu, J. H., Wang, R., Chen, X., Mi, L. Z., Walz, T., et al. (2011). Latent TGF-beta structure and activation. *Nature* 474 (7351), 343–U370. doi: 10.1038/nature10152

Song, G. Q., Pacher, M., Balakrishnan, A., Yuan, Q. G., Tsay, H. C., Yang, D. K., et al. (2016). Direct Reprogramming of Hepatic Myofibroblasts into Hepatocytes In Vivo Attenuates Liver Fibrosis. *Cell Stem Cell* 18 (6), 797–808. doi: 10.1016/j.stem.2016.01.010

Song, L. Y., Ma, Y. T., Fang, W. J., He, Y., Wu, J. L., Zuo, S. R., et al. (2019). Inhibitory effects of oxymatrine on hepatic stellate cells activation through TGF-/miR-195/Smad signaling pathway. *BMC Complementary Altern. Med.* 19, 9. doi: 10.1186/s12906-019-2560-2

Stefanovic, A., Kotur-Stevuljevic, J., Spasic, S., Bogavac-Stanojevic, N., and Bujisic, N. (2008). The influence of obesity on the oxidative stress status and the concentration of leptin in type 2 diabetes mellitus patients. *Diabetes Res. Clin. Pract.* 79 (1), 156–163. doi: 10.1016/j.diabres.2007.07.019

Sunami, Y., Leithauser, F., Gul, S., Fiedler, K., Guldiken, N., Espenlaub, S., et al. (2012). Hepatic activation of IKK/NF kappa B signaling induces liver fibrosis via macrophage-mediated chronic inflammation. *Hepatology* 56 (3), 1117–1128. doi: 10.1002/hep.25711

Tang, Y. C., and Chen, A. P. (2010). Curcumin Protects Hepatic Stellate Cells against Leptin-Induced Activation in Vitro by Accumulating Intracellular Lipids. *Endocrinology* 151 (9), 4168–4177. doi: 10.1210/en.2010-0191

Tang, Y. C., Zheng, S. Z., and Chen, A. P. (2009). Curcumin Eliminates Leptin's Effects on Hepatic Stellate Cell Activation via Interrupting Leptin Signaling. *Endocrinology* 150 (7), 3011–3020. doi: 10.1210/en.2008-1601

Teratani, T., Tomita, K., Suzuki, T., Oshikawa, T., Yokoyama, H., Shimamura, K., et al. (2012). A High-Cholesterol Diet Exacerbates Liver Fibrosis in Mice via Accumulation of Free Cholesterol in Hepatic Stellate Cells. *Gastroenterology* 142 (1), 152–U331. doi: 10.1053/j.gastro.2011.09.049

Tomasek, J. J., Gabbiani, G., Hinz, B., Chaponnier, C., and Brown, R. A. (2002). Myofibroblasts and mechano-regulation of connective tissue remodelling. *Nat. Rev. Mol. Cell Biol.* 3 (5), 349–363. doi: 10.1038/nrm809

Tomita, K., Teratani, T., Suzuki, T., Shimizu, M., Sato, H., Narimatsu, K., et al. (2014). Acyl-CoA:cholesterol acyltransferase 1 mediates liver fibrosis by regulating free cholesterol accumulation in hepatic stellate cells. *J. Hepatol.* 61 (1), 98–106. doi: 10.1016/j.jhep.2014.03.018

Troeger, J. S., Mederacke, I., Gwak, G. Y., Dapito, D. H., Mu, X. R., Hsu, C. C., et al. (2012). Deactivation of Hepatic Stellate Cells During Liver Fibrosis Resolution in Mice. *Gastroenterology* 143 (4), 1073–107+. doi: 10.1053/j.gastro.2012.06.036

Tu, C. T., Yao, Q. Y., Xu, B. L., Wang, J. Y., Zhou, C. H., and Zhang, S. C. (2012). Protective effects of curcumin against hepatic fibrosis induced by carbon tetrachloride: Modulation of high-mobility group box 1, Toll-like receptor 4 and 2 expression. *Food Chem. Toxicol.* 50 (9), 3343–3351. doi: 10.1016/j.fct.2012.05.050

Van Rooyen, D. M., Gan, L. T., Yeh, M. M., Haigh, W. G., Larter, C. Z., Ioannou, G., et al. (2013). Pharmacological cholesterol lowering reverses fibrotic NASH in obese, diabetic mice with metabolic syndrome. *J. Hepatol.* 59 (1), 144–152. doi: 10.1016/j.jhep.2013.02.024

Wake, K. (1971). Sternzellen in liver - perisinusoidal cells with special reference to storage of vitamin-A. *Am. J. Anat.* 132 (4), 429–. doi: 10.1002/aja.1001320404

Wang, Y. P., Zhao, W., Xue, R., Zhou, Z. X., Liu, F., Han, Y. X., et al. (2011). Oxymatrine inhibits hepatitis B infection with an advantage of overcoming drug-resistance. *Antiviral Res.* 89 (3), 227–231. doi: 10.1016/j.antiviral.2011.01.005

Wang, R., Yu, X. Y., Guo, Z. Y., Wang, Y. J., Wu, Y., and Yuan, Y. F. (2012). Inhibitory effects of salvianolic acid B on CCl4-induced hepatic fibrosis through regulating NF-kappa B/I kappa B alpha signaling. *J. Ethnopharmacol.* 144 (3), 592–598. doi: 10.1016/j.jep.2012.09.048

Wang, Z. C., Xiang, M. P., Li, Q. Q., Zhang, F. Y., Wei, D. Y., Wen, Z. X., et al. (2017). Astragaloside Alleviates Hepatic Fibrosis Function via PAR2 Signaling Pathway in Diabetic Rats. *Cell. Physiol. Biochem.* 41 (3), 1156–1166. doi: 10.1159/000464122

Watanabe, S., Yaginuma, R., Ikejima, K., and Miyazaki, A. (2008). Liver diseases and metabolic syndrome. *J. Gastroenterol.* 43 (7), 509–518. doi: 10.1007/s00535-008-2193-6

Wei, R. D., Liu, H. D., Chen, R., Sheng, Y. J., and Liu, T. (2019). Astragaloside IV combating liver cirrhosis through the PI3K/Akt/mTOR signaling pathway. *Exp. Ther. Med.* 17 (1), 393–397. doi: 10.3892/etm.2018.6966

Wong, L., Yamasaki, G., Johnson, R. J., and Friedman, S. L. (1994). Induction of beta-platelet-derived growth-factor receptor in rat hepatic lipocytes during cellular activation in-vivo and in culture. *J. Clin. Invest.* 94 (4), 1563–1569. doi: 10.1172/jci117497

Wu, X. N., and Wang, G. J. (2004). Experimental studies of oxymatrine and its mechanisms of action in hepatitis B and C viral infections. *Chin. J. Digest. Dis.* 5 (1), 12–16.

Wu, C. S., Piao, X. X., Piao, D. M., Jin, Y. R., and Li, C. H. (2005). Treatment of pig serum-induced rat liver fibrosis with Boschniakia rossica, oxymatrine and interferon-alpha. *World J. Gastroenterol.* 11 (1), 122–126. doi: 10.3748/wjg.v11.i1.122

Wu, X. L., Zeng, W. Z., Jiang, M. D., Qin, J. P., and Xu, H. (2008). Effect of Oxymatrine on the TGFbeta-Smad signaling pathway in rats with CCl4-induced hepatic fibrosis. *World J. Gastroenterol.* 14 (13), 2100–2105. doi: 10.3748/wjg.14.2100

Wu, S. J., Tam, K. W., Tsai, Y. H., Chang, C. C., and Chao, J. C. J. (2010). Curcumin and Saikosaponin A Inhibit Chemical-Induced Liver Inflammation and Fibrosis in Rats. *Am. J. Chin. Med.* 38 (1), 99–111. doi: 10.1142/s0192415x10007695

Wu, L. W., Zhang, Q. H., Mo, W. H., Feng, J., Li, S. N., Li, J. J., et al. (2017). Quercetin prevents hepatic fibrosis by inhibiting hepatic stellate cell activation and reducing autophagy via the TGF-beta 1/Smads and PI3K/Akt pathways. *Sci. Rep.* 7, 13. doi: 10.1038/s41598-017-09673-5

Wu, C., Chen, W., Ding, H., Li, D., Wen, G., Zhang, C., et al. (2019a). Salvianolic acid B exerts anti-liver fibrosis effects via inhibition of MAPK-mediated phospho-Smad2/3 at linker regions in vivo and in vitro. *Life Sci.* 239, 116881. doi: 10.1016/j.lfs.2019.116881

Wu, S. W., Liu, L. C., Yang, S., Kuang, G., Yin, X. R., Wang, Y. Y., et al. (2019b). Paeonol alleviates CCl4-induced liver fibrosis through suppression of hepatic stellate cells activation via inhibiting the TGF-beta/Smad3 signaling. *Immunopharmacol. Immunotoxicol.* 41 (3), 438–445. doi: 10.1080/08923973.2019.1613427

Xu, Y. J., Liu, W. D., Fang, B. W., Gao, S. N., and Yan, J. (2014). Artesunate ameliorates hepatic fibrosis induced by bovine serum albumin in rats through regulating matrix metalloproteinases. *Eur. J. Pharmacol.* 744, 1–9. doi: 10.1016/j.ejphar.2014.09.035

Yan, J., Tung, H. C., Li, S., Niu, Y., Garbacz, W. G., Lu, P., et al. (2019). Aryl Hydrocarbon Receptor Signaling Prevents Activation of Hepatic Stellate Cells and Liver Fibrogenesis in Mice. *Gastroenterology* 157793-806 (3), e714. doi: 10.1053/j.gastro.2019.05.066

Yang, S. M., Chen, J. G., Guo, Z., Xu, X. M., Wang, L. P., Pei, X. F., et al. (2003). Triptolide inhibits the growth and metastasis of solid tumors. *Mol. Cancer Ther.* 2 (1), 65–72.

Yang, L., Kwon, J., Popov, Y., Gajdos, G. B., Ordog, T., Brekken, R. A., et al. (2014). Vascular Endothelial Growth Factor Promotes Fibrosis Resolution and Repair in Mice. *Gastroenterology* 146 (5), 1339–133+. doi: 10.1053/j.gastro.2014.01.061

Yang, T., Liu, S., Zheng, T. H., Tao, Y. Y., and Liu, C. H. (2015). Comparative pharmacokinetics and tissue distribution profiles of lignan components in normal and hepatic fibrosis rats after oral administration of Fuzheng Huayu recipe. *J. Ethnopharmacol.* 166, 305–312. doi: 10.1016/j.jep.2015.03.024

Yao, Q. Y., Xu, B. L., Wang, J. Y., Liu, H. C., Zhang, S. C., and Tu, C. T. (2012). Inhibition by curcumin of multiple sites of the transforming growth factor-beta1 signalling pathway ameliorates the progression of liver fibrosis induced by carbon tetrachloride in rats. *BMC Complementary Altern. Med.* 12, 11. doi: 10.1186/1472-6882-12-156

Yin, M. F., Lian, L. H., Piao, D. M., and Nan, L. X. (2007). Tetrandrine stimulates the apoptosis of hepatic stellate cells and ameliorates development of fibrosis in a thioacetamide rat model. *World J. Gastroenterol.* 13 (8), 1214–1220. doi: 10.3748/wjg.v13.i8.1214

Yuan, X. X., Gong, Z. Q., Wang, B. Y., Guo, X. Y., Yang, L., Li, D. D., et al. (2018). Astragaloside Inhibits Hepatic Fibrosis by Modulation of TGF-beta 1/Smad Signaling Pathway. *Evid. Based Complementary Altern. Med.* 13, 1–13. doi: 10.1155/2018/3231647

Zhang, X. P., Zhang, F., Zhang, Z. L., Ma, J., Kong, D. S., Ni, G. X., et al. (2012). Acupuncture combined with curcumin disrupts platelet-derived growth factor beta receptor/extracellular signal-regulated kinase signalling and stimulates extracellular matrix degradation in carbon tetrachloride-induced hepatic fibrosis in rats. *Acupuncture Med.* 30 (4), 324–330. doi: 10.1136/acupmed-2012-010167

Zhang, J., Wang, M., Zhang, Z. W., Luo, Z. G., Liu, F., and Liu, J. (2015). Celecoxib derivative OSU-03012 inhibits the proliferation and activation of hepatic stellate cells by inducing cell senescence. *Mol. Med. Rep.* 11 (4), 3021–3026. doi: 10.3892/mmr.2014.3048

Zhang, D. Q., Sun, P., Jin, Q., Li, X., Zhang, Y., Zhang, Y. J., et al. (2016). Resveratrol Regulates Activated Hepatic Stellate Cells by Modulating NF-kappa B and the PI3K/Akt Signaling Pathway. *J. Food Sci.* 81 (1), H240–H245. doi: 10.1111/1750-3841.13157

Zhang, F., Hao, M., Jin, H. H., Yao, Z., Lian, N. Q., Wu, L., et al. (2017). Canonical hedgehog signalling regulates hepatic stellate cell-mediated angiogenesis in liver fibrosis. *Br. J. Pharmacol.* 174 (5), 409–423. doi: 10.1111/bph.13701

Zhang, F., Lu, S., He, J. L., Jin, H. H., Wang, F. X., Wu, L., et al. (2018). Ligand Activation of PPAR gamma by Ligustrazine Suppresses Pericyte Functions of Hepatic Stellate Cells via SMRT-Mediated Transrepression of HIF-1 alpha. *Theranostics* 8 (3), 610–626. doi: 10.7150/thno.22237

Zhao, H. W., Zhang, Z. F., Chai, X., Li, G. Q., Cui, H. R., Wang, H. B., et al. (2016). Oxymatrine attenuates CCl4-induced hepatic fibrosis via modulation of TLR4-dependent inflammatory and TGF-beta 1 signaling pathways. *Int. Immunopharmacol.* 36, 249–255. doi: 10.1016/j.intimp.2016.04.040

Zhou, L. M., Zuo, Z., and Chow, M. S. S. (2005). Danshen: An overview of its chemistry, pharmacology, pharmacokinetics, and clinical use. *J. Clin. Pharmacol.* 45 (12), 1345–1359. doi: 10.1177/0091270005282630

Zhou, Y. P., Tong, X., Ren, S., Wang, X. L., Chen, J. M., Mu, Y. P., et al. (2016). Synergistic anti-liver fibrosis actions of total astragalus saponins and glycyrrhizic acid via TGF-beta 1/Smads signaling pathway modulation. *J. Ethnopharmacol.* 190, 83–90. doi: 10.1016/j.jep.2016.06.011

Zhu, J., Wang, R. W., Xu, T., Zhang, S., Zhao, Y., Li, Z. L., et al. (2018). Salvianolic Acid A Attenuates Endoplasmic Reticulum Stress and Protects Against Cholestasis-Induced Liver Fibrosis via the SIRT1/HSF1 Pathway. *Front. Pharmacol.* 9, 12. doi: 10.3389/fphar.2018.01277

Zoubek, M. E., Trautwein, C., and Strnad, P. (2017). Reversal of liver fibrosis: From fiction to reality. *Best Pract. Res. Clin. Gastroenterol.* 31 (2), 129–141. doi: 10.1016/j.bpg.2017.04.005

Zuo, L. Q., Zhu, Y. Q., Hu, L. L., Liu, Y. Y., Wang, Y. H., Hu, Y. M., et al. (2019). PI3-kinase/Akt pathway-regulated membrane transportation of acid-sensing ion channel 1a/Calcium ion influx/endoplasmic reticulum stress activation on PDGF-induced HSC Activation. *J. Cell. Mol. Med.* 23 (6), 3940–3950. doi: 10.1111/jcmm.14275

Herbal Medicine in the Treatment of Non-Alcoholic Fatty Liver Diseases-Efficacy, Action Mechanism, and Clinical Application

Yu Xu, Wei Guo, Cheng Zhang, Feiyu Chen, Hor Yue Tan, Sha Li, Ning Wang and Yibin Feng*

School of Chinese Medicine, Li Ka Shing Faculty of Medicine, The University of Hong Kong, Hong Kong, Hong Kong

Non-alcoholic fatty liver disease (NAFLD) is a common chronic liver disease with high prevalence in the developed countries. NAFLD has been considered as one of the leading causes of cryptogenic cirrhosis and chronic liver disease. The individuals with obesity, insulin resistance and diabetes mellitus, hyperlipidaemia, and hypertension cardiovascular disease have a high risk to develop NAFLD. The related critical pathological events are associated with the development of NAFLD including insulin resistance, lipid metabolism dysfunction, oxidative stress, inflammation, apoptosis, and fibrosis. The development of NAFLD range from simple steatosis to non-alcoholic steatohepatitis (NASH). Hepatic steatosis is characterized by fat accumulation, which represents the early stage of NAFLD. Then, inflammation triggered by steatosis drives early NAFLD progression into NASH. Therefore, the amelioration of steatosis and inflammation is essential for NAFLD therapy. The herbal medicine have taken great effects on the improvement of steatosis and inflammation for treating NAFLD. It has been found out that these effects involved the multiple mechanisms underlying lipid metabolism and inflammation. In this review, we pay particular attention on herbal medicine treatment and make summary about the research of herbal medicine, including herb formula, herb extract and naturals compound on NAFLD. We make details about their protective effects, the mechanism of action involved in the amelioration steatosis and inflammation for NAFLD therapy as well as the clinical application.

Keywords: non-alcoholic fatty liver disease, herb medicine, fatty acids, steatosis, inflammation

BACKGROUND

Non-alcoholic fatty liver disease (NAFLD) is a common chronic liver disease, and it is associated high metabolic risk of health problem such as dyslipidemia, insulin resistance, obesity and type II diabetic disease. In parallel with the prevalence of metabolic syndrome, NAFLD comprised of a spectrum of fatty liver that encompasses three typical pathological subtypes including liver steatosis, non-alcoholic steatohepatitis (NASH) and fibrosis. The least severe stage is simple liver steatosis induced by a largely build-up of fat in liver cell (Clapper et al., 2013). The progression of steatosis

can be slowed or reversed by lifestyle modification and physical exercise. Otherwise, Non-Alcoholic Steatohepatitis (NASH), a severer form characterized by fat build-up, varying degrees of inflammation and ballooning degeneration of liver cells could be developed. More seriously, NASH continues to develop liver fibrosis and cirrhosis when the long term of liver injury leads to irreversible scarring of the liver (Bertot and Adams, 2019). As the late stage of fibrosis, Cirrhosis could irreversibly disrupt liver function and finally increased the risk of hepatocellular carcinoma development in patients.

Currently, there is no pharmacological agent that is being officially approved in NAFLD therapy. For one thing, the recommended intervention in NAFLD is lifestyle modification including energy intake restriction and physical activity enhancement. Lifestyle modification can reduce body weight and a moderate decrease of body weight could improve hepatic pathologic syndrome and decrease hepatic fat accumulation. For the other thing, some pharmacological interventions classified as antioxidants, insulin sensitizers and lipid-lowering drugs have been applied. For example, the antioxidant reagent such as Vitamin E has been suggested to treat non-diabetic patients with NASH as evidenced by a recent clinical trial (Sanyal et al., 2010); The use of lipid-lowering agents such as statin has been shown to reduce the risk of mortality or liver transplant in NAFLD patients (German et al., 2019); As sodium-glucose co-transporter 2 (SGLT2) inhibitors, Dapagliflozin and Canagliflozin could decrease hepatic lipid accumulation and significantly improve liver function (Arase et al., 2019). However, Most of these pharmacological agents are still at various stages of new drug development. For example, the natural farnesoid X receptor (FXR) agonist (obeticholic acid) and dual peroxisome proliferator-activated receptor α-δ (PPARα-δ) agonist (elafibranor), as well as glucagon-like peptide-1 antagonists were still investigated in phase IIA or IIB clinical trials (Sarwar et al., 2018). Meanwhile, several anti-diabetic medications such as pioglitazone (Brunner et al., 2019), metformin and thiazolidinediones have been applied for the pharmacologic management of NAFLD in clinical practice due to their ability to reverse insulin resistance. Although the advances in conventional medicine, herbal medicine are easily accessible and do not require artificial synthesis, thus herbal medicine seems highly attractive for the effective management of NAFLD. Herbal medicine, defined as whole medicinal plants and unpurified plant extracts with medical properties, has been traditionally used in different countries of the world to improve liver conditions. A special term Traditional Chinese Medicine (TCM) was particularly given to refer to herbal medicines that have been applied since the ancient time of China, though TCM might also include medicines with origins of animals and minerals. TCM includes various forms of herbal medicine that has been proved to take effects on treatment of NAFLD. In recent years, progress in drug development of NAFLD has been found major advances with herbal medicines which are regarded as abundant sources of natural bioactive chemicals that improve hepatic functions. In this paper, we have provided an overview of herbal medicine (including herbal formula, crude extract, and pure bioactive compound form medicinal plants) approaches which have demonstrated their ability to counteract NAFLD in human patients and animal models.

THE EFFECTIVE MANAGEMENT OF HERBAL MEDICINE ON NAFLD

Herbal Medicine Improve Hepatic Lipid Metabolism

Overload lipid is the main initial reason that triggers hepatic steatosis. Excessive free fatty acids (FFAs) delivery from the adipose to the liver and result in the intrahepatic pool expansion of FFAs in the form of triglycerides. Fat accumulation evokes hepatic lipo-toxicity, which induces liver cells to release pro-inflammatory cytokines, trigger oxidative stress and hepatic stellate cell activation, ultimately lead to hepatic inflammatory injury. Improvement of fatty acid metabolism is an effective measure for in treating NAFLD, and the efficacy of herbal medicine targeting fatty acid metabolism has examined in both preclinical and clinical research of NAFLD. Firstly, The beneficial effects of herbal medicine on patients with liver dyslipidemia can improve lipid metabolic parameters such as decreasing the levels of triglycerides (TG), total cholesterol (TC) and low-density lipoprotein (LDL-C), alanine aminotransferase (ALT), aspartate aminotransferase (AST), as well as increasing the production of high-density lipoprotein (HDL-C). The interference of herbal medicine on dyslipidemia has been proved to be related to the regulation of fatty acid production or consumption. It has been found out that many herbal medicine (including herbal formula, crude extract and pure bioactive compound form medicinal plants) depressed the hepatic lipogenesis *via* reducing the expression of the key transcriptional factors and lipogenic enzymes such as Sterol Regulatory Element Binding Protein 1c (SREBP-1c), Peroxisome-Proliferator-Activated Receptor γ (PPAR-γ), Acetyl-CoA Carboxylase (ACC), Fatty Acid Synthase (FAS) and SCD1. For example, Gypenosides (extracted from *Gynostemma pentaphyllum*) (Li et al., 2017a), the chloroform fraction of *Cyclocarya paliurus* (Lin et al., 2016), total alkaloids extracted from *Rubus aleaefolius* Poir. (Li et al., 2014b), *Lonicera caerulea* L. extract (Park et al., 2019) and the crude extract from the peels of *Citrus aurantium* L. *(Rutaceae)* (Han et al., 2019) effectively attenuates high fat diet (HFD) induced triglyceride accumulation *via* reducing the high production of SREBP-1c, PPAR-γ, FAS, and ACC.

AMPK Pathway Involves in Herbal Medicine Modulation of Hepatic Lipogenesis and β-Oxidation

Adenosine monophosphate-activated Protein Kinase (AMPK) is a key energy sensor of intracellular energy metabolism, which could cause the reduction of cellular triglyceride and cholesterol production. The activation of AMPK phosphorylation could attenuate free fatty acid-regulated *de novo* lipogenesis genes

and hepatic lipid accumulation. AMPK phosphorylation have been mentioned frequently in hepatic lipid metabolism to be activated in response to many herbal medicine such as BaiHuJia RenShen Decoction (Liu et al., 2015a), Qushi Huayu Decoction (Feng et al., 2013), *Lonicera caerulea* L. extract (Park et al., 2019), nobiletin (a polymethoxylated flavonoid derived from citrus fruits) (Yuk et al., 2018), ginsenoside Rb1 (Shen et al., 2013), betulinic acid (Kim et al., 2019b), and berberine (Zhu et al., 2019). Sophocarpine (derived from foxtail-like sophora herb and seed) influences adipocytokine production *via* AMPK signaling in NASH rats (Song et al., 2013), and salvianolic acid B (isolated from *Salvia miltiorrhiza* Bge.) reduces dyslipidemia and hyperglycemia *via* AMPK activation (Huang et al., 2016). It has been reported that some herbal medicine such as *Lonicera caerulea* L. extract (Park et al., 2019) and methanolic extract of *Alisma orientalis* (Hong et al., 2006) increases fatty acid β-oxidation *via* activating lipid antioxidant enzymes such as Carnitine Palmitoyltransferase-1 (CPT-1) and lessening peroxidation. This beneficial effects of herbal medicine on β-oxidation involved the activation of AMPK/PPAR-α and its downstream pathway. For example, the methanolic extract of *Alisma orientalis* (Hong et al., 2006), the ethanol extract of *Leonurus japonicus* Houtt (Lee et al., 2017), *Lycopus lucidus* Turcz. ex Benth (Lee et al., 2019) and Hugan Qingzhi formula (Yin et al., 2014) increases hepatic β-oxidation *via* upregulation of the phosphorylated AMPK and PPARα expression (Cao et al., 2016; Lee et al., 2017). AMPK activation in hepatic lipid β-oxidation also requires the activity of silent information regulator 1 (SIRT1), which interferes with PPARs activation. Silibinin shows its potential natural antioxidant effects on restoration of NAD$^+$ levels *via* AMPK/SIRT1 pathway. Licochalcone A (isolated from *Glycyrrhiza uralensis*) significantly induces the AMPK/SIRT-1 pathway to inhibit hepatic lipogenesis synthesis and improve β-oxidation (Liou et al., 2019). Dioscin mediated SIRT1/AMPK signal pathway and LXRα action (Cheng et al., 2018) to modulate the expression of SREBP-1c, CPT-1, FAS, SCD, FoxO1, and ATGL(Yao et al., 2018). Ursolic acid has been treated as a novel Liver X receptor α (LXRα) antagonist and Ursolic acid stimulated AMPK phosphorylation to inhibit steroid receptor coactivator-1 (SRC-1) recruitment and promote small heterodimer partner-interacting leucine zipper protein to the SREBP-1c promoter region (Lin et al., 2018). Thus, AMPK action activated by herbal medicine involves in *de novo* lipid synthesis associated with the suppression of SREBP-1c, FAS, ACC, and SCD-1expression, and increase β-oxidation defense that improves hepatic fatty acids efflux *via* the modulation of CPT-1 and PPARα production.

Oxidative Stress Action Involves in Herbal Medicine Modulation of Lipid Metabolism

Oxidative stress reflected an imbalance between the reactive species production and antioxidant defense, which can lead to liver damage in the progression of NAFLD. The lipid metabolic disorder influences the production of reactive oxygen species (ROS), specifically, fatty acid β-oxidation seems to generate more ROS in NAFLD. The lipid lowering effect of herbal medicine shows its

correlation with anti-oxidative stress action. For example, Bangpungtongseong-san attenuates the transcriptional response of oxidative phosphorylation (OXPHOS) in NAFLD liver (Choi J. Y. et al., 2019). Korea red ginseng shows anti-oxidant activity to improve hepatic lipid profiles in fatty rat (Hong et al., 2013). The ethyl acetate extract of *Aristolochia manshuriensis* Kom suppresses hepatic oxidative stress *via* improving the SOD, GR and GPx enzymes, subsequently increases hepatic lipid peroxidation of CYPE21 to promote hepatic lipolysis (Kwak et al., 2016). LiGanShiLiuBaWei San can significantly promote fatty acid oxidation *via* activation of PPARα and PPARβ, and reduce oxidative stress *via* the inhibition of iNOS production (Jiang et al., 2015). The down-regulation of hepatic HO-1, NF-E2-related factor 2 (Nrf2), and SOD2 as well as up-regulation KEAP1 were detected in the NAFLD models, and the expression of these oxidative stress markers can be all reversed by Dioscin (Liu et al., 2015b). The Nrf2 activation mediated by herbal medicine can improve NAFLD *via* inhibiting oxidative stress pathway. It has been reported that scutellarin (a flavonoid glycoside), swertiamarin (a secoiridoid glycoside) (Yang Y. et al., 2019) and gastrodin (isolated from *Gastrodia elata* Bl) enhance Nrf2-mediated antioxidant system *via* activating the mRNA and protein levels of PPARγ and its coactivator-1α, HO-1, GST, and NQO1 expressions (Ahmad et al., 2019), thus ameliorate NAFLD. Isochlorogenic acid B [extracted from *Laggera alata* (Asteraceae)] shows its protective effects on fibrosis in NASH by Nrf2 signaling pathway, and reverse the downregulation of miR-122 level and upregulation of hepatic HIF-1α expression to inhibit multiple profibrogenic factors (COL1α1, MCP-1, LOX, TGF-β1, and TIMP-1) (Liu et al., 2019c).

Mitochondria Function Involves in Herbal Modulation of Hepatic Lipid Metabolism

Mitochondria plays a specialized role in lipid metabolism and could contact lipid droplets *via* Mitochondria oxidation in liver. Mitochondria dysfunction contribute to the progression of NAFLD since it influences hepatic lipid metabolism, promote the generation of ROS, and lipid peroxidation. Previous research has proved that herbal medicine such as *cyclocarya paliurus*, *sida rhomboidea*.roxb, *punica granatum* L., resveratrol, mangosteen pericarp, epigallocatechin gallate, and shexiang baoxin pill, were shown to be effective on mitochondrial dysfunction during treating the NAFLD (Yang X. et al., 2019). More detail, Shizukaol D (extracted from *Chloranthus japonicas*) improved mitochondrial dysfunction, leading to hepatic AMPK-dependent lipid content reduction (Hu et al., 2013). Polygonati Rhizoma and *Polygonatum kingianum* promote mitochondrial β-oxidation *via* increasing the CPT-1 activity to block long-chain fatty acid enter mitochondria, and improve mitochondrial function *via* inhibiting HFD-induced excessive production of ROS and malondialdehyde (MDA) (Yang X. et al., 2019). Nobiletin (Qi et al., 2018) and diosgenin (Fang et al., 2019) could lead to the reduction of ROS level and restoration of mitochondrial membrane potential. This mitochondrial interference suppressed lipid peroxidation that involved the increase of vital scavenger levels of glutathione peroxidase (GSH-Px) and superoxide dismutase (SOD). Dioscin (isolated

from *Polygonatum Zanlanscianense* Pamp) has been proved to increase the expression of SOD, GSH and GSH-Px, and decrease the production of iNOS, MDA and NO. Puerarin (extracted from Radix *Pueraria lobate*) evoked the activation of PARP-1/PI3K/AKT signaling that facilitated the transcripts (Acox1, MCAD, Cpt1 and Cox5a) in β-oxidation and reversed the decreased level of mitochondrial respiration complex I and II activities, further improved the fatty acid metabolism (Wang S. et al., 2019).
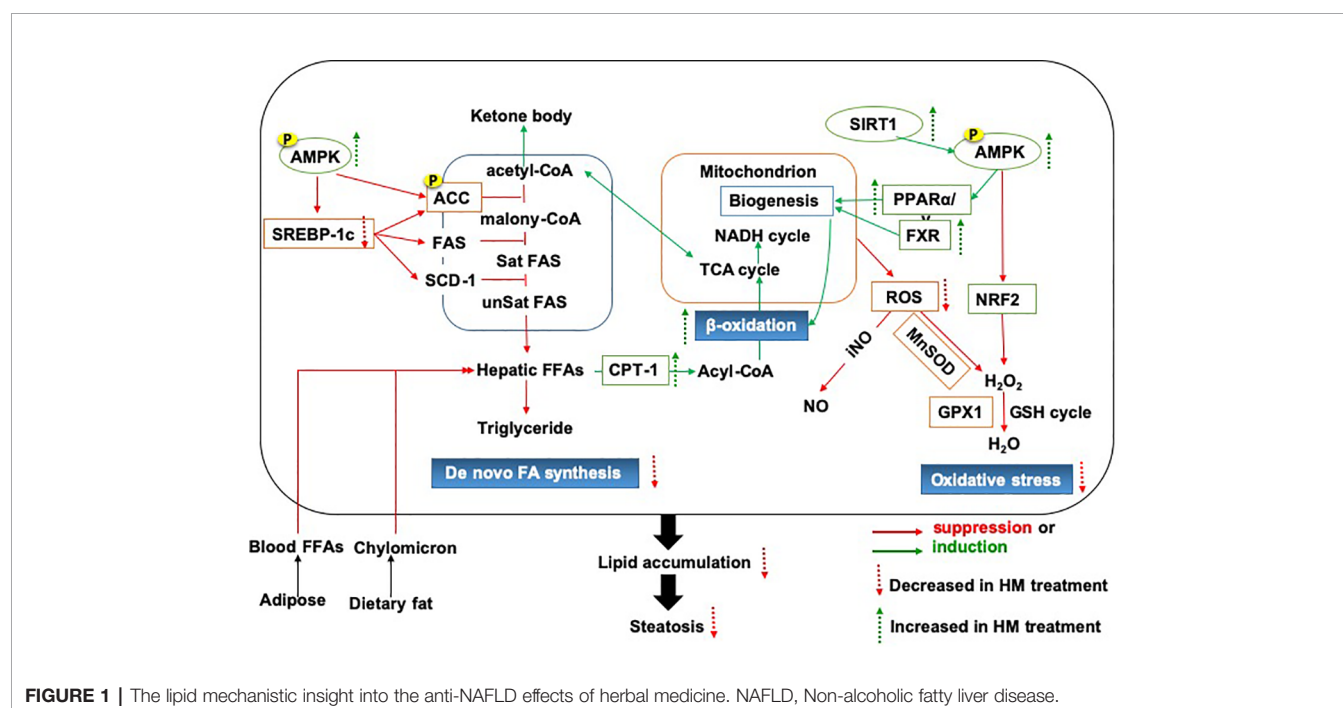
Bile Acid Synthesis Involves in Herbal Medicine Modulation of Lipid Metabolism

Bile acids are synthesized in the liver and act as biological detergent to metabolite lipids and cholesterol into the bile. Gypenosides (extracted from *Gynostemma pentaphyllum*) (Li et al., 2017a), palmatine and jatrorrhizine (extracted from Coptidis Rhizoma) promote bile acid synthesis to prevent NAFLD, which involved the expression of cholesterol 7α-hydroxylase A1 (CYP7A1). Punicalagin and pomegranate ellagic acid (isolated from *Punica granatum* L.) activate the CYP7A1/PPARγ signaling to promote hepatic diversion of cholesterol into bile acid (Ji et al., 2019). *Celastrus orbiculatus* Thunb. accelerated the hepatic cholesterol excretion in guinea pigs through suppressing oxidative stress *via* upregulation of the mRNA abundance of 3-hydroxy-3-methyl-glutaryl-CoA reductase (HMG-CoAR) and CYP7A1 (Zhang et al., 2013). Glycyrrhizin (extracted from Glycyrrhizae Radix Et Rhizoma) modulated serum bile acid metabolism in MCD diet-fed mice by restoring inflammation-mediated hepatic farnesoid X receptor (FXR) inhibition (Yan et al., 2018). The modulation of herbal medicine on lipid and cholesterol absorption and transport involved the bile acid regulation and shows its beneficial effects on treating NAFLD.

Above all, we provided an important lipid mechanistic insight into the anti-NAFLD effects of herbal medicine, which was shown in **Figure 1**. The commonly used herbal medicine inhibited fatty acid or diet-induced lipogenesis *via* SREBP-1c pathway and promoted the lipolysis focusing on fatty acid β-oxidation, which involved oxidative stress and mitochondrial function. The underlying mechanism of action might be achieved through the modulation of AMPK signaling pathway (Ding et al., 2019).

Herbal Medicine Ameliorates the Hepatic Inflammation

Hepatic inflammation promotes lipid deposition and redistribution from adipose to liver and drives liver inflammatory injury. Hepatic inflammation triggers the development of NAFLD from hepatic steatosis to steatohepatitis and fibrosis (Marra and Lotersztajn, 2013). Amelioration of heaptic inflammation is vital for NAFLD therapy. It has been indicated that herbal medicine has exerted the protective effects against the progression from hepatic steatosis to steatohepatitis and the underlying mechanism have been proved to be involved in inhibiting the inflammatory signaling pathway as shown in **Figure 2**, thereby regulating dyslipidemia and improving liver function in NAFLD. Many herbal medicine (including herbal formula, crude extract and pure bioactive compound form medicinal plants) possessed anti-inflammatory properties for slowing down the NAFLD progression, such as Sinai san dection (Zhang et al., 2005), Hugan Qingzhi tablet (Tang et al., 2015), betulinic acid (Kim et al., 2019b), *Alisma orientalis* (Choi E. et al., 2019), gastrodin (Ahmad et al., 2019), the peel extract of *Citrus aurantium L.* (Rutaceae) (Han et al., 2019) and swertiamarin (Yang Y. et al.,
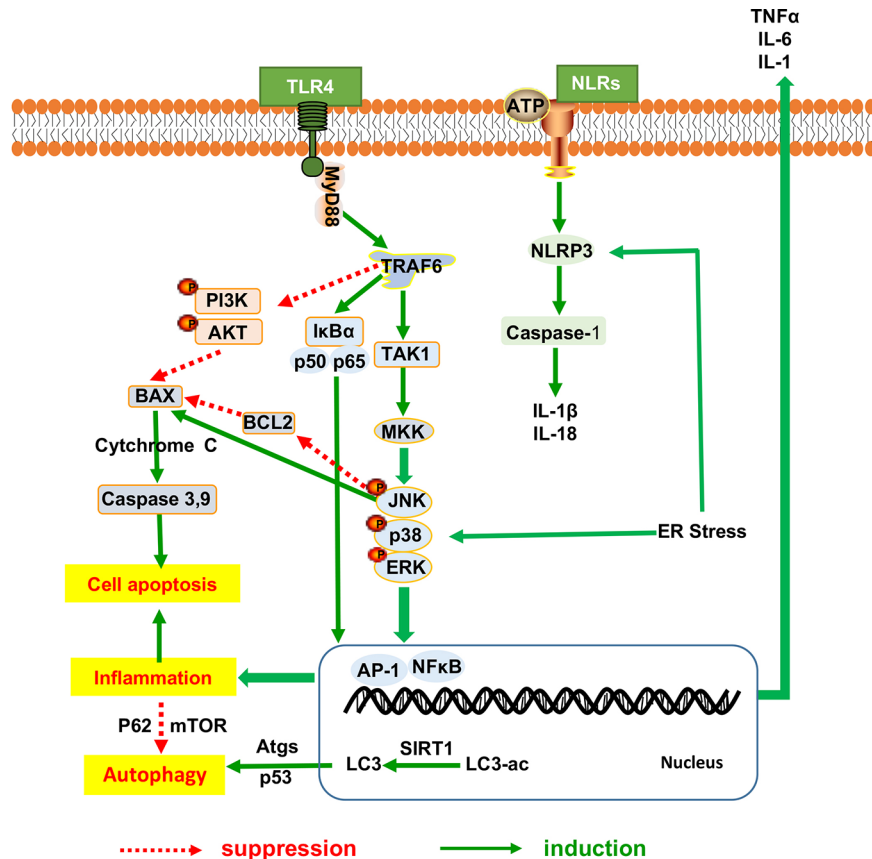

FIGURE 1 | The lipid mechanistic insight into the anti-NAFLD effects of herbal medicine. NAFLD, Non-alcoholic fatty liver disease.

FIGURE 2 | The inflammatory mechanistic insight into the anti-NAFLD effects of herbal medicine. NAFLD, Non-alcoholic fatty liver disease.

2019), and all of these medicine reduces the expression levels of hepatic inflammatory cytokines (TNFα, IL-6, and IL1β). Baicalin (extracted from *Scutellaria baicalensis* Georgi) (Zhang J. et al., 2018) and aqueous extract of *Salvia miltiorrhiza* Bunge (Hong et al., 2017) show the anti-inflammatory action, further improve liver fibrosis by inhibition of α-SMA, Col1A1, and TGF-β1 production.

NF-κB Pathway Involves in Herbal Medicine Modulation of Hepatic Inflammation

We found out that the NF-κB signaling mentioned frequently in the anti-inflammatory response of herbal medicine in treating NAFLD. Jianpi Huoxue formula (Feng et al., 2019), baicalin (Zhang J. et al., 2018) and *Lycium barbarum* polysaccharides showed ameliorative effects on hepatic inflammatory response involved with the reduction in Monocyte Chemotactic Protein-1 (MCP-1) expression, macrophage influx and hepatocyte apoptosis, partially owing to its power to suppress nuclear factor-κB (NF-κB) activation and the autophagic process of cleaved caspase-3 (Xiao et al., 2014; Zhai et al., 2015). Moreover, as a necessary prerequisite for triggering other inflammasome, the NF-κB signaling medicated the regulation of other inflammasome including NLRP3, the toll-like receptors

and apoptosis mediators, all of which has been proved to be involved in the anti-inflammatory research of herbal medicine for NAFLD. Firstly, the palmitate acid-induced hepatocytes steatosis involved the activation of NLRP3 inflammasome and increased secretion of IL-1β and IL-18. And the NOD-, LRR- and pyrin domain-containing protein 3 (NLRP3) activation can be reversed by nobiletin and andrographolide (extracted from *Andrographis paniculata* (burm.f.)Nees) (Cabrera et al., 2017), as described by the downregulation of Caspase1, IL1β and IL18 expression *via* a NF-κB-dependent mechanism (Askari et al., 2014). Secondly, TLRs initiated signaling by binding to Myeloid Differentiation primary-response protein 88 (MyD88) triggers recruitment of TRAF6, TAK1, and MKK, which thereby activated the downstream signaling pathway of the extracellular signal-regulated kinase (ERK), p38MAPK, and c-jun N-terminal kinase (JNK). This activity leads to NF-κB nuclear translocation and the induction of gene transcription mediated by proinflammatory cytokines and chemokines. Toll-like receptors (TLRs) signaling pathways have been proved to participate in the anti-inflammatory response of herbal medicine in treating NAFLD. BuShenKangShuai tablet improved liver adiponectin resistance *via* inhibiting TLR4/NF-κB p65 signaling pathway, followed by the inhibition of TNF-α, IL-1β,

MCP-1 and Vascular Vell Adhesion Molecule-1(VCAM-1), as well as the promotion of interleukin-10 and adiponectin production (Pang et al., 2019). Sparstolonin B (derived from *Sparganium stoloniferum* Buch.-Ham.) attenuated liver fibrosis through antagonizing TLR4 induced TGF-β signaling. Sparstolonin B augmented the hepatic TGFβ pseudo-receptor expression in mice, leading to downregulation of extracellular matrix deposition and hepatic stellate cell activation (Dattaroy et al., 2018). Moreover, Sparstolonin B obviously inhibited Kupffer cell activities as evidenced by the decrease in MCP-1 and CD68 levels with concomitant suppression of macrophage infiltration *via* blocking NADPH oxidase-driven TLR4 trafficking to the lipid rafts in NASH (Dattaroy et al., 2016). Dioscin rehabilitated inflammation (Liu et al., 2015b) that was associated with the decreased expression levels of p50, p65, and IκBα *via* regulation of MyD88-dependent TLR4 signaling pathway (Zhang E. et al., 2016; Yang L. et al., 2019). Garlic-derived S-allylmercaptocysteine mitigated NAFLD-induced inflammation *via* the restoration of the phosphorylated FFAs-dependent mitogen-activated protein kinases (MAPKs) and diminishment of the AP-1 and NF-κB activation (Xiao et al., 2013a). Berberine prevent NASH-derived hepatocellular carcinoma in mice *via* suppressing the phosphorylation of p38MAPK, ERK and COX2 expression (Luo et al., 2019).

Apoptosis Signaling Involves in Herbal Medicine Modulation of Hepatic Inflammation

The interference with the TLR mediated inflammatory response has proved to be involved into intracellular apoptosis signaling. These have been supported by the evidence that total aralosides from *aralia elata* (Miq) seem protected mice against HFD-induced cellular apoptosis, as suggested by TUNEL staining, and ameliorated NASH by inhibiting the NF-κB/IRE1α/JNK/IκB activation in ApoE$^{-/-}$ mice (Luo et al., 2015); *Lycium barbarum* polysaccharides partially modulated hepatocyte apoptosis process *via* NF-κB/MAPK pathways, which has been proved to be related to the biological activity of l-arabinose and β-carotene in polysaccharides (Xiao et al., 2014). Resveratrol and Sparstolonin B exerted a promising role on the modulation of cell proliferation and apoptosis *via* TLR4/phosphatidylinositol 3-kinase- (PI3K-)/AKT signaling pathway (Dattaroy et al., 2016). *Psoralea corylifolia* L. inhibited NF-κB activation in the portal area to alleviate inflammatory cell infiltration and fibroplasia, further enhanced PI3K/Akt signaling to reduce hepatic superoxide anion expression, and NADPH oxidase activity as well as p47(phox) protein level and PKCα activation (Zhou et al., 2017). Since the apoptosis signaling involves in herbal medicine modulation of hepatic inflammation, herbal medicine reduces the apoptotic cytokines such as caspases and Bcl-2 family proteins expression in the progression of hepatic inflammation. For instance, dioscin increased Bcl-2 production and blocked the activation of Bak, Caspase-3/9, FasL, Fas, p53 proteins *via* reducing IRF9 production against apoptosis (Liu et al., 2015b; Shen et al., 2015; Zhang W. et al., 2016). Polygonati Rhizoma could notably remedy mitochondrial apoptosis and alleviate HFD-induced NAFLD *via* increasing the expression levels of

caspase 3, caspase 9, and Bax, while decreasing the Bcl-2 level in hepatocytes and cytchrome C in mitochondria (Yang et al., 2019b). Furthermore, herbal medicine showed an effective role in inhibition of apoptotic cytokines, partially involved in the JNK-induced hepatocyte apoptosis for the treatment of NAFLD/NASH. Jianpi Huoxue formula (mainly consists of Atractylodis macrocephalae Rhizoma, Salvia miltiorrhizae Radix Et Rhizoma, Paeonia Radix Alba, Alismatis Rhizoma, and Schisandrae Chinensis Fructus) may have beneficial effects on MCD induced liver inflammation and apoptosis *via* the inhibition of the JNK phosphorylation and the activation of caspase 3 and 7 proteins (Feng et al., 2019). The ethyl acetate extract of *Aristolochia manshuriensis* Kom inhibited hepatic apoptosis *via* the suppression of ERK1/2 and JNK1/2 phosphorylation (Kwak et al., 2016); Silibinin (a flavonolignan from milk thistle) ameliorated various symptoms of NASH by activating death domain-like apoptosis regulator (CFLAR)-JNK pathway, and thereby modulated its downstream target genes to promote the fatty acid β-oxidation (PPARα, SREBP-1C, and PNPLA3), anti-oxidase action (CAT, HO-1, and GSH-Px) and inhibition of pro-oxidase action (NRF2, CYP4A, and CYP2E1) to ameliorate oxidative stress, as well as inflammatory response (Wang et al., 2017; Liu et al., 2018; Liu et al., 2019d). Therefore, activated hepatic apoptosis exerted a wide range of biological actions involved facilitating inflammation with oxidative stress modulation. And combined with the beneficial effects on liver steatosis, herbal medicine also relived the reliable growth in indicators of hepatocyte cytokine proinflammatory status, apoptosis, and fibrosis in the development of steatohepatitis.

Autophagy Involves in Herbal Medicine Modulation of Hepatic Inflammation

The lysosomal-mediated degradation process of autophagy is beneficial for removing the damaged cellular proteins and organelles, including mitochondria, peroxisomes, and endoplasmic reticulum (ER), thus the autophagy activation takes metabolic intermediates necessary for protein metabolism. And herbal medicine induced autophagy had been considered as an anti-inflammatory strategy to show the obvious effects on reducing the NAFLD progression. Resveratrol promoted the autophagy pathway to restore liver injury, which was linked with NF-κB activation (Ji et al., 2015); *Lycium barbarum* polysaccharides showed ameliorative effects on autophagic proteins (LC3II and Atg5), and deceased autophagic negative modulators (p62 and p-mTOR) *via* the NF-κB/MAPK pathways (Xiao et al., 2014). Herbal medicine rehabilitated inflammation, reduced apoptosis and enhanced autophagy through both extrinsic and intrinsic apoptotic pathways, thereby counteracting the effects of NAFLD. For example, Dioscin inhibits collagen synthesis through modulating the expressions of autophagic flux (P62 LC-I LC-II) (Xu et al., 2017). Administration of Akebia saponin D (extracts from *Akebia quinata*) resulted in the upregulation of autophagic flux (e.g., decreased P62 accumulation and increased the level of LC3-II expression) in the liver of ob/ob mice (Gong et al., 2016); Glycycoumarin (a coumarin compound isolated

from Rhizoma Glycyrrhizae) inhibited hepatocyte lipo-apoptosis through reactivation of impaired autophagy and inactivation of GSK-3. In line with autophagy activation, mitochondrial apoptotic activation, and ER stress-mediated JNK pathway were also blocked by glycycoumarin (Zhang A. et al., 2016); Nobiletin (Yuk et al., 2018), ginsenoside Rb2 (extracted from *Panax Ginseng* C.A.Mey) and Tangshen formula (Wang Y. et al., 2019), could reverse the repression of autophagic pathways in AMPK-SIRT1 dependent manner (Huang et al., 2017). The AMPK/SIRT1 pathway mediated the activation of fork head box transcription factors that increased Atg proteins production, additionally, SIRT1 could combine with Atgs (Atg7 and Atg8) to form a molecular complex to deacetylate the core autophagy machinery. Resveratrol (a pharmacological SIRT1 activator) significantly prevented hepatocyte ballooning and steatosis, along with the changed levels of LC3-II, Beclin 1, and P62, as well as ER stress (Ding et al., 2017). It could be confirmed that resveratrol potentiated SIRT1 secretion and its deacetylase activity, which decreased p53 and increased autophagy. Further studies demonstrated that the effect of resveratrol on hepatic steatosis was achieved partially *via* the cAMP-PRKA-AMPK-SIRT1 autophagy pathway (Zhang et al., 2015). Meanwhile, mTOR, another famous negative autophagic regulator, was decreased after some herbal treatments, such as Garlic-derived S-allylmercaptocysteine enhanced the levels of autophagic markers expression in the liver, with a concomitant decrease the mTOR activity (Xiao et al., 2013b).

Herbal Medicine Triggers Other Pathways in NAFLD

Endoplasmic Reticulum (ER) Stress

ER stress involved the increase of JNK and caspase-12 expression serves a primary role in the procession of NAFLD and pathogenesis to NASH. The pharmacological activation of FXR induced by betulinic acid alleviated the hepatic ER stress-mediated hepatic steatosis (Gu et al., 2019). The farnesoid X receptor (FXR) activation suppresses the expression of ER stress markers (PERK, EIF2α and ATF4) and CHOP signaling, thereby reducing hepatocellular ER stress. Betulinic acid could serve as an FXR agonist that effectively attenuates the pathogenesis of HFD and MCD induced NAFLD, and *Alisma orientalis* could restore the hepatocellular ER homeostasis by stimulating the FXR activation, particularly, Alisol A 24 (B 23)-acetate accounts for this action (Choi E. et al., 2019).

Insulin Signaling Pathway

Insulin-induced insulin receptor phosphorylation recruited the insulin receptor substrate-1 (IRS-1) and subsequently activated phosphoinositide 3-kinase (PI3K)/AKT pathway, leading to the activation of PKA and SGK-3β and ultimately encouraging glycogen and lipolysis synthesis, and subduing gluconeogenesis and lipogenesis (Kwon et al., 2018). Naringenin (Mulvihill et al., 2009), Ginsenoside Rb1(Yu et al., 2015) and *Leonurus japonicus* Houtt extract (Lee et al., 2017) prevented hyperinsulinemia, leading to the correction of NAFLD associated metabolic disturbance that was linked to glucose utilization and insulin

sensitivity (Lee et al., 2017). It has been found that nobiletin (Kim et al., 2017) and ursolic acid (Li et al., 2014a) ameliorated insulin resistance and takes effects on amplifying glucose uptake through IRS-1/AKT stimulation (Yuk et al., 2018) in treatment of NAFLD; Jwa Kum Whan ameliorated insulin resistance and reduced hepatic triglyceride and cholesterol accumulation *via* significant triggered the phosphorylation of IRS-1 and PI3K (Lim et al., 2019). The potential underlying mechanism of Erchen decoction for the treatment of obesity, hyperlipidemia and fatty liver is to increase the CDKAL1 production, improve islet cell function and insulin level (Gao et al., 2015). A related study indicated that yangonin increased insulin sensitivity *via* increasing the expression of phosphorylated IRS-1 and IRS-2 (Dong et al., 2019).

Herbal Medicine Induced Gut Microbiota Alteration in NAFLD

It has been suggested that gut dysbiosis in patients have different shift in the development of NAFLD. There is an inverse association between the presence of NAFLD and the abundance of *Bacteroidetes* in gut microbiota, indicating that the intestine microbiota takes a vital role in the progression of NAFLD (Mouzaki et al., 2013). Therefore, the modulation of intestine microbiota has become a potential therapeutic strategy for the treatment of NAFLD. Supplementation of prebiotic, probiotic compounds, or herbal medicine (Porras et al., 2017), have taken a modulatory effect on the intestine microbiota. Lingguizhugan decoction reduced hepatic steatosis and improved glycemic control through the modulation of gut microbiota (Liu et al., 2019b). Microbiome analysis revealed that herbal formula shenling baizhu powder promoted the relative percentage of short-chain fatty acid-producing microbiota, such as *Bifidobacterium* and *Anaerostipes* (Zhang Y. et al., 2018). Mechanistic studies found that herbal formula such as shenling baizhu powder alleviated hepatic steatosis and repaired colon mucosa *via* decreasing the expression level of endotoxin and inflammatory mediators (TNF-α, IL-1β) *via* the TLR4 pathway (Zhang Y. et al., 2018b). Diammonium glycyrrhizinate is a medicinal form of glycyrrhizic acid and has been proved to modify gut microbiota composition to decrease the intestinal low-grade inflammation and restore intestinal barrier function in NAFLD mice. Diammonium glycyrrhizinate reduced the abundance of the endotoxin-producing bacteria such as *Desulfovibrio* and elevates the level of probiotics such as *Lactobacillus* and *Proteobacteria*, as well as augmented the abundance of short-chain fatty acid (SCFA)-producing bacteria such as *Ruminococcaceae* and *Lachnospiraceae* to promote SCFA production (Li et al., 2018).

Clinical Application of Herbal Medicine on NAFLD

In the clinical setting, clinical trials could confirm the experimental benefits of herbal medicine application in NAFLD patients. Clinical trials for NAFLD have been seen improvement with herbal medicine therapy. Randomized controlled trials comparing either herbal medicine alone or in

combination with other interventions or pharmaceutical agents have been investigated and the results indicated that herbal medicine had a better effect on the normalization of AST and the disappearance of radiological steatosis in the treatment of NAFLD patients (Shi et al., 2012). For instance, the daily consumption of resveratrol plus with lifestyle modification for 12 weeks showed superior effect than lifestyle change alone. Meanwhile, after resveratrol supplementation, the decreased level of insulin resistance, ALT, AST, LDLC, TC, and TNF-α were showed in NAFLD patients (Berman et al., 2017). It is essential to prove the efficacy and safety of herb medicine in treating NAFLD, because the side-effects of herb medicine need to be confirmed and investigated further (Rahmani et al., 2016) in clinical application. Because some herbal medicines such as *Phyllanthus urinaria* L. that has been suggested as the hepatoprotective herb in animal studies showed unsatisfactory effect in improving NAFLD activity score in NASH patients (Wong et al., 2013). The development of Radom Control Trials for herbal medicine is important and essential for making validation about the efficacy of herbal medicine in treating NAFLD. We made summery about the clinical trials about the effective herbal medicine (including herbal formula, crude extract and pure bioactive compound form medicinal plants) that have proved to take positive effects on the biochemical and physiological features of NAFLD (Liu et al., 2013).

Herbal Formula Against NAFLD

According to Chinese Medicine theory and prescription principles, the herbal formula is developed with selection of appropriate medicinal plants and the dosage of each herb for treating patients with NAFLD. The meta-analysis of 62 randomized controlled trial was conducted to investigate the herbal medicine therapy for NAFLD. It indicated that 246 Chinese herbs have been found to be included and clinical applied for NAFLD with an average of ten species in each formulation. It was found out that herbal medicine take effective action on the therapy of NAFLD, and Crataegi Fructus (Shan-Zha) was the most common used herbal medicine for 321 times in 17,670 patients (Shi et al., 2012). Many herbal formulas have been reported to show anti-NAFLD function in clinical application. For example, Yinchenhao Decoction has been used in treatment of gallbladder and liver diseases for centuries and it was composed of *Artemisia capillaris* (Thunb), *Gardenia jasminoides* (Ellis), and *Rheum palmatum* (L) (Yao et al., 2016); Oral administration of Danning Tablet (composed of Rhei Radix Et Rhizoma, Polygoni Cuspidati Rhizoma Et Radix, dried green orange peel and dried old orange peel) for three month in 232 patients can improve the clinical symptoms of NAFLD (Fan, 2004); The results of meta-analysis showed that HuoXueHuaYu improved B ultrasonic level in patients with NAFLD. As to lipids, HuoXueHuaYu showed effective action on reduction of TC, TG, ALT, and AST levels (Cai et al., 2019); Bangpungtongseong-san is an ancient Chinese herbal medicine formula and has been clinically applied in Korea, Japan (Bofu-tsusho-san), and China (Fang feng tong sheng-san) for obesity and its associated metabolic syndrome (Kobayashi et al., 2017); Erchen Decoction is used for the treatment of obesity, hyperlipidemia, and fatty liver diseases. Seven randomized controlled trials with a total of 1951 participants were investigated for the effects of Erchen Decoction on patients with NAFLD. The meta-analysis results of Erchen Decoction investigation showed that patients receiving Erchen Decoction with conventional treatment showed more effective in clinical improvement of NAFLD compared with conventional treatment alone (Li et al., 2017b); The Dava AL-balgham (composed of *Nigella Sativa*, *Zataria Multiflora*, *Trachyspermum ammi*, *Pistacia lentiscus* have shown anti-inflammatory, anti-atherogenic, and anti-oxidant effects. A double blind randomized trial of Dava AL-balgham has been applied for 76 patients with fatty liver disease. After three month treatment, Dava AL-balgham could improve the serum level of liver enzymes in patients with fatty liver (Hormati et al., 2019).

Single Herb Against NAFLD

The meta-analysis was performed to confirm the efficiency and safety of *Salvia miltiorrhiza* Bunge (Danshen) in eight randomized controlled trials with 800 patients. It indicated that *Salvia miltiorrhiza* Bunge showed positive effects on the levels of ALT, AST, TC and TG, LDL, and liver/spleen computed tomography ratio in patients with NAFLD. Future randomized clinical trials of higher quality are still required to evaluate the efficacy and safety of *Salvia miltiorrhiza* Bunge in NAFLD (Peng et al., 2016). *Panax Ginseng* C.A.Mey has been often applied against multiple metabolic conditions, including hepato-steatosis, Korean Red Ginseng shows anti-inflammatory and anti-fatigue effects on 80 patients with NAFLD (Hong et al., 2016).

Pure Natural Compound Against NAFLD

Curcumin (a natural polyphenol from *Curcuma longa* L.) owed the lipid-modifying, anti-inflammatory and antioxidant properties. Panahi et al. reported a randomized placebo controlled trial of curcumin in 87 subjects with NAFLD (Panahi et al., 2017) and concluded that daily supplementation of curcumin for 8 weeks decreased liver lipid accumulation and the levels of AST and ALT in patients of NAFLD without any issues of tolerance (Liu et al., 2019a). Diammonium glycyrrhizinate, a medicinal form of glycyrrhizic acid possesses anti-inflammatory and antioxidant effects. It has been applied for the treatment and control of chronic hepatopathy including NAFLD(Li et al., 2018); Cinnamon (Blevins et al., 2007) showed the improvement of the serum glucose and lipid levels in people with non-insulin dependent type 2 diabetes mellitus (NCT00237640). Further studies with 50 patients NAFLD were tested to investigate whether Cinnamon exerts the insulin sensitizer action in NAFLD patients. The results showed that daily intake of Cinnamon (1.5 g) for 12 weeks has beneficial effects on lipid profile, insulin resistance, liver enzymes, and high-sensitivity C-reactive protein in NAFLD patients (Askari et al., 2014). Ginger possess strong antioxidant ability to reduce lipids peroxidation (Si et al., 2018). The Early Phase I clinical investigation of Ginger in treatment of NAFLD in patients with type 2 diabetes mellitus (NCT02289235) is in progress to test whether Ginger takes effects on the liver biomarkers (ALT, AST,

and γ-glutamyl transpeptidase) and fatty liver score in fibro-scan. A multi-center, phase III, double-blind clinical trial reported that oral administration of silybin combined with phosphatidylcholine and vitamin E for 12 months can improve insulin resistance, liver enzymes, and liver histology (Loguercio et al., 2012). The clinical trial study of Silymarin (IRCT201202159018N1) was conducted on 64 patients with NASH and after 8 weeks treatment, the patients with NASH experience obvious fall in hepatic enzymes (Solhi et al., 2014).

Others

At present, the clinical trials recorded in U.S. National Library of Medicine mentioned the herbal medicine in treating NAFLD includes YiQiSanJu formula (NCT01677325, Phase I completed), Phyllanthus urinaria (NCT01210989, N/A completed), Zhenzhu Tiaozhi capsules (NCT03375580, N/A Recruiting), Fermented ginseng powder (NCT03260543, N/A completed), Trigonella Foenum-graecum Seed Extract (NCT02303314, Phase II, and III completed), *Zataria Multiflora* Boiss. (Shirazi's thyme) (NCT02983669, N/A completed), and Ginger (NCT02535195, Phase II and III completed), as well as some bioactive natural compounds such as Berberine (NCT04049396, NCT03198572 Recruiting, Phase IV), Curcumin (NCT03864783, Recruiting), Silymarin (NCT02006498, Phase II completed and NCT02973295, Phase IV Recruiting), Resveratrol (NCT02030977, Phase II and III completed; NCT01464801, N/A completed; NCT01446276 N/A completed), Anthocyanin (NCT01940263, Early Phase I completed), Pioglitazone and Berberine (NCT00633282, phase II Completed), Anthocyanin (NCT01940263, phase II Completed) and Siliphos (NCT00443079, phase II Completed).

Conclusion and Discussion

Following the general requirement of the pharmacological research of herbal medicine (Heinrich et al., 2020), we firstly made assessment of the pharmacological research literature on herbal medicine, focusing on the experiment design, we checked the methodological details such as group size, controls and animal species. Specifically, we observed the dosage, route and frequency of drug administration in the research literature, and checked the tested dose range that should be pharmacological relevant. After the assessment, the literature of herbal medicine that reach the general requirement of the pharmacological research are included in our review. As shown in **Table 1**, a large number of natural compounds, whole extract and herb formula have been widely investigated against different pathologies of NAFLD with promising results (Porras et al., 2018). Increasing evidence has shown polyphenols (Porras et al., 2018) including resveratrol (Aguirre et al., 2014), quercetin (green tea, soy isoflavones) silymarin (extracted from *Sylbum marianum*), silybin and rutin (Van De Wier et al., 2017) are the frequently investigated natural compounds, along with the satisfactory effectiveness in NAFLD. As shown in **Figure 3**, herbal medicine mediated the key pathological events in the procession of NAFLD include lipid metabolism dysfunction, insulin resistance, fibrosis, oxidative stress, inflammation, and

apoptosis (Wang et al., 2016). The satisfactory improvement of NAFLD disease outcomes and endpoints mentioned the amelioration or reduction of fat mass, insulin resistance, serum level of FFA, AST, and ALT, hepatic lipid accumulation and fibrosis, as well as hepatic oxidative stress, inflammatory response, and apoptosis. Thus, we made a review of the usage and role of herbal medicine in NAFLD. Steatosis, characterized by fat accumulation, represented the early stage of NAFLD and inflammation that interfered with the insulin signaling pathway is the key process that makes early steatosis develop into steatohepatitis (Bai and Li, 2019). Therefore, amelioration of steatosis and inflammation is vital for NAFLD therapy. Herbal medicine therapy has shown promising anti-inflammatory, antioxidant, and anti-apoptotic properties that might take beneficial effects on curtailing the inflammatory progression of NAFLD. Their action was always involved in multi-pathways to improved NAFLD, such as baicalin exerted anti-inflammation and anti-oxidant effects that can reduce hepatic lipid accumulation, suppress induced hepatic inflammation, and prevent liver fibrosis involved inhibiting hepatocyte apoptosis (Zhang J. et al., 2018). Gegenqinlian decoction influence NAFLD *via* improving PPARγ to inhibit inflammation and modulated lipid metabolism (Wang et al., 2015). *Alisma orientalis* protected against *de novo* lipogenesis to upregulate hepatic lipid export. Additionally, it modulated oxidative stress cytokines, inflammatory and fibrotic mediators, eventually influenced lipo-apoptosis and liver injury panels (Choi E. et al., 2019). Resveratrol can be considered as a pharmacological SIRT1 activator (Zhang et al., 2015) and take effects on hepatic steatosis by improving lipid-related gene transcriptional expression, oxidative stress and inflammation (Cheng et al., 2019), meanwhile decreasing ER stress (Ding et al., 2017) *via* the autophagy (Liu et al., 2015a). In addition, it has shown that herbal medicine combined with other interventions exhibited a much better beneficial effect than single interference alone. For example, Lingguizhugan decoction and calorie-restriction therapy together could enhance the reduction of fasting blood lipid levels (Yuanyuan et al., 2015; Cao et al., 2016). The combination of Korean red ginseng and probiotic *Lactobacillus* synergistically ameliorated hepatic inflammation (Kim et al., 2019a). The combination of Ganmaidazao and Shengmai-Yin decoction is applied as adjuvant therapy for Type II diabetes mellitus *via* activation of HSL, PPARα, and AMPK/PI3K/AKT, and inhibition of SREBP-1/FAS, influencing insulin sensitivity, and lipid biosynthesis (Li et al., 2019). Two types of anti-dyslipidemia herb formulas (Fenofibrate and xuezhikang) have been simultaneously applied in the treatment of NAFLD (Hong et al., 2007) as well as combined use of *Fructus Schisandrae* with statin showed anti-oxidative effect and inhibitory effect against liver toxicity (Wat et al., 2016). *Schisandra chinensis* Baill has been used as a complementary therapy for rosiglitazone and alleviated NASH with significantly lower levels of LDLC and SOD in liver than rosiglitazone (Yao et al., 2014; Wat et al., 2016). Therefore, herbal medicine supplement combined with other therapeutic approaches

TABLE 1 | The recent research for herb medicine in the setting of NAFLD therapy.

Herbal Medicine	Source organism	Pharmacological model	Treatment (Pharmacological model and Duration)	Effective Dosage	Reported mechanism of action		
					Lipogenesis	Modulation of inflammatory parameters	others
S-allylmercaptocysteine	Garlic-derived	HFD induced obese rat	i.p, 3 times/week	200 mg/kg	↓	↓NF-κB and AP-1	↓Collagen formation ↓Oxidative stress ↑Autophagy
Dioscin	Polygonati Rhizoma	HFD induced obese rats	Orally,	60 mg/kg		↓ IκBα, p50 and p65	↓Collagen formation
		HFD induced obese Wistar rats and mice	Orally, 8 weeks	15–80mg/kg	↑SIRT1/AMPK		↓**Apoptosis**
		Dimethylnitrosamine-induced acute liver injury mice	Orally,	80 mg/kg	↓LXRα	↓	↓**Oxidative stress(**↑SIRT1, Nrf2)
Resveratrol		MCD diet induced NAFLD mice	Orally,	100 or 250 mg/kg/day		↓TBARS	↑**Autophagy**
		AML12 cells		25, 50, or 100 µmol/L	↓ FFA uptake.		
		C57BL/6J mice and as ULK1+/− mice with HFD	Orally, 4 weeks.	50 mg/kg		↓ IκBα-NF-κB	↓ **Oxidative stress** ↓Fibrosis
		Mice with HFD for 4 weeks	Orally, 4 weeks.	0.40%			↓**Oxidative stress**
		HepG2 cells	24 h	20, 40, and 80µM			
		Wistar rats with HFD	Orally, 18 weeks	200 mg/kg		↑ cAMP-PRKA-AMPK-SIRT1	↓ ER stress(↑SIRT1)
Naringenin	Citrus-derived flavonoid	LDLR−/− mice with HFD	Orally, 4 weeks	1% or 3% wt/wt	↓ VLDL		↑ insulin resistance
Yangonin	Piper methysticum	Mouse fed with HFD	Orally, 16 weeks	10, 20, or 40 mg/kg	↓SREBP-1c pathway;↑ fatty acid β-oxidation		↑insulin sensitivity ↓Fibrosis (↑ FXR)
Berberine	Coptidis Rhizoma	Mice fed with HFD	Orally; for 4 weeks	300 mg/kg/day	↓ SCD1 via AMPK-SREBP-1c pathway	p38MAPK/ERK-COX2 pathways	↓Fibrosis
		AML12		20 µM			
		NASH-HCC mice model	Orally, 12 week	250 mg/kg			
Betulinic acid	Outer bark of tree species	Mice fed with HFD	Orally, 11 weeks	50 mg/kg,	↓ SREBP-1c, ApoC2, RBP4, FAS, and SCD-1; ↑AMPK ↑ fatty acid oxidation	↓F4/80, IL-1α, IL-1β, IL-6, TNF-α	↓Fibrosis (↑ FXR)
		AML12 treated with palmitic acid (PA)		50 µg/ml			
		Mice fed with MCD and HFD	Orally, 6 weeks	100 mg/100 g diet			
Glycyrrhizin	Glycyrrhizae Radix Et Rhizoma	Mice fed with MCD diet	i.p, 2 weeks	50 mg/kg per day	↓ lipogensis	↓NLRP3 ↑FXR	
Gastrodin	*Gastrodia elata* Bl	Larval zebrafish fed with HFD		10, 25, 50 mg/L	↓ lipogensis	↓TNFα, IL-6, and IL1β	↓Fibrosis ↓TGFβ1) **Oxidative stress** ↑NRF2, HO-1
Naringenin	Citrus-derived flavonoid	*Ldlr*−/− mice fed a Western diet	Orally, 4 weeks	1 or 3%	↓ SREBP1c; ↓VLDL;↑ fatty acid oxidation		↓ hyperinsulinemia
Puerarin	*Pueraria lobate* (Willd.) Ohwi	Mice fed with a high-fat +high-sucrose diet	Orally, 18 weeks	0.2,0.4g/kg/day	↓liver steatosis	↓	↓Fibrosis ↓TGFβ1)

(Continued)

TABLE 1 | Continued

Herbal Medicine	Source organism	Pharmacological model	Treatment (Pharmacological model and Duration)	Effective Dosage	Reported mechanism of action		
					Lipogenesis	Modulation of inflammatory parameters	others
Silibinin	*Silybum martanum* (L.) Gaertn.	MCD diet induced NASH mice	Orally, 6 weeks	10 and 20 mg/kg/day	↑ β-oxidation	↓NASH *via* CFLAR-JNK pathway,	**Oxidative stress** ↑CAT, GSH-Px and HO-1; ↓CYP2E1, CYP4A
		NCTC-1469 cells treated with OA plus PA		50 and 100 μmol/L			
		HepG2 cells treated with OA		5, 20, 50, and 100 μM	↓PPARα, SREBP-1C and PNPLA3	↓NO	↓glucose uptake (PI3K-AKT) **↓oxidative stress** (NRF2, CYP2E1, CYP4A)
Sparstolonin B	*Sparganium stoloniferum* Buch-Ham	High-fat-fed mice	ip, for 4 week	3 mg/kg, twice a week	↓TLR4 lipid raft trafficking	↓ TLR4 pathway	↓Fibrosis ↓TGFβ1) ↓NADPH oxidase activation.
		Kupffer cell line		100 μg/ml			
		LX2 cells with LPS (100 ng/ml)		10, 100 μM			
Isochlorogenic acid B	Laggera alata (Asteraceae)	Mice fed with MCD diet	Orally, 4 weeks	5, 10 and 20 mg/kg.			↓Fibrosis (↓TGFβ1, LXO,MCP-1, COL1α1 and TIMP-1.) ↓ oxidative stress (↑Nrf2)
Swertiamarin	Swertia bimaculata	Fructose-fed mice for 12 week	Orally, 4 weeks	25, 50 and 100 mg/kg	↓ SREBP-1/ FAS/ACC	↓hepatic pro-inflammation	↓ hepatic xanthine oxidase (XO) ↑Nrf2
Baicalin	*Scutellaria baicalensis* Georgi	MCD diet-induced NASH	Orally, 4weeks.	50 and 100,200 mg/kg	↓	↓ inflammation	↓Fibrosis ↓ hepatic apoptosis.
Ursolic acid(UA)		Mice fed with HFD	Orally, 16 week	0.05% (w/w) UA diet			↓Fibrosis
		T090-induced mouse model.	Orally, 7 days	100, 250 mg/kg/day	Liver X Receptor α antagonist ↓ lipid accumulation		
		L02 cells treated with PA		10–30 μg/ml			↓oxidative stress.
		Rat fed with HFD	Orally, 6 weeks.	0.125%, 0.25%, 0.5% UA diet		↓ inflammation	↓ insulin resistance
Andrographolide	*Andrographis paniculata* (Burm. f.)Nee	Mice fed with CDAA diet	i.p, 22 weeks	1 mg/kg, 3 times/week		↓hepatic inflammation	↓collagen formation
		Fat-laden HepG2 cells.		50 μM		↓ NF-κB	
Ginsenoside Rb1	*Panax Ginseng* C.A.Mey	Rat fed with HFD	ip	10 mg/kg	↑CPT1		
		db/db mice	i.p, 14 days.	20 mg/kg	↓	↓	
Nobiletin	*Citrus reticulata* Blanco	Mice fed a high-fat diet	Orally, 16 weeks.	0.02%, w/w		↓ NLRP3	
		High glucose induced hepG2 cells		5, 25, and 50 μM	↑AMPK		
Ginsenoside Rb2	*Panax Ginseng* C.A.Mey	HepG2 cells		50 μmol/L			↑Autophagy
		db/db mice	i.p, 4 weeks	10 mg/kg	↑AMPK or SIRT1		
Akebia saponin D	*Dipsacus asper* Wall.ex Henry	ob/ob mice fed with HFD	i.p, 4 weeks	30,60,120 mg/kg,			**↑Autophagy**
		OA stressed Buffalo rat liver cells		1, 10, and 100 μM			↑ LC3-II ↓P62
Glycycoumarin	Rhizoma Glycyrrhizae	PA stressed cells (HepG2, AML-12, and L02)		10–40μM			↓Mitochondrial apoptosis(↓GSK-3,↓JNK)
		MCD diet induced NASH mice	i.p. 4 weeks	GCM 15 mg/kg/day	↓Lipogenesis	↓Inflammation	↓ Fibrosis; Oxidative stress
ethanol extract	*Lycopus lucidus* Turcz. ex Benth	HepG2 cells treated with OA plus PA		250–1000 mg/ml.	↑PPARα, AMPK ↓SREBP-1c		

(Continued)

TABLE 1 | Continued

Herbal Medicine	Source organism	Pharmacological model	Treatment (Pharmacological model and Duration)	Effective Dosage	Reported mechanism of action		
					Lipogenesis	Modulation of inflammatory parameters	others
		Mice fed with HFD	Orally,14 weeks.	100 or 200 mg/kg/day		↓TNF-α	
Danshen aqueous extract	*Salviae miltiorrhiza* Bge.	Mice fed with ethanol	Orally, 9 days	0.093, 0.28, 0.84 g/kg	↓Lipogenesis	↓Inflammation	↓ Fibrosis
Jwa Kum Whan	Scutellariae Radix and Euodiae Fructus	Mice fed with HFD	Orally, 15 week	100,200 mg/kg daily			↑Insulin Signaling
		HepG2 cells		10, 25, 50, 75, or 100 µg/ml			
Ethanol Extract	*Leonurus japonicus* Houtt.	Mice fed with HFD	Orally, 14 weeks	100 or 200 mg/kg	↑ AMPK, PPARα		↑Insulin Signaling
		1 mM free fatty acid induced HepG2 cells		250, 500, 750, or 1000 µg/ml	↑ AMPK, PPARα		
honeyberry extract	*Lonicera caerulea*	Mice fed with HFD	Orally, 6 weeks.	0.5%, 1%	↑ AMPK, CPT-1,PPARα		
polysaccharides	*Lycium barbarum* L.	Rat treated with HFD	Orally, 4 weeks	1 mg/kg,	↓lipid accumulation ↑ fatty acid oxidation		
methanolic extract	*Alisma orientale* (Sam.) Juzep.	Rats fed with HFD for 6 weeks	Orally, 6 week	150, 300, and 600 mg/kg	↑AMPK, PPARα	↓Inflammation	↓apoptosis;↓ oxidative stress;↑insulin sensitive
Seed Extract	*Psoralea corylifolia* L.	Mice fed a HFD	orally, 12 weeks	300 or 500 mg/g/d,	↓Lipogenesis	↓Inflammation	↑Insulin Signaling
Extract	*Schisandra chinensis* (Turcz)Baill	Wister rats fed with HFD	56 days	100 mg/kg/day	↓ LDLC		↓Endoplasmic reticulum (ER) stress
Total saponins	*Aralia elata* Seem.	ApoE-/- mouse fed with HFD.	i.g., 12 weeks.	75, 150 mg/kg/day		↓Inflammation	↓oxidative stress.
Total alkaloids	*Rubus aleaefolius* Poir.	HFD for 8 weeks	orally, 4 weeks	1.44, 0.72 g/kg	↓FAS, ACC ↑CPT		
Polygonatum kingianum		Rat fed with HFD	Orally, 14 weeks	1, 2, 4g/kg			Remedy mitochondrial dysfunction
Ethyl acetate extract	*Aristolochia manshuriensis* Kom	HFD-induced NASH model	15 weeks	2.5 mg/kg		↓Inflammation	↓oxidative stress. ↓apoptosis
Fructus Schisandrae		SD rats fed with HFD for 8 weeks:	orally, 8 weeks	0.45% FS+0.3% Atorvastatin			↓oxidative stress.
Aqueous extract	*Salvia miltiorrhiza* Bunge	Ovariectomized (OVX)+ hyperlipidemic SD rats	Orally, 12 weeks	600 mg/kg/d			↓ Fibrosis
The chloroform extract	*Cyclocarya paliurus*	SD rats fed with HFD for 6 weeks	Orally, 4 weeks.				↓ Fibrosis
Saponins Raw and processed	*Panax Notoginseng* (Burk.) F.H.Chen	CCl₄ induced fibrosis in rat	i.p	130 mg/kg		↓Inflammation	↓ Fibrosis
Citrus aurantium Peel Extract	*Citrus aurantium* L. (Rutaceae)	Mice fed with HFD	orally, 8 weeks	50, 100 mg/kg	↓PPAR-γ, SREBP-1c	↓ inflammation	
Korea red ginseng	*Panax ginseng* C.A.Mey	Fatty Rats	orally, 2 months	200 mg/kg/day		↓ inflammation	↓oxidative stress.
Celastrus orbiculatus Thunb.		ApoE(-/-) mice	Orally, 6 weeks	10.0 g/kg/d	↑adiponectin	↓TLR4 and NF-κB p65, TNF-α.	
		A guinea pig of NAFLD	Orally, 8 weeks		↑CYP7A1 and HMGCR		↓NO and iNOS levels

(Continued)

TABLE 1 | Continued

Herbal Medicine	Source organism	Pharmacological model	Treatment (Pharmacological model and Duration)	Effective Dosage	Reported mechanism of action		
					Lipogenesis	Modulation of inflammatory parameters	others
BaiHuJia RenShen Decoction	Anemarrhenae Rhizoma, Gypsum Fibrosum, Glycyrrhizae Radix Et Rhizoma,Ginseng Radix Et Rhizoma	HuS-E/2 cell with PA db/db mice	orally, 6 weeks	900 mg/kg	↑P-AMPK;P-ACC; ↓SCD1 ↑CPT		
BuShenKangShuai tablet		ApoE (-/-) mice	Gavage, 6 weeks	BSKS or atorvastatin		↑adiponectin ↓TLR4 and NF-κB p65	
LiGanShiLiuBaWei San	Punica granatum, Cinnamomum cassia, Elettaria cardamomum, Piper longum, Carthamus tinctorius, Amomum tsao-ko	Rat with HFD HepG2 with FFAs	Orally, 4 weeks	0.75 and 1.5 g/kg	↑PPARα ↑PPARβ		↓iNOS levels
Hugan Qingzhi tablet	Alismatis Rhizoma, Crataegi Fructus, Typhae Pollen, Nelumbinis Folium, Notoginseng Radix Et Rhizoma	L02 and HepG2 cells induced by FFA Rat with HFD	Orally, 12 weeks	2.16/1.08/0.54 g/kg		↑SIRT1 ↓Ac-NF-κB-p65	
Sinai san decoction	Bupleuri Radix, Paeoniae Radix, Aurantii Fructus Immaturus, Glycyrrhizae Radix Et Rhizoma	Rat with HFD+CCL4	Orally, 8 weeks	0.1 ml/kg/day		↓ inflammation	
Gegenqinlian Decoction	PuerariaeLobataeRadix, Coptidis Rhizoma, Scutellariae Radix, Glycyrrhizae Radix Et Rhizoma	Rat with HFD	Orally, 8 weeks	5.04, 10.08 g/kg/day	↓PPARγ		
Tangzhiqing Decoction	Mori Folium, Nelumbinis, Crataegi Folium, Salviae Miltiorrhizae Radix Et Rhizoma, Paeoniae Radix Rubra	Rat with HFD	Orally, 4 weeks	540 mg/kg/d	↓steatosis		
Qushi Huayu Decoction	Artemisiae scopaiae Herba, Polygoni cuspidati Rhizoma Et Radix, Hyperici Japonici Herba, Curcumae longae Rhizoma, Gardenia jasminoides Ellis	Rat with HFD	Orally, 4 weeks	0.1 ml/kg·d,	↑AMPK and ACC		
		L02 cells		5%–15% QHD serum	↓ cellular TG		
Hugan Qingzhi tablet	Alismatis Rhizoma, Crataegi Fructus, Typhae Pollen, Nelumbinis Folium,	Rat with HFD	Orally,	10% HQT-medicated serum	↓	↓IL-6, ↓P65	

(Continued)

TABLE 1 | Continued

Herbal Medicine	Source organism	Pharmacological model	Treatment (Pharmacological model and Duration)	Effective Dosage	Reported mechanism of action		
					Lipogenesis	Modulation of inflammatory parameters	others
	Notoginseng Radix Et Rhizoma			90 mg/kg, combination with calorie restriction			
Lingguizhugan decoction	Poria, Ramulus Cinnamomi, Atractylodis Macrocephalae Rhizoma, Glycyrrhizae Radix Et Rhizoma	Mice with HFD	16 weeks	Fecal microbiota transplantation	↓		
Tangshen formula	Puerariae Radix, Astragalus, Ligustrum lucidum Ait, Ganoderma, Salvia miltiorrhizae Radix Et Rhizoma, Rhei Radix Et Rhizoma	Mice with HFD	Orally, 16 weeks	2.4 g/kg/day	↑AMPK/SIRT1		
Fenofibrate and Xuezhikang		HepG2 cells Rat fed with HFD	Orally, 6 weeks	25, 50, 100 µg/ml F (100 mg/kg) and X (300 mg/kg)	↑PPARα	↓TNF-α.	
Bangpungtongseong-san	Talcum, Glycyrrhiza uralensis,Gypsum, Scutellaria baicalensis, Platycodon grandiflorum, Ledebouriella seseloides, Cnidium officinale, Angelica gigas,Paeonia lactiflora,Rheum undulatum, Ephedra sinica, Mentha pulegium, Forsythia koreana, Erigeron canadensis, Schizonepeta tenuifolia, Atractylodes japonica, Gardenia jasminoides, Zingiber officinale	HFD induced obese mice	12 weeks	1.5% w/w	↑ mitochondrial function		antioxidant
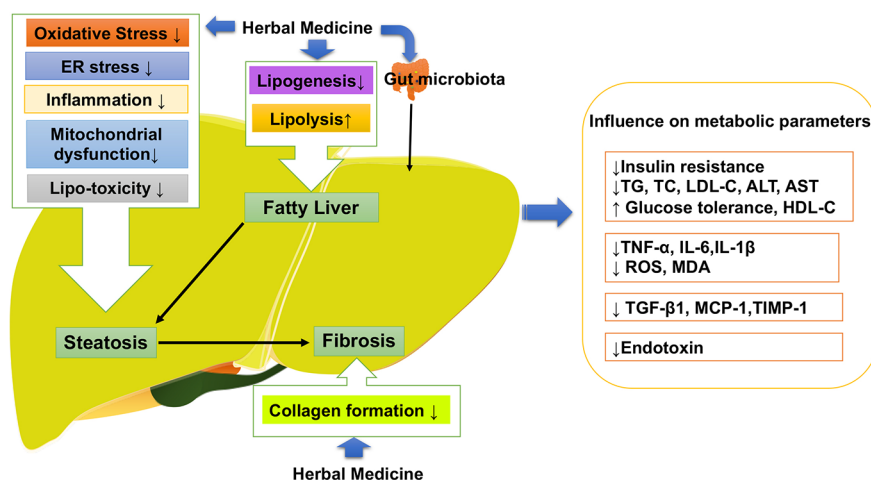
FIGURE 3 | Herbal medicine mediated the key pathological events in the procession of NAFLD. NAFLD, Non-alcoholic fatty liver disease.

might provide feasible therapeutic strategies for patients with NAFLD (Porras et al., 2018).

AUTHOR CONTRIBUTIONS

YF and designed and conceived the study. YX, NW, and YF retrieved, analyzed the data and drafted the manuscript. WG, CZ, FC, HT, SL, and NW discussed and revised the manuscript. All authors confirmed final version of the manuscript.

FUNDING

REFERENCES

Aguirre, L., Fernández-Quintela, A., Arias, N., and Portillo, M. P. (2014). Resveratrol: anti-obesity mechanisms of action. Molecules (Basel, Switzerland). 19, 18632–18655. doi: 10.3390/molecules191118632

Ahmad, O., Wang, B., Ma, K., Deng, Y., Li, M., Yang, L., et al. (2019). Lipid Modulating Anti-oxidant Stress Activity of Gastrodin on Nonalcoholic Fatty Liver Disease Larval Zebrafish Model. *Int. J. Mol. Sci.* 20, 1984. doi: 10.3390/ijms20081984

Arase, Y., Shiraishi, K., Anzai, K., Sato, H., Teramura, E., Tsuruya, K., et al. (2019). Effect of Sodium Glucose Co-Transporter 2 Inhibitors on Liver Fat Mass and Body Composition in Patients with Nonalcoholic Fatty Liver Disease and Type 2 Diabetes Mellitus. *Clin. Drug Invest.* 39, 631–641. doi: 10.1007/s40261-019-00785-6

Askari, F., Rashidkhani, B., and Hekmatdoost, A. (2014). Cinnamon may have therapeutic benefits on lipid profile, liver enzymes, insulin resistance, and high-sensitivity C-reactive protein in nonalcoholic fatty liver disease patients. *Nutr. Res.* 34, 143–148. doi: 10.1016/j.nutres.2013.11.005

Bai, L., and Li, H. (2019). Innate immune regulatory networks in hepatic lipid metabolism. *J. Mol. Med. (Berl)* 97, 593–604. doi: 10.1007/s00109-019-01765-1

Berman, A. Y., Motechin, R. A., Wiesenfeld, M. Y., and Holz, M. K. (2017). The therapeutic potential of resveratrol: a review of clinical trials. *NPJ Precis. Oncol.* 1, 35. doi: 10.1038/s41698-017-0038-6

Bertot, L. C., and Adams, L. A. (2019). Trends in hepatocellular carcinoma due to non-alcoholic fatty liver disease. *Expert Rev. Gastroenterol. Hepatol.* 13, 179–187. doi: 10.1080/17474124.2019.1549989

Blevins, S. M., Leyva, M. J., Brown, J., Wright, J., Scofield, R. H., and Aston, C. E. (2007). Effect of cinnamon on glucose and lipid levels in non insulin-dependent type 2 diabetes. *Diabetes Care* 30, 2236–2237. doi: 10.2337/dc07-0098

Brunner, K. T., Henneberg, C. J., Wilechansky, R. M., and Long, M. T. (2019). Nonalcoholic Fatty Liver Disease and Obesity Treatment. *Curr. Obes. Rep.* 8, 220–228. doi: 10.1007/s13679-019-00345-1

Cabrera, D., Wree, A., Povero, D., Solis, N., Hernandez, A., Pizarro, M., et al. (2017). Andrographolide Ameliorates Inflammation and Fibrogenesis and Attenuates Inflammasome Activation in Experimental Non-Alcoholic Steatohepatitis. *Sci. Rep.* 7, 3491. doi: 10.1038/s41598-017-03675-z

Cai, Y., Liang, Q., Chen, W., Chen, M., Chen, R., Zhang, Y., et al. (2019). Evaluation of HuoXueHuaYu therapy for nonalcoholic fatty liver disease: a systematic review and meta-analysis of randomized controlled trial. *BMC Complement. Altern. Med.* 19, 178. doi: 10.1186/s12906-019-2596-3

Cao, G.-S., Li, S.-X., Wang, Y., Xu, Y.-Q., Lv, Y.-N., Kou, J.-P., et al. (2016). A combination of four effective components derived from Sheng-mai san attenuates hydrogen peroxide-induced injury in PC12 cells through inhibiting Akt and MAPK signaling pathways. *Chin. J. Natural Medicines* 14, 508–517. doi: 10.1016/S1875-5364(16)30060-7

Cheng, S., Liang, S., Liu, Q., Deng, Z., Zhang, Y., Du, J., et al. (2018). Diosgenin prevents high-fat diet-induced rat non-alcoholic fatty liver disease through the AMPK and LXR signaling pathways. *Int. J. Mol. Med.* 41, 1089–1095. doi: 10.3892/ijmm

Cheng, K., Song, Z., Zhang, H., Li, S., Wang, C., Zhang, L., et al. (2019). The therapeutic effects of resveratrol on hepatic steatosis in high-fat diet-induced obese mice by improving oxidative stress, inflammation and lipid-related gene

transcriptional expression. *Med. Mol. Morphol.* 52, 187–197. doi: 10.1007/s00795-019-00216-7

Choi, E., Jang, E., and Lee, J. H. (2019). Pharmacological Activities of Alisma orientale against Nonalcoholic Fatty Liver Disease and Metabolic Syndrome: Literature Review. *Evid. Based. Complement. Alternat. Med.* 2019, 2943162. doi: 10.1155/2019/2943162

Choi, J. Y., Kwon, E. Y., and Choi, M. S. (2019). Elucidation of the Metabolic and Transcriptional Responses of an Oriental Herbal Medicine, Bangpungtongseongsan, to Nonalcoholic Fatty Liver Disease in Diet-Induced Obese Mice. *J. Med. Food.* doi: 10.1089/jmf.2018.4383

Clapper, J. R., Hendricks, M. D., Gu, G., Wittmer, C., Dolman, C. S., Herich, J., et al. (2013). Diet-induced mouse model of fatty liver disease and nonalcoholic steatohepatitis reflecting clinical disease progression and methods of assessment. *Am. J. Physiol. Gastrointest. Liver Physiol.* 305, G483–G495. doi: 10.1152/ajpgi.00079.2013

Dattaroy, D., Seth, R. K., Das, S., Alhasson, F., Chandrashekaran, V., Michelotti, G., et al. (2016). Sophocarpine alleviates hepatocyte steatosis through activating AMPK signaling pathway. *Am. J. Physiol. Gastrointest. Liver Physiol.* 310, G510–G525. doi: 10.1016/j.tiv

Dattaroy, D., Seth, R. K., Sarkar, S., Kimono, D., Albadrani, M., Chandrashekaran, V., et al. (2018). Sparstolonin B (SsnB) attenuates liver fibrosis via a parallel conjugate pathway involving P53-P21 axis, TGF-beta signaling and focal adhesion that is TLR4 dependent. *Eur. J. Pharmacol.* 841, 33–48. doi: 10.1016/j.ejphar.2018.08.040

Ding, S., Jiang, J., Zhang, G., Bu, Y., Zhang, G., and Zhao, X. (2017). Resveratrol and caloric restriction prevent hepatic steatosis by regulating SIRT1-autophagy pathway and alleviating endoplasmic reticulum stress in high-fat diet-fed rats. *PloS One* 12, e0183541. doi: 10.1371/journal.pone.0183541

Ding, J., Zhang, B., Wang, P. J., He, G. N., Wei, D. M., Ding, J. L., et al. (2019). Analysis on mechanisms and medication rules of herbal prescriptions for nonalcoholic fatty liver disease based on methods of data mining and biological information. *Zhongguo Zhong Yao Za Zhi* 44, 1689–1695. doi: 10.19540/j.cnki.cjcmm

Dong, R., Yang, X., Wang, C., Liu, K., Liu, Z., Ma, X., et al. (2019). Yangonin protects against non-alcoholic fatty liver disease through farnesoid X receptor. *Phytomedicine* 53, 134–142. doi: 10.1016/j.phymed.2018.09.006

Fan, J.-G. (2004). Evaluating the efficacy and safety of Danning Pian in the short-term treatment of patients with non-alcoholic fatty liver disease: a multicenter clinical trial. *Hepatobiliary Pancreatic Dis. Int.* 3, 375–380.

Fang, K., Wu, F., Chen, G., Dong, H., Li, J., Zhao, Y., et al. (2019). Diosgenin ameliorates palmitic acid-induced lipid accumulation via AMPK/ACC/CPT-1A and SREBP-1c/FAS signaling pathways in LO2 cells. *BMC Complement Altern. Med.* 19, 255. doi: 10.1186/s12906-019-2671-9

Feng, Q., Gou, X. J., Meng, S. X., Huang, C., Zhang, Y. Q., Tang, Y. J., et al. (2013). Qushi Huayu Decoction Inhibits Hepatic Lipid Accumulation by Activating AMP-Activated Protein Kinase In Vivo and In Vitro. *Evid. Based. Complement. Alternat. Med.* 2013, 184358. doi: 10.1155/2013/184358

Feng, Y., Chen, Y., Yang, B., Lan, Q., Wang, T., Cui, G., et al. (2019). Hepatoprotective Effect of Jianpi Huoxue Formula on Nonalcoholic Fatty Liver Disease Induced by Methionine-Choline-Deficient Diet in Rat. *BioMed. Res. Int.* 2019, 7465272. doi: 10.1155/2019/7465272

Gao, B. Z., Chen, J. C., Liao, L. H., Xu, J. Q., Lin, X. F., and Ding, S. S. (2015). Erchen Decoction Prevents High-Fat Diet Induced Metabolic Disorders in C57BL/6 Mice. *Evid. Based. Complement. Alternat. Med.* 2015, 501272. doi: 10.1155/2015/501272

German, M. N., Lutz, M. K., Pickhardt, P. J., Bruce, R. J., and Said, A. (2019). Statin Use is Protective Against Hepatocellular Carcinoma in Patients With Nonalcoholic Fatty Liver Disease: A Case-control Study. *J. Clin. Gastroenterol.* 8, 876. doi: 10.1097/MCG.0000000000001260

Gong, L. L., Li, G. R., Zhang, W., Liu, H., Lv, Y. L., Han, F. F., et al. (2016). Akebia Saponin D Decreases Hepatic Steatosis through Autophagy Modulation. *J. Pharmacol. Exp. Ther.* 359, 392–400. doi: 10.1124/jpet.116.236562

Gu, M., Zhao, P., Zhang, S., Fan, S., Yang, L., Tong, Q., et al. (2019). Betulinic acid alleviates endoplasmic reticulum stress-mediated nonalcoholic fatty liver disease through activation of farnesoid X receptors in mice. *Br. J. Pharmacol.* 176, 847–863. doi: 10.1111/bph.14570

Han, H. Y., Lee, S. K., Choi, B. K., Lee, D. R., Lee, H. J., and Kim, T. W. (2019). Preventive Effect of Citrus aurantium Peel Extract on High-Fat Diet-Induced Non-alcoholic Fatty Liver in Mice. *Biol. Pharm. Bull.* 42, 255–260. doi: 10.1248/bpb.b18-00702

Heinrich, M., Appendino, G., Efferth, T., Fürst, R., Izzo, A. A., Kayser, O., et al. (2020). Best practice in research – Overcoming common challenges in phytopharmacological research. *J. Ethnopharmacol.* 246, 112230. doi: 10.1016/j.jep.2019.112230

Hong, X., Tang, H., Wu, L., and Li, L. (2006). Protective effects of the Alisma orientalis extract on the experimental nonalcoholic fatty liver disease. *J. Pharm. Pharmacol.* 58, 1391–1398. doi: 10.1211/jpp.57.10.0013

Hong, X. Z., Li, L. D., and Wu, L. M. (2007). Effects of fenofibrate and xuezhikang on high-fat diet-induced non-alcoholic fatty liver disease. *Clin. Exp. Pharmacol. Physiol.* 34, 27–35. doi: 10.1111/j.1440-1681.2007.04547.x

Hong, S. H., Suk, K. T., Choi, S. H., Lee, J. W., Sung, H. T., Kim, C. H., et al. (2013). Anti-oxidant and natural killer cell activity of Korean red ginseng (Panax ginseng) and urushiol (Rhus vernicifera Stokes) on non-alcoholic fatty liver disease of rat. *Food Chem. Toxicol.* 55, 586–591. doi: 10.1016/j.fct.2013.01.022

Hong, M., Lee, Y. H., Kim, S., Suk, K. T., Bang, C. S., Yoon, J. H., et al. (2016). Anti-inflammatory and antifatigue effect of Korean Red Ginseng in patients with nonalcoholic fatty liver disease. *J. Ginseng Res.* 40, 203–210. doi: 10.1016/j.jgr.2015.07.006

Hong, M., Li, S., Wang, N., Tan, H. Y., Cheung, F., and Feng, Y. (2017). A Biomedical Investigation of the Hepatoprotective Effect of Radix salviae miltiorrhizae and Network Pharmacology-Based Prediction of the Active Compounds and Molecular Targets. *Int. J. Mol. Sci.* 18, 620. doi: 10.3390/ijms18030620

Hormati, A., Tooiserkany, F., Mohammadbeigi, A., Aliasl, F., and Dehnavi, H. M. (2019). Effect of an Herbal Product on the Serum Level of Liver Enzymes in Patients with Non-Alcoholic Fatty Liver Disease: A Randomized, Double-Blinded, Placebo-Controlled Trial. *Iran. Red Crescent Med. J.* 21, 7. doi: 10.5812/ircmj.91024

Hu, R., Yan, H., Hao, X., Liu, H., and Wu, J. (2013). Shizukaol D isolated from Chloranthus japonicas inhibits AMPK-dependent lipid content in hepatic cells by inducing mitochondrial dysfunction. *PloS One* 8, e73527. doi: 10.1371/journal.pone.0073527

Huang, M. Q., Zhou, C. J., Zhang, Y. P., Zhang, X. Q., Xu, W., Lin, J., et al. (2016). Salvianolic Acid B Ameliorates Hyperglycemia and Dyslipidemia in db/db Mice through the AMPK Pathway. *Cell Physiol. Biochem.* 40, 933–943. doi: 10.1159/000453151

Huang, Q., Wang, T., Yang, L., and Wang, H. Y. (2017). Ginsenoside Rb2 Alleviates Hepatic Lipid Accumulation by Restoring Autophagy via Induction of Sirt1 and Activation of AMPK. *Int. J. Mol. Sci.* 18, 1063. doi: 10.3390/ijms18051063

Ji, G., Wang, Y., Deng, Y., Li, X., and Jiang, Z. (2015). Resveratrol ameliorates hepatic steatosis and inflammation in methionine/choline-deficient diet-induced steatohepatitis through regulating autophagy. *Lipids Health Dis.* 14, 134. doi: 10.1186/s12944-015-0139-6

Ji, X., Shi, S., Liu, B., Shan, M., Tang, D., Zhang, W., et al. (2019). Bioactive compounds from herbal medicines to manage dyslipidemia. *BioMed. Pharmacother.* 118, 109338. doi: 10.1016/j.biopha.2019.109338

Jiang, Y., Chen, L., Wang, H., Narisi, B., and Chen, B. (2015). Li-Gan-Shi-Liu-Ba-Wei-San improves non-alcoholic fatty liver disease through enhancing lipid oxidation and alleviating oxidation stress. *J. Ethnopharmacol.* 176, 499–507. doi: 10.1016/j.jep.2015.11.019

Kim, Y. J., Choi, M. S., Woo, J. T., Jeong, M. J., Kim, S. R., and Jung, U. J. (2017). Long-term dietary supplementation with low-dose nobiletin ameliorates hepatic steatosis, insulin resistance, and inflammation without altering fat mass in diet-induced obesity. *Mol. Nutr. Food Res.* 61, 1600889. doi: 10.1002/mnfr.201600889

Kim, J. C., Jeon, J. Y., Yang, W. S., Kim, C. H., and Eom, D. W. (2019a). Combined Amelioration of Ginsenoside (Rg1, Rb1, and Rg3)-enriched Korean Red Ginseng and Probiotic Lactobacillus on Non-alcoholic Fatty Liver Disease. *Curr. Pharm. Biotechnol.* 20, 222–231. doi: 10.2174/1389201020666190311143554

Kim, K. D., Jung, H. Y., Ryu, H. G., Kim, B., Jeon, J., Yoo, H. Y., et al. (2019b). Betulinic acid inhibits high-fat diet-induced obesity and improves energy balance by activating AMPK. *Nutr. Metab. Cardiovasc. Dis.* 29, 409–420. doi: 10.1016/j.numecd.2018.12.001

Kobayashi, S., Kawasaki, Y., Takahashi, T., Maeno, H., and Nomura, M. (2017). Mechanisms for the anti-obesity actions of bofutsushosan in high-fat diet-fed obese mice. *Chin. Med.* 12, 8. doi: 10.1186/s13020-017-0129-x

Kwak, D. H., Kim, J. S., Chang, K. T., and Choo, Y. K. (2016). Aristolochia manshuriensis Kom ethyl acetate extract protects against high-fat diet-induced non-alcoholic steatohepatitis by regulating kinase phosphorylation in mouse. *J. Vet Sci.* 17, 279–287. doi: 10.4142/jvs.2016.17.3.279

Kwon, E. Y., Shin, S. K., and Choi, M. S. (2018). Ursolic Acid Attenuates Hepatic Steatosis, Fibrosis, and Insulin Resistance by Modulating the Circadian Rhythm Pathway in Diet-Induced Obese Mice. *Nutrients* 10, 1719. doi: 10.3390/nu10111719

Lee, M. R., Park, K. I., and Ma, J. Y. (2017). Leonurus japonicus Houtt Attenuates Nonalcoholic Fatty Liver Disease in Free Fatty Acid-Induced HepG2 Cells and Mice Fed a High-Fat Diet. *Nutrients* 10, 20. doi: 10.3390/nu10010020

Lee, M. R., Yang, H. J., Park, K. I., and Ma, J. Y. (2019). Lycopus lucidus Turcz. ex Benth. Attenuates free fatty acid-induced steatosis in HepG2 cells and non-alcoholic fatty liver disease in high-fat diet-induced obese mice. *Phytomedicine* 55, 14–22. doi: 10.1016/j.phymed.2018.07.008

Li, S., Liao, X., Meng, F., Wang, Y., Sun, Z., Guo, F., et al. (2014a). Therapeutic role of ursolic acid on ameliorating hepatic steatosis and improving metabolic disorders in high-fat diet-induced non-alcoholic fatty liver disease rats. *PloS One* 9, e86724. doi: 10.1371/journal.pone.0086724

Li, Y., Zhao, J., Zheng, H., Zhong, X., Zhou, J., and Hong, Z. (2014b). Treatment of Nonalcoholic Fatty Liver Disease with Total Alkaloids in Rubus aleaefolius Poir through Regulation of Fat Metabolism. *Evid. Based. Complement. Alternat Med.* 2014, 768540. doi: 10.1155/2014/768540

Li, H., Ying, H., Hu, A., Hu, Y., and Li, D. (2017a). Therapeutic Effect of Gypenosides on Nonalcoholic Steatohepatitis via Regulating Hepatic Lipogenesis and Fatty Acid Oxidation. *Biol. Pharm. Bull.* 40, 650–657. doi: 10.1248/bpb.b16-00942

Li, W. S., Wu, Y., Ge, W. Z., Fan, L., and Sun, W. (2017b). A herbal formula Erchen decoction for non-alcoholic fatty liver disease: a systematic review and meta-analysis of randomized controlled trials. *Int. J. Clin. Exp. Med.* 10, 9110–9116.

Li, Y., Liu, T., Yan, C., Xie, R., Guo, Z., Wang, S., et al. (2018). Diammonium Glycyrrhizinate Protects against Nonalcoholic Fatty Liver Disease in Mice through Modulation of Gut Microbiota and Restoration of Intestinal Barrier. *Mol. Pharm.* 15, 3860–3870. doi: 10.1021/acs.molpharmaceut.8b00347

Li, S., Qian, Y., Xie, R., Li, Y., Jia, Z., Zhang, Z., et al. (2019). Exploring the protective effect of ShengMai-Yin and Ganmaidazao decoction combination against type 2 diabetes mellitus with nonalcoholic fatty liver disease by network pharmacology and validation in KKAy mice. *J. Ethnopharmacol.* 242, 112029. doi: 10.1016/j.jep.2019.112029

Lim, D. W., Kim, H., Lee, S. J., Yu, G. R., Kim, J. E., and Park, W. H. (2019). Jwa Kum Whan Attenuates Nonalcoholic Fatty Liver Disease by Modulating Glucose Metabolism and the Insulin Signaling Pathway. *Evid. Based. Complement. Alternat. Med.* 2019, 4589810. doi: 10.1155/2019/4589810

Lin, Z., Wu, Z. F., Jiang, C. H., Zhang, Q. W., Ouyang, S., Che, C. T., et al. (2016). The chloroform extract of Cyclocarya paliurus attenuates high-fat diet induced non-alcoholic hepatic steatosis in Sprague Dawley rats. *Phytomedicine* 23, 1475–1483. doi: 10.1016/j.phymed.2016.08.003

Lin, Y. N., Wang, C. C. N., Chang, H. Y., Chu, F. Y., Hsu, Y. A., Cheng, W. K., et al. (2018). Ursolic Acid, a Novel Liver X Receptor alpha (LXRalpha) Antagonist Inhibiting Ligand-Induced Nonalcoholic Fatty Liver and Drug-Induced Lipogenesis. *J. Agric. Food Chem.* 66, 11647–11662. doi: 10.1021/acs.jafc.8b04116

Liou, C. J., Lee, Y. K., Ting, N. C., Chen, Y. L., Shen, S. C., Wu, S. J., et al. (2019). Protective Effects of Licochalcone A Ameliorates Obesity and Non-Alcoholic Fatty Liver Disease Via Promotion of the Sirt-1/AMPK Pathway in Mice Fed a High-Fat Diet. *Cells* 8, 447. doi: 10.3390/cells8050447

Liu, Z. L., Xie, L. Z., Zhu, J., Li, G. Q., Grant, S. J., and Liu, J. P. (2013). Herbal medicines for fatty liver diseases. *Cochrane Database Syst. Rev.* 8, CD009059. doi: 10.1002/14651858.CD009059.pub2

Liu, H.-K., Hung, T.-M., Huang, H.-C., Lee, I. J., Chang, C.-C., Cheng, J.-J., et al. (2015a). Bai-Hu-Jia-Ren-Shen-Tang Decoction Reduces Fatty Liver by Activating AMP-Activated Protein Kinase In Vitro and In Vivo. *Evid. Based. Complement. Altern. Med.* 2015, 651734. doi: 10.1155/2015/651734

Liu, M., Xu, L., Yin, L., Qi, Y., Xu, Y., Han, X., et al. (2015b). Potent effects of dioscin against obesity in mice. *Sci. Rep.* 5, 7973. doi: 10.1038/srep07973

Liu, Y., Yu, Q., and Chen, Y. (2018). Effect of silibinin on CFLAR-JNK pathway in oleic acid-treated HepG2 cells. *Biomed. Pharmacother.* 108, 716–723. doi: 10.1016/j.biopha.2018.09.089

Liu, K., Luo, M., and Wei, S. (2019a). The Bioprotective Effects of Polyphenols on Metabolic Syndrome against Oxidative Stress: Evidences and Perspectives. *Oxid. Med. Cell. Longevity* 2019, 1–16. doi: 10.1155/2019/6713194

Liu, M. T., Huang, Y. J., Zhang, T. Y., Tan, L. B., Lu, X. F., and Qin, J. (2019b). Lingguizhugan decoction attenuates diet-induced obesity and hepatosteatosis via gut microbiota. *World J. Gastroenterol.* 25, 3590–3606. doi: 10.3748/wjg.v25.i27.3590

Liu, X., Huang, K., Niu, Z., Mei, D., and Zhang, B. (2019c). Protective effect of isochlorogenic acid B on liver fibrosis in non-alcoholic steatohepatitis of mice. *Basic Clin. Pharmacol. Toxicol.* 124, 144–153. doi: 10.1111/bcpt.13122

Liu, Y., Xu, W., Zhai, T., You, J., and Chen, Y. (2019d). Silibinin ameliorates hepatic lipid accumulation and oxidative stress in mice with non-alcoholic steatohepatitis by regulating CFLAR-JNK pathway. *Acta Pharm. Sin. B* 9, 745–757. doi: 10.1016/j.apsb.2019.02.006

Loguercio, C., Andreone, P., Brisc, C., Brisc, M. C., Bugianesi, E., Chiaramonte, M., et al. (2012). Silybin combined with phosphatidylcholine and vitamin E in patients with nonalcoholic fatty liver disease: a randomized controlled trial. *Free Radical Biol. Med.* 52, 1658–1665. doi: 10.1016/j.freeradbiomed.2012.02.008

Luo, Y., Dong, X., Yu, Y., Sun, G., and Sun, X. (2015). Total aralosides of aralia elata (Miq) seem (TASAES) ameliorate nonalcoholic steatohepatitis by modulating IRE1alpha-mediated JNK and NF-kappaB pathways in ApoE-/- mice. *J. Ethnopharmacol.* 163, 241–250. doi: 10.1016/j.jep.2015.01.017

Luo, Y., Tian, G., Zhuang, Z., Chen, J., You, N., Zhuo, L., et al. (2019). Berberine prevents non-alcoholic steatohepatitis-derived hepatocellular carcinoma by inhibiting inflammation and angiogenesis in mice. *Am. J. Transl. Res.* 11, 2668–2682.

Marra, F., and Lotersztajn, S. (2013). Pathophysiology of NASH: perspectives for a targeted treatment. *Curr. Pharm. Des.* 19, 5250–5269. doi: 10.2174/13816128113199990344

Mouzaki, M., Comelli, E. M., Arendt, B. M., Bonengel, J., Fung, S. K., Fischer, S. E., et al. (2013). Intestinal microbiota in patients with nonalcoholic fatty liver disease. *Hepatology* 58, 120–127. doi: 10.1002/hep.26319

Mulvihill, E. E., Allister, E. M., Sutherland, B. G., Telford, D. E., Sawyez, C. G., Edwards, J. Y., et al. (2009). Naringenin Prevents Dyslipidemia, Apolipoprotein B Overproduction, and Hyperinsulinemia in LDL Receptor–Null Mice With Diet-Induced Insulin Resistance. *Diabetes* 58, 2198–2210. doi: 10.2337/db09-0634

Panahi, Y., Kianpour, P., Mohtashami, R., Jafari, R., Simental-Mendía, L. E., and Sahebkar, A. (2017). Efficacy and Safety of Phytosomal Curcumin in Non-Alcoholic Fatty Liver Disease: A Randomized Controlled Trial. *Drug Res.* 67, 244–251. doi: 10.1055/s-0043-100019

Pang, S. C., Wang, S., Chen, M. L., Zhang, J. P., Wang, Y. Y., Jia, H. Y., et al. (2019). BuShenKangShuai Tablet Alleviates Hepatic Steatosis via Improving Liver Adiponectin Resistance in ApoE(-/-) Mice. *Evid. Based. Complement. Alternat. Med.* 2019, 8986038. doi: 10.1155/2019/8986038

Park, M., Yoo, J. H., Lee, Y. S., and Lee, H. J. (2019). Lonicera caerulea Extract Attenuates Non-Alcoholic Fatty Liver Disease in Free Fatty Acid-Induced HepG2 Hepatocytes and in High Fat Diet-Fed Mice. *Nutrients* 11, 494. doi: 10.3390/nu11030494

Peng, H., He, Y., Zheng, G., Zhang, W., Yao, Z., and Xie, W. (2016). Meta-analysis of traditional herbal medicine in the treatment of nonalcoholic fatty liver disease. *Cell Mol. Biol. (Noisy-le-grand)* 62, 88–95.

Porras, D., Nistal, E., Martinez-Florez, S., Pisonero-Vaquero, S., Olcoz, J. L., Jover, R., et al. (2017). Protective effect of quercetin on high-fat diet-induced non-alcoholic fatty liver disease in mice is mediated by modulating intestinal microbiota imbalance and related gut-liver axis activation. *Free Radic. Biol. Med.* 102, 188–202. doi: 10.1016/j.freeradbiomed.2016.11.037

Porras, D., Nistal, E., Martínez-Flórez, S., González-Gallego, J., García-Mediavilla, M. V., and Sánchez-Campos, S. (2018). Intestinal Microbiota Modulation in Obesity-Related Non-alcoholic Fatty Liver Disease. *Front. Physiol.* 9, 1813–1813. doi: 10.3389/fphys.2018.01813

Qi, G., Guo, R., Tian, H., Li, L., Liu, H., Mi, Y., et al. (2018). Nobiletin protects against insulin resistance and disorders of lipid metabolism by reprogramming of circadian clock in hepatocytes. *Biochim. Biophys. Acta Mol. Cell Biol. Lipids* 1863, 549–562. doi: 10.1016/j.bbalip.2018.02.009

Rahmani, S., Asgary, S., Askari, G., Keshvari, M., Hatamipour, M., Feizi, A., et al. (2016). Treatment of Non-alcoholic Fatty Liver Disease with Curcumin: A

Randomized Placebo-controlled Trial. *Phytother. Res.* 30, 1540–1548. doi: 10.1002/ptr.5659

Sanyal, A. J., Chalasani, N., Kowdley, K. V., Mccullough, A., Diehl, A. M., Bass, N. M., et al. (2010). Pioglitazone, Vitamin E, or Placebo for Nonalcoholic Steatohepatitis. *New Engl. J. Med.* 362, 1675–1685. doi: 10.1056/NEJMoa0907929

Sarwar, R., Pierce, N., and Koppe, S. (2018). Obesity and nonalcoholic fatty liver disease: current perspectives. *Diabetes Metab. Syndr. Obes.* 11, 533–542. doi: 10.2147/DMSO.S146339

Shen, L., Xiong, Y., Wang, D. Q., Howles, P., Basford, J. E., Wang, J., et al. (2013). Ginsenoside Rb1 reduces fatty liver by activating AMP-activated protein kinase in obese rats. *J. Lipid Res.* 54, 1430–1438. doi: 10.1194/jlr.M035907

Shen, K., Wang, Y., Zhang, Y., Zhou, H., Song, Y., Cao, Z., et al. (2015). Cocktail of Four Active Components Derived from Sheng Mai San Inhibits Hydrogen Peroxide-Induced PC12 Cell Apoptosis Linked with the Caspase-3/ROCK1/MLC Pathway. *Rejuvenation Res.* 18, 517–527. doi: 10.1089/rej.2015.1697

Shi, K. Q., Fan, Y. C., Liu, W. Y., Li, L. F., Chen, Y. P., and Zheng, M. H. (2012). Traditional Chinese medicines benefit to nonalcoholic fatty liver disease: a systematic review and meta-analysis. *Mol. Biol. Rep.* 39, 9715–9722. doi: 10.1007/s11033-012-1836-0

Si, W., Chen, Y. P., Zhang, J., Chen, Z. Y., and Chung, H. Y. (2018). Antioxidant activities of ginger extract and its constituents toward lipids. *Food Chem.* 239, 1117–1125. doi: 10.1016/j.foodchem.2017.07.055

Solhi, H., Ghahremani, R., Kazemifar, A. M., and Hoseini Yazdi, Z. (2014). Silymarin in treatment of non-alcoholic steatohepatitis: A randomized clinical trial. *Caspian J. Internal Med.* 5, 9–12.

Song, C. Y., Shi, J., Zeng, X., Zhang, Y., Xie, W. F., and Chen, Y. X. (2013). Sophocarpine alleviates hepatocyte steatosis through activating AMPK signaling pathway. *Toxicol. In Vitro* 27, 1065–1071. doi: 10.1016/j.tiv.2013.01.020

Tang, W., Zeng, L., Yin, J., Yao, Y., Feng, L., Yao, X., et al. (2015). Hugan Qingzhi Exerts Anti-Inflammatory Effects in a Rat Model of Nonalcoholic Fatty Liver Disease. *Evidence-Based Complementary Altern. Med.* 2015, 810369. doi: 10.1155/2015/810369

Van De Wier, B., Koek, G. H., Bast, A., and Haenen, G. R. (2017). The potential of flavonoids in the treatment of non-alcoholic fatty liver disease. *Crit. Rev. Food Sci. Nutr.* 57, 834–855. doi: 10.1080/10408398.2014.952399

Wang, Y.-L., Liu, L.-J., Zhao, W.-H., and Li, J.-X. (2015). Intervening TNF-α via PPARγ with Gegenqinlian Decoction in Experimental Nonalcoholic Fatty Liver Disease. *Evidence-Based. Complement. Altern. Med.* 2015, 715638. doi: 10.1155/2015/715638

Wang, Y., Liu, Q., Xu, Y., Zhang, Y., Lv, Y., Tan, Y., et al. (2016). Ginsenoside Rg1 Protects against Oxidative Stress-induced Neuronal Apoptosis through Myosin IIA Related Cytoskeletal Reorganization. *Int. J. Biol. Sci.* 12, 1341–1356. doi: 10.7150/ijbs.15992

Wang, Y., Xu, Y., Liu, Q., Zhang, Y., Gao, Z., Yin, M., et al. (2017). Myosin IIA-related Actomyosin Contractility Mediates Oxidative Stress-induced Neuronal Apoptosis. *Front. Mol. Neurosci.* 10, 75. doi: 10.3389/fnmol.2017.00075

Wang, S., Yang, F. J., Shang, L. C., Zhang, Y. H., Zhou, Y., and Shi, X. L. (2019a). Puerarin protects against high-fat high-sucrose diet-induced non-alcoholic fatty liver disease by modulating PARP-1/PI3K/AKT signaling pathway and facilitating mitochondrial homeostasis. *Phytother. Res.* 33, 2347–2359. doi: 10.1002/ptr.6417

Wang, Y., Zhao, H., Li, X., Li, N., Wang, Q., Liu, Y., et al. (2019b). Tangshen Formula Alleviates Hepatic Steatosis by Inducing Autophagy Through the AMPK/SIRT1 Pathway. *Front. Physiol.* 10, 494. doi: 10.3389/fphys.2019.00494

Wat, E., Ng, C. F., Wong, E. C., Koon, C. M., Lau, C. P., Cheung, D. W., et al. (2016). The hepatoprotective effect of the combination use of Fructus Schisandrae with statin–A preclinical evaluation. *J. Ethnopharmacol.* 178, 104–114. doi: 10.1016/j.jep.2015.12.004

Wong, V. W.-S., Chan, R. S.-M., Wong, G. L.-H., Cheung, B. H.-K., Chu, W. C.-W., Yeung, D. K.-W., et al. (2013). Community-based lifestyle modification programme for non-alcoholic fatty liver disease: a randomized controlled trial. *J. Hepatol.* 59, 536–542. doi: 10.1016/j.jhep

Xiao, J., Ching, Y. P., Liong, E. C., Nanji, A. A., Fung, M. L., and Tipoe, G. L. (2013a). Garlic-derived S-allylmercaptocysteine is a hepato-protective agent in non-alcoholic fatty liver disease in vivo animal model. *Eur. J. Nutr.* 52, 179–191. doi: 10.1007/s00394-012-0301-0

Xiao, J., Guo, R., Fung, M. L., Liong, E. C., Chang, R. C., Ching, Y. P., et al. (2013b). Garlic-Derived S-Allylmercaptocysteine Ameliorates Nonalcoholic Fatty Liver Disease in a Rat Model through Inhibition of Apoptosis and Enhancing Autophagy. *Evid. Based. Complement Alternat. Med.* 2013, 642920. doi: 10.1155/2013/642920

Xiao, J., Xing, F., Huo, J., Fung, M. L., Liong, E. C., Ching, Y. P., et al. (2014). Lycium barbarum polysaccharides therapeutically improve hepatic functions in non-alcoholic steatohepatitis rats and cellular steatosis model. *Sci. Rep.* 4, 5587. doi: 10.1038/srep05587

Xu, L., Yin, L., Tao, X., Qi, Y., Han, X., Xu, Y., et al. (2017). Dioscin, a potent ITGA5 inhibitor, reduces the synthesis of collagen against liver fibrosis: Insights from SILAC-based proteomics analysis. *Food Chem. Toxicol.* 107, 318–328. doi: 10.1016/j.fct.2017.07.014

Yan, T., Wang, H., Cao, L., Wang, Q., Takahashi, S., Yagai, T., et al. (2018). Glycyrrhizin Alleviates Nonalcoholic Steatohepatitis via Modulating Bile Acids and Meta-Inflammation. *Drug Metab. Disposition* 46, 1310–1319. doi: 10.1124/dmd.118.082008

Yang, L., Ren, S., Xu, F., Ma, Z., Liu, X., and Wang, L. (2019). Recent Advances in the Pharmacological Activities of Dioscin. *BioMed. Res. Int.* 2019, 5763602. doi: 10.1155/2019/5763602

Yang, X. X., Wang, X., Shi, T. T., Dong, J. C., Li, F. J., Zeng, L. X., et al. (2019). Mitochondrial dysfunction in high-fat diet-induced nonalcoholic fatty liver disease: The alleviating effect and its mechanism of Polygonatum kingianum. *BioMed. Pharmacother.* 117, 109083. doi: 10.1016/j.biopha.2019.109083

Yang, Y., Li, J., Wei, C., He, Y., Cao, Y., Zhang, Y., et al. (2019). Amelioration of nonalcoholic fatty liver disease by swertiamarin in fructose-fed mice. *Phytomedicine* 59, 152782. doi: 10.1016/j.phymed.2018.12.005

Yao, Z., Liu, X. C., and Gu, Y. E. (2014). Schisandra chinensis Baill, a Chinese medicinal herb, alleviates high-fat-diet-inducing non-alcoholic steatohepatitis in rats. *Afr. J. Tradit. Complement. Altern. Med.* 11, 222–227. doi: 10.4314/ajtcam.v11i1.35

Yao, H., Qiao, Y.-J., Zhao, Y.-L., Tao, X.-F., Xu, L.-N., Yin, L.-H., et al. (2016). Herbal medicines and nonalcoholic fatty liver disease. *World J. Gastroenterol.* 22, 6890–6905. doi: 10.3748/wjg.v22.i30.6890

Yao, H., Tao, X., Xu, L., Qi, Y., Yin, L., Han, X., et al. (2018). Dioscin alleviates non-alcoholic fatty liver disease through adjusting lipid metabolism via SIRT1/AMPK signaling pathway. *Pharmacol. Res.* 131, 51–60. doi: 10.1016/j.phrs.2018.03.017

Yin, J., Luo, Y., Deng, H., Qin, S., Tang, W., Zeng, L., et al. (2014). Hugan Qingzhi medication ameliorates hepatic steatosis by activating AMPK and PPARα pathways in L02 cells and HepG2 cells. *J. Ethnopharmacol.* 154, 229–239. doi: 10.1016/j.jep.2014.04.011

Yu, X., Ye, L., Zhang, H., Zhao, J., Wang, G., Guo, C., et al. (2015). Ginsenoside Rb1 ameliorates liver fat accumulation by upregulating perilipin expression in adipose tissue of db/db obese mice. *J. Ginseng Res.* 39, 199–205. doi: 10.1016/j.jgr.2014.11.004

Yuanyuan, W., Minghua, J., Lina, Z., Suhua, L., Jiayu, Z., Yongzhi, S., et al. (2015). Effect of a combination of calorie-restriction therapy and Lingguizhugan decoction on levels of fasting blood lipid and inflammatory cytokines in a high-fat diet induced hyperlipidemia rat model. *J. Tradit. Chin. Med.* 35, 218–221. doi: 10.1016/S0254-6272(15)30031-5

Yuk, T., Kim, Y., Yang, J., Sung, J., Jeong, H. S., and Lee, J. (2018). Nobiletin Inhibits Hepatic Lipogenesis via Activation of AMP-Activated Protein Kinase. *Evid. Based. Complement. Alternat. Med.* 2018, 7420265. doi: 10.1155/2018/7420265

Zhai, K., Tang, Y., Zhang, Y., Li, F., Wang, Y., Cao, Z., et al. (2015). NMMHC IIA inhibition impedes tissue factor expression and venous thrombosis via Akt/GSK3β-NF-κB signalling pathways in the endothelium. *Thromb. Haemostasis* 114, 173–185. doi: 10.1160/TH14-10-0880

Zhang, Q., Zhao, Y., Zhang, D.-B., and Sun, L.-J. (2005). Effect of Sinai san decoction on the development of non-alcoholic steatohepatitis in rats. *World J. Gastroenterol.* 11, 1392–1395. doi: 10.3748/wjg.v11.i9.1392

Zhang, Y., Si, Y., Zhai, L., Yang, N., Yao, S., Sang, H., et al. (2013). Celastrus orbiculatus Thunb. ameliorates high-fat diet-induced non-alcoholic fatty liver disease in guinea pigs. *Pharmazie* 68, 850–854.

Zhang, Y., Chen, M. L., Zhou, Y., Yi, L., Gao, Y. X., Ran, L., et al. (2015). Resveratrol improves hepatic steatosis by inducing autophagy through the

cAMP signaling pathway. *Mol. Nutr. Food Res.* 59, 1443–1457. doi: 10.1002/mnfr.201500016

Zhang, E., Yin, S., Song, X., Fan, L., and Hu, H. (2016). Glycycoumarin inhibits hepatocyte lipoapoptosis through activation of autophagy and inhibition of ER stress/GSK-3-mediated mitochondrial pathway. *Sci. Rep.* 6, 38138. doi: 10.1038/srep38138

Zhang, W., Yin, L., Tao, X., Xu, L., Zheng, L., Han, X., et al. (2016). Dioscin alleviates dimethylnitrosamine-induced acute liver injury through regulating apoptosis, oxidative stress and inflammation. *Environ. Toxicol. Pharmacol.* 45, 193–201. doi: 10.1016/j.etap.2016.06.002

Zhang, J., Zhang, H., Deng, X., Zhang, N., Liu, B., Xin, S., et al. (2018). Baicalin attenuates non-alcoholic steatohepatitis by suppressing key regulators of lipid metabolism, inflammation and fibrosis in mice. *Life Sci.* 192, 46–54. doi: 10.1016/j.lfs.2017.11.027

Zhang, Y., Tang, K., Deng, Y., Chen, R., Liang, S., Xie, H., et al. (2018). Effects of shenling baizhu powder herbal formula on intestinal microbiota in high-fat diet-induced NAFLD rats. *BioMed. Pharmacother.* 102, 1025–1036. doi: 10.1016/j.biopha.2018.03.158

Zhou, L., Tang, J., Xiong, X., Dong, H., Huang, J., Zhou, S., et al. (2017). Psoralea corylifolia L. Attenuates Nonalcoholic Steatohepatitis in Juvenile Mouse. *Front. Pharmacol.* 8, 876. doi: 10.3389/fphar.2017.00876

Zhu, X., Bian, H., Wang, L., Sun, X., Xu, X., Yan, H., et al. (2019). Berberine attenuates nonalcoholic hepatic steatosis through the AMPK-SREBP-1c-SCD1 pathway. *Free Radic. Biol. Med.* 141, 192–204. doi: 10.1016/j.freeradbiomed.2019.06.019

Chlorogenic Acid Decreases Malignant Characteristics of Hepatocellular Carcinoma Cells by Inhibiting DNMT1 Expression

Yao Liu[1†], Ying Feng[1†], Yuxin Li[1†], Ying Hu[1], Qun Zhang[1], Yunyi Huang[2], Ke Shi[2], Chongping Ran[1], Jie Hou[2], Guiqin Zhou[1*] and Xianbo Wang[1*]

[1] Center of Integrative Medicine, Beijing Ditan Hospital, Capital Medical University, Beijing, China, [2] Department of Gastroenterology, Dongzhimen Hospital, Beijing University of Chinese Medicine, Beijing, China

Background: Hepatocellular carcinoma (HCC) is the most common malignant tumor of the adult liver, exhibiting rapid progression and poor prognosis. Chlorogenic acid (CGA), a polyphenol, has several biological activities, including the suppression of liver cancer cell invasion and metastasis. Increased levels or alterations in the function of DNMT1 are associated with the inactivation of tumor suppressor genes. However, the CGA-affected DNMT1 expression mediated mechanism is still unclear.

Methods: The human hepatocellular carcinoma (HCC) HepG2 cells were treated with a positive control drug (5-AZA) or varying doses of CGA. DNA methyltransferase 1 (DNMT1) protein levels and other relevant proteins were evaluated using Western blotting and immunocytochemistry. Cell-cycle analysis was performed by flow cytometry-based PI staining, and cell viability was assessed using 3-(4,5-dimethylthiazol-2-yl)-2,5-diphenyltetrazolium bromide (MTT) assay. The transwell invasion and wound healing assays were used to evaluate cell migration and invasion. In vivo proliferation of the HCC cells was detected. We investigated the expression of DNMT1, p53, p21, p-ERK, MMP-2, and MMP-9 in tumors using immunohistochemical analysis.

Results: Our results showed that CGA inhibited the proliferation, colony formation, invasion, and metastasis of HepG2 cells both *in vitro* and *in vivo* by down-regulating DNMT1 protein expression, which enhanced p53 and p21 activity, and resulting in a significant reduction in cell proliferation and metastasis. Moreover, CGA inactivated ERK1/2 and reduced MMP-2 and MMP-9 expression in HepG2 cells.

Conclusions: CGA can suppress liver cancer cell proliferation, invasion, and metastasis through several pathways. CGA could serve as a candidate chemopreventive agent for HCC.

Keywords: chlorogenic acid, DNMT1, hepatocellular carcinoma, proliferation, migration

INTRODUCTION

Hepatocellular carcinoma (HCC) is the most common adult liver malignancy exhibiting rapid progression and poor prognosis (Shimada et al., 1996; Ma et al., 2014). Many signaling pathways participate in the development of HCC. In addition to several possibilities causing HCC development, studies have implicated the accumulation of genetic abnormalities (e.g., epigenetic changes and gene amplification, as well as chromosomal variations) in triggering the development of HCC (Nishida and Goel, 2011). Epigenetic alterations are heritable variations that are not attributed to DNA sequence variations. DNA methylation is an important research topic in epigenetics.

DNA methylation is the addition of a methyl group to a cytosine (C) residue assisted by an enzyme, DNA methyltransferase 1 (DNMT1); it is the most prevalent epigenetic modification (Jones and Baylin, 2002; Hegi et al., 2009). Gene promoter hypermethylation has been considered as a vital mechanism to inhibit the expression of genes involved in tumor development. In sporadic cancers, roughly half the tumor-suppressor genes are reported to be inactivated by epigenetic rather than genetic mechanisms (Xu et al., 2018). Protein-protein interactions (PPIs) were used to identify the interactions between DNMT1 and tumor progression-related proteins (https://string-db.org/). The results showed a link between DNMT1 and p53.

p53 is a tumor-suppressor protein. Under normal conditions, p53 is turned off and activated during stress when cells divide and proliferate uncontrollably (Vogelstein et al., 2000; Harris and Levine, 2005). As cell growth is out of control, p53 induces p21 expression, which results in cell-cycle arrest (Faria et al., 2007; Georgakilas et al., 2017). Previous studies have shown a relationship between the methylation of CpG dinucleotide located in the p53 promoter region with low p53 expression levels, leading to tumor progression and growth.

Since tumor-suppressor gene promoter hypermethylation is considered as one of the principal factors facilitating tumor progression, demethylation drugs have become the primary research focus for molecularly targeted therapy (Sajadian et al., 2016). Many different in vitro studies showed that 5-azacytidine (5-AZA), a potent DNA methyltransferase inhibitor (DNMTi), triggers the re-expression of silenced genes, alters the expression of genes participating in tumor suppression (Christman, 2002), and is used as a positive control drug. Chlorogenic acid (CGA), a polyphenol, is an ester in which the acid (part of the caffeic acid) binds to the hydroxyl group at 5′ of the quinic acid (5′-coffee-derived quinic acid). Epidemiological studies suggested that CGA has antioxidant, anti-inflammatory, antiviral, and anticancer properties, and other biological characteristics (Shi et al., 2009; Xu et al., 2010; Yun et al., 2012; Zhao et al., 2012; Ji et al., 2013; Shi et al., 2013). A recent study showed that CGA could prevent HCC progression by inactivating ERK1/2 and suppressing MMP-2 and MMP-9 expressions (Yan et al., 2017). Furthermore, by inhibiting the activity of the anti-apoptotic proteins Bcl2 and Bcl-xL and activating the pro-apoptotic proteins annexin V, Bax, and caspase 3/7, CGA promoted regorafenib's apoptotic effect (Refolo et al., 2018). However,

the CGA-affected DNMT1 expression-mediated mechanisms are still unclear.

In this study, we evaluated the direct effect of CGA on the HCC cells. CGA inhibited in vitro HepG2 cell proliferation by inactivating DNMT1 and activating P53 and increasing the expression of p21. In addition, CGA inactivated ERK1/2 and reduced the expression of MMP-2 and MMP-9 in HepG2 cells. Based on the data mentioned above, CGA exhibits anti-proliferative activity and could be a potential therapeutic agent for the treatment of HCC.

MATERIALS AND METHODS

Materials

CGA was provided by J&K Scientific. Ltd (Beijing, China), was dissolved in sterile H_2O, the solution filtered using a 0.22-μm filter, incubated at $-20°C$, and diluted with the cell culture medium. 5-Azacytidine was obtained from Melone Pharmaceutical Co. Ltd (Dalian, China), dissolved in sterile Dimethyl Sulfoxide (DMSO, Sigma), and incubated at $-20°C$. The cells in the CGA group were treated for 48 h with graded doses of CGA (0, 250, 500, and 1000 μM). The cells in the 5-AZA group were treated for 48 h with varying doses of 5-AZA (0, 1, 5, and 10 μM), and vehicle DMSO was present at an equal concentration in the control group (CON). The antibodies for DNMT1, p21, MMP2, MMP9, and GAPDH were procured from Cell Signaling Technology, Inc. (Danvers, MA, USA). The antibodies against p53 were obtained from Proteintech Group, Inc. (Wuhan, Hubei, China).

Cell Culture

The HCC cell lines (HuH-7, HepG2, MHCC97H, and MHCC97L) were provided by the China Infrastructure of Cell Line Resources. Cells were cultured with Dulbecco's modified Eagle's medium (DMEM) containing 1% glutamine, 1% penicillin/streptomycin, and 10% fetal bovine serum (FBS; Hyclone, USA). Cells were incubated at $37°C$ with 5% CO_2 and were passaged once every 2–3 days, and cells in the mid-log phase were used for all experiments.

Cell Viability Assay

Cell viability was assessed with the 3-(4,5-dimethylthiazol-2-yl)-2,5-diphenyltetrazolium bromide (MTT) method. HepG2 cells were seeded in 96-well plates (4×10^3 cells/well) and incubated for 96 h at $37°C$ with 5% CO2 in the presence of increasing concentrations of CGA and 5-AZA. At the end of 96 h, 20 μl of MTT solution (5 mg/ml) was added to each well and incubated for 4 h at $37°C$. Next, the optical density was measured at 490 nm, and for normalization of the number of live cells, the absorbance values of cells dissolved in 150 μl of DMSO were used.

Colony Formation Assays

We conducted colony formation assays for 48 h with 500 cells plated in six-well plates from each group treated with a fixed dose

of 5-AZA (5 µM) and varying doses of CGA (250, 500, and 1000 µM). After 7 days of incubation, each well was washed with PBS and stained with crystal violet. The colonies were counted using a Leica DM6000B microscope with 10×0.25 NA objective lens (Leica, Wetzlar, Germany).

Cell Cycle Analysis

Cells pretreated for 48 h with 5-AZA (5 µM), and different doses of CGA (250, 500, and 1000 µM) were harvested by trypsinization, and 1×10^6 cells were used for analysis. The cells were washed twice with PBS and fixed in 75% ethanol at 4°C overnight. The cells were stained with propidium iodide for 30 min in the dark at 37°C following the manufacturer's instructions (BD, USA). Later, cells were collected, and cell-cycle analysis conducted using a flow cytometer (BD), and the histograms were analyzed using the ModFit software (Becton-Dickinson, USA).

Transwell Invasion Assay

For the transwell chamber assays, we used a filter membrane with an 8 µm pore size, pre-coated with Matrigel (BD Biosciences, CA, USA) for invasion assays, while ECM was omitted for performing cell migration assays (Costar, NY, USA). We added 600 µl of complete medium (DMEM, 10% FBS) to the lower chamber. Later, diluted HepG2 (5×10^5/ml) cells and 200 µl of the suspensions of CGA (250, 500, and 1000 µM)-, 5-AZA (5 µM)-pretreated cells and the vehicle DMSO control group (CON) were added to the upper chamber. For invasion assays, HepG2 cells were incubated for 24 and 48 h at 37°C in a humidified incubator with 5% CO_2. The non-migratory cells over the top of the filter were removed, and the invaded cells were kept stationary using anhydrous ethanol and stained using crystal violet. Images were captured at 100× magnification and the number of invaded cells was counted in five image fields. No fewer than five random microscopic fields were observed using Leica DM6000B microscope with a 10×0.25 NA objective lens (Leica, Wetzlar, Germany).

Wound Healing Assay

Cells pretreated with CGA (250, 500, and 1000 µM) were seeded in six-well plates, and when cells reached 90% confluence, the cells were scratched using a sterile pipette tip (10 µl). The scratched cells were washed with PBS and imaged using a Leica DM6000B microscope with 10×0.25 NA objective lens (Leica, Wetzlar, Germany). Later, 10% FBS in DMEM was added to cells for 48 h, and images of the wound were taken using the Image-Pro Plus (Media Cybernetics, USA), for measuring the scratch area.

Western Blot Analysis

Cells were lysed in RIPA buffer supplemented with protease inhibitors. The protein concentrations were measured using the BCA Protein Assay kit (Pierce). Equal amounts of each protein sample (20 µg) were added to the sample wells and electrophoresed on 10% SDS-polyacrylamide gels. The separated proteins were transferred to polyvinylidene difluoride membranes. The blotted membranes were blocked for 1 h with 5% skim milk, followed by incubation with anti-rabbit antibodies against DNMT1 (CST, 1:500 dilution), p53 (Proteintech, 1:500 dilution), p21$^{waf/Cip1}$ (CST, 1:500 dilution), MMP2 (CST, 1:500 dilution), MMP9 (CST, 1:500 dilution), and GAPDH (CST, 1:1000 dilution). Horseradish peroxidase-conjugated IgG secondary antibodies were used to visualize the immunoreactive bands with optimized chemiluminescence, and the band intensity was measured by the Alpha View software (Protein Simple, USA).

Immunocytochemistry Staining

For immunocytochemistry, HepG2 cells pretreated with CGA (500 µM) and 5-AZA (5 µM) for 48 h on glass coverslips were washed three times with phosphate-buffered saline, fixed for 30 min in absolute alcohol, followed by immunocytochemical staining for DNMT1 (1:500 dilution, CST), p53 (1:500 dilution, Proteintech), and p21 (1:500 dilution, CST). All steps were performed following the immunohistochemistry kit instructions. Diaminobenzidine (DAB) was used for color development. No fewer than five random microscopic fields were observed under Leica DM6000B microscope (Leica, Wetzlar, Germany), and the degree of immunostaining was measured using the Image-Pro Plus (Media Cybernetics, USA).

Subcutaneous Xenograft Nude Mouse Models

The animal center at the Beijing Vital River provided nude mice (BALB/c-A, 4 weeks old, male); they were housed under specific pathogen-free conditions. The mice were given free access to aseptic water and food. Before the experiment, the nude mice were acclimatized for at least seven days. Then, HepG2 cells (5×10^6 cells) were injected subcutaneously into the right flank of the mice. Tumors were measured using calipers every 5 days for 25 days, and the tumor size was calculated using the formula: V = 1/2 ab^2, where "a" is the maximum tumor diameter and "b" is the minimum tumor diameter. When the subcutaneous tumors of the nude mice reached 100 to 200 mm^3, the mice were divided randomly into four groups and received an intraperitoneal injection once per day (CON [normal saline], CGA [120 and 480 mg/kg], and 5-AZA [5 mg/kg]). Mice bearing subcutaneous tumors were euthanized after 35 days. The tumor tissues were surgically resected, fixed in formalin, and embedded in paraffin. For the immunohistochemistry analysis, we used the paraffin-embedded tissues. The study protocol was approved by the Vital River Institutional Animal Care and Use Committee (Document Number: RSD-SOP-002-01, and Protocol Number: P2019037). All animal experiments were conducted in accordance with the recommendations in the Guide for the Care and Use of Laboratory Animals of the National Institutes of Health. Every effort was made to reduce the number of the animals used and minimize animal suffering.

Immunohistochemistry

Formalin-fixed, paraffin-embedded tissue sections were de-paraffinized using washing steps with a graded range of alcohol solutions, and subsequent antigen retrieval and blocking with 5% BSA for 60 min. Tissue sections were incubated with antibodies

against DNMT1 (1:400 dilution, Abcam), p53 (1:80 dilution, CST), p21 (1:50 dilution, CST), p-ERK (1:200 dilution, CST), MMP-2 (1:50 dilution, CST), and MMP-9 (1:50 dilution, CST) over-night at 4°C. After washing, the secondary goat anti-mouse IgG antibody (ZSGB-BIO, Beijing, China) was added and incubated for 1 h at room temperature. The tissue sections were stained with 3,3′-diaminobenzidine (ZSGB-BIO, Beijing, 121 China) and hematoxylin (Solarbio, Beijing, China). Images were captured using a ZEISS microscope (Carl Zeiss AG, Baden-Württemberg, Germany), and the degree of the immunostaining was measured using Image-Pro Plus (Media Cybernetics, USA).

Statistical Analysis

Statistical analysis was by using the SPSS 20.0 (IBM, NY, USA) software, and results presented using the GraphPad software (GraphPad Software, CA, USA). The number of observations represents the categorical data. The mean ± standard deviation denoted the variables consistent with normal distributions. One-way ANOVA was used to analyze the differences in cell numbers, number of colonies, and tumor cell proliferation during various stages of the cell cycle among the experimental groups. A p value of < 0.05 was considered significant.
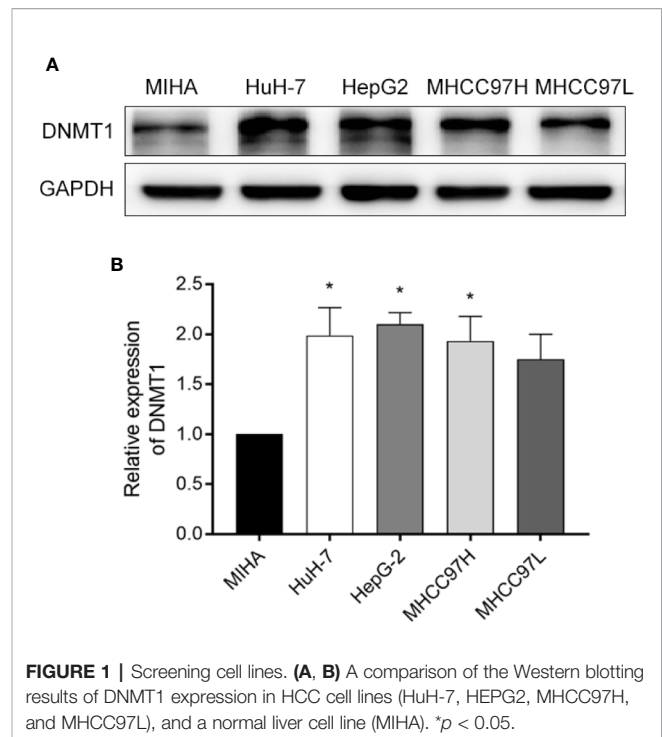

FIGURE 1 | Screening cell lines. (A, B) A comparison of the Western blotting results of DNMT1 expression in HCC cell lines (HuH-7, HEPG2, MHCC97H, and MHCC97L), and a normal liver cell line (MIHA). *$p < 0.05$.

RESULTS

Suppression of Cell Proliferation and Cell Cycle Progression in HepG2 Cells

We confirmed DNMT1 expression in four commonly used HCC cell lines, HuH-7, HepG2, MHCC97H, MHCC97L, as well as MIHA, a normal liver cell line. The Western blot results showed a high expression of DNMT1 in HepG2 cells (**Figures 1A, B**).

Cell proliferation was evaluated using MTT and colony formation assays. Cell proliferation was suppressed dose-dependently by CGA and 5-AZA, as shown by the MTT assay. At 500 and 1000 μM concentrations, CGA decreased the cell viability to 64.63%, and 53.88%, respectively; at 1 and 5 μM concentrations, 5-AZA decreased the cell viability by 69.10%, and 47.56%, respectively, at 48 h ($p < 0.001$, **Figures 2A–D**). Colony formation assay results showed that cells pretreated with CGA and 5-AZA exhibited fewer and smaller colonies than the control group, and with increasing CGA concentrations, the effect was more significant (**Figures 2E, F**).

Furthermore, cell cycle analysis was conducted to evaluate the CGA- and 5-AZA-mediated suppression of HepG2 cell viability. The data showed that both CGA and 5-AZA caused S-phase arrest in HepG2 cells (**Figures 2G, H**). These *in vitro* results suggest the CGA-mediated inhibition of HepG2 cell proliferation.

CGA and 5-AZA Inhibit *In Vitro* Invasion and Migration of HCC Cells

Rapid invasion and migration of HCC cells lead to disappointing liver cancer treatment outcomes. For investigating the *in vitro* effect of CGA and 5-AZA on HCC cell invasion and migration

processes, cells were treated with CGA at doses of 0, 250, 500, and 1000 μM and 5-AZA at 5 μM. HepG2 cell invasion and migration abilities were analyzed in transwell chambers. CGA suppressed the invasion of HCC cells dose-dependently (**Figures 3A, B**), with significant inhibition by CGA at 500 and 1000 μM. At 1000 μM, the percent suppression of invasion was 52.5% at 48 h in HepG2 cells compared to the control group. CGA inhibited the migration of HepG2 cells (**Figures 3C, D**). In Boyden chamber assays without Matrigel, CGA caused considerable suppression of HepG2 cell migration by 50.7% compared to the control group at 24 h. In contrast, 5 μM 5-AZA reduced the invasion ability by 70.5% and suppressed migration by 39.1% compared to the cells in the control group at 48 and 24 h, respectively.

In addition, to characterize the effect of CGA on HepG2 cells' migration, we performed wound healing assays. Treatment with CGA at doses of 500 and 1,000 μM significantly reduced the migratory ability of HepG2 in would healing assays over 24 and 48 h (**Figures 3E, F**). Altogether, based on the data mentioned above, CGA and 5-AZA can suppress HCC cells from metastasizing *in vitro*.

CGA Suppresses DNMT1 and Up-Regulates p53 and p21

P21 is a vital signal transducer for proliferation processes. Western blot assays were performed to confirm the effect of CGA on DNMT1 activity, p53, and p21, and the results show decreased levels of DNMT1 in cells after treatment with CGA or 5-AZA for 48 h. However, the levels of p53 and p21 increased
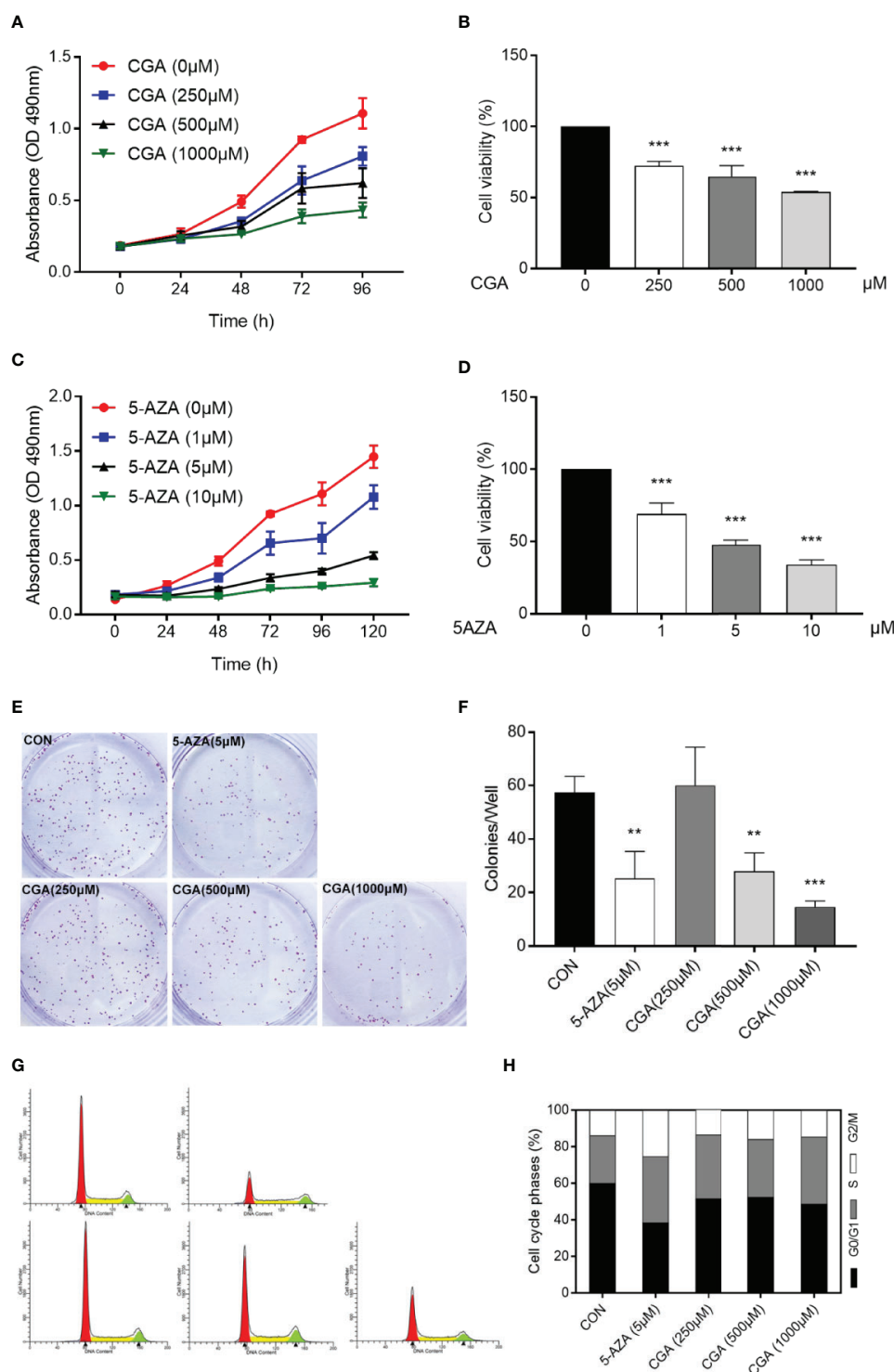
FIGURE 2 | CGA and 5-AZA inhibit proliferation and trigger cell cycle arrest of human HepG2 cells. Human HepG2 cells were treated for 96 h with increasing concentration of CGA (A, B) and a fixed concentration of 5-AZA (C, D). Subsequently, MTT assay assessed the cell viability as described in the Materials and Methods section. (E, F) HepG2 colony formation ability decreased remarkably after 48 h treatment with CGA and 5-AZA. (G, H) Cell cycle analysis shows increased S-phase arrest in cells from the CGA (1000 μM), and 5-AZA (5 μM) groups, compared to those from the CON group. **$p < 0.01$ and ***$p < 0.001$. CON, vehicle DMSO control group.
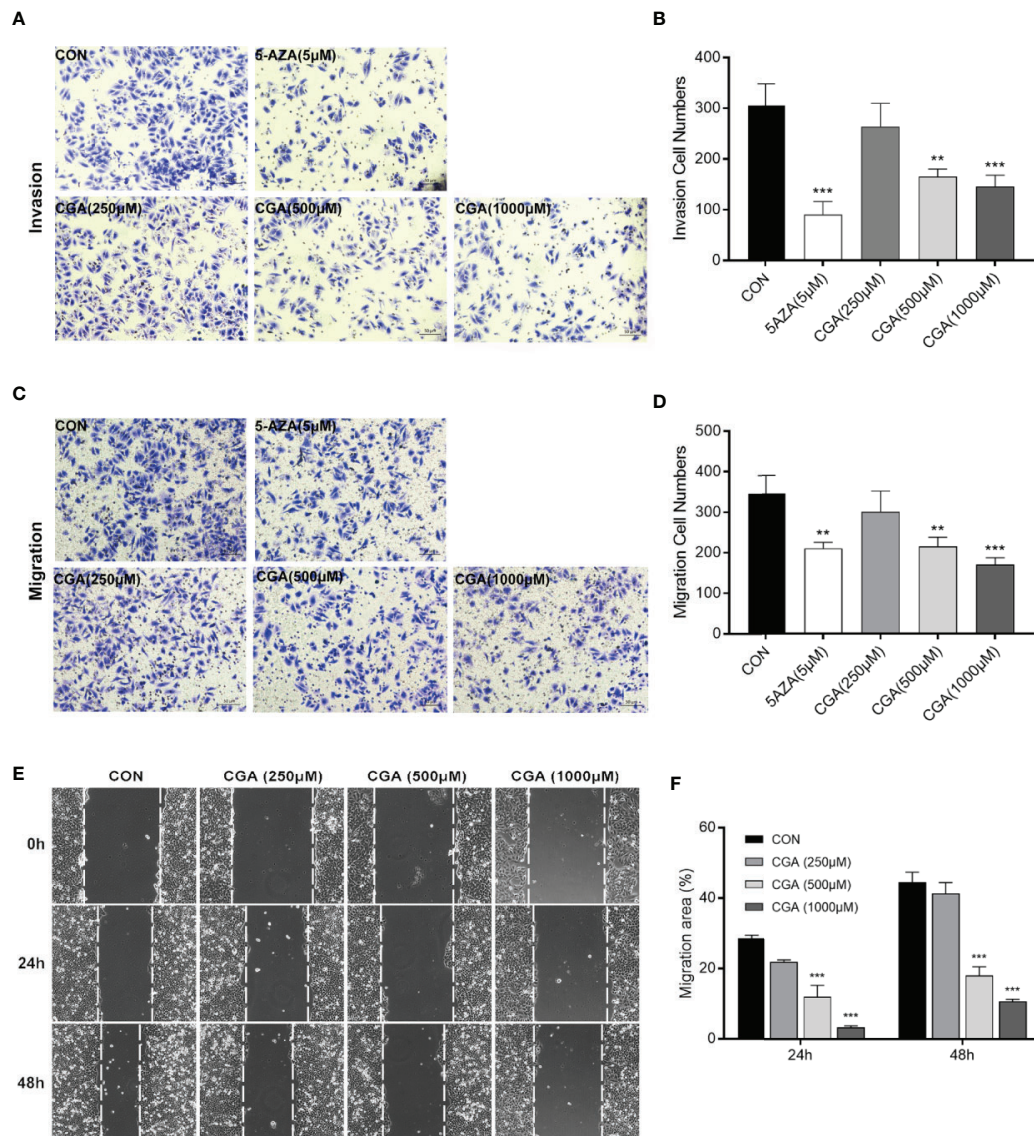
FIGURE 3 | CGA and 5-AZA inhibit invasion and migration of HEPG2 cells. After treatment with CGA (250, 500, 1000 µM) or 5-AZA (5 µM), cell invasion **(A, B)** and migration **(C, D)** abilities were detected by transwell invasion assays, and the migration rate was measured by the wound healing assay **(E, F)** in HepG2 cells. *******p* < 0.01, ********p* < 0.001. CON, vehicle DMSO control group.

as the DNMT1 levels decreased (**Figure 4A**). The protein levels in the cells from the CGA (500 µM) and 5-AZA (5 µM) group varied considerably compared to those from the control group. The grey values of DNMT1, p53, and p21 in the Western blots were analyzed for estimating the protein amount (**Figure 4B**).

CGA Inhibits the Activation of ERK1/2 and MMP2/9 in HepG2 Cells

The mitogen-activated protein kinases (MAPK) signaling pathway is critical to cell proliferation. Immunoblotting results confirmed

ERK1/2 activation based on the phosphorylated ERK1/2 level. After 48 h of treatment, CGA suppressed ERK1/2 phosphorylation and MMP2/9 expression in HepG2 cells (**Figures 4C, D**).

CGA Decreased DNMT1 Levels in HepG2 Cells by Immunocytochemistry Staining

Figure 5 shows positive immunocytochemical staining of DNMT1, p53, and p21 in the cytoplasm of HepG2 cells. DNMT1 and p53 showed diffuse staining, whereas p21 showed a granular staining pattern. CGA pretreated cells showed a significantly lower DNMT1 immunoreactivity than control
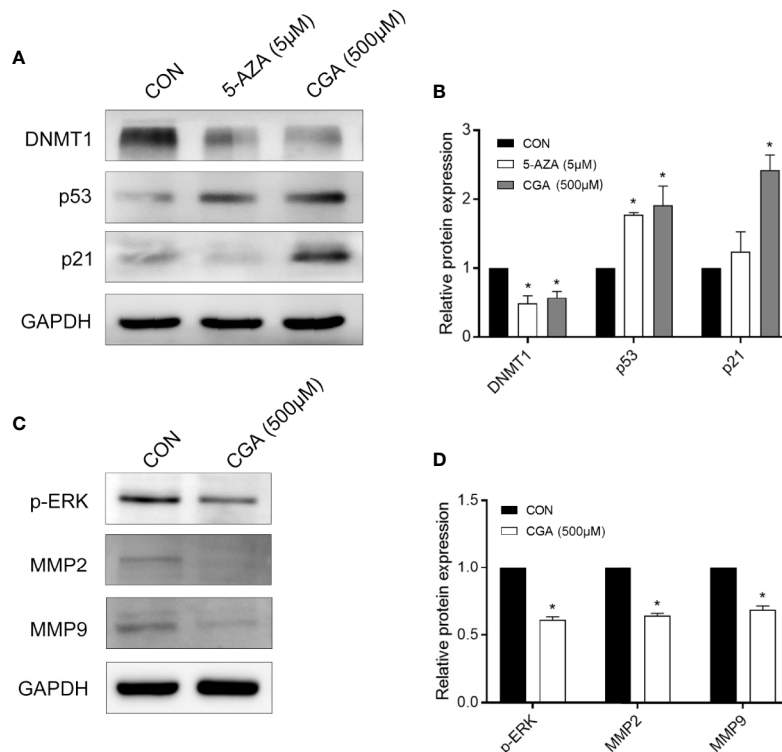
FIGURE 4 | CGA and 5-AZA inhibit the expression of DNMT1 and up-regulate p53, p21waf/Cip1, to suppress HCC cell proliferation. **(A)** CGA inhibits the expression of ERK1/2 and MMP2/9 to suppress HCC growth. **(C)** Evaluation of the protein expression levels involved in the DNMT1/p53/p21 pathway and p-ERK/MMP2/MMP9 pathway. **(B, D)** The gray value statistics of protein DNMT1, p53, p21, p-ERK, MMP2, and MMP9. *$p < 0.05$. CON, vehicle DMSO control group.

cells, and similar results were observed with 5-AZA treated cells (**Figure 5A**). CGA pretreated cells showed a considerably stronger immunoreactivity toward p53 and p21 than control cells (**Figures 5C, E**). The intensity of the immunocytochemical staining of DNMT1, p53, and p21 was analyzed in addition to protein levels, and significant differences were observed in case of cells from the CGA (500 μM), and 5-AZA (5 μM) groups, compared to those from the control group (**Figures 5B, D, F**). The results showed that in comparison to the control group, the DNMT1 protein levels were considerably lower in the CGA group. In contrast, in cells treated with CGA, the p53 and p21 levels were markedly higher than those in the cells from the control group. These results showed that decrease in DNMT1 expression inhibits HCC cell proliferation by up-regulating p53 and p21.

Anticancer Effect of CGA Against HepG2 Xenografts

The *in vivo* anticancer effect of CGA was evaluated in immunodeficient HepG2 xenograft nude mouse models. The mice were divided randomly into four groups: Group 1, injected with saline, groups 2 and 3, injected with CGA at 120 and 480 mg/kg, respectively, and Group 4, injected with 5-AZA 5 mg/kg every day from the first day of tumor formation. Compared to

the control (Group 1), treatment with CGA at 120 mg/kg (Group 2), 480 mg/kg (group 3), and 5-AZA at 5 mg/kg (Group 4) inhibited tumor growth, especially in case of 480 mg/kg CGA and 5 mg/kg 5-AZA (**Figures 6A, B**). All the mice were healthy. Slight differences were observed in body weight among the four groups (**Figure 6C**). Tumor volumes of mice xenografts in groups 3 and 4 were reduced considerably by 18.5% and 28.0%, respectively, compared to the control (Group 1) (**Figure 6D**), while the weights of the xenograft tumors in mice from groups 3 and 4 were reduced by 30.7% and 33.4%, respectively, compared to those in case of mice from the control (Group 1) (**Figure 6E**). These results showed that CGA inhibits the *in vivo* tumor growth in HepG2 xenograft mice.

Additionally, the protein levels of DNMT1, p53, p21, p-ERK, MMP-2, and MMP-9 in tumors were assessed by immunohistochemical analysis, and the results showed that compared to the control group, the levels of these proteins in the CGA and 5-AZA groups were reduced (**Figure 7A**). The *in vivo* results showed an apparent decrease in the levels of DNMT1 after treatment with CGA or 5-AZA, and this effect was higher with increasing CGA concentrations. By maintaining the stability and localization of p53 and p21, a low level of DNMT1 inhibits the formation and growth of the HCC xenograft tumor. Moreover, CGA inhibits the HepG2 xenograft growth by inactivating ERK
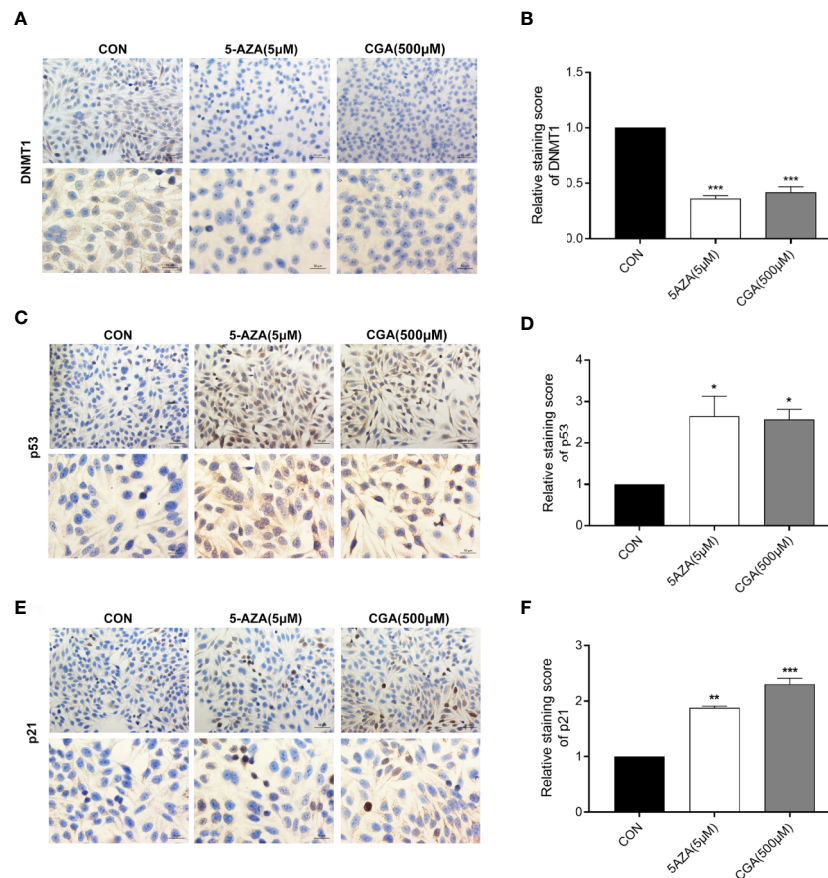
FIGURE 5 | Immunocytochemical staining intensity after treatment with CGA (250, 500, 1000 µM) and 5-AZA (5 µM) (200 × and 400 × magnification). **(A–F)** DAB staining showed a considerable decrease in DNMT1 expression and an increase in p53 and p21 expression in the CGA group. *$p < 0.05$, **$p < 0.01$, ***$p < 0.001$. CON, vehicle DMSO control group.

and decreasing MMP-2/9, thus inhibiting extracellular matrix degradation and HepG2 xenograft development (**Figure 7B**).

DISCUSSION

HCC treatment methods should explore effective chemoprevention strategies. Epidemiological studies showed that CGA ameliorates certain chronic diseases and cancers (Feng et al., 2005; Wang et al., 2011; Intisar et al., 2012). However, the CGA-affected DNMT1 expression-mediated mechanism is not yet understood.

In this study, we used the HCC cell line HepG2, and HepG2 nude mice xenografts, to evaluate inhibition of HCC growth both *in vivo* and *in vitro*. At higher concentrations, CGA reduced *in vitro* HepG2 cell viability, colony formation, invasion and migration (**Figures 2** and **3**), and *in vivo*, CGA treatment inhibited growth of HepG2 xenograft tumors, at both 120 and 480 mg/kg of CGA causing reduction in tumor weight and tumor volume (**Figure 6**).

At concentrations higher than 250 µM, CGA showed a significant inhibitory effect, and at a concentration of 1000 µM, it caused considerable S-phase arrest in HepG2 cells, which was consistent with other studies (Yan et al., 2017).

The regulation of genes involved in epigenetic processes is critical to understanding cancer development. DNA methylation is an essential epigenetic event in maintaining cellular function and regulating gene expression, probably facilitating cancer development (Butt et al., 2009; Lai et al., 2012; Bayan et al., 2014). DNMT1 is a maintenance methylase, critical throughout DNA methylation (Dan and Chen, 2016). The p53 protein is a tumor repressed gene, involved in regulating uncontrolled cell division, DNA replication, and cell cycle during tumor growth(Luo et al., 2017). When p53 protein loses its regulatory function, it may cause tumor progression and growth. Cyclin-dependent kinase (CDK) inhibitors (e.g., the cip/Kip family proteins, such as p21waf/cip1) bind to, and inhibit the activity of cyclin-CDK complexes, thereby participating as a negative regulator of cell cycle progression (Elledge et al., 1996; Harper and Elledge,
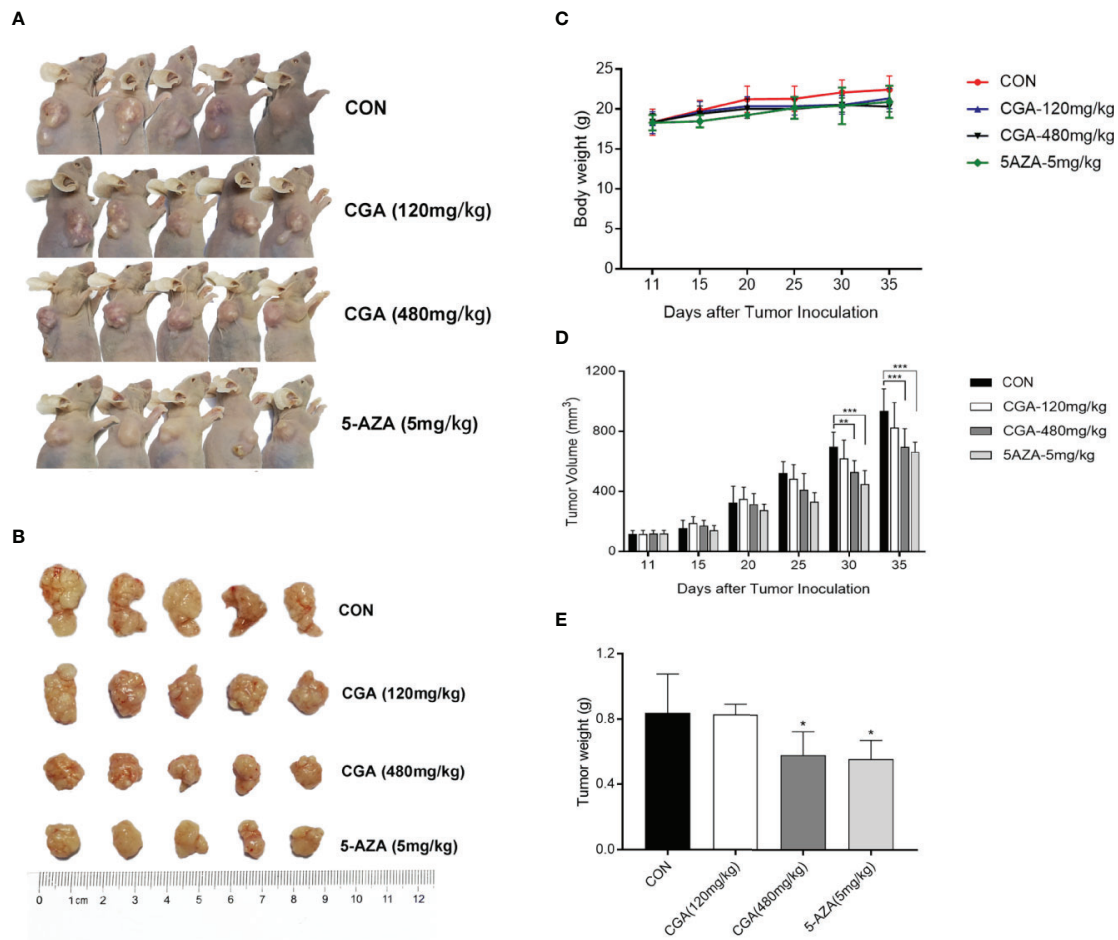
FIGURE 6 | CGA reduces HepG2 tumor xenograft's weight and volume. HepG2 cells were transplanted into nude mice and divided randomly into four groups: CON, CGA (120 and 480 mg/kg), and 5-AZA (5 mg/kg), and treated every day for 24 days from 11 days after tumor inoculation **(A, B)**. **(C)** Mouse body weights were measured every five days, from day 11 to day 35. **(D)** HepG2 xenograft tumor progression was assessed by tumor volume measurement every five days. **(E)** After 35 days, the tumor was resected, and weights measured. *$p < 0.05$, **$p < 0.01$, ***$p < 0.001$. CON, control group receiving intraperitoneal injection of normal saline.

1996). In addition, a previous study indicated that DNMT1 could translocate into the nucleus, inhibiting p53 transcription and leading to breast cancer progression by the activation of autophagy (Du et al., 2018). The inhibition of p53 expression was relieved in the absence of DNMT1, leading to the apoptosis of pancreatic progenitor cells (Georgia et al., 2013). Long noncoding RNA ATB could accelerate the proliferative and migratory rates of renal cell carcinoma cells and inhibit cell apoptosis through downregulation of p53 *via* binding to DNMT1 (Song et al., 2019). In this study, we showed a link between DNMT1 and p53, p21. The Western blotting analysis showed that CGA treatment resulted in decreased DNMT1 levels and increased p53 and p21 levels in HepG2 cells (**Figure 4**). This study reports for the first time, the effect of CGA on the expression of DNMT1 in HCC. Protein expression in HepG2 cells

examined by immunocytochemical methods showed a significant decrease in DNMT1 expression and increased p53, p21 in the CGA group (**Figure 5**). The above data showed the variable effect of CGA on the levels of DNMT1, p53, and p21 in HepG2 cells, leading to suppression of HCC proliferation.

ERK abnormalities participate in HCC cell proliferation processes and tumor progression (Shimizu et al., 2015). MMPs are critical for tumor invasion and metastasis by degenerating matrix proteins located on or outside the cells (e.g., proteoglycans and collagens) (Fassina et al., 2000; Mannello et al., 2005). Our results also showed that CGA inhibited HepG2 cell proliferation and HCC growth by inactivation of ERK and down-regulation of MMP-2/9, which prevented the degradation of the extracellular matrix (**Figure 4**); thus, these mechanisms may be involved in its anti-tumor effect.
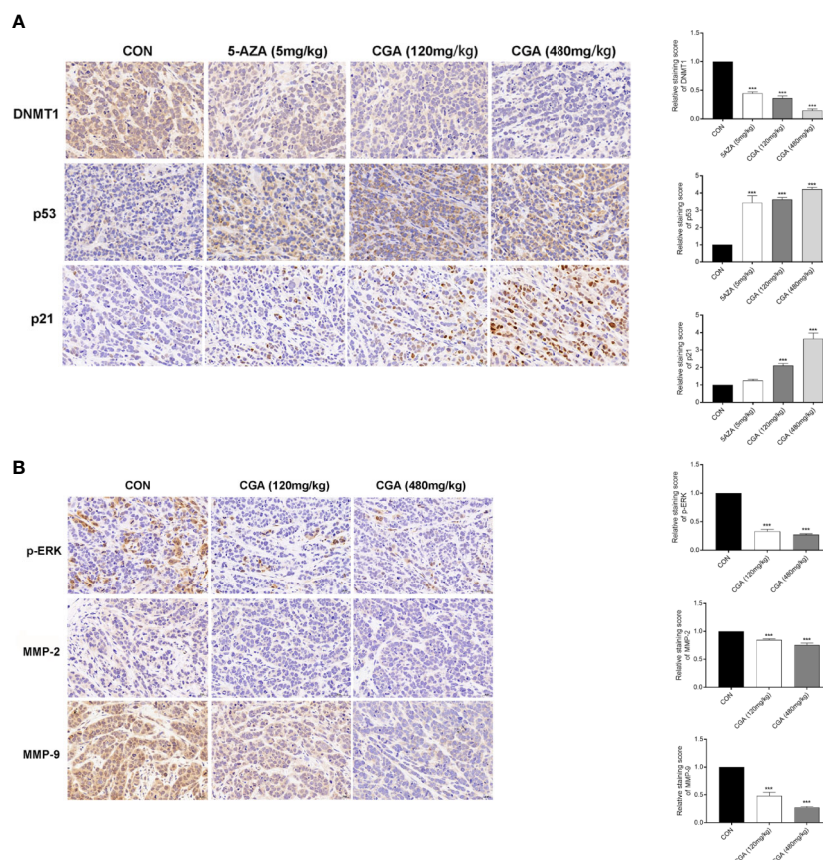
FIGURE 7 | Detection of DNMT1, p53, p21, p-ERK, MMP-2, and MMP-9 expression in HepG2 xenografts by immunohistochemistry (400× magnification). **(A)** Compared with the CON group, DAB staining showed a considerable decrease in DNMT1 expression and an increase in p53 and p21 expression in the CGA group. **(B)** And a considerable decrease in p-ERK, MMP-2 and MMP-9 expression in the CGA group. ***$p < 0.001$. CON, control group receiving intraperitoneal injection of normal saline.

DATA AVAILABILITY STATEMENT

The datasets generated for this study are available on request to the corresponding authors.

ETHICS STATEMENT

The animal study was reviewed and approved by Vital River Institutional Animal Care and Use Committee.

AUTHOR CONTRIBUTIONS

YF and XW designed this study and supervised the entire process. YaL performed IHC, carried out the majority of the vitro experiments, and performed cell viability and migration/invasion assay. GZ supervised the vivo experiments. YuL conducted the majority of the vivo experiments. YiH reviewed IHC slides. YaL wrote the manuscript. All authors contributed to the article and approved the submitted version.

FUNDING

REFERENCES

Bayan, L., Koulivand, P. H., and Gorji, A. (2014). Garlic: a review of potential therapeutic effects. *Avicenna J. Phytomed.* 4, 1–14.

Butt, M. S., Sultan, M. T., Butt, M. S., and Iqbal, J. (2009). Garlic: nature's protection against physiological threats. *Crit. Rev. Food Sci. Nutr.* 49, 538–551. doi: 10.1080/10408390802145344

Christman, J. K. (2002). 5-Azacytidine and 5-aza-2′-deoxycytidine as inhibitors of DNA methylation: mechanistic studies and their implications for cancer therapy. *Oncogene* 21, 5483–5495. doi: 10.1038/sj.onc.1205699

Dan, J., and Chen, T. (2016). Genetic Studies on Mammalian DNA Methyltransferases. *Adv. Exp. Med. Biol.* 945, 123–150. doi: 10.1007/978-3-319-43624-1_6

Du, W. W., Yang, W., Li, X., Awan, F. M., Yang, Z., Fang, L., et al. (2018). A circular RNA circ-DNMT1 enhances breast cancer progression by activating autophagy. *Oncogene* 37, 5829–5842. doi: 10.1038/s41388-018-0369-y

Elledge, S. J., Winston, J., and Harper, J. W. (1996). A question of balance: the role of cyclin-kinase inhibitors in development and tumorigenesis. *Trends Cell Biol.* 6, 388–392. doi: 10.1016/0962-8924(96)10030-1

Faria, M. H., Patrocinio, R. M., Moraes Filho, M. O., and Rabenhorst, S. H. (2007). Immunoexpression of tumor suppressor genes p53, p21 WAF1/CIP1 and p27 KIP1 in humam astrocystic tumors. *Arq. Neuropsiquiatr.* 65, 1114–1122. doi: 10.1590/S0004-282X2007000700004

Fassina, N., Ferrari, N., Brigati, C., Benelli, R., Santi, L., Noonan, D. M., et al. (2000). Tissue inhibitors of metalloproteases: regulation and biological activities. *Clin. Exp. Metastasis* 18, 111–120. doi: 10.1023/A:1006797522521

Feng, R., Lu, Y., Bowman, L. L., Qian, Y., Castranova, V., and Ding, M. (2005). Inhibition of activator protein-1, NF-kappaB, and MAPKs and induction of phase 2 detoxifying enzyme activity by chlorogenic acid. *J. Biol. Chem.* 280, 27888–27895. doi: 10.1074/jbc.M503347200

Georgakilas, A. G., Martin, O. A., and Bonner, W. M. (2017). p21: A Two-Faced Genome Guardian. *Trends Mol. Med.* 23, 310–319. doi: 10.1016/j.molmed.2017.02.001

Georgia, S., Kanji M Fau - Bhushan, A., and Bhushan, A. (2013). DNMT1 represses p53 to maintain progenitor cell survival during pancreatic organogenesis. *Genes Dev.* 27, 372–377. doi: 10.1101/gad.207001.112

Harper, J. W., and Elledge, S. J. (1996). Cdk inhibitors in development and cancer. *Curr. Opin. Genet. Dev.* 6, 56–64. doi: 10.1016/S0959-437X(96)90011-8

Harris, S. L., and Levine, A. J. (2005). The p53 pathway: positive and negative feedback loops. *Oncogene* 24, 2899–2908. doi: 10.1038/sj.onc.1208615

Hegi, M. E., Sciuscio, D., Murat, A., Levivier, M., and Stupp, R. (2009). Epigenetic deregulation of DNA repair and its potential for therapy. *Clin. Cancer Res.* 15, 5026–5031. doi: 10.1158/1078-0432.CCR-08-1169

Intisar, A., Zhang, L., Luo, H., Kiazolu, J. B., Zhang, R., and Zhang, W. (2012). Anticancer constituents and cytotoxic activity of methanol-water extract of Polygonum bistorta L. *Afr. J. Tradit. Complement. Altern. Med.* 10, 53–59. doi: 10.4314/ajtcam.v10i1.9

Ji, L., Jiang, P., Lu, B., Sheng, Y., Wang, X., and Wang, Z. (2013). Chlorogenic acid, a dietary polyphenol, protects acetaminophen-induced liver injury and its mechanism. *J. Nutr. Biochem.* 24, 1911–1919. doi: 10.1016/j.jnutbio.2013.05.007

Jones, P. A., and Baylin, S. B. (2002). The fundamental role of epigenetic events in cancer. *Nat. Rev. Genet.* 3, 415–428. doi: 10.1038/nrg816

Lai, K. C., Kuo, C. L., Ho, H. C., Yang, J. S., Ma, C. Y., Lu, H. F., et al. (2012). Diallyl sulfide, diallyl disulfide and diallyl trisulfide affect drug resistant gene expression in colo 205 human colon cancer cells in vitro and in vivo. *Phytomedicine* 19, 625–630. doi: 10.1016/j.phymed.2012.02.004

Luo, Q., Beaver, J. M., Liu, Y., and Zhang, Z. (2017). Dynamics of p53: A Master Decider of Cell Fate. *Genes (Basel)* 8, 66. doi: 10.3390/genes8020066

Ma, L., Chua, M. S., Andrisani, O., and So, S. (2014). Epigenetics in hepatocellular carcinoma: an update and future therapy perspectives. *World J. Gastroenterol.* 20, 333–345. doi: 10.3748/wjg.v20.i2.333

Mannello, F., Tonti, G., and Papa, S. (2005). Matrix metalloproteinase inhibitors as anticancer therapeutics. *Curr. Cancer Drug Targets* 5, 285–298. doi: 10.2174/1568009054064615

Nishida, N., and Goel, A. (2011). Genetic and epigenetic signatures in human hepatocellular carcinoma: a systematic review. *Curr. Genomics* 12, 130–137. doi: 10.2174/138920211795564359

Refolo, M. G., Lippolis, C., Carella, N., Cavallini, A., Messa, C., and D'Alessandro, R. (2018). Chlorogenic Acid Improves the Regorafenib Effects in Human Hepatocellular Carcinoma Cells. *Int. J. Mol. Sci.* 19, 1518. doi: 10.3390/ijms19051518

Sajadian, S. O., Tripura, C., Samani, F. S., Ruoss, M., Dooley, S., Baharvand, H., et al. (2016). Vitamin C enhances epigenetic modifications induced by 5-azacytidine and cell cycle arrest in the hepatocellular carcinoma cell lines HLE and Huh7. *Clin. Epigenet.* 8, 46. doi: 10.1186/s13148-016-0213-6

Shi, H., Dong, L., Bai, Y., Zhao, J., Zhang, Y., and Zhang, L. (2009). Chlorogenic acid against carbon tetrachloride-induced liver fibrosis in rats. *Eur. J. Pharmacol.* 623, 119–124. doi: 10.1016/j.ejphar.2009.09.026

Shi, H., Dong, L., Dang, X., Liu, Y., Jiang, J., Wang, Y., et al. (2013). Effect of chlorogenic acid on LPS-induced proinflammatory signaling in hepatic stellate cells. *Inflammation Res.* 62, 581–587. doi: 10.1007/s00011-013-0610-7

Shimada, M., Takenaka, K., Gion, T., Fujiwara, Y., Kajiyama, K., Maeda, T., et al. (1996). Prognosis of recurrent hepatocellular carcinoma: a 10-year surgical experience in Japan. *Gastroenterology* 111, 720–726. doi: 10.1053/gast.1996.v111.pm8780578

Shimizu, M., Shirakami, Y., Sakai, H., Kubota, M., Kochi, T., Ideta, T., et al. (2015). Chemopreventive potential of green tea catechins in hepatocellular carcinoma. *Int. J. Mol. Sci.* 16, 6124–6139. doi: 10.3390/ijms16036124

Song, C. A.-O., Xiong, Y., Liao, W., Meng, L., and Yang, S. (2019). Long noncoding RNA ATB participates in the development of renal cell carcinoma by downregulating p53 via binding to DNMT1. *J. Cell Physiol.* 234, 12910–12917. doi: 10.1002/jcp.27957

Vogelstein, B., Lane, D., and Levine, A. J. (2000). Surfing the p53 network. *Nature* 408, 307–310. doi: 10.1038/35042675

Wang, Q., Chen, Q., He, M., Mir, P., Su, J., and Yang, Q. (2011). Inhibitory effect of antioxidant extracts from various potatoes on the proliferation of human colon and liver cancer cells. *Nutr. Cancer.* 63, 1044–1052. doi: 10.1080/01635581.2011.597538

Xu, Y., Chen, J., Yu, X., Tao, W., Jiang, F., Yin, Z., et al. (2010). Protective effects of chlorogenic acid on acute hepatotoxicity induced by lipopolysaccharide in mice. *Inflammation Res.* 59, 871–877. doi: 10.1007/s00011-010-0199-z

Xu, Y., Su, D., Zhu, L., Zhang, S., Ma, S., Wu, K., et al. (2018). S-allylcysteine suppresses ovarian cancer cell proliferation by DNA methylation through DNMT1. *J. Ovarian Res.* 11, 39. doi: 10.1186/s13048-018-0412-1

Yan, Y., Liu, N., Hou, N., Dong, L., and Li, J. (2017). Chlorogenic acid inhibits hepatocellular carcinoma in vitro and in vivo. *J. Nutr. Biochem.* 46, 68–73. doi: 10.1016/j.jnutbio.2017.04.007

Yun, N., Kang, J. W., and Lee, S. M. (2012). Protective effects of chlorogenic acid against ischemia/reperfusion injury in rat liver: molecular evidence of its antioxidant and anti-inflammatory properties. *J. Nutr. Biochem.* 23, 1249–1255. doi: 10.1016/j.jnutbio.2011.06.018

Zhao, Y., Wang, J., Ballevre, O., Luo, H., and Zhang, W. (2012). Antihypertensive effects and mechanisms of chlorogenic acids. *Hypertens. Res.* 35, 370–374. doi: 10.1038/hr.2011.195

Advantages of publishing in Frontiers

OPEN ACCESS
Articles are free to read for greatest visibility and readership

FAST PUBLICATION
Around 90 days from submission to decision

HIGH QUALITY PEER-REVIEW
Rigorous, collaborative, and constructive peer-review

TRANSPARENT PEER-REVIEW
Editors and reviewers acknowledged by name on published articles

REPRODUCIBILITY OF RESEARCH
Support open data and methods to enhance research reproducibility

DIGITAL PUBLISHING
Articles designed for optimal readership across devices

FOLLOW US
@frontiersin

IMPACT METRICS
Advanced article metrics track visibility across digital media

EXTENSIVE PROMOTION
Marketing and promotion of impactful research

LOOP RESEARCH NETWORK
Our network increases your article's readership